

#### รายงานวิจัยฉบับสมบูรณ์

โครงการ การจำลองแบบของระบบไม่เชิงเส้นในชีววิทยาและการแพทย์: ทฤษฎีและการประยุกต์

# Modeling of Nonlinear Systems in Biology and Medicine: Theory and Applications

โดย ศาสตราจารย์ ดร. ยงค์วิมล เลณบุรี และคณะ

กรกฎาคม 2548

#### รายงานวิจัยฉบับสมบูรณ์

# ห้องสมุ

### โครงการ การจำลองแบบของระบบไม่เชิงเส้นในชีววิทย<del>์ โเละการ</del>แพทย์: ทฤษฎีและการประยุกต์

# Modeling of Nonlinear Systems in Biology and Medicine: Theory and Applications

	ผู้วิจัย	สังกัด			
1.	ศ. ดร. ยงค์วิมล	เลณบุรี	มหาวิทยาลัยมหิดล		
2.	ศ. ดร. อิ มิง	ถัง	มหาวิทยาลัยมหิดล		
3.	รศ. ดร. เบญจวรรณ	วิวัฒนปฐพี	มหาวิทยาลัยมหิดล		
4.	รศ. ดร. มนต์ทิพย์	เทียนสุวรรณ	มหาวิทยาลัยมหิดล		
5.	ดร. ปิยะพงศ์	เนียมทรัพย์	มหาวิทยาลัยเชียงใหม่		
6.	ผศ. ดร. วรรณพงษ์	เตรียมโพธิ์	มหาวิทยาลัยมหิดล		

สนับสนุนโดย สำนักงานกองทุนสนับสนุนการวิจัย

(ความเห็นในรายงานนี้เป็นของผู้วิจัย สกว. ไม่จำเป็นต้องเห็นด้วยเสมอไป)

#### TABLE OF CONTENT

	Content		page no		
1.	PROJECT TIT	LE ,	1		
2.	RESEARCH TI	EAM	1		
3.	RESEARCH FIELD				
4.	BACKGROUND AND RATIONALE				
5.	PROJECT OBJ	UECTIVES «	8		
<ol> <li>3.</li> <li>4.</li> <li>6.</li> </ol>	RESEARCH A	CTIVITIES	8		
	Subproject 1:	Dynamical Modeling of Systems in Medical Science	9		
	Subproject 2:	Mathematical Modeling of Blood Flow in the Coronary	24		
	4	Artery Bypass Grafting			
	Subproject 3:	Mathematical Modeling of Disease Transmission	57		
/	Subproject 4:	Application of Log-linear and Logistic Models to Cancer	60		
		Patients: A Case Study of the National Cancer Institute			
	Subproject 5:	Modeling and Computer Simulation in Cancer Research:	66		
		Theory and Modeling of the Growth of Tumors			
	Subproject 6:	Research on Asymptotic Stability of Difference Equations	88		
		with Delays			
7.	OVERALL OU	TPUT	94		
	7.1 Summary t	able	94		
<ol> <li>3.</li> <li>4.</li> <li>6.</li> </ol>	7.2 Rank promotions		95		
	7.3 Publication	95			
	7.4 Publication	98			
	7.5 Names of g	101			
8.	ADDITIONAL	COMMENTS	102		
	8.1 First annua	102			
	8.2 Second annual meeting				
	8.3 The final report meeting				
9.	APPENDICES		103		
	9.1 Manuscripts of newly accepted / appeared papers				
	9.2 Announcer	ments of Special Seminars	107		

#### **CONTRACT # RTA4580005**

#### **Final Report**

#### REPORT PERIOD

31 July 2002 - 30 July 2005

1. PROJECT TITLE: Modeling of Nonlinear Systems in Biology and Medicine: Theory and Applications

การจำลองแบบของระบบไม่เชิงเส้นในชีววิทยาและการแพทย์: ทฤษฎีและการประยุกต์

#### 2. RESEARCH TEAM:

#### Team Leader:

Prof. Yongwimon Lenbury, Ph.D. (Mathematics)

Address: Department of Mathematics, Faculty of Science, Mahidol University

Tel.: 02-644-5419 Fax: 02-644-5419 e-mail: scylb@mahidol.ac.th

Devoted Time per Week: 60 hours

# Subproject 1: Dynamical Modeling of Systems in Medical Science Principal Investigator:

Prof. Yongwimon Lenbury, Ph.D. (Mathematics)

Address: Department of Mathematics, Faculty of Science, Mahidol University

Tel.: 02-644-5419 Fax: 02-644-5419 e-mail: scylb@mahidol.ac.th

Devoted Time per Week: 60 hours

#### **Team Members:**

2 University lecturers:

• Miss Pornsarp Pornsawad, M.Sc. (Applied Mathematics)

Address: Department of Mathematics, Faculty of Science, Silpakorn University

Tel.: (034) 243-428 Fax: (034) 243-428 e-mail: ppornsup@hotmail.com

Devoted Time per Week: 20 hours

Responsibility: research assistant in analysis and computer simulations.

▶ Miss Wannapa Kunphasuruang, M.Sc. (Applied Mathematics)

Address: Department of Mathematics, Faculty of Science, Silpakorn University

Tel.: (034) 243-428 Fax: (034) 243-428 e-mail: wannapa@su.ac.th

Devoted Time per Week: 25 hours

Responsibility: research assistant in analysis and computer simulations.

- 5 Ph.D. students
- 1 M.Sc. student

#### **Expert Contacts:**

- Prof. Phillip S. Crooke (Vanderbilt University, U.S.A.)
- Prof. Glenn F. Webb (Vanderbilt University, U.S.A.)

## Subproject 2: Numerical Analysis of Pressure and Blood Flow in Artery Bifurcation with Surgical Reconstruction

#### **Principal Investigator:**

Assoc. Prof. Benchawan Wiwatanapataphee, Ph.D. (Mathematics)

Address: Department of Mathematics, Faculty of Science, Mahidol University

Tel.: 02-201-5345 Fax: 02-644-5419 e-mail: scbww@mahidol.ac.th

Devoted Time per Week: 30 hours

#### Team Members:

- 1 University lecturer:
- Dr. Mahosut Punpocha, Ph.D. (Mathematics)

Address: Department of Mathematics, Faculty of Applied Science,

King Mongkut's Institute of Technology North Bangkok

Tel.: 02-5878258 Fax: 02-5878258 e-mail: mpc@kmitnb.ac.th

Devoted Time per Week: 30 hours

Responsibility: research assistant with computational and modeling skills in Fluid Dynamics.

6 Ph.D. students

#### **Expert Contacts:**

> Dr. Permyos Ruengsakulrach (The Saint Louis Hospital, Thailand)

Prof. Yong Hong Wu (Curtin University of Technology, Australia)

### Subproject 3: Mathematical Modeling of Disease Transmission Principal Investigator:

Prof. I. Ming Tang, Ph.D. (Physics)

Address: Department of Physics, Faculty of Science, Mahidol University

Tel.: 02-201-5773 Fax: 02-246-1381 e-mail: scimt@mahidol.ac.th

Devoted Time per Week: 20 hours

#### Team Members:

4 Ph.D. students

#### **Expert Contacts:**

Dr. Jean-Paul Gonzalas (Institutde Recherche pour Developpement, France)

Dr. Phillippe Barbazan (Institutde Recherche pour Developpement, France)

Prof. Dr. Warren Brockelmann (Conservation Biology Center)

Prof. Dr. Suthee Yoksan (Center for Vaccine Development)

# Subproject 4: Application of Log-linear and Logistic Models to Cancer Patients: A Case Study of the National Cancer Institute

#### Principal Investigator:

Assoc. Prof. Montip Tiensuwan, Ph.D. (Applied Statistics)

Address: Department of Mathematics, Faculty of Science, Mahidol University

Tel.: 02-201-5762 Fax: 02-644-5419 e-mail: scmts@mahidol.ac.th

Devoted Time per Week: 20 hours

#### Team Members:

- 3 Ph.D. students
- 2 M.Sc. students

#### **Expert Contacts:**

Prof. Bimal K. Sinha (University of Maryland, Baltimore County, U.S.A.)

Subproject 5: Modeling and Computer Simulation in Cancer

Research: Theory and Modeling of the Growth of

Tumors

#### Principal Investigator:

Asst. Prof. Wannapong Triampo, Ph.D. (Physics)

Address: Department of Physics, Faculty of Science, Mahidol University

Tel.: 02-201-5770 Fax: 02-246-1381 e-mail: wtriampo@yahoo.com

Devoted Time per Week: 40 hours

#### **Team Members:**

5 Ph.D. students

#### **Expert Contacts:**

Prof. Timothy Newman (University of Virginia, U.S.A.)

# Subproject 6: Research on Asymptotic Stability of Difference Equations with Delays

#### Principal Investigator:

Dr. Piyapong Niamsup, Ph.D. (Mathematics)
 Address: Department of Mathematics, Faculty of Science, Chiangmai University
 Tel.: (053) 943-327 Fax: (053) 892-280 e-mail: scipnmsp@chiangmai.ac.th
 Devoted Time per Week: 30 hours

#### .Team Members:

• 1 Ph.D./M.Sc. student

#### **Expert Contacts:**

> Prof. Julian J. Palmore (University of Illinois, U.S.A.))

3. RESEARCH FIELD: Mathematical Science (Modeling, Nonlinear Systems, Biomathematics).

#### 4. BACKGROUND AND RATIONALE:

Characterization of biological systems has reached an unparalled level of interest and concentration. In order to arrive at a better fundamental understanding of life processes, it is imperative that powerful conceptual tools from mathematics and the physical sciences be applied to the frontier problems in biology. As stated in the 1996 report of the National Science Foundation (NSF) of the United States, "modeling of biological systems is evolving into an important partner of experimental work. All facets of biology, environmental, organism, cellular and molecular biology are becoming more accessible to chemical, physical and mathematical approaches".

The goals of mathematical, statistical, and computational approaches are to elucidate mechanisms for seeming disparate phenomena. The NSF report also voiced its belief in the tremendous potential of mathematical and computational approaches in leading to fundamental insights and important practical benefits in research on biological systems. "Mathematical and computational approaches have long been appreciated in physics and in the last twenty years have played an ever-increasing role in chemistry. It is our opinion, they are just coming into their own in biology".

As evidenced by the NSF report and the establishment of several research centers in biomathematics all over the world, it is clear that mathematical/computational methods which are based on fundamental physical laws, theory of nonlinear systems, empirical data analyses, and their combination, are providing a key element in biological research. These methods can provide hypotheses that let one go beyond the empirical data and be ready for constant testing for their range of validity. It is, in the opinion of this research team, our undeniable task to try to keep pace with this high speed development.

Despite its recognized relevance, the science of mathematical modeling still encounters resistance from some members of the professional field who might feel they have no need for unrealistic mathematical models. According to Novak (1991), there can be two answers to this skepticism. The first is that cellular and population interactions are highly nonlinear, and that many examples show intuition alone is a poor guide to predicting the behavior of nonlinear systems. Thus, although all good biologists and medical researchers already use theory, that theory could be more rigorously defined and more productively explored if it were expressed in mathematical form and its consequences investigated on this ground.

The second answer is to point out that even though the past two centuries have provided us with a rapidly growing catalog of organisms, as well as increasing detailed information about the interactions among them, it is still incomplete. Real advances in understanding how individual populations, or communities of interacting populations, respond to natural or artificial disturbance has come from combinations of mathematical models and experimental programs deliberately focused on population-level properties. The models, some of which are meant to contemplate specific systems in a detailed way, while others are constructed to answer larger questions in a relatively abstract fashion, have foundations on field and laboratory observations of the constituent individuals. All share the common purpose of helping to construct a broad theoretical framework within which to assemble an otherwise indigestible mass of field and laboratory data, and of helping us understand how seemingly simple properties at the level of individual organisms can give rise to surprising, and often bizarre, outcomes at the level of populations (Novak et al., 1991).

Recent scientific advances has made it now possible to analyze complex biological phenomena, including disease processes. Indeed, some of the most promising discoveries in biomedicine have resulted from the insights of investigators with strong backgrounds in physics, mathematics, and chemistry. Yet strong organizational barriers often impede efforts to bring scientists and students with training focused in the physical, mathematical, chemical, or quantitative sciences into research or graduate/postdoctoral programs in the biomedical science. This research team has been an instrument in the effort to encourage collaborations across disciplines and lower the barriers for interdisciplinary research. This is clearly reflected by the six subprojects carried out by the members of this research team.

The key role of interdisciplinary research and training perhaps is nowhere more evident than in the hot new field of "bioinformatics"—the study of how information is represented and transmitted in biological systems. In nerve cells, information is transmitted through electrical impulses which cause muscles to contract and endocrine cells to secrete hormones. Quite often, impulses are generated in high-frequency bursts, followed by periods of quiescence. This is particularly true in endocrine systems. It is believed that modulation of amplitudes and/or frequencies of these temporal hormone secretory patterns plays an important role in the regulation of receptor synthesis, internalization, and cellular functions. Therefore, Subproject 1.1 has been involved with investigating such cascade

feedback endrocrine systems in terms of the temporal secretion characteristics which exhibit time lags in their response mechanism.

Moreover, recent advances in instrumentation have made it possible to measure motions and mechanical forces with high speed and efficiency. These techniques have begun to supply data that has revived interest in cellular mechanics. It is now possible to make realistic models of bio-mechanical processes that can be related directly to experimentally observable, and controllable, parameters (Peskin and Oster, 1995). Subprojects 1.2 and 1.3, on mechanical ventilation and antibiotic models respectively, have taken advantage of these advances in experimental technology.

Furthermore, because of the ongoing revolution in computation theory and technology, we can now solve fluid dynamics problems in the three spatial dimensions and time (Ellington and Pedly, 1995). This opens up biological opportunities on many different scales and sizes (NSF report, 1996). For example, one can now perform fluid dynamics simulations of the embryonic and fetal heart at different stages of development. Such models will help to elucidate the role of fluid forces and flows in the control mechanisms of the human physiology. The research in Subproject 2. tackled the problem of blood flow simulation under variable boundary conditions. The difficulty in measuring and simulation of microscopic fluid flows and the dependence on access to large-scale scientific computing make it important that the best technology be made available to scientists on a scale sufficient to sustain this kind of research.

ç:

On the other hand, on the scale of populations, opportunities also exist for substantial advances in immunology by the use of modeling techniques. During the last decade mathematical modeling has had a major impact on research in immunology and virology (NSF report, 1996). Serious collaborations between theorists and experimentalists have provided break through discoveries. For example, in AIDS research experiments in which patients were given anti-retroviral drugs as perturbations of a nonlinear dynamical system, mathematical modeling combined with analysis of data obtained during drug clinical trials established for the first time that HIV is rapidly cleared from the body and that approximately 10 billion virus particles are produced daily (Ho et al., 1995). Such successes indicate that opportunities exist for developing realistic and useful models of many viral diseases, studied as a nonlinear problem. Subproject 3. has met this challenge by concentrating on modeling transmission of re-emerging viral diseases, such as dengue haemorrhagic fever, Japanese encephalites, malaria, West Nile virus, SARs, and Peptosprosis.

Considering all the above mentioned research activities with which this project has been involved, it is clear that crucial component of any research in modeling has to do with data analysis and statistical techniques and concepts. Biological and biochemical research is producing exponentially-growing data sets. Thus, a statistical component such as the group proposing Subprojects 4. and 5. has been an important integral unit in this research team. They have been devoted to modeling of processes which involve the progression of tumor, incorporating useful concepts in statistics and stochastic principles.

Last, but not least, mathematical analysis is needed to interpret the results of numerical simulations and modeling, as well as incorporate the insights into nonlinear models. There are fundamental limits to predictability of biologically interesting quantities since we are dealing with nonlinear systems with possible chaotic dynamics. This is the reason why theory and modeling studies should develop in parallel fashion. Additional theory of nonlinear systems should be made available as a necessary basis for modeling as well as experimental measurements, so that it becomes and iterative, interactive process, and thus the proposal of Subproject 6. It has provided us with the necessary theoretical foundation for asymptotic stability analysis of nonlinear systems with delays.

#### **5. PROJECT OBJECTIVES:**

- Develop necessary theory, techniques and tools to construct and analyze models of nonlinear systems.
- Construct appropriate models of nonlinear systems such as the hormone secretion system, mechanical ventilation, bacteria growth in the presence of antibiotics, blood flow, tumor growth, disease transmission, and other biological processes of current interest.
- 3. Analyze the models theoretically and numerically to gain insights leading to useful suggestions for control/management strategies.

#### 6. RESEARCH ACTIVITIES:

This research team has in fact been studying, as well as those originally proposed for this project, several other biological systems which were not specifically mentioned in the proposal, yielding a lot more international publications than what has been promised. The following is the detailed description of activities and outputs of each subproject in the past 3 years.

#### Subproject 1: Dynamical Modeling of Systems in Medical Science

Principal Investigator: Prof. Dr. Yongwimon Lenbury

In general, mathematical models can be used to promote an understanding of the system of interest and they can be used to predict its behavior (Zahalak, 1992). An enhanced understanding can be achieved by describing a complicated phenomenon in terms of a limited number of simpler concepts. A good model thus allows insights into the relevant processes of the system. It can also enable one to assess how a system will behave in situations that cannot be experimentally validated.

It is important to note that the model must be developed to match the task. To choose a model, one must select a suitable model form, an appropriate level of model complexity, and a set of model parameters. Two general types of model form are structural models and phenomenological models. Structural models (sometimes called 'parametric' models) are based on fundamental physical properties of the system and may be most appropriate to gain insight into physiological processes. Phenomenological models (sometimes called 'empirical' or 'non-parametric' models) are based on observations of input/output relationships and may sometimes be suitable for simulation studies or control implementation.

Another concern in selecting a model is that of model complexity. In general, a model should be kept as simple as possible, i.e. its order and number of parameters should be as low as possible (Zahalak, 1992). Only those physiological effects should be considered that are relevant for the specific task.

The activities in this subproject can be categorized into 3 headings as follows.

#### 1.1 Investigation of time lags in signaling responses in feedback cascade systems.

ŀ:

In many biological systems, information is transferred by hormonal ligands, and it is assumed that these hormone signals encode developmental and regulatory programs in mammalian organisms. Recently, it became apparent that hormone pulses contribute to this hormonal pool which modulates the responsiveness of receptors within the cell membrane by regulation of the receptor synthesis, movement within the membrane layer, coupling to signal transduction proteins and internalization.

In simple organisms, the detection of nonlinear or chaotic behavior in information transfer is associated with differentiation and proliferation. Modulation of the amplitude and/or the frequency of the hormone pulses in higher organisms is believed to be capable of modifying intracellular signaling pathways, gene expression, cell proliferation, and cellular functions. Modeling of episodic hormone secretion and identification of nonlinear

deterministic dynamics in an apparently irregular hormonal rhythm in human physiology can lead to valuable insights into the physiological linkage between functional and genetic programs of the living organisms.

Many hormone secretion systems incorporate some form of cascade mechanism into their operation. A system with a cascade mechanism is an amplification process where an initial reaction results in the generation of multiple second reactions, each of which sets off multiple third reactions, and so on.

An example of cascade processes is found in eco-systems such as in the plantherbivore-carnivore food chain. In general, the biomass and the reproductive rates of the components in the cascade increase as we proceed down the trophic levels. Another example of systems which incorporate the cascade mechanism involves the central nervous system, the hypothalamus, pituitary, and the distal hormone secretion glands.

Up to date, little attention to our knowledge has been devoted to analysis of cascade systems and the time lags in their response mechanisms. Although several workers have developed stability and oscillation theory for differential equations with delay (Hamada and Anderson, 1983; Lee and Zak, 1986; Bainov, 1991; and Hennet and Tarbouriech, 1997), they are concerned mainly with second order systems most of which are linear. In 1995, Campbell et al. analyzed a second-order, nonlinear delay-differential equation with negative feedback, dealing with existence for limit cycles, tori, and complex dynamics. Typically these equations take the form

$$\ddot{\mathbf{x}} + \beta \dot{\mathbf{x}} + \alpha \mathbf{x} = \mathbf{f}(\mathbf{x}_{\star}) \tag{1.1}$$

where  $\alpha, \beta$  are positive constants,  $\tau$  is the time delay,  $x, x_{\tau}$  are the values of the controlled variable evaluated at, respectively, times t and  $t - \tau$ , and the function f(u) is a nonnegative, monotone decreasing function of u which describes negative feedback.

Most recently, Michiels et al. (2000) reported on the stability of perturbed delay differential equations and stabilization of nonlinear cascade systems. They studied nonlinear time delay systems of the form

$$\dot{z} = f(z, z(t-\tau)) + \Psi(z, z(t-\tau))w \tag{1.2}$$

where  $z \in \Re^n$ ,  $w \in \Re$ . Investigation was carried out to find conditions under which global stability would be preserved and if not, whether semi-global stabilization was possible by reducing the size of the perturbation or modifying its shape.

We have been able to identify 3 types of delay mechanism which have been observed in biological/medical systems. The first type of delays is associated with the maturation time required before a member of the population may procreate or produce off springs. In this case, the reproduction rate r(t) at time t is a function which depends on the population density x at a time  $t-\tau$ ; namely,

$$r(t) = f(x(t-\tau))$$

In past research works, f has been assumed to be a monotonic function. The theories concerning existence, uniqueness, persistence, or stability of a solution to the model equation usually depend on very stringent conditions on the function f. They are therefore applicable only to limited number of population models. We have investigated this type of delays as reported in Part a) below.

The second type of delays is found in cascade systems in which different components in the system possess diversified dynamics. When we move down the cascade, the components respond with drastically different speeds. A delayed response of one component to change in another component is then due to this diversified characteristics. This type of delay mechanisms can have very significant applications in the management and control of nonlinear systems in biology and medicine. We have studied a system with this type of delays as detailed in Part b) below.

The third type of delays is associated by the transport time required for a signal to travel or an increased level in one component at the peripheral region to arrive at the target organ and take its effects. For example, an injected dose of supplementary insulin may require time in transport before its increase may be felt at the target site to give rise to a reduction in the glucose level as intended. We have investigated this type of delays as detailed in Part c) below.

a) New analytical tools necessary for tackling the nonlinear system models have been developed. We have successfully proved theorems for the existence, stability, and persistance of solutions to delayed differential equations of the form

$$\dot{x}(t) = -\mu x(t) + f(x(t - \tau)) \tag{1.3}$$

which is a delayed population model capable of modelling several dynamical systems of interest in medical science, such as viral proliferation or cell divisions, etc., the rate of which is delayed by the maturation time. The function f utilized in (1.3) was assumed

٠i

in past research works to be monotone. We however allowed f to be non-monotone, and sometimes not continuous, which is more general.

The following theorems have been proved.

**Theorem 1** If  $f(u) < \mu u$  for all u > 0 then every solution x(t) of (1.3) converges to 0 as  $t \to \infty$ .

Conversely, if every solution of (1.3) converges to 0 then  $f(u) < \mu u$  for all u > 0.

**Theorem 2** Assume that f(x) > 0 for all x > 0 and

$$\limsup_{x \to \infty} \frac{f(x)}{x} < \mu$$

$$\liminf_{x\to 0+} \frac{f(x)}{x} > \mu$$

Then, every solution x(t) of (1.3) is persistent.

**Theorem 3** Suppose that f(x) is monotonically increasing and

$$\limsup_{x \to \infty} \frac{f(x)}{x} < \mu, \tag{1.4}$$

$$\liminf_{x \to 0} \frac{f(x)}{x} > \mu.$$
(1.5)

Then, every solution x(t) of (1.3) converges to the unique  $\overline{x}$  such that  $f(\overline{x}) = \overline{x}$ .

**Theorem 4** Suppose that f(x) is monotonically decreasing and the following system

$$a = \frac{f(b)}{\mu}$$

$$b = \frac{f(a)}{u}$$

has a unique solution  $a = b = \overline{x}$ . Then, every solution x(t) of (1.3) converges to  $\overline{x}$ .

**Theorem 5** Suppose that  $f(y_0) = \max_{x \ge 0} f(x) \le \mu y_0$ . Also, (1.4) and (1.5) are assumed to

be true. Let x(t) be a persistent solution of (1.3). Then  $\lim_{t\to\infty} x(t) = \overline{x}$ .

**Theorem 6** Suppose that (1.5) holds. Suppose, moreover, that the solution of the following system of difference equations

$$\begin{aligned} a_{n+1} &= \inf_{x \in [a_n, b_n]} \frac{f(x)}{\mu} \\ b_{n+1} &= \sup_{x \in [a_n, b_n]} \frac{f(x)}{\mu} \qquad (n = 1, 2, ...), \\ a_1 &= \inf_{x > 0} \frac{f(x)}{\mu} \qquad b_1 = \sup_{x > 0} \frac{f(x)}{\mu} \end{aligned}$$

converges to  $\overline{x}$ . Then every persistent solution of (1.3) converges to  $\overline{x}$ .

This part of our work has been published in the international journal *Mathematical*1 and Computer Modelling. Please see the paper that has appeared in Appendix # 1.1.

We have continued to work on the model (1.3) and given further stability conditions which depend on the delay  $\tau$ , as well as conditions under which periodic solutions would exist. This portion of work has yielded another paper which has been accepted for publication in the *Journal of Mathematical Analysis and Applications*. Please see the full paper in Appendix # 1.2.

Further, since many systems involve many interacting components, the analysis of the system models needs more sophisticated techniques. We have therefore developed a higher order singular perturbation technique for the analysis of cascade systems involving n+3 components ( $n \ge 1$ ). The arguments yield separation conditions on the system parameters by pivoting about the slow component of the cascade. This result has been published in *Mathematical and Computer Modelling* as can be seen in Appendix # 1.3.

Also, in many of these nonlinear system models, chaotic behavior has been often discovered which poses serious problems for control. In order to investigate how we can control such chaotic phenomena in biological systems, we considered a Komolgorov type model of cascade systems, such as food webs, with external input and removals. Applying a feedback control technique proposed by Isidori (1985), we were able to derive the rules under which chaotic solution can be counteracted and system stability or robustness may be assured. This result is published in *ScienceAsia* (appendix #1.4).

b) Modelling of bone formation has been carried out, the mathematical formulation of which was based biologically on clinical evidence observed in various reports such as that of Hock and Gera (1992), Dempster et al. (1993), Momsen and Schwarz (1997), Kong et al. (1999), Takahashi et al. (1999), Burgess et al. (1999), or Kroll (2000) amongst several others.

Firstly, since activated osteoclasts result from differentiation and activation of osteoclast precursors, we assume that a high level in osteoclast precursors is reflected in the high level of the resulting activated osteoclastic population C(t). Secondly, osteoclasts resorb bone and liberate calcium, in order to counter balance the high level of calcium in blood the rate of PTH secretion will decrease (Momsen and Schwarz, 1997). The equation for the rate of PTH secretion is then assumed to take the form

$$\frac{dP}{dt} = \frac{c_1}{k_1 + C} - d_1 P \tag{1.6}$$

where P(t) denotes the level of PTH above the basal level. The first term on the right-hand side represents the secretion rate of PTH from the parathyroid grand which decreases with the increase in the number of active osteoclastic cells C(t), c<sub>1</sub> and k<sub>1</sub> being positive constants. This accounts for the above mentioned observation that as active osteoclasts C resorb bone and liberate calcium, the rate of PTH secretion will decrease to counter balance the high level of calcium in blood. Therefore, a higher C should lead to lower PTH secretion rate. Finally, it is assumed that the hormone is removed from the system at the rate which is proportional to its current level with the removal rate constant d<sub>1</sub>.

The dynamics of the osteoclastic population, on the other hand, can be described by the following equation

$$\frac{dC}{dt} = \frac{(c_2 + c_3 P)BC}{k_2 + P^2} - d_2 C$$
 (1.7)

where the first term on the right-hand side represents the reproduction of active osteoclasts which requires the production of osteoclast differentiation factor (ODF) and its receptor on osteoclasts (Kroll, 2000). The more C means the more ODF receptors available for the reproduction of active osteoclasts, and hence the term is taken to depend on the number of osteoclasts C at that moment in time.

Moreover, osteoclasts precursors possess RANK, a receptor of tumor necrosis factor (TNF) family that recognizes ODF through a cell-to-cell interaction with osteoblasts (Kong et al., 1999; Takahashi et al., 1999; Burgess et al.,1999; Kroll, 2000), hence the rate of reproduction is taken to depend also on the number of active osteoblastic cells B(t) at any time t. Based on the well founded theory on mathematical modeling and population dynamics known as the law of mass action (Leah, 1988), when an event occurs through cell-to-cell interaction of the two populations involved, the rate may then be assumed to

vary as their product, provided that the event occurs randomly. However, the rate of reproduction of C increases with the increase in the level of PTH (Dempster et al., 1993; Weryha and Leclere, 1995). On the other hand, it has been clinically observed (Kroll, 2000) that as PTH level increases further, it begins to inhibit osteoclastic reproduction, and hence the saturation expression  $(c_2 + c_3 P)/(k_2 + P^2)$  is assumed for the stimulating effect of PTH, where  $c_2, c_3$ , and  $k_2$  are positive constants.

Thus, without any active osteoclasts or osteoblasts (C = 0, B = 0), the reproductive rate of C should vanish. On the other hand, C will be produced at the rate which varies directly as the product BC, by the law of mass actions mentioned before, with the variation constant  $c_2/k_2$  at vanishing P. With PTH mediation, however, this variation parameter increases initially with increasing P but decreases when P becomes too high according to the saturation function utilized in Eq. (1.7), where  $c_3$  is a measure of how late the inhibition effect will set in.

Finally, the dynamics of the active osteoblastic population B(t) can be described by the following equation

÷į

$$\frac{dB}{dt} = c_4 P - \frac{c_5 PB}{k_1} + P - d_3 B \tag{1.8}$$

where  $c_4$  is the specific rate at which PTH stimulates reproduction of active osteoblasts (Brown, 1991; Isogai et al., 1996), while the second term on the right-hand side of Eq. (1.8) accounts for the clinically observed inhibition of osteoblastic differentiation due to the PTH (Kroll, 2000). PTH stimulates osteoblast differentiation in immature osteoblasts but inhibits it in more mature cells (Isogai et al., 1996), through the process of down-regulation of the PTH receptors on osteoblasts. IL-6, a cytokine produced by osteoblasts, enhances the anti-proliferative effects of PTH by suppressing the PTH-induced  $Ca^{2+}$  transients in addition to the down-regulation of the PTH receptor caused by chronic activation of the protein kinase A signal pathway. Therefore, PTH and IL-6 produced by osteoblasts exert a receptor-mediated negative feedback on the conversion of preosteoblasts to osteoblasts (Kroll, 2000). The inhibition effect is assumed here to take the form of the Holling type response function  $c_5P/(k_3 + P)$  which means that there should be no such inhibition if B or P vanishes. The inhibition term  $c_5PB/(k_3 + P)$  then tends to  $c_5B$  at high PTH level, so that the osteoblastic formation is predominantly stimulated positively by PTH according to

the first term  $c_4P$  in Eq. (1.4) at higher levels of this hormone. This is consistent with observed clinical data reported by both Tam et al. (1982) and Hock and Gera (1992). The parameters  $c_5$  and  $k_3$  may then be varied to accommodate different physiological data of different individuals. The higher  $k_3$  means the inhibition remains effective still at higher level of PTH. The last terms in Eqs. (1.6)-(1.8) are the removal rates of the three components of the remodeling process with rate constants  $d_1, d_2$  and  $d_3$ , respectively.

Our reference core model, therefore, consisted of Eqs. (1.6)-(1.8), possessing highly diversified nonlinear characteristics, upon which analysis and investigation were carried out in an attempt to explain several mystifying empirical observations.

A singular perturbation analysis was carried out to yield conditions under which periodic solutions can be expected. A bifurcation diagram was then constructed to identify the ranges of a system parameter which permitted chaotic hormone secretory patterns. Our theoretical results and numerical experiments conformed with observed clinical data. Moreover, investigation of the effects of estrogen supplements suggested to us that, in order to prevent severe osteoporosis, it might be possible to give estrogen supplements only for disjointed periods and not for the entire time. The effect of a high enough dose, given during a long enough period, can last for some time after the supplement has be cut off. This lagged or delayed effect, due to the diversified time responses inherent to this cascade, can last long enough to overlap with the next period of estrogen supplement. Such dosing regimen may reduce the danger of side effects due to prolonged estrogen treatment, such as cancer.

The result of this piece of research has already been accepted and appeared in *BioSystems*, an international journal with impact factor 0.736. (Please see manuscript in Appendix # 1.5)

c) Modelling of endocrine systems has been carried out by incorporating time delays into a mathematical model of the hypothalamus adrenal cortex axis, which resulted in the following system of nonlinear delay differential equations.

$$\frac{\mathrm{dR}}{\mathrm{dt}} = -\delta_1 R + \kappa_1 e^{\beta_1 (1 - A^2 (t - \tau_2))} \tag{1.9}$$

$$\frac{dA}{dt} = -\delta_2 A + \kappa_2 e^{\beta_2 (1 - C^2 (t - \tau_2))} R(t - \tau_1)$$
 (1.10)

$$\frac{dC}{dt} = -\delta_3 C + \kappa_3 A(t - \tau_2)$$
 (1.11)

where R(t), A(t), and C(t) are plasma concentrations of corticotropin releasing hormone (CRH), adrenocorticotropic hormone (ACTH), and cortisol (C), respectively, while  $\delta_1, \delta_2$ , and  $\delta_3$  are the respective hormone removal rates, and  $\kappa_1, \kappa_2$ , and  $\kappa_3$  are the respective hormone secretion rate constants.  $\beta_1$  and  $\beta_2$  are the feedback response potencies. The feedforward response is assumed to have a delay of  $\tau_1$  due to traveling time required before the target is reached, while the feedback effect of cortisol on ACTH or ACTH on CRH is assumed to have a delay of  $\tau_2$ .

We analyzed the model system (1.9)-(1.11) by the Hopf bifurcation theory to investigate the possibility of periodic solution and chaotic dynamics. The paper on the results has been published in the *Mathematical Medicine and Biology* with impact factor 0.368. (Please see manuscript in Appendix # 1.6).

We also applied these analytical techniques to a model of Liutinizing hormone secretion system and published another paper in *Pure and Applied Chemistry* (Appendix # 1.7)

#### 1.2 Mathematical modeling of non-invasive mechanical ventilation

ì

ł

1

;

Many forms of pressure preset ventilation have been introduced to clinical practice, each characterized by the abrupt and periodic application and release of a set level of airway pressure at the airway opening (Boysen and McGough, 1988; Stock et al., 1987, Tharatt et al., 1988).

Although numerous attempts have been made to model the behavior of the respiratory system (Ligas et al., 1990; Burke et al., 1993; Venegas et al., 1998), few have accounted for the nonlinear pressure-flow relationships which characterize biological systems. Linear approximations sometimes serve quite well, however, the frictional component of pressure loss (influenced by changes in flow regime) varies non-linearly with the flow rate (Crooke and Marini, 1993).

In 1993, Marini and Crooke developed a general mathematical model for the dynamic behavior of a single-compartment respiratory system in response to an arbitrary applied airway pressure. It provided the means to compute most ventilation and pressure variables of clinical interest from clinician-selected and patient-specific impedance parameters. A general two-compartment model was considered by Crooke et al. in 1996. In both models, clinically important outcome variables, such as tidal volume, end-expiratory

pressure, minute ventilation and mean alveolar pressure were computed for an arbitrary applied inspiratory airway pressure.

In 1993, Crooke and Marini also presented and analyzed a nonlinear mathematical model of pressure preset ventilation which accounts for the interactive behavior of inspiratory and expiratory half cycles. It comprises a set of nonlinear differential equations which incorporates a variably nonlinear relationship between the resistive component of applied pressure and flow rate. This model was compared to the linear model of pressure preset ventilation which served to link the clinical input variables of pressure level, frequency, inspiratory time fraction, and impedance with the key outcome variables of clinical interest: tidal volume, minute ventilation, mean alveolar pressure, and end-expiratory pressure. Predictive differences arise between linear and nonlinear formulations.

In 1998, dynamics of the elastic pressure-volume (Pet-V) curve were determined during a single prolonged insufflation before and after the recruitment manoeuvre by Svantesson et al. A mathematical three-segment model of the curve including a linear intermediate segment, delineated by the lower (LIP) and upper (UIP) inflection points, was used for illustration of the recorded curves. This was due to the fact that the model was based on the concept that compliance varied with volume.

Our reference mathematical model for pressure support ventilation incorporates pressure support ventilation that is applied to a single compartment lung with compliance C, inspiratory resistance  $R_i$ , and expiratory resistance  $R_e$ . The ventilator cycle is split into two parts: inspiration of duration  $t_i$ , and expiration of duration  $t_e$ . The total length of each cycle is  $t_{tot} = t_i + t_e$ . During inspiration, a preset pressure  $P_{set}$  is applied to the airway, and during expiration, the ventilator applies a constant pressure  $P_{peep}$ .

At any instant of time in  $[0,t_{tot}]$ , there is a pressure balance between applied pressures to the compartment ( $P_{vent}$ ), pressures due to elastic forces ( $P_{elastic}$ ), pressures due to resistive forces ( $P_{resistive}$ ), and residual pressures ( $P_{residual}$ ). The volume of the compartment, V(t), is modeled by differential equations that correspond to the pressure balances in the system:

$$P_{\text{vent}} = P_{\text{resistive}} + P_{\text{elastic}} + P_{\text{residual}}.$$
 (1.12)

During inspiration,  $P_{vent} = P_{set}$  and during expiration  $P_{vent} = P_{peep}$ .

This part of our work has yielded one published paper to date. In the paper, a one-compartment, mathematical model for pressure controlled ventilation, incorporating volume dependent compliances, linear and nonlinear resistances, is constructed and compared with data obtained from healthy and (oleic acid) lung-injured pigs. Experimental data is used to find parameters in the mathematical model and was collected in two forms. Firstly, the  $P_e$  – V curves for healthy and lung injured pigs were constructed; this data is used to compute compliance functions for each animal. Secondly, dynamic data from pressure controlled ventilation for a variety of applied pressures is used to estimate resistance parameters in the model. The model was then compared against the collected dynamic data. The best mathematical model is the one with compliance functions of the form C(V) = a + bV, where A0 and A1 are constants obtained from the A2 curves, and the resistive pressures during inspiration change from a linear relation A3 curves, and nonlinear relation A4 where A5 where A6 is the flow into the one-compartment lung and A6 is a positive number. The form of the resistance terms in the mathematical model indicates the possible presence of gas-liquid foams in the experimental data.

The model of non-invasive mechanical ventilation which incorporates variable compliances can then be written as follows.

#### Inspiration

$$R_{1}\left(\frac{dV_{i1}}{dt}\right) + \frac{V_{i1}}{a_{i} + b_{i}V_{i1}} + P_{ex} = P_{set}, \ 0 \le t \le t_{i1}$$
 (1.13)

$$R_{2}\sqrt{\frac{dV_{i2}}{dt}} + \frac{V_{i2}}{a_{i} + b_{i}V_{i2}} + P_{ex} = P_{set}, \ t_{i1} \le t \le t_{i}$$
 (1.14)

#### Expiration

$$R_{e}\left(\frac{dV_{e}}{dt}\right) + \frac{V_{e}}{a_{e} + b_{e}V_{e}} + P_{ex} = P_{peep}, t_{i} \le t \le t_{tot}$$

$$(1.15)$$

where  $V_{i1}, V_{i2}$ , and  $V_e$  are lung volumes during inspiration period 1, period 2, and that during expiration period, respectively.  $R_i$  and  $R_e$  are the resistances;  $a_i, b_i, a_e$ , and  $b_e$  are the compliance constants;  $P_{ex}$  is the end-expiratory pressure,  $P_{set}$  the preset pressure, and  $P_{peep}$  the ventilator applied pressure. Here, we use  $\varepsilon = 1$  during  $0 \le t \le t_{i1}$ , and  $\varepsilon = \frac{1}{2}$  during  $t_{i1} \le t \le t_i$ , since these give the best fit to the experimental data. Also, the value of

 $t_{i1}$  is chosen to be the time when a sharp change in the slope of the pressure-flow curve is observed.

We have determined the system parameters in the model from experimental data, then used the model to compute key ventilatory outcome variables and compared them with clinical data. The result has been published in *Mathematical Medicine and Biology* with impact factor 0.368. (Please see manuscript in Appendix # 1.8).

#### 1.3 Mathematical modeling of bacteria growth in the presence of antibiotics

Antibiotic resistance of bacteria is a growing problem. Mathematical models have played an important part in understanding antibiotic resistance, such as the work of Ganusov et al. (2000) which elaborated a structural approach to studying the regularities of the population dynamics of unstable recombinant bacteria strain in a chemostat. The approach was based on the mathematical modelling of all distribution in a population with different numbers of plasmid copies. In another recent study, Dibdin et al. (1996) presented a mathematical model that describes penetration of an antibacteria agent into a bacteria biofilm. As well as dealing with penetration, and the consequent bacterial lysis, the model considered diffusion of the released beta-lactamases in the extra cellular space and the consequent inactivation there of further incoming antibiotic.

As observed by McGowan et al. (2001), pharmacokinetic models of infection can make an important contribution to the study of the pharmacodynamics properties of an antibacteria agent. Apart from providing data to allow for the optimization of drug dosing regimens, such models can be used to describe the effect of a drug on a bacteria population, and provide data for more-analytical studies, as well as hypothesis testing. Analysis of the model can yield information on the pharmacodynamic parameters best correlated to the chosen outcome. Pharmacokinetic models thus play a crucial role in ensuring antibiotic efficacy and in reducing the chance of resistance.

The process of treatment of bacteria infections with antibiotics involves a multitude of variables. Many factors effect the therapeutic efficacy, such as bacteria susceptibility to antibiotics, physicochemical properties of the drug product, specific properties of the infected tissue, metabolism and elimination of antibiotic, host factors, and dosing regimen. According to Nolting and Derendorf (1995), some of the central questions for addressing this problem are

- 1. What factors govern antibacterial activity?
  - 2. How can antibiotic efficacy be quantified to permit reliable comparison between different antibiotics?
- 1 3. How can efficacy of antibiotical treatment be optimized?

In the past, dosing regimens are often based on trial and error rather than on rational design. An important step in addressing the above problem is the development and analysis of a model of antibacterial activity. The most commonly used method was the utilization of the killing curves which describe the time course of the antibacteria effect in order to find the important parameters describing the killing behavior of the antibiotic over time. Although widely employed to characterize the susceptibility of a bacterium, the method does not reflect the situation in vivo, where the antibiotic concentration is subject to considerable fluctuation due to elimination and multiple dosing regimens (Mouton et al., 1997)

In order to simulate more closely the in vivo conditions, we attempt to derive a kinetic model of the dynamics of continuous flow peritoneal dialysis with single-pass flow of fresh dialysate. We thus assume an open habitat, such as a chemostat for continuous culture of microorganisms. Two strains of microorganisms compete for a single limiting resource in the presence of an inhibitor (antibiotic) to which one strain of microorganisms is sensitive and the other resistant. Let C and X be the concentrations of the resource and the inhibitor, respectively, while S and R are the respective densities of the sensitive and resistant strains. We arrive at the following system model.

$$\frac{dC}{dt} = (C_0 - C)\omega - \frac{\varepsilon_S \psi_S SC}{(1 + \gamma X_0)(k_S + C)} - \frac{\varepsilon_R \psi_R CR}{k_R + C}$$
(1.16)

$$\frac{dS}{dt} = \frac{\psi_{S}SC}{(1 + \gamma X_{0})(k_{S} + C)} - \omega S - \frac{\varepsilon_{r}RS}{k_{r} + R} - \frac{\varepsilon_{k}X_{0}S}{k_{k} + X_{0}}$$
(1.17)

$$\frac{dR}{dt} = \frac{\psi_R CR}{k_R + C} - \omega R + \frac{\varepsilon_r SR}{k_r + R}$$
 (1.18)

Application of the singular perturbation technique led us to necessary conditions for the existence of limit cycle behavior. However, we have found that the conditions may not be satisfied simultaneously since they are self contradictory. Thus, we have concluded that the system model (1.16)-(1.18) does not permit periodic solutions. In such a case, the model is deemed not suitable, since clinical data invariably shows oscillatory behavior. We have therefore considered a modification of (1.16)-(1.18) as follows.

$$\frac{dC}{dt} = (C_0 - C)\omega - \frac{\varepsilon_S \psi_S SC}{(1 + \gamma X_0)(k_S + C)} - \frac{\varepsilon_R \psi_R CR}{k_R + C}$$
(1.19)

$$\frac{dS}{dt} = \frac{\psi_s CS(r-S)}{(1+\gamma X_0)(k_s+C)} - \omega S - \frac{\varepsilon_r RS}{k_r-S} - A_4 S$$
 (1.20)

$$\frac{dR}{dt} = \frac{\psi_R CR}{k_R + C} - \omega R + \frac{\varepsilon_r SR}{k_r + S}$$
 (1.21)

so that the susceptible bacteria S is limited by the physiological environment to grow only up to the level r.

We have used experimental data supplied by Prof. John Hotchkiss at University of Minnesota and Prof. Philip S. Crooke at Vanderbilt University to support our choices of the terms utilized in the above model. The data has been collected from a culture of two separate bacteria (Methicillin Susceptible Staphylococcus Aurens (MSSA) and Methicillin Resistant Staphylococcus Aurens (MRSA)) growing in dialysis broth. The antibiotics used were amoxicllian and vancomycin (Vanco).

The model analysis by the singular perturbation technique has been completed, yielding conditions under which different dynamic behaviors may occur. We have written the paper in a form ready to be submitted for publication. Our modelling results have been interpreted in terms of bacteria-antibiotics interaction in patients receiving dialysis treatments. Although each dialysis treatment should be regarded as a batch process, a sequence of treatments, one after the other, may be modeled as a continuous process.

However, Prof. Hotchkiss and Prof. Crooke are supplying additional measurements on the gastrointestinal tract data which is more appropriate for modelling as a continuous process. We are therefore waiting on these extra data to validate our model further. The paper shall then be submitted in short order.

Table I: Plan and Actual Activity for Subproject 1.

Activity: Proposed (	Months	Months	Months	Months	Months	Months
$   \text{Actual}  (\longleftrightarrow)$	1-6	7-12	13-18	19-24	25-30	31-36
1. Carry out extensive literature	<>					
search to select the best	$\longleftrightarrow$					
approach and analytical tools						
to develop and analyze the						
model.						
2. Develop new analytical tools	<u> </u>					
if necessary, or modify the	<	<b></b>				
existing ones to be more						
capable of tackling the						
systems of interest.	:					
3. Develop models of cascade		<u> </u>				
systems characterized by	,	$\longleftrightarrow$				
delay in response mechanism.						
4. Develop a model of	<	>				
mechanical ventilation.	<	$\rightarrow$				
5. Develop a model of bacteria		<b></b>		<b></b>		
growth.		<del>&lt;</del>		<del>                                     </del>		
6. Analyze the resulting models.			<			
			<del></del>		<del></del>	
7. Simulate the model to		<				
compare with experimental		←		<u> </u>	<del>&gt;</del>	
data and make model			•			
modification, if necessary.						
8. Make clinical interpretations		<	***************************************			
and conclusions.	,	<				<del>                                     </del>

#### Outputs of Subproject 1

Papers appeared/accepted in international journals	8
Papers presented in international conferences	2
Ph.D. graduates	6
Master graduate	1

# Subproject 2: Mathematical Modeling of Blood Flow in the Coronary Artery Bypass Grafting

Principal Investigator: Assoc. Prof. Dr. Benchawan Wiwatanapataphee

Heart acts as a pump creating the pulsatile pressure to propel blood from the heart through arteries in which pressure is around 100 mmHg to channel the blood to arterioles to capillaries. The blood is transported back to the heart through a series of vessels: capillaries to venules to veins in which pressure is around 20 mmHg. The walls of arteries consist of three layers which are the tunica externa, the tunica media and the tunica intima. The intima is the innermost layer composed of the endothelium and connective tissue. Flow in the arteries is considered as a continuum. The arterial stretches when the pressure rises during systole and it recoils when the pressure drops during diastole. When the coronary artery is affected by a stenosis, critical flow conditions occur, for example negative pressure, high shear rate at the arterial wall and wall compression, which are thought to be the significant factors in the onset of coronary heart disease. In order to understand the genesis of coronary diseases, a number of vivo using animal model and vitro experiments have been conducted. It has been established that (i) blood behaves like a viscoelastic and a shear-thinning liquid [Fung (1984), Chien et al. (1984)], (ii) blood flow is controlled by the constriction or dilation of vessel wall, (iii) high shear stress at the wall (WSS) is correlated with various degree of stenotic artery [Holme et al. (1997), Marano et al (1998)], (iv) intimal thickening and WSS are correlated in the affected vessel [Lee et al. (1998), Kraiss et al. (1991), Krams et al (1998)] and (v) when the WSS reaches a value higher than 400 dyne/cm<sup>2</sup> the endothelial surface is irreversibly damaged [Ku (1997)]. In 1998, Marano et al. estimated WSS in collared carotid arteries of rabbits. They found that the magnitudes of the wall shear rate (WSR) are 420  $s^{-1}$  in the healthy small arteries and between 2600-15000  $s^{-1}$  in the stenotic arteries.

Due to a difficult task of determining the critical flow conditions for both in vivo and vitro experiments, the exact mechanism involved is still not well understood. In general, mathematical modeling and numerical simulation can give better understanding of the phenomena involved in vascular diseases. Over the last 2 decades, a number of mathematical models based on Finite Element Method (FEM) have been proposed to describe the rheological behavior of blood in the stenotic arteries using 1-D to 3-D with rigid or compliant wall. The models with particular assumptions that blood acts like a Newtonian fluid with constant viscosity and vessel is rigid seem not to be satisfactory to

predict the dynamics of real pulsatile blood flow in the artery. In 1990, Mann and Tarbell used a non-Newtonian model to determine a nonlinear dependence of the viscosity of blood on the strain rate in order to study the flow of blood analog fluids in rigid curved and straight artery models. Grigioni et al (2002) investigated the wall shear stress and velocity field via the vivo experiment in unsteady vascular dynamics and proposed a non-Newtonian model for an unsteady flow in rigid pipe driven by a known oscillatory pressure gradient. Comparison to all the validated velocity points along the vessel's lumen indicates that the results of the model in a rigid pipe are not directly related to the data in vivo experiment. However, the use of mathematical models and vivo experiments in the present works allows us to understand the importance of the rheology in blood flow, at least from a qualitative point of view. Therefore, the further development of mathematical model to study blood flow is necessary. Once a satisfactory model has been generated, the benefits to the future management of human health are unlimited.

In this study, a mathematical model is developed to study steady and unsteady state blood flow through a stenotic artery with different severity. Blood is considered as a non-Newtonian fluid. Using three geometry domains of straight tube with three different sizes of stenosis: 25%, 50% and 65%. Numerical simulations based on FEM are carried out for the flow field, temperature field and shear rate in the flow channel. Dependence of the flow on the severity of stenosis has been investigated.

#### 2.1 Numerical simulation of blood flow in a small artery channel with solid wall

This study focuses on the blood flow in stenotic artery. A mathematical model based on FEM is developed to simulate blood flow with distribution of pressure. Blood is considered as an incompressible and non-Newtonian fluid. The flow pattern with the distribution of pressure and shear rate, are computed. The results show how the blood flows through the present stenotic area. The quadratic profile is present in the flow channel except in the stenosis area. Blood speed at the throat of the stenosis is blunt, resulting in high shear rate and dropping of pressure there. Bigger size of stenosis gives bigger shear rate and higher jumping pressure in the channel, especially around the stenosis.

#### 2.1.1 Mathematical model

·

The computational domain is considered in the lumen channel. Blood is assumed to be an incompressible fluid. The non-Newtonian model based on Carreau model is used to determine the viscosity of blood. The fluid motion is governed by the continuity

equation, Navier-Stokes equations and defined in the domain  $\Omega$  which is bounded by the boundary  $\partial\Omega=\partial\Omega_{\rm in}\cup\partial\Omega_{\rm wall}\cup\partial\Omega_{\rm out}$ :

$$\mathbf{u}_{i,i} = \mathbf{0},\tag{2.1}$$

$$\rho \frac{\partial u_i}{\partial t} - \nabla \cdot \eta \left( u_{i,j} + u_{j,i} \right) + \rho u_j u_{i,j} + p_{,i} = F_i, \qquad (2.2)$$

where  $\rho$  denotes the blood density of 1.06g cm<sup>-3</sup>,  $u_i$  represents the component of velocity vector in the *i*th direction, p denotes pressure in the channel, and F is the volume force affecting the fluid. The quantity  $\eta$  is the blood viscosity. We here use a Carreau model for describing viscosity by the following four-parameter equation

$$\eta = \eta_m + (\eta_0 - \eta_m)[1 + (\lambda \dot{\gamma})^2]^{(n-1)/2}, \tag{2.3}$$

where  $\lambda = 3.313s$ , the zero shear rate viscosity  $\eta_0 = 0.56 \, dyn \cdot s/cm^2$ , the infinite shear rate viscosity  $\eta_{\infty} = 0.0350 \, dyn \cdot s/cm^2$  and n = 0.3568.

The quantity  $\dot{\gamma}$  in equation (3) represents the shear rate given by

$$\dot{\gamma} = \sqrt{\frac{1}{2}(4u_X^2 + 4v_Y^2 + 4w_Z^2 + 2(u_Y + v_X)^2 + 2(v_Z + w_Y)^2 + 2(u_Z + w_X)^2)}.$$
 (2.4)

For three-dimensional problem, the above system of equations can be manipulated to yield a closed system of four partial differential equations in terms of four coordinates and time-dependent unknown functions  $u_1, u_2, u_3$  and p. The system, once supplemented by the initial and boundary conditions, can be solved numerically to yield the velocity field with pressure distribution and to determine the wall shear stress. In this work, we study both steady state and unsteady state flow in the stenotic tube. The boundary conditions considered for velocity field and pressure field include the Dirichlet type and the Neumann/Robin type, i.e, for i, j = 1, 2, 3

$$\begin{aligned} \boldsymbol{u}_{i} &= \overline{\boldsymbol{u}}_{i} & \partial \Omega_{in} \\ \\ \boldsymbol{u}_{i} &= 0 & \partial \Omega_{wall} \\ \\ \boldsymbol{p} &= \boldsymbol{p}_{0}, & \eta (\boldsymbol{u}_{i,i} + (\boldsymbol{u}_{j,i})^{T}) \cdot \boldsymbol{n} = 0 & \partial \Omega_{out} \end{aligned}$$

In this work, we assumed that blood flows into an artery tube with constant velocity of 20.13 cm s<sup>-1</sup> for steady state problem and flow with the pulsatile velocity for unsteady state problem. We chose a pulsatile flow rate in the right coronary artery of 65 years old patient given by Bertolotti et al (2001) [20] and assumed that blood flows out with constant pressure 1.865×10<sup>5</sup> dyn/cm<sup>2</sup> or 140 mmHg.

#### † 2.1.2 Weak formulation

To develop the variational statement for the boundary value problem, we consider the following representation of the problem.

Find  $u_1, u_2, u_3$  and p such that for all test functions  $\hat{u}_1, \hat{u}_2, \hat{w}_3 \in H^1_{0u}(\Omega)$  and  $\hat{p} \in H^1_{0p}(\Omega)$ , all the Dirichlet boundary conditions for the unknown functions are satisfied and

$$(\mathbf{u}_{::},\hat{\mathbf{p}}) = 0,$$
 (2.5)

$$\left(\rho \frac{\partial u_{i}}{\partial t}, \hat{u}_{i}\right) + \left(\rho u_{j} u_{i,j}, \hat{u}_{i}\right) - \left(\left(\eta \left(u_{i,j} + u_{j,i}\right)_{,j}\right), \hat{u}_{i}\right) + \left(p_{,i}, \hat{u}_{i}\right) = (F_{i}, \hat{u}_{i}), \quad (2.6)$$

where  $(\cdot,\cdot)$  denotes the inner product on the square integrable function space  $L^2(\Omega)$ ,  $H^1(\Omega)$  is the Sobolev space  $W^{1,2}(\Omega)$  with norm  $\|\cdot\|_{1,2,\Omega}$ ,  $H^1_{0q}(\Omega) = \left\{v \in H^1(\Omega) \mid v = 0 \text{ on } \partial\Omega_q\right\}$ . A standard procedure is then carried out to reduce the second-order derivatives involved in the above problem into the first-order ones using integration by parts and ensuring that all integrals involved are well defined.

To find the numerical solution of the problem, we pose the variational problem into an N-dimension subspace. The computation domain  $\Omega$  is discretized into a finite number of elements connected by N nodes. Let U and P denote respectively the global vectors of velocity and pressure fields with each i th entry representing the value of the corresponding unknown function at the ith node of the finite element mesh. Then, by using the Galerkin finite element formulation, we obtain the ordinary differential equations:

$$D_{u}U = 0,$$

$$M\dot{U} + A_{u}U + A_{p}P = F,$$
(2.7)

where the superposed dot represents differentiation with respect to time and all coefficient matrices are global matrices assembled from element matrices. Matrix M corresponds to the transient term, matrices  $A_u$  and  $D_u$  correspond to the advection and diffusion terms,

matrix  $A_p$  corresponds to the pressure term and vector  $\mathbf{F}$  provides forcing functions for the Navier-Stokes equations.

#### 2.1.3 Numerical results

A test example is given here to demonstrate the validity of mathematical model. The example under consideration is a stenotic artery with a 25%, 50% or 65% stenosis as shown in Fig.2.1. The artery is modeled by a straight tube with the length of 5 cm and diameter of 0.2 cm containing stenosis in the middle part at one side of the internal wall. In this work, a spherical shape with radius of 0.15 cm was used to define the stenosed disease. We assumed that no volume force affects the fluid.

Fig. 2.2 shows the velocity vectors and streamlines of blood at stenosis in the middle part of the domain. The flow patterns and streamlines clearly outline the path of the blood and show how the blood flows through the stenosis. The maximum speed is present at throat of the stenosis as shown in Fig. 2.3. The parabolic profile of velocity is present in the upper part and lower part of the stenosis. Fig. 2.4 shows the distribution of pressure and shear rate along a longitudinal line of the artery. It indicates that pressure drops very fast and high shear rate occurs near the stenosis.

Comparing the results obtained from three tubes with 25%, 50% and 65% stenosis, blood speed profile at the throat of the stenosis in all domains is blunt. This results in high shear rate and dropping of pressure there as shown in Fig. 2.3. Bigger size of stenosis gives bigger shear rate and higher jumping pressure in the channel, especially near the stenosis.

To study the transient flow in stenotic artery, we chose the artery with 50% stenosis and used a flow rate wave form in the right coronary artery of a 65 years old patient as an inlet flow [20]. Fig. 2.5 and Fig. 2.6 show the velocity vectors and streamlines of blood along the arterial axis at time t=0, 0.3, 0.8 and t=1.2 s. Fig. 2.7 shows the distribution of pressure and shear rate along a longitudinal line of the artery at different times. The results show that the critical flow occurs at all time, especially between t=0.3 to t=0.5 s with pressure between  $1.96 \times 10^5$  to  $2.23 \times 10^5$  dyn/cm<sup>2</sup> and shear rate between  $1.96 \times 10^5$  to  $2.23 \times 10^5$  dyn/cm<sup>2</sup> and shear rate between  $1.96 \times 10^5$  to  $2.23 \times 10^5$  dyn/cm<sup>2</sup> and shear rate between

t(s)	0	0.1	0.2	0.3	0.4	0.5	0.6	0.7	0.8
$\mathrm{U}_{max}$	32	31	70	215	200	161	117	73	63
$p_{\text{max}} \times 10^5$	1.87	1.89	1.92	2.03	1.98	1.96	1.92	1.90	1.90
$\dot{\gamma}_{max} \times 10^5$	0.19	0.23	0.63	2.5	2.23	1.69	1.13	0.63	0.53
Re	47	42	100	389	359	276	191	109	90
t(s)	0.9	1.0	1.1	1.2	1.3	1.4	1.5	1.6	1.7
U <sub>max</sub>	78	102	121	125	113	91	66	47	35
$p_{max} \times 10^5$	1.91	1.93	1.94	1.54	1.93	1.91	1.90	1.89	1.88
$\dot{\gamma}_{max} \times 10^5$	0.70	0.97	1.19	1.25	1.10	0.83	0.56	0.36	0.26
Re	117	160	195	205	183	141	97	65	47

#### 2.1.4. Conclusions

A mathematical model for simulating blood flow in stenotic artery has been constructed. The model is used to study the critical flow in stenotic artery with severity of 25%, 50% and 65%. The result shows the significant effect of the stenosis size on fluid flow, pressure field and shear rate. The quadratic profile is present in the flow channel except in the stenosis area. The blood speed at the throat of the stenosis is blunt, resulting in high shear rate and dropping of pressure there. Bigger size of stenosis gives bigger shear rate and higher jumping pressure in the channel, especially around the stenosis. For 50% stenotic artery, the critical flow occurs at all time, especially during systolic period.

It should be addressed here that blood flow in a small stenotic artery is an extremely complex phenomenon and there are still many unsolved modeling problems. The presented work focuses on blood flow in the lumen channel without the effect of the wall. Further work could be carried out to incorporate the fluid-wall interaction in a stenotic artery.

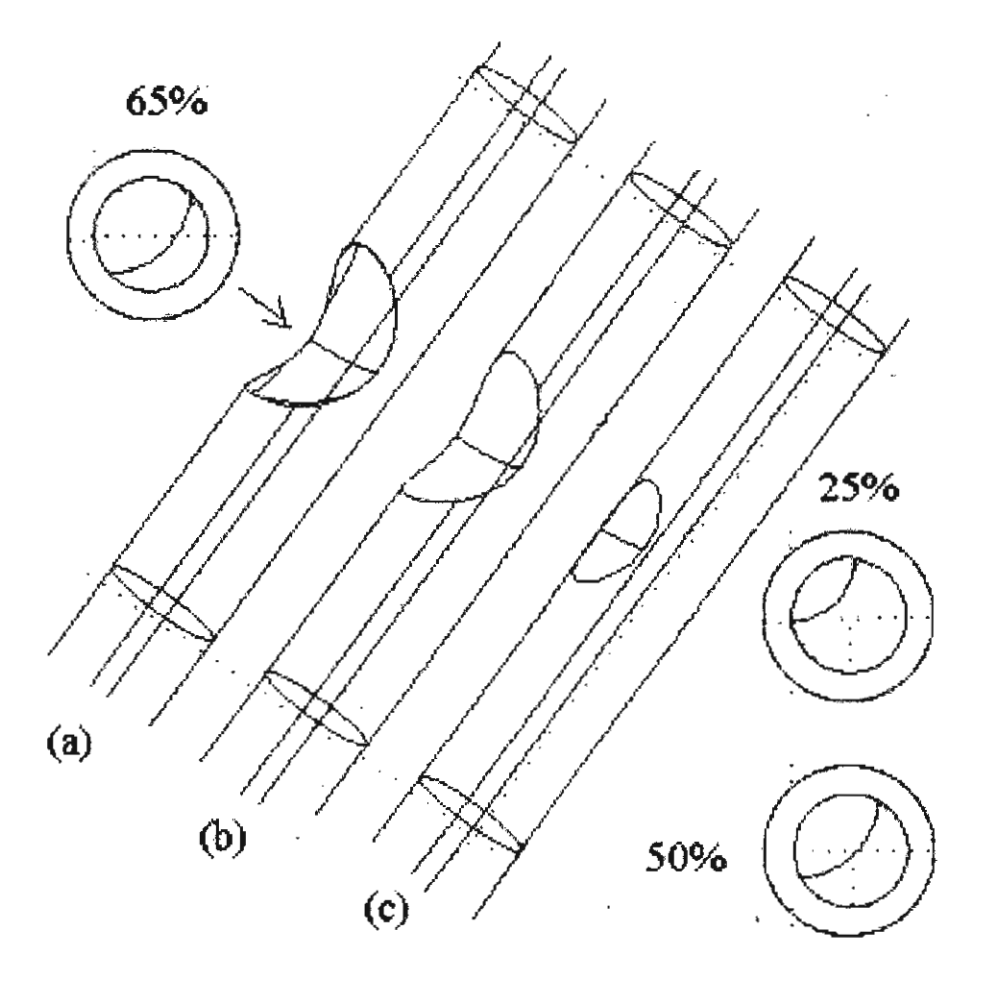


Figure 2.1 Computational domain (a) 25% stenotic tube (b) 50% stenotic tube (c) 65% stenotic tube.

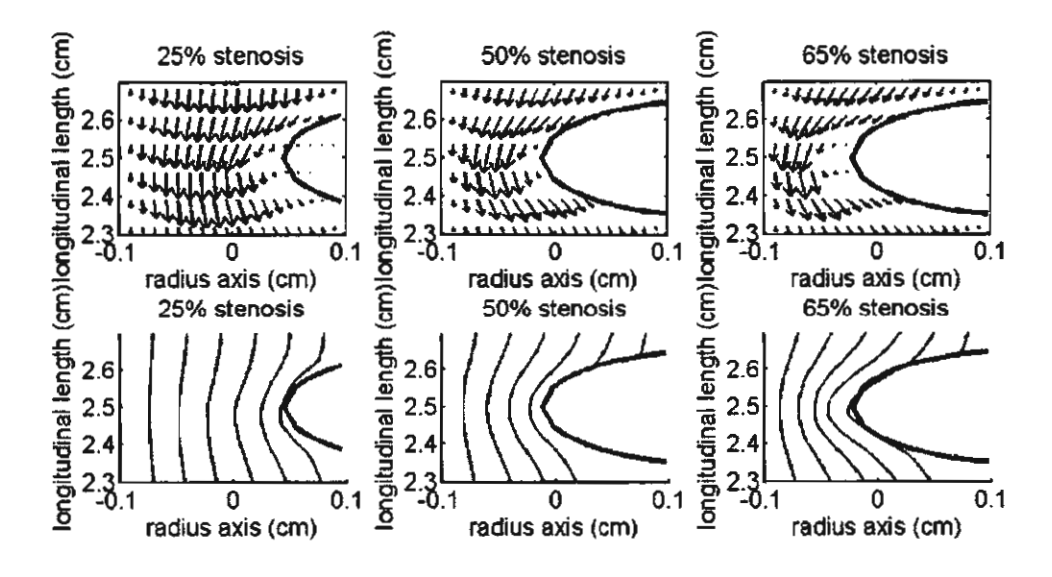


Figure 2.2 Velocity vector and streamline along the stenotic artery with different severity.

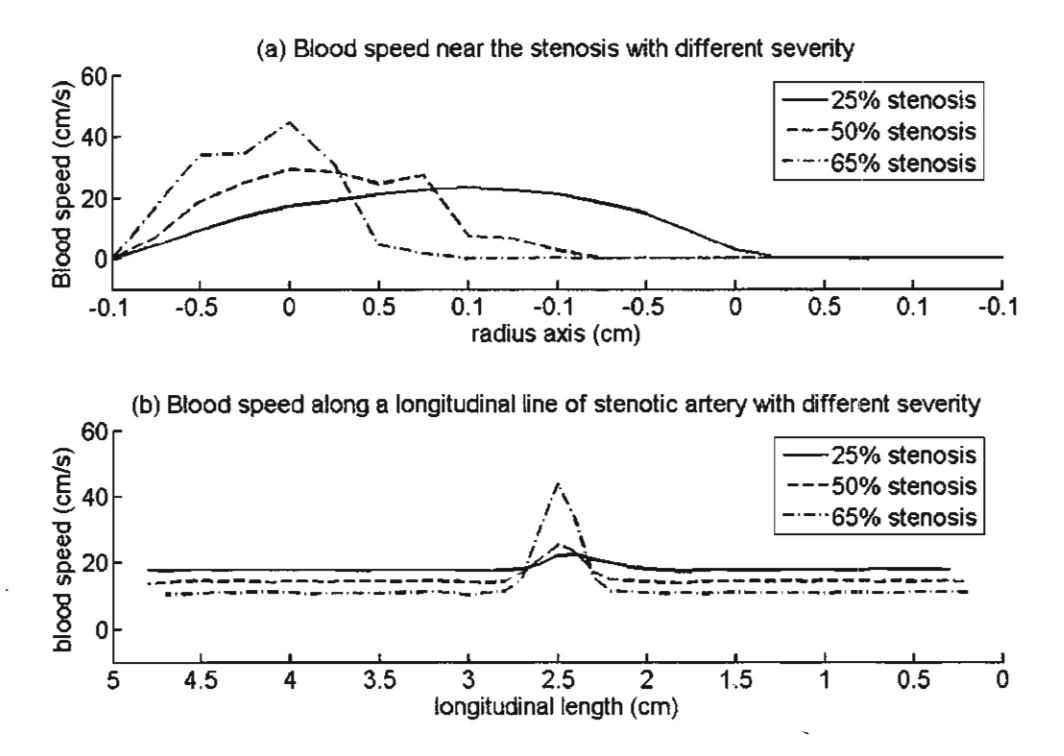


Figure 2.3 Blood speed (cm/s) at (a) mid plane of stenosis site (b) a line along the arterial axis.

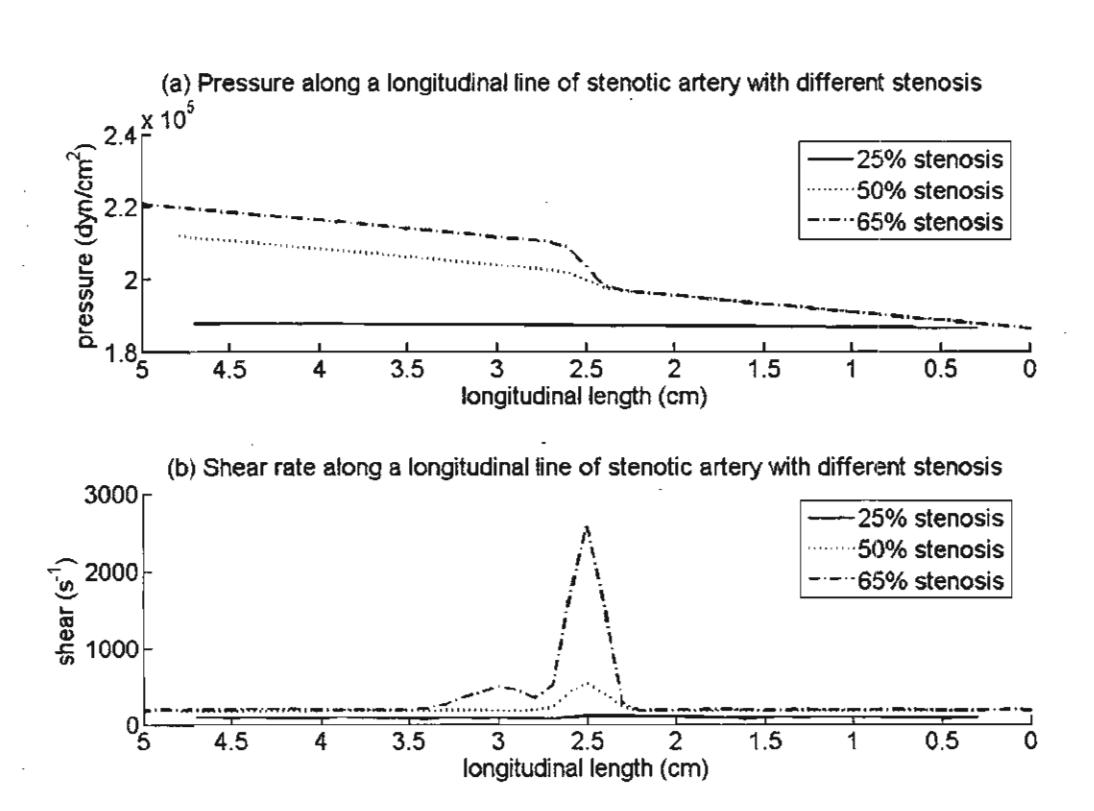


Figure 2.4 Distribution of (a) pressure (dyn/cm<sup>2</sup>) (b) shear rate (1/s) along the stenotic artery with different severity.

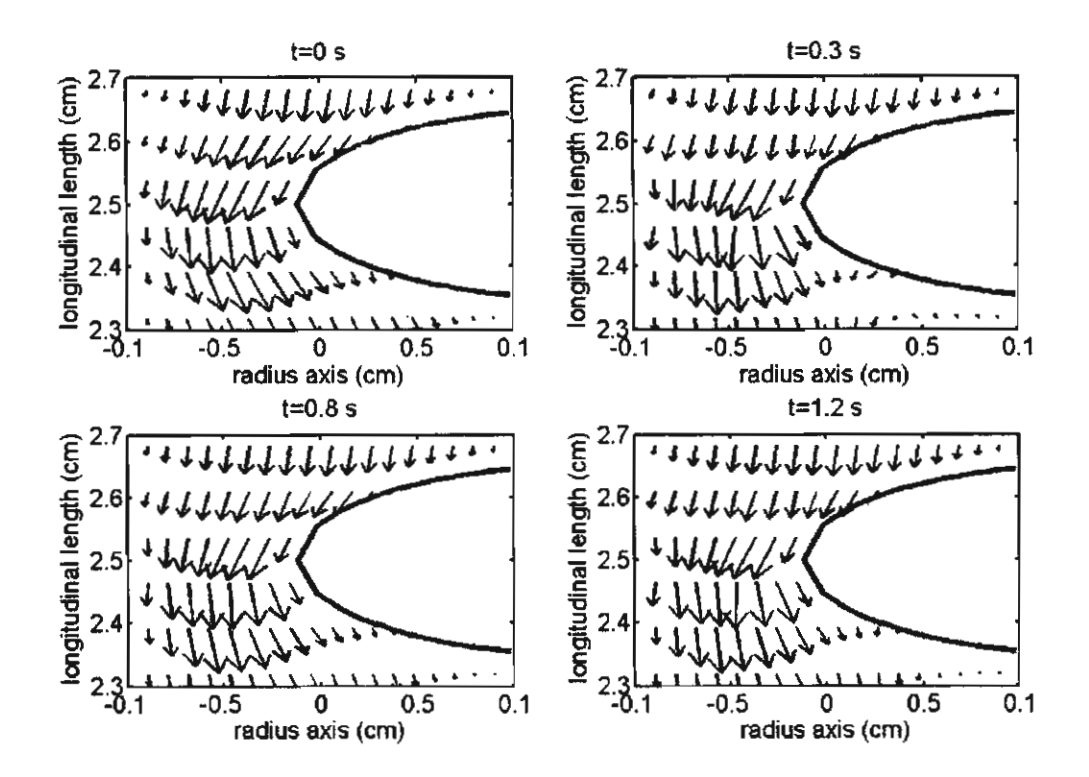


Figure 2.5 Velocity profile along a 50% stenotic artery at different time t.

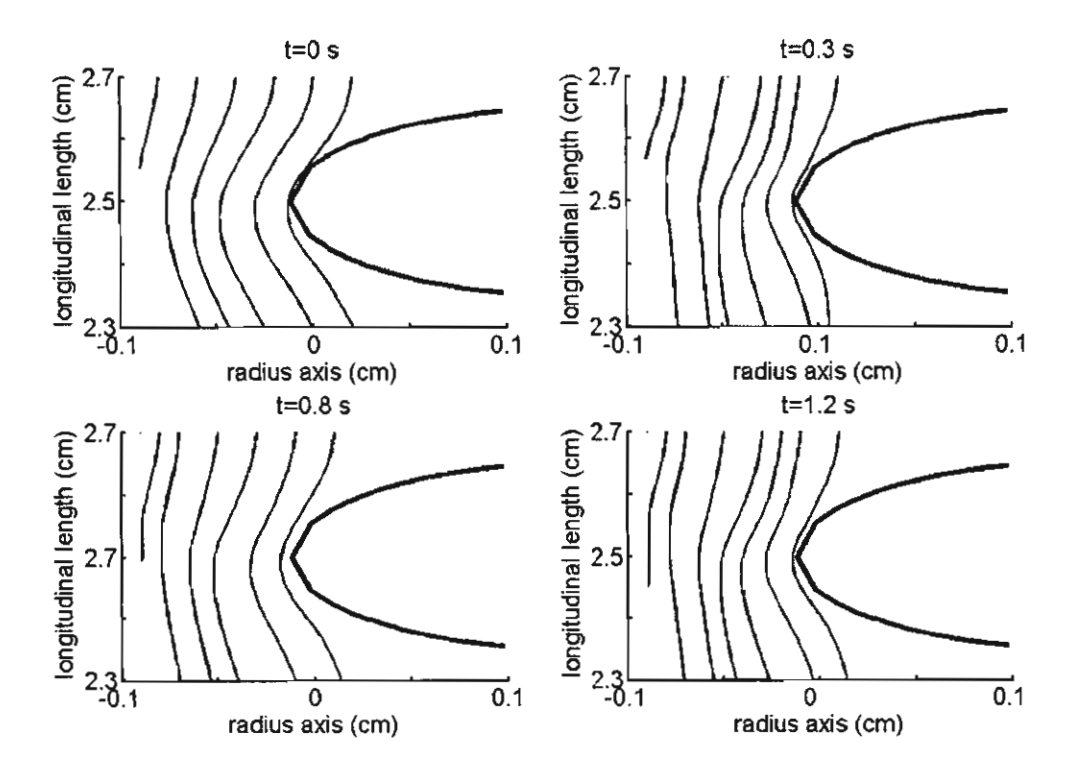


Figure 2.6 Streamline of blood flow along a 50% stenotic artery at different times t.

٤

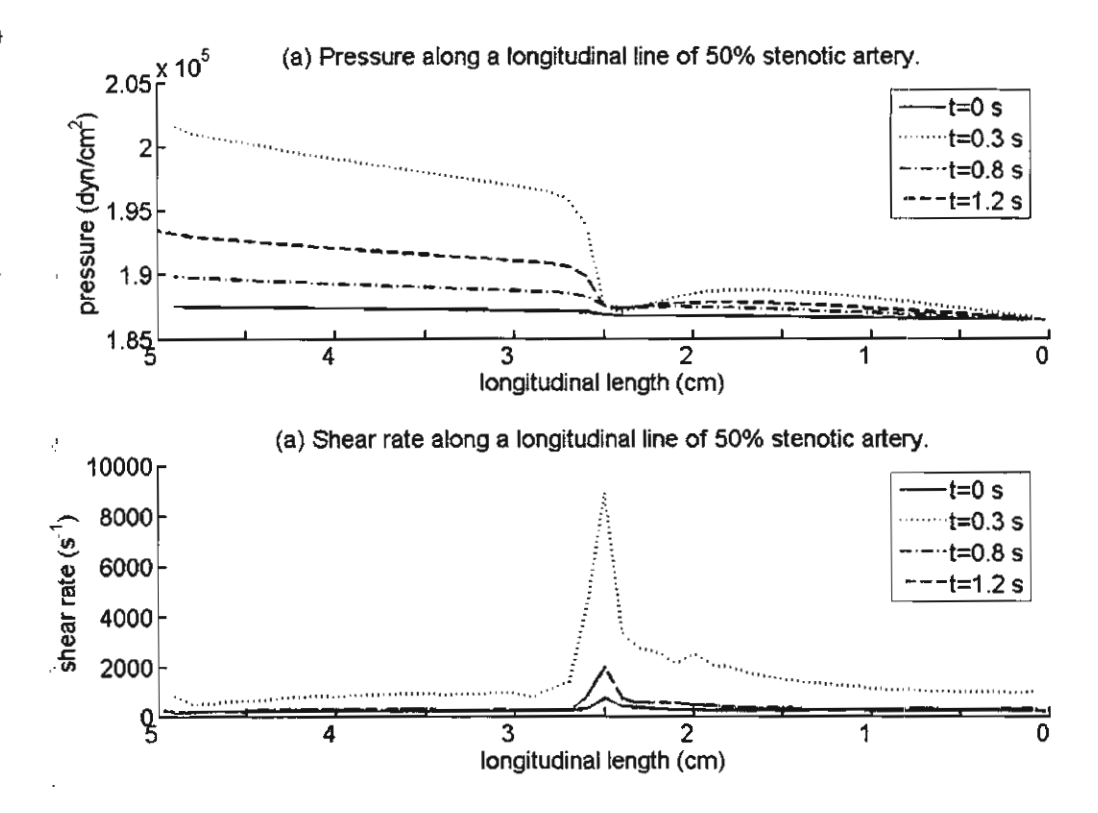


Figure 2.7 Distribution of (a) pressure (dyn/cm<sup>2</sup>) (b) shear rate (1/s) along the stenotic artery at different times t.

#### References

- [1] K.B. CHANDRAN, J.H. MUN, K.K.CHOI, J.S. CHEN, A.HAMILTON, A. NAGARAJ AND D.D. McPherson, A method for in-vivo analysis for regional arterial wall material property alterations with atherosclerosis: preliminary results, Medical Engineering and Physisa, 25 (2003), pp. 289-298.
- [2] F.N. VAN DE VOSSE, J. DEHART, C.H.G.A. VAN OIJEN, D. BESSEMS, T.W.M. GUNTHER, A. SEGAL, B.J.B.M. WOLTERS, J.M.A. STIJNEN AND F.P.T. BAAIJENS, Finite-element-based computational methods for cardiovascular fluid-structure interaction, Journal of Engineering Mathematics, 47 (2003), pp. 335-368.
- [3] B. CHAHBOUNE AND J.M. CROLET, Numerical simulation of the blood-wall interaction in the human left ventricle, The European Physical Journal: Applied Physics, 2 (1998), pp. 291-297.
- [4] B.M. JOHNSTON, P.R. JOHNSON, S. CORNEY, D. KILPATRICK, Non-Newtonian blood flow in human right coronary arteries: steady state simulations, Journal of Biomechanics, 37 (2004), pp. 709-720.
- [5] Y.I. CHO AND K.R. KENSEY, Effects of the non-Newtonain viscosity of blood on flows in a diseased arterial vessel. Part 1: steady flows, Biorheology, 28 (1991), pp. 241-262.

- [6] D.K. STANGEBY AND C.R. ETHIER, Coupled computational analysis of arterial LDL transport-effects of Hypertension, Journal of Biomechanical Engineering, 5:3 (2002), pp. 233-241.
- [7] P. RUENGSAKULRACH, R. SINCLAIR, M. KOMEDA, J. RAMAN, I. GORDAN, B. BUXTON, Comparative histopathology of radial artery versus internal thoracic artery and risk factors for development of intimal hypeplasia and altherosclerosis, Circulation, November 9:2 (1999), pp. 139-144.
- [8] G. KARNER AND K. PERKTOLD, Effect of endothelial injury and increased blood pressue on albumin accumulation in the arterial wall: a numerical study, Journal of Biomechanics, 33 (2000), pp. 709-715.
- [9] G.A. HOLZAPFEL, T.C> GASSER, M. STADLER, A structural model for the viscoelastic behavior of arterial walls: Continuum formulation and finite element analysis, Eoropean Journal of Mechanics A/Solids, 21 (2002), pp. 441-463.
- [10] X. ZHANG, M. FATEMI, AND J.F. GREENLEAF, Vibro-Acoustography for modal analysis of arterial vessels, IEEE, (2002), pp. 513-516.
- [11] G-T LIU, X-J WANG, B-Q AI, AND L-G LIU, Numerical study of pulsating flow through a tapered artery with stenosis, Chinese Journal of Physisc, 42:4-I (2004), pp.401-409.
- [12] F.G. BASOMBRIO, E.A. DARI, G.C. BUSCAGLIA AND R.A. FEIJOO, Numerical experiments in compleax hamodynamic flows. Non-Newtonian effects, International Journal of Computational Fluid Dynamics, 16:4 (2002), pp. 231-246.
- [13] M.R. KAAZEMPUR-MOFRAD AND C.R. ETHIER, Mass transport in an Anatomically realistic human right coronary artery, Annals of Biomedical Engineering, 29 (2001), pp. 121-127.
- [14] S. DEPARIS, M.A. FERNANDEZ, L. FORMAGGIA, F. NOBILE, Modified fixed point algorithm in fluid-structure interation, Comptes Rendus Mecanique, 331 (2003), pp. 525-530.
- [15] J-F GERBEAU, M. VIDRASCU, P. FREY, Fluid-structure interaction in blood flows on geometries based on medical imaging, Computers and Strucutres, 83 (2005), pp. 155-165.
- [16] M.A. FERNANDEZ, M. MOUBACHIR, An exact-Newton algorithm for solving fluidstructure interaction problems, Comptes Rendus Mathematique, 1336 (2003), pp. 681-686.

- [17] D. TANG, C. YANG, S. KOBAYASHI, D.N. Ku, Steady flow and wall compression in stenotic arteries: a three-dimensional thick-wall model with fluid-wall interation, Transactions of the ASME, 123 (2001), pp. 548-557.
  - [18] B.R. SIMON, M.V. KAUFMANN, M.A. MCAFEE, A.L. BALDWIN, Finite element models for arterial wall mechanics, Journal of Biomechanical Engineering, 115 (1993), pp. 489-496.
  - [19] F. ARMERO, E. LOVE, An arbitrary Lagrangian-Eulerian finite element method for finite strain plasticity, International Journal for Numerical Methods in Engineering, 57 (2003), pp. 471-508.
  - [20] C. Bertolotti, V. Deplano, J. Fuseri, P. Dupouy, Numerical and experimental methods of post-operative realistic flows in stenosed coronary artery bypasses, Journal of Biomechanics, 34 (2001), pp. 1049-1064.

## 2.2 Numerical study of blood flow in stenotic arteries with solid wall and permeable wall

This study focuses on the blood flow in stenotic arteries with solid wall and permeable wall. A mathematical model based on Finite element method is developed to simulate blood flow with distribution of pressure and shear rate in the lumen region and arterial wall. Blood in the lumen is considered as incompressible and non-Newtonian fluid and arterial wall is modeled as porous layer. The results show that the model with solid wall generates linear distribution of pressure along the arterial line except at the stenosis whereas the model with permeable wall gives oscillating pressure along an arterial line. High shear rate and Higher dropping pressure occurs at the stenosis. Bigger size of stenosis gives higher shear rate and higher pressure with bigger dropping pressure around the stenosis.

#### 2.2.1 Mathematical model

**`**,.

The computational domain consists of two regions: the arterial wall and the arterial lumen. The velocity field in the artery lumen and in the arterial wall are computed in a fully coupled manner through the use of the lumen/wall condition. Blood is assumed to be incompressible fluid and non-Newtonian fluid. The non-Newtonian model based on Carreau model is used to determine the viscosity of blood. The artery wall is assumed to be porous media with permeability of  $1.0 \times 10^{-14}$ . The fluid motion is governed by the

continuity equation, Navier-Stokes equations and defined in the domain  $\Omega = \Omega_{\text{lumen}} \cup \Omega_{\text{wall}}$  which is bounded by the boundary  $\partial \Omega = \partial \Omega_{\text{in}} \cup \partial \Omega_{\text{interface}} \cup \partial \Omega_{\text{outerwall}} \cup \partial \Omega_{\text{out}}$ .

$$\nabla \cdot \mathbf{v} = 0, \tag{2.8}$$

$$-\nabla \cdot \eta \left(\nabla \mathbf{v} + (\nabla \mathbf{v})^{\mathrm{T}}\right) + \rho(\mathbf{v} \cdot \nabla)\mathbf{v} + \nabla \mathbf{p} = \mathbf{f}, \tag{2.9}$$

where  $\rho$  denotes the blood density,  ${\bf v}$  represents the 3D velocity vector,  ${\bf p}$  denotes pressure in the channel, and  ${\bf f}$  is the volume force affecting the fluid. For this model, we assume that no volume force is affecting the fluid, so  ${\bf f}=0$ . The quantity  $\eta$  is the blood viscosity defined by the following four-parameter equation

$$\eta = \eta_{\infty} + (\eta_0 - \eta_{\infty})[1 + (\lambda \dot{\gamma})^2]^{(n-1)/2}, \tag{2.10}$$

where  $\lambda=3.313s$ , the zero shear rate viscosity  $\eta_0=0.56 \ dyn \cdot s/cm^2$ , the infinite shear rate viscosity  $\eta_\infty=0.0.0345 \ dyn \cdot s/cm^2$  and n=0.3568.

The quantity  $\dot{\gamma}$  in equation (3) represents the shear rate given by

$$\dot{\gamma} = \sqrt{\frac{1}{2}(4u_X^2 + 4v_Y^2 + 4w_Z^2 + 2(u_Y + v_X)^2 + 2(v_Z + w_Y)^2 + 2(u_Z + w_X)^2)}$$
 (2.11)

In arterial wall (porous domain), flow is described by the Brinkman equations according to the following.

$$\nabla \cdot \mathbf{u} = 0, \tag{2.12}$$

$$-\mu \Delta \mathbf{u} + \frac{\mu}{\kappa} \mathbf{u} + \nabla \mathbf{p} = \mathbf{g}, \tag{2.13}$$

where  $\mu$  denotes viscosity in porous layer,  $\kappa$  is permeability,  $\mathbf{u}$  represents the 3D velocity vector, and  $\mathbf{g}$  is the volume force affecting the fluid in artery. For this model, we assume that no volume force is affecting the fluid in the artery, so  $\mathbf{g} = 0$ .

For three-dimensional problem, the above system of equations can be manipulated to yield a closed system of eight partial differential equations in terms of eight coordinate and time-dependent unknown functions  $v_1, v_2, v_3, u_1, u_2, u_3$  and  $p_v, p_u$ . The system, once supplemented by the initial and boundary conditions, can be solved numerically to yield the velocity field with pressure distribution and to determine shear rate.

The boundary conditions considered for velocity field and pressure field include the Dirichlet type and the Neumann/Robin type, i.e, for i, j = 1, 2, 3

$$\mathbf{v} = \overline{\mathbf{v}} \quad \partial \Omega_{in} \tag{2.14}$$

$$\mathbf{p}_{\mathbf{v}} = \mathbf{p}_{0}, \quad \eta(\nabla \mathbf{v} + (\nabla \mathbf{v})^{\mathsf{T}}) \cdot \mathbf{n} = 0 \ \partial\Omega_{\text{out}}$$
 (2.15)

For steady state flow, blood speed at inlet boundary  $\partial\Omega_m$  is set to the mean flow of 20.13 cm/s, and we assumed that blood flows out with constant pressure 1.865 ×10<sup>5</sup> dyn/cm<sup>2</sup> or 140 mmHg at  $\partial\Omega_{out}$ .

At the interface between lumen and artery wall, the expression for the pressure and velocity must be continuous across the interface. We thus set

$$p_{\nu}|_{\text{wall}} = p_{u}|_{\text{wall}} \qquad \partial \Omega_{\text{interface}},$$
 (2.16)

and

١:

$$\mathbf{u}\big|_{wall} = \mathbf{v}\big|_{wall} \tag{2.17}$$

We also assumed that no slip condition is applied on the external wall. To this end, the boundary value problem for blood flow in a stenotic artery is as follows.

**BVP**: Find  $\mathbf{v}, \mathbf{p}_{\mathbf{v}}$  and  $\mathbf{u}, \mathbf{p}_{\mathbf{u}}$  such that the field equations (2.8) and (2.13) are respectively satisfied in the computational domain  $\Omega$  and all boundary conditions are satisfied.

#### 2.2.2 Weak formulation

To develop the variational statement for the boundary value problem, we consider the following representation of the problem.

Find  $\mathbf{v}, \mathbf{p}_{v}$  and  $\mathbf{u}^{T}, \mathbf{p}_{u}$  such that for all test function  $\hat{\mathbf{v}} \in H^{1}_{0\mathbf{v}}(\Omega)$ ,  $\hat{\mathbf{p}}_{v} \in H^{1}_{0\mathbf{p}_{u}}(\Omega)$ ,  $\hat{\mathbf{p}}_{u} \in H^{1}_{0\mathbf{p}_{u}}(\Omega)$ , all the Dirichlet boundary conditions for the unknown functions are satisfied and

$$(\nabla \mathbf{v}, \hat{\mathbf{p}}_{\mathbf{v}}) = 0, \tag{2.18}$$

$$(\rho \mathbf{v} \cdot \nabla \mathbf{v}, \hat{\mathbf{v}}) - (\nabla \cdot \eta (\nabla \mathbf{v} + (\nabla \mathbf{v})^{\mathsf{T}}), \hat{\mathbf{v}}) + (\nabla p_{\mathsf{v}}, \hat{\mathbf{v}}) = (\mathbf{f}, \hat{\mathbf{v}}), \tag{2.19}$$

$$(\nabla \mathbf{u}, \hat{\mathbf{p}}_{\mathbf{u}}) = 0, \tag{2.20}$$

$$-\mu(\Delta \mathbf{u}, \hat{\mathbf{u}}) + \frac{\mu}{\kappa}(\mathbf{u}, \hat{\mathbf{u}}), +(\nabla p_{u}, \hat{\mathbf{u}}) = (\mathbf{g}, \hat{\mathbf{u}}), \tag{2.21}$$

where  $(\cdot,\cdot)$  denotes the inner product on the square integrable function space  $L^2(\Omega)$ ,  $H^1(\Omega)$  is the Sobolev space  $W^{1,2}(\Omega)$  with norm  $\left|\cdot\right|_{1,2,\Omega}$ ,  $H^1_{0q}(\Omega) = \{v\epsilon H^1(\Omega) \mid v=0 \text{ on } \partial\Omega_q\}$ . A standard procedure is then carried out to reduce the second-order derivatives involved in the above problem into the first-order ones using integration by parts and ensuring that all integrals involved are well defined.

To find the numerical solution of the problem, we pose the variational problem into an N-dimension subspace. The computation domain  $\Omega$  is discretized into a finite number of elements connected by N nodes. Let  $\mathbf{V}, \mathbf{P}_{v}$  and  $\mathbf{U}, \mathbf{P}_{u}$  denote respectively the global vectors with each i th entry representing the value of the corresponding unknown function at the ith node of the finite element mesh. Then, by using the Galerkin finite element formulation, we obtain the ordinary differential equations:

$$D_{v}V = 0,$$

$$A_{v}V + A_{pv}P_{v} = F_{v},$$
(2.22)

$$D_{u}U = 0,$$

$$A_{u}U + A_{pu}P_{u} = F_{u},$$
(2.23)

where and all coefficient matrices are global matrices assembled from element matrices. Matrices  $A_v$ ,  $A_u$  and  $D_v$ ,  $D_u$  correspond to the advection and diffusion terms, matrix  $A_{pv}$ ,  $A_{pu}$  corresponds to the pressure term and vector  $\mathbf{F}$  provides forcing functions for the Navier-Stokes equations.

#### 2.2.3 Numerical results

A test example is given here to demonstrate the validity of mathematical model. The example under consideration is a stenotic artery with severity of 25%, 50% and 65%. The artery is modeled by a straight tube with the length of 5 cm and diameter of 0.2 cm containing stenosis in the middle part at one side of the internal wall. Wall thickness is 0.05 cm and diameter of the flow channel (lumen) is 0.2 cm. A spherical shape with radius of 0.15 cm was used to define the stenosed disease. The computational domains are shown in Section 1.

Fig. 2.8-2.10 show the velocity vectors and streamline of blood near 25%, 50% and 65% stenoses in the middle part of the solution, respectively. The flow patterns and streamlines clearly outline the path of the blood and show how the blood flows through the stenosis. The maximum speed is present at throat of the stenosis as shown in Fig. 2.11 and Fig 2.12.

Fig. 2.13 shows the distribution of pressure along a longitudinal line of stenotic artery obtained from a model with solid wall and permeable wall. It is noted that (1) for 25% stenotic artery, both models with solid wall and with permeable wall give the same pressure distribution which is a linear function along the longitudinal line of the artery; (2) blood flow in the 50% stenotic artery with solid wall generates linear distribution of pressure along an arterial line except at the stenosis where dropping pressure occurs, whereas the model with permeable wall gives the oscillating pressure along the arterial line; (3) comparison to a model with 50% stenosis, higher dropping pressure is present in the model with 65% stenosis. The model with solid wall generates linear distribution of pressure except at the stenosis whereas the model with permeable wall gives oscillating pressure along an arterial line.

Fig 2.14 shows shear rate along a longitudinal line of 25%, 50% and 65% stenotic arteries obtained from a model with solid wall and permeable wall. The results indicate that high shear rate occurs at stenosis. Comparison to a model with solid wall, it is found that (1) a model with permeable wall and 25% stenosis gives almost the same shear rate from inlet boundary to the front hill of stenosis, lower shear rate from the hill to throat of stenosis and then higher shear rate after leaving the throat of stenosis; (2) Blood flow obtained from a model with permeable wall and 50% stenosis (1) generates oscillating shear rate along the longitudinal line from inlet boundary to the back hill of stenosis, and gives the same shear rate after traveling 3 cm from inlet boundary; (3) Blood flow obtained from a model with permeable wall and 65% stenosis gives the same shear rate along the longitudinal length except the area near the stenosis where shear rate is much higher.

#### 2.2.4. Conclusions

The results show the significant effect of permeable wall on the flow pattern of blood, especially at the stenosis area. In general, we conclude that blood speed at the throat of the stenosis is blunt, resulting in high shear rate and dropping of pressure there. Bigger size of stenosis gives bigger shear rate and higher jumping pressure in the channel, especially near the stenosis. Comparison the results obtained from the model with solid

wall and permeable wall, it is found that the model with solid wall generates linear distribution of pressure except at the stenosis and the model with permeable wall gives oscillating pressure along an arterial line. Higher dropping pressure occurs at the stenosis. Bigger size of stenosis gives bigger dropping pressure around there.

It should be addressed here that blood flow in a small stenotic artery is an extremely complex phenomenon and there are still many unsolved modeling problem. The presented work focuses on blood flow in a stenotic artery with solid wall and permeable wall. Further work could be carried out to incorporate the fluid-wall interaction in a stenotic artery when arterial wall is poroelastic material.

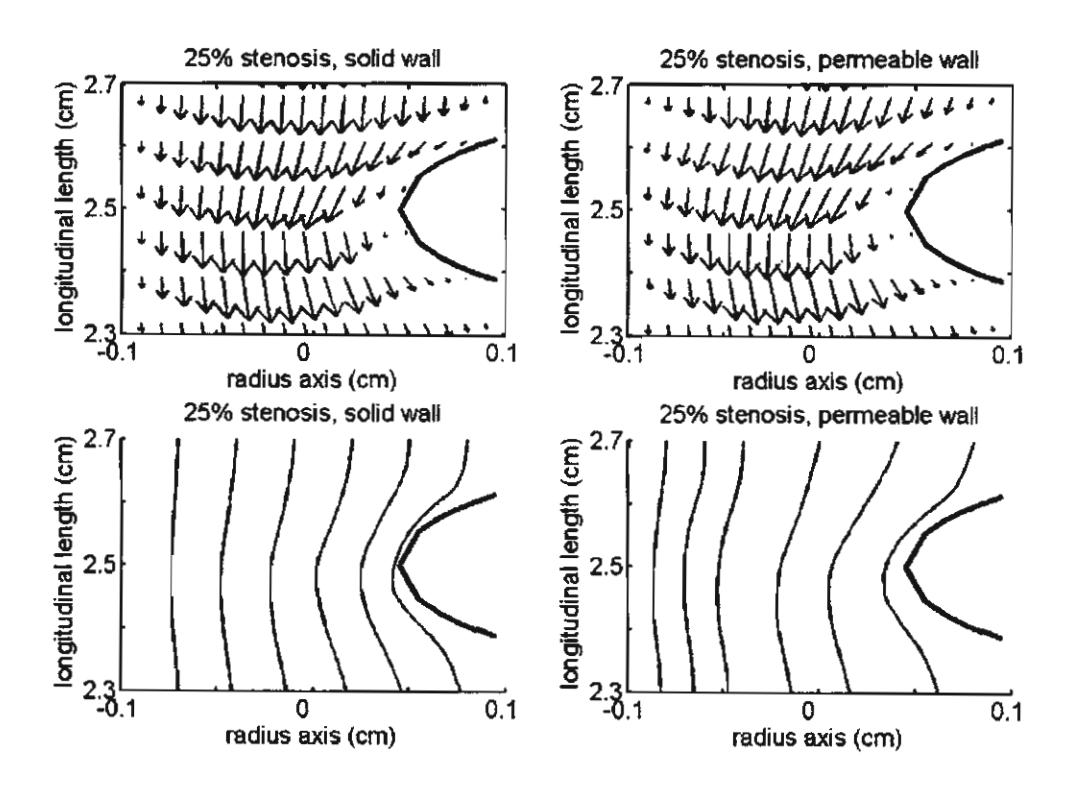


Figure 2.8 Velocity profile along 25% stenotic artery obtained from a model with solid wall and permeable wall.

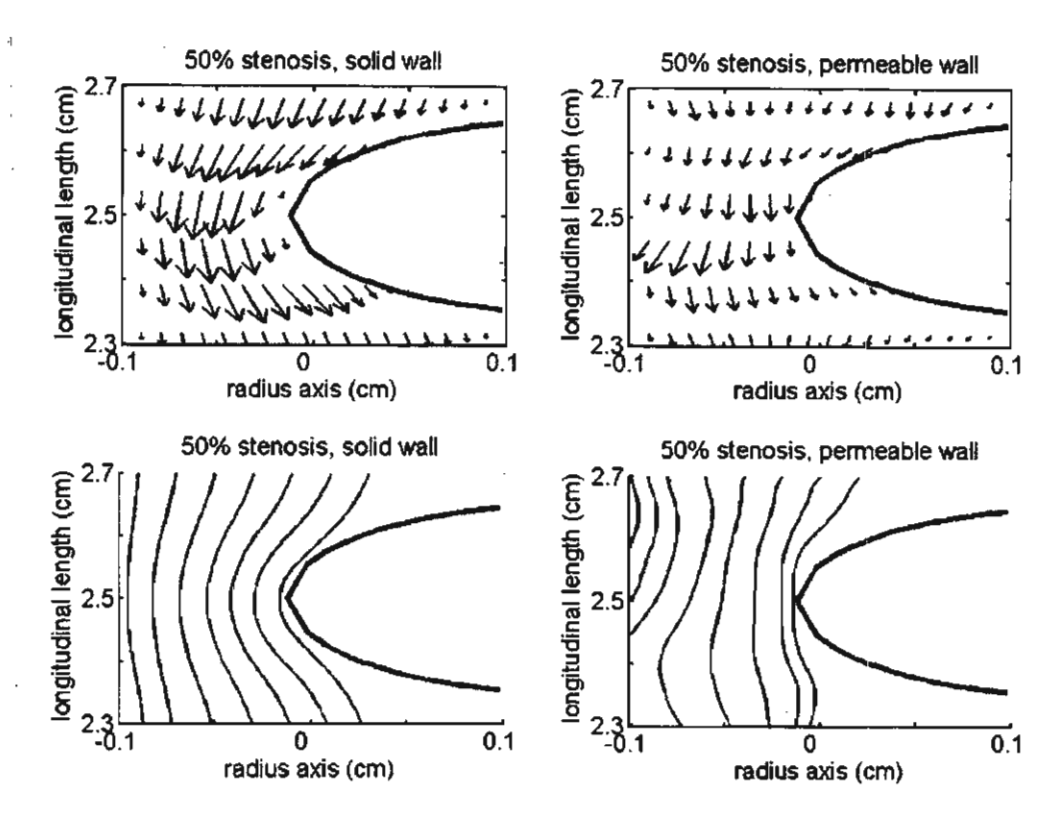


Figure 2.9 Velocity profile along 50% stenotic artery obtained from a model with solid wall and permeable wall.

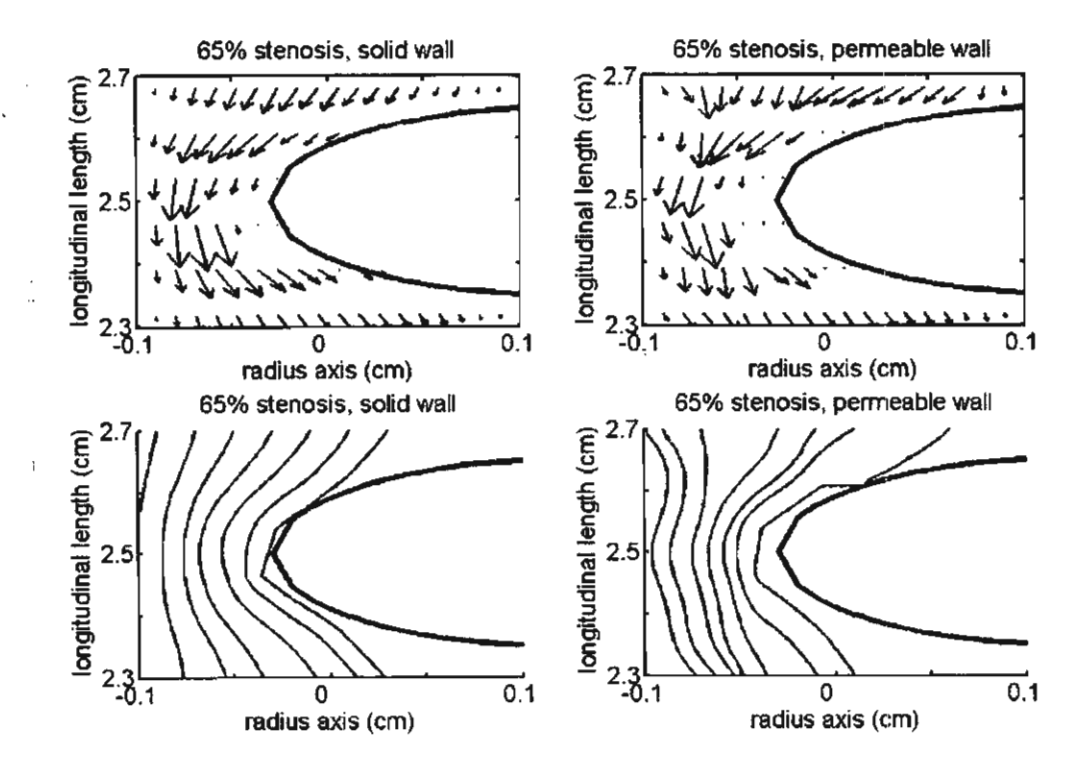


Figure 2.10 Velocity profile along 65% stenotic artery obtained from a model with solid wall and permeable wall.

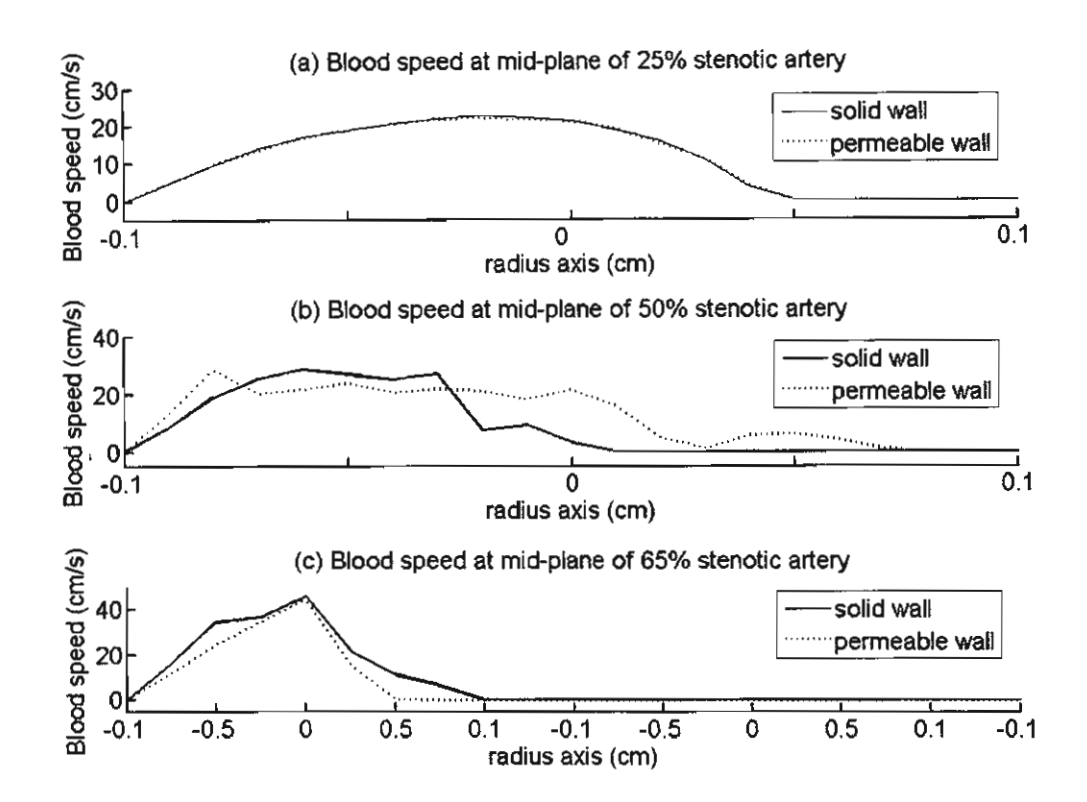


Figure 2.11 Blood speed at (a) mid plane of stenosis with different severity obtained from a model with solid wall and permeable wall.

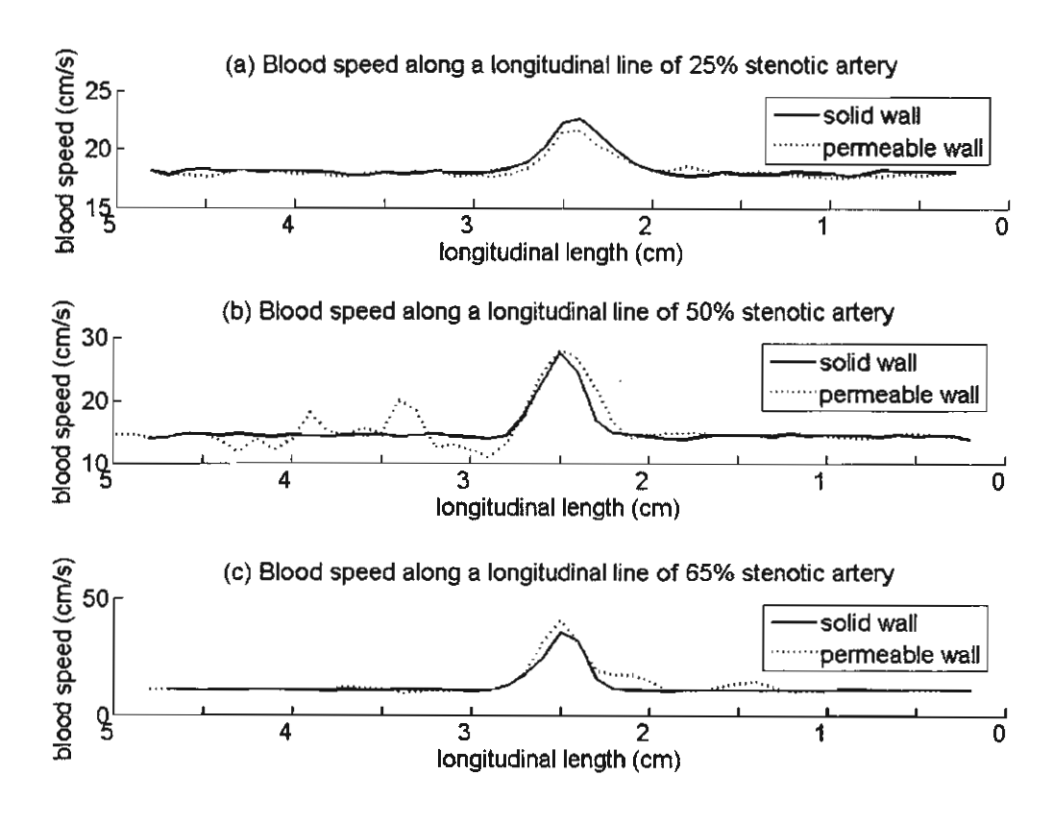


Figure 2.12 Blood speed along a longitudinal line of stenotic artery with different severity obtained from a model with solid wall and permeable wall.

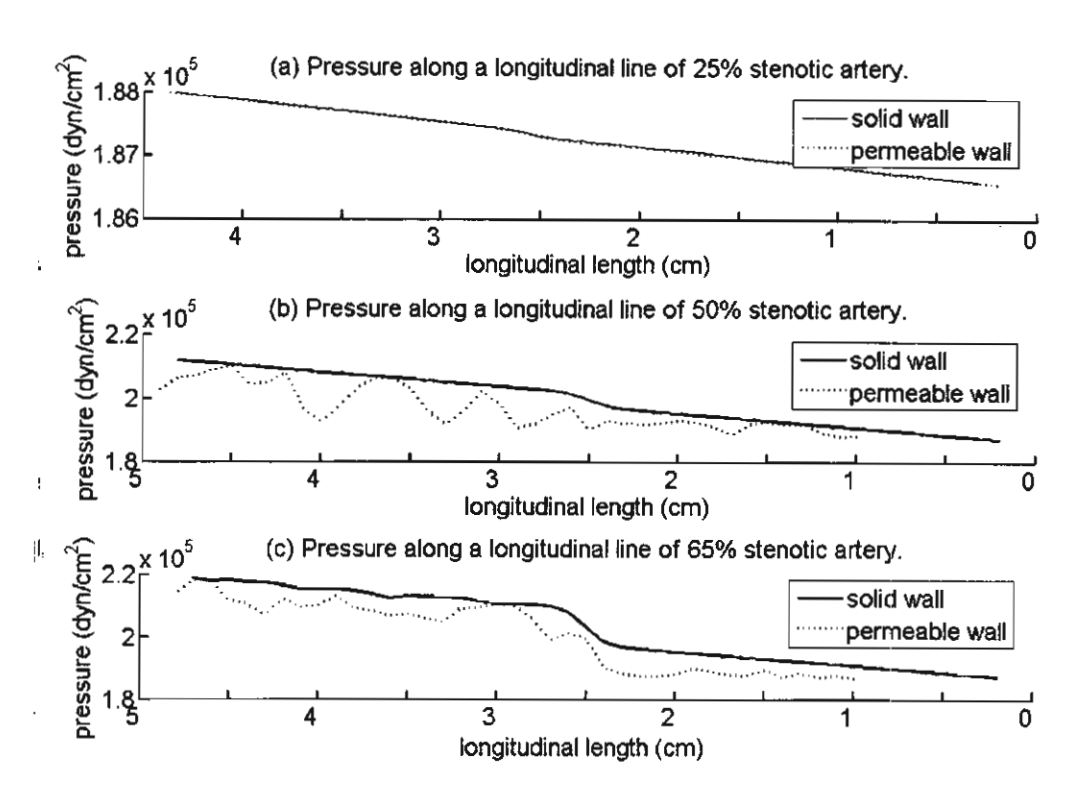


Figure 2.13 Pressure along a longitudinal line of stenotic arteries with different severity obtained from a model with solid wall and permeable wall.

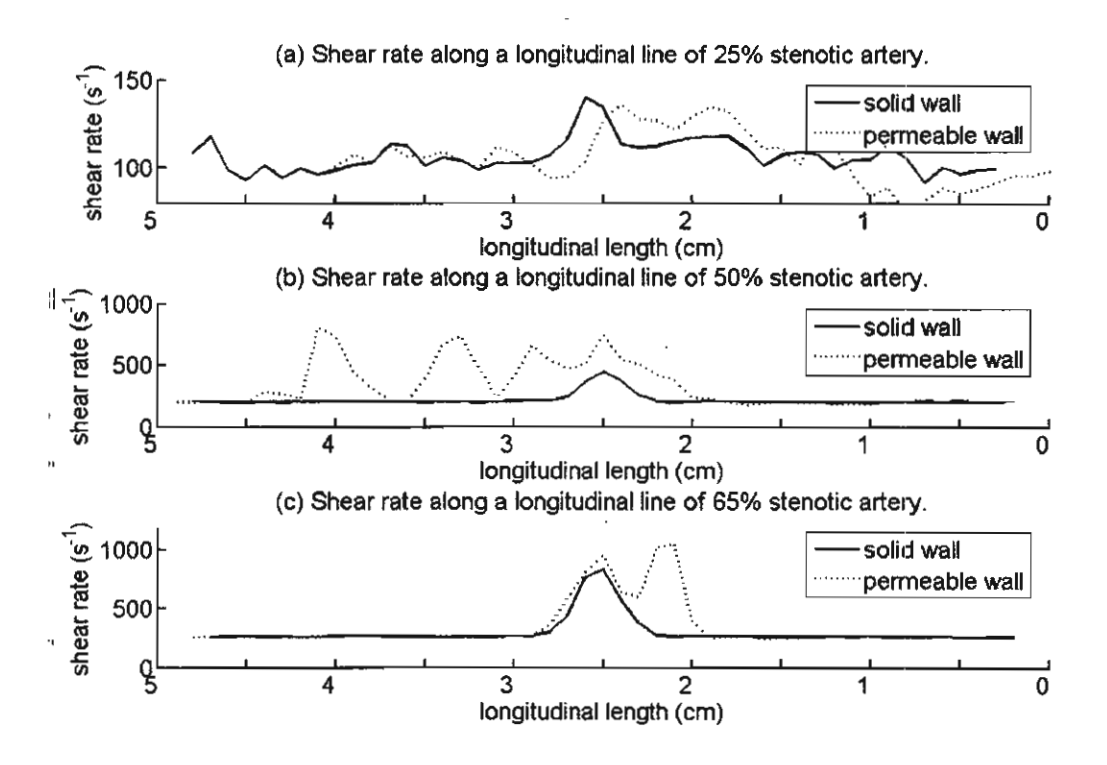


Figure 2.14 Shear rate along stenotic arteries with different severity obtained from a model with solid wall and permeable wall.

\*

ĄĀ

## 2.3 A Numerical study of non-Newtonian blood flow in stenosed coronary artery bypass graft

It has been reported that cardiovascular disease is the leading cause of death in developed countries [1, 2]. In recent years, surgical treatments of cardiovascular diseases have been developed rapidly, and coronary artery bypass grafting (CABG) has been widely used for patients with severe coronary artery diseases. The bypass grafts are worldwide implanted each year. However, up to 25% of the grafts become occluded in one year and up to 50% occluded in ten years [3]. Intimal hyperplasia which is related to the distribution of wall shear stress (WSS) is an importance factor in failure of the coronary bypass surgery. In general, atherosclerotic lesions in the coronary arteries have been related to low and oscillating WSS [5, 4].

Another important factor in simulating blood flow is the behavior of blood. The blood is a non-Newtonian fluid with low shear rate, less than  $100 \, s^{-1}$  [10]. Some numerical studies assumed the blood to be Newtonian under the assumption that the shear rate is larger than this value [11, 12, 13]. It has been known that near the center of the arteries the shear rate is small. Therefore, a non-Newtonian behavior must be taken into account in the model.

#### 2.3.1 Mathematical model

The blood is assumed as an incompressible fluid and blood flow is laminar. The governing equations consist of the continuity equation and the Navier-Stokes equations, which can be expressed in vector notation as follows:

$$\nabla \cdot \mathbf{u} = 0, \tag{2.24}$$

$$\frac{\partial \mathbf{u}}{\partial t} + \mathbf{u} \cdot \nabla \mathbf{u} = \frac{1}{\rho} \nabla \cdot \mathbf{\sigma},\tag{2.25}$$

where  $\mathbf{u}$  and the blood velocity vector,  $\rho$  is the density of blood.  $\sigma$  is total stress tensor which is defined by  $\sigma = -\mathbf{p}\mathbf{I} + \tau$ , p is pressure,  $\tau$  is the stress tensor and linearly dependent on the rate of deformation tensor  $\mathbf{D}$  with the relation  $\tau = 2\eta(\dot{\gamma})\mathbf{D}$ ,  $\mathbf{D} = \frac{1}{2}(\nabla \mathbf{u} + \nabla \mathbf{u}^T)$ ,  $\eta$  and  $\dot{\gamma}$  denote the viscosity of blood and shear rate respectively. For the non-Newtonian property of blood,  $\eta$  depends on the shear rate  $\dot{\gamma}$ . The complex rheology of blood is approximated using a shear-thinning model by Carreau model.

$$\eta = \eta_{\infty} + (\eta_0 - \eta_{\infty}) [1 + (\lambda \dot{\gamma})^2]^{n-1/2}. \tag{2.26}$$

For  $\dot{\gamma}$ , a scalar measure of the rate of deformation tensor,  $\dot{\gamma} = \sqrt{2 \text{tr}(\mathbf{D}^2)}$ ,  $\eta_0$  and  $\eta_{\infty}$  denote zero shear viscosity and infinite shear viscosity. The consistency index, n is the parameter between 0 and 1. The other parameters in equation (2.26) are based on Cho and Kensey [6],  $\eta_{\infty} = 0.0345 \text{ g cm}^{-1} \text{ s}^{-1}$ ,  $\eta_0 = 0.56 \text{ g cm}^{-1} \text{ s}^{-1}$ , n = 0.3568,  $\lambda = 3.313 \text{ s}$ .

To completely define the flow problem, boundary conditions for the velocity and pressure fields must be specified. For a typical CABG system, the boundary of the computation region consists of four parts, namely the inflow surfaces of the native artery and the bypass graft, the artery wall and the outflow boundary.

On the inflow surfaces, The pulsatile velocity used in this study is shown in Figure 2.15 [7]. The flow pattern is very large during systole and small during diastole.

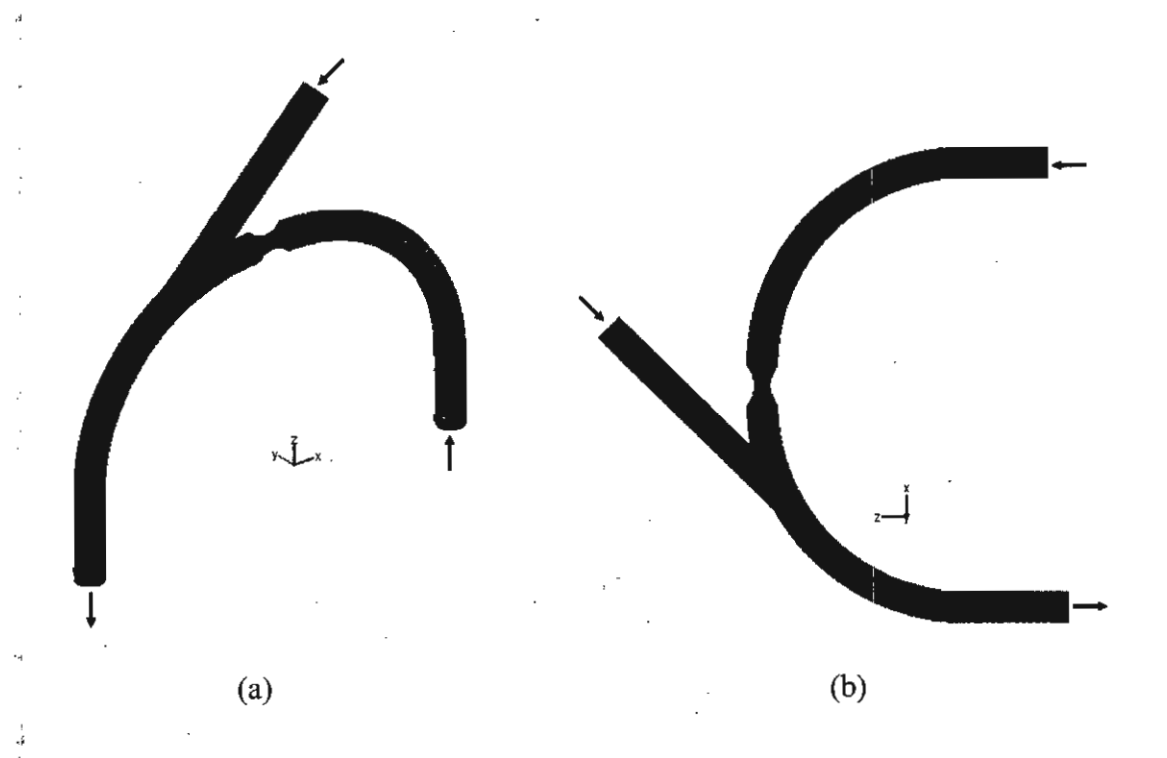


Figure 2.15 Geometry of three-dimensional 75% stenosed right coronary artery with bypass grafting model: (a) global view; (b) x-z view.

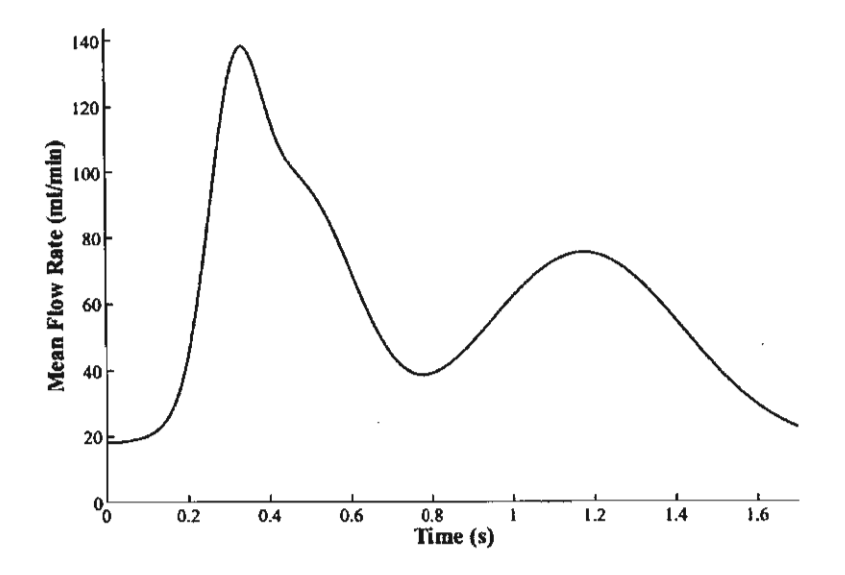


Figure 2.16 The right coronary artery volume flow rate [7].

No-slip condition is applied to the artery wall. The outflow boundary is assumed to be

$$\sigma \cdot \mathbf{n} = p_n$$

where **n** is the unit normal vector to the outlet surface. We assume pressure at the outlet of 140 mmHg.

In summary, the fluid flow problem in CABG is governed by the following boundary value problem.

BVP: Find  $\mathbf{u}$  and  $\mathbf{p}$  such that the field equations (1) and (2) are satisfied in  $\Omega$  and all boundary condition are satisfied.

#### 2.3.2 A Numerical algorithm based on the finite element method

The variational statement corresponding to the BVP is then VBVP: Find  $\mathbf{u}$  and  $\mathbf{p} \in H^1(\Omega)$  such that for all  $\mathbf{w}^u$  and  $\mathbf{w}^p \in H^1(\Omega)$ , all boundary conditions are satisfied and

$$(\nabla \cdot \mathbf{u}, \mathbf{w}^{\mathsf{p}}) = 0, \tag{2.27}$$

$$\left(\frac{\partial \mathbf{u}}{\partial t}, \mathbf{w}^{\mathrm{u}}\right) + \left(\mathbf{u} \cdot \nabla \mathbf{u}, \mathbf{w}^{\mathrm{u}}\right) = \frac{1}{\rho} \left(\nabla \cdot \sigma, \mathbf{w}^{\mathrm{u}}\right), \tag{2.28}$$

where  $(\cdot,\cdot)$  denotes the inner product on the square integrable function space  $L^2(\Omega), H^1(\Omega)$  is the Sobolev space  $W^{1,2}(\Omega)$  with norm  $\|\cdot\|_{1,2,\Omega}$  and  $H^1_0(\Omega) = \{v \in H^1(\Omega) \mid v = 0 \text{ on the Dirichlet type boundary}\}$ .

To find the Galerkin numerical solution of the above problem, we pose the problem into a finite dimension subspace. The Galerkin finite element formulation was used in the calculation. Then, we obtained the system of ordinary differential equation,

$$C^{\mathsf{T}}U = 0,$$

$$\dot{U} + A(U)U - \overline{C}P = 0,$$
(2.29)

#### 2.3.3 Numerical example

ij

北

Flow simulations were conducted under a typical physiological condition. The fluid properties are typical of human blood with density of 1.06 gcm<sup>-3</sup> [8]. The computation region, as shown in Figure 2.15, represents the right coronary artery with 75% stenosis located at 3.95 cm from the inlet boundary. Diameter of the native artery is equal to 0.3 cm (D), and diameter of grafts is equal to 0.96×D [9]. The length of investigation is about 8.5 cm.

We simulate the blood flow through stenosis right coronary artery with 45°, 60° and 90° bypass operations in three-dimensions. The mesh as shown in Figure 2.15 consists of 27030 nodes and 15819 elements. To get flow patterns in successive cycles, each of which is divided into 280 time steps with step size 3.57 ms.

Table1: Mean/maximum velocities, pressures and mean/maximum and minimum wall shear stress

				·	
RCA with	t	U <sub>max</sub>	P <sub>max</sub>	WSS <sub>max</sub>	$\overline{\mathrm{WSS}}_{\mathrm{min}}$
75% stenosis	(s)	(cm/s)	(mmHg)	(dyn/cm <sup>2</sup> )	(dyn/cm <sup>2</sup> )
	0.4	150.68	145.99	449.70	0.53
Without	0.8	47.55	141.56	113.75	0.55
bypass graft	1.2	92.91	143.38	255.98	0.79
	1.6	36.91	140.91	80.61	0.34
	0.4	154.16	147.72	442.03	1.422
With 45°	0.8	48.28	142.06	111.13	0.40
bypass graft	1.2	94.71	144.52	253.79	0.85
	1.6	37.09	141.17	82.18	0.46
	0.4	157.51	148.15	2760.47	0.00
With 60°	0.8	46.75	142.01	916.00	0.00
bypass graft	1.2	91.75	144.48	1765.31	0.00
	1.6	36.62	141.15	692.76	0.00
	0.4	183.61	147.80	520.25	0.00
With 90°	0.8	49.78	141.75	123.35	0.00
bypass graft	1.2	94.54	143.96	273.83	0.00
	1.6	38.05	141.01	87.22	0.00

Table 1 shows the maximum blood speed, pressures and maximum and minimum wall shear stress. Maximum speed at the throat of stenosis obtained from each domain is very high at the peak systolic. The results indicated that pressure drops along the arterial axis. Figure 2.17 shows, in x-z plane, that the retrograde flows occur along the vessel wall in the neighborhood of heel part in the native artery. Bypass graft with 45° produces the re-circulation zone in the cardiac cycle. The re-circulating jet flow tends to decrease as the anastomosis angle increases as shown in Figure 2.18.

Figures 2.19 and 2.20 show the wall shear stress along the lines A and B, respectively. The results indicate that very high WSS occurs during systole period. Figure 2.19 shows that wall shear stress at the bed of graft (line A) tends to increase after bypass operation for all graft angles. Figure 2.20 shows WSS at the toe part of the graft (line B). High WSS is present at the toe part as shown in Figure 2.20.

#### 2.3.4 Conclusions

A mathematical model of blood flow patterns in the 75% right coronary artery bypass grafting is presented based on the Bubnov-Galerkin Finite Element formulation. The three-dimensional non-Newtonian flow is calculated. On comparing the results with other angles of bypass grafts, the ones of 45° graft angle seem to be satisfied. It can be stated that the proper choice of the diameter of the graft might improve the balance of inflow and outflow in the coronary artery. It should be addressed that to improve the accuracy of results, the effect of porous wall and wall deformation must be included. Therefore, further research work is required.

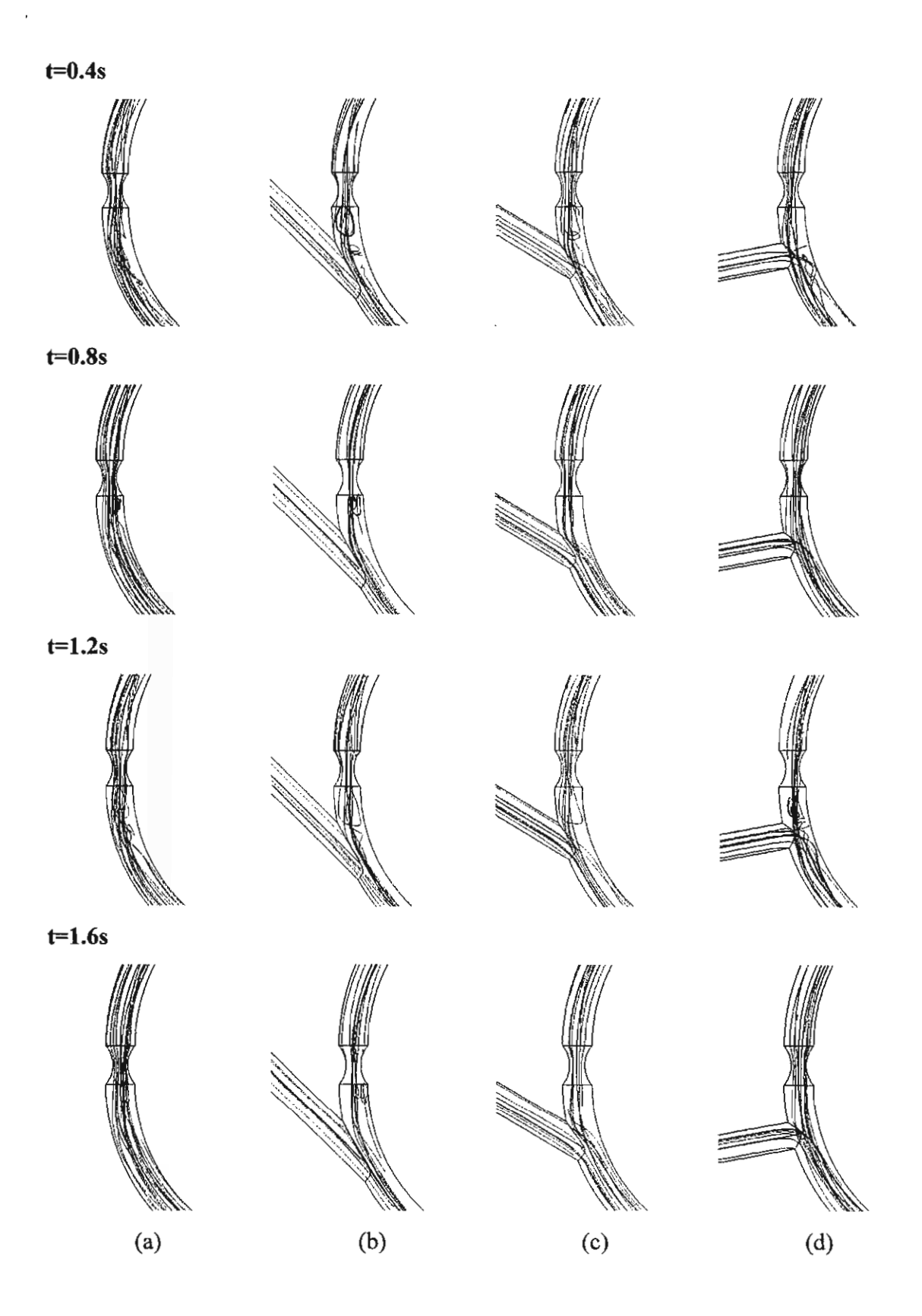


Figure 2.17 The streamline velocity field in RCA (a) without and (b)-(d) with bypass operation  $45^{\circ}$ ,  $60^{\circ}$  and  $90^{\circ}$ , respectively, in x-z plane at specific times.

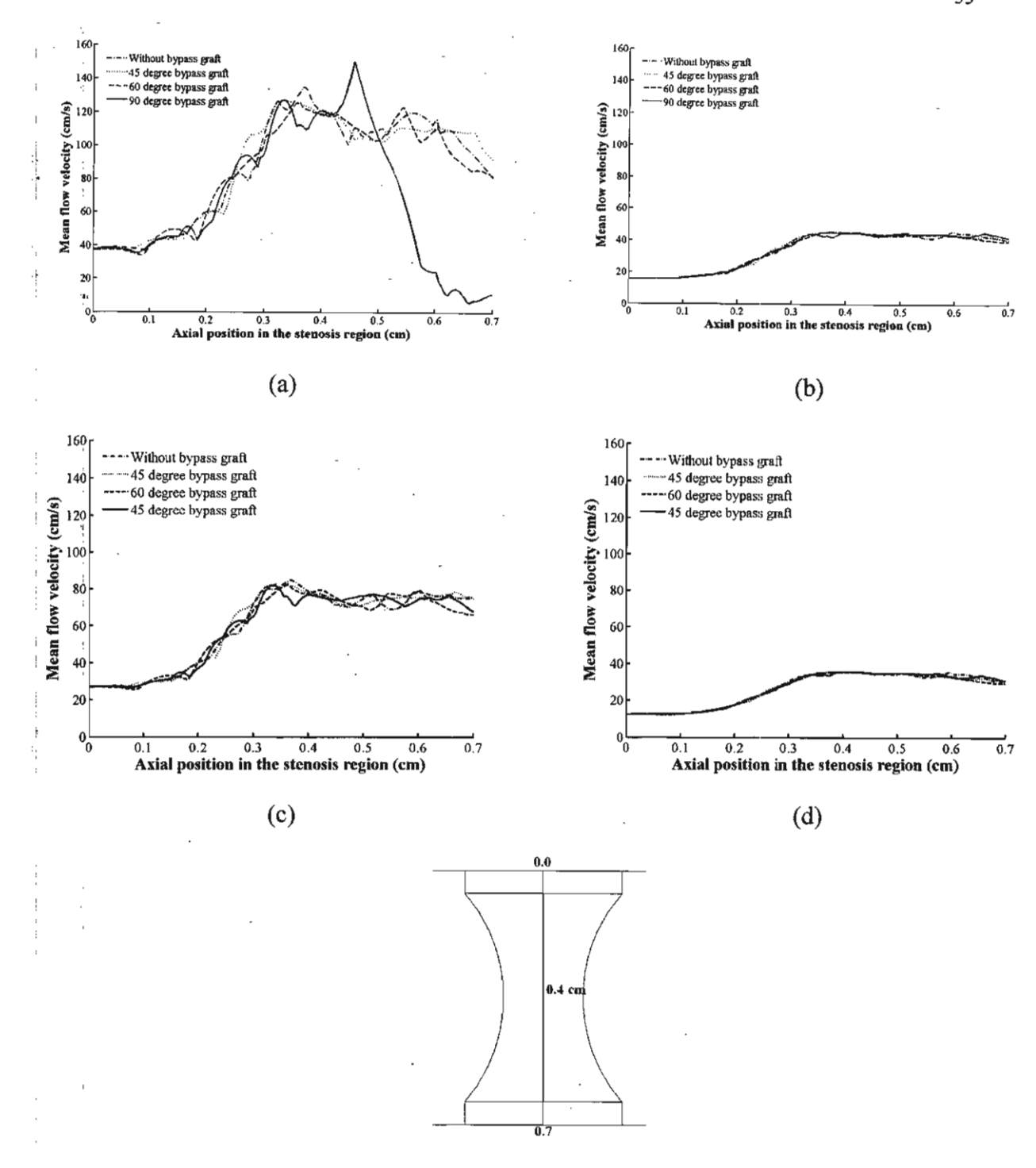


Figure 2.18 Axial distribution of mean axial velocity in the stenosis region at specific times: (a) t=0.4s, (b) t=0.8s, (c) t=1.2s and (d) t=1.6s.

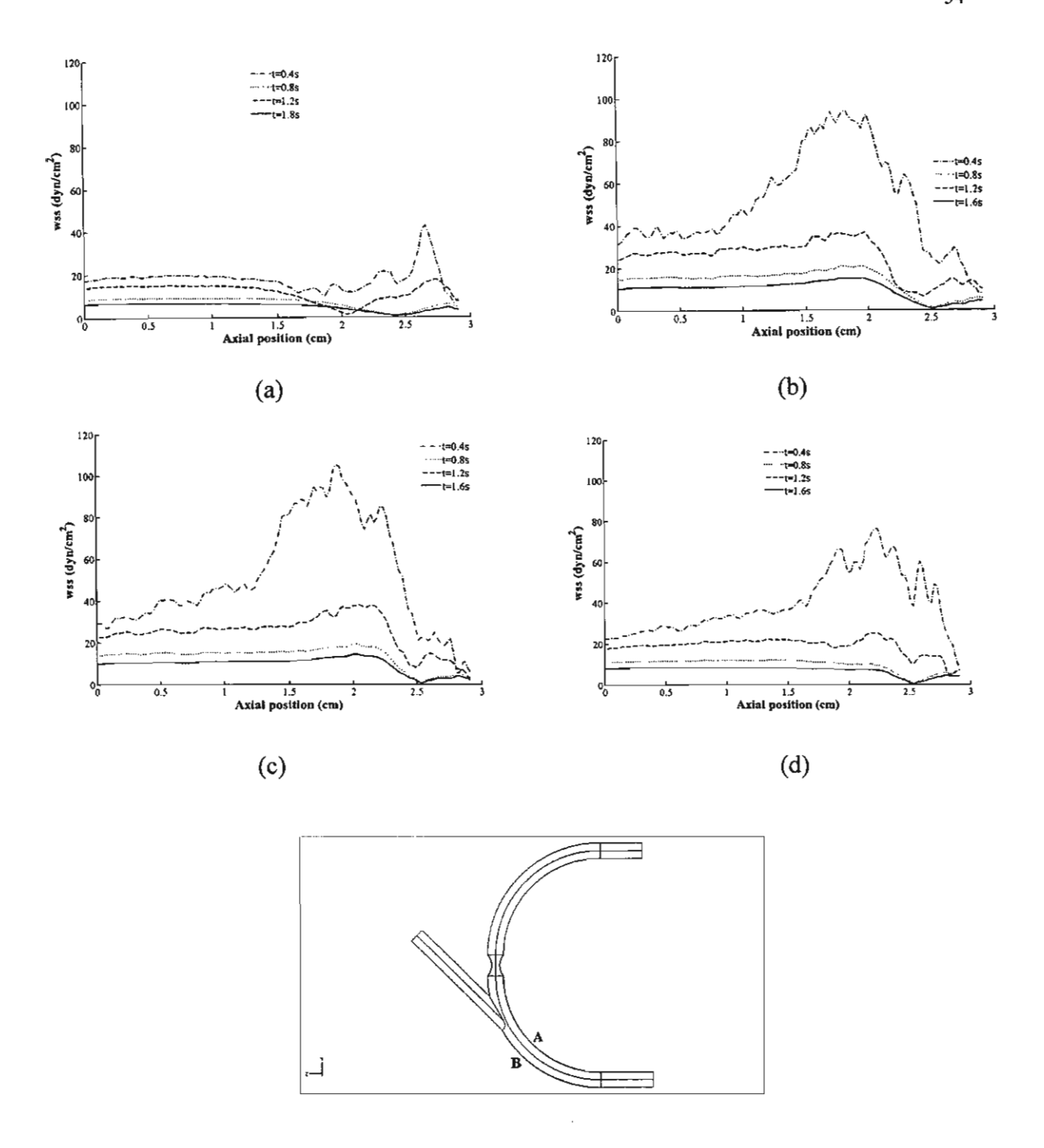


Figure 2.19 The wall shear stress evaluation along line A: (a) without bypass grafting and with bypass grafting of angles (b)  $45^{\circ}$ , (c)  $60^{\circ}$  and (d)  $90^{\circ}$ .

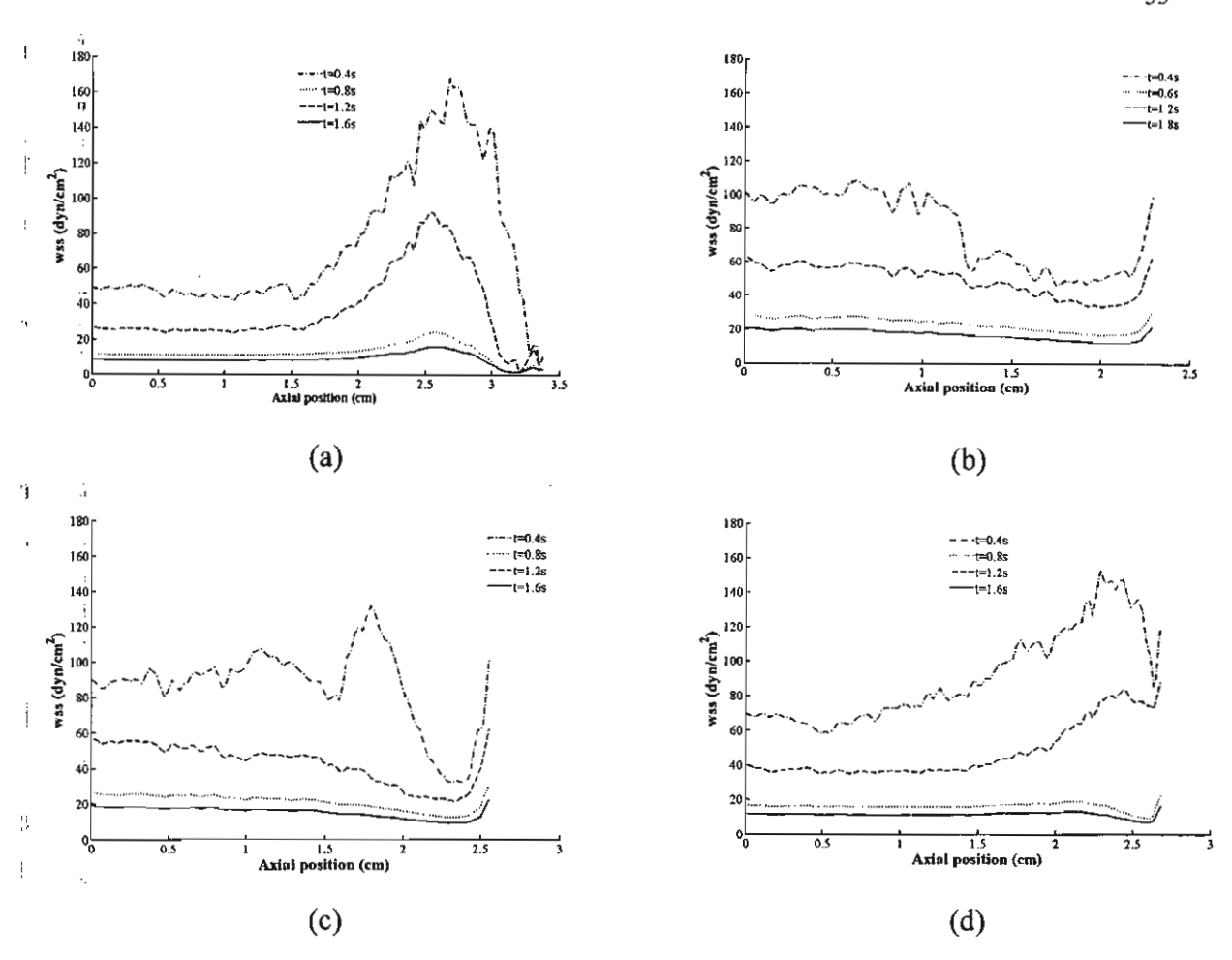


Figure 2.20 The wall shear stress evaluation along line B: (a) without bypass grafting and (b)-(d) with bypass grafting of angles  $45^{\circ}$ ,  $60^{\circ}$  and  $90^{\circ}$ , respectively.

#### References

- [1] CARO, C.G., FITZ-GERALD, J.M., SCLIROTER, R.C, Atheroma and arterial wall shear: observation, correlation and proposal of a shear dependent mass transfer mechanism for atherogenesis, Proc. Roy. Soc. B, 177 (1971), pp. 109-159.
- [2] Organisation Mondiale de la Sante (OMS). Annual Report, 1999.
- [3] Y. PAPAHARILAOU, D.J. DOORLY, S.J. SHERWIN, The influence of out-of plane geometry on pulsatile flow within a distal end-to-side anastomosis, J Biomech, 35 (2002), pp. 1255-39.
- [4] C.R. ETHIER, D.A. STEINMAN, X. ZHANG, S.R. KARPIK, M. OJHA, Flow waveform efects on end-to-side anastomotic patterns, J Biomech, 31 (1998), pp. 609-17.
- [5] E.S. WEYDAHL, J.M. MOORE JR., Dynamic curvature strongly affects wall shear rates in a coronary artery bifercation model, J Biomech, 34 (2001), pp. 1189-96.

- [6] Y.I. Cho, K.R. Kensey, Effects of the non-Newtonian viscosity of blood on flows in a diseased arterial vessel. Part 1: steady flows, Biorheology. 28 (1991), pp. 241-262.
- [7] C. Bertolotti, V. Deplano, J. Fuseri, P. Dupouy, Numerical and experimental models of post-operative realistic flows in stenosed coronary bypasses, J Biomech, 34 (2001), pp. 1049-64.
- [8] D. TANG, C. YANG, S. KOBAYASHI, KU DN, Steady flow and wall compression in stenotic arteries: a three-dimensional thick-wall model with fluid-wall interactions, J Biomech Eng, 123 (2001), pp. 548-57.
- [9] A. QUANTERONI, L. FORMAGIA, Mathematical modelling and numeriacal simulation of the cardiovascular system in modelling of living system, Handbook of Numerical Analysis Series (P.G. Ciarlet, J.L. Lions Eds), Elsevier, Amsterdam, 2003.
- [10] M.J BARBARA, R.J. PETER, C. STUART, K. DAVID, Non-Newtonian blood flow in human right coronary arteries: steady state simulations. J Biomech, 37 (2004), pp. 709-720.
- [11] D.Y. FEI, J.D. THOMAS, S.E. RITTGERS, The effect of angle and flow rateupon hemodynamics in distal vascular graft anatomoses: a numerical model study. J Biomech Eng, 116 (1994), pp. 331-6.
- [12] M. Bonert, J. G. Myers, S. Fremes, J. Williams, C. R. Ethier, A Numerical Study of Blood Flow in Coronary Artery Bypass Graft Side-to-Side Anastomoses, Annals of Biomedical Engineering, 30(2002), pp. 599-611.
- [13] M-H. Song, M. Sato, Y. Ueda, Three-dimensional simulation of coronary artery bypass grafting with the use of computational fluid dynamics, Surg Today, 30 (2000), pp. 993-8.

Table II: Proposed and Actual Activity for Subproject 2.

Activity: Proposed (<->)	Months	Months	Months	Months	Months	Months
Actual (←→)	1-6	7-12	13-18	19-24	25-30	31-36
Construction of mathematical model.	<	>				
Development of numerical technique	<					
Design of numerical     method (NM)						
Implementation of NM in     a computer			-			
3. Validation  • Design of schemes &			<			<u> </u>
analysis  Computation & analysis						

#### **Outputs of Subproject 2**

Papers appeared/accepted in international journals	1
Papers presented in international conferences	2
Ph.D. graduates	2

### Subproject 3: Mathematical Modeling of Disease Transmission

Principal Investigator: Prof. Dr. I. Ming Tang

The project commenced around the end of the first academic semester of 2002. As a program director in the Institute of Science & Technology for Research & Development, Mahidol University, the investigator of this subproject met on a regular basis with the program directors of the Center for Vaccine Development (CVD) and the Conservation Biology Center (CVB). Through his acquaintance with Prof. Sutee of CVD, he met with the French scientists at the Institute Recherche pour Development (IRD) who were working on the transmission of infectious diseases in Thailand. Dr. Tang established very close collaboration with them, especially Dr. Phillippe Barbazan. Dr. Barbazan served as the co-advisor to three of Dr. Tang's Ph.D. students, who have subsequently graduated with their Ph.D. They are now working at three universities in Thailand.

Due to the interests of the investigator's collaborators, he has worked on the following diseases:

- 1. Dengue Fever
- Malaria
- 3. West Nile Virus
- 4. Japanese Encepthalitis
- 5. Tuberculosis
- 6. Severe acute respiratory syndrome (SARS)
- 7. Leptosprosis
- 8. Smallpox

and has published papers on these diseases. Please see Appendices # 3.1-3.14 for full papers.

To further improve the research capabilities of the students, Dr. Tang have joined up with Dr. Phillippe Barbazan to set up a Franco-Thai Collabrative Research network involving six institutions and three units in France. We have been informed that our proposal (one of fifteen accepted) has been accepted and it is now running. This is a four year proposal. The title of the proposal is Spatial approach and mathematical modeling of emerging infectious diseases transmission and development of resistance. It is under the Franco – Thai Cooperation Program in Higher Education and Research. My team is only interested in that part of the proposal that is underlined.

Several officials in the Ministry of Public Health have indicated interests in the net-work of local surveillance centers in the provinces. Dr. Suwich Thammapalo, Chief, Dengue Fever Control Section, Bureau of Vector Borne Disease Control, MOPH is interested in my proposed network. Professor Dr. Virasakdi Chonsuvivatwong, Epidemiology Unit, Faculty of Medicine, Prince of Songkla University, who is the Ph.D. thesis advisor of Dr. Suwich is interested in the work of Dr. Puntani Pongsumpun. Dr. Suwich is working on a statistical model to correlate the data on the DHF cases, rain fall, rain days, max. and min. temp. and humidity in the monthly records over the past 20 years (1977-1997). Dr. Viroj Tangcharoensathien, Director of IHPP-Thailand, MOPH is working on projecting the HIV/AIDS incidences in different population groups in Thailand over the next forty years to help in determining the public health policies on AIDS from an economic viewpoint. The output of our work could assist the MOPH.

The MOPH are interested in our proposed network because it will be based in the provinces and not in Bangkok. This being the reason we recruited the students from the Rajabhat Institutes. The undergraduate students at these institutes are from the local villages in the provinces. They would return to the local villages and become teachers at the tamboon schools. They might be able to get the local people interested in public health issues of direct concern to them. Leptosprosis is a disease affecting the poorer provinces in Thailand where the medical care is not as advanced as in Bangkok and the other big cities. Having local people as part of a community-based public health surveillance units fits into the governmental plan of getting local people involved in thier own development.

Leptosprosis is also being used as the bacterium to determine the toxicity of nanoparticles, a project being undertaken in the Capacity Building Unit in Nanoscience & Nanotechnology of the Faculty of Science. This unit is also being headed by Prof. Dr Tang.

Table III: Proposed and Actual Activity for Subproject 3.

Activity: Proposed (	Months	Months	Months	Months	Months	Months
Actual $(\longleftrightarrow)$	1-6	7-12	13-18	19-24	25-30	31-36
1. Modelling transmission of	<				***************************************	
dengue hemorrhagic fever.	<del></del>		,			<del>&gt;</del>
2. Modelling cannibalism in an	<b></b>					
age structured predator-prey system.	<	>				
3. Modelling P. falcipurum			<u> </u>			
malaria transmission.			<del></del>	<b>→</b>		
4. Modelling of P. vivax malaria transmission.			<del></del>			
5. Analysis of feedback control			*	******************************	***************************************	***************************************
of blood platelet regulation by						
TPO.						
6. Study EPO regulation of				*		
erythrocytes production.						
7. Model the spread of seeds in tropical forests.				<u> </u>		

<sup>\*</sup> The investigator has become interested in SARs, Leptosporosis, and other diseases instead.

#### Outputs of Subproject 3

Papers appeared/accepted in international journals	14
Papers presented in international conferences	3
Ph.D. graduates	4
Master graduates	9

# Subproject 4: Application of Log-linear and Logistic Models to Cancer Patients: A Case Study of the National Cancer Institute

Principal Investigator: Assoc. Prof. Dr. Montip Tiensuwan

The activities in this subproject have followed the proposed plan, that is,

- (1) Application of log-linear models to cancer patients: a case study of data from the National Cancer Institute.
- (2) Application of logistic regression models to cancer patients: a case study of data from the National Cancer Institute.

We finished number (1) and submitted our paper to the Southeast Asian Journal of Tropical Medicine and Public Health (see the manuscript in Appendix 4.1).

For number (2), application of logistic regression models, the aims of the study are as follows:

- 1. To analyze the cancer data by using logistic regression models to identify factors associated with the status of last contact of all cancer patients and estimate parameters of the models which indicate association between cancer variables.
- 2. To analyze the cancer data by using logistic regression models to identify factors associated with the status of last contact of cancer patients for individual gender and estimate parameters of the models which indicate association between cancer variables.
- 3. To analyze the cancer data by using logistic regression models to identify factors associated with the status of last contact of cancer patients for the specific site and estimate parameters of the models which indicate association between cancer variables.

#### Results of the completed study

The subjects were cancer patients treated at the National Cancer Institute. We collected cancer data by using a cancer notification form of the National Cancer Institute. The classification and coding of primary site and morphology are given in cancer notification form, that is ICD-O (9). This data set includes the number of new cancer patients who were admitted between January 2000 and December 2001 at the National

Cancer Institute. In this data set, there were 5,946 cancer patients which consisted of 2,042 male patients and 3,904 female patients.

The cancer data were considered according to the sex of cancer patients: male patients and female patients. In addition, each sex was classified into two parts as follows:

Part I Personal data. This part consists of age, region, marital status, race and religion.

Part II Cancer/clinical data. Factors being important variables in this part were as follows: Diagnostic evidence, site of cancer, pathological, stage of diagnosis, sites of metastasis, treatment which consists of surgery, radiation, chemotherapy, hormone and support and status of last contact.

#### Summary of general data of most patients

Part I: personal data. More patients were females than males. The majority of male patients ranges from 56 to 65 years of age, while female patients ranges from 46 to 55 years of age. We found that many of the patients were middle aged. Most of the patients were of Thai race, Buddhist religion, married / divorced / widowed patients and lived in the central part of Thailand.

Part II: cancer/clinical data. Most patients were diagnosed by using the histology of primary. A large number of female patients had cancer at their breasts and female genital organs, whereas, digestive organs were the positions at which cancer occurred most often for male patients. The majority of male patients had squamous cell neoplasms, while female patients had ductal, lobular and medullary neoplasms. Most patients were in the direct extension stage. Since more male patients were in the distant metastasis stage than female patients, more male patients had the sites of metastasis than the female patients. For treatments, radiation, surgery and chemotherapy, by order of preference, were used in male patients. While female patients were treated by surgery, radiation and chemotherapy, by order of preference. Most of patients survived with cancer.

#### Model for all cancer patients

The best logistic regression model to identify factors associated with the status of last contact for all cancer patients is given by the following equation:

$$\log it(\hat{\pi}) = -3.477 + 0.557X1 - 0.030X9 - 2.082X10 - 0.113X18 + 0.209X19 - 2.124X20 - 0.784X21 - 1.229X22 - 0.891X23 + 0.559X36 + 1.429X37 + 0.101X38 + 0.511X39 - 0.615X40 + 1.424X41 + 1.06X42 - 0.677X44 + 2.001X47 - 1.755(X18 × X47) - 1.360(X19 × X47) + 1.462(X20 × X47) + 0.162(X21 × X47) - 6.936(X22 × X47) + 0.133(X23 × X47).$$

According to this model, the factors which effect the status of last contact are sex  $\{X1\}$ , marital status  $\{X9, X10\}$ , site of cancer  $\{X18 - X23\}$ , sites of metastasis  $\{X36 - X42\}$ , radiation  $\{X44\}$ , support  $\{X47\}$  and site of cancer  $\times$  support  $\{(X18 - X23) \times X47\}$ .

#### Model for male cancer patients

By using the logistic regression models, the best model for male cancer patients that identify factors associated with the status of last contact is given by the equation below.

$$logit(\hat{\pi}) = -2.939 + 0.546X8 - 1.472X9 + 0.107X16 + 0.760X17 - 1.013X18 - 0.923X19$$
$$-1.450X39 - 0.842X40 + 1.661(X39 \times X40).$$

According to the above model, the factors which effect the status of last contact are marital status  $\{X8, X9\}$ , site of cancer  $\{X16 - X19\}$ , radiation  $\{X39\}$ , chemotherapy  $\{X40\}$  and radiation  $\times$  chemotherapy  $\{X39 \times X40\}$ .

#### Model for female cancer patients

The best logistic regression model to identify factors associated with the status of last contact for female cancer patients is given by the following equation.

$$\begin{aligned} \log &\mathrm{it}(\hat{\pi}) = & -11.030 + 0.009\mathrm{X1} - 0.438\mathrm{X14} + 0.095\mathrm{X15} - & 2.343\mathrm{X16} - 0.634\mathrm{X17} - \\ & 0.244\mathrm{X18} + 6.026\mathrm{X25} + 8.594\mathrm{X26} + 5.731\mathrm{X27} + 0.428\mathrm{X28} + 7.583\mathrm{X37} + \\ & 3.072\mathrm{X38} - 1.712(\mathrm{X14} \times \mathrm{X38}) - 12.126(\mathrm{X15} \times \mathrm{X38}) + 1.327(\mathrm{X16} \times \mathrm{X38}) - \\ & 1.074(\mathrm{X17} \times \mathrm{X38}) - 0.802(\mathrm{X18} \times \mathrm{X38}) - 7.538(\mathrm{X25} \times \mathrm{X37}) - 6.276(\mathrm{X26} \times \mathrm{X37}) - 7.109(\mathrm{X27} \times \mathrm{X37}) + 0.744(\mathrm{X28} \times \mathrm{X37}) + 0.007(\mathrm{X1} \times \mathrm{X25}) - \\ & 0.043(\mathrm{X1} \times \mathrm{X26}) + 0.041(\mathrm{X1} \times \mathrm{X27}) - 0.027(\mathrm{X1} \times \mathrm{X28}) - 10.034(\mathrm{X37} \times \mathrm{X38}). \end{aligned}$$

According to the above model, the factors which effect the status of last contact are age  $\{X1\}$ , site of cancer  $\{X14 - X18\}$ , stage of diagnosis (extent)  $\{X25 - X28\}$ , chemotherapy  $\{X37\}$ , support  $\{X38\}$ , age × stage of diagnosis (extent)  $\{X1 \times (X25 - X28)\}$ , site of cancer × support  $\{(X14 - X18) \times X38\}$ , stage of diagnosis (extent) × chemotherapy  $\{(X25 - X28) \times X37\}$  and chemotherapy × support  $\{X37 \times X38\}$ .

#### Models for the specific site in cancer patients

We classified the specific sites in cancer patients into five groups.

Group 1: Lip, oral cavity and pharynx

Group 2: Digestive organs

Group 3: Respiratory system and intrathoracic organs

Group 4: Female breast and female genital organs

Group 5: Thyroid gland, endocrine glands, eye, brain, central nervous system, lymph nodes, skin, blood, connective tissue, urinary tract, peritoneum and bones.

#### Model for Group 1

By using the logistic regression models, the best model for the patients who have cancer sites classified in this group, identifying factors associated with the status of last contact, is given by the equation below:

$$logit(\hat{\pi}) = -3.609 + 2.310X15$$

According to the above model, the factor which effects the status of last contact is support {X15}.

#### Model for Group 2

The best model for the patients who have cancer sites classified in this group identifying factors associated with the status of last contact is given by the following equation:

$$\log it(\hat{\pi}) = -3.648 + 0.925X1 + 1.218X26 + 0.204X27 - 0.404X28 - 0.529X29 + 1.945X30 + 0.466X31$$

According to this model, the factors which effect the status of last contact are sex {X1} and sites of metastasis {X26 - X31}.

Using the logistic regression models with the dependent variable being the status of last contact, for the male patients who have cancer sites in this group, the best model is given by the following equation.

$$logit(\hat{\pi}) = -2.400 - 0.950X31$$

According to the above model, the factor which effects the status of last contact is chemotherapy {X31}.

#### Model for Group 3

For the patients who have cancer sites classified in this group, the best logistic regression model to identify factors associated with the status of last contact is given by the following equation:

$$logit(\hat{\pi}) = -3.631 + 0.940X18 + 2.083X19 + 3.120X20 + 1.362X21 + 0.197X22 + 1.028X23 + 2.378X24 + 2.650X28 - 2.444(X18 \times X28) - 2.489(X19 \times X28) - 9.341(X20 \times X28) - 2.779(X21 \times X28) - 6.418(X22 \times X28) - 2.127(X23 \times X28) - 2.784(X24 \times X28)$$

According to the above model, the factors which effect the status of last contact are sites of metastasis  $\{X18 - X24\}$ , support  $\{X28\}$  and sites of metastasis  $\times$  support  $\{(X18 - X24) \times X28\}$ .

#### Model for Group 4

By using the logistic regression models, the best model for the female patients who have cancer sites classified in this group that identify factors associated with the status of last contact is given by the equation below:

$$logit(\hat{\pi}) = -6.630 + 1.708X17 + 1.459X18 + 3.273X19 + 2.205X27$$

According to the above model, the factors which effect the status of last contact are stage of diagnosis (extent) {X17 - X19} and support {X27}.

#### Model for Group 5

For the patients who have cancer sites classified in this group, the best logistic regression models to identify factors associated with the status of last contact is given by the following equation:

$$logit(\hat{\pi}) = -3.647 - 0.025X1 - 1.844X24 + 1.764X25 - 17.490X26 + 0.325(X1 \times X26)$$

According to this model, the factors which effect the status of last contact are age  $\{X1\}$ , radiation  $\{X24\}$ , chemotherapy  $\{X25\}$ , support  $\{X26\}$  and age  $\times$  support  $\{X1 \times X26\}$ .

In all the best models, the fitted value of each model is  $\hat{\pi} = \frac{e^{\log it(\hat{\pi})}}{1 + e^{\log it(\hat{\pi})}}$ .

Table IV: Proposed and Actual Activity for Subproject 4.

Months Mo	Months	Months	Months	Months	(←→)	: Proposed	ctivit
25-30 31	19-24	13-18	7-12	1-6	$(\longleftrightarrow)$	Actual	
-				<>	e: statistical	rch literature	. Se
				$\longleftrightarrow$		hods	me
					lence	t of independ	Te
					al log-linear	o-dimensiona	Tv
						dels	mo
					nal log-	ee-dimensior	, Th
						ar models	lin
		}			ion models	istic regressi	i Lo
			<>			a collection.	. · Da
			$\longleftrightarrow$				!
. —	<u> </u>	<b></b>				gress report.	. Pr
	$\stackrel{\widehat{\longleftarrow}}{\longleftrightarrow}$						ı
		<b> </b>			lence	t of independ	. Te
		$\longleftrightarrow$			ncer	ween two can	be
						ables.	va
		<b>~</b>			wo	olication of tw	. Ај
		←>			-linear	ensional log-	di
						dels.	mo
		<b>~</b>			hree	olication of th	. A
		$\longleftrightarrow$			-linear	ensional log-	di
						dels.	me
					ogistic	olication of lo	. Ap
<del></del>	<u>-</u>				els	ression mode	re
		l			port	l progress rep	. Fu
←						Ì	!
	<				els	plication of lo	. Ap

### Outputs of Subproject 4

Papers presented in international conferences

3

Master graduates

3

Subproject 5: Modeling and Computer Simulation in Cancer
Research: Theory and Modeling of the Growth of
Tumors

Principal Investigator: Asst. Prof. Dr. Wannapong Triampo

#### **Proposed activities**

We now have completed our work on the stochastic cellular automata *in silico* model for immune system- avascular tumor interactions *in vivo*: self-organized vascular growth, pattern formation and fractal analysis. Also the final draft of the manuscript is about to be finished and is expected to be submitted in a few weeks. It can be summarized as follows. The stochastic discrete model on two-dimensional square lattice has been developed. The cellular automata method was presented to describe the growth of an avascular tumor based on microscopic scale of immune system response, cell proliferation, cell death and degradation. The Monte-Carlo method was applied in this model which enables us to idealize three regimes of Gompertzian growth. We have used scaling techniques to analyze the fractality of tumor colony, proliferating tumor colony as well as statistical properties to make conclusions about the fractality of the boundary.

#### 5.1 The model

#### 5.1.1 The microscopic scale

The basic biological principles, which is represented by the microscopic scale change, are cell proliferation as well as its interaction with the immune system as shown in Fig. 5.1.

It is established that the immune system has an important role which influences the development of avascular tumor growth. The immune system is very complicated. Let us consider a simplified process of a growing avascular tumor which effects an immune response in the host immune system. By [10, 29 and 31], the tumor can be effectively eliminated by tumor-infiltrating cytotoxic lymphocytes (TICLs). Practically, TICLs may be cytotoxic lymphocytes, natural killer-like cells and/or lymphokine activated killer. TICLs are assumed to interact with the tumor cell and then lymphocyte-tumor cell complexes are formed. These lymphocyte-tumor cells complexes detachment results in either the death of tumor cells by a program of lysis or by TICLs without damaging the proliferating tumor cells.

The host tissue is represented by a lattice of size L x L. And any site has coordinates  $(x_n, y_n)$ , where  $x_n, y_n = 1, 2, ..., L$ . We let the proliferating tumor cells, the dead tumor cells, the cytotoxic lymphocyte, and TICLs-tumor cell complexes be represented by P, D, TICLs, and C, respectively. Then, the kinetics of fundamental feature of tumor development could be represented as in Fig. 5.1.

$$P \xrightarrow{r'_{prolif.}} 2P$$

$$P + TICLs \xrightarrow{r_{binding}} C \xrightarrow{r_{lysis}} D + TICLs$$

$$D \xrightarrow{r_{decay}}.$$

Fig. 5.1 Kinetic mechanisms of development of cancer with immune response (modified from [1, 10]).

The parameters  $r_{prolif}$ ,  $r_{binding}$ ,  $r_{detach}$ ,  $r_{lysis}$ , and  $r_{decay}$  are non-negative kinetic constants where  $r_{prolif}$  describes the base rate of tumor proliferation.  $r_{binding}$  represents the rate of binding of TICLs to tumor cells,  $r_{detach}$  is the rate of detachment of TICLs from cancer cell without damaging cells,  $r_{lysis}$  is the rate of detachment of TICLs from dead tumor cells, resulting in an irreversible programming of the tumor cells for lysis, and  $r_{decay}$  describes dissolution of the dead cancer cells. Additionally, we may define the function  $r'_{prolif}$  as an avascular tumor growth rate in vivo, by assuming  $r'_{prolif}(t) = r_{prolif}(1 - \frac{p}{K})$ , where P(t) denotes the number of proliferating tumor cells, and K denotes the carrying capacity, which can be indicated as the restriction of nutrient for proliferation of cancer cells and/or increasing waste product accumulation indices, decreasing the rate of proliferation of cancer cells [27,28].

We investigated the influences of the parameters on the Gompertz growth curve. By Fig. 5.5 (g),  $r'_{prolif}$  decreases with increasing cancer cells, and this function incorporates the fact that the proliferating tumor cells growth depends on the competition for resources among the proliferating tumor cells. These effects are assumed in avascular microscopic tumor growth *in vivo* [17] as illustrated in the first reaction of Fig. 5.1. By the second reaction, the parameter  $r_{detach}$  indicates the tumor's potential for escaping the host's

<del>4</del>

3

ť

=

immune surveillance whereas  $r_{binding}$  corresponds to the TICLs' response in a chemotactic manner towards tumor cells and  $r_{lysis}$  describes the TICLs' detachment rate of activation from tumor cells, being an irreversible programming of the tumor cells for lysis, and  $r_{decay}$  represents the dissolution process in which the dead tumor cells turn into normal tissues and reflects the degraded dead tumor cells.

Table 5.1 Summary of functions and input constant parameters for the model.

#### Functions in the model

 $r'_{prolif}$  Rate of proliferation of cancer cells (varying with the number of proliferating tumor cells)

#### **Parameters**

 $r_{prolif.}$  Base rate of proliferation of cancer cells

 $r_{binding}$  Rate of TICLs' binding to the tumor cell to become cell complexes

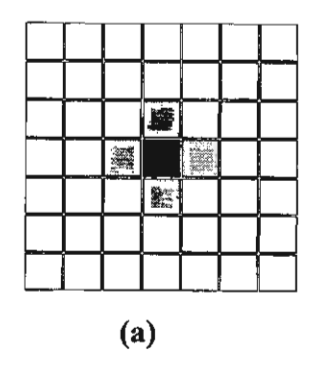
 $r_{detach}$  Rate of TICLs' detachment from the cell complexes without cell damage

 $r_{lysis}$  Rate of TICLs' detachment from the cell complexes resulting in the lysis of tumor cells

 $r_{decay}$  Death rate of tumor cells degrading to normal cells

K The maximum proliferating tumor cells extent

<sup>\*</sup> The parameter values of  $r_{prolif}$ ,  $r_{binding}$ ,  $r_{lysis}$  and  $r_{decay}$  have been modified from Qi, et. al. [1], and  $r_{detach}$  and  $r_{lysis}$  have been modified from Matzavinos, A., et. al [10, 13, 30].



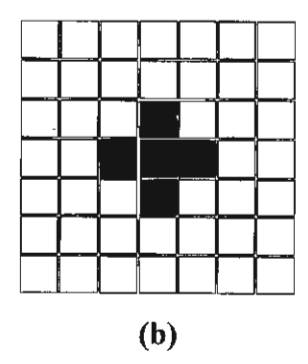


Fig. 5.2 (a) The four nearest neighboring sites (gray) of the tumor site (black): with the nearest neighboring rule of the so-called von Neumann neighborhood.

(b) The initial configuration: five cancer cells in the center of the square lattice.

#### 5.1.2 The methodology for stochastic CA

Time runs in discrete steps. The lattice compartment may accommodate either: proliferating tumor cell (P), TICLs-tumor cell complexes (C), or dead tumor cell (D), on host normal tissue. The flowchart of the simulation procedure is shown in Fig. 5.4. A simulation is terminated after 1000 individual simulations with determined timesteps. A random number (a), in the series of random generating numbers has the value in the range of 0 < a < 1. We distinguish the total tumor cells to one of two possible states:

- (1) proliferating state (i.e. cancer or proliferating tumor cells, P), and
- (2) non-proliferating state or stationary state (i.e. C and D).

For each simulated tumor colony the tumor progress is simulated by the following algorithm:

- (I) At t=0: Initial configuration is five cancer cells in the center of the normal tissue as shown in Fig 5.2 (b).
- (II) At each time step: The rules of cellular automaton are applied to each tumorous cell one by one sequentially selected at random with the same probability and carry out one of the actions upon its state as shown in schematic diagram (Fig. 5.3), described as follows:
- (1) Proliferating state: If the selected cell is the cancer cell, the cancer cell takes one of the following three actions with the function  $r'_{prolif}$  and parameter  $r_{binding}$ .
- (i) The cancer cell may invade the normal cell with the probability  $r'_{prolif}$  if this cancer cell has at least one nearest neighbor normal cell (as shown in Fig. 5.2 (a)) randomly chosen with the same probability.
- (ii) The cancer cell is bound by the TICLs with probability  $r_{binding}$ .
- (iii) The cancer cell may not change with probability  $1 (r'_{prolif} + r_{binding})$  or there is no nearest neighboring normal site in the case of invasion with probability  $r'_{prolif}$ .
- (2) Stationary state: If the selected cell is in the non-proliferating state, which consists of dead cancer cells and TICLs –tumor complexes that maybe defined as cell complexes.
- (2.1) The complexes: If the selected cell is a complex. The cell may take one of the following three actions with parameters  $r_{detach}$ ,  $r_{binding}$  and  $r_{lysis}$ .
- (i) The complexes revert into cancer cells with probability  $r_{detach}$ .
- (ii) The complexes may go thru lysis and become dead cancer cells with the probability  $r_{lysis}$ .

- (iii) The complexes may not change state with the probability  $1 (r_{detach} + r_{lysis})$ .
- (2.2) The dead cancer cells: If the selected cell is a dead cancer cell, it takes one of two actions.
- (i) The dead tumor cell may dilute into normal cell with probability  $r_{decay}$ .
- (ii) The dead tumor cell may not change with probability  $1 r_{decay}$ .
- (III) Step (II) continues until the set number of timesteps is reached.

**Remark:** By this methodology we have to satisfy  $r_{prolif.} + r_{binding.} \le 1$  and  $r_{detach.} + r_{lysis.} \le 1$ .

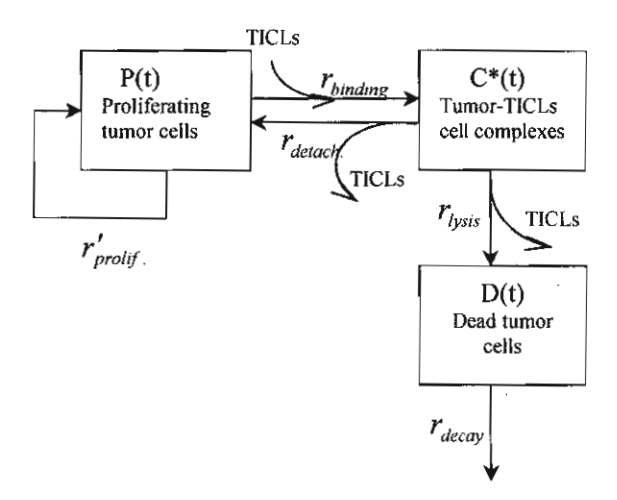


Fig. 5.3 Schematic diagram of cellular automaton model of tumor growth reveals the possible actions, reactions and changing states of each type of tumor cells.

Initial Configuration (t=0): with five proliferating tumor cells in the middle of the tissue model

**Setting parameters** 

:  $r_{prolif.}$  ,  $r_{binding}$  ,  $r_{inavt.}$  ,  $r_{lysis}$  ,  $r_{decay.}$  and K

Setting variables

: n, p, c, d with n(t) = p(t)+c(t)+d(t)

Setting function

: r'\_prolif.

Setting timestep

: t from 0 to Ts

Setting simulation : s from 1 to Ss

Initial simulation number, s = 0 Initial timestep, t = 0 with initial configuration Calculate the proliferating rate of avascular tumor,  $r'_{prolif.} = r_{prolif.} (1 - \frac{P}{K})$ Randomly choosing a cell one by one and then select action by using random generating number and checking conditions. Yes  $t < T_s$ No s = s+1Yes  $s < = S_s$ No Print "The average of the total number of tumor cells in each timestep for Ss simulated tumors",  $\bar{n}(t)$ 

End

#### 5.1.3 Simulation Results

The methodology described in Section 2 has been transformed into a computer simulation programming. Computer simulation experiments and computational representation of the results in a two-dimensional spatial visualization of tumor invasion of normal tissues are shown in Figures 5.5 (a), 5.5 (b), 55. (f), and 5.5 (g). We denote by P(t) the number of proliferating tumor cells at time t,  $C^*(t)$  the number of TICL-tumor cells complexes at time t, and D(t) the number of dead tumor cells at time t. To investigate the evolution of tumor growth, we also denote the total number of tumor cells by  $N(t) = P(t) + C^*(t) + D(t)$  Clearly, N(t) can indicate the size of the tumor at time t.

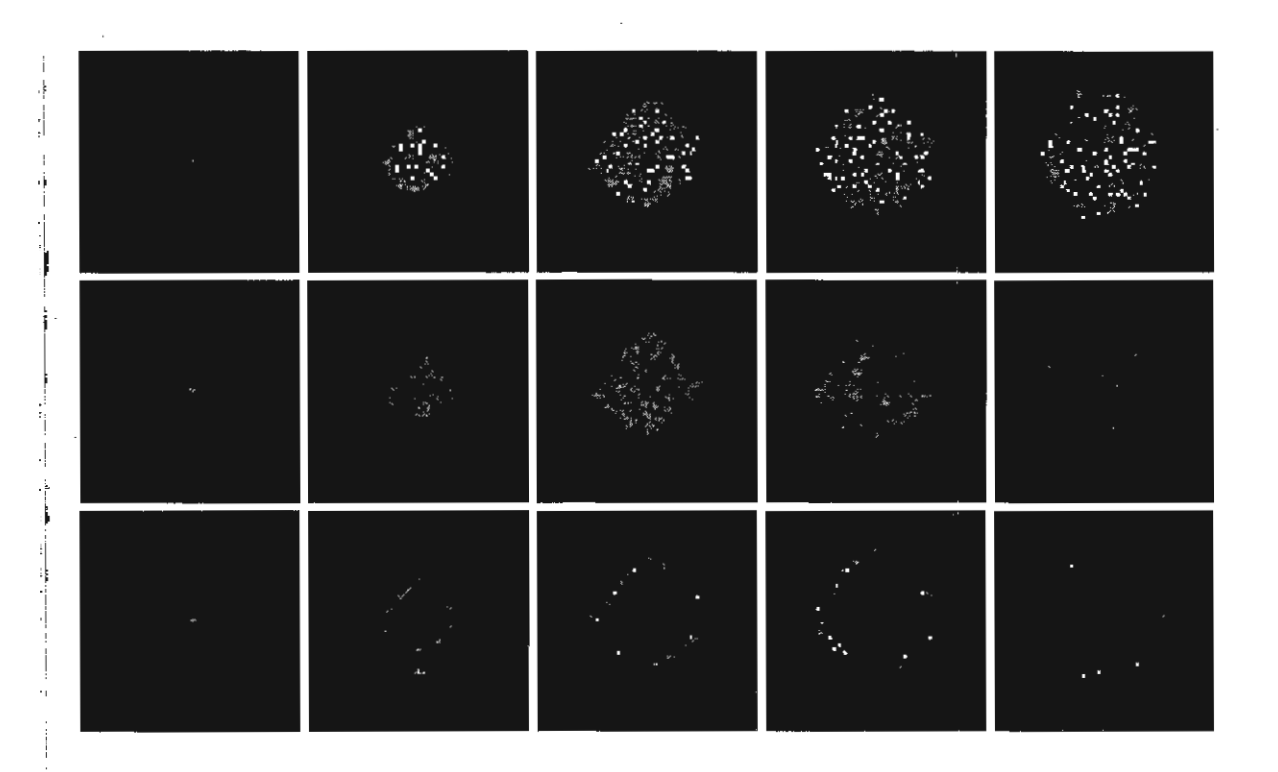


Fig. 5.5 (a) Snapshots of the simulated tumor 61x 61 squared lattice, proliferating cell cluster, and its boundary colony at timesteps 0,15,30,50, and 80. The simulation setting is  $r_{prolif.} = 0.85, r_{binding} = 0.1, r_{det ach.} = 0.5, r_{lysis} = 0.35, r_{decay} = 0.35$  and K = 550. Exproliferating tumor cells, : TICLs-tumor cell complexes, Expression dead tumor cells, and Expression cells.

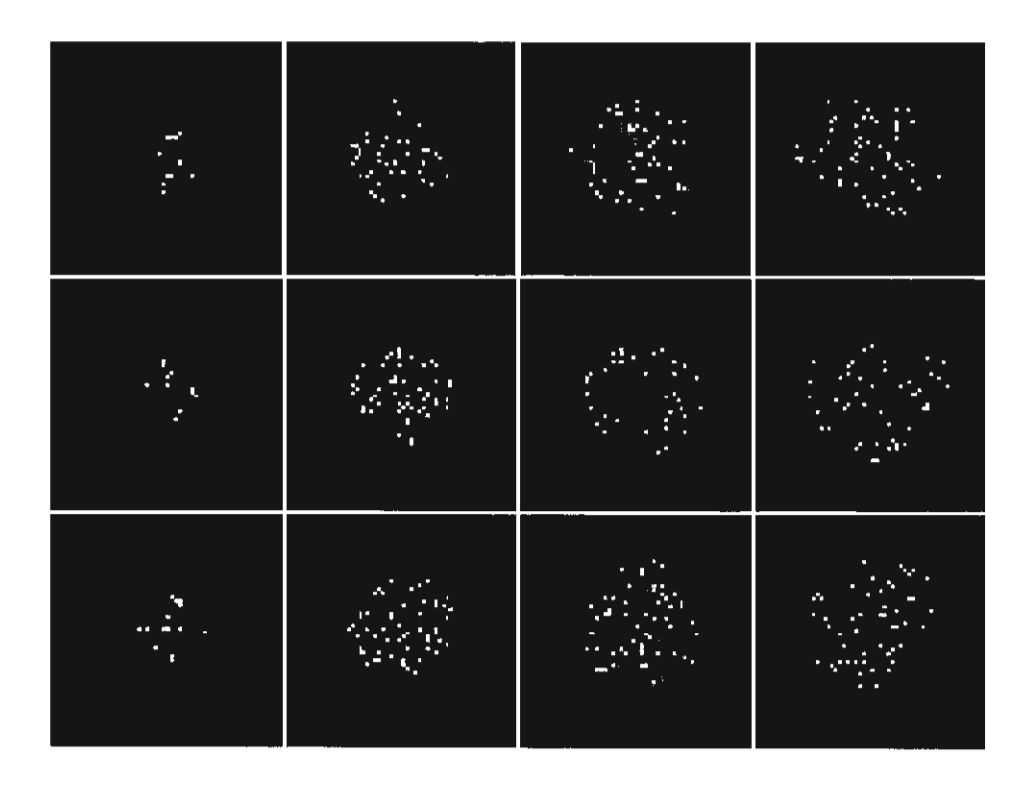


Fig. 5.5 (b) Snapshots of the typical configuration of simulated tumor colonies (61x 61 squared lattice) with the different generating random number and the same simulation setting at timesteps 15, 30, 50, and 80. The simulation setting is  $r_{prolif.} = 0.85, r_{binding} = 0.1, r_{detach.} = 0.5, r_{lysis} = 0.35 r_{decay} = 0.35$  and K = 550.  $\blacksquare$ : proliferating tumor cells, : TICLs-tumor cell complexes,  $\blacksquare$ : dead tumor cells, and  $\blacksquare$ : normal cells.

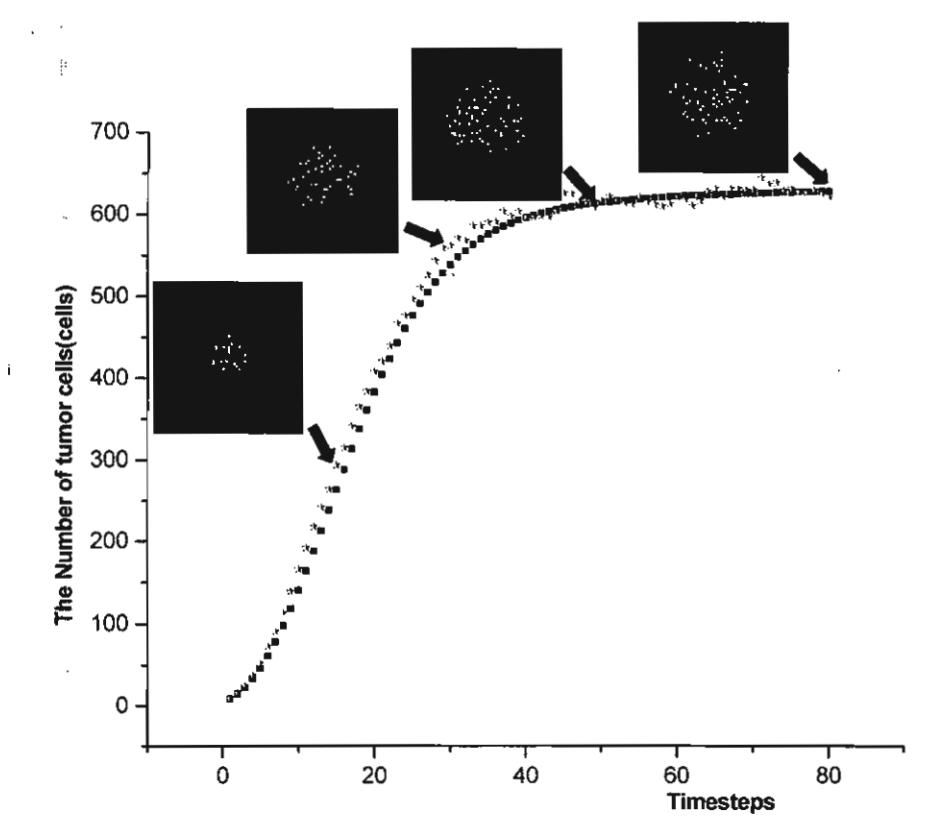
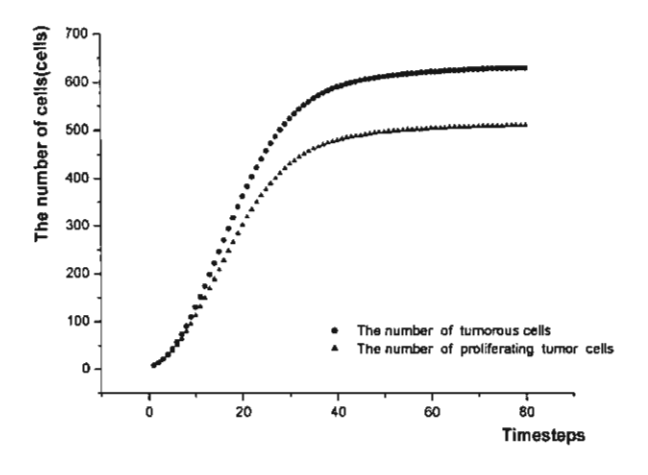


Fig. 5.5 (c) Plots of the time evolutions of the number of cancerous cells dual show with the qualitative shape of simulated multicell tumor. The simulation results are shown for one simulation (star)and averaging over 1000 individual simulations (square), at timesteps 0, 15, 30, 50, and 80. The simulation setting is  $r_{prolif.} = 0.85$ ,  $r_{binding} = 0.1$ ,  $r_{detach} = 0.5$ ,  $r_{lysis} = 0.35$ ,  $r_{decay} = 0.35$  and K = 550.



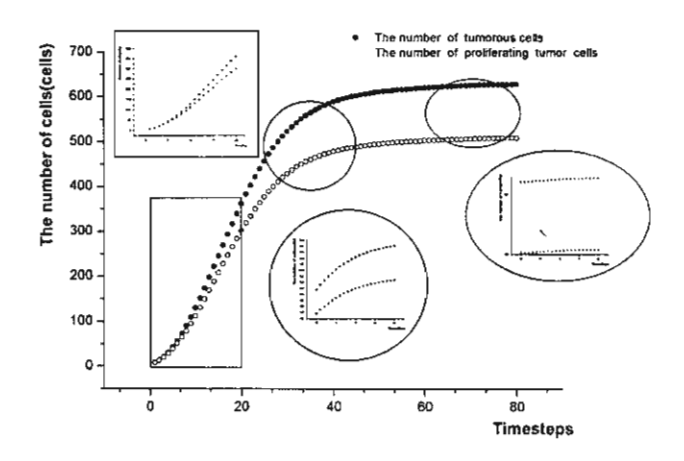


Fig. 5.5 (d) Plots of the time evolutions of the number of tumoral cells (solid circle) and proliferating tumor cells (hollow circle). A part of the curve in typical different figures shows different dynamic growth. The simulational results are the average of 1000 individual simulations, with  $r_{prolif.} = 0.85$ ,

 $r_{binding} = 0.1, r_{det\,ach.} = 0.5, r_{lysis} = 0.35, r_{decay} = 0.35$  and K = 550.

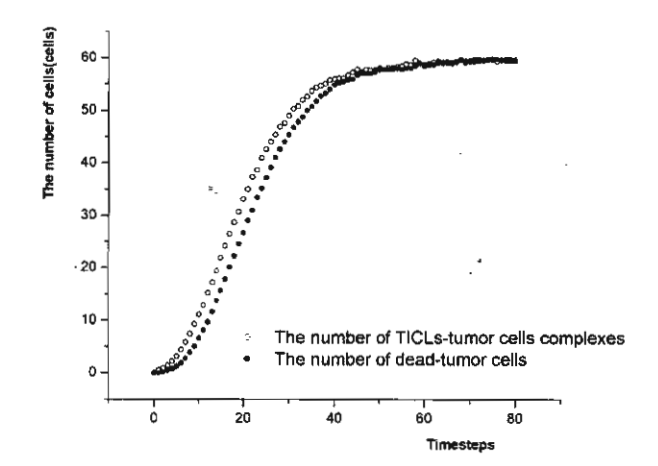


Fig. 5.5 (e) the time evolutions of the number of TICLs-tumor cells complexes (circle) and dead tumor cells (solid circle). The simulational results are the average of 1000 individual simulations, with  $r_{prolif.} = 0.85, r_{binding} = 0.1, r_{detach.} = 0.5, r_{lysis} = 0.35, r_{decay} = 0.35$  and K = 550.

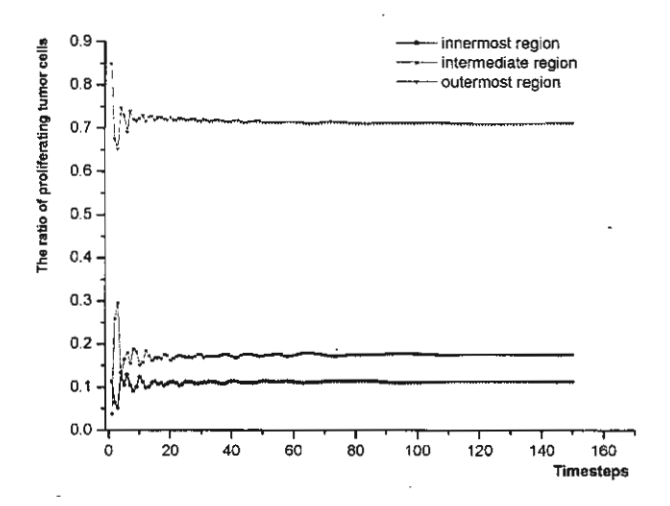


Fig. 5.5 (f) Plots of the ratio of proliferating tumor cell in each region, the innermost, the intermediate and outermost region. The simulation results are the average of 1000 individual simulations, with  $r_{prolif.} = 0.85, r_{binding} = 0.1, r_{detach.} = 0.5, r_{lysis} = 0.35, r_{decay} = 0.35$  and K = 550.

1

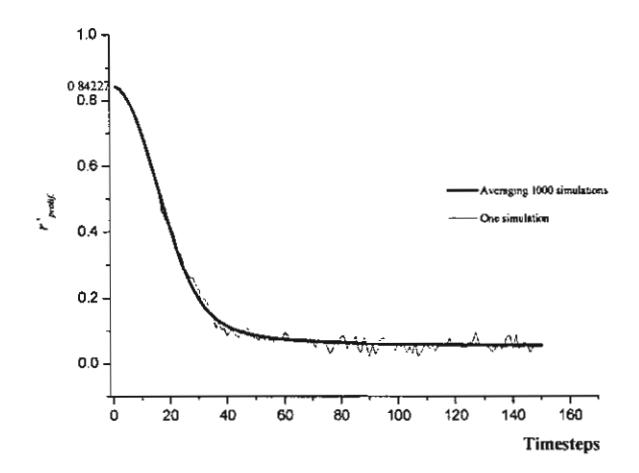


Fig. 5.5 (g) The proliferating function value of avascular tumor growth,  $r'_{prolif}$  versus time. The function is defined by  $r'_{prolif} = r_{prolif} (1 - \frac{p}{K})$ . The average of 1000 individual values of  $r'_{prolif}$  from simulated tumor growth (the black solid line) and a typical simulation (gray) have been obtained with  $r_{prolif} = 0.85$ ,  $r_{binding} = 0.1$ ,  $r_{detach} = 0.5$ ,  $r_{lysis} = 0.35$ ,  $r_{decay} = 0.35$  and K = 550.

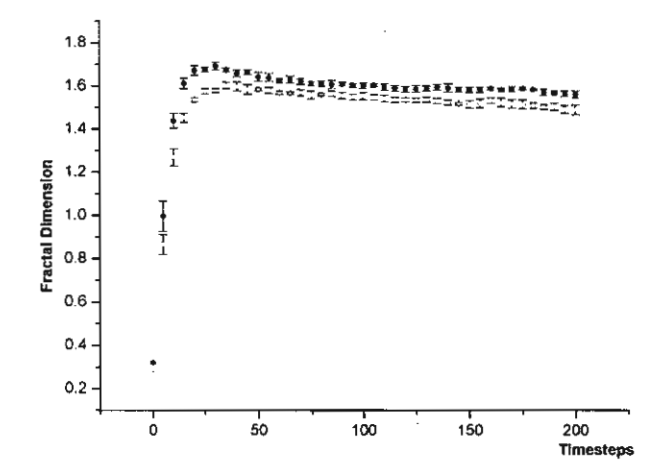


Fig. 5.5 (h) The evolution of fractal dimension of expanding tumor colony (solid circle) proliferating tumor colony by box counting method, using 5 individual colonies. The parameter setting of the five tumor colonies is  $r_{prolif.} = 0.85, r_{binding} = 0.1, r_{detach} = 0.5, r_{lysis} = 0.35, r_{decay} = 0.35$  and K = 550.

By the methodology of Cellular automaton model, starting the simulation by placing five proliferating tumor cells in the center of the square lattice, then both later invade and change their states by a series of random generating number to govern the simulated tumor pattern as shown a typical snapshot in different timesteps in Fig. 5.5 (a). Fig. 5.5 (b) reveals a number of simulated colonis made by the different seeds caused by different series of random generating number. Apparently, the morphology of different simulated tumor patterns are different. The growth curve of a typical simulated colony (red star) and the average of 1000 colonies are shown in Fig. 5.5 (c).

The Gompertz growth curve is the best known model, which is successfully used to characterize the experimental data of tumor growth *in vivo* [1, 16, 17], and can be written as

$$V(t) = V_0 \exp\left(\frac{A}{B}(1 - \exp(-Bt))\right), \tag{5.1}$$

where V(t) is the size of tumor at time t,  $V_0$  is the initial volume, while the positive parameters A and B are evaluated by the method of least squares. Based on the CA's model which is described in Section 2.2, the averaged growth curve, as shown in Fig. 5.5 (a) can be described mathematically by Gompertz function approach to Enrich carcinoma mouse growth *in vivo* [17] with the coefficient of nonlinear regression  $r^2 = 0.9997$  by computational simulation setting  $r_{prolif.} = 0.85$ ,  $r_{binding} = 0.1$ ,  $r_{det ach.} = 0.5$ ,  $r_{lysis} = 0.35$ ,  $r_{decay} = 0.35$ , and K=550, and Gompertz parameter setting  $V_0 = 2.26 \times 10^{-2} \text{ (cm)}^3$ ,  $A = 0.456 \text{ (days}^{-1})$ ,  $B = 0.102 \text{ (days}^{-1})$ . Ultimately, we normalized the data with  $V_{max} = 1.94 \text{ (cm)}^3$ , and  $N_0 = 8.394$ ,  $N_{max} = 625$ , as shown in both growth curves in Fig. 5.6. By the growth curves of Fig. 5.6 and the typical five colonies, cell-doubling time versus number of total tumor cells were plotted as shown in Fig. 5.7 with linear relationship.

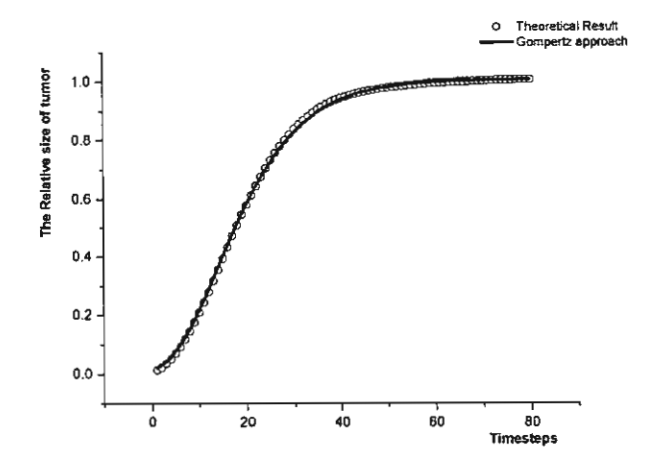


Fig. 5.6 The comparison between the theoretial prediction and the Gompertz approach for the mouse carcinoma Ehrlich with the coefficient of nonlinear regression  $r^2 = 0.9997$ . Gompertz parameters:  $V_0 = 2.26 \times 10^{-2} \, (\text{cm})^3$ ,  $A = 0.456 \, (\text{day})^{-1}$ ,  $B = 0.102 \, (\text{day})^{-1}$  and  $V_{max} = 1.94 \, (\text{cm})^3$ . The parameters of the model are: with  $N_0 = 8.381$ ,  $N_{max} = 627.379$ ,  $r_{prolif.} = 0.85$ ,  $r_{binding} = 0.1$ ,  $r_{detach} = 0.5$ ,  $r_{lysis} = 0.35$ ,  $r_{decay} = 0.35$  and K = 550.

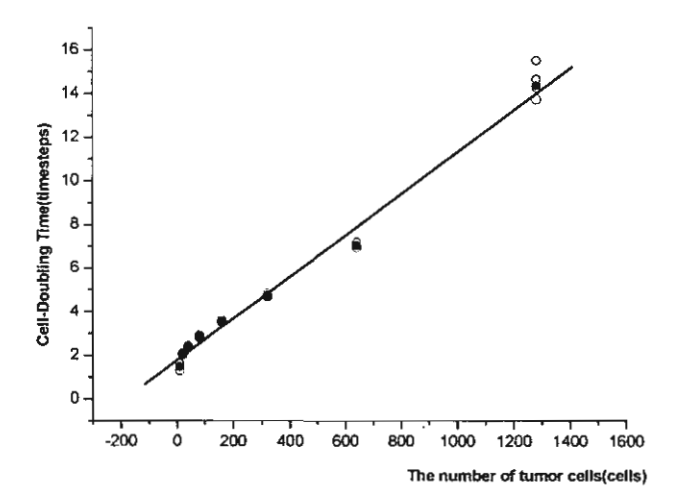


Fig. 5.7 Cells-doubling time versus the number of tumor cells from 1000 individual simulated tumor (solid circle) with five typical individual simulated colonies. The plot of the cell-doubling time of tumor cell number against the number of tumor cells in each colony shows their linear relationship, when parameter setting  $r_{prolif.} = 0.85, r_{binding} = 0.1, r_{det\,ach} = 0.5, r_{lysis} = 0.35, r_{decay} = 0.35$  and K = 2000.

The Gompertz curve can be mathematically divided into three regimes as done in [17, 20]. The first regime or early phase, reflects the dynamics of the initial stages of tumorigenesis until the number of tumor cells reaches the value equal to 0.37 of their maximum number of tumor cells within referring time step, which is the time at the infection point on the curve and is defined by  $t_1$ . The second regime, or intermediate phase, of the growth curve is the curve from the first segment, the curve being concave downward until number of tumor cells at crossover time is reached, and the third regime, or saturated phase, begins at the crossover time and lasts until saturated state is reached as seen in Fig. 5.8. In other words, the Gompertzain growth curve can be divided into three regimes by the time at infection point and the crossover time.

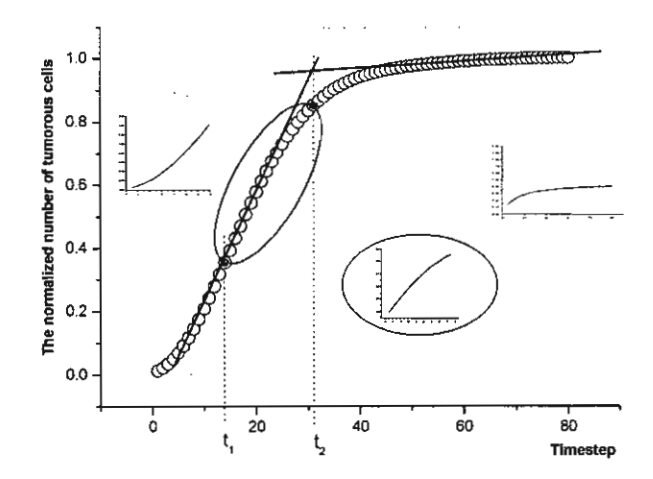


Fig. 5.8 The three segments of sigmoidal Gompertzian curve from simulation result of Fig. 5.4. The first segment has the range from 0 to 14 timesteps within the first solid circle; the second phase covers days 15 until 31; the third phase begins at 32 days beyond the second solid circle.

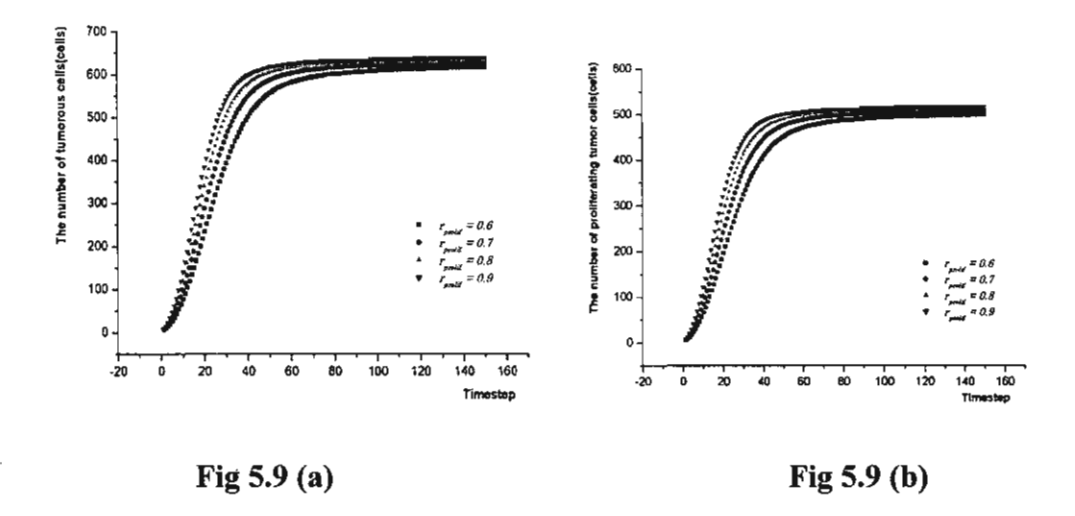
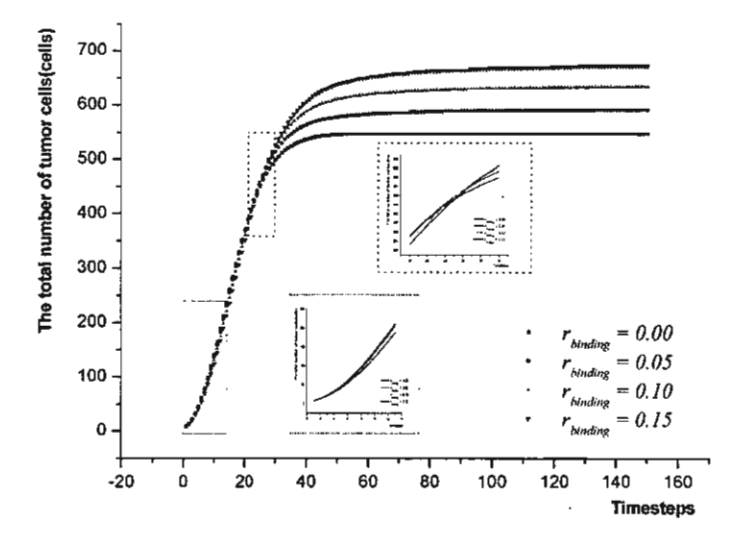


Fig. 5.9 (a) and (b) Plots of the time evolutions of the number of tumoral cells and proliferating tumor cells, respectively. The simulation results are the average of 1000 individual simulations, with parameter  $r_{prolif.}$  varying from 0.6 to 0.9 in steps of 0.1, and fixed parameters  $r_{binding} = 0.1$ ,  $r_{detach} = 0.5$ ,  $r_{lysis} = 0.35$ ,  $r_{decay} = 0.35$  and K = 550.

Fig. 5.9 shows the simulation results when only  $r_{prolif}$  was varied from 0.6 to 0.9 in steps of 0.1, whereas the other parameters were fixed. Fig. 5.9 (a) shows the growth curve of the tumor with varying proliferating rate. We found that the growth rate and saturated tumor cell number are increased with increasing proliferating rate. With the recent finding of crossover time process, the growth curves of a greater proliferating rate will take the shorter crossover time together with the increase in saturated tumor size. By Fig. 5.9 (b), we also reach the same conclusion on the growth curve of total tumor cells as that from Fig. 5.9 (a).



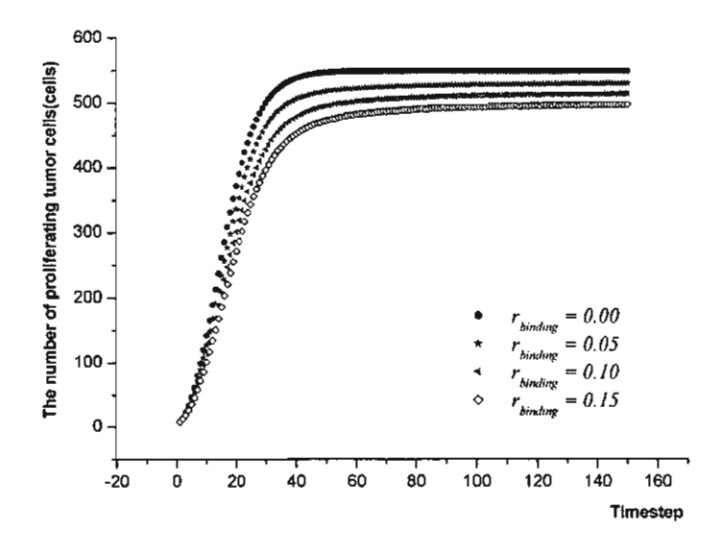
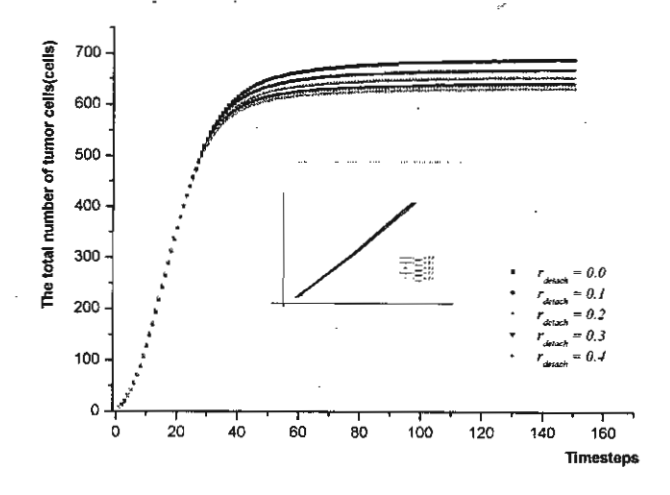


Fig. 5.10 (a) and (b) Plots of the time evolutions of the total number of tumor cells and the number of proliferating tumor cells. The simulation results are the average of 1000 individual simulations, with varying parameter  $r_{binding}$ , and fixed parameters  $r_{prolif.} = 0.85, r_{det\,ach} = 0.5, \ r_{lysis} = 0.35, \ \text{and} \ K = 550$ .

In order to investigate the role of immune system within this model which is represented by the values of the parameters  $r_{binding}$  and,  $r_{detach}$ . We consider the growth curve of tumor when only  $r_{binding}$  is varied, with other parameters fixed as illustrated in Fig. 5.10 (a), while the growth curve of tumor with varying  $r_{detach}$  and other parameters fixed is shown in Fig. 5.11 (a). Certainly, increasing the binding rate of TICLs, will increase the binding rate effect in delaying or inhibiting tumor proliferation. Figures 5.10 (a) and (b) show that when  $r_{binding}$  is increased, the growth curve will have more crossover time, which means that the system will take more time to reach the saturated phase. In more detail, considering the first regime of the growth curves in Fig. 5.10 (a) (t = 1 to 13), the growth will decrease with increasing  $r_{binding}$ , which shows that the first regime is effected by the number of proliferating cells more than other cell types. Between timesteps 25 and 29, each growth curve flips until the growth increases with increasing  $r_{binding}$ , and the third regime is reached with higher saturated size of tumor for higher value of  $r_{binding}$ . Apparently, according to Fig. 5.10 (b), the growth of proliferating cells decreases and the saturated number of proliferating cell decreases with increasing  $r_{binding}$ , since the binding role of immune system is to decrease the number of proliferating tumor cells. According to Figures 5.10 (a) and (b), varying the parameter  $r_{binding}$  indicates that higher number of proliferating cells does not necessary mean larger tumor size. Moreover,  $r_{binding} = 0.0$  refers to the proliferating tumor cells growing stochastically on two-dimensional square lattice with von Neuman neighborhood.



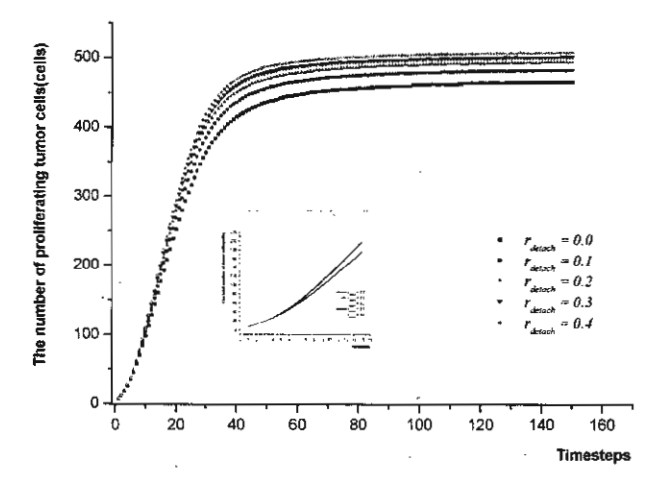


Fig. 5.11 (a) and (b) Plots of the time evolutions of the total number and the number of proliferating tumor cells of simulated tumor. The simulation results are the average of 1000 individual simulations with  $r_{detach}$ , varying from 0.0 to 0.4 in steps of 0.1, and fixed parameters  $r_{prolif.} = 0.85$ ,  $r_{binding} = 0.1$ ,  $r_{lysis} = 0.35$ ,  $r_{decay} = 0.35$  and K = 550.

To investigate the influence of the  $r_{detach}$ , we fixed the other parameters and vary this rate from 0.0 to 0.4 in steps of 0.1. According to Fig. 5.11 (a), we found that increasing  $r_{detach}$  will decrease the crossover time of the growth curve, which means that the system will use shorter time to reach the saturated regime. However, the saturated size of the tumor will decrease with lower  $r_{detach}$ . Considering Fig. 5.11 (b), increasing  $r_{detach}$  will lead to an increase in the number of proliferating tumor cell, larger saturated tumor size and less crossover time.

investigating the morphology of simulated tumor colony. Clinically, Bru et al. [27] have defined the three regions of avascular tumor via the radius of tumor (R), namely, an innermost region  $(0 \le r_i < \frac{R}{2})$ , an intermediate region  $(\frac{R}{2} \le r_i < \frac{4R}{5})$ , and an outermost region  $r_i \ge \frac{4R}{5}$ , where  $r_i$  is the radius of tumor colony from the origin. They measured the proliferating cell of human colon adenocarcinoma colony in each region, the innermost region covers 6% of proliferating cells and 25% of the whole colony surface, the intermediate region covers 14% of proliferating cells and 39% of the whole colony surface, and the outermost region consists of 80% of proliferating cells and 36% of the whole colony surface. We also measured this quantity by computational algorithm applied to each simulated tumor colony and we also found that the averaging ratio of proliferating cell in the outtermost region is greater than those of both other regions by 70%, 18% and 12% respectively as shown in Fig. 5.5 (f). The simulation results indicated that proliferating cells are located mainly to the outtermost region which corresponds to the experimental data *in vivo* of Bru et al [27].

We have been interested in the qualitative result of avascular tumor growth model,

It is found that the colonies obtained from the stochastic model have an approximately circular shape with a rough boundary as shown in Figures 5.5 (a) and (b). A few researchers [6, 7, 8, 22, 23, 25, 26] were interested in the fractal dimension of the stochastic growth model. We defined the boundary cells of the simulated tumor growth by assuming that the boundary cells are the outtermost cells covering the colony in each row and each column in the lattice. We also found the fractal dimension of the expansion of multicell tumor colony and the proliferating tumor cell against timesteps using Beniot 1.3 [36] as shown in Fig. 5.5 (h).

At each time step, if we let S be the number of tumor cells on the tumour periphery. The center of mass of the boundary with coordinates  $(x_n, y_n)$  is defined as

$$(\overline{x}, \overline{y}) = \frac{1}{S} \sum_{\text{periphery}} (x_n, y_n)$$
 (5.2)

The mean radius of the boundary is defined as

$$R = \frac{1}{S} \sum_{\text{periphery}} \sqrt{\left(x_{n} - \overline{x}\right)^{2} + \left(y_{n} - \overline{y}\right)^{2}}$$
 (5.3)

A

The squared mean thickness of the boundary is defined as

$$\sigma^{2} = \frac{1}{S} \sum_{\text{periphery}} \left[ \sqrt{\left(x_{n} - \overline{x}\right)^{2} + \left(y_{n} - \overline{y}\right)^{2}} - R \right]^{2}$$
 (5.4)

For each colony, using least square method to find  $\alpha$  and  $\beta$  in the relation

$$\sigma = \alpha R^{\beta} \tag{5.5}$$

By equation (5.5), the value of  $\beta$  indicates how the dynamics of boundary growth depends on the power law. We used the individuals of 1000 colonies for each timestep through to 35 timesteps, from the simulated result in Fig. 5.5, then we obtained  $\alpha = 0.23439 \pm 0.01456$ , and  $\beta = 0.63339 \pm 0.02581$  with  $r^2 = 0.96746$ . Our results are different from the result given in [23] and [26], the stochastic cluster growth on a plane, which found that  $\beta = 0.468 \pm 0.092$ .

However, we obtained the same conclusion on the fractality of the boundary. Thus, we can conclude from the fractional value of  $\beta$  that the boundary is fractal. Which means that it has the same amount of roughness when enlarged [23]. By the equation (5.5), Wang et al. [26] concluded that if  $\beta$ < 1, the larger colonies have smaller relative boundary thickness.

In conclusion, the CA model showed that the macroscopic behavior of a tumor can be affected by setting the presence of an immune system response at microscopic scale. In addition, the analysis of the morphology of simulated patterns by scaling law and the growth rate of tumor in each phase of the Gompertzian curve were presented.

The cellular automata model on a three-dimensional square lattice with simulation results is in progress.

#### Other related activities

Apart from the work explained above on what has been proposed in this project, we have spent some of our time in investigating different techniques of modelling and simulation of cell division in various aspects. This part of our work has resulted in 3 published papers as can be seen in Appendices # 5.1-5.3. The work on growth of Leptospire (in Appendix # 5.1) is done in support of the research work in Subproject 3, while the work on bacteria cell division (Appendix # 5.3) will be of great use to the continued research on bacterial growth and drug resistance in Subproject 1.

Table V: Proposed and Actual Activity for Subproject 5.

Months	Month	Months	Months	Months	Months
1-6	7-12	13-18	19-24	25-30	31-36
<>					
$\longleftrightarrow$		ļ			
	<del></del>				
	$\longleftrightarrow$				
	<b></b>			Ì	
	←				
		:			
		<b>~</b>			
		·	$\longrightarrow$	:	
				<u></u>	
				$\longleftrightarrow$	
				<b>_</b>	
				<u> </u>	
		j		*	
				`	
		· 			
	1-6	1-6 7-12 <	1-6 7-12 13-18  <	1-6 7-12 13-18 19-24	1-6 7-12 13-18 19-24 25-30

<sup>\*</sup> The investigator has become interested in investigation of different simulation techniques for other cell divisions instead.

## **Outputs of Subproject 5**

Papers appeared/accepted in international journals 3

Paper presented in international conference

1

# Subproject 6: Research on Asymptotic Stability of Difference Equations with Delays

Principal Investigator: Dr. Piyapong Niamsup

The research work in this subproject may be summarized year by year as follows.

## 6.1 Year 1:

During the first year, we mainly studied the asymptotic stability of linear difference equations of the form

$$x_{n+1} - a^2 x_{n-1} + b x_{n-k} = 0 ag{6.1}$$

where a and b are arbitrary real numbers, k is a positive integer and n = 0,1,2,... The motivation for studying the above difference equations came from a paper of S.A. Kuruklis [1] in which he gave the necessary and sufficient conditions for asymptotic stability for the linear difference equation of the form

$$x_{n+1} - ax_n + bx_{n-k} = 0 ag{6.2}$$

where a and b are arbitrary real numbers, k is a positive integer and n = 0,1,2,... The main result in [1] reads as follows:

Theorem A Let a be a nonzero real, b an arbitrary real, and k a positive integer greater than 1. Equation (6.2) is asymptotically stable if and only if  $|a| < \frac{k+1}{k}$ , and

$$|a|-1 < b < {a^2 - 2|a|\cos\phi + 1}^{\frac{1}{2}}$$
 for k odd  
 $|b-a| < 1$  and  $|b| < {a^2 - 2|a|\cos\phi + 1}^{\frac{1}{2}}$  for k even

where  $\phi$  is the solution in  $\left(0, \frac{\pi}{k+1}\right)$  of  $\frac{\sin k\theta}{\sin(k+1)\theta} = \frac{1}{|a|}$ .

Our main result on asymptotic stability of equation (6.1) is obtained as follows:

Theorem 1 Let a be a nonzero real, b an arbitrary real, and k a positive integer greater than

1. Equation (6.1) is asymptotically stable if and only if

$$|a| < 1$$
 and  $a^2 + |b| < 1$  for k even 
$$|a| < \sqrt{\frac{k+1}{k-1}} \text{ and } a^2 - 1 < b < \{a^4 - 2a^2 \cos 2\phi + 1\}^{\frac{1}{2}} \text{ for k odd}$$

where  $\phi$  is the solution in  $\left(0, \frac{\pi}{k+1}\right)$  of  $\frac{\sin(k-1)\theta}{\sin(k+1)\theta} = \frac{1}{a^2}$ .

**Remark** 1. Note that when a = 0 or k = 1 it is easy to show that the necessary and sufficient conditions for (6.1) to be asymptotically stable is that  $|a^2 - 1| < 1$ .

2. The technique of proof in a main step of Theorem 1 is somewhat different from that in Theorem A so that we pointed out an error of the proof of Theorem A in [1].

#### References

[1] S.A. Kuruklis, The Asymptotic Stability of  $x_{n+1} - ax_n + bx_{n-k} = 0$ , J. Math. Anal. Appl. 188 (1994), 719-731.

## 6.2 Year 2:

Continuing from the first year, in the beginning of the second year we have investigated the necessary and sufficient conditions for asymptotic stability of the following linear delayed difference equation:

$$X_{n+1} - X_{n-1} + p \sum_{i=1}^{N} X_{n-k+(j-i)l} = 0$$
 (6.3)

where n is a nonnegative integer, p is a real number, k, l and N are positive integers where k > (N-1)1. The idea of this investigation began when we read through a paper written by R. Ogita, H. Matsunaga, and T. Hara [1], where they gave the necessary and sufficient conditions for the asymptotic stability of the following linear delayed difference equation

$$x_{n+1} - x_n + p \sum_{i=1}^{N} x_{n-k+(j-1)i} = 0$$
 (6.4)

where n is a nonnegative integer, p is a real number, k, l and N are positive integers where k > (N-1)1. The following is the main result obtained in [1]:

Theorem 1 Let k, l and N be positive integers with k > (N-1)1. Then the zero solution of (6.4) is asymptotically stable if and only if

$$0$$

where M = 2k + 1 - (N-1)1.

Using similar technique as in [4] we are able to obtain the necessary and sufficient conditions for the asymptotic stability of (3) as follows:

Theorem 2 Let k, l and N be positive integers with k odd, l even and k > (N-1)1. Then the zero solution of (6.4) is asymptotically stable if and only if

$$0$$

where M = 2k - (N-1)1.

<u>Theorem 3</u> Let k, l and N be positive integers with k and l odd and k > (N-1)l. Then the zero solution of (6.4) is asymptotically stable if and only if

$$0$$

where 
$$M = 2k - (N-1)l$$
,  $p_0^* = min\{p_0, p^*\}$ ,  $p_0 = \frac{2sin\left(\frac{\pi}{M}\right)sin\left(\frac{l\pi}{2M}\right)}{sin\left(\frac{Nl\pi}{2M}\right)}$ ,

$$p' = \min \left\{ p_m : m = \left[ \frac{M}{4} - \frac{1}{2} \right] + 1, \left[ \frac{M}{4} - \frac{1}{2} \right] + 2, \dots, \frac{M}{2} - 1 \right\},$$

$$p_{m} = 2(-1)^{m+1} \frac{\sin w_{m} \sin \frac{lw_{m}}{2}}{\sin \frac{Nlw_{m}}{2}} \text{ and } w_{m} = \frac{2m+1}{M}\pi.$$

We note that the main tool in the proof is the analysis of the locations of the roots of the characteristic equation of (6.3) to obtain the criterion for these roots to be located inside the unit disk which imply the asymptotic stability of the zero solution of (6.3).

Similarly, we have the following result:

<u>Theorem 4</u> Let k, l and N be positive integers with  $k \ge (N-1)1$ . Then the zero solution of

$$X_{n+1} + p \sum_{i=1}^{N} X_{n-k+(i-1)1} = 0$$
 (6.5)

is asymptotically stable if and only if

$$-\frac{1}{N}$$

where  $p_{min}$  is the smallest positive real value of p for which the characteristic equation of (6.5) has a root on the boundary of the unit circle.

The other topics that we have been studying are the controllability and stability of Chen chaotic dynamical system given by

$$\dot{x} = a(y - x)$$

$$\dot{y} = (c - a)x - xz + cy$$

$$\dot{z} = xy - bz$$
(6.6)

where a, b, c are positive real parameters. In [2], H.N. Agiza and M.T. Yassen studied synchronization of system (6.6) using adaptive control. In [3], Y. Wang, Z.H. Guan and X. Wen studied adaptive synchronization of system (6.6) with fully unknown parameters. In [4], M.T. Yassen studied the optimal control of system (6.6). Motivated by these results we are interested in controllability and stability of the following modified Chen chaotic dynamical system

$$\dot{x} = a(y-x)$$

$$\dot{y} = (c-a)x - xz + cy$$

$$\dot{z} = xy - bz + dx^{2}$$
(6.7)

where a, b, c, d are positive real parameters. We are interested in studying the control of chaos in the system (6.7) using linear feedback controls and bounded feedback controls, the sufficient conditions on parameters which ensure the stabilities of equilibrium points, and the synchronization of system (6.7) using adaptive control and active control.

#### References

- [1] R. Ogita, H. Matsunaga, and T. Hara, Asymptotic Stability for a Class of Linear Delay Difference Equations of Higher Order, *J. Math. Anal. Appl.* 248 (2000), 83-96.
- [2] H.N. Yagiza and M.T. Yassen, Synchronization of Rossler and Chen Chaotic Dynamical System, *Physic Letter A*, 278 (2001), 191-197.
- [3] Y. Wang, Z.H. Guan and X. Wen, Adaptive Synchronization for Chen Chaotic System with Fully Unknown Parameters, *Chaos Solitons and Fractals*, 19 (2004), 899-903.
- [4] M.T. Yassen, The Optimal Control of Chen Cahotic Dynamical System, Applied Math. Comput., 131 (2002), 171-180.

## 6.3 Year 3:

In year 3, one of our papers has appeared, namely

1. T. Kaewong, P. Niamsup and Y. Lenbury, A note on asymptotic stability conditions for delay difference equations. *International Journal of Mathematics and Mathematical Sciences*. 7 (2005) 1007-1013.

Note that in this manuscript, we have studied the asymptotic stability of  $x_{n+l} + p \sum_{i=1}^{N} x_{n-k+(j-l)i} = 0 \text{ and we obtained the following result:}$ 

<u>Theorem 1</u> Let k, l and N be positive integers with  $k \ge (N-1)1$ . Then the zero solution of

$$X_{n+1} + p \sum_{i=1}^{N} X_{n-k+(j-1)1} = 0$$
 (6.8)

is asymptotically stable if and only if

$$-\frac{1}{N}$$

The idea of this investigation began when we read through a paper written by R. Ogita, H. Matsunaga, and T. Hara [1], where they gave the necessary and sufficient conditions for the asymptotic stability of the following linear delayed difference equation

$$x_{n+1} - x_n + p \sum_{i=1}^{N} x_{n-k+(j-1)i} = 0$$
 (6.9)

where n is a nonnegative integer, p is a real number, k, l and N are positive integers where k > (N-1)l. The following is the main result obtained in [1]:

<u>Theorem 2</u> Let k, l and N be positive integers with k > (N-1)1. Then the zero solution of (6.4) is asymptotically stable if and only if

$$0$$

where M = 2k + 1 - (N-1)1.

We have been investigating the following difference equation similar to (6.8) and (6.9):

$$X_{n+1} - \alpha X_n + p \sum_{j=1}^{N} X_{n-k+(j-1)1} = 0$$
 (6.10)

where  $0 \le \alpha \le 1$ . We note that when  $\alpha = 0$ , (6.10) becomes (6.8); and when  $\alpha = 1$ , (6.10) becomes (6.9). Thus, it is natural to study the asymptotic stability of (6.10).

In year 2, we studied the controllability and stability of perturbed Chen chaotic dynamical system given by

$$\dot{x} = a(y-x)$$

$$\dot{y} = (c-a)x - xz + cy$$

$$\dot{z} = xy - bz + dx^{2}$$
(6.11)

where a, b, c, d are positive real parameters.

We continue our work to the perturbed Chua's circuit system given by

$$\dot{x} = p \left( y - \frac{1}{7} (2x^3 - x) \right)$$

$$\dot{y} = x - y + z$$

$$\dot{z} = -qy + rx^2$$
(6.12)

where p, q, r are positive real parameters. We are interested in studying the control of chaos in the system (6.12) using linear feedback controls and bounded feedback controls, the sufficient conditions on parameters which ensure the stabilities of equilibrium points, and the synchronization of the system (6.12) when the parameters of the drive system are fully unknown and different with those of the response system using adaptive control and active control. See [1]-[3] for more details.

#### References

[1] J.H. Park, Chaos Synchronization between Two Different Chaotic Systems Using Active Control, Chaos, Solitons and Fractals, 2005, in press.

- [2] M.T. Yassen, Adaptive Control and Synchronization of a Modified Chua's Circuit System, *Applied Mathematics and Computation*, 135(2003), 13-128.
- [3] M.T. Yassen, Adaptive Synchronization of Rossler and Lu Systems with Fully Uncertain Parameters, Chaos, Solitons and Fractals, 23(2005), 1527-1536.

Table VI: Proposed and Actual Activity for Subproject 6.

Activity: Proposed (<->)	Months	Month	Months	Months	Months	Months
Actual $(\longleftrightarrow)$	1-6	7-12	13-18	19-24	25-30	31-36
1. Collect papers, books.	<>					
2. Study techniques used in		·>				
papers and books.	<b>←</b>	<del></del>				
3. Research to obtain new	<		-			
results.	<del></del>				<del>&gt;</del>	
4. Submit papers for		-	<b>&lt;</b>			
publications.			<del>&lt;</del>			<del>                                     </del>

## **Outputs of Subproject 6**

Papers appeared/accepted in international journals 4

Master graduates 6

## 7. OVERALL OUTPUT

## 7.1 Summary table

Ėį.

Subproject	Appeared/ Accepted	Inter. Conference	Ph.D. graduates	Masters graduates
1	8	2	6	1
2	1	2	2	-
3	14	3	4	9
4 .	-	3	-	3
5	3	1	-	-
6	4		-	. 6
Total	30	11	12	19

## 7.2 Rank promotions

4 rank promotions:

Dr. Julian Poulter promoted to Full Professor
 Asst. Prof. Nardtida Tumrasvin promoted to Associate Professor
 A. Somkid Amornsamankul promoted to Assistant Professor
 Dr. Wannapong Triampo promoted to Assistant Professor

## 7.3 Publications output of the project

#### Subproject 1

- Dumrongpokaphan, T., Lenbury, Y. Cascade Mechanism in a Selfregulatory Endocrine System: Modelling Pulsatile Hormone Secretion. *Pure* and Applied Chemistry. 74(6) (2002) 881-890.
- Lenbury, Y., Pansuwan, A., Tumrasvin, N. Chaos and Control Action in a Kolmogorov Type Model for Food Webs with Harvesting or Replenishment. Science Asia. 28(3) (2002) 205-215.
- 3. Rattanakul, C., Lenbury, Y., Krishnamara, N., Wollkind, D.J. Modeling of Bone Formation and Resorption Mediated by Parathyroid Hormone: Response to Estrogen/PTH Therapy. *BioSystems*. **70(1)** (2003) 55-72.
- Dumrongpokaphan, T., Lenbury, Y., Crooke, P.S. The Analysis of Higher-Order Cascade Systems with Separation Conditions Pivoting on the Slow Components: Application to a Model of Migration for Survival of the Species. *Mathematical and Computer Modelling*. 38 (2003) 671-690.
- Lenbury, Y., Giang, D.V. Nonlinear Delay Differential Equations Involving Population Growth. Mathematical and Computer Modelling. 40 (2004) 586-590.
- Lenbury, Y., Pornsaward, P. A Delay-differential Equation Model of the Feedback-controlled Hypothalamus-pituitary-adrenal Axis in Humans. *Mathematical Medicine and Biology: A Journal of the IMA*. 22 (2005) 15-33.
- 7. Crooke, P.S., Kongkul, K., Lenbury, Y., Adams, A.B., Carter, C.S., Marini, J.J., Hotchkiss, J.R. Mathematical Models for Pressure Controlled Ventilation of Oleic Acid-injured Pigs. *Mathematical Medicine and Biology.* **22** (2005) 99-112.

 Giang, D.V., Lenbury, Y., Seidman, T.I. Delay Effect in Models of Population Growth. *Journal of Mathematical Analysis and Applications*. 305 (2005) 631-643.

## Subproject 2

4

ä

4

• 1

.

:1

ij

ij,

1

ì

d

ij.

H

 Poltem, D., Wiwatanapataphee, B., Ruengsakulrach, P., Lenbury, Y., Punpocha, M., Wu, Y.H. A Numerical Study of Blood Flow Patterns in Coronary Artery Bypass Grafts. *Quantitative Methods*. 1(1) (2004) 1-7.

## Subproject 3

- Pongsumpun, P., Yoksan, S., Tang, I.M. A Comparison of the Age Distributions in the Dengue Hemorrhagic Fever Epidemics in Santiago de Cuba (1997) and Thailand (1998). Southeast Asian Journal of Tropical Medicine and Public Health. 33 (2002) 255.
- Pongsumpun, P., Lenbury, Y., Tang, I.M. Age Structure in a Model for the Transmission of Dengue Hemorrhagic Fever in Thailand. *East-West Journal* of Mathematics. Special Volume (2002) 93-103.
- Kammanee, A., Lenbury, Y., Tang, I.M. Transmission of Plasmodium Vivax
   Malaria. East-West Journal of Mathematics. Special Volume (2002)
- Kanyamee, N., Lenbury, Y., Tang, I.M. The Effect of Migrant Workers on the Transmission of Malaria. East-West Journal of Mathematics. Special Volume (2002) 297-308.
- 5. Pongsumpun, P., Tang, I.M. Transmission of Dengue Hemorrhagic Fever in an Age Structured Population. *Math. Comp. Model.* **37** (2003) 949-961.
- Kaewmanee, C., Tang, I.M. Cannibalism in an Age-structured Predator-prey System. Ecol. Modelling 167 (2003) 213-220.
- Sriprom, M., Pongsumpun, P., Yoksan, S., Barbazan, P., Gonzales, J.P., Tang, I.M. Dengue Haemorrhagic Fever in Thailand 1998-2003: Primary or Secondary. *Dengue Bulletin*. 27 (2003) 39-45.
- 8. Nishiura, H., Tang, I.M., Kakehashi, M. The Impact of Initial Attack Size on Sars Epidemic for SARS Free Countries: Possible Reason for Japan without a Domestic Transmission. *Journal of Medical Safety*. **1(1)** (2003) e1-e6.
- Pongsumpun, P., Patanarapelert, K., Sriprom, M., Varamit, S., Tang, I.M. Infection Risk to Travellers Going to Dengue Fever Regions. Southeast Asian Journal of Tropical Medicine and Public Health. 35 (2004) 155.

- Naowarat, S., Tang, I.M. Effect of Bird-to-bird Transmission of the West Nile Virus on the Dynamics of the Transmission of this Disease. Southeast Asian Journal of Tropical Medicine and Public Health. 35 (2004) 162.
- Nishiura, H., Patanaraspelert, K., Sriprom, M., Sarakorn, W., Sriyab, S., Tang, I.M. Modelling Potential Responses to Severe Acute Respiratory Syndrome (SARS) in Japan: the Role of Initial Attack Size, Precaution and Quarantine. J. Epid. Commun. Health. 58(3) (2004) 156.
- Nishiura, H., Tang, I.M. Modeling for a Smallpox-vaccination Policy against Possible Bio-terrorism in Japan: The Impact of Long-lasting Vaccinal Immunity. J. Epid. 14(2) (2004) 41.
- Nishiura, H., Patanarapelert, K., Khortwong, P., Tang, I.M., Pasakorn, A.
   Predicting the Future Trend of Drug-resistant Tuberculosis in Thailand:
   Assessing the Impact of Control Strategy. Southeast Asian Journal of Tropical Medicine and Public Health. 35 (2004) 1.
- 14. Kaewpradit, C., Triampo, W., Tang, I.M. Limit Cycle of a Herbuvire-plantbee Model Containing a Time Delay. *ScienceAsia*. **31** (2005) 193.

## Subproject 4

- Tiensuwan, M.; Yimprayoon, P.; Lenbury, Y. Application of Log-linear Models to Cancer Patients: A Case Study of Data from the National Cancer Institute of Thailand, submitted to Southeast Asian Journal of Tropical Medicine and Public Health.
- Tiensuwan, M., Rattanapornpong, S., Lenbury, Y. Applications of Logistic Regression Models to Cancer Patients: A Case Study of the National Cancer Institute. (In preparation).

## Subproject 5

 Triampo, W., Doungchawee, G., Triampo, D., Wong-Ekkabut, J., Tang, I.M. Effects of Static Magnetic Field on Growth of Leptospire, Leptospira interrogans serovar canicola: Immunoreactivity and Cell Division. Journal of Bioscience and Bioengineering. 98(3) (2004) 182-186.

- Ngamsaad, W., Triampo, W., Kanthang, P., Modchang, C., Nuttavut, N., Tang, I.M., Lenbury, Y. A Lattice Boltzann Method for Modeling the Dynamic Pole-to-pole Oscillations of Min Proteins for Determining the Position of the Midcell Division Plane. J. Korean Phys. Soc. 46(4) (2005) 1025-1030.
- Modchang, C., Kanthang, P., Triampo, W., Ngamsaad, W., Nuttavut, N., Tang, I.M., Lenbury, Y. Modeling of the Dynamic Pole-to-pole Oscillations of the *Min* Proteins in Bacterial Cell Division: The Effect of an External Field. J. Korean Phys. Soc. 46(4) (2005) 1031-1036.

## Subproject 6

1

Ž,

٠

£ .

1

1

ķ

ŧ

4

- Kaewong, T., Niamsup, P., Lenbury, Y. A Note on Asymptotic Stability Conditions for Delay Difference Equations. *International Journal of Mathematics and Mathematical Sciences*. 7 (2005), 1007-1013.
- Plienpanich, T., Niamsup, P., Lenbury, Y. Controllability and Stability of the Perturbed Chen Chaotic Dynamical System. Applied Mathematics and Computations. In Press.
- 3. Niamsup, P., Lenbury, Y. The Asymptotic Stability of  $x_{n+1} a^2 x_{n-1} + b x_{n-k} = 0$ , accepted in *Kyungpook Mathematical Journal*. (under minor revision).
- 4. Niamsup, P., Lenbury, Y. M, -Factors and Q, -Factors for Near Quasi-Norm on Certain Sequence Spaces, to appear in to *International Journal of Mathematics and Mathematical Sciences*, 2005.

## 7.4 Publications output of P.I. (Prof. Y. Lenbury) in last 3 years

- 30. Kunphasuruang, W., Lenbury, Y., Hek, G. A Nonlinear Mathematical Model for Pulsatile Discharges of Luteinizing Hormone Mediated by Hypothalamic and Extra-Hypothalamic Pathways. *Mathematical Models* and Methods in Applied Sciences. 12(5) (2002) 607-624. (Impact factor 0.816)
- 31. Dumrongpokaphan, T., Lenbury, Y. Cascade Mechanism in a Self-regulatory Endocrine System: Modelling Pulsatile Hormone Secretion. *Pure and Applied Chemistry.* **74(6)** (2002) 881-890. (Impact factor 1.750)

- 32. Lenbury, Y., Pansuwan, A., Tumrasvin, N. Chaos and Control Action in a Kolmogorov Type Model for Food Webs with Harvesting or Replenishment. *ScienceAsia*. **28(3)** (2002) 205-215. (Impact factor 0.06)
- 33. Suwanwongse, S., Chasreechai, S., Lenbury, Y., Kataunyuthita, S. Modeling of AIDS Incidence and the Response of Transmission Rates to Increased Awareness: a Case Study of the Thai Province of Nakorn Pathom. Southeast Asian Journal of Tropical Medicine and Public Health. 33(3) (2002) 581-588. (Impact factor 0.097)
- 34. Siripunvaraporn, W., Egbert, G., Lenbury, Y. Numerical Accuracy of Magnetotelluric Modeling: A Comparison of Finite Difference Approximations. *Earth Planets and Space*. **54(6)** (2002) 721-725. (Impact factor 0.822)
- Pongsumpun, P., Lenbury, Y., Tang, I.M. Age Structure in a Model for the Transmission of Dengue Haemorrhagic Fever in Thailand. *East-West Journal of Mathematics*. Special Volume (2002) 93-103. (Reviewed by Math. Review)
- 36. Kammanee, A., Lenbury, Y., Tang, I.M. Transmission of *Plasmodium Vivax* Malaria. *East-West Journal of Mathematics*. **Special Volume** (2002) 277-284. (Reviewed by Math. Review)
- 37. Kanyamee, N., Lenbury, Y., Tang, I.M. The Effect of Migrant Workers on the Transmission of Malaria. *East-West Journal of Mathematics*. **Special Volume** (2002) 297-308. (Reviewed by Math. Review)
- Rattanakul, C., Lenbury, Y., Krishnamara, N., Wollkind, D.J. Modeling of Bone Formation and Resorption Mediated by Parathyroid Hormone: Response to Estrogen/PTH Therapy. *BioSystems*. 70(1) (2003) 55-72. (Impact factor 0.846)
- 39. Maneesawarng, C., Lenbury, Y. Total Curvature and Length Estimate for Curves in CAT(K) spaces. *Differential Geometry and its Applications*. 19 (2003) 211-222. (Impact factor 0.704)
- 40. Dumrongpokaphan, T., Lenbury, Y., Crooke, P.S. The Analysis of Higher-Order Cascade Systems with Separation Conditions Pivoting on the Slow Components: Application to a Model of Migration for Survival of the Species. *Mathematical and Computer Modelling*. 38 (2003) 671-690. (Impact factor 0.426)

41. Triampo, W., Triampo, D., Tang, I.M., Lenbury, Y. Random Walk on a Plane-Spin-Rotator System: Continuum Theory and Monte Carlo Simulations. *ScienceAsia*. **29** (2003) 289-299. (Impact factor 0.06)

pt 2

抻

e k

ħį

į

1

- 42. Wong-ekabut, J., Triampo, W., Tang, I.M., Triampo, D., Baowan, D., Lenbury, Y., Vacancy-Mediated Disordering Process in Binary Alloys at Finite Temperatures: Monte Carlo Simulation. *Journal of the Korean Physical Society*. **45(2)** (2004) 310-317. (Impact factor 0.505)
- 43. Poltem, D., Wiwatanapataphee, B., Ruengsakulrach, P., Lenbury, Y., Punpocha, M., Wu, Y.H. A Numerical Study of Blood Flow Patterns in Coronary Artery Bypass Grafts. *Quantitative Methods*. **1(1)** (2004) 1-7.
- 44. Lenbury, Y., Giang, D.V. Nonlinear Delay Differential Equations Involving Population Growth. *Mathematical and Computer Modelling*. **40** (2004) 586-590. (Impact factor 0.426)
- 45. Lenbury, Y., Pornsaward, P. A Delay-differential Equation Model of the Feedback-controlled Hypothalamus-pituitary-adrenal Axis in Humans. *Mathematical Medicine and Biology: A Journal of the IMA*. **22** (2005) 15-33.
- Crooke, P.S., Kongkul, K., Lenbury, Y., Adams, A.B., Carter, C.S., Marini, J.J., Hotchkiss, J.R. Mathematical Models for Pressure Controlled Ventilation of Oleic Acid-injured Pigs. *Mathematical Medicine and Biology.* 22 (2005) 99-112.
- Giang, D.V., Lenbury, Y., Seidman, T.I. Delay Effect in Models of Population Growth. *Journal of Mathematical Analysis and Applications*.
   305 (2005) 631-643. (Impact factor 0.458)
- 48. Siripunvaraporn, W., Egbert, G., Lenbury, Y., Uyeshima, M. Three-Dimension Magnetotelluric Inversion: Data Space Method. *Physics of the Earth and Planetary Interiors*. **150** (2005) 3-14. (Impact factor 1.246)
- 49. Ngamsaad, W., Triampo, W., Kanthang, P., Tang, I.M., Nuttawut, N., Modjung, C., Lenbury, Y. A Lattice Boltzmann Method for Modeling the Dynamic Pole-to-Pole Oscillations of Min Proteins for Determining the Position of the Midcell Division Plane. *Journal of the Korean Physical Society*. 46(4) (2005) 1025-1030. (Impact factor 0.790)
- 50. Modchang, C., Kanthang, P., Triampo, W., Ngamsaad, W., Nuttawut, N., Tang, I.M., Sanguansin, S., Boondirek, A., Lenbury, Y. Modeling of the

- 50. Modchang, C., Kanthang, P., Triampo, W., Ngamsaad, W., Nuttawut, N., Tang, I.M., Sanguansin, S., Boondirek, A., Lenbury, Y. Modeling of the Dynamic Pole-to-Pole Oscillations of the Min Proteins in Bacterial Cell Division: the Effect of an External Field. *Journal of the Korean Physical Society*. 46(4) (2005) 1031-1036. (Impact factor 0.790)
- Kaewong, T., Lenbury, Y., Niamsup, P. A Note on Asymptotic Stability Conditions for Delay Difference Equations. *International Journal of Mathematics and Mathematical Sciences*. 7 (2005) 1007-1013.
- 52. Pansuwan, A., Rattanakul, C., Lenbury, Y., Wollkind, D.J., Harrison, L., Rajapakse, I. Nonlinear Stability Analyses of Pattern Formation on Solid Surfaces During Ion-Sputtered Erosion. *Mathematical and Computer Modelling*. In Press. (Impact factor 0.426)
- Plienpanich, T., Niamsup, P., Lenbury, Y. Controllability and Stability of the Perturbed Chen Chaotic Dynamical System. *Applied Mathematics and Computations*. In Press. (Impact factor 0.359)
- 54. Yanarojana, S., Chantharaksria, U., Wilairat, P., Lenbury, Y. Kinetic Modeling of Lipoprotein Peroxidation Initiated by Copper and Azo Compounds. *ScienceAsia*. In Press. (Impact factor 0.06)

## 7.5 Names of graduated students

## 7.5.1 Ph.D. students

## Subproject 1

- 1. Rujira Ouncharoen
- 2. Thongchai Dumrongpokaphan
- 3. Chontita Rattanakul
- 4. Konvika Kongkul
- 5. Sahattaya Rattanamongkonkul
- 6. Adoon Pansuwan

## Subproject 2

- 1. Jutatip Archapitak
- 2. Bundit Unyong

## Subproject 3

- 1. Puntani Pongsumpun
- 2. Surapol Noaowarat

- 3. Malee Sriprom
- 4. Somporn Punpocha

## 7.5.2 Master students

## Subproject 1

1. Pornsup Pornsawad

## Subproject 2

1. Sineenart Srimongkol

## Subproject 3

jŀ

ŧļ.

.

- 1. Ratchanee Muangyai
- 2. Somchai Sriyab
- 3. Charn Khetchaturat
- 4. Kot Patanarapelert
- 5. Athassawat Kammanee
- 6. Nairat Kanyamee
- 7. Weerachai Sarakorn
- 8. Charn Khetchaturat
- 9. Eakchai Navapunyakul

## Subproject 4

- 1. Sompit Thammasurat
- 2. Ngamphol Sunthornworasiri
- 3. Sugunya Rattanapornpong

## Subproject 6

- 1. Jutarat Kongson
- 2. Teeranush Suebcharoen
- 3. Tidarut Plienpanich
- 4. Kreangkri Ratchgit
- 5. Thongchai Botmart
- 6. Thasanai Chamnanpet

## 8. ADDITIONAL COMMENTS

Two annual progress report meetings have been organized.

## 8.1 First annual meeting: May 8-9, 2003

The program

- i) 2 invited lectures by Prof. Yuesheng Xu form West Verginia University.
- ii) 13 contributed papers.

Attendance

- i) On May 8, 86 participants.On May 9, 61 participants.
- ii) Participants were from 16 universities.
- 8.2 Second annual meeting: January 7-8, 2004.

The program

- i) 4 invited lectures by
  - Prof. Charles Micchelli from University at Albany, New York, U.S.A.
  - Prof. Hideaki Kaneko from Old Dominion University, Virginia, U.S.A.
  - Asst. Prof. Massimiliano Pontil from University College, London, U.K.
  - Assoc. Prof. Wayne Michael Lawton from National University of Singapore,
     Singapore.
- ii) 7 contributed papers.

Attendance

- i) On January 7, 55 participants.On January 8, 58 participants.
- ii) Participants were from 11 universities.
- 8.3 The final report meeting is being organized as an international conference (ICMA-MU 2005) during December 15-17, 2005. Announcement has been posted in the web (www.sc.mahidol.ac.th/scma/).

## 9. APPENDICES

9.1 Manuscripts of newly accepted / appeared papers

Subproject 1 pages 108-219

- 1.1 Dumrongpokaphan, T., Lenbury, Y., Crooke, P.S. The Analysis of Higher-Order Cascade Systems with Separation Conditions Pivoting on the Slow Components: Application to a Model of Migration for Survival of the Species. *Mathematical and Computer Modelling*. 38 (2003) 671-690.
- 1.2 Giang, D.V., Lenbury, Y., Seidman, T.I. Delay Effect in Models of Population Growth. *Journal of Mathematical Analysis and Applications*. 305 (2005) 631-643.
- 1.3 Lenbury, Y., Giang, D.V. Nonlinear Delay Differential Equations Involving Population Growth. *Mathematical and Computer Modelling*. **40** (2004) 586-590.

- 1.4 Lenbury, Y., Pansuwan, A., Tumrasvin, N. Chaos and Control Action in a Kolmogorov Type Model for Food Webs with Harvesting or Replenishment. Science Asia. 28(3) (2002) 205-215.
- 1.5 Rattanakul, C., Lenbury, Y., Krishnamara, N., Wollkind, D.J. Modeling of Bone Formation and Resorption Mediated by Parathyroid Hormone: Response to Estrogen/PTH Therapy. *BioSystems*. 70(1) (2003) 55-72.
- 1.6 Lenbury, Y., Pornsaward, P. A Delay-differential Equation Model of the Feedback-controlled Hypothalamus-pituitary-adrenal Axis in Humans. Mathematical Medicine and Biology: A Journal of the IMA. 22 (2005) 15-33.

ij

li

- 1.7 Dumrongpokaphan, T., Lenbury, Y. Cascade Mechanism in a Self-regulatory Endocrine System: Modelling Pulsatile Hormone Secretion. Pure and Applied Chemistry. 74(6) (2002) 881-890.
- 1.8 Crooke, P.S., Kongkul, K., Lenbury, Y., Adams, A.B., Carter, C.S., Marini, J.J., Hotchkiss, J.R. Mathematical Models for Pressure Controlled Ventilation of Oleic Acid-injured Pigs. *Mathematical Medicine and Biology.* 22 (2005) 99-112.

Subproject 2 pages 220-224

2.1 Poltem, D., Wiwatanapataphee, B., Ruengsakulrach, P., Lenbury, Y., Punpocha, M., Wu, Y.H. A Numerical Study of Blood Flow Patterns in Coronary Artery Bypass Grafts. *Quantitative Methods*. 1(1) (2004) 1-7.

## Subproject 3 pages 225-341

- 3.1 Pongsumpun, P., Yoksan, S., Tang, I.M. A Comparison of the Age Distributions in the Dengue Hemorrhagic Fever Epidemics in Santiago de Cuba (1997) and Thailand (1998). Southeast Asian Journal of Tropical Medicine and Public Health. 33 (2002) 255.
- 3.2 Pongsumpun, P., Lenbury, Y., Tang, I.M. Age Structure in a Model for the Transmission of Dengue Hemorrhagic Fever in Thailand. *East-West Journal of Mathematics*. **Special Volume** (2002) 93-103.
- 3.3 Kammanee, A., Lenbury, Y., Tang, I.M. Transmission of Plasmodium Vivax Malaria. East-West Journal of Mathematics. Special Volume (2002) 277-284.

- 3.4 Kanyamee, N., Lenbury, Y., Tang, I.M. The Effect of Migrant Workers on the Transmission of Malaria. East-West Journal of Mathematics. Special Volume (2002) 297-308.
- 3.5 Pongsumpun, P., Tang, I.M. Transmission of Dengue Hemorrhagic Fever in an Age Structured Population. *Math. Comp. Model.* **37** (2003) 949-961.
- 3.6 Kaewmanee, C., Tang, I.M. Cannibalism in an Age-structured Predator-prey System. *Ecol. Modelling* **167** (2003) 213-220.
- 3.7 Sriprom, M., Pongsumpun, P., Yoksan, S., Barbazan, P., Gonzales, J.P., Tang, I.M. Dengue Haemorrhagic Fever in Thailand 1998-2003: Primary or Secondary. *Dengue Bulletin.* 27 (2003) 39-45.
- 3.8 Nishiura, H., Tang, I.M., Kakehashi, M. The Impact of Initial Attack Size on Sars Epidemic for SARS Free Countries: Possible Reason for Japan without a Domestic Transmission. *Journal of Medical Safety*. **1(1)** (2003) e1-e6.
- 3.9 Pongsumpun, P., Patanarapelert, K., Sriprom, M., Varamit, S., Tang, I.M. Infection Risk to Travellers Going to Dengue Fever Regions. Southeast Asian Journal of Tropical Medicine and Public Health. 35 (2004) 155.
- 3.10 Naowarat, S., Tang, I.M. Effect of Bird-to-bird Transmission of the West Nile Virus on the Dynamics of the Transmission of this Disease. Southeast Asian Journal of Tropical Medicine and Public Health. 35 (2004) 162.
- 3.11 Nishiura, H., Patanaraspelert, K., Sriprom, M., Sarakorn, W., Sriyab, S., Tang, I.M. Modelling Potential Responses to Severe Acute Respiratory Syndrome (SARS) in Japan: the Role of Initial Attack Size, Precaution and Quarantine. J. Epid. Commun. Health. 58(3) (2004) 156.
- 3.12 Nishiura, H., Tang, I.M. Modeling for a Smallpox-vaccination Policy against Possible Bio-terrorism in Japan: The Impact of Long-lasting Vaccinal Immunity. J. Epid. 14(2) (2004) 41.
- 3.13 Nishiura, H., Patanarapelert, K., Khortwong, P., Tang, I.M., Pasakorn, A. Predicting the Future Trend of Drug-resistant Tuberculosis in Thailand: Assessing the Impact of Control Strategy. Southeast Asian Journal of Tropical Medicine and Public Health. 35 (2004) 1.
- 3.14 Kaewpradit, C., Triampo, W., Tang, I.M. Limit Cycle of a Herbuvire-plant-bee Model Containing a Time Delay. *ScienceAsia*. **31** (2005) 193.

Subproject 5 pages 342-358

5.1 Triampo, W., Doungchawee, G., Triampo, D., Wong-Ekkabut, J., Tang, I.M. Effects of Static Magnetic Field on Growth of Leptospire, Leptospira interrogans serovar canicola: Immunoreactivity and Cell Division. Journal of Bioscience and Bioengineering. 98(3) (2004) 182-186.

- 5.2 Ngamsaad, W., Triampo, W., Kanthang, P., Modchang, C., Nuttavut, N., Tang, I.M., Lenbury, Y. A Lattice Boltzann Method for Modeling the Dynamic Pole-to-pole Oscillations of Min Proteins for Determining the Position of the Midcell Division Plane. *Journal of the Korean Physical Society.* 46(4) (2005) 1025-1030.
- 5.3 Modchang, C., Kanthang, P., Triampo, W., Ngamsaad, W., Nuttavut, N., Tang, I.M., Lenbury, Y. Modeling of the Dynamic Pole-to-pole Oscillations of the Min Proteins in Bacterial Cell Division: The Effect of an External Field. Journal of the Korean Physical Society. 46(4) (2005) 1031-1036.

Subproject 6 pages 359-393

- 6.1 Kaewong, T., Niamsup, P., Lenbury, Y. A Note on Asymptotic Stability Conditions for Delay Difference Equations. *International Journal of Mathematics and Mathematical Sciences*. 7 (2005), 1007-1013.
- 6.2 Plienpanich, T., Niamsup, P., Lenbury, Y. Controllability and Stability of the Perturbed Chen Chaotic Dynamical System. Applied Mathematics and Computations. In Press.
- 6.3 Niamsup, P., Lenbury, Y. The Asymptotic Stability of  $x_{n+1} a^2 x_{n-1} + b x_{n-k} = 0$ , accepted in *Kyungpook Mathematical Journal*. (under minor revision).
- 6.4 Niamsup, P., Lenbury, Y. M, Factors and Q, Factors for Near Quasi-Norm on Certain Sequence Spaces, to appear in to International Journal of Mathematics and Mathematical Sciences, 2005.

## 9.2 Announcements of Special Seminars

111 seminars have been organized by members of the project in the past 3 years.

(Appendix # 7) pages 394-452

Signature

Prof. Yongwimon Lenbury

(Project Leader)



Mathematical and Computer Modelling 38 (2003) 671-690

MATHEMATICAL AND COMPUTER MODELLING

www.elsevier.com/locate/mcm

# The Analysis of Higher-Order Cascade Systems with Separation Conditions Pivoting on the Slow Components: Application to a Model of Migration for Survival of the Species

T. DUMRONGPOKAPHAN AND Y. LENBURY\*

Department of Mathematics
Faculty of Science, Mahidol University
Bangkok, Thailand

P. S. CROOKE

Department of Mathematics, Vanderbilt University Nashville, TN 37240, U.S.A.

(Received August 2001; accepted August 2002)

Abstract—Cascade systems, characterized by highly diversified time responses, are considered in this paper. Singular perturbation principles, which have been used to analyze relaxation oscillations in second-order dynamical systems, will be extended here to accommodate nonlinear systems in which more state variables are involved in multiscale interactions. Separation conditions will be derived for the identification of limit cycle behavior in a higher-dimensional  $(n \ge 4)$  cascade system. It is found that when appropriate regularity and boundedness requirements are met by the slow components of the dynamical system, pivoting on the slow components can lead to separation conditions which identify limit cycle behavior as well as other dynamic behavior permitted by the model. The principle is then applied to a model of two communities coupled by migration. Through such analysis, we can examine how the mechanisms of migration, variations in reproduction, recruitment, mortality, and feeding success, exploited by interacting species, may achieve survival and coexistence of the populations concerned. © 2003 Elsevier Ltd. All rights reserved.

Keywords—Cascade systems, Singular perturbation, Sustained oscillation, Persistence, Migration.

#### INTRODUCTION

Several important cascade systems are found in nature which incorporate some form of diversities in their dynamics. Many endocrine systems are considered to constitute a cascade mechanism for being an amplification system where an initial reaction gives rise to the generation of multiple second reactions, each of which sets off multiple third reactions, and so on.

<sup>\*</sup>Author to whom all correspondence should be addressed.

Deepest appreciation is extended to the Thailand Research Fund for the financial support (Contract Numbers RTA/02/2542 and PHD/0029/2543).

An example of endocrine cascade systems involves the hypothalamus, pituitary, and distal endocrine secreting glands. A signal, in either the external or internal environment, is sent to the limbic system and then the hypothalamus, resulting in the secretion of a releasing hormone into the closed portal system connecting the hypothalamus and anterior pituitary. Releasing hormones may be secreted in nanogram amounts and have half-lives of about 3–7 min [1]. They then stimulate the release of the appropriate anterior pituitary hormones, which may be secreted in microgram amounts with half-lives on the order of 20 min or longer. These hormones in turn signal the secretion of the ultimate hormones, which may be secreted in many micrograms or milligrams and may be fairly stable. Thus, the stability and amounts of the hormones increase as one proceeds down the cascade.

Such cascade effects can be found also in ecosystems, in the majority of food chains where the size and time needed for reproduction and growth of the individuals of each population are increasing with the trophic levels. Phytoplankton-zooplankton-fish is a typical example [2]. In fact, almost all food chains belonging to the class vegetation-herbivore-carnivore have time responses increasing along the chain from bottom to top, an exception of which is the chain "tree-defoliator-bird" in which the second trophic level is that with the fastest dynamics [2].

It is well known that such systems characterized by highly diversified dynamics can be analyzed with the singular perturbation method [2], under suitable regularity assumptions. Such arguments have been used to analyze relaxation oscillations in slow-fast second-order dynamical systems and have been extended successfully to apply to three-dimensional systems by Muratori and Rinaldi [3]. However, in a complex system where more than three state variables are involved, analysis and identification of sustained oscillation become a formidable task. Since a great deal of understanding and insights can be gained from such analysis which cannot be achieved from numerical work alone, we attempt here to extend the concept to accommodate higher-dimensional systems. Lenbury et al. [4] was able to derive the separation condition for a higher-dimensional system by pivoting about the fast components of the system, upon certain assumptions of their boundedness and regularity. Here, we show that in a different circumstance where pivoting about the slow components is allowed, existence of sustained oscillations may be ascertained at relative ease through the singular perturbation analysis. We derive the separation and delineating conditions, which help us to identify different dynamical behavior permitted by a nonlinear system of order greater than or equal to four.

Application is then made to a model of predator-prey communities coupled by migration in order to investigate how certain species can survive by exploiting the mechanisms which involve a combination of migration, variations in rates of reproduction, consumption, and mortality.

According to Matsumoto and Seno [5], population persistence is influenced by both biotic and abiotic environmental heterogeneity, namely, resource distribution, temperature, humidity, stochastic disturbance, and so on. Some effect of local environmental heterogeneity is transferred through population migration processes and affects the whole population to affect population persistence.

Whitehead [6], in his report on the variation in the feeding success of sperm whales, stated that a consideration of scale should be central in ecology. At the species level, patterns of environmental variation over a wide range of spatial and temporal scales determine population ecology and define evolutionary selective pressure. "Populations of particular species track spatial and temporal variability in their environment at some scales but not others. Tracking at temporal scales longer than the organism's lifetime and spatial scales broader than its home range is largely achieved through variations in reproduction, recruitment, mortality, and migration." Environmental variability over smaller scales usually results in changes in the feeding success, nutritional status, and, sometimes, the behavior of individual organisms.

Whitehead's study [6] found that sperm whales maintain high biomass and very low reproductive rates in an environment which shows great variability over time scales of one or more years. As the environmental variation has little coherence over scales of about 300 km or more, the study

found that sperm whales are able to use migration as their principal strategy for surviving in an uncertain habitat. During periods characterized by low feeding success groups of sperm whales moved greater distances and are able to maintain high biomass and low reproductive rates in an environment which, at any location, contains long, unpredictable periods of food shortage. Groups have been found to move more consistently in particular directions when feeding success is low, and doubling back on their tracks when it is high.

Walde [7] also presented field data which indicated that population densities were higher and persistence was greater where immigration rates were higher. Most importantly, it appeared that temporal patterns of density and, perhaps, probability of persistence, were dependent on the amount of migration between populations.

As commented by Walde [7], most of the current debate is centered on the question of the mechanisms underlying the stability among interacting species. One of the two alternative hypotheses in such a debate is that the predator-prey interaction is stable at a relatively small spatial scale due to mechanisms such as foraging behavior, or due to fine-scale physical biotic heterogeneity. The other hypothesis is that the interaction is stable at a larger spatial scale due to migration among partially subdivided populations.

We, therefore, study a simple model of two communities, assuming that predators can migrate between communities, while prey cannot. Prey populations in the two communities are assumed to exhibit different reproductive behavior to take into account the difference in abundance, and different parameters are assigned to the predators response functions to model the variation in the foraging success in the two communities. The condition for migration is the difference in predator population densities. We derive the higher-dimensional separation conditions developed in this paper to identify limit cycle behavior and carry out an analysis of the dynamics of the four-dimensional model in order to provide partial support for the arguments concerning the stability of the system and the persistence of the populations in the coupled communities.

#### Singular Perturbation Arguments in the Lower-Dimensional Case

In order to understand how the singular perturbation arguments can be used to detect limit cycles in a three component cascade system, let us consider a third-order system of the form

$$\dot{x} = f(x, y, z; \alpha),\tag{1}$$

$$\dot{y} = \varepsilon g(x, y, z; \alpha),\tag{2}$$

$$\dot{z} = \varepsilon \delta h(x, y, z; \alpha),\tag{3}$$

where  $\varepsilon$  and  $\delta$  are small positive parameters. Thus, when the right sides of equations (1)-(3) are finite and different from zero,  $|\dot{y}|$  is of the order  $\varepsilon$  and  $|\dot{z}|$  is of the order  $\varepsilon\delta$ . Therefore, x is the fast variable, z is the slow one, while y has intermediate dynamics.

As explained by Muratori and Rinaldi [2,3], system (1)–(3) with small  $\varepsilon$  and  $\delta$  can be analyzed with the singular perturbation method which, under suitable regularity conditions, allows approximating the solution of system (1)–(3) with a sequence of simple dynamic transitions occurring at different speeds. The argument, following that of Muratori and Rinaldi's [2,3], goes as follows.

Given an initial condition (x(0), y(0), z(0)), the slow z and intermediate (y) variables are frozen, and the "fast system"

$$\dot{x}(\tau_1) = f(x(\tau_1), y(0), z(0); \alpha), \qquad \tau_1 = \frac{t}{\varepsilon \delta}$$

$$(4)$$

is considered with initial condition x(0). Thus, the fast component x varies very quickly according to equation (4), and eventually tends toward a stable equilibrium  $\bar{x}(x(0), y(0), z(0))$  of (4). Then, still keeping z frozen at z(0), we now consider the "intermediate system"

$$\dot{y}(\tau_2) = g(\bar{x}(x(0), y(\tau_2), z(0)), y(\tau_2), z(0); \alpha), \qquad \tau_2 = \frac{t}{\delta}.$$
 (5)

where  $\ddot{x}(x(0),y,z(0))$  is a stable equilibrium of the fast system (4) with y(0) replaced by y.

Referring to Figure 1, where slow, intermediate, and high-speed transitions are indicated, respectively, by one, two, and three arrows, a transition at high speed  $(\tau_1 = t/\varepsilon\delta)$  first develops at constant y and z and brings the system from the point (x(0), y(0), z(0)), point A in Figure 1, to point B on a stable equilibrium of the slow manifold f = 0. Then a second intermediate speed  $(\tau_2 = t/\delta)$  transition is made on the manifold at constant z until an equilibrium  $\bar{y}(x(0), y(0), z(0))$  of system (5) is approached (point C in Figure 1). A third transition then follows at low speed along the line obtained by intersecting the slow manifold f = 0 and the intermediate manifold g = 0. The transition may end at an equilibrium point where f = g = h = 0 or a situation may occur in which the stability of the manifold f = 0 is lost first at a bifurcation point f = 0 in Figure 1). Then, a fast catastrophic transition may bring the state of the system to a point on the other stable branch of the manifold f = 0 (point f = 0).

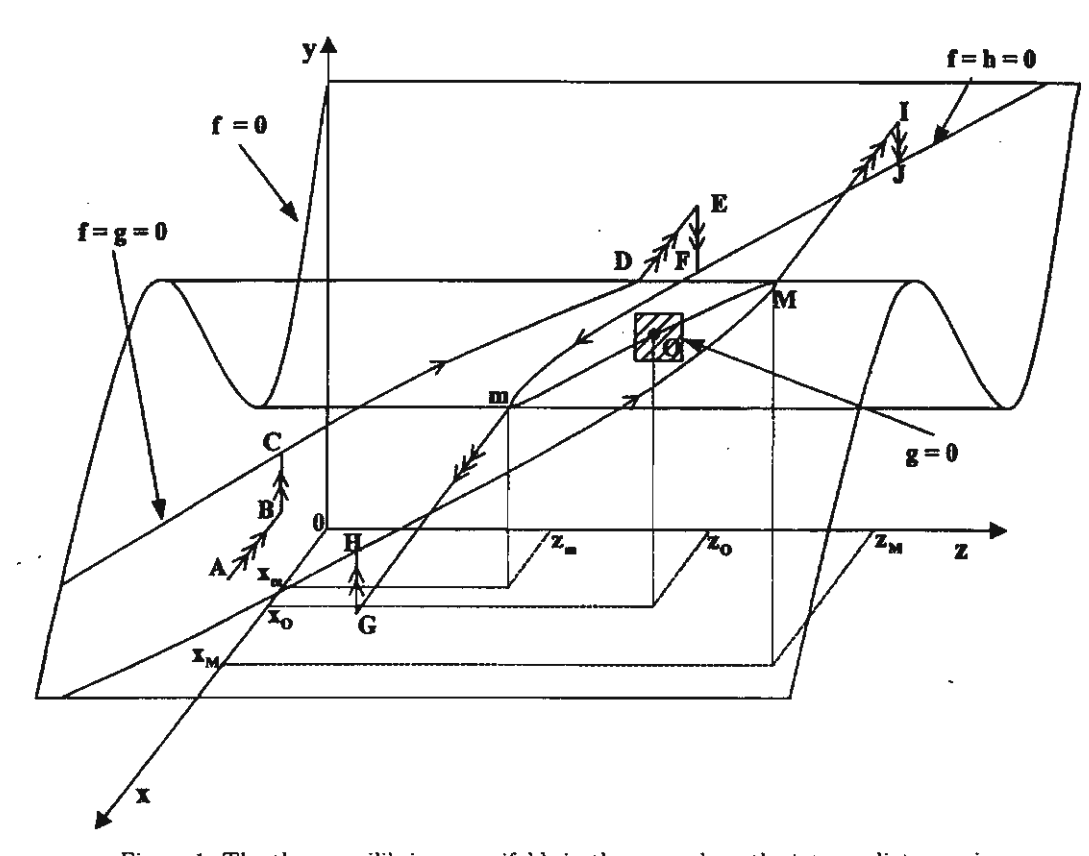


Figure 1. The three equilibrium manifolds in the case where the intermediate manifold g=0 separates the two stable branches of the curve f=h=0.

Now, if the manifold g=0 is positioned in such a way that point O, where f=g=h=0, is located between the two bifurcation points m and M on the curve f=h=0 so that the manifold g=0 separates the two stable branches of the curve as shown in Figure 1, then g>0 on one branch (the front one in Figure 1) and g<0 on the other (the back one).

In this case, once the system reaches point E, a transition develops at intermediate speed downward towards point F located on the intersection between f=0 and h=0 and follows this curve at slow speed in the direction of decreasing g until the bifurcation point g is reached. A catastrophic transition then brings the system to point g on the front part of g of followed by a transition at intermediate speed to point g on the front part of g of a slow transition will develop in the direction of increasing g until the stability of the manifold is lost again at point g on the first point g on the back portion of g of the system to point g on the back portion of g of g is now negative. A transition at intermediate speed then develops downward until point g on g is reached. A slow transition then follows along this curve until g is reached again. A quick jump to g closes up the cycle g and g is intermediate speed.

Obviously, the cycle can be much more complex if, for suitable values of its parameters, system (1)-(3) has multiple equilibria. However, we shall assume that for appropriately chosen parametric values, the manifold g=0 intersects the curve f=h=0 at only one point, namely the point  $O(x_O,y_O,z_O)$  and the two bifurcation points on f=h=0 are  $M(x_M,y_M,z_M)$  and  $m(x_m,y_m,z_m)$ . Then if, for a particular value of the system parameter  $\alpha$ , the separation condition

$$x_m < x_O < x_M \tag{6}$$

holds, then the system of equations (1)-(3) has a stable limit cycle which is contained in a tube around the transitions described above, and the radius of the tube goes to zero with  $\varepsilon$  and  $\delta$ .

#### Extension to Higher-Dimensional Systems Pivoting about the Slow Components

In order to extend the above concept to higher-dimensional systems, let us consider a system of n+3 differential equations which may be written in the form

$$\dot{x} = f(x, y, z, w; \alpha), \tag{7}$$

$$\dot{y} = \varepsilon g(x, y, z, w; \alpha), \tag{8}$$

$$\dot{z} = \varepsilon \delta h(x, y, z, w; \alpha), \tag{9}$$

$$\dot{w} = \varepsilon \delta \eta k(x, y, z, w; \alpha), \tag{10}$$

where  $\varepsilon$ ,  $\delta$ , and  $\eta$  are small positive constants,  $\alpha \in \mathbb{R}^N$  is the N-dimensional vector of system parameters, while

 $\begin{bmatrix} x \\ y \\ z \end{bmatrix} \in \Re^3$ 

and

$$w = \begin{bmatrix} w_1 \\ w_2 \\ \vdots \\ w_n \end{bmatrix} \in \Re^n$$

are the n+3 state variables, and

$$k = \begin{bmatrix} k_1(x, y, z, w; \alpha) \\ k_2(x, y, z, w; \alpha) \\ \vdots \\ k_n(x, y, z, w; \alpha) \end{bmatrix}.$$

Hence, x is the fast variable, y the intermediate, z the slow, and  $w_i$ , i = 1, 2, ..., n, the very slow components of the system.

Employing the same line of arguments as above, we first assume that w is varying extremely slowly in comparison to the first three components x, y, and z. Then, we may initially assume that w is kept frozen at a constant value w(0) while x, y, and z vary according to the three-dimensional system

$$\dot{x} = f(x, y, z, w(0); \alpha), \tag{11}$$

$$\dot{y} = \varepsilon g(x, y, z, w(0); \alpha), \tag{12}$$

$$\dot{z} = \varepsilon \delta h(x, y, z, w(0); \alpha). \tag{13}$$

Thus, if, for suitable parametric values  $\alpha$ , the relative positions of the three equilibrium manifolds of system (11)-(13) are the same as those three shown in Figure 1, then trajectories will

develop as described earlier. However, as w varies with time, though very slowly, the shapes and positions of the three manifolds shift slowly as time passes. The coordinates of points m, M, and O are, in this case,  $(x_m(w;\alpha), y_m(w;\alpha), z_m(w;\alpha))$ ,  $(x_M(w;\alpha), y_M(w;\alpha), z_M(w;\alpha))$ , and  $(x_O(w;\alpha), y_O(w;\alpha), z_O(w;\alpha))$ , respectively, since f, g, and h are all functions of w.

Moreover, since w may not equilibrate and the manifolds  $k_i(x, y, z, w; \alpha) = 0$ , i = 1, 2, ..., n, may not be stable, as the transitions develop around the curve shown in Figure 1, the value of w can swing about off the manifolds

$$k_i(x, y, z, w; \alpha) = 0, \qquad i = 1, 2, \dots, n.$$
 (14)

If we further assume that each of the equations in (14) can be solved for z as an explicit function of the other components

$$z = Z_i(x, y, w; \alpha), \qquad i = 1, 2, \dots, n, \tag{15}$$

then we see that extra separation conditions are needed to ensure that the manifolds described by the equations in (15) are positioned in between the two stable branches of the curve f = h = 0 as well, in order that a limit cycle exists. These conditions are stated in the following theorem, under all the assumptions mentioned above.

THEOREM. Suppose that the functions  $f(x, y, z, w; \alpha)$ ,  $g(x, y, z, w; \alpha)$ ,  $h(x, y, z, w; \alpha)$ , and  $k(x, y, z, w; \alpha)$  are continuous, and that the functions  $x_M(w; \alpha)$ ,  $z_M(w; \alpha)$ , z

$$\sup_{w} x_m(w; \alpha) < \inf_{w} x_O(w; \alpha), \tag{16}$$

$$\sup_{w} x_{\mathcal{O}}(w; \alpha) < \inf_{w} x_{\mathcal{M}}(w; \alpha), \tag{17}$$

$$\sup_{w} z_{m}(w; \alpha) < \min_{i} \inf_{\Delta_{i}} Z_{i}, \tag{18}$$

$$\max_{i} \sup_{\alpha} Z_{i} < \inf_{w} z_{M}(w; \alpha), \tag{19}$$

where the supremum and infemum of  $Z_i$  are taken over its domain  $\Delta_i$  which is a subset of  $\Re^{n+2}$ , then a limit cycle exists for the system of equations (7)-(10), provided that  $\varepsilon$ ,  $\delta$ , and  $\eta$  are sufficiently small.

PROOF. Since the functions involved are assumed to be bounded in their respective domains, the infema and suprema in inequalities (16)–(19) exist. The separating conditions (16),(17) and the continuity of the functions concerned guarantee that, as w ranges over time, the intermediate equilibrium manifold g=0 will remain in the appropriate position, separating the two stable branches of the submanifold f=h=0, under the regularity assumptions already mentioned above. The transitions will develop as shown in Figure 1, even as w varies slowly. The separation conditions (18) and (19) ensure that, as the transition reaches the highest value of z at point M in Figure 1, which keeps shifting with w, the trajectory in the (n+3)-dimensional space swings to one side of the manifolds given by (15), and when the transition reaches the lowest value of z at point m in Figure 1, the trajectory has swung over to the other side of the manifolds given by (15). This guarantees that w shall not increase or decrease without bound, but remain close to the manifolds  $z=Z_i$ ,  $i=1,2,\ldots,n$ , permitting sustained oscillation around a closed cycle as identified in Figure 1, provided that  $\varepsilon$ ,  $\delta$ , and  $\eta$  are sufficiently small.

## APPLICATION TO A MODEL OF COMMUNITIES COUPLED BY MIGRATION

In order to illustrate how the technique can be applicable to practical situations, we consider a model of two predator-prey communities coupled by migration, consisting of the following

677

nonlinear differential equations:

$$\dot{x} = r_1 x (1 - x) - \frac{\gamma_1 x y}{x + M_1},\tag{20}$$

$$\dot{y} = \frac{C_1 \gamma_1 x y}{x + M_1} - D_1 y - \mu_1 (y - z), \tag{21}$$

$$\dot{z} = \frac{C_2 \Gamma_2 z w}{w + M_2} - D_2 z + \mu_2 (y - z), \tag{22}$$

$$\dot{w} = \frac{R_2 w}{w + r_3} - \frac{\Gamma_2 z w}{w + M_2},\tag{23}$$

where x, y, z, and w are the population densities of prey in the first community, predators in the first community, predators in the second community, and prey in the second community, respectively. The growth rate of prey in the first community is assumed to be logistic, while a saturation function is assumed for prey in the second community in order to incorporate the effect of resource variability in the two environments. Holling type response functions are assumed for both predators with conversion factors  $C_1$  and  $C_2$  specifying the numbers of newly born predators for each captured prey. Parameters  $\gamma_1$  and  $\Gamma_2$  are the maximum predation rates,  $M_1, M_2, r_3$  the half-saturation constants,  $D_1, D_2$  the corresponding death rates, and  $R_2$  is the maximum birth rate of prey in the second community. Parameters  $\mu_1$  and  $\mu_2$  are the variation constants of migration from one community to the other, which are allowed to be different to account for the difference in spatial capacities available in the two habitats.

We assume that prey has very fast dynamics and the feeding success of the predators is higher in the first community. After a period of successful foraging, predator population density greatly increases while the level of prey continuously drops leading to shortage of food due to intrapopulation competition. Migration is then adopted as the predators' strategy for surviving in an uncertain habitat. The rate of migration from one community to the other is assumed to vary directly as the difference in the population densities. As Sherry observed in his recent study [8], habitats are considered saturated when some individuals are unable to secure or defend their ground due to competition, forcing settlement in less preferred areas. Thus, intraspecific competition in the first community may drive the predators to migrate to a less favorable habitat in which prey multiplies more slowly. However, evidence [6] shows that, confronted with low food availability, organisms may die, fast, or move. An adjustment in their reproductive rate and foraging behavior is a common strategy for survival in a less favorable environment and a decline of body mass is found in individuals occupying the most drought-stressed habitats. Therefore, predators in the second community are assigned slower dynamics than those in the first. Consequently, we scale the dynamics of the four components of the system by means of three small positive parameters  $\epsilon$ ,  $\delta$ , and  $\eta$  as follows.

Letting  $c_1 = C_1 \gamma_1/\varepsilon$ ,  $d_1 = D_1/\varepsilon$ ,  $v_1 = \mu_1/\varepsilon$ ,  $c_2 = C_2 \Gamma_2/\varepsilon \delta$ ,  $d_2 = D_2/\varepsilon \delta$ ,  $v_2 = \mu_2/\varepsilon \delta$ ,  $r_2 = R_2/\varepsilon \delta \eta$ , and  $\gamma_2 = \tau_2/\varepsilon \delta \eta$ , we are led to the following model equations:

$$\dot{x} = r_1 x (1 - x) - \frac{\gamma_1 x y}{x + M_1} \equiv f(x, y, z, w), \tag{24}$$

$$\dot{y} = \varepsilon \left[ \frac{c_1 x y}{x + M_1} - d_1 y - \upsilon_1(y - z) \right] \equiv \varepsilon g(x, y, z, w), \tag{25}$$

$$\dot{z} = \varepsilon \delta \left[ \frac{c_1 z w}{w + M_2} - d_2 z + \upsilon_2 (y - z) \right] \equiv \varepsilon \delta h(x, y, z, w), \tag{26}$$

$$w = \varepsilon \delta \eta \left[ \frac{r_2 w}{w + r_3} - \frac{\gamma_2 z w}{w + M_2} \right] \equiv \varepsilon \delta \eta k(x, y, z, w). \tag{27}$$

Thus, if  $\varepsilon$ ,  $\delta$ , and  $\eta$  are small, prey and predators in the first community have the fastest and intermediate dynamics, respectively. In the second community, the predator population has a relatively slow time response, while the prey population has the slowest dynamics.

We now study each of the equilibrium manifolds in detail.

The Manifold f = 0. This consists of the trivial manifold x = 0 and the nontrivial one given by the equation

$$y = \frac{r_1}{\gamma_1}(x + M_1)(1 - x), \tag{28}$$

which intersects the (y, z)-plane along the line

$$y=\frac{r_1}{\gamma_1}M_1.$$

The maximum point on this manifold is located at the point where

$$y = \frac{r_1(1+M_1)^2}{4\gamma_1} \equiv y_M \tag{29}$$

and

$$x = \frac{(1 - M_1)}{2} \equiv x_M,\tag{30}$$

as shown in Figure 2a.

THE MANIFOLD q = 0. This is the surface

$$z = \frac{y}{v_1} \left( d_1 + v_1 - \frac{c_1 x}{x + M_1} \right), \tag{31}$$

which intersects the trivial manifold x = 0 along the line

$$z = \frac{y}{v_1} (d_1 + v_1) \tag{32}$$

and intersects the nontrivial manifold f = 0 along the curve

$$z = \frac{r_1}{\gamma_1 \nu_1} (1 - x)((d_1 + \nu_1 - c_1)x + M_1(d_1 + \nu_1)). \tag{33}$$

Moreover, the curve f = g = 0 in (33) intersects the (x, y)-plane at the point where z = 0 and

$$x = \frac{M_1(d_1 + \nu_1)}{c_1 - (d_1 + \nu_1)} \equiv \hat{x},\tag{34}$$

which is positive provided that

$$c_1 > d_1 + v_1. (35)$$

The Manifold h = 0. This is a surface given by

$$z = \frac{\upsilon_2 y(w + M_2)}{(d_2 + \upsilon_2 - c_2)w + (d_2 + \upsilon_2)M_2},$$
(36)

which intersects the nontrivial manifold f = 0 along the curve given by

$$z = \frac{r_1 v_2}{\gamma_1} \left[ \frac{(x + M_1)(1 - x)(w + M_2)}{(d_2 + v_2 - c_2)w + (d_2 + v_2)M_2} \right]. \tag{37}$$

The maximum point of the curve f = h = 0 in (37) is attained when  $x = x_M$  given in (30) and, on substituting (30) into (37),

$$z = z_M(w) = \frac{r_1 \nu_2}{4\gamma_1} \left[ \frac{(1+M_1)^2 (w+M_2)}{(d_2 + \nu_2 - c_2)w + (d_2 + \nu_2)M_2} \right].$$
(38)

Analysis of Higher-Order Cascade Systems

679

On differentiating  $z_M(w)$ , we find that

$$\frac{d}{dw}z_{M}(w)>0,$$

for all parametric values. Thus,

$$\inf_{w} z_{M}(w) = z_{M}(w)|_{w=0}$$

$$= \frac{r_{1}v_{2}(1+M_{1})^{2}}{4\gamma_{1}(d_{2}+v_{2})},$$
(39)

$$\sup_{w} z_{M}(w) = \lim_{w \to \infty} z_{M}(w)$$

$$= \frac{r_{1}v_{2}(1 + M_{1})^{2}}{4\gamma_{1}(d_{2} + v_{2} - c_{2})},$$
(40)

which is positive if

$$d_2 + v_2 > c_2. (41)$$

The point where the curve f = h = 0 in (37) intersects the (y, z)-plane is found by substituting x = 0 in (37), yielding

$$z = \frac{r_1 \nu_2 M_1(w + M_2)}{\gamma_1 \left[ (d_2 + \nu_2 - c_2)w + (d_2 + \nu_2) M_2 \right]} \equiv z_m(w). \tag{42}$$

Differentiating  $z_m(w)$ , we find that

$$\frac{d}{dw}z_m(w) > 0,$$

for all parametric values. Thus,

$$\sup_{w} z_{m}(w) = \lim_{w \to \infty} z_{m}(w) 
= \frac{r_{1}v_{2}M_{1}}{\gamma_{1}(d_{2} + v_{2} - c_{2})},$$
(43)

$$\inf_{w} z_{m}(w) = z_{m}(w)|_{w=0} = \frac{r_{1} \nu_{2} M_{1}}{\gamma_{1} (d_{2} + \nu_{2})},$$
(44)

which is always positive.

-

Finally, the curve f = g = 0 in (33) intersects the curve f = h = 0 in (37) at the point where  $x = x_O(w)$  and

$$x_O(w) = \frac{M_1([(d_1+v_1)(d_2+v_2-c_2)-v_1v_2]w + [(d_1+v_1)(d_2+v_2)-v_1v_2]M_2)}{[v_1v_2 - (d_1+v_1-c_1)(d_2+v_2-c_2)]w + [v_1v_2 - (d_1+v_1-c_1)(d_2+v_2)]M_2}.$$
 (45)

On differentiating  $x_O(w)$ , one finds that

$$\frac{d}{dw}x_O(w) < 0$$

for all parametric values, and therefore,

$$\inf_{w} x_{O}(w) = \lim_{w \to \infty} x_{O}(w)$$

$$= \frac{M_{1} \left[ (d_{1} + v_{1})(d_{2} + v_{2} - c_{2}) - v_{1}v_{2} \right]}{\left[ v_{1}v_{2} - (d_{1} + v_{1} - c_{1})(d_{2} + v_{2} - c_{2}) \right]}$$
(46)

680

T. DUMRONGPOKAPHAN et al.

and

$$\sup_{w} x_{O}(w) = x_{O}(w)|_{w=0} 
= \frac{\left[ (d_{1} + v_{1})(d_{2} + v_{2}) - v_{1}v_{2} \right] M_{1}}{\left[ v_{1}v_{2} - (d_{1} + v_{1} - c_{1})(d_{2} + v_{2}) \right]}.$$
(47)

In a similar manner, one can find

$$\inf_{w} z_O(w) = \frac{r_1}{\gamma_1 v_1} \left( 1 - \sup_{w} x_O(w) \right) \left( M_1(d_1 + v_1) + (d_1 + v_1 - c_1) \sup_{w} x_O(w) \right) \tag{48}$$

and

$$\sup_{w} z_{O}(w) = \frac{r_{1}}{\gamma_{1} \nu_{1}} \left( 1 - \inf_{w} x_{O}(w) \right) \left( M_{1}(d_{1} + \nu_{1}) + (d_{1} + \nu_{1} - c_{1}) \inf_{w} x_{O}(w) \right)$$
(49)

provided that (35) holds.

Moreover, we observe that the manifold h=0 intersects the (y,z)-plane along the line given by (36) whose slope is, for a given value of w,

$$\frac{\upsilon_2(w+M_2)}{(d_2+\upsilon_2-c_2)w+(d_2+\upsilon_2)M_2},$$

which has a minimum value when w = 0 of  $v_2/(d_2 + v_2)$ . However, the slope of the line where g=0 intersects the (y,z)-plane is found from (32) as  $(d_1+v_1)/v_1$ . Since

$$(d_1+\upsilon_1)(d_2+\upsilon_2) \ge \upsilon_1\upsilon_2$$

as long as  $d_1 > 0$  and  $d_2 > 0$ , the line where g = 0 intersects the (y, z)-plane is always above the one where h = 0 intersects that plane, as shown in Figure 2a.

The Manifold k=0. This consists of a trivial manifold w=0 and a nontrivial one given by the equation

$$z = \frac{r_2(w + M_2)}{\gamma_2(w + r_3)} \equiv Z_1(w), \tag{50}$$

whose graph is shown projected onto the (w, z)-plane in Figure 3. Since

$$\frac{d}{dw}Z_1(w) = \frac{r_2(r_3 - M_2)}{\gamma_2(w + r_3)^2},$$

which is negative if

$$r_3 < M_2, \tag{51}$$

one finds

and

$$\inf_{w} Z_{1}(w) = \lim_{w \to \infty} Z_{1}(w) = \frac{r_{2}}{\gamma_{2}}.$$
 (53)

We are now in the position to classify the different dynamic behavior exhibited by the system of equations (24)–(27).

CASE 1. This case is identified by inequalities (35), (41), (51), and the separation conditions

$$0 < \inf_{w} x_O(w) \quad \text{and} \quad \sup x_O(w) < x_M, \tag{54}$$

$$0 < \inf_{w} x_{O}(w) \quad \text{and} \quad \sup_{w} x_{O}(w) < x_{M},$$

$$\sup_{w} z_{m}(w) < \inf_{w} Z_{1}(w) \quad \text{and} \quad \sup_{w} Z_{1}(w) < \inf_{w} z_{M}(w),$$
(54)

681

with

$$0 < x_M < \hat{x} < 1, \tag{56}$$

where the infemum and supremum values are as given earlier in (39), (40), (43), (44), and (46)–(49). The inequalities in (54) are the separation conditions required in (16) and (17) of the above theorem, while (55) are those required in (18) and (19). As w varies with time, point O remains between the two stable branches of the curve f = h = 0 and the trajectory will develop into a closed limit cycle, as seen in Figure 2a, which slowly shifts its position with the slowly varying w.

Starting from a generic point, say point A in Figure 2a, a fast transition will develop towards point B on the manifold f=0. Here, g>0 and a transition at intermediate speed will be made in the direction of increasing y until point C on the curve f=g=0 is reached. A slow transition then follows along this curve to point D where the stability will be lost and a catastrophic transition will bring the system to point E on the other stable branch of f=0. Here, g<0 and a transition at intermediate speed will develop in the direction of decreasing y toward point F on the curve f=h=0. A slow transition then follows along f=h=0 until at some point m the stability of the submanifold will be lost. During this time, m will be increasing since m0 here, due to the first inequality in (55). A jump to point m1 followed by a slow transition brings the system to the bifurcation point m2. A catastrophic transition then brings the system to point m3 on the trivial manifold m4 on the trivial manifold m5 of during which time m6 will be decreasing since m6 of here, due to

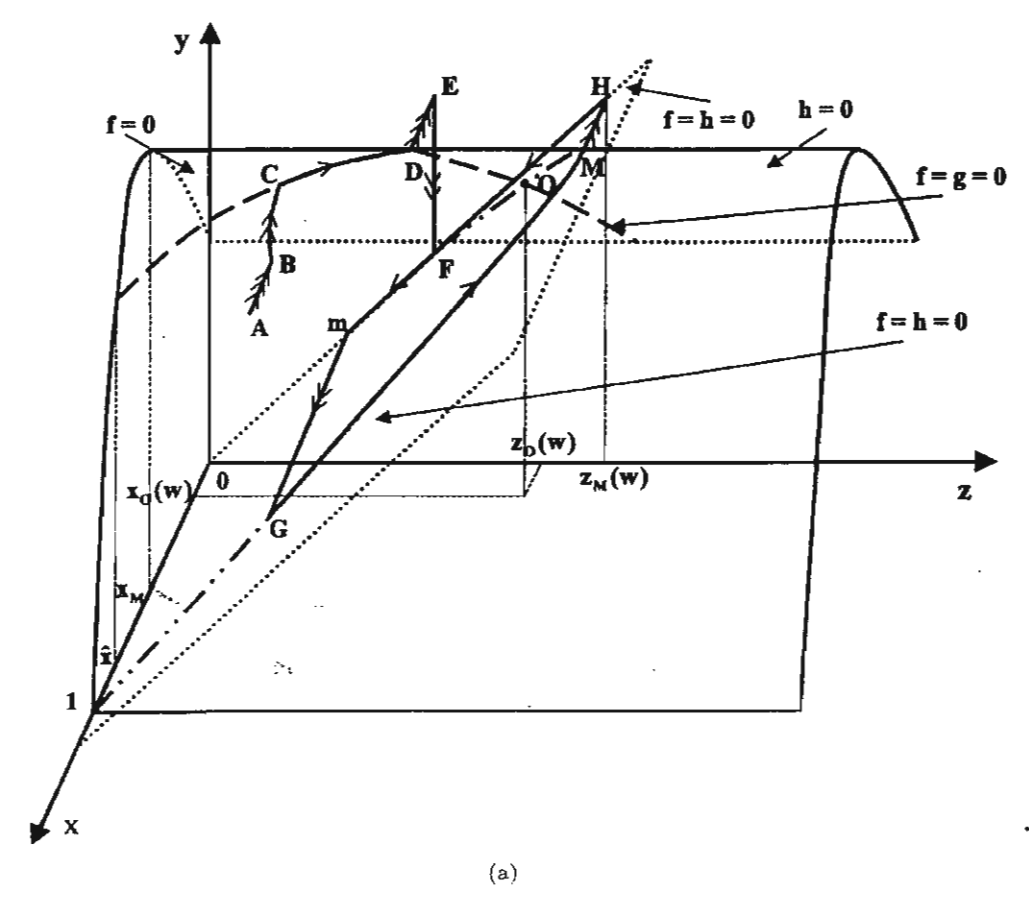
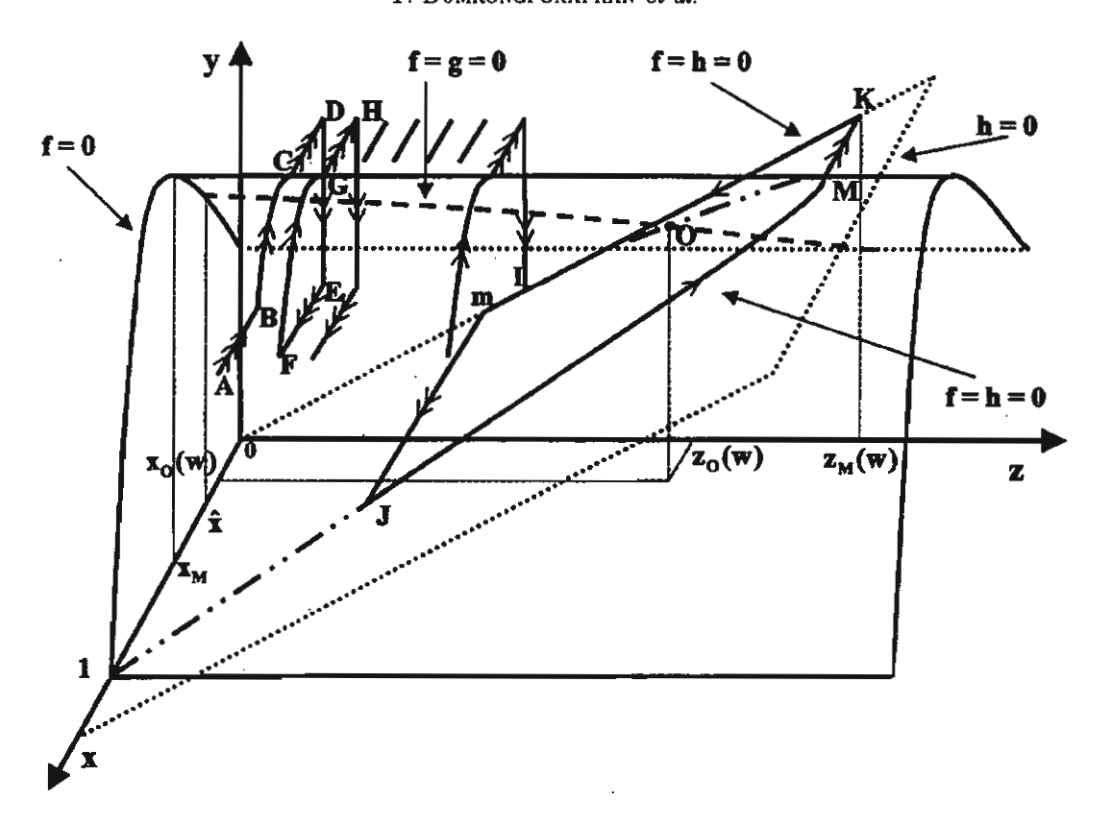
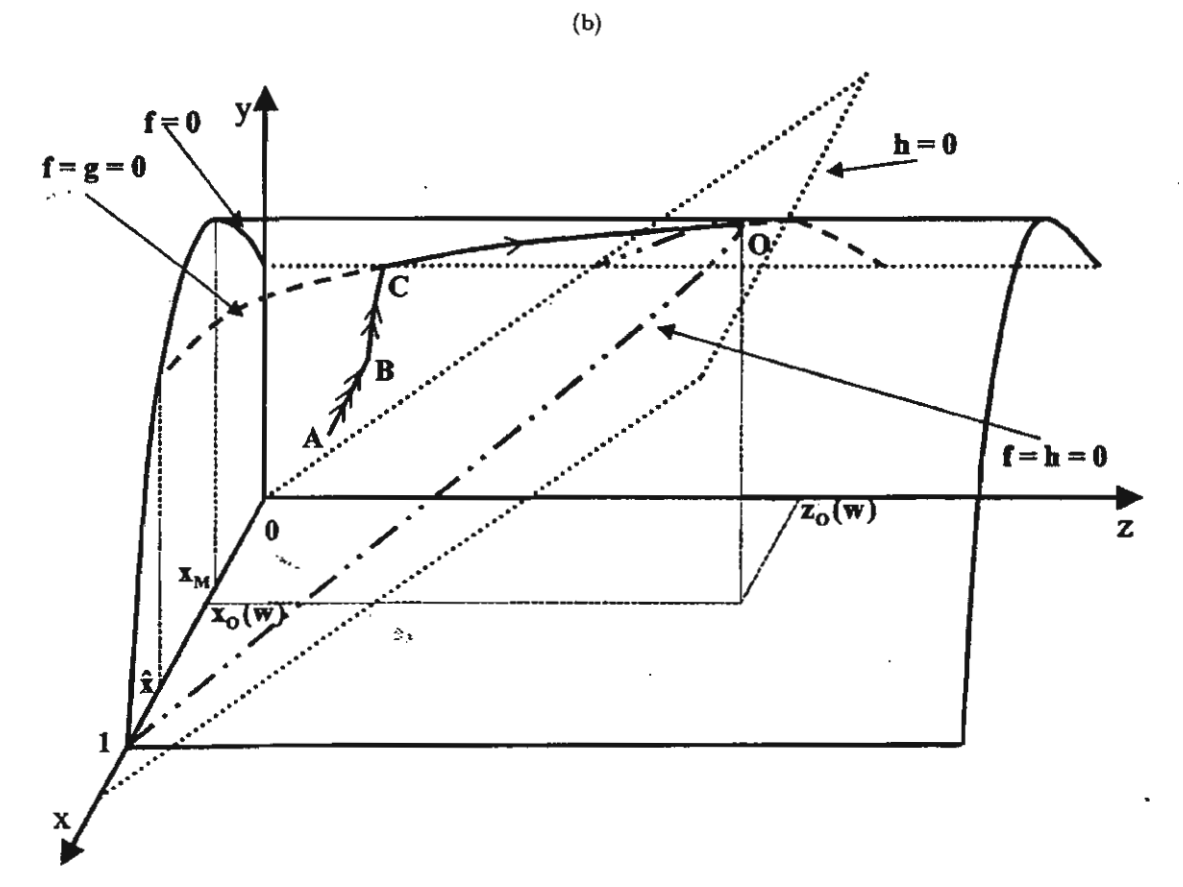


Figure 2. The three equilibrium manifolds f = 0, g = 0, and h = 0 in the (x, y, z)-space for a particular value of w, in the five cases identified in the text. The transitions develop into closed cycles in Figures 2a and 2b, approach the stable equilibrium point O in the positive octant in Figures 2c and 2c, and approach the washout steady state (x, y, z) = (1, 0, 0) in Figure 2d.

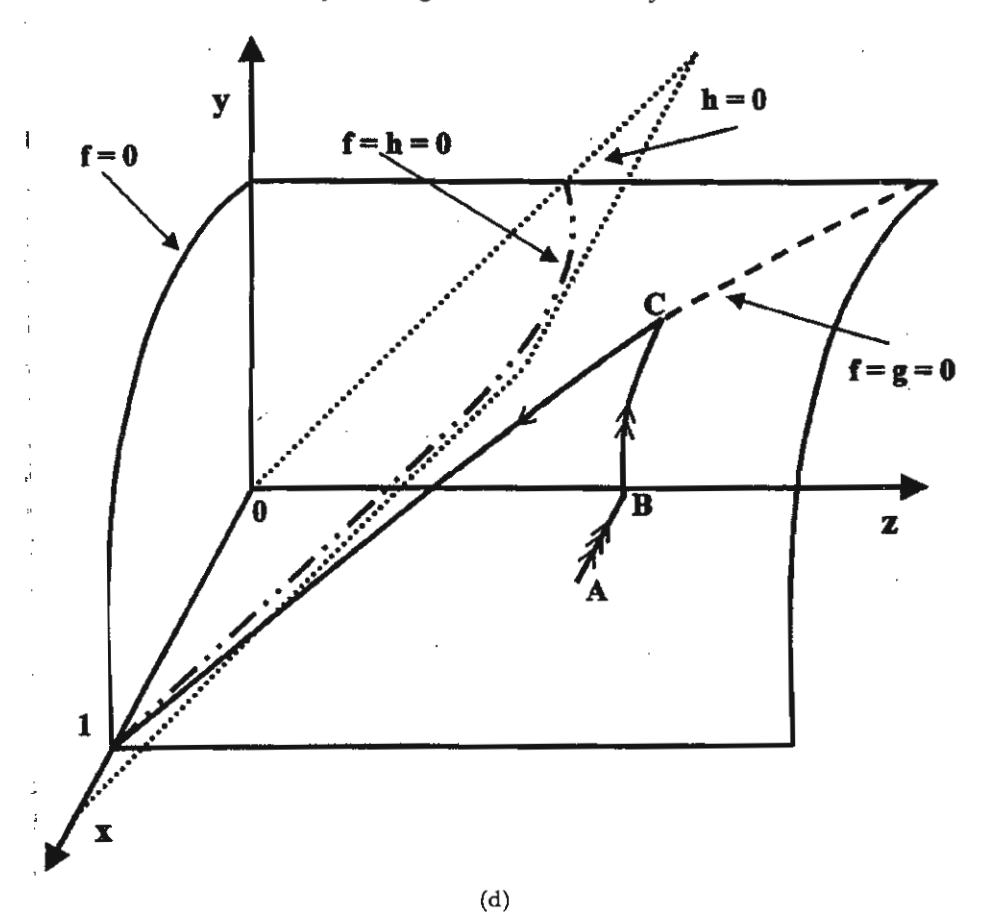
#### T. DUMRONGPOKAPHAN et al.





(c)

Figure 2. (cont.)



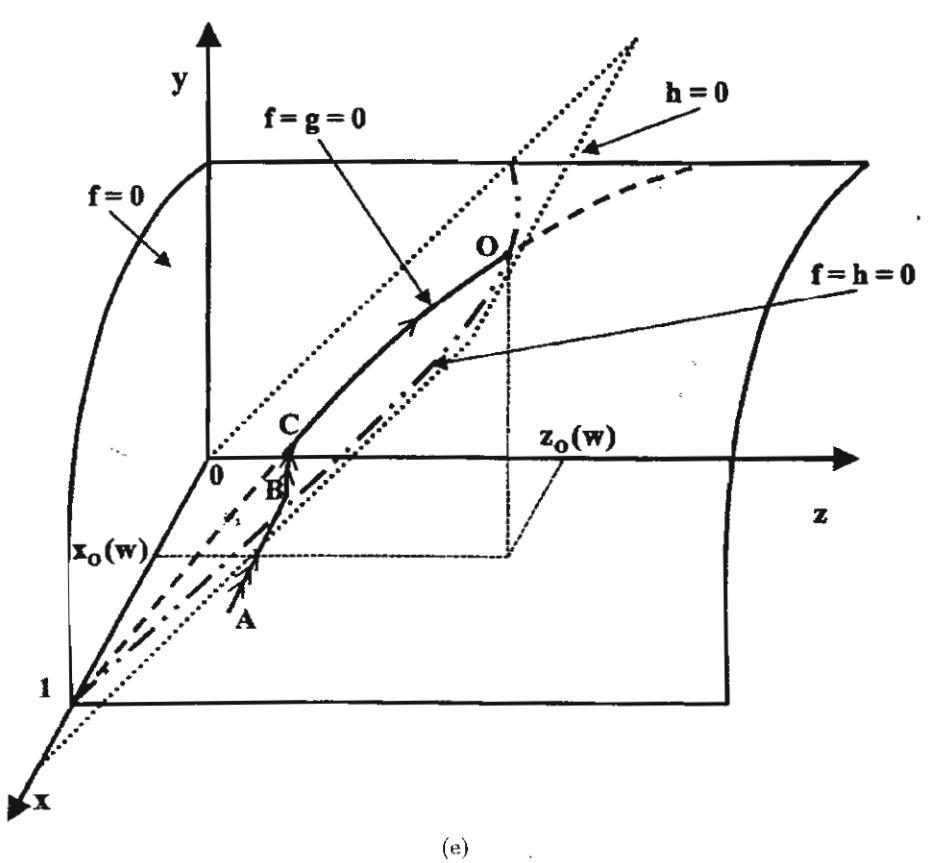


Figure 2. (cont.)

the second inequality in (55). A slow transition will now develop to point m which closes up the cycle mGMHm and thereby a limit cycle has been identified.

CASE 2. In this case, inequalities (35), (41), (51), (54), and (55) still hold, while (56) is now violated and

$$0 < \hat{x} < x_M. \tag{57}$$

The relative positions of the manifolds f = 0, g = 0, and h = 0 are as shown in Figure 2b, slowly shifting with time.

The transition will develop from point A in Figure 2b to B as before. However, a transition at intermediate speed from B will continue upward until the bifurcation point C is reached, where a catastrophic transition will bring the system to point D on the trivial manifold x=0. A transition at intermediate speed follows downward until the stability is lost at some point E and a quick jump takes the system to point E on the other stable branch of E which almost closes up the cycle. However, E has been varying slowly and so point E just misses E and the transition continues upward to point E, then to E and so on, until a point E on the curve E is reached, from which point the transitions will trace out a closed cycle in the same manner as in Case 1.

CASE 3. In this case, inequalities (35), (41), (51), and (56) hold, while the separation condition (54) is violated and we have instead that

$$0 < x_M < \inf_{w} x_O(w). \tag{58}$$

The trajectory will develop as in Case 1, initially. However, since now point O (in Figure 2c) is located on the stable branch of f = 0, the transition from point C on f = g = 0 will first reach point O where f = g = h = 0.

Considering the manifold k = 0 projected onto the (w, z)-plane in Figure 3, we see that w may behave in three different manners. First, if it is further required that

$$\inf_{w} z_O(w) > \sup_{w} Z_1(w) = \frac{r_2 M_2}{\gamma_2 r_3}.$$
 (59)

Then the trajectory eventually stays in the region where  $\dot{w} < 0$  and w tends to zero as time passes. Thus, this is the case where the predators can persist on the supply of only one prey pop-

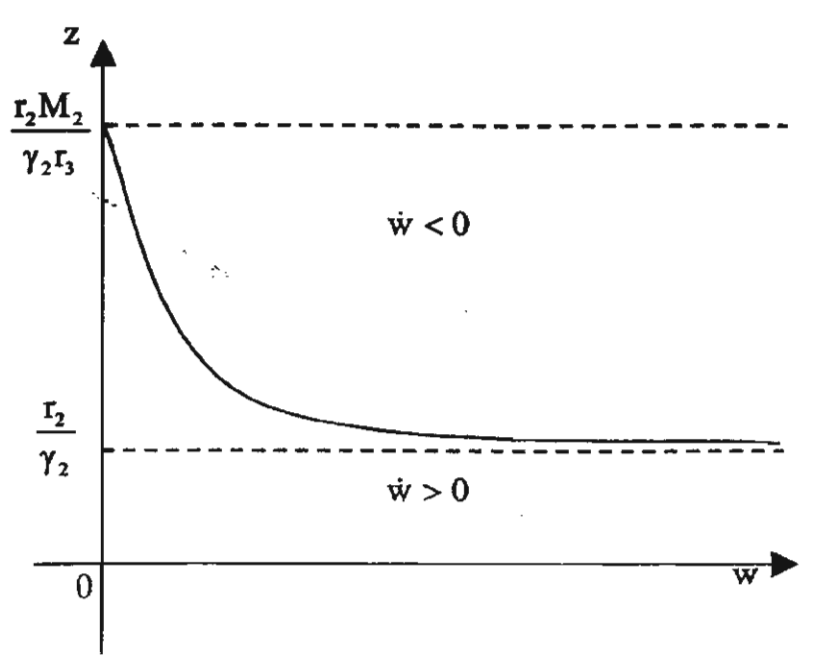


Figure 3. The graph of the manifold k = 0 projected on the (w, z)-plane.

ulation in one community. The mechanism of migration into the other community can be taken as hibernation or fasting periods during which some predators choose abstinence to insure survival. Second, if it is required, on the other hand, that

$$\sup_{w} z_{O}(w) < \inf_{w} Z_{1}(w) = \frac{r_{2}}{\gamma_{2}}, \tag{60}$$

then the trajectory eventually stays in the region where  $\dot{w} > 0$  and we will find that w increases unboundedly as time passes.

Finally, if we require

$$\frac{r_2}{\gamma_2} < \inf_{w} z_O(w) \quad \text{and} \quad \sup_{w} z_O(w) < \frac{r_2 M_2}{\gamma_2 r_3}$$
 (61)

instead of inequality (59) or (60), then it is guaranteed that w will tend towards a stable nonzero equilibrium value on the manifold k = 0. This is then the case where all four populations persist at constant levels.

CASE 4. If inequalities (35), (51), and (60) hold, but

$$\hat{x} > 1, \tag{62}$$

then we must have  $x_M < 0$  as well, from considering equations (30) and (34). We also note that the curve f = h = 0 can be shown to be concave up, while f = g = 0 is concave down as z increases along the surface f = 0. Therefore, the two curves will not intersect at a point where z > 0 if we make sure that the curve f = h = 0 is steeper than f = g = 0 at the point z = 0, namely, we need to require

$$(M_1+1)(d_1+\nu_1)-c_1>\frac{\nu_1\nu_2(M_1+1)}{d_2+\nu_2}. (63)$$

Then, the three manifolds are positioned as shown in Figure 2d and the transitions will develop from the starting point A to point C on f=g=0 as before. Here, however, h<0 and so a slow transition will develop downward in the direction of decreasing z to end at the equilibrium point (x,y,z)=(1,0,0) where f=g=h=0. Thus, in this case the predator populations vanish in both communities. Prey in the first community eventually reaches the steady level 1, and prey in the second one increases unboundedly since  $\dot{w}>0$  once z=0.

CASE 5. On the other hand, if, apart from (35), (51), and (62), we also have

$$(M_1+1)(d_1+\upsilon_1)-c_1<\frac{\upsilon_1\upsilon_2(M_1+1)}{d_2+\upsilon_2},$$
(64)

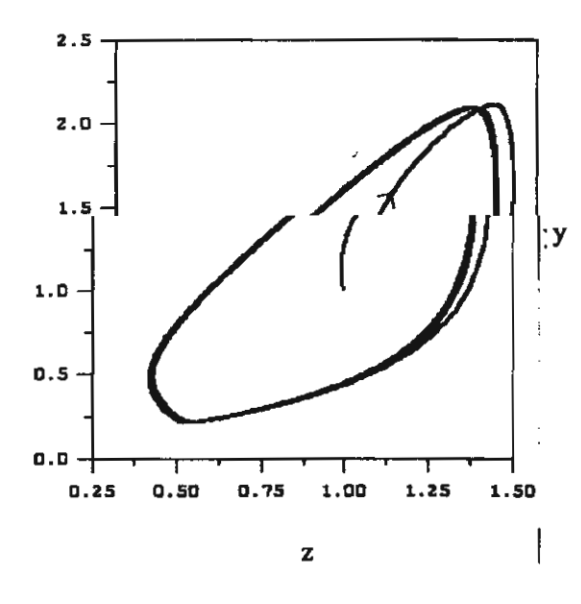
then the curve f = g = 0 is steeper than f = h = 0 at the point z = 0, and they will intersect at some point where z > 0 as shown in Figure 2c. The trajectory will, therefore, develop in the same manner as in Case 3: The populations x, y, and z tend toward steady positive levels, while w either vanishes, establishes a positive constant level, or becomes unbounded, depending on whether inequality (59), (60), or (61) holds, respectively.

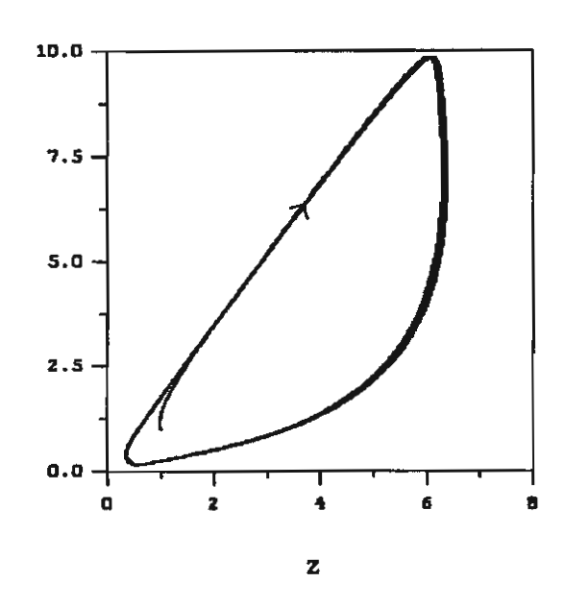
#### DISCUSSION AND CONCLUSION

We present, in Figure 4, a computer simulation of system (24)–(27) with parametric values chosen to satisfy the delineating conditions in Cases 1–5 described above. Figures 4a–4e show the solution trajectories projected onto the (z, y)-plane, corresponding to Cases 1–5, identified earlier, respectively. The numerical results are in agreement with our theoretical predictions.

Figure 5 shows the corresponding time courses of the state variables in each of the five cases shown in Figure 4. The population levels are seen to develop into sustained oscillations in Cases 1

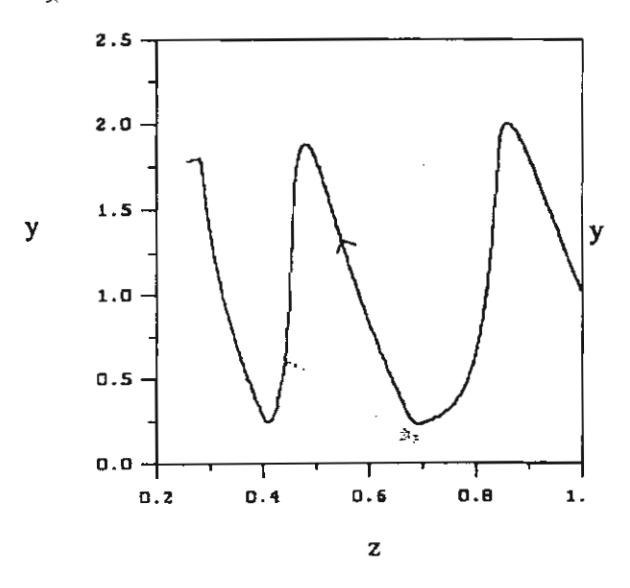
and 2 (Figures 5a and 5b, respectively), and tend toward steady-state levels in Cases 3 and 5 (Figures 5c and 5e, respectively). Case 5 is shown here with (60) being satisfied and all four populations persist, while Case 3 is shown here with inequality (59) being satisfied, and only the first three populations persist, while prey in the second community becomes extinct eventually. Inequality (59) may be interpreted to say that even the lowest value of  $z_O$ , the level of predators in the second community, at the point where f = g = 0, below which the levels of both predators

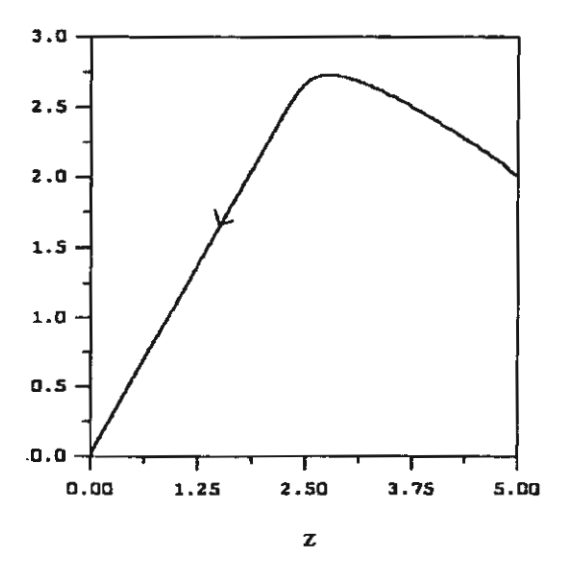




(a)  $c_1 = 0.8$ ,  $c_2 = 0.075$ ,  $d_1 = 0.5$ ,  $d_2 = 0.3$ ,  $\gamma_1 = 1$ ,  $\gamma_2 = 3$ ,  $M_1 = 0.1$ ,  $M_2 = 2$ ,  $r_1 = 6$ ,  $r_2 = 2$ ,  $r_3 = 1$ ,  $v_1 = 0.2$ ,  $v_2 = 2$ ,  $\varepsilon = 1$ ,  $\delta = 0.1$ ,  $\eta = 0.5$ , x(0) = 1.2, y(0) = 1, z(0) = 1, and w(0) = 1.

(b)  $c_1 = 0.7$ ,  $c_2 = 0.1$ ,  $d_1 = 0.5$ ,  $d_2 = 0.3$ ,  $\gamma_1 = 0.2$ ,  $\gamma_2 = 1$ ,  $M_1 = 0.05$ ,  $M_2 = 3$ ,  $r_1 = 6$ ,  $r_2 = 2$ ,  $r_3 = 2$ ,  $v_1 = 0.1$ ,  $v_2 = 2$ ,  $\varepsilon = 1$ ,  $\delta = 0.1$ ,  $\eta = 0.5$ , x(0) = 1.2, y(0) = 1, z(0) = 1, and w(0) = 1.

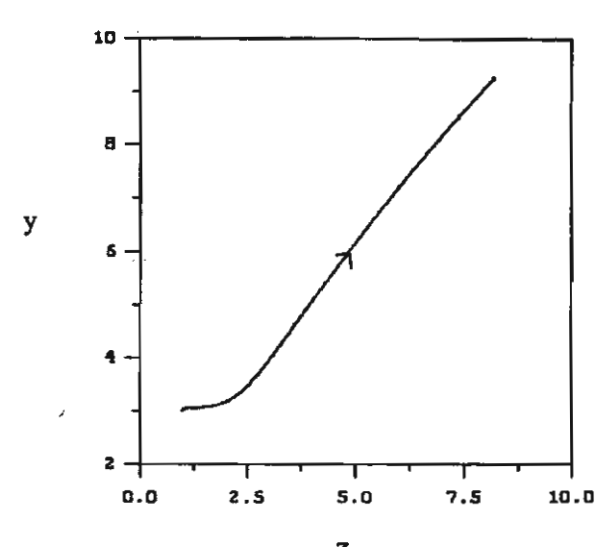




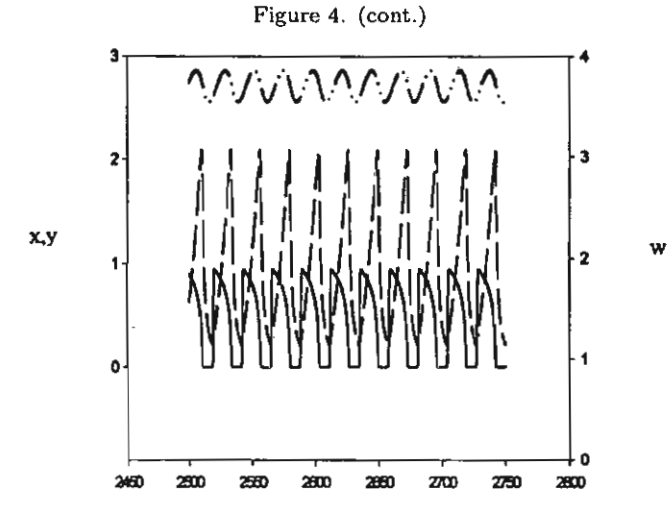
(c)  $c_1 = 0.8$ ,  $c_2 = 0.075$ ,  $d_1 = 0.5$ ,  $d_2 = 0.3$ ,  $\gamma_1 = 1$ ,  $\gamma_2 = 3$ ,  $M_1 = 0.1$ ,  $M_2 = 2$ ,  $r_1 = 6$ ,  $r_2 = 0.3$ ,  $r_3 = 1$ ,  $v_1 = 0.2$ ,  $v_2 = 0.05$ ,  $\epsilon = 1$ ,  $\delta = 0.1$ ,  $\eta = 0.5$ , x(0) = 1.2, y(0) = 1, z(0) = 1, and w(0) = 1.

(d)  $c_1=0.43,\ c_2=0.075,\ d_1=0.1,\ d_2=0.3,\ \gamma_1=1,\ \gamma_2=3,\ M_1=3,\ M_2=8,\ r_1=6,\ r_2=15,\ r_3=1,\ \upsilon_1=0.1,\ \upsilon_2=2,\ \varepsilon=1,\ \delta=0.1,\ \eta=0.5,\ x(0)=2,\ y(0)=2,\ z(0)=5,\ {\rm and}\ w(0)=1.$ 

Figure 4. Computer simulations of the model equations (26)-(29) in the five cases mentioned in Figure 2. The simulation results agree with our theoretical prediction set out in Figure 2.



(e)  $c_1=0.7,\ c_2=0.075,\ d_1=0.1,\ d_2=0.3,\ \gamma_1=1,\ \gamma_2=3,\ M_1=3,\ M_2=8,\ r_1=6,\ r_2=15,\ r_3=1,\ v_1=0.1,\ v_2=2,\ \varepsilon=1,\ \delta=0.1,\ \eta=0.5,\ x(0)=2,\ y(0)=3,\ z(0)=1,\ {\rm and}\ w(0)=1.$ 



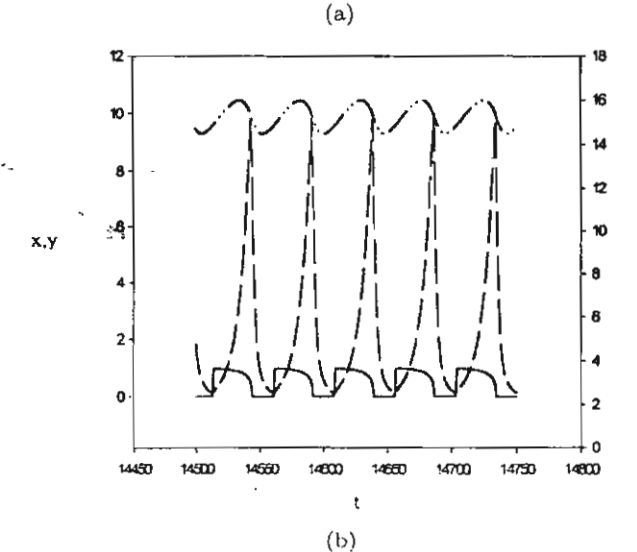
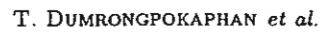


Figure 5. The time courses of three populations  $\pi(t)$ , y(t), and w(t) in the corresponding five cases shown in Figure 4.



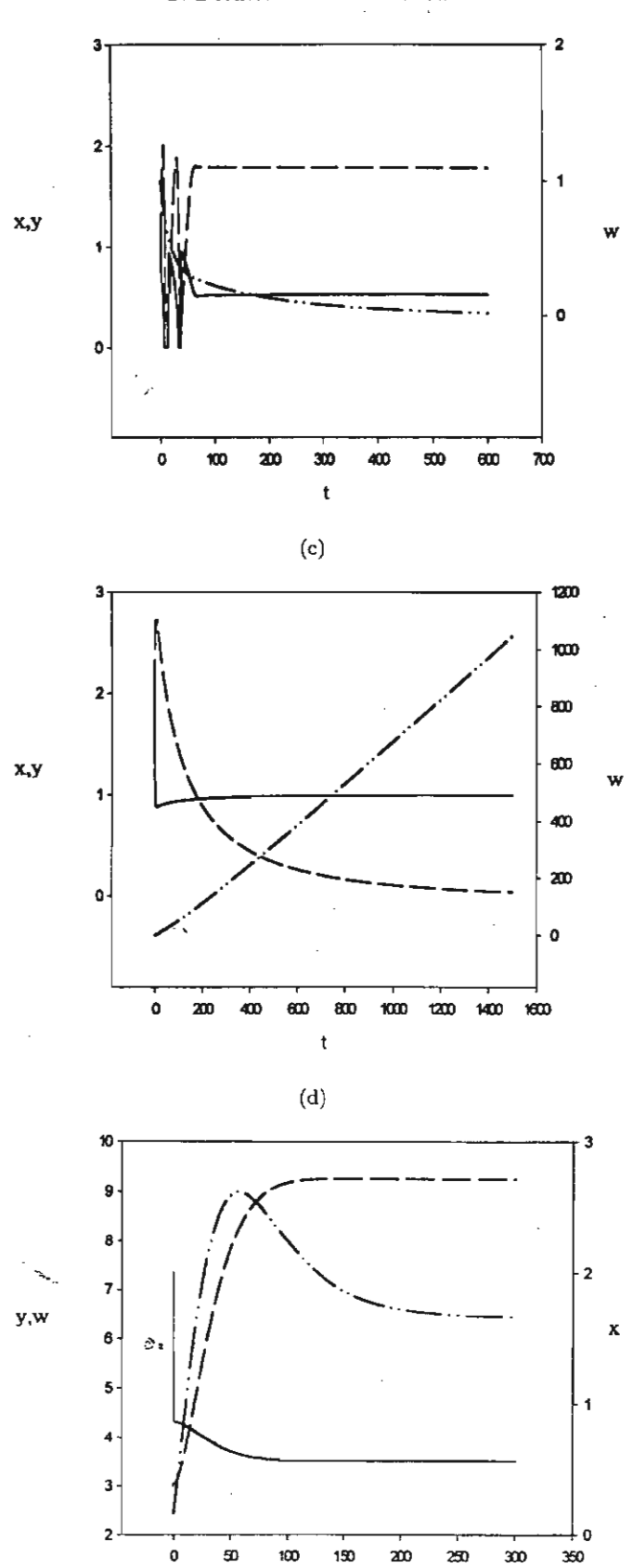


Figure 5. (cont.)

(e)

t

must be rising, is still too high to be sustainable by the preys in the second community, whose slow dynamics then drive them to extinction. Thus, to ensure survival in this case, some predators migrate out of the community or, equivalently, escape into hibernation when sustenance is low in that community.

The separation conditions in (54) for sustained oscillation may be interpreted as follows. The value  $y_M$  is the highest possible level of predators in the first community, above which the level of prey x in that community must decline (f < 0). On the other hand,  $y_O$  is the level of predators, at the point where f = g = h = 0, above which the levels of prey x and predators y must decline while z begins to rise. The level  $x_M$  of prey in the first community, which sustains the first event, must be high enough to exceed the level  $x_O$ , which sustains the latter, over all levels of prey w in the second community. The first inequality in (55) may be interpreted as follows. The value  $Z_1(w)$  is the level of predators in the second community below which the level of prey w must rise (k > 0). On the other hand,  $z_m(w)$  is the level of predators in the second community below which its level must begin to rise when there is no prey in the first community (x = 0). The levels of  $Z_1$ , over all w, must exceed the levels of  $z_m$  over all w. A similar interpretation can be made of the second inequality in (55).

Moreover, the requirement that  $Z_1(w)$  is bounded above simply means that there should be an upper bound for the levels of predators above which the prey population density in the second community must begin to decline  $(\dot{w} < 0)$ . Similarly, the condition that  $Z_1(w)$  should be bounded below by a positive number means that there must be a positive level of predators below which point the prey population density, whatever it is, must be increasing  $(\dot{w} > 0)$ .

If the requirements stated above are satisfied, then the surrounding conditions are suitable for sustained oscillations in all four persisting populations. Field data which exhibits oscillatory behavior in connection with migration have often been reported [9,10].

We further note that extinction of predators in both communities is discovered in this system in Case 4 when  $\hat{x} > 1$  and (63) holds as presented in Figure 5d. Considering the value of  $\hat{x}$  given by (34),  $\hat{x}$  will be less than one if

$$d_1 + \upsilon_1 < \frac{c_1}{M_1 + 1}. (65)$$

This means that, to keep from extinction, the predators in the first community must keep the death and migration rates from being too high.

On the other hand, for persistence and stability in the case that  $\hat{x} < 1$ , we need inequality (41) to hold for the existence of a positive attractor to be assured. This inequality can be satisfied if the migration constant  $v_2$  is large enough while the death rate  $d_2$  can still be low. Thus, migration must be balanced in a proper way to achieve sustainability. In the case that  $v_1 = v_2 = v$ , then (41) and (65) lead to the requirement that

$$c_2 - d_2 < v < \frac{c_1 - d_1(M_1 + 1)}{M_1 + 1},$$

which gives the bounds for the migration rate v to keep the populations from extinction.

We have, thus, demonstrated the crucial role of migration, variation in reproductive rates, foraging success, and mortality as a mechanism which effects population survival, by the application of the higher-dimensional separation conditions, which in this case pivots about the slow component. Field data has been reported [7,11] which strongly suggests that increasing the number of interacting population, and thus, migration rates, slows down the tendency to extinction. In trying to model such a multipopulated system, the separation conditions can then become more complex. There are several sophisticated computer programs, however, which can render the calculations of bounds and parametric values easy to accomplished. Studies of several other cascade systems may be undertaken through similar analyses which invariably yield valuable insights into the systems under sindy.

#### T. DUMRONGPOKAPHAN et al.

#### REFERENCES

- 1. A.W. Norman and G. Litwack, Hormones, Second Edition, pp. 8-9, Academic Press, San Diego, CA, (1997).
- S. Muratori and S. Rinaldi, Low- and high-frequency oscillations in three-dimensional food chain systems, Siam J. Appl. Math. 52, 1688-1706, (1992).
- S. Muratori and S. Rinaldi, A separation condition for the existence of limit cycles in slow-fast systems, Appl. Math. Modelling 15, 312-318, (1991).
- Y. Lenbury, R. Ouncharoen and N. Tumrasvin, Higher dimensional separation principle for the analysis
  of relaxation oscillations in nonliner systems: Application to a model of HIV infection, IMA Journal of
  Mathematics Applied in Medicine and Biology 17, 243-261, (2000).
- 5. H. Matsumoto and H. Seno, On predator invasion into multi-patchy environment of two kinds of patches, *Ecological Modelling* 79, 131-147, (1995).
- H. Whitehead, Variation in the feeding success of sperm whales: Temporal scale, spatial scale and relationship to migrations, Journal of Animal Ecology 65, 429-438, (1996).
- S.J. Walde, Immigration and the dynamics of a predator-prey interaction in biological control, Journal of Animal Ecology 63, 337-346, (1994).
- 8. T.W. Sherry and R.T. Holmes, Winter habitat quality, population limitation, and conservation of neotropical-nerctic migrant birds, *Ecology* 77, 36-48, (1996).
- 9. F.J. Ebling, A.D. Hawkins, J.A. Kitching, L. Muntz and V.M. Pratt, The ecology of Lough Ine XVI. Predation and diurnal migration in the paracentrotus community, *Journal of Animal Ecology* 35, 559-566, (1966).
- 10. J.E. Diffendorfer, M.S. Gaines and R.D. Holt, Habitat fragmentation and movements of three small mammals (sigmodon, microtus, and peromyscus), *Ecology* 73, 827-839, (1995).
- 11. B.W. Dale, L.G. Adams and R.T. Bowyer, Functional response of wolves preying on barren-ground caribou in a multiple-prey ecosystem, *Journal of Animal Ecology* 63, 644-652, (1994).

Ó٦



## Available online at www.sciencedirect.com

J. Math. Anal. Appl. 305 (2005) 631-643

Journal of
MATHEMATICAL
ANALYSIS AND
APPLICATIONS

www.elsevier.com/locate/jmaa

### Delay effect in models of population growth

Dang Vu Giang a, Yongwimon Lenbury b,\*, Thomas I. Seidman c

<sup>a</sup> Hanoi Institute of Mathematics, 18 Hoang Quoc Viet, 10307 Hanoi, Viet Nam
<sup>b</sup> Department of Mathematics, Faculty of Science, Mahidol University, Rama 6 Road,

Bangkok 10400, Thailand

<sup>c</sup> Department of Mathematics and Statistics, University of Maryland Baltimore County,
Baltimore, MD 21250, USA

Received 29 June 2004

Available online 20 January 2005

Submitted by P.G.L. Leach

#### Abstract

First, we systematize earlier results on the global stability of the model  $\dot{x} + \mu x = f(x(\cdot - \tau))$  of population growth. Second, we investigate the effect of delay on the asymptotic behavior when the nonlinearity f is a unimodal function. Our results can be applied to several population models [Elements of Mathematical Ecology, 2001 [7]; Appl. Anal. 43 (1992) 109–124; Math. Comput. Modelling, in press; Funkt. Biol. Med. 256 (1982) 156–164; Math. Comput. Modelling 35 (2002) 719–731; Mat. Stos. 6 (1976) 25–40] because the function f does not need to be monotone or differentiable. Specifically, our results generalize earlier result of [Delay Differential Equations with Applications in Population Dynamics, 1993], since our function f may not be differentiable. © 2004 Elsevier Inc. All rights reserved.

Keywords: Delay differential equations; Comparison theorem; ω-limit set of a persistent solution; One-parameter semi-group; Convergence to equilibrium; Nicholson's blowfly model; Periodic solutions

<sup>\*</sup> Corresponding author.

E-mail addresses: dangvugiang@yahoo.com (D.V. Giang), scylb@mucc.mahidol.ac.th (Y. Lenbury), seidman@math.umbc.edu (T.I. Seidman).

 <sup>0022-247</sup>X/\$ – see front matter © 2004 Elsevier Inc. All rights reserved. doi:10.1016/j.jmaa.2004.12.018

#### 1. Introduction

Given a continuous function  $f: \mathbb{R}_+ \to \mathbb{R}_+$  and a nonnegative function  $\xi \neq 0$  on  $[-\tau, 0]$ , we consider the delay differential equation

$$\dot{x} + \mu x = f(x(\cdot - \tau)), \qquad x(s) = \xi(s) \quad \text{for } s \in [-\tau, 0]. \tag{1.1}$$

For simplicity, we assume throughout that  $\xi$  is bounded. It follows that (1.1) has a unique solution—e.g., one can proceed by intervals of length  $\tau$ —with  $x_{f,\xi}(\cdot)$  nonnegative and continuous for  $t \ge 0$ . We denote the solution of the delay differential equation (1.1) by  $x(\cdot) = x_{f,\xi}(\cdot)$ . It is easily seen that one has the equivalent integrated formulation:

$$x(t) = e^{-\mu(t-a)}x(a) + \int_{a}^{t} e^{-\mu(t-s)} f(x(s-\tau)) ds$$
 (1.2)

for  $t \ge 0$ . (Actually, continuity of f is not needed for (1.2), only enough regularity to ensure the requisite integrability.) We further note the following

**Lemma 1.** Given real constants  $\mu$ ,  $\nu$  and  $\tau > 0$ , there is a function X = X(t) such that the solution y of the autonomous linear delay differential equation

$$\dot{y} + \mu y + \nu y(t - \tau) = g(t), \quad y|_{[-\tau,0]} = \eta,$$
 (1.3)

has the integral representation

$$y(t) = y_0(t; \eta) + \int_0^t X(t - s)g(s) ds,$$
 (1.4)

where  $y_0 = y_0(\cdot; \eta)$  is the solution of the associated homogeneous initial value problem. Both  $X(\cdot)$  and  $y_0$  decay exponentially if

$$h(z) := z + \mu + \nu e^{-\tau z} = 0 \quad \Rightarrow \quad \Re(z) < 0,$$
 (1.5)

i.e., if every root of the characteristic equation has (strictly) negative real part, and grow exponentially if  $h(\cdot)$  has any root with positive real part.

Proof. See, e.g., [6]. Note that

$$||X||_1 = \int_0^\infty |X(t)| dt < \infty \tag{1.6}$$

when X decays exponentially.  $\square$ 

A standard calculation shows that (1.5) holds for all  $\tau > 0$  when  $|\nu| < \mu$  and, conversely, fails when  $|\nu| > \mu$  unless  $\tau$  is restricted so that

$$\tau < \tau_* = \tau_*(\mu, \nu) = \frac{\arccos[-\mu/\nu]}{\sqrt{\nu^2 - \mu^2}}$$
 (1.7)

(cf., e.g., [1,5]). We will later focus our attention on delay equations of the form (1.1) in which the nonlinearity f satisfies:

- $\bullet f: \mathbb{R}_+ = [0, \infty) \to \mathbb{R}_+$  is continuous.
- There is a unique equilibrium  $\hat{r} > 0$ , so  $\mu \bar{r} = f(\bar{r}) > 0$ .

$$\bullet \begin{cases} f(r) > \mu r & \text{for } 0 < r < \hat{r}, \\ f(r) < \mu r & \text{for all } r > \bar{r}. \end{cases}$$
(1.8)

#### 2. Comparison theorem and consequences

An easy argument then provides the following basic comparison theorem.

**Theorem 2.** Let  $f, \xi$  and correspondingly  $g, \eta$  be as above with g nondecreasing. Set  $x := x_{f,\xi}$  and  $y := x_{g,\eta}$ .

- (1) Suppose  $f \leq g$  where relevant (i.e.,  $f(r) \leq g(r)$  for each r in the range of f(x)) and suppose  $\xi \leq \eta$  on  $[-\tau, 0]$ . Then  $x(t) \leq y(t)$  for all t.
- (2) Suppose  $f \ge g$  where relevant and  $\xi \ge \eta$  on  $[-\tau, 0]$ . Then  $x(t) \ge y(t)$  for all t.

**Proof.** Both cases go in essentially the same fashion, so we only consider the first case (with  $f \leq g$ , etc.). Now suppose the result were false. We could then find a largest  $t_*$  such that  $x(s) \leq y(s)$  on  $[-\tau, t_*)$ . For any  $t < t_* + \tau$  we would have  $r = t - s - \tau < t_*$  for  $0 \leq s < t$  whence  $x(r) \leq y(r)$  for such r so  $f(x(r)) \leq g(x(r)) \leq g(y(r))$ . It follows from (1.2) and the corresponding integrated formulation involving g that  $x(t) \leq y(t)$  for such  $t \in [t_*, t_* + \tau)$  as well, contradicting the definition of  $t_*$ .  $\square$ 

We remark that this comparison theorem generalizes to equations in partially ordered Banach spaces, etc., but we do not pursue this here.

**Corollary 3.** Let  $f, \xi, x$  be as above in (1.1).

- (1) Suppose there is some M > 0 such that  $f(r) \le \mu \max\{r, M\}$  and suppose  $x \le M$  on  $[t_* \tau, t_*]$ . Then, also  $x(t) \le M$  for all  $t \ge t_*$ .
- (2) Suppose there is some m > 0 such that  $f(r) \ge \mu \min\{r, m\}$  and suppose  $x \ge m$  on  $[t_* \tau, t_*]$ . Then, also  $x(t) \ge m$  for all  $t \ge t_*$ .

**Proof.** Again, both cases go in essentially the same fashion so we need only consider the first. Further, since we can restart at any  $t_*$  it is sufficient to consider  $t_* = 0$  so we may assume  $\xi \leq M$  on  $[-\tau, 0]$ .

Take  $\eta \equiv M$  and  $g(r) := \mu \max\{r, M\}$ . Clearly, g is nondecreasing and the hypotheses yield  $\xi \leqslant \eta$  and  $f \leqslant g$ . We immediately verify that  $y \equiv M$  satisfies the delay differential equation to have  $y = x_{g,\eta}$  so that the result follows from Theorem 2.  $\square$ 

We will be seeking asymptotic upper and lower bounds for solutions x(t) of (1.1) and to this end it is convenient to introduce

$$\tilde{m} = \tilde{m}(x) = \liminf_{t \to \infty} x(t), \qquad \tilde{M} = \tilde{M}(x) = \limsup_{t \to \infty} x(t).$$
 (2.1)

**Lemma 4.** Let f be bounded with  $0 < f(r) \le B$ . Then  $\overline{M} \le B/\mu$ .

**Proof.** From (1.2) we have

$$x(t) \le e^{-\mu t} x(0) + \int_{-\tau}^{t} B e^{-\mu(t-s)} ds,$$

which gives the desired result as  $t \to \infty$ .  $\square$ 

We also note some information about the  $\omega$ -limit set of a nontrivial solution x, e.g., as used in [10].

**Lemma 5.** For any bounded solution  $x = x_{f,\xi}$  of (1.1), there are functions u, v defined on  $\mathbb{R}$  such that

- (i) u, v satisfy (1.1) on  $\mathbb{R}$ .
- (ii)  $\bar{m} \leq u(t), v(t) \leq \bar{M}$ .

(iii) 
$$u(0) = \bar{M}, \quad \dot{u}(0) = 0; \quad v(0) = \hat{m}, \quad \dot{v}(0) = 0,$$
 (2.2)

with  $\bar{m} = \bar{m}(x)$ ,  $\bar{M} = \bar{M}(x)$  as in (2.1).

For completeness, we sketch a proof here.

**Proof.** By the definition of  $\bar{M}$  there is a sequence  $t_k \to \infty$  such that  $x(t_k) \to \bar{M}$  and we set  $u_k(t) = x(t_k + t)$ —e.g., for  $t \ge -t_k$ . The set  $\{u_k(\cdot)\}$  is uniformly bounded with uniformly bounded derivatives, so there is a function u such that  $u_k \to u$  uniformly on compact sets in  $\mathbb{R}$ . Since the derivatives also converge uniformly on compact subsets and each  $u_k$  satisfies (1.1), so does u. Since, for compact set  $\mathcal{I}$  and any  $\varepsilon > 0$ , the definition of  $\bar{M}$  gives  $\bar{m} - \varepsilon < u_k < \bar{M} + \varepsilon$  for large enough k, we have (ii) in the limit. Since  $u_k(0) = x(t_k) \to \bar{M}$ , we have  $u(0) = \bar{M}$  and, as that is necessarily a maximum, we also have  $\dot{u}(0) = 0$ . The construction of  $v(\cdot)$  is similar.  $\square$ 

#### 3. Asymptotic bounds and attraction

**Theorem 6.** Let f,  $\xi$ , and x be as above in (1.1).

(1) Suppose there is some  $\bar{r} \geqslant 0$  such that

$$f(r) \leq \mu \bar{r}$$
 for  $0 < r \leq \bar{r}$ ,  
 $f(r) < \mu r$  for all  $r > \bar{r}$ . (3.1)

Then,  $\bar{M} \leqslant \bar{r} < \infty$  and there is a nonincreasing positive function  $z_+$  such that

$$x(t) := x_{f,\xi}(t) \leqslant z_{+}(t) \quad \text{with } z_{+}(t) \to \bar{r} \text{ as } t \to \infty.$$
 (3.2)

(2) Suppose there is some  $\bar{r} \geqslant 0$  such that

$$f(r) \geqslant \mu \bar{r}$$
 for  $r \geqslant \bar{r}$ ,  
 $f(r) > \mu r$  for all  $0 < r < \bar{r}$ . (3.3)

Then,  $\tilde{m} \geqslant \tilde{r}$  and there is a nondecreasing nonnegative function  $z_{-}$  such that

$$x(t) := x_{f,\xi}(t) \geqslant z_{-}(t) \quad \text{with } z_{-}(t) \to \tilde{r} \text{ as } t \to \infty.$$

$$(3.4)$$

**Proof.** Yet again, both cases go in essentially the same fashion. For the first case we begin by fixing  $M > \bar{r}$ ,  $M \ge \xi$ , and any  $\varepsilon = \varepsilon_0 > 0$  with  $\bar{r} + \varepsilon < M$ . We then let

$$\gamma_{\varepsilon} := \max\{f(r)/r \colon \bar{r} + \varepsilon \leqslant r \leqslant M\} < \mu \tag{3.5}$$

and, choosing  $\gamma$  so  $\gamma_{\varepsilon} \leqslant \gamma < \mu$ , set

$$g(r) = g_{\varepsilon}(r) := \max \{ \mu(\bar{r} + \varepsilon), \gamma r \}. \tag{3.6}$$

Now, let  $\lambda_{\varepsilon} > 0$  satisfy the characteristic equation

$$\lambda_{\varepsilon} + \gamma e^{\lambda_{\varepsilon} \tau} = \mu \tag{3.7}$$

and set

$$y^*(t) := y_{\varepsilon}^*(t) := Me^{-\lambda_{\varepsilon}t}. \tag{3.8}$$

If we did not have  $\xi$  bounded on  $[-\tau, 0]$ , we note that x is continuous for  $t \ge 0$  so we could restart at  $\tau$  with bounded initial data. Note also that, since f was assumed continuous and  $[\bar{r} + \varepsilon, M]$  is compact and nonempty, the 'max' in (3.5) is achieved and  $\gamma_{\varepsilon} < \mu$ .

Moreover, one easily sees that (3.7) has a unique positive solution since  $\gamma < \mu$ .

The construction yields  $y^*$  which satisfies the delay differential equation

$$\dot{y}(t) = -\mu y(t) + \gamma y(t - \tau) \tag{3.9}$$

so, taking  $\eta = \eta_{\varepsilon}$  to be  $y^*$  on  $[-\tau, 0]$ , this  $y^*$  must coincide with  $y = x_{g,\eta}$  so long as  $y^*(t-\tau) \geqslant \bar{r} + \delta$ , where  $\gamma(\bar{r} + \delta) = \mu(\bar{r} + \varepsilon)$ . Note that we can—and do—choose  $\gamma$  close enough to  $\mu$  to ensure that  $\delta \leqslant 2\varepsilon$ .

To apply Theorem 2, we note that g, as given by (3.6), is clearly nondecreasing and observe that our hypotheses ensure directly that  $f(r) \leq g(r)$  for  $r \leq \bar{r}$  and for  $\bar{r} \leq r \leq \bar{r} + \varepsilon$ , while choosing  $\gamma \geqslant \gamma_{\varepsilon}$  ensures that  $f(r) \leq g(r)$  for  $\bar{r} + \varepsilon \leq r \leq M$ . Since Corollary 3 ensures  $x(t) \leq M$ , it follows that  $f \leq g$  where relevant and that  $\xi \leq M \leq \eta$ . Thus, Theorem 2 applies and we have  $x \leq y := x_{g,\eta}$ —whence  $x \leq y^*$  as long as  $y^*$  coincides with y. Noting that this includes an interval of length  $\tau$  on which  $y \leq \bar{r} + \delta \leq \bar{r} + 2\varepsilon$ , we can apply Corollary 3 again (now restarting at the end of this interval) to see that x thereafter remains below  $\bar{r} + 2\varepsilon$ —i.e., we have shown that

$$x(t) \leqslant z_{\varepsilon}(t) := \max\{Me^{-\lambda_{\varepsilon}t}, \bar{r} + 2\varepsilon\}$$

for all t. Since this holds for arbitrarily small  $\varepsilon > 0$ , we have (3.2), as desired, with  $z_+(t) := \inf\{z_{\varepsilon}(t): \varepsilon > 0\}$ . This completes the proof for the first case.

Using the second case in Theorem 2, we will get a corresponding lower bound. First, however, we note that (1.2) gives

$$x(\tau) = e^{-\mu \tau} x(0) + \int_{-\tau}^{0} e^{-\mu(\tau+s)} f(\xi(s)) ds,$$

which will be strictly positive for nonnegative, nontrivial  $\xi$ —and then x(t) will be strictly positive for all  $t \ge \tau$ . We can therefore assume, restarting if necessary, that  $\xi \ge m$  for some m > 0. The rest of the proof is then almost exactly like that for the first case.  $\square$ 

**Theorem 7.** Let  $f, \xi, x$  be as above in (1.1) and suppose there is some  $\bar{r} \ge 0$  such that

$$f(r) > \mu r \quad for \ 0 < r < \bar{r},$$
  
$$f(r) < \mu r \quad for \ all \ r > \bar{r}.$$
 (3.10)

Suppose, also, that

either 
$$f(r) \leq \mu \bar{r}$$
 for  $0 < r < \bar{r}$   
or  $f(r) \geq \mu \bar{r}$  for all  $r \geq \bar{r}$ . (3.11)

Then,  $x_{f,\xi}(t) \to \hat{r}$  as  $t \to \infty$  for every nontrivial initial data  $\xi \geqslant 0$ —i.e.,  $\bar{m} = \bar{r} = \bar{M}$ .

**Proof.** We consider explicitly only the first alternative in (3.11). Since this with (3.10) include (3.1), the first case of Theorem 6 applies to give  $\bar{M} \leq \bar{r}$ . If  $\bar{r} = 0$ , we are now done so we need only show  $\bar{m} \geqslant \bar{r}$  when  $\bar{r} > 0$ . For any  $\varepsilon > 0$  we can choose  $\delta > 0$  so  $f(r) \geqslant f(\bar{r}) - \mu \varepsilon$  on  $[\bar{r}, \bar{r} + \delta]$  and there is some  $t_{\delta}$  such that  $x(t) \leqslant \bar{r} + \delta$  for all  $t \geqslant t_{\delta} - \tau$ . Setting  $\bar{r} = \bar{r} - \varepsilon$ , this gives  $f(r) \geqslant \mu \bar{r}$  for  $\bar{r} \leqslant r \leqslant \bar{r} + \delta$ . Restarting at  $t_{\delta}$ , and noting that only values of r below  $\bar{r} + \delta$  are relevant, we thus have the hypotheses for the second case of Theorem 6 for the restarted problem with  $\bar{r}$  replaced by  $\bar{r}$ . Thus,  $\bar{m} \geqslant \bar{r} = \bar{r} - \varepsilon$  for arbitrary  $\varepsilon > 0$  so  $\bar{m} \geqslant \bar{r}$ . Combining these upper and lower asymptotic bounds is just the desired result.  $\square$ 

We henceforth will consider equations of the form (1.1) subject to the hypotheses (1.8). If  $\max\{f(r): r > 0\} = B \le \mu \bar{r}$ , giving the first case of (3.11), then we already know from Theorem 7 that all solutions converge to the equilibrium  $\bar{r}$ , so we will also assume henceforth that  $B > \mu \bar{r}$  with  $y_0 < \bar{r}$ : (1.8) then gives (3.10) but we have neither case of (3.11).

#### 4. Attraction dependent on the delay

As noted, we henceforth assume (1.8):

•  $f: \mathbb{R}_+ = [0, \infty) \to \mathbb{R}_+$  is continuous.

• There is a unique equilibrium 
$$\bar{r} > 0$$
, so  $\mu \bar{r} = f(\bar{r}) > 0$ .

$$\bullet \begin{cases}
f(r) > \mu r & \text{for } 0 < r < \bar{r}, \\
f(r) < \mu r & \text{for all } r > \bar{r}.
\end{cases}$$
(4.1)

Lemma 8. Assume (4.1). Then, for every nontrivial solution x of (1.1) we have

$$e^{-\mu\tau}\bar{r} \leqslant \bar{m} \leqslant \bar{r} \leqslant \bar{M} \leqslant \max_{e^{-\mu\tau}\bar{r} \leqslant r \leqslant \bar{r}} f(r)/\mu$$
 (4.2)

with  $\bar{m} = \bar{m}(x)$ ,  $\bar{M} = \bar{M}(x)$  as in (2.1).

**Proof.** From Corollary 3 we know x is bounded and let u, v be as in Lemma 5. Then, as  $\dot{u}(0) = 0 = \dot{v}(0)$ ,

$$f(u(-\tau)) = \mu u(0) = \mu \tilde{M} \geqslant \mu u(-\tau)$$

and, similarly,  $f(v(-\tau)) = \mu v(0) \leqslant \mu v(-\tau)$ . But  $f(r) > \mu r$  if and only if  $x < \bar{r}$ , so  $u(-\tau) \leqslant \bar{r} \leqslant v(-\tau)$ . Thus,

$$v(0) = \bar{m} \leqslant u(-\tau) \leqslant \bar{r} \leqslant v(-\tau) \leqslant \bar{M}. \tag{4.3}$$

Since u, v satisfy (1.1) on all of  $\mathbb{R}$ , we may apply (1.2) with t = 0,  $a = -\tau$  to get, as  $f(\cdot) \ge 0$ ,

$$\tilde{m} = v(0) = e^{-\mu\tau} v(-\tau) + \int_{-\tau}^{0} e^{\mu s} f(x(s-\tau)) ds \geqslant e^{-\mu\tau} v(-\tau) \geqslant e^{-\mu\tau} \bar{r}$$

and consequently,  $u(-\tau) \geqslant v(0) \geqslant e^{-\mu \tau} \bar{r}$ . Therefore,

$$u(0) = f(u(-\tau))/\mu \leqslant \max_{e^{-\mu\tau}\bar{r} \leqslant r \leqslant \bar{r}} f(r)/\mu.$$

The proof is complete.  $\Box$ 

Our next objective is to show global attraction to the equilibrium when the delay  $\tau$  is not too large.

**Theorem 9.** Assume (4.1) and the following pair of one-sided Lipschitz conditions:

$$0 \leq f(r) - \mu \bar{r} \leq L_1(\bar{r} - r) \quad \text{for } e^{-\mu \tau} \bar{r} \leq r < \bar{r},$$

$$0 \leq \mu \bar{r} - f(r) \leq L_2(r - \bar{r}) \quad \text{for } \bar{r} < r \leq B.$$

$$(4.4)$$

Suppose t is such that

$$(1 - e^{-\mu \tau}) < \frac{\mu}{\sqrt{L_1 L_2}}. (4.5)$$

Then, every nontrivial solution of (1.1) converges to the equilibrium  $\bar{r}$ .

**Proof.** Let u, v be as in Lemmas 5 and 8. It then follows from (4.3) that there is some  $a \in [-\tau, 0]$  such that  $u(a) = \bar{r}$  and we set

$$\mathcal{A} = \left\{ s \in [a, 0] \subset [-\tau, 0] \colon u(s - \tau) \leqslant \tilde{r} \right\}.$$

Note that for  $s \in [-\tau, 0] \setminus A$  we have  $u = u(s - \tau) > \bar{r}$  so  $f(u) - \mu \bar{r} \le 0$  by (4.1), while for  $t \in A$  we have  $u \le \bar{r}$  and  $e^{-\mu \tau} \bar{r} \le \bar{m} \le u$  from (4.2) in Lemma 8 so (4.4) gives

$$f(u) - \mu \bar{r} \leqslant L_1(\bar{r} - u) \leqslant L_1(\bar{r} - \bar{m}).$$

638

Thus.

$$\int_{A} e^{\mu s} [f(u) - \mu \bar{r}] ds \leqslant L_{1}(\bar{r} - \bar{m}) \int_{-\tau}^{0} e^{\mu t} ds = L_{1}(\bar{r} - \bar{m})(1 - e^{-\mu \tau}).$$

Applying (1.2) with t = 0 and this a, we then have

$$\bar{M} - \bar{r} = \left[ u(0) - e^{\mu a} u(a) \right] + \mu \int_{a}^{0} e^{\mu s} ds = \int_{a}^{0} e^{\mu s} \left[ f(u(s - \tau)) - \mu \bar{r} \right] ds$$

$$\leq \int_{A} e^{\mu s} \left[ f(u) - \mu \bar{r} \right] ds \leq L_{1} (\bar{r} - \bar{m}) (1 - e^{-\mu \tau}) / \mu.$$

Somewhat similarly, we have some  $a \in [-\tau, 0]$  such that  $v(a) = \bar{r}$  and now set  $A = \{s \in [a, 0]: v(s - \tau) \ge \bar{r}\}$ , noting that (4.4) ensures that  $f(r) \ge \mu \bar{r}$  for  $r \in [e^{-\mu \tau} \bar{r}, \bar{r}]$ . Much as before we then get

$$\bar{r} - \bar{m} \leqslant L_2(\bar{M} - \bar{r})(1 - e^{-\mu\tau})/\mu$$

and combining gives  $(\bar{r} - \bar{m}) \le [L_1 L_2 (1 - e^{-\mu \tau})^2 / \mu^2] (\bar{r} - \bar{m})$ . Thus, using the assumption (4.5), we have  $\bar{m} = \bar{r}$  and then  $\bar{M} = \bar{r}$  as well.  $\Box$ 

Essentially the same argument gives a localized version when, instead of (4.4) and (4.5), we have |f'| suitably small near  $\bar{r}$ .

#### 5. Another stability result

We now return to the integral formula (1.4), noting that if x is a solution of (1.1), then  $y = x - \bar{r}$  is a solution of (1.3) and an appropriate choice of g:

$$g(t) = f_1(y(t-\tau)) \text{ with } f_1(r) := [f(\bar{r}+r) - f(\bar{r})] + \nu r,$$
 (5.1)

where, of course, we anticipate taking  $v = -f'(\bar{r})$  for differentiable functions f, although this is not required.

It is worth noting that with this choice of  $\nu$  we necessarily have  $L_1, L_2 \ge |f'(\bar{r})| = \nu$  in Theorem 9 so that Lemma 1 suggests that we could not expect asymptotically stable convergence to equilibrium when  $\nu > \mu$  if we do not have (1.7); indeed, as we will note in more detail in the following section, (1.1) will then have a nontrivial periodic solution. Even ignoring the constraint on  $\tau$  in requiring that  $f(r) \ge \mu \bar{r}$  for  $r \in [e^{-\mu \tau} \bar{r}, \bar{r}]$ , the assumption (4.5) taking  $L_1 = L_2 = -f'(\bar{r}) = \nu$  leads to  $(1 - e^{-\mu \tau}) < \mu/\nu$  or

$$\tau < \frac{1}{\mu} \ln \left[ \frac{1}{1 - \mu/\nu} \right]. \tag{5.2}$$

Since we anticipate having f(0) = 0, this part of (4.4) must be treated as a significant constraint on  $\tau$ .

Clearly this, as a sufficient condition for convergence to equilibrium, is the best one can obtain using Theorem 9 and it is interesting to compare with the (necessarily weaker) condition (1.7). There is obviously a gap between these, and we now seek to handle intermediate delays under appropriate conditions.

**Theorem 10.** Suppose f is a unimodal function and  $\tau > 0$  satisfies (1.7) with  $\nu = -f'(\bar{r})$ . Further, suppose

$$\left| f(\bar{r} + r) - f(\bar{r}) + \nu r \right| \le L|r| \quad \text{for } e^{-\mu \tau} \bar{r} - \bar{r} \le r \le B - \bar{r}. \tag{5.3}$$

If f is 'flat enough near equilibrium' such that (5.3) holds with

$$L < 1/\|X\|_1,\tag{5.4}$$

where X is as in (1.4), then every nontrivial nonnegative solution of (1.1) converges to the equilibrium  $\bar{r}$  as  $t \to \infty$ .

**Proof.** Set  $\hat{M} = \max\{\bar{M} - \bar{r}, \bar{r} - \bar{m}\}$  and, again, let u, v be as in Lemmas 5 and 8. First suppose  $\hat{M} = \bar{M} - \bar{r}$ . We then let  $y(t) = u(t - T) - \bar{r}$  so  $\hat{M} = u(0) - \bar{r} = y(T)$  with T > 0 arbitrary. We note that  $\bar{m} \leq y \leq \hat{M}$  gives  $|y| \leq \hat{M}$ . Therefore, (5.3) gives  $|f_1(y)| \leq L\hat{M}$  uniformly. Thus, using (1.3) with (5.1), we have

$$\hat{M} = y_0(T) + \int_0^T X(T - s) f_1(y(s - \tau)) ds \le \bar{y}_0(T) + \int_0^T |X(T - s)| L \hat{M} ds$$

$$\le \bar{y}_0(T) + L ||X||_1 \hat{M}$$
(5.5)

using (1.6) and letting  $\bar{y}_0 = y_0(\cdot; \hat{M})$ . For the alternative case  $\hat{M} = \bar{r} - \bar{m}$ , we let  $y(t) = v(t-T) - \bar{r}$  and, similarly, again obtain (5.5) for arbitrary T. Since  $\bar{y}_0(T) \to 0$  as  $T \to \infty$ , (5.4) ensures that  $\hat{M} = 0$  so  $x(t) \to \bar{r}$  as  $t \to \infty$ .  $\square$ 

#### 6. Nonconstant periodic solution for large delay

In this section we will use Hopf bifurcation and fixed point theory to prove the existence of a nonconstant periodic solution when the delay  $\tau$  is large enough. To see more clearly the effect of delay we let  $\mu=1$ . The usual linearized analysis lets  $x=\bar{r}+\varepsilon y$  and notes that, to first order in  $\varepsilon$ , the perturbation satisfies

$$\dot{y} + y = f'(\bar{r})y(\cdot - \tau).$$

Seeking a solution of the form  $y(t) = \exp(\lambda t)$ , we obtain the characteristic equation for  $\lambda$ :

$$\lambda + 1 = f'(r) \exp(-\tau \lambda).$$

We will have linearized stability if all complex roots of this characteristic equation have negative real parts. If |f'(r)| < 1 we have the local convergence to the positive equilibrium for all delays. If |f'(r)| > 1, the effect of delay will occur. More exactly, in this case with

$$\tau > \tau_* = \frac{1}{\sqrt{|f'(\bar{r})|^2 - 1}} \arccos \frac{1}{f'(\bar{r})}$$

there is a nonconstant periodic solution of Eq. (1.1).

Atay [1] used the Schauder fixed point theory to prove that there is a nonconstant periodic solution of the equation

$$\dot{y} = \tau h(y, y(\cdot - 1)),$$

provided

$$\tau > \tau_* = \frac{1}{\sqrt{D^2 - C^2}} \arccos\left(-\frac{C}{D}\right),$$

where h(u, v) is differentiable at the origin, h(0, 0) = 0 and

$$0 < C := -\frac{\partial h}{\partial u}(0,0) < D := -\frac{\partial h}{\partial v}(0,0).$$

We let  $y(t) = x(\tau t) - \bar{r}$  and

$$h(u, v) = \bar{r} - u + f(v + \bar{r}).$$

Then,

$$C=1,$$
  $D=-f'(\bar{r})$ 

and we reproduce

$$\tau_* = \frac{1}{\sqrt{|f'(\bar{r})|^2 - 1}} \arccos \frac{1}{f'(\bar{r})}.$$

Here, we assume that  $f'(\bar{r}) < -1$  and the function arc cosine takes its value in  $[0, \pi]$ .

**Lemma 11.** If a positive solution x of (1.1) does not oscillate around the positive equilibrium  $\bar{r}$  then x(t) tends to  $\bar{r}$  as  $t \to \infty$ . Consequently, every nonconstant positive periodic solution should oscillate around the positive equilibrium.

**Proof.** If x does not oscillate around  $\bar{r}$ , then either

$$\limsup_{t\to\infty} x(t) \leqslant \bar{r} \quad \text{or} \quad \liminf_{t\to\infty} x(t) \geqslant \bar{r}.$$

From Lemma 8, in the first case, we have  $\limsup x(t) = \bar{r}$ . For the second case, we have  $\liminf x(t) = \bar{r}$ . So it is enough to consider the second case. Using the proof of Lemma 8, we get  $\bar{r} \ge u(-\tau) \ge v(0) = \bar{r}$ . Hence,  $u(-\tau) = \bar{r}$  and  $u(0) = f(u(-\tau)) = \bar{r}$ . The proof is now complete.  $\Box$ 

Y. Cao [2] proved that for  $\tau \le \tau_*$  there is no periodic solution which is larger than  $y_0$  and oscillates slowly around the only positive equilibrium  $\bar{r}$ . For  $\tau > \tau_*$ , there is at most one periodic solution which is larger than  $y_0$  and oscillates slowly around  $\bar{r}$ . Recall that a T-periodic solution is called *slowly oscillated around the positive equilibrium*, if  $T > \tau$ ,  $x(0) = x(T) = \bar{r}$ , and there is  $t_0 \in (0, T - \tau)$  such that

$$x(t_0) = \overline{r},$$
  $x(t) > \overline{r}$  for  $t \in (0, t_0)$  and  $x(t) < \overline{r}$  for  $t \in (t_0, T)$ .

Cao assumes that f is decreasing from  $y_0 < \bar{r}$  until  $f(y_0)$ . He also requires that the function h(x) = xf'(x)/f(x) is monotonically increasing in  $[y_0, \bar{r}]$  and decreasing in

 $[\bar{r}, f(y_0)]$ . Recall that  $f(y_0)$  is the maximal value of f(y), when y > 0. Without these assumptions on h one can construct several slowly oscillated periodic solutions for (1.1). Also, it is known that, if a periodic solution is not oscillated slowly, it should be unstable. Of course, Cao did not prove these results directly, but from his works one can deduce this.

#### 7. Some applications

Equation (1.1) with unimodal f has been proposed as a model for a variety of physiological processes, where in most cases, one of the model functions

$$f(x) = kx^{c} \exp(-x) \tag{7.1}$$

or

$$f(x) = \frac{kx}{1 + x^c},\tag{7.2}$$

with parameters k > 0 and c > 0, is considered [3,4,9,11–13].

The population dynamics of Nicholson's blowflies have been studied [9,12] using a function f of the form (7.1) with c = 1. In such a case, f is differentiable and one has

$$\bar{r} = \ln \frac{k}{\mu},\tag{7.3}$$

and

$$\nu = -f'(\bar{r}) = \mu \left( \ln \frac{k}{\mu} - 1 \right).$$

Thus, Theorem 9 yields, using (5.2),

$$\tau < \frac{1}{\mu} \ln \left[ \frac{\ln(k/\mu) - 1}{\ln(k/\mu) - 2} \right]$$

as a sufficient condition for convergence to equilibrium  $\bar{r}$  given in (7.3), provided  $k > \mu e^2$ . Moreover, there is a nonconstant periodic solution to the model equation if

$$\tau > \tau^* = \frac{1}{\mu \sqrt{(\ln(k/\mu) - 2) \ln(k/\mu)}} \arccos\left[\frac{1}{1 - \ln(k/\mu)}\right],$$

using (1.7)

In respiratory studies, (1.1) has been employed in which the response function takes the form (7.2). In such a case, one has the positive equilibrium

$$\bar{r} = \left(\frac{k}{\mu} - 1\right)^{1/c},\tag{7.4}$$

provided  $k/\mu > 1$ . Then,

$$v = -f'(\bar{r}) = \frac{\mu}{k} [(c-1)k - c\mu].$$

Thus, Theorem 9 yields, using (5.2),

$$\tau < \frac{1}{\mu} \ln \left[ \frac{c(1-\mu/k) - 1}{c(1-\mu/k) - 2} \right]$$

as a sufficient condition for convergence to equilibrium  $\bar{r}$  given in (7.4), provided

$$c\left(1-\frac{\mu}{k}\right) > 2.$$

Moreover, there is a nonconstant periodic solution to the model equation (1.1) with f as in (7.2) if

$$\tau > \tau^* = \frac{1}{\mu \sqrt{c(c(1-\mu/k)-2)(1-\mu/k)}} \arccos \left[ \frac{1}{1-c(1-\mu/k)} \right],$$

using (1.7).

#### 8. Conclusion

We have given a basic comparison theorem and discussed some of their consequences. The effect of delay on the asymptotic behavior has then been studied and the periodicity of positive solutions investigated for large delays. Our discussions allow the nonlinearity f to be nonmonotonic and nondifferentiable which are then more general than those of [8]. Thus, our results should be applicable to a wider range of population models; for example, models arising from the study of an optically bistable device [3,4], blood cells production, respiration dynamics, or cardiac arrhythmias [11,13]. We can also find application with a system in which the growth function is not smooth, such as a population where growth occurs in birth pulses (during the breeding season) and not continuously throughout the year.

**Open problem.** Investigate the stability of periodic solutions of (1.1) and the structure of  $\omega$ -limit sets when the delay is large enough!

#### Acknowledgment

Deepest appreciation is extended towards the National Research Council of Thailand and the Thailand Research Fund for the financial support.

#### References

- [1] F.M. Atay, Periodic solutions of a delay-differential equation with a restorative condition, Nonlinear Anal. 45 (2001) 555-576.
- [2] Y. Cao, Uniqueness of periodic solution for differential delay equations, J. Differential Equations 128 (1996)
- [3] M.W. Derstine, H.M. Gibbs, F.A. Hopf, D.L. Kaplan, Bifurcation gap in a hybrid optically bistable system, Phys. Rev. A 26 (1982) 3720-3722.
- [4] M.W. Derstine, H.M. Gibbs, F.A. Hopf, D.L. Kaplan, Alternate paths to chaos in optical bistability, Phys. Rev. A 27 (1983) 3200-3208.
- [5] K.P. Hadeler, J. Tomiuk, Periodic solutions of difference differential equations, Arch. Rational Mech. Anal. 65 (1977) 87-95.

- [6] J. Hale, Introduction to Functional Differential Equations, Springer-Verlag, 1993.
- [7] M. Kot, Elements of Mathematical Ecology, Cambridge Univ. Press, 2001.
- [8] Y. Kuang, Delay Differential Equations with Applications in Population Dynamics, Academic Press, 1993.
- [9] M. Kulenovic, G. Ladas, Y. Sficas, Global attractivity in Nicholson's blowflies, Appl. Anal. 43 (1992) 109– 124.
- [10] Y. Lenbury, D.V. Giang, Nonlinear delay differential equations involving population growth, Math. Comput. Modelling, in press.
  - [11] M.C. Mackey, U. an der Heiden, Dynamical diseases and bifurcations: understanding functional disorders in physiological systems, Funkt. Biol. Med. 256 (1982) 156-164.
  - [12] S.H. Saker, S. Agarwal, Oscillation and global attractivity in a periodic Nicholson's blowflies model, Math. Comput. Modelling 35 (2002) 719-731.
  - [13] M. Wazewska-Czyewska, A. Lasota, Mathematical models of the red cell system, Mat. Stos. 6 (1976) 25-40 (in Polish).



# Available online at www.sciencedirect.com

MATHEMATICAL AND COMPUTER MODELLING

Mathematical and Computer Modelling 40 (2004) 583-590

www.elsevier.com/locate/mcm

## Nonlinear Delay Differential Equations Involving Population Growth

Y. LENBURY\*

Department of Mathematics, Mahidol University Rama 6, Bangkok, 10400 Thailand scylb@mahidol.ac.th

D. V. GIANG

Hanoi Institute of Mathematics
18 Hoang Quoc Viet, 10307 Hanoi, Vietnam dangvugiang@yahoo.com

(Received June 2003; revised and accepted September 2003)

Abstract—Conditions are given on the function f, such that population x(t) given by

$$\dot{x}(t) = -\mu x(t) + f(x(t-\tau)),$$

becomes extinct or remains globally stable. Our theorems are shown to be applicable to the Nicholson's model of blowfiles and the population dynamics of baleen whales. In some of these cases, the function f is unimodal rather than monotone. © 2004 Elsevier Ltd. All rights reserved.

Keywords—Constant variation formula, Positivity of population models,  $\omega$ -limit set of a persistent solution, One parameter semigroup.

#### 1. INTRODUCTION

Consider the following delay differential equation,

$$\dot{x}(t) = -\mu x(t) + f(x(t-\tau)), \tag{1.1}$$

for t > 0, where  $f : [0, \infty) \to [0, \infty)$  is a continuous function, f(0) = 0, while  $\mu$  and  $\tau$  are positive parameters. The initial condition  $x|_{[-\tau,0]} = \phi$  is given by a positive continuous function in  $[-\tau,0]$ . The corresponding constant variation formula is given as

$$x(t) = e^{-\mu t}x(0) + \int_0^t e^{-\mu(t-\xi)} f(x(\xi-\tau)) d\xi, \quad \text{for } t > 0.$$
 (1.2)

This can be proved by differentiating both sides. This formula also shows that x(t) > 0, for all t > 0, hence, (1.1) really is a model for population growth. The following theorem gives a sufficient and necessary condition for the population to become extinct.

0895-7177/04/\$ - see front matter © 2004 Elsevier Ltd. All rights reserved. doi:10.1016/j.mcm.2003.09.038

Typeset by AMS-TEX

<sup>\*</sup>Author to whom all correspondence should be addressed. The authors would like to extend their deepest appreciation to the Thailand Research Fund for the financial support of this research project, which is also partially funded by a grant from the Ministry of University Affairs.

THEOREM 1. If  $f(u) < \mu u$ , for all u > 0, then, every solution x(t) of (1.1) converges to 0 as  $t \to \infty$ . Conversely, if every solution of (1.1) converges to 0, then,  $f(u) < \mu u$ , for all u > 0.

PROOF. First, assume that  $f(u) < \mu u$ , for all u > 0. Let x(t) be a positive solution of (1.1) and  $M = \max_{-\tau \le \xi \le 0} x(\xi) + 1$ . We prove that x(t) < M, for all t > 0. Indeed, assume, for the sake of contradiction, that  $t_0$  is the *first positive point*, such that  $x(t_0) = M$ . The "first positive point" only means that  $x(\xi - \tau) < M$ , for all  $\xi < t_0$ . Then, by the constant variation formula

$$\begin{split} M &= x(t_0) = e^{-\mu t_0} x(0) + \int_0^{t_0} e^{-\mu(t_0 - \xi)} f(x(\xi - \tau)) \, d\xi, \\ &< e^{-\mu t_0} M \left( 1 + \int_0^{t_0} e^{\mu \xi} \mu \, d\xi \right) = M, \end{split}$$

which is a contradiction. Therefore, x(t) < M, for all t. Let

$$\ell_1 = \limsup_{t \to \infty} x(t),$$
  
$$\ell_2 = \limsup_{t \to \infty} f(x(t - \tau)).$$

Let  $\epsilon > 0$  be a small number, and let  $T = T(\epsilon)$  be, such that  $f(x(t - \tau)) < \ell_2 + \epsilon$ , for all t > T. Now, if t > T, then, we have

$$\begin{split} x(t) &= e^{-\mu t} x(0) + \int_0^T e^{-\mu(t-\xi)} f(x(\xi-\tau)) \, d\xi + \int_T^t e^{-\mu(t-\xi)} f(x(\xi-\tau)) \, d\xi \\ &\leq e^{-\mu t} x(0) + e^{-\mu t} \int_0^T e^{\mu \xi} f(x(\xi-\tau)) \, d\xi + (\ell_2 + \epsilon) e^{-\mu t} \int_T^t e^{\mu \xi} \, d\xi \\ &\leq e^{-\mu t} x(0) + e^{-\mu t} \int_0^T e^{\mu \xi} f(x(\xi-\tau)) \, d\xi + \frac{(\ell_2 + \epsilon)}{\mu} \left(1 - e^{-\mu(t-T)}\right). \end{split}$$

Taking lim sup on both sides, we have

$$\ell_1 \leq \frac{\ell_2 + \epsilon}{\mu}.$$

Since  $\epsilon$  is as small as we wish, this gives

$$\mu \ell_1 \le \ell_2. \tag{1.3}$$

On the other hand, from the definition of  $\limsup$ , we can choose a sequence  $\{t_k\}$  tending to infinity for which

$$\ell_{2} = \lim_{k \to \infty} f\left(x\left(t_{k} - \tau\right)\right).$$

The sequence  $\{x(t_k - \tau)\}$  is bounded because the function x(t) is bounded. Hence, this sequence should contain some convergent subsequence. Without loss of generality, we assume that the sequence  $\{x(t_k - \tau)\}$  converges to a limit  $\ell_3$ , say. Since the function f is continuous, we have

$$\ell_{2} = \lim_{k \to \infty} f(x(t_{k} - \tau)) = f(\ell_{3}).$$

If  $\ell_3 > 0$ , then,

$$\ell_2 = f(\ell_3) < \mu \ell_3.$$

Clearly,  $\ell_3 \leq \ell_1$ . Therefore,  $\ell_2 < \mu \ell_1$ . Considering (1.3), we have a contradiction. Consequently,  $\ell_3 = 0$ . However,  $\ell_2 = f(\ell_3)$ , and so,  $\ell_2$  is zero also. Combining this with (1.3), we have  $\ell_1 = 0$ , and hence, the solution x(t) tends to 0 as  $t \to \infty$ .

Conversely, suppose that  $f(u) < \mu u$  is not satisfied, for all u > 0. Two cases are possible.

- (i)  $f(a) = \mu a$ , for some a > 0.
- (ii)  $f(u) > \mu u$ , for all u > 0.

In the first case,  $x(t) \equiv a$  is a positive solution which does not tend to 0. For the second case, let x(t) = 2 for  $t \in [-\tau, 0]$ . We shall prove that x(t) > 1, for all t. Suppose, for the sake of contradiction, that  $t_0 > 0$  is the the first point, such that  $x(t_0) = 1$ , and x(t) > 1, for all  $0 \le t < t_0$ . Then,

$$\begin{split} 1 &= x(t_0) = 2e^{-\mu t_0} + e^{-\mu t_0} \int_0^{t_0} e^{\mu \xi} f(x(\xi - \tau)) \, d\xi \\ &> e^{-\mu t_0} \left( 2 + \int_0^{t_0} e^{\mu \xi} \mu \, d\xi \right) = e^{-\mu t_0} \left( 1 + e^{\mu t_0} \right) > 1, \end{split}$$

which is a contradiction. Therefore, x(t) > 1, for all t, which does not tend to 0. The proof is complete.

#### 2. THE PERSISTENCE

A positive solution x(t) is called persistent if

$$0 < \liminf_{t \to \infty} x(t) \le \limsup_{t \to \infty} x(t) < \infty.$$

The following theorem gives a sufficient condition for the population to be persistent.

THEOREM 2. Assume that f(x) > 0, for all x > 0 and

$$\limsup_{x \to \infty} \frac{f(x)}{x} < \mu,\tag{2.1}$$

$$\liminf_{x \to 0+} \frac{f(x)}{x} > \mu.$$
(2.2)

Then, every solution x(t) of (1.1) is persistent.

PROOF. First, we prove that  $\{x(t)\}$  is bounded from above. Assume, for the sake of contradiction, that  $\limsup x(t) = \infty$ . For each  $t \ge -\tau$ , we define

$$\alpha(t) := \max \left\{ \rho \le t : x(\rho) = \max_{-\tau \le \xi \le t} x(\xi) \right\}.$$

Observe that  $\alpha(t) \to \infty$  and that

$$\lim_{t\to\infty}x(\alpha(t))=\infty.$$

But  $x(\alpha(t)) = \max_{\xi \le t} x(\xi)$  and so,  $\dot{x}(\alpha(t)) \ge 0$ . Therefore,

$$0 \le \dot{x}(\alpha(t)) = -\mu x(\alpha(t)) + f(x(\alpha(t) - \tau)),$$

and consequently,

$$\mu x(\alpha(t)) \leq f(x(\alpha(t) - \tau)).$$

Since f is a continuous function, combining this inequality with the fact that

$$\lim_{t\to\infty}x(\alpha(t))=\infty,$$

we obtain

$$\lim_{t\to\infty}x(\alpha(t)-\tau)=\infty.$$

Therefore.

$$\limsup_{x\to\infty}\frac{f(x)}{x}\geq \limsup_{t\to\infty}\frac{f(x(\alpha(t)-\tau))}{x(\alpha(t)-\tau)}\geq \mu,$$

which contradicts (2.1). Thus, x(t) is bounded from above.

Next, we prove that  $\liminf_{t\to\infty} x(t) > 0$ . Suppose, for the sake of contradiction, that  $\liminf x(t) = 0$ . For each  $t \ge -\tau$ , we define

$$\beta(t) := \max \left\{ \rho \leq t : x(\rho) = \min_{-\tau \leq \xi \leq t} x(\xi) \right\}.$$

Observe that  $\beta(t) \to \infty$  and that

$$\lim_{t\to\infty}x(\beta(t))=0.$$

However,  $x(\beta(t)) = \min_{\xi \le t} x(\xi)$ , and so  $\dot{x}(\beta(t)) \le 0$ . Therefore,

$$0 \ge \dot{x}(\beta(t)) = -\mu x(\beta(t)) + f(x(\beta(t) - \tau))$$

and consequently,

$$\mu x(\beta(t)) \ge f(x(\beta(t) - \tau)).$$

Since f is a continuous function, combining this inequality with the fact that

$$\lim_{t\to\infty}x(\beta(t))=0,$$

we obtain

$$\lim_{t\to\infty}x(\beta(t)-\tau)=0.$$

Therefore,

$$\liminf_{x\to 0+}\frac{f(x)}{x}\leq \liminf_{t\to \infty}\frac{f(x(\beta(t)-\tau))}{x(\beta(t)-\tau)}\leq \mu,$$

which contradicts (2.2). The proof is complete.

Inequalities (2.1) and (2.2) give the lower and upper bounds for the death rate  $\mu$  in order that the population may persist. As x becomes very large, to prevent the population from overflowing, the lim sup of the ratio of the growth function f(x) and the population density x should be smaller than the death rate  $\mu$ . On the other hand, as x becomes very small, the lim inf of that ratio should remain bigger that the death rate  $\mu$  to keep the population from extinction.

In what follows, we will assume that  $x(\cdot)$  is a persistent solution of (1.1) with  $x|_{[-\tau,0]} = \psi$ . We let s be a variable in the interval  $[-\tau,0]$  and denote by  $\mathcal{C}[-\tau,0]$ , the Banach space of continuous functions in the interval  $[-\tau, 0]$ . For each persistent solution  $x(\cdot)$  and  $t \ge 0$ , let  $x_t(s) = x(t+s)$ be a function with the variable  $s \in [-\tau, 0]$ . We consider the semigroup  $\{T(t)\}_{t>0}$  of operators from  $\mathcal{C}[-\tau,0]$  into itself defined by letting  $T(t)\psi=x_t$ , where x is a persistent solution beginning from  $\psi$ . Clearly, the operator T(t) is injective, for all  $t \geq 0$ . The  $\omega$ -limit set of  $\psi$  is defined to be the set of all limit points of the set  $\{x_t:t\geq 0\}$ . This  $\omega$ -limit set is often denoted by  $\omega(x)$  and is (nonempty) compact and invariant under T(t), for each  $t \geq 0$ . Moreover, T(t) is a bijective mapping from this  $\omega$ -limit set into itself, for each  $t \geq 0$  (see [1]). Therefore, we can define T(t) = T(-t), for all t < 0, to obtain a one-parameter group  $\{T(t)\}_{t \in R}$  of operators from  $\omega(x)$  into itself. Letting  $u_0$  and  $v_0$  be functions in  $\omega(x)$ , such that  $u_0(0) = \sup\{\phi(0) : \phi \in \omega(x)\}$ and  $v_0(0) = \inf\{\phi(0) : \phi \in \omega(x)\}$ , it is easy to see that  $u_0(0) = \limsup_{t \to \infty} x(t)$  and  $v_0(0) = \max_{t \to \infty} x(t)$  $\liminf_{t\to\infty} x(t)$ . We now let  $u(t)=T(t)u_0(0)$  and  $v(t)=T(t)v_0(0)$ . Then, both u and v are solutions of (1.1), which can be extended to the whole real line. Moreover,  $u(t), v(t) \in [v(0), u(0)]$ , for all  $t \in \mathbb{R}$ . The constant variation formulae for the two full time solutions u(t) and v(t) are as follows:

$$u(t) = \int_{-\infty}^{t} e^{-\mu(t-\xi)} f(u(\xi-\tau)) d\xi,$$
 (2.3)

$$v(t) = \int_{-\infty}^{t} e^{-\mu(t-\xi)} f(v(\xi - \tau)) d\xi.$$
 (2.4)

587

# 3. THE STABILITY

In what follows, we shall assume that the algebraic equation,

$$\mu K = f(K),$$

has the unique solution  $K = \bar{x}$  in  $(0, \infty)$ .

THEOREM 3. Suppose that f(x) is monotonically increasing and

$$\limsup_{x \to \infty} \frac{f(x)}{x} < \mu,\tag{3.1}$$

$$\lim_{x \to 0} \inf \frac{f(x)}{\tau} > \mu.$$
(3.2)

Then, every solution x(t) of (1.1) converges to  $\bar{x}$ .

PROOF. By Theorem 2, every solution x(t) of (1.1) is persistent. We can, therefore, choose two (full time) solutions u(t) and v(t), such that

$$u(0) = \limsup_{t \to \infty} x(t), \qquad v(0) = \liminf_{t \to \infty} x(t). \tag{3.3}$$

Using the constant variation formula, we have

$$u(0) = \int_{-\infty}^{0} e^{\mu\xi} f(u(\xi - \tau)) d\xi \le \int_{-\infty}^{0} e^{\mu\xi} f(u(0)) d\xi = \frac{f(u(0))}{\mu}$$
(3.4)

and similarly,

$$v(0) = \int_{-\infty}^{0} e^{\mu\xi} f(v(\xi - \tau)) d\xi \ge \int_{-\infty}^{0} e^{\mu\xi} f(v(0)) d\xi = \frac{f(v(0))}{\mu}, \tag{3.5}$$

If we let

$$\varphi(x)=\frac{f(x)}{x}-\mu,$$

then, it follows from (3.4) that  $\varphi(u(0)) \geq 0$  and from (3.5) that  $\varphi(v(0)) \leq 0$ . On the other hand, it follows from (3.1) that  $\limsup_{x\to\infty} \varphi(x) < 0$ , and from (3.2) that  $\liminf_{x\to 0} \varphi(x) > 0$ . If v(0) < u(0), we have at least 2 distinct zeros of  $\varphi(x)$  in (0, v(0)), (v(0), u(0)) and in  $(u(0), \infty)$ . This contradicts our assumption that  $\bar{x}$  is the only zero of  $\varphi$ . Thus,  $v(0) = u(0) = \bar{x}$ . We conclude that

$$\lim_{t\to\infty}x(t)=\bar{x}.$$

The proof is complete.

Theorem 4. Suppose that f(x) is monotonically decreasing and the following system

$$a = \frac{f(b)}{\mu},$$
$$b = \frac{f(a)}{\mu},$$

has a unique solution  $a = b = \bar{x}$ . Then, every solution x(t) of (1.1) converges to  $\bar{x}$ .

PROOF. By Theorem 2, every solution x(t) of (1.1) is persistent. We can, therefore, choose two (full time) solutions u(t) and v(t), such that

$$u(0) = \limsup_{t \to \infty} x(t), \qquad v(0) = \liminf_{t \to \infty} x(t). \tag{3.3'}$$

588

Using the constant variation formula, we have

$$u(0) = \int_{-\infty}^{0} e^{\mu \xi} f(u(\xi - \tau)) d\xi \le \int_{-\infty}^{0} e^{\mu \xi} f(u(0)) d\xi \le \frac{f(u(0))}{\mu} := b_1$$
 (3.4')

and similarly,

$$v(0) = \int_{-\infty}^{0} e^{\mu \xi} f(v(\xi - \tau)) d\xi \ge \int_{-\infty}^{0} e^{\mu \xi} f(v(0)) d\xi \ge \frac{f(v(0))}{\mu} := a_1.$$
 (3.5')

We now let

$$a_{n+1} = \frac{f(b_n)}{\mu}, \quad b_{n+1} = \frac{f(a_n)}{\mu}, \quad \text{for } n = 1, 2, \dots$$

Similarly to (3.4') and (3.5'), u(0) and v(0) belong to the interval  $[a_n, b_n]$ , for all  $n = 1, 2, \ldots$  On the other hand, the sequence  $\{a_n\}$  is monotonically increasing and the sequence  $\{b_n\}$  is monotonically decreasing so that they converge. Let a and b be their respective limits. Then, a and b satisfy the above system in the statement of our theorem. Our assumptions assure that  $a = b = \bar{x}$ . Therefore,  $u(0) = v(0) = \bar{x}$ . The proof is complete.

From this point on, we shall assume that, for some  $y_0 > 0$ , we have

$$f(y_0) = \max_{x > 0} f(x)$$

and f(x) is increasing in  $[0, y_0]$  and decreasing in  $(y_0, \infty)$ . That is, f(x) is called a unimodal function as we have mentioned in the abstract. Suppose further that x(t) is a persistent solution of (1.1). Let u(t) and v(t) be two (full time) solutions of (1.1) with respect to a persistent solution x. Using the constant variation formula, we have

$$u(0) = \int_{-\infty}^{0} e^{\mu \xi} f(x(\xi - \tau)) d\xi \le \int_{-\infty}^{0} e^{\mu \xi} f(y_0) d\xi = \frac{f(y_0)}{\mu}.$$
 (3.6)

THEOREM 5. Suppose that  $f(y_0) \le \mu y_0$ . Also, (3.1) and (3.2) are assumed to be true. Let x(t) be a persistent solution of (1.1). Then,  $\lim_{t\to\infty} x(t) = \bar{x}$ .

PROOF. From (3.6), we have  $u(t) \le u(0) < f(y_0)/\mu \le y_0$ . Since the function f is increasing in  $[0, y_0]$ , it follows from the constant variation formula that

$$u(0) = \int_{-\infty}^{0} e^{\mu\xi} f(u(\xi - \tau)) d\xi \le \int_{-\infty}^{0} e^{\mu\xi} f(u(0)) d\xi = \frac{f(u(0))}{\mu}$$
(3.4")

and similarly,

$$v(0) = \int_{-\infty}^{0} e^{\mu \xi} f(v(\xi - \tau)) d\xi \ge \int_{-\infty}^{0} e^{\mu \xi} f(v(0)) d\xi = \frac{f(v(0))}{\mu}.$$
 (3.5")

Let

$$\varphi(x) = \frac{f(x)}{x} - \mu.$$

It follows from (3.4") that  $\varphi(u(0)) \geq 0$  and from (3.5") that  $\varphi(v(0)) \leq 0$ . On the other hand, it follows from (3.1) that  $\limsup_{x\to\infty} \varphi(x) < 0$ , and from (3.2) that  $\liminf_{x\to 0} \varphi(x) > 0$ . If v(0) < u(0), we have at least 2 distinct zeros of  $\varphi(x)$  in (0,v(0)), (v(0),u(0)) and in  $(u(0),\infty)$ . This contradicts our assumption that  $\bar{x}$  is the only zero of  $\varphi$ . Therefore,  $v(0) = u(0) = \bar{x}$ . We conclude that

$$\lim_{t\to\infty}x(t)=\bar x$$

The proof is complete.

We can now state the following result.

THEOREM 6. Suppose that (3.2) holds. Suppose, moreover, that the solution of the following system of difference equations

$$a_{n+1} = \inf_{x \in [a_n, b_n]} \frac{f(x)}{\mu},$$

$$b_{n+1} = \sup_{x \in [a_n, b_n]} \frac{f(x)}{\mu}, \qquad n = 1, 2, ...,$$

$$a_1 = \inf_{x > 0} \frac{f(x)}{\mu},$$

$$b_1 = \sup_{x > 0} \frac{f(x)}{\mu}$$

converges to  $\bar{x}$ . Then, every persistent solution of (1.1) converges to  $\bar{x}$ .

## 4. APPLICATION

Consider the Nicholson's model of a population of blowflies [2],

$$\dot{N}(t) = -\mu N(t) + \alpha N(t-\tau) \exp\left(-\beta N(t-\tau)\right).$$

Here,  $\alpha$  and  $\beta$  are positive parameters and

$$f(x) = \alpha x \exp(-\beta x).$$

If  $\alpha \leq \mu$ , using Theorem 1, we have  $\lim N(t) = 0$ . This means that if the death rate  $\mu$  is higher than  $\alpha$ , then, the population becomes extinct. On the other hand, if we now let  $\alpha > \mu$ , then using Theorem 2, we have

$$0 < \liminf N(t) \le \limsup N(t) < \infty$$

and the population persists. Moreover,

$$f'(x) = \alpha(1 - \beta x) \exp(-\beta x),$$

and the (only) positive equilibrium is

$$\bar{x} = \frac{1}{\beta} \ln \left( \frac{\alpha}{\mu} \right).$$

We have  $f'(1/\beta) = 0$  and  $f(1/\beta) = \max f(x) = \alpha/(e\beta)$ . From (3.6), we have

$$\limsup_{t\to\infty}N(t)<\frac{\alpha}{e\mu\beta}.$$

If  $\alpha \leq e\mu$ , then, from Theorem 5, we conclude that

$$\lim_{t\to\infty}N(t)=\bar{x}.$$

Next, we consider the population dynamics of baleen whales [2]:

$$\dot{N}(t) = -\mu N(t) + \mu N(t-\tau) \left\{ 1 + q \left[ 1 - \left( \frac{N(t-\tau)}{K} \right)^z \right] \right\}.$$

Here, all parameters are positive and

$$f(x) = \mu x \left\{ 1 + q \left[ 1 - \left( \frac{x}{K} \right)^z \right] \right\}$$

satisfies conditions (2.1) and (2.2), and so this population is persistent. Moreover,

$$f'(x) = \mu \left\{ 1 + q \left[ 1 - \left( \frac{x}{K} \right)^z \right] \right\} + \mu x q \left[ \left( -\frac{z}{K} \right) \left( \frac{x}{K} \right)^{z-1} \right] = \mu \left[ 1 + q - \frac{q(1+z)}{K^z} \cdot x^z \right],$$

and hence,

$$\max f(x) = f(y_0) = \mu y_0(1+q) \cdot \frac{z}{1+z},$$

where

$$y_0 = K \sqrt[z]{\frac{1+q}{q(1+z)}}$$

and the only positive equilibrium is

$$\bar{x} \approx K$$
.

From (3.6), we have

$$\limsup_{t\to\infty} N(t) < y_0(1+q) \cdot \frac{z}{1+z}.$$

To use Theorem 5, we must assume that  $f(y_0) \le \mu y_0$  or, equivalently,  $qz \le 1$ . In this case, we have  $\lim N(t) = K$ .

# 5. CONCLUSION

We have given conditions on the function f, such that the solution of the population model equation

$$\dot{x}(t) = -\mu x(t) + f(x(t-\tau))$$

will persist or remain globally stable. We then discussed the applications of our results to the population dynamics of Nicholson's model of blowflies and that of baleen whales.

Finally, we note that the results proven here have not been shown by earlier researchers, who have worked only with delay differential equations where the function f is monotone decreasing [3-6]. The assumptions imposed on f in our theorems are less stringent than in any previous work so that they should be applicable to a large variety of ecological models.

# REFERENCES

- 1. J. Hale, Introduction to functional differential equations, Springer Verlag, (1993).
- 2. M. Kot, Elements of Mathematical Ecology, Cambridge University Press, (2001).
- 3. Y. Kuang, Delay Differential Equations, Academic Press, (1977).
- Kubiaczyk and S. Saker, Oscillation and stability in nonlinear delay differential equations of population dynamics, Mathl. Comput. Modelling 35 (3/4), 295-301, (2002).
- S.H. Saker and S. Agarwal, Oscillation and global attractivity in a periodic nicholson's blowfiles model, Mathl. Comput. Modelling 35 (7/8), 719-731, (2002).
- S. Saker, Oscillation and global attractivity in hematopoiesis model with delay time, Appl. Math. Comput. 136, 241-250, (2003).



ScienceAsia 28 (2002) : 205-215

# Chaos and Control Action in a Kolmogorov Type Model for Food Webs with Harvesting or Replenishment

# Yongwimon Lenbury\*, Adoon Pansuwan, Nardfida Tumrasvin

Department of Mathematics Faculty of Science, Mahidol University, Rama 6 Rd, Bangkok 10400, Thailand.

\* Corresponding author, E-mail: scylb@mahidol.ac.th

Received 11 Sep 2001 Accepted 8 Feb 2002

**ABSTRACT** In this paper, we apply the feedback decoupling technique to a Kolmogorov type model for three species food webs with harvesting or replenishment. A feedback control law is derived to decouple the effect of predators from prey dynamics. It is found that the necessary and sufficient conditions for the existence of the decoupling control law rely on the persistence of the prey population and the fact that the specific growth rate of prey depends explicitly on the superpredator population density at any moment in time. It is shown that, without any control action of regulated replenishment or harvesting, irregular or chaotic behavior is possible in such a process for certain ranges of the system parameters. This is illustrated by the construction of a bifurcation diagram for a model of a three-species food web with response functions of the Holling type II. To make the system output or variables less sensitive to irregular disturbances, the feedback control technique is applied which produces the desirable effect of stabilizing the system. When such a model is applied to an activated sludge process, the objective of the control action can also be to regulate the inputs in order to obtain satisfactory water quality.

KEYWORDS: Kolmogorov model - control - chaos - stabilization.

# INTRODUCTION

Ecological models may be classified as either strategic or tactical, as identified by Holling (1966). Tactical models are relatively more complex. They usually rely on a great amount of supporting data, and are used for making specific predictions. Strategic models, on the other hand, can provide broader insights into possible behaviors of the system based on simple assumptions (McLean and Kirkwood, 1990), such as the model considered by Hadeler and Freedman (1989) for predator-prey populations with parasitic infection, or the model of continuous bioreactor analyzed by Lenbury and Orankitjaroen (1995).

As Mosetti (1992) has observed, the control of ecological systems for management purposes is a difficult task due to the amount of supporting data needed as well as the conflicting management goals. In this respect, a simple reduced strategic model which requires fewer data for calibration can be quite a useful tool as a building block for the study of real problems in order to give a decision-maker some preliminary results.

The Kolmogorov model of population growth is, mathematically, probably the most general model of the types considered to date. It incorporates the principle that the growth rate of species is proportional to the number of interacting species present. The classical ecological models of interacting populations have typically focussed on two species. The first Kolmogorov model, developed in 1936, was expanded on by several researchers, including May (1972) and Albrecht et al (1974). Such models have been applied to plant and animal dynamics both in aquatic and terrestrial environments (Hastings and Powell, 1991). However, mathematical developments reveal that community models involving only two species as the building blocks may miss a great deal of important ecological behavior. In fact, it is now recognized that in community studies the essence of the behavior of a complex system may only be understood when attempts are made to incorporate the interactions among a larger number of species.

Researchers in the last decade or so have turned their attention to the theoretical study of food webs as the "building blocks" of ecological communities and have been faced with the problem of how to couple the large number of interacting species. Behavior of the entire community is then assumed to arise from the coupling of strongly interacting pairs. The approach is attractive by its virtue of being tractable to theoretical analysis (Hastings and Powell, 1991). Yet, many researchers have demonstrated that

very complex dynamics can arise in model systems with three species (Gilpin, 1979; Rai and Sreenivasan, 1993). For example, an investigation by Hastings and Powell (1991) showed that a continuous time model of a food chain incorporating nonlinear functional responses can exhibit chaotic dynamics in long-term behavior when reasonable parametric values are chosen. The key feature observed in this chaotic dynamics is the sensitive dependence on initial conditions.

In this paper, we first study the possibility of making the ecosystem output or variables less sensitive to irregular disturbances by applying the feedback control technique in order to stabilize the system. A feedback control law is derived to decouple the effect of the predators from the prey dynamics in a three-species food web of the Kolmogorov type. It is found that the necessary and sufficient conditions for the existence of the decoupling control law rely on the persistence of the prey population and the fact that the specific growth rate of prey depends explicitly on the superpredator population density at any moment in time.

We demonstrate by the construction of a bifurcation diagram for a model with response functions of the Holling type II that, without any control action, chaotic behavior may result through period doubling bifurcations. Once, the feedback decoupling control action is in place, the system can be stabilized and, in this context, we obtain a process which is more easily controllable.

Moreover, when the Kolmogorov type model with input / removal terms is applied to an activated sludge process, the main objective is perhaps to regulate the inputs in order to obtain satisfactory water quality. By simply fine-tuning the point in time when the control action is set in motion, the control technique considered here can be adjusted to give the desirable outcome.

# THE KOLMOGOROV TYPE MODEL AND THE STATIC DECOUPLING PROBLEM

We consider a general Kolmogorov type model of n-species food webs, which may be written as follows

$$X_i = X_i F_i + u_i, i = 1, 2, ..., n$$
 (1)

where  $X_i$  is the *i-th* species population density,  $u_i$  is the input/removal (replenishment/harvesting) rate

of the species which depends on the population densities of all n-species in the food web, and

$$F_i = F_i(X_1, X_2, ...X_n), i = 1, 2, ..., n$$

Such a system (1) can be used to model population dynamics of plant or animal interactions in an aquatic or terrestorial environment such as in the work of Lenbury and Siengsanan (1993), where an activated sludge process was analyzed using a three-species Kolmogorov type model. Also, in the study by Lenbury and Likasiri (1994), the dynamic behavior of a model for a food web was investigated through the application of the singular perturbation technique.

To formulate the static feedback decoupling problem, we let

$$X = (X_1, X_2, ... X_n)^t$$
  

$$F = (F_1, F_2, ... F_n)^t$$
  

$$U = (u_1, u_2, ... u_{n-1})^t$$

and

$$G(X) = \begin{pmatrix} 1 & 0 & 0 & \cdots & 0 \\ 0 & 1 & 0 & \cdots & 0 \\ \vdots & \vdots & \ddots & \cdots & \vdots \\ 0 & 0 & 0 & \cdots & 1 \\ 0 & 0 & 0 & \cdots & 0 \end{pmatrix}$$

an  $n \times (n-1)$  matrix.

Then, the system of equations (1) with  $u_n = 0$  can be rewritten as

$$X_i = X_i F_i + [GU]_i, \quad i = 1, 2, ..., n$$
 (2)

If we now take  $X_1$  to be the state variable which is more easily regulated externally, the "outcome" or output of equation (2) is then assumed to be

$$H(X) \equiv (X_n, X_2, \dots X_{n-1})^t$$
 (3)

The static feedback decoupling problem, as stated in the work by Mosetti (1992) and explained in greater detail by Isidori (1985), can be defined as follows. "Given equations (2) and (3), we need to find a feedback law  $\alpha(X)$  and a state-dependent change of coordinates  $\beta(X)$  in the input space  $\mathfrak{R}^n$  such that the closed-loop system formed by the combination of (2) and (3) with the control law

$$U = \alpha(X) + \beta(X)V$$
,  $U \in \Re^{n-1}$ ,  $V \in \Re^{n-1}$ 

has the i-th output dependent only on the i-th component of the new input V".

In order to accomplish this, we introduce the following notation. Letting

$$\nabla^* = \left( X_1 \frac{\partial}{\partial X_1} \quad X_2 \frac{\partial}{\partial X_2} \quad \cdots \quad X_n \frac{\partial}{\partial X_n} \right)$$

then the operator  $\nabla_F$  is defined as

$$\nabla_F H_i = F \nabla^* H_i$$

where  $H_i$  is the *i-th* component of the vector H(x)defined in (3).

We then understand that

$$\nabla_F^k H_i = \nabla_F (\nabla_F^{k-1} H_i)$$

while  $\nabla_{F}^{0}H_{i}=H_{i}$ .

Further, the characteristic number  $\rho_i$  associated with the output  $H_i$  can be defined as the largest integer such that for all  $k < \rho_i$ 

$$grad(\nabla_F^k H_i)G_j = 0$$
 ,  $j = 1, 2, ..., n-1$ 

where  $G_i$  is the *j-th* column of the matrix G.

Accordingly, the decoupling matrix A(X)associated with equations (2) and (3) is the (n-1)x(n-1) matrix

$$A(X) = \left(a_{ij}\right)$$

where

$$a_{ij} = \operatorname{grad}(\nabla_F^{\rho_i} H_i) G_j$$

The static state-feedback decoupling theory (Mosetti, 1992) can be stated as follows.

Theorem 1A necessary and sufficient condition for the existence of  $(\alpha, \beta)$  which solves the decoupling problem is that the decoupling matrix A(x) is nonsingular. If this is the case then a possible decoupling control is given by

$$\alpha(X) = -A^{-1}(X)J$$
 and 
$$\beta(X) = A^{-1}(X)$$

where

$$J = (\nabla_F^{\rho_1+1} H_1, \nabla_F^{\rho_2+1} H_2, ..., \nabla_F^{\rho_n+1} H_n)'$$

provided that the decoupling matrix A(X) is nonsingular.

Proof We refer readers to Isidori's work (1985) for the proof of this theorem in the general case.

In order to establish the control law for the Kolmogorov type model, we need to first prove the following Lemma.

**Lemma** 1The characteristic number  $\rho_1 = 1$  and  $\rho_i$ = 0, i = 2, 3, ..., n - 1.

Proof In the case of  $\rho_1$  (i = 1), we first consider grad  $(\nabla_F^k H_1)G_j$ , j=1, 2, ..., n-1, when k=0. We find that

$$\operatorname{grad}\left(\nabla_{F}^{0}H_{1}\right)G_{j}=\operatorname{grad}\left(X_{n}\right)G_{j}$$

$$= \left(\frac{\partial X_n}{\partial X_1} \frac{\partial X_n}{\partial X_2} \dots \frac{\partial X_n}{\partial X_n}\right) \begin{bmatrix} 0 \\ 0 \\ \vdots \\ 0 \\ 1 \\ 0 \\ \vdots \\ 0 \end{bmatrix} \leftarrow j - th \text{ row}$$

$$= \begin{pmatrix} 0 & 0 & \dots & 0 & 1 \end{pmatrix} \begin{pmatrix} 0 \\ 0 \\ \vdots \\ 0 \\ 1 \\ 0 \\ \vdots \\ 0 \end{pmatrix} \leftarrow j - th \text{ row}$$

$$= 0$$

since j < n.

However, when k = 1, we find  $\operatorname{grad} \left( \nabla_F^1 H_1 \right) G_j = \operatorname{grad} \left( \nabla_F^1 X_n \right) G_j$ 

$$= \operatorname{grad} \left\{ \begin{pmatrix} F_1 & F_2 & \cdots & F_n \end{pmatrix} \middle| \begin{array}{c} X_1 \frac{\partial X_n}{\partial X_1} \\ X_2 \frac{\partial X_n}{\partial X_2} \\ \vdots \\ X_n \frac{\partial X_n}{\partial X_n} \end{array} \right\} G_j$$

= grad  $(F_n X_n) G_n$ 

$$= \left(\frac{\partial}{\partial X_{1}} \left(F_{n} X_{n}\right) \frac{\partial}{\partial X_{2}} \left(F_{n} X_{n}\right) \dots \frac{\partial}{\partial X_{n}} \left(F_{n} X_{n}\right)\right) \begin{vmatrix} 0\\0\\\vdots\\0\\1\\0\\\vdots\\0 \end{vmatrix}$$

$$\leftarrow j - th \text{ row}$$

$$= \frac{\partial}{\partial X_{j}} (X_{n} F_{n}) = X_{n} \frac{\partial F_{n}}{\partial X_{j}}$$

$$\neq 0$$

if we assume that  $F_n$  is an explicit function of  $X_i$  for all  $j=1,\,2,\,...,\,n-1$ . Therefore,  $\rho_1=1$ .

Now, for  $\rho_i$ , i = 2, 3, ..., n - 1, we consider grad  $(\nabla_F^k H_i)G_j$  for  $i \ge 2$  when k = 0, and obtain  $\operatorname{grad}\left(\nabla_{F}^{0}H_{i}\right)G_{i}=\operatorname{grad}\left(X_{i}\right)G_{i}$ 

$$= \left(\frac{\partial X_{i}}{\partial X_{1}} \frac{\partial X_{i}}{\partial X_{2}} \cdots \frac{\partial X_{i}}{\partial X_{j}} \cdots \frac{\partial X_{i}}{\partial X_{n}}\right) \begin{bmatrix} 0\\0\\\vdots\\0\\1\\0\\\vdots\\0 \end{bmatrix} \leftarrow j-th \text{ row}$$

$$A(x) = \begin{bmatrix} X_{n} \frac{\partial F_{n}}{\partial X_{1}} & X_{n} \frac{\partial F_{n}}{\partial X_{2}} & \cdots & \cdots & X_{n} \frac{\partial F_{n}}{\partial X_{n-1}}\\0 & 1 & 0 & 0 & \cdots & 0\\0 & 0 & 1 & 0 & \cdots & 0\\\vdots & \vdots & \vdots & \vdots & \vdots & \cdots & \vdots\\0 & 0 & 0 & 0 & \cdots & 1 \end{bmatrix}$$

$$= \begin{cases} 1 & \text{if } i = j \\ 0 & \text{if } i \neq j \end{cases}$$

Thus, grad  $(\nabla_F^0 H_i)G_j \neq 0$  for some j, which means that  $\rho_i = 0$  for i = 2, 3, ..., n - 1.

We can now derive the entries  $a_{ij}$  of the decoupling matrix A(x) as follows.

$$a_{ij} = \operatorname{grad} \left( \nabla^{1}_{F} H_{i} \right) G_{j}$$

$$= \operatorname{grad} \left\{ \left( F_{1} \quad F_{2} \quad \cdots \quad F_{n} \right) \left( \begin{array}{c} X_{1} \frac{\partial X_{n}}{\partial X_{1}} \\ X_{2} \frac{\partial X_{n}}{\partial X_{2}} \\ \vdots \\ X_{n} \frac{\partial X_{n}}{\partial X_{n}} \end{array} \right) \right\} G_{j}$$

= grad 
$$(F_n X_n) G_j$$
  
=  $X_n \frac{\partial F_n}{\partial X_j}$ 

for j = 1, 2, ..., n - 1.

On the other hand, for  $i \ge 2$ ,  $\rho_i = 0$ , we therefore obtain -

$$a_{ij} = \operatorname{grad} \left( \nabla_F^0 H_i \right) G_j$$
$$= \begin{cases} 1 & \text{if } i = j \\ 0 & \text{if } i \neq j \end{cases}$$

for j = 1, 2, ..., n - 1 and i = 2, 3, ..., n - 1. Thus, the decoupling matrix is

$$A(x) = \begin{bmatrix} X_{n} \frac{\partial F_{n}}{\partial X_{1}} & X_{n} \frac{\partial F_{n}}{\partial X_{2}} & \cdots & \cdots & X_{n} \frac{\partial F_{n}}{\partial X_{n-1}} \\ 0 & 1 & 0 & 0 & \cdots & 0 \\ 0 & 0 & 1 & 0 & \cdots & 0 \\ \vdots & \vdots & \vdots & \vdots & \cdots & \vdots \\ 0 & 0 & 0 & 0 & \cdots & 1 \end{bmatrix}$$

209

ScienceAsia 28 (2002)

# APPLICATION TO THREE SPECIES FOOD WEBS

The control law

We now derive the control law for the Kolmogorov type model for a three species food web which can be written as

$$x = x f(x, y, z) + u_1$$
 (4)

$$y = y g(x, y, z) + u_2$$
 (5)

$$z = z h (x, y, z)$$
 (6)

where z is the prey population density, y and x are the predator and superpredator, respectively, while  $u_1$  and  $u_2$  are the corresponding input rates. Then,

$$X = \begin{pmatrix} x & y & z \end{pmatrix}'$$

$$F = (f & g & h)$$

$$U = \begin{pmatrix} u_1 & u_2 \end{pmatrix}'$$

$$G(X) = \begin{pmatrix} 1 & 0 \\ 0 & 1 \\ 0 & 0 \end{pmatrix}$$

and the output is

$$H(X) = \begin{pmatrix} z & \nu \end{pmatrix}' \tag{7}$$

The main result of the static state-feedback decoupling theory can be stated as follows.

Theorem 2A necessary and sufficient condition for the existence of  $(\alpha, \beta)$  which solves the decoupling problem for equations (4)-(6) is that the prey population persists and the specific growth rate of prey h depends explicitly on the superpredator population density. If this is the case, then a possible decoupling control is given by:

$$\alpha(X) = \left(-xf - \frac{h}{h_x}(zh_z + h) - yg\right)^{t}$$

$$\beta(X) = \left(\frac{1}{zh_x} - \frac{h_y}{h_x}\right)$$

and

$$u_1 = -xf - \frac{h}{h_x}(zh_z + h) + \frac{1}{zh_x}v_1 - \frac{h_y}{h_x}v_2$$
 (8)

$$u_2 = -yg + V_2 \tag{9}$$

**Proof** From Lemma 1, we found that  $\rho_1 = 1$  and  $\rho_2 = 0$ . We then obtain

$$\nabla^* H_1 = \begin{pmatrix} 0 & 0 & z \end{pmatrix}'$$

so that  $\nabla^1_F H_1 = zh$ , and  $\nabla^0_F H_2 = y$ . Therefore, we are led to the decoupling matrix

$$A(X) = \begin{pmatrix} zh_x & zh_y \\ 0 & 1 \end{pmatrix} \tag{10}$$

Thus, A(X) is nonsingular if and only if det  $A \neq 0$ , namely

$$zh_{\nu} \neq 0$$
 (11)

This leads to the requirement that prey persists, in which case z > 0, and that  $h_x \neq 0$  or, equivalently, h depends explicitly on x.

Moreover, we have

$$\nabla_F^{\rho_1+1} H_1 = \nabla_F^2(z) = \nabla_F \{\nabla F(z)\}$$

$$= \nabla_{F} \left\{ \left( f \quad g \quad h \right) \begin{pmatrix} x \frac{\partial z}{\partial x} \\ y \frac{\partial z}{\partial y} \\ z \frac{\partial z}{\partial z} \end{pmatrix} \right\}$$

$$=\nabla_{F}(hz)$$

$$= \begin{pmatrix} f & g & h \end{pmatrix} \begin{pmatrix} x \frac{\partial}{\partial x} (hz) \\ y \frac{\partial}{\partial y} (hz) \\ z \frac{\partial}{\partial z} (hz) \end{pmatrix}$$

$$= xzfh_x + yzgh_y + z^2hh_z + zh^2$$

Also,

.

$$\nabla_F^{\rho_2+1} H_2 = \nabla_F^1(y)$$

$$= \begin{pmatrix} f & g & h \end{pmatrix} \begin{pmatrix} x \frac{\partial y}{\partial x} \\ y \frac{\partial y}{\partial y} \\ z \frac{\partial y}{\partial z} \end{pmatrix}$$

$$= gy$$

Therefore,

$$J = (\nabla_E^{\rho_1+1} H_1 \quad \nabla_E^{\rho_2+1} H_2)$$

$$= \begin{pmatrix} xzfh_x + yzgh_y + z^2hh_z + zh^2 \\ gz \end{pmatrix}$$

which leads us to

$$\alpha(X) = -A^{-1}(X)J$$

$$= -\left(\frac{1}{zh_x} \frac{h_y}{h_x}\right) \left(xzfh_x + yzgh_y + z^2hh_z + zh^2\right)$$

$$gy$$

$$= \begin{pmatrix} -xf - zh\frac{h_z}{h_x} - \frac{h^2}{h_x} \\ -gv \end{pmatrix}$$

while

$$\beta(X) = A^{-1}(X)$$

$$= \begin{pmatrix} \frac{1}{zh_x} & \frac{h_y}{h_x} \\ 0 & 1 \end{pmatrix}$$

as claimed.

If we now let

$$\xi = \frac{dz}{dt} \tag{12}$$

then, since z = zh, we have

$$\frac{d\xi}{dt} = \frac{\partial(zh)}{\partial x}x + \frac{\partial(zh)}{\partial y}y + \frac{\partial(zh)}{\partial z}z$$

$$= zh_x(xf + u_1) + zh_y(yg + u_2) + (zh_z + h)zh = V_1$$

by applying the law in equations (8) and (9). Also, using (9), we find

$$\frac{dy}{dt} = yg + u_2 = v_2$$

Therefore, in the new coordinate system  $(\xi, y, z)$  we have

$$\frac{d\xi}{dt} = V_1 \tag{13}$$

$$\frac{dy}{dt} = v_2 \tag{14}$$

$$\frac{dz}{dt} = \xi \tag{15}$$

which clearly shows the decoupled structure, namely, each of the control variables acts only on one state variable. In fact, to keep the system decoupled, one approach is to set  $v_1=0$ . Then,  $\xi$  now remains constant, say at  $\xi(t_0)$ .

Integrating (15), we obtain

$$z(t) = \xi(t_0)t = z(t_0)$$

Thus, if  $\xi(t_0) = 0$  at a given initial time  $t = t_0$  when the control is activated, then

$$z(t) = z(t_0)$$

for any subsequent time t, whatever the fluctuation of  $v_2$ . This means that the prey population will not depend upon variations in the predator or superpredator. This is the essential feature of this technique, whereby the variations in the predator and superpredators are decoupled from the prey dynamics.

#### Persistence conditions

The question of persistence has been dealt with in various literature in all its versions: weak persistence; strong persistence; and uniform persistence ScienceAsia 28 (2002) 211

(Huaping and Zhien, 1991). We shall give, in the following Lemma, the persistence conditions for the standard food web consisting of equations (4)-(6) with

$$f(x, y, z) = \frac{c_2 y}{b_2 + y} + \frac{c_3 z}{b_3 + z} - d$$
 (16)

$$g(x, y, z) \equiv \frac{c_1 z}{b_1 + z} + \frac{a_2 x}{b_2 + y} - d$$
 (17)

$$h(x, y, z) = r(1 - \frac{z}{k}) - \frac{a_1 y}{b_1 + z} - \frac{a_3 x}{b_1 + z}$$
 (18)

where d is the specific removal rate, and the terms

$$\frac{c_i z}{b_i + z}, \quad i = 1, 3$$

and

$$\frac{c_2y}{b_2+y}$$

ţ

are the population response functions of the Holling type II in which  $c_i$  is the maximum growth rate and  $b_i$  is the so-called half-saturation constant. The construction and analysis of the model in the case that  $u_1 = u_2 = 0$  may be found in the work of Lenbury and Likasiri (1994).

A standard food web given by equations (4)-(6) with (16)-(18) generally possesses only one positive equilibrium  $\hat{E} = (0, \hat{y}, \hat{z})$  and possibly only one

positive limit cycle  $\hat{\Gamma} = (0, \hat{y}(t), \hat{z}(t))$  for its subsystem (5)-(6) with x set equal to zero. Under this assumption, we are led to the following Lemma.

Lemma 2The food web given by equations (4)-(6) with (16)-(18) is persistent if

$$\frac{c_2 \stackrel{\circ}{y}}{\underset{b_2 + y}{\wedge}} + \frac{c_3 \stackrel{\circ}{z}}{\underset{\circ}{\wedge}} > d \tag{19}$$

and (in the case that  $\hat{\Gamma}$  exists)

$$\frac{1}{T} \int_{0}^{T} \left( \frac{c_{2} \dot{y}(t)}{b_{1} + \dot{y}(t)} + \frac{c_{3} \dot{z}(t)}{b_{1} + \dot{z}(t)} \right) dt > d \quad (20)$$

where T is the period of the limit cycle  $\Gamma$ , provided that  $u_1$  and  $u_2$  are identically zero. Otherwise, the population persists if

$$u_1(0, y, z) > 0$$
 (21)

and (in the case that  $\stackrel{\hat{}}{\Gamma}$  exists)

$$\frac{1}{T} \int_0^T u_1(0, \hat{y}(t), \hat{z}(t)) dt > 0$$
 (22)

**Proof** This is a straight forward extension of the result given in one of our earlier papers (Lenbury and Likasiri, 1994) with the addition of the input/removal terms  $u_1$  and  $u_2$ .

Consequently, on substituting (16)-(18) into (8) and (9), one obtains the following decoupling feedback law.

$$u_{1} = -x \left( \frac{c_{2}y}{b_{2} + y} + \frac{c_{3}z}{b_{3} + z} - d \right)$$

$$+ \frac{z(b_{3} + z)}{a_{3}} \left( r(1 - \frac{z}{k}) - \frac{a_{1}y}{b_{1} + z} + \frac{a_{3}x}{b_{3} + z} \right) \left( r(1 - \frac{2z}{k}) - \frac{a_{1}b_{1}y}{(b_{1} + z)^{2}} + \frac{a_{3}b_{3}x}{(b_{2} + z)^{2}} \right)$$

$$-\frac{b_3+z}{a_3z}V_1 - \frac{a_1(b_3+z)}{a_2(b_1+z)}V_2$$
 (25)

$$u_2 = -y \left( \frac{c_1 z}{b_1 + z} - \frac{a_2 x}{b_2 + y} - d \right) + v_2$$
 (26)

Figure 1 shows the time courses of the three state variables and the discharge rates  $u_1$  and  $u_2$  under normal conditions. We then chose to start our control action at the time  $t = t_0$  shown in the Figure

where  $z = \xi(t_0) = 0$ . Thus, the effect of the control action is seen in Figure 2 when the new input  $v_1$  is set equal to zero and  $v_2$  is taken to be of the form

$$V_2 = Ae^{-\mu} \sin \omega t$$

which corresponds to a damped sinusoidal input. The prey population density z becomes constant after the time  $t_0$ , while the predator and superpredator vary in a sinusoidal fashion with damping amplitude. As time passes, the new input rate  $\mathbf{v}_2$  becomes negligibly small and the corresponding population densities of all three species are maintained at constant levels as a result.

# CONTROL ACTION ON A CHAOTIC SYSTEM

In the work by Lenbury and Likasiri (1994), the model of a food web given by equations (4)-(6) with (16)-(18) and  $u_1 = u_2 = 0$  have been analyzed using the singular perturbation method. Explicit conditions were derived which separate the various dynamic structures and identify the limit cycles composed of alternately slow and fast transitions. In particular, it was found that the system will have a unique global attractor in the first octant which is a low-frequency limit cycle with a period of high-frequency oscillation if the following conditions hold on the system parameters.

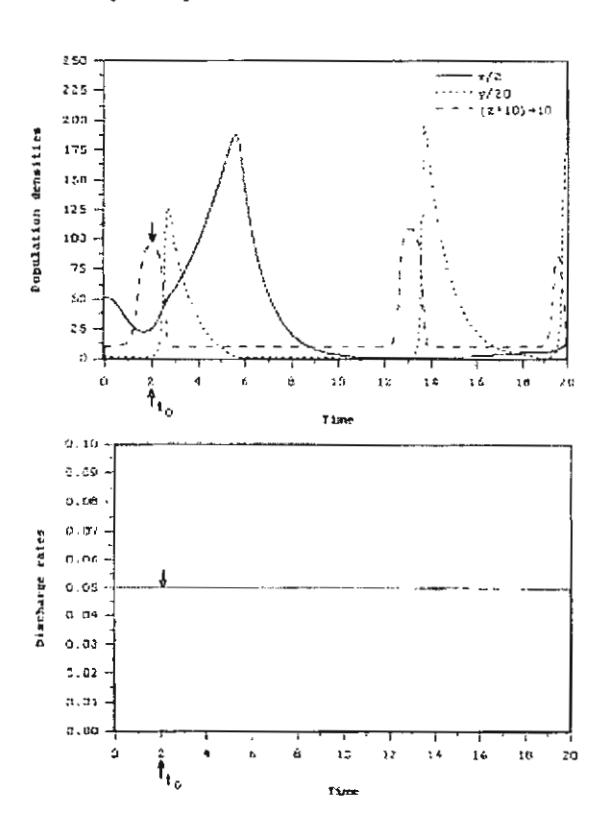


Fig 1. Time evolution of superpredator x (———), predator y (………), and prey z ( \_ \_ \_ \_ \_ \_ ), and constant discharge rates  $u_1$  and  $u_2$  with no control action. Here,  $a_1 = 0.05$ ,  $a_2 = 0.5$ ,  $a_3 = 0.5$ ,  $b_1 = 4.0$ ,  $b_2 = 8.0$ ,  $b_3 = 8.0$ ,  $c_1 = 15.0$ ,  $c_2 = 1.5$ ,  $c_3 = 1.5$ , d = 1.0, k = 10.0, r = 10.0,  $u_1 = 0.05$ , and  $u_2 = 0.05$ .

$$\frac{4a_1b_1b_2c_1k}{(b_1+k)^2} < \frac{r(b_3-b_1)[c_1(k-b_1)-d(b_1+k)]}{2b_3+k-b_1}$$
 (27)

$$k(c_1 - d) > b_1(c_1 + d)$$
 (28)

$$\frac{b2(c_1k-b_1d-dk)}{a_2(b_1+k)} < \frac{b_1b_3(a_1+r)[c_1(k-b_3)-d(2b_1+k-b_3)]}{(a_1b_3-a_3b_1d)(2b_1+k-b_3)+a_3b_1c_1(k-b_3)}$$
(29)

and 
$$\frac{c_i}{d}$$
 ( $i=1,2,3$ ) are sufficiently high.

We now carry out a numerical investigation to determine the ranges of parametric values where chaotic dynamics were likely. Our choice of parameters was guided by two factors. First, we follow the example of the work by Lenbury and Likasiri (1994) and assume that the ecological system under study may be characterized by highly diversified dynamics. Accordingly, we chose parametric values so that the time response of the

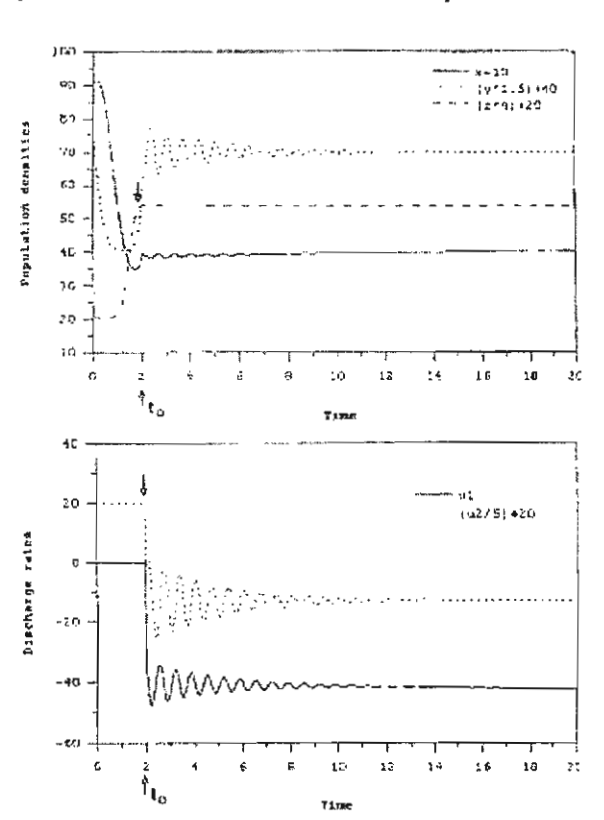


Fig 2. Time evolution of superpredator x, predator y, and prey z, and discharge rates  $u_1$  and  $u_2$  under control operations starting at  $t=t_0$  with  $v_1=0$  and  $v_2=100e^{\nu/3}\sin 3\pi t$ , and other system parameters as in Figure 1.

system equations (4)-(6) increases from top to bottom. The prey is assumed to have very fast dynamics, while the predator and superpredator have intermediate and slow dynamics, respectively. Phytoplankton - zooplankton - fish is a typical example of an ecosystem where the time response increases with the trophic levels. In fact, most food chains observed in nature have time responses increasing along the chain from top to bottom.

Second, as has been noted by many previous workers (Hastings and Powell, 1991; Rai and Sreenivasan, 1993), one may be able to generate chaos in a nonlinear system which already exhibits limit cycle behavior. We therefore chose parametric values to satisfy the conditions (27)-(29) found by Lenbury and Likasiri (1994) to lead to a solution trajectory on a low frequency limit cycle with bursts of high frequency oscillations.

Our investigation involves letting the system run for 100,000 time steps and examining only the last 80,000 time steps to eliminate transient behavior. We use values of  $b_1$  between 4.0 and 4.5, changing  $b_1$  in steps of 0.01. The relative maximum values  $\mathbf{x}_{\text{max}}^{1}$  of  $\mathbf{x}$ , collected during the last 80,000 time steps, are plotted as a function of  $b_1$  as shown in Figure 3.

We discover in this bifurcation diagram the appearance of a period doubling route to chaos, similar to those exhibited by one-dimensional difference equations such as the logistic population model. Apparently, the system of equations (4)-(6) with (16)-(18) exhibits chaotic dynamics for the values of  $b_1$  between 4.22 and 4.32. Windows in the bifurcation diagram are observed for  $b_1$  in the ranges of  $4.26 < b_1 < 4.32$  and  $4.34 < b_1 < 4.40$ , for example, where periodicity is re-established.

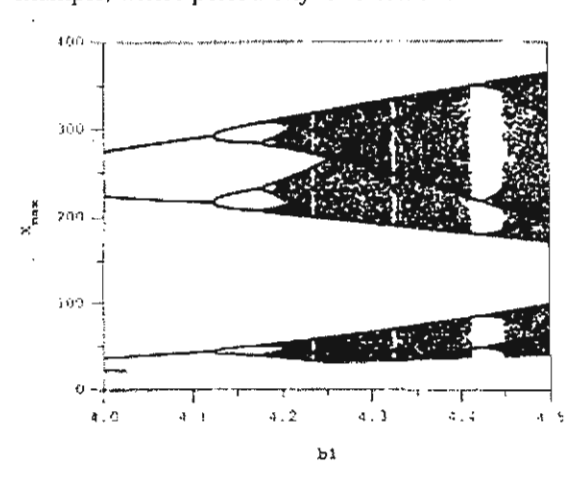


Fig 3. Bifurcation diagram for the model system (4)-(6) with (16)-(18), using the value of b<sub>1</sub> from 4.0 to 4.5, and other parametric values as in Figure 1. Plots are of the relative maximum values of x vs b<sub>1</sub>.

Figure 4 shows the solution trajectory of the model system (4)-(6) with (16)-(18) using  $b_1$  = 4.3 in the chaotic range identified in the bifurcation diagram. The strange attractor is projected onto the (y, z)-plane in Figure 4, and the corresponding chaotic time courses of x, y and z in uncontrolled conditions are shown in Figure 5 with the discharge rates  $u_1$  and  $u_2$ .

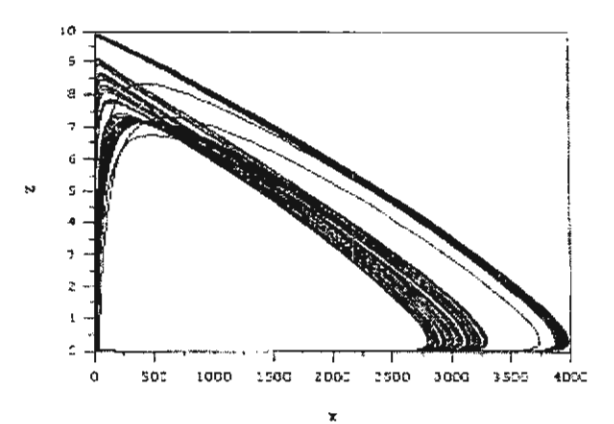


Fig 4. Projection onto the (y,z)-plane of the strange attractor obtained on simulating the model system (4)-(6) with (16)-(18) using  $b_1 = 4.3$  in the chaotic range identified in the bifurcation diagram, and other parametric values as in Figure 1.

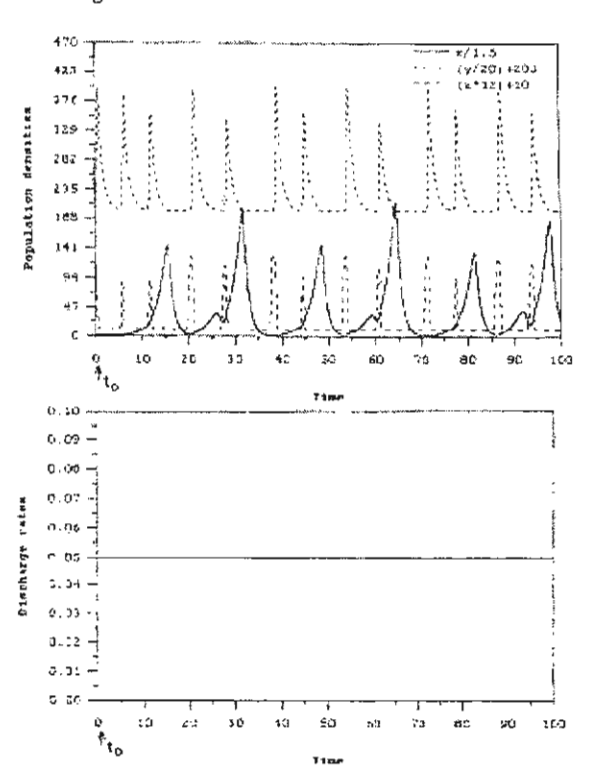


Fig 5. Time courses of the three state variables exhibiting chaotic behavior when there is no control action, and parametric values are as in Figure 4.

214 ScienceAsia 28 (2002)

Figure 6 shows the time courses of z starting from two different initial conditions. The difference in the two starting values of z is merely 0.01. We observe that, while the two plots follow indistinguishable paths during the initial short period, they begin to diverge and follow noticeably different paths eventually. This clearly demonstrates the sensitivity to initial conditions which is the essential characteristics of chaotic behavior.

Figure 7 then shows the effect of the control action on the chaotic system of Figure 4 with  $v_1$  set equal to zero and  $v_2$  irregular. Here, the control is ... initiated at the point where  $z(t_0) = 0$  and  $z(t_0) < 0$ . Once the control action is in place, prey is maintained at a constant high level, while the variations in predator, superpredator, and the discharge rates  $u_1$  and  $u_2$  are irregular.

On applying the model to an activated sludge process, the state variables can be nutrient-bacteria-protozoa, for example, and the objective of the control action is perhaps to regulate the inputs in order to obtain satisfactory water quality. In such a case, it is desirable to start the control action when the variable z falls to its first lowest point  $(z(t_0) = 0)$  and  $z(t_0) > 0$ . We will then be able to maintain z at a constant low level.

# CONCLUSION

It has been demonstrated that while some inherent properties of a nonlinear model permit the emergence of chaotic dynamics, they also allow the existence of a feedback decoupling control mechanism. Since the behavior of the entire community is believed to arise from the coupling of these strongly interacting species, the detection and possibility of control of a chaotic system is of critical importance. If a generalization from a food web model depends crucially upon behavior after a long time, then the role of chaos may be extremely relevant.

On a cautious note, the question of whether or not deterministic chaos actually occurs in a real ecosystem is still open to discussion. As has been observed by Sabin and Summers (1993), "... there is still no generally accepted example of a chaotic ecosystem in nature. Moreover, some traditional ecologists believe that irregular oscillations in natural populations are attributed to random perturbations or noise in the environment rather than being the result of the intrinsic nonlinear dynamics of the system".

Perhaps the first concrete example of occurrence of chaos in nature is due to Sugihara and May (1990) who showed that there underlies a three-dimensional chaotic attractor in the dynamics of marine planktonic diatoms. Despite the fact that the corresponding time series is very noisy, they have been able to extract the information which allows them to describe some of the dynamics as deterministic chaos.

Such irregular behavior is not desirable when one is interested in managing a system, since chaos allows

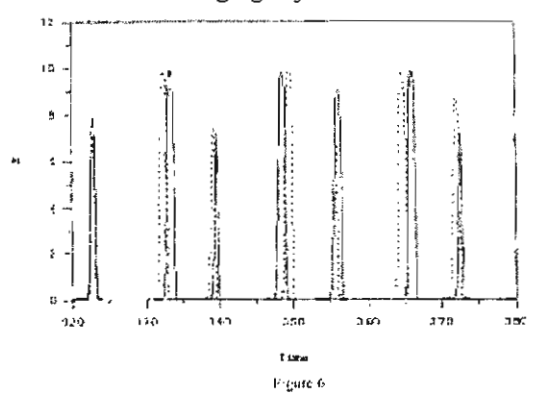


Fig 6. Divergence of solutions when the system exhibits chaotic dynamics. Prey densities are plotted for two different initial conditions ( \_\_\_\_\_ and \_\_\_\_), differing only by 0.01 in z.

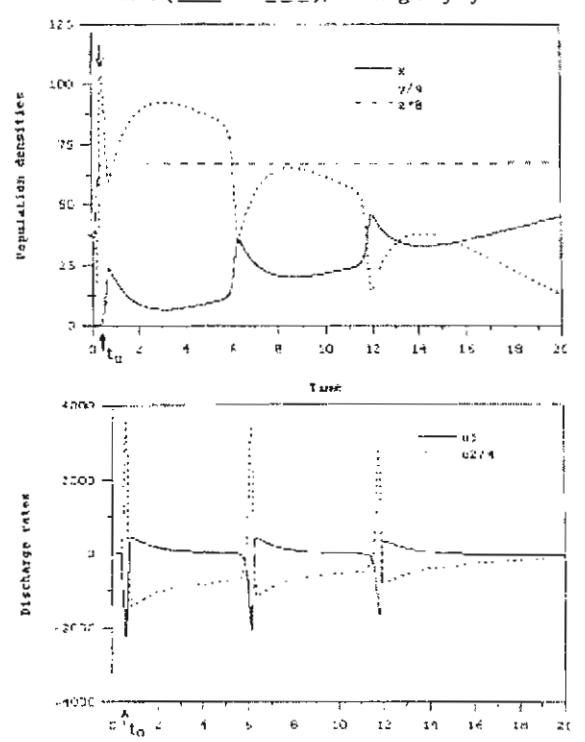


Fig 7. Time evolution of the three state variables, using parametric values of Figure 5. The chaotic system becomes stabilized when the control action is initiated at  $t = t_0$  with  $v_1 = 0$  and  $v_2$  irregular.

ScienceAsia 28 (2002) 215

only short-term predictions. Thus, a feedback control mechanism such as the one we have been discussing provides an attractive and useful tool to regulate the process since it can stabilize the system and make it less sensitive to the exogenous disturbances or noise input. The present study has potential to act as a spring board for a generalization to more complex models in the hope of obtaining a more manageable system.

# **ACKNOWLEDGMENT**

Appreciation is expressed to the Thailand Research Fund and the National Research Council of Thailand for the financial support which has made this research project possible.

#### REFERENCES

- Albrecht F, A Gatzke, A Haddad and N Wax (1974) The dynamics of two interacting populations. J Math Anal Appl 46, 658-70. Gilpin ME (1979) Spiral chaos in a predator-prey model. American Naturalist 107, 306-8.
- Hadeler KP and HI Freedman (1989) Predator-prey populations with parasitic infection. J Math Biol 28, 609-31.
- Hastings A and T Powell (1991) Chaos in a three-species food chain. *Ecology* 72(3), 896-903.
- Holling CS (1966) In Systems Analysis in Ecology KEF Watt (ed) p 195. New York: Academic Press.
- Huaping L and M Zhien (1991) The threshold of survival for system of two species in a polluted environment. J Math Biol 30, 46-61.
- Isidori A. (1985) Non-linear Control Systems: An Introduction. Springer Lecture Notes in Control and Information Sciences. 297 pp Berlin: Springer-Verlag.
- Lenbury Y and S Orankitjareon (1995) Dynamic behavior of a membrane permeability sensitive model for a continuous bioreactor exhibiting culture rhythmicity. J Sci Soc Thailand 21, 97-116
- Lenbury Y and M Siengsanan (1993) Coexistence of competing microbial species in a chemostat where on population feeds on another. *Acta Biotechnol* 13, 1-18.
- Lenbury Y and C Likasiri (1994) Low- and high-frequency oscillations in a food chain where one of the competing species feeds on the other. Mathl Comput Modelling 20(7), 71-89.
- May RM (1972 Limit cycles in predator-prey communities. Science 177, 900-2.
- McLean AR and TBL Kirkwood (1990) A model of human immunodeficiency virus in T helper cell clones. J Theor Biol 147, 177-203.
- Mosetti R (1992) On the control of phytoplankton growth via a decoupling feedback law. Ecol Model 62, 71-81.
- Muratori S and S Rinaldi (1992) Low- and high-frequency oscillations in three dimensional food chain systems. SIAM J APPL MATH 52(6), 1688-1706.
- Rai V and R Sreenivasan (1993) Period-doubling bifurcations leading to chaos in a model food chain. Ecol Model 69, 63-77.
- Sabin GCW and D Summers (1993) Chaos in a periodically forced predator-prey ecosystem model. Math Biosci 113, 91-113.
- Sugihara G and RM May (1990) Nonlinear forecasting as a way of distinguishing chaos from measurement error in time series. Nature 344, 734-41.



BioSystems 70 (2003) 55-72



www.elsevier.com/locate/biosystems

# Modeling of bone formation and resorption mediated by parathyroid hormone: response to estrogen/PTH therapy

Chontita Rattanakul<sup>a</sup>, Yongwimon Lenbury<sup>a,\*</sup>, Nateetip Krishnamara<sup>b</sup>, David J. Wollkind<sup>c</sup>

Department of Mathematics, Faculty of Science, Mahidol University, Rama 6 Road, Bangkok 10400, Thailand
Department of Physiology, Faculty of Science, Mahidol University, Rama 6 Road, Bangkok 10400, Thailand
Department of Mathematics, Faculty of Science, Washington State University, Washington, WA 99164-3113, USA

Received 18 January 2002; received in revised form 11 September 2002; accepted 27 January 2003

#### Abstract #

Bone, a major reservoir of body calcium, is under the hormonal control of the parathyroid hormone (PTH). Several aspects of its growth, turnover, and mechanism, occur in the absence of gonadal hormones. Sex steroids such as estrogen, nonetheless, play an important role in bone physiology, and are extremely essential to maintain bone balance in adults. In order to provide a basis for understanding the underlying mechanisms of bone remodeling as it is mediated by PTH, we propose here a mathematical model of the process. The nonlinear system model is then utilized to study the temporal effect of PTH as well as the action of estrogen replacement therapy on bone turnover. Analysis of the model is done on the assumption, supported by reported clinical evidence, that the process is characterized by highly diversified dynamics, which warrants the use of singular perturbation arguments. The model is shown to exhibit limit cycle behavior, which can develop into chaotic dynamics for certain ranges of the system's parametric values. Effects of estrogen and PTH administrations are then investigated by extending on the core model. Analysis of the model seems to indicate that the paradoxical observation that intermittent PTH administration causes net bone deposition while continuous administration causes net bone loss, and certain other reported phenomena may be attributed to the highly diversified dynamics which characterizes this nonlinear remodeling process.

© 2003 Elsevier Science Ireland Ltd. All rights reserved.

Keywords: Bone remodeling; Parathyroid hormone control; Estrogen therapy

#### 1. Introduction

Bone is a highly organized tissue which differs from reproductive tissues in many aspects of its growth and turnover, are not dependent on gonadal hormones. It, however, provides support and protection as well as provides the environment for hemopoiesis. Moreover,

E-mail address: scylb@mahidol.ac.th (Y. Lenbury).

bone is the major calcium reservoir of the body since over 99% of total body calcium is stored in the skeleton (Heersche and Cherk, 1989).

In order to maintain its structural integrity, a great deal of new cells must be produced continuously (Heersche and Cherk, 1989). This involves two types of cells: the osteoblasts which are responsible for bone formation, and the osteoclasts which are responsible for bone resorption. The knowledge of how these cell types are regulated and how their proliferation and differentiation are stimulated is most important to our

<sup>\*</sup> Corresponding author. Tel.: +66-2-201-5341; fax: +66-2-201-5343.

3

understanding of factors regulating their number and activity in healthy or diseased human.

The skeleton undergoes continuous changes during growth and, until recently, was believed to reach its permanent shape after sexual maturation. However, it has now become clear that bone never attains permanent state (Albright and Sauders, 1990). After maximum skeletal mass has been reached, the final adult phase begins. A steady loss of bone mass, together with progressive architectural alterations continues throughout life, with the rate of change increasing with age. The severe loss of bone, especially cancellous (trabecular) bone, and the "spontaneous" fracturing of the remaining bone, characterizes the condition called osteoporosis (Whitfield et al., 1998).

Osteoporosis, a condition of generalized skeletal fragility caused by a reduction in bone mass as well as by a disruption of skeletal architecture, is a major cause of morbidity and mortality in postmenopausal women. It is estimated that women have lost 10% of their bone mass by the time they go through menopause and that 35% of cortical bone, and 50% of trabecular bone are lost over a lifetime (DeCherney, 1993).

Prevention and reversal of bone loss require a thorough understanding of the remodeling process in bone, the mechanism of bone formation, resorption, including the action of hormones such as estrogen and parathyroid hormone (PTH).

Albright et al. (1941), first called attention to estrogen deficiency as the cause of postmenopausal osteoporosis. It has now been widely accepted that estrogen deficiency plays an important role in the pathogenesis of osteoporosis and that estrogen therapy can prevent menopausal bone loss and reduces the risk of fracture. The mechanisms by which estrogen exerts its effects on bone remodeling process are not entirely understood, however, and several puzzling discoveries cannot be completely explained still. Recent studies (Albright et al., 1941; Prestwood et al., 1994) surprisingly indicated that short-term estrogen treatment of elderly women decreased values for biochemical markers of bone turnover significantly. Since estrogen therapy has some risks and side effects, the beneficial effect of prolonged estrogen treatment is put in question. Estrogen has important pharmacological side effects on skeletal tissues. Bone blood flow appears to be depressed by estrogen (Turner et al., 1994). A

change in blood flow might have profound effects on bone cell metabolism. High doses of estrogen result in weight loss in rats (Moon et al., 1991), and an increase in tumor formation was noted in aging rats following long-term treatment with estrogen.

The PTH has been proposed as an alternative agent that can replace lost bone and restore bone strength (Whitfield et al., 1998). Several researchers have investigated pulsatile PTH secretion in health and osteoporosis (Harms et al., 1989; Schmitt et al., 1996), concluding that pulsatile secretion of PTH in healthy young men is the physiological mode of secretion. Low pulsatile secretion of PTH might be related to low turnover osteoporosis. Paradoxically, however, PTH has been found (Kroll, 2000) to cause net bone loss (resorption) when administered in a continuous fashion, and net bone formation (deposition) when administered intermittently.

A sensible model of the process of bone formation and bone resorption should be capable of addressing and, to a certain extent, explain the puzzling discoveries mentioned before. We shall, therefore, develop a mathematical model for the differentiation of osteoblastic and osteoclastic populations in bone, based on the differential effects of PTH. The model is shown to admit pulsatile and chaotic secretory patterns in PTH levels conformal to clinical observations reported by Prank et al. (1995) recently. By expanding on the model, the question about the marked effect of short-term estrogen treatment, or the paradoxical effect of intermittent versus continuous PTH administrations mentioned before, can be explained as attributes of the highly diversified nonlinear dynamics which characterize this remodeling process.

#### 2. Model development

Bone, being a major reservoir of body calcium, is under the hormonal control of PTH (Kroll, 2000). Osteoclasts resorb bone and liberate calcium, but they lack receptors for PTH. The preosteoblastic precursors and preosteoblasts possess receptors for PTH, upon which the hormone induces differentiation from the precursors to preosteoblasts and from the preosteoblasts to osteoblasts. The osteoblasts, consequently generate IL-6, which induces preosteoclasts to differentiate into osteoclasts (Kroll, 2000).

Thus, bone remodeling is a continuous cycle of destruction and renewal of bone that is carried out by teams of osteoclasts and osteoblasts (Marcus, 1994). Osteoclasts and osteoblasts differentiate from less mature precursors, which line bone surfaces in an inactive state. In bone remodeling process, osteoclasts appear on a previously inactive surface of bone and then, they excavate a lacuna on the surface of cancellous bone or resorption tunnel in cortical bone. Osteoclasts are subsequently replaced by osteoblasts and finally, osteoblasts refill the resorption cavity. After osteoblasts have laid down their protein-based matrix, known as osteoid, they bury themselves in bony matrix, becoming osteocytes, or revert to an inactive cell form and line the bone surfaces as surface osteocytes or resting osteoblasts (Turner et al., 1994).

Therefore, the rate of bone deposition can be determined by the number of osteoblasts (B) while the rate of bone resorption can be determined by the number of osteoclasts (C), the balance between the number and activity of osteoblasts and osteoclasts determines whether net bone deposition or net bone resorption occurs. An excessively deep resorption space produced by osteoclasts, or an incomplete replenishment of the resorption space by the activation of osteoblasts can result in bone imbalance. If a remodeling imbalance exists after the completion of a remodeling cycle, the degree of bone loss will be exacerbated and that leads to osteoporosis (Turner et al., 1994).

We now proceed to construct our core model, the mathematical formulation of which is based biologically on clinical evidence observed in various reports such as that of Hock and Gera (1992), Dempster et al. (1993), Momsen and Schwarz (1997), Kong et al. (1999), Takahashi et al. (1999), Burgess et al. (1999), or Kroll (2000) amongst several others.

Firstly, since activated osteoclasts result from differentiation and activation of osteoclast precursors, we shall assume in what follows that a high level in osteoclast precursors is reflected in the high level of the resulting activated osteoclastic population C(t). Secondly, osteoclasts resorb bone and liberate calcium, in order to counter balance the high level of calcium in blood the rate of PTH secretion will decrease (Momsen and Schwarz, 1997). The equation for the rate of PTH secretion is then assumed to take the

form

$$\frac{\mathrm{d}P}{\mathrm{d}t} = \frac{c_1}{k_1 + C} - d_1 P \tag{1}$$

where P(t) denotes the level of PTH above the basal level. The first term on the right-hand side represents the secretion rate of PTH from the parathyroid grand which decreases with the increase in the number of active osteoclastic cells C(t),  $c_1$  and  $k_1$  being positive constants. This accounts for the above-mentioned observation that as active osteoclasts C resorb bone and liberate calcium, the rate of PTH secretion will decrease to counter balance the high level of calcium in blood. Therefore, a higher C should lead to lower PTH secretion rate. Finally, it is assumed that the hormone is removed from the system at the rate which is proportional to its current level with the removal rate constant  $d_1$ .

The dynamics of the osteoclastic population, on the other hand, can be described by the following equation

$$\frac{dC}{dt} = \frac{(c_2 + c_3 P)BC}{k_2 + P^2} - d_2 C \tag{2}$$

where the first term on the right-hand side represents the reproduction of active osteoclasts which requires the production of osteoclast differentiation factor (ODF) and its receptor on osteoclasts (Kroll, 2000). The more C means the more ODF receptors available for the reproduction of active osteoclasts, and hence the term is taken to depend on the number of osteoclasts C at that moment in time.

Moreover, osteoclasts precursors possess RANK, a receptor of tumor necrosis factor (TNF) family that recognizes ODF through a cell-to-cell interaction with osteoblasts (Kong et al., 1999; Takahashi et al., 1999; Burgess et al., 1999; Kroll, 2000), hence the rate of reproduction is taken to depend also on the number of active osteoblastic cells B(t) at any time t. Based on the well founded theory on mathematical modeling and population dynamics known as the law of mass action (Leah, 1988), when an event occurs through cell-to-cell interaction of the two populations involved, the rate may then be assumed to vary as their product, provided that the event occurs randomly. However, the rate of reproduction of C increases with the increase in the level of PTH (Dempster et al., 1993; Weryha and Leclere, 1995). On the other hand, it has been clinically observed (Kroll, 2000) that as PTH level

increases further, it begins to inhibit osteoclastic reproduction, and hence the saturation expression  $(c_2 + c_3 P)/(k_2 + P^2)$  is assumed for the stimulating effect of PTH, where  $c_2$ ,  $c_3$ , and  $k_2$  are positive constants.

Thus, without any active osteoclasts or osteoblasts (C=0, B=0), the reproductive rate of C should vanish. On the other hand, C will be produced at the rate which varies directly as the product BC, by the law of mass actions mentioned before, with the variation constant  $c_2/k_2$  at vanishing P. With PTH mediation, however, this variation parameter increases initially with increasing P but decreases when P becomes too high according to the saturation function utilized in Eq. (2), where  $c_3$  is a measure of how late the inhibition effect will set in.

Finally, the dynamics of the active osteoblastic population B(t) can be described by the following equation

$$\frac{\mathrm{d}B}{\mathrm{d}t} = c_4 P - \frac{c_5 PB}{k_3 + P} - d_3 B \tag{3}$$

where c4 is the specific rate at which PTH stimulates reproduction of active osteoblasts (Brown, 1991; Isogai et al., 1996), while the second term on the right-hand side of Eq. (3) accounts for the clinically observed inhibition of osteoblastic differentiation due to the PTH (Kroll, 2000). PTH stimulates osteoblast differentiation in immature osteoblasts but inhibits it in more mature cells (Isogai et al., 1996), through the process of down-regulation of the PTH receptors on osteoblasts. IL-6, a cytokine produced by osteoblasts, enhances the anti-proliferative effects of PTH by suppressing the PTH-induced Ca<sup>2+</sup> transients in addition to the down-regulation of the PTH receptor caused by chronic activation of the protein kinase A signal pathway. Therefore, PTH and IL-6 produced by osteoblasts exert a receptor-mediated negative feedback on the conversion of preosteoblasts to osteoblasts (Kroll, 2000). The inhibition effect is assumed here to take the form of the Holling type response function  $c_5P/(k_3 +$ P) which means that there should be no such inhibition if B or P vanishes. The inhibition term  $c_5PB/(k_3+P)$ then tends to  $c_5 B$  at high PTH level, so that the osteoblastic formation is predominantly stimulated positively by PTH according to the first term  $c_4P$  in Eq. (3) at higher levels of this hormone. This is consistent with observed clinical data reported by both Tam et al. (1982) and Hock and Gera (1992), some of which

is shown in Fig. 1. The parameters  $c_5$  and  $k_3$  may then be varied to accommodate different physiological data of different individuals. The higher  $k_3$  means the inhibition remains effective still at higher level of PTH. The last terms in the above three equations are the removal rates of the three components of the remodeling process with rate constants  $d_1$ ,  $d_2$ , and  $d_3$ , respectively.

Our reference core model, therefore, consists of Eqs. (1)–(3), possessing highly diversified nonlinear characteristics, upon which further analysis and investigation may be carried out in an attempt to explain the mystifying empirical observations previously mentioned.

#### 3. Theoretical analysis

Now, the argument for our assumption that the system is characterized by highly diversified dynamics goes as follows. According to Whitfield et al. (1998), the need to repair microdamage in a patch of cortical bone is sensed by an interconnected network of cells called osteocytes, each of which is locked in a tiny cubicle inside the dense cortical bone. The damage may only strain the osteocytes or it may be severe enough for them to suicidally trigger a process called apoptosis. When osteocytes are injured or die, they stop producing a major suppressor of osteoclastic biosynthesis. This removes a major restraint on the production of new osteoclasts, each of which will live and dig for the next 2 weeks (Whitfield et al., 1998).

When the osteoclasts dissolve the bone mineral, a lot of Ca<sup>2+</sup> is released. The Ca<sup>2+</sup> concentration serves as a 2-way switch: "off" for the osteoclasts and "on" for the bone-making osteoblasts (Whitfield et al., 1998). Osteoblasts take about five times longer to fill the tunnels and trenches than osteoclasts take to dig them. When the patch is finally repaired 6–9 months later, the distress signals have stopped, the approximately 3-month-old members of the last osteoblast crew are now out of work, so they "commit apoptotic suicide," as explained in great detail by Whitfield et al. (1998).

In view of the above discussion, therefore, it is reasonable to assume that PTH, being the stimulating agent in both bone resorption and formation, should possess very fast dynamics, responding quickly to

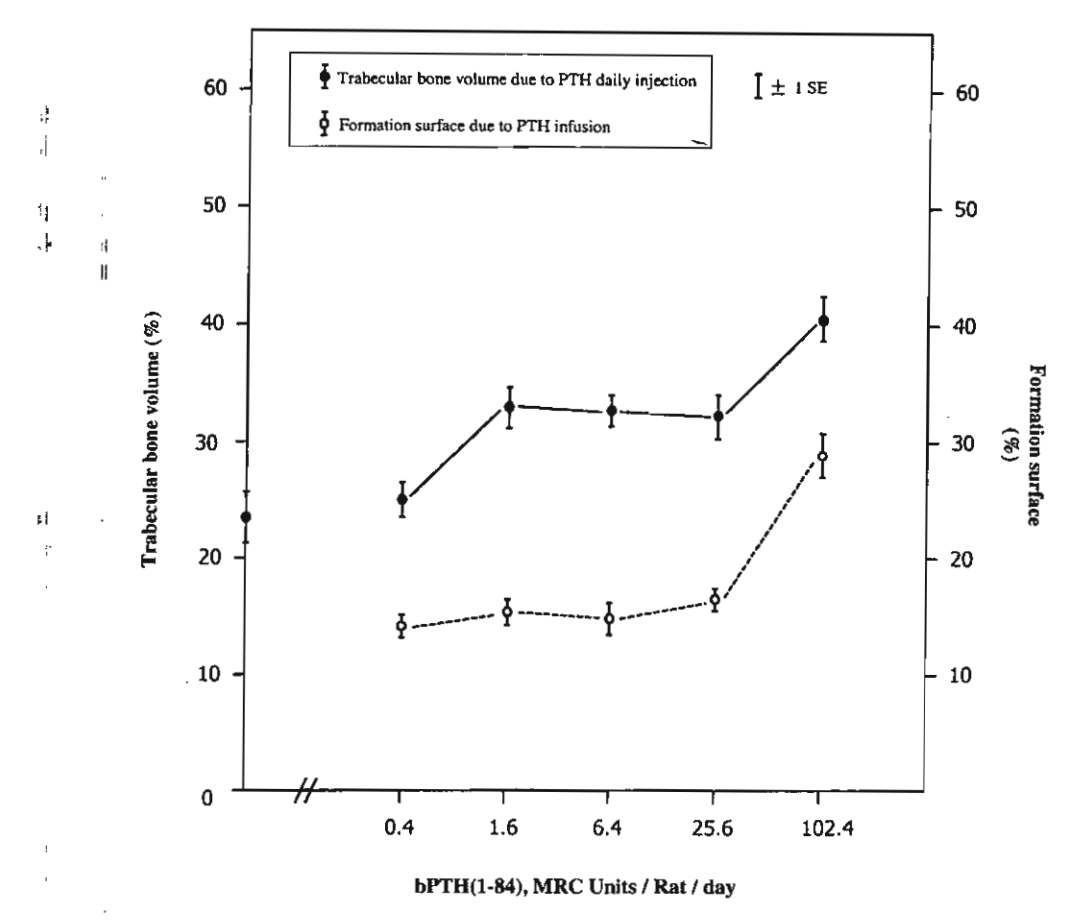


Fig. 1. Effects of PTH administration on bone surface formation and volume. (Adapted from Tam et al. (1982).)

changes in the cellular environment, specifically the Ca<sup>2+</sup>, concentration. The osteoclastic population is the component with intermediate dynamics and more stable than PTH, while the osteoblastic population possesses the slowest dynamics, lasting up to approximately 3 months, and therefore is the most stable of the three components in this system.

Supported by such well-documented clinical observation (Whitfield et al., 1998), we scale the components and parameters in terms of small parameters  $0 < \varepsilon \ll 1$  and  $0 < \delta \ll 1$  as follows. Letting x = P, y = C, z = B,  $a_1 = c_1$ ,  $a_2 = c_2/\varepsilon$ ,  $a_3 = c_3/\varepsilon$ ,  $a_4 = c_4/\varepsilon\delta$ ,  $a_5 = c_5/\varepsilon\delta$ ,  $b_1 = d_1$ ,  $b_2 = d_2/\varepsilon$ , and  $d_3 = d_3/\varepsilon\delta$ , we are led to the following system of differential equations.

$$\frac{dx}{dt} = \frac{a_1}{k_1 + y} - b_1 x \equiv F(x, y, z)$$
 (4)

$$\frac{\mathrm{d}y}{\mathrm{d}t} = \varepsilon \left[ \frac{(a_2 + a_3 x)yz}{k_2 + x^2} - b_2 y \right] \equiv \varepsilon G(x, y, z) \tag{5}$$

$$\frac{\mathrm{d}z}{\mathrm{d}t} = \varepsilon \delta \left[ a_4 x - \frac{a_5 x z}{k_3 + x} - b_3 z \right] \equiv \varepsilon \delta H(x, y, z) \quad (6)$$

which means that during transitions, when the right-hand sides of Eqs. (4)-(6) are finite and non-zero,  $|\dot{y}|$  is of the order  $\varepsilon$  and  $|\dot{z}|$  is of the order  $\varepsilon\delta$ . In the sequel, we will adopt the notation  $\dot{y} = O(\varepsilon)$  and  $\dot{z} = O(\varepsilon\delta)$ .

The system of Eqs. (4)–(6), with small  $\varepsilon$  and  $\delta$ , can be analyzed with geometric singular perturbation methods which, under suitable regularity conditions, allow approximation of solutions of the system by a sequence of simple dynamic transitions occurring at different speeds. A resulting singular curve, composed of these transitions, approximates an actual solution in

the sense that the real trajectory is contained in a tube around the curve, and that the radius of the tube tends to zero with  $\varepsilon$  and  $\delta$ . Examples where this technique has been applied to biological systems can be found in the work of Muratori and Rinaldi (1992) and that of Lenbury et al. (1997). A detailed description of singular perturbation theory can for instance be found in the work of O'Malley (1974) on this subject. The works by Jones (1994) and Kaper (1999) give good overviews of geometric singular perturbation methods. See also the classical text by Eckhaus (1979).

We call the system of Eqs. (4)–(6) the fast system. In the form of an intermediate system, where  $\varepsilon$  and  $\delta$  are positive, it can be written as follows

$$\varepsilon \frac{\mathrm{d}x}{\mathrm{d}\tau_1} = F(x, y, z) \tag{7}$$

$$\frac{\mathrm{d}y}{\mathrm{d}\tau_1} = G(x, y, z) \tag{8}$$

$$\frac{\mathrm{d}z}{\mathrm{d}\tau_1} = \delta H(x, y, z) \tag{9}$$

where  $\tau_1 = \varepsilon t$ , or in the form of the slow system

$$\varepsilon \delta \frac{\mathrm{d}x}{\mathrm{d}\tau_2} = F(x, y, z) \tag{10}$$

$$\delta \frac{\mathrm{d}y}{\mathrm{d}\tau_2} = G(x, y, z) \tag{11}$$

$$\frac{\mathrm{d}z}{\mathrm{d}\tau_2} = H(x, y, z) \tag{12}$$

with  $\tau_2 = \varepsilon \delta t$ . Evolution on the time-scale t is said to be fast, evolution on the time-scale  $\tau_1$  is intermediate, and evolution on the time-scale  $\tau_2$  is slow.

Geometric singular perturbation theory allows us to analyze the system of Eqs. (4)–(6) for small positive  $\varepsilon$  and  $\delta$  by suitably combining the dynamics of the fast, intermediate, and slow limits. Under certain regularity conditions and provided that the sets of critical points (critical manifolds) are normally hyperbolic for  $\varepsilon=0$ , and  $\delta=0$ , compact subsets of these critical manifolds persist as locally invariant slow or intermediate manifolds of the full problem Eqs. (4)–(6) for  $\varepsilon\neq0$ , and  $\delta\neq0$  but sufficiently small. These manifolds are  $O(\varepsilon)$  or  $O(\varepsilon\delta)$  close to  $\{F(x,y,z)=0\}$  and  $\{F(x,y,z)=0\}$ , respectively.

#### 4. Analysis of the manifolds

The shapes and relative positions of the manifolds  $\{F=0\}$ ,  $\{G=0\}$ , and  $\{H=0\}$  determine the directions, speeds, and shapes of the resulting solution trajectories. Therefore, we shall analyze each of the equilibrium manifolds in detail. The delineating conditions for the existence of limit cycle are arrived at from the close inspection of these manifolds.

#### 4.1. The manifold $\{F=0\}$

This manifold is given by the equation

$$x = \frac{a_1}{b_1(k_1 + y)} \equiv U(y) \tag{13}$$

We see that this manifold is independent of the slow variable z, thus this manifold is parallel to the z-axis and intersects the (x, z)-plane at the point where

$$x = \frac{a_1}{b_1 k_1} \equiv x_1 \tag{14}$$

Moreover, U(y) is a decreasing function of y, so that  $x \to 0$  as  $y \to \infty$  along this curve.

#### 4.2. The manifold $\{G=0\}$

This manifold consists of two submanifolds. One is the trivial manifold y = 0, while the other is the nontrivial manifold given by the equation

$$z = \frac{b_2(k_2 + x^2)}{a_2 + a_3 x} \equiv V(x) \tag{15}$$

We see that this nontrivial manifold, shown in Fig. 2, is independent of the intermediate variable y, and thus this manifold is parallel to the y-axis. It intersects the (x, z)-plane along a curve which is asymptotic to the line

$$x = -\frac{a_2}{a_3} \tag{16}$$

The curve intersects the z-axis at the point where x = 0, and

$$z = \frac{b_2 k_2}{a_2} \equiv z_0 \tag{17}$$

attaining its minimum at the point where

$$x = -\frac{a_2}{a_3} + \sqrt{\left(\frac{a_2}{a_3}\right)^2 + k_2} \equiv x_{\rm m} \tag{18}$$

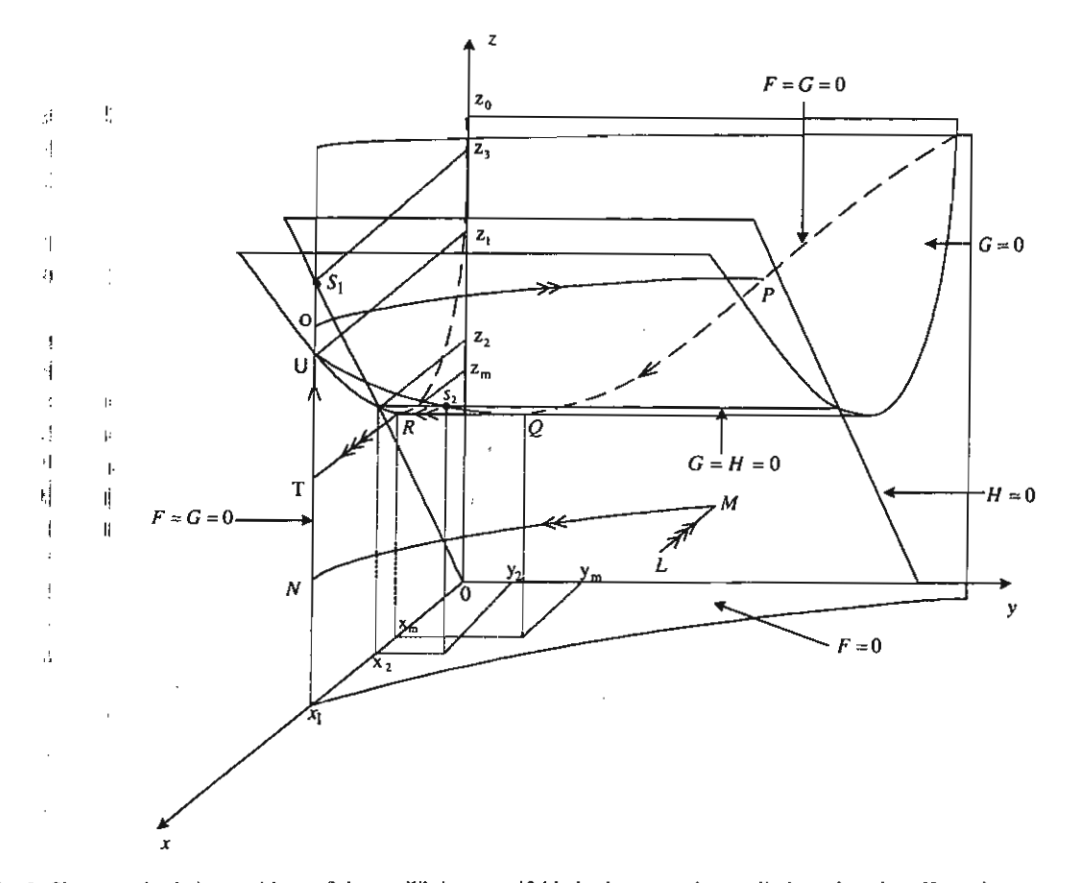


Fig. 2. Shapes and relative positions of the equilibrium manifolds in the case where a limit cycle exists. Here, three arrows indicate fast transitions, two arrows indicate transitions at intermediate speed, and a single arrow indicates slow transitions.

and 
$$z = V(x_m) \equiv z_m$$
 (19)

in the first octant.

Moreover, the manifold  $\{F=0\}$  intersects the trivial manifold y=0 along the line  $x=x_1$  on the (x,z)-plane. On the other hand, the manifold  $\{F=0\}$  intersects the nontrivial manifold given by (15) along the curve

$$z = \frac{b_2(k_2 + U^2(y))}{a_2 + a_3 U(y)}$$

which has a minimum point  $Q(x_m, y_m, z_m)$  where

$$y_{\rm m} \equiv \frac{a_{\rm 1-1}}{b_{\rm 1}x_{\rm m}} - k_{\rm 1} \tag{20}$$

utilizing (13). Also, the curve  $\{F = G = 0\}$  intersects the (x, z)-plane at the point U where y = 0,  $x = x_1$ ,

and

$$z = \frac{b_2}{b_1 k_1} \left( \frac{b_1^2 k_1^2 k_2 + a_1^2}{a_2 b_1 k_1 + a_1 a_3} \right) \equiv z_1$$
 (21)

Finally,  $z \to z_0$  as  $y \to \infty$  along this curve as shown in Fig. 2.

# 4.3. The manifold $\{H=0\}$

This manifold is given by the equation

$$z = \frac{a_4 x (k_3 + x)}{(a_5 + b_3) x + b_3 k_3} \equiv W(x)$$
 (22)

which is independent of y. Thus, this manifold is parallel to the y-axis, and intersects the (y, z)-plane along the y-axis. We also observe that W(x) is an increasing function of x in the first octant.

The manifold  $\{H = 0\}$  intersects the manifold  $\{G = 0\}$  along the straight line

$$\left\{ x = x_2, \quad z = \frac{b_2(k_2 + x_2^2)}{a_2 + a_3 x_2} \equiv z_2 \right\}$$
 (23)

which is parallel to the y-axis,  $x_2$  being the real solution of

$$(b_2a_5 + b_2b_3 - a_3a_4)x^3 + (b_2b_3k_3 - a_2a_4 - a_3a_4k_3)x^2 + (a_5b_2k_2 + b_2b_3k_2 - a_2a_4k_3)x + b_2b_3k_2k_3 = 0$$
(24)

which exists in the positive octant and is unique provided

$$b_2 a_5 + b_2 b_3 - a_3 a_4 < 0 (25)$$

$$b_2b_3k_3 - a_2a_4 - a_3a_4k_3 < 0 (26)$$

and

$$a_5b_2k_2 + b_2b_3k_2 - a_2a_4k_3 > 0 (27)$$

The manifold  $\{H = 0\}$  intersects the (x, z)-plane along the curve z = W(x) which intersects the line  $x = x_1$  at the point  $S_1 = (x_1, 0, z_3)$  where

$$z_3 = \frac{a_1 a_4 (b_1 k_1 k_3 + a_1)}{b_1 k_1 [a_1 (a_5 + b_3) + b_1 b_2 k_1 k_3]}$$
(28)

seen in Fig. 2.

Moreover, the curve  $\{F = G = 0\}$  intersects the curve  $\{G = H = 0\}$  at the point  $S_2 = (x_2, 0, z_2)$  located on the unstable portion QU of the curve  $\{F = G = 0\}$  as shown in Fig. 2, provided that

$$x_{\rm m} < x_2 < x_1$$

#### 5. Existence of an attracting limit cycle

The relative positions of the manifolds  $\{F = 0\}$ ,  $\{G = 0\}$ ,  $\{H = 0\}$ , and in particular the existence and position of the point  $S_2$  are apparently important for the existence of a limit cycle. After the calculations of the previous section, we are ready to state the main result of this paper.

**Theorem 1.** Suppose inequalities (25)–(27) hold. If  $\varepsilon$  and  $\delta$  are sufficiently small, and

$$x_{\rm m} < x_2 < x_1$$
 (29)

$$z_1 < z_3 < z_0 \tag{30}$$

where all parametric values are defined as before, then the system of Eqs. (4)–(6) has a global attractor, in the positive octant of the phase-space. This attractor is a limit cycle that is singular in the limit  $\varepsilon \to 0$ ,  $\delta \to 0$ . In that limit it can formally be constructed by concatenating various transitions occurring at three different speeds.

The proof of the theorem is based on geometric singular perturbation methods, which are elaborated by Jones (1994) and Kaper (1999) and utilized successfully in many areas. These methods rely heavily on using the different types of flows that can be distinguished: the fast O(1) flow, the intermediate O( $\varepsilon$ ) flow, and the slow O( $\varepsilon$  $\delta$ ) flow. Orbits can consist of various parts; in Fig. 2 the fast parts are indicated by three arrows, the intermediate parts by two arrows, and the slow parts by a single arrow. Under the conditions identified in the theorem, the shapes and relative positions are as in Fig. 2.

Take an initial point  $L = (x_0, y_0, z_0)$ , with  $F(x_0, y_0, z_0) \neq 0$ . Under the conditions in Theorem 1, without loss of generality we assume that the position of L is as in Fig. 2. L lies in the fast field on an orbit governed by

$$\frac{\mathrm{d}x}{\mathrm{d}t} = F(x, y, z), \quad \frac{\mathrm{d}y}{\mathrm{d}t} = 0, \quad \frac{\mathrm{d}z}{\mathrm{d}t} = 0$$
 (31)

and the  $\varepsilon=0$  orbit through L tends to the point M on the fast stable manifold F=0 while y and z remain constant. Generically,  $G(x, y, z) \neq 0$  at this point M. Then, on this manifold the flow with respect to the intermediate time  $\tau_1$  is given by

$$0 = F(x, y, z), \quad \frac{\mathrm{d}y}{\mathrm{d}\tau_1} = G(x, y, z),$$
$$\frac{\mathrm{d}z}{\mathrm{d}\tau_1} = \delta H(x, y, z) \tag{32}$$

For sufficiently small  $\delta$ ,  $0 < \delta \ll 1$ , this is again a singularly perturbed system. Inspection of G yields that  $\{G=0\}$  is normally hyperbolic attracting for the  $\delta=0$  flow restricted to  $\{F=0\}$ , and that the full manifold  $\{F=0\}$  serves as a stable manifold of  $\{G=0\}$  for the restricted  $\delta=0$  flow. The flow on

 ${F = 0, G \neq 0}$  is given by

$$0 = F(x, y, z), \quad \frac{dy}{d\tau_1} = G(x, y, z), \quad \frac{dz}{d\tau_1} = 0$$
(33)

and is hence  $O(\varepsilon)$  or intermediate in the direction of decreasing y, since G < 0 here. As long as  $G \neq 0$  the orbits on  $\{F = 0\}$  have constant x and z coordinates. Then, the orbit reaches the point N on the stable part of  $\{F = 0, G = 0\}$ , where the flow is prescribed by

$$0 = F(x, y, z), \quad 0 = G(x, y, z),$$

$$\frac{dz}{d\tau_2} = H(x, y, z)$$
(34)

and is hence  $O(\varepsilon\delta)$  or slow in the direction of increasing z, since H > 0 here, until the point O is reached, where the stability of  $\{F = 0, G = 0\}$  is lost. (The existence and location of the point O has been discussed and proved by Schecter (1985) and Osipove'et al. (1986).) The  $O(\varepsilon)$  time-scale becomes dominant once again. Hence, the orbit follows an intermediate path to the point P on the other stable part of  $\{F = 0, G = 0\}$ . Then, it tends to the point Q during which the flow is  $O(\varepsilon\delta)$  in the direction of decreasing z, since H<0here. Once the point Q is reached, a saddle node bifurcation occurs and the stability of  $\{F = 0, G = 0\}$ will again be lost. The  $O(\varepsilon)$  time-scale becomes dominant again. This yields an intermediate trajectory to the point R followed by a fast transition to the point T on the stable part  $\{F = 0, G = 0\}$ . Consequently, a slow transition with increasing z, since H > 0here, will bring the system back to the point O, followed by flows along the same path described before repeatedly, resulting in the closed cycle OPQRTO.

Thus, the existence of a limit cycle in the system for  $\varepsilon$  and  $\delta$  sufficiently small is assured. Finally, since L was arbitrary, the limit cycle is a global attractor.

A computer simulation of Eqs. (4)–(6) is presented in Fig. 3, with parametric values chosen to satisfy the inequalities identified in Theorem 1. The solution trajectory, shown in Fig. 3a projected onto the (x, y)-plane, tends to a limit cycle as theoretically predicted. The corresponding time courses of PTH and active osteoclastic population level C are shown in Fig. 3b and c, respectively. Such oscillatory behavior in the level of PTH has often been observed in clinical data (Albright et al., 1941; Prank et al., 1995, 1994).

On comparing the spaces between PTH peaks in our numerical simulation to those in available clinical data, we are able to estimate that the scale of 1 day is equivalent to 917 time steps in our model simulations.

#### 6. Nonlinear dynamics in PTH secretion

Several researchers (Albright et al., 1941; Prank et al., 1995, 1994) have reported evidence of non-linear dynamics in pulsatile secretion of PTH in normal human subjects. Prank et al. (1994) reported low-dimensional deterministic chaos in the pulsatile secretion of PTH in three young subjects. It appears that a phase-space analysis may allow the definition of health and disease by identifying the dynamic differences in the subjects' PTH secretory patterns.

In order to investigate the possibility of chaotic dynamics in the secretory pattern of PTH in our system, we carried out a numerical experiment on our model Eqs. (4)-(6). A bifurcation diagram was constructed by choosing parametric values that would lead to cycling in the x, y, and z components, guided by our work in the previous section, then letting the system run for  $10^5$  time steps. We retained only the last  $8 \times 10^4$  time steps to eliminate transient behavior, using the values of  $k_1$  between 0.08 and 0.1, and changing  $k_1$  in steps of  $10^{-5}$ . The relative maximum values  $x_{\text{max}}$  of x were collected during the last  $8 \times 10^4$  time steps and plotted against  $k_1$  as shown in Fig. 4. We discovered in this bifurcation diagram that periodic orbits of period 2 can be expected in the model system for values of  $k_1 > 0.097$ . Chaotic dynamics occur for  $k_1$  between 0.087 and 0.089, emerging through a period doubling route. In this chaotic range, the system is very sensitive to initial conditions. From experimenting numerically, we found that the time courses of solutions in this situation, which start at very slightly different initial values, will stay close for only a short time, before diverging and following drastically different paths as time passes.

A computer simulation of the model systems (4)–(6), with parametric values chosen under the above-mentioned guidelines and  $k_1 = 0.087$  in the chaotic range, is presented in Fig. 5. The strange attractor is shown projected onto the (x, y)-plane in Fig. 5a, and the corresponding chaotic time course of PTH is presented in Fig. 5b.

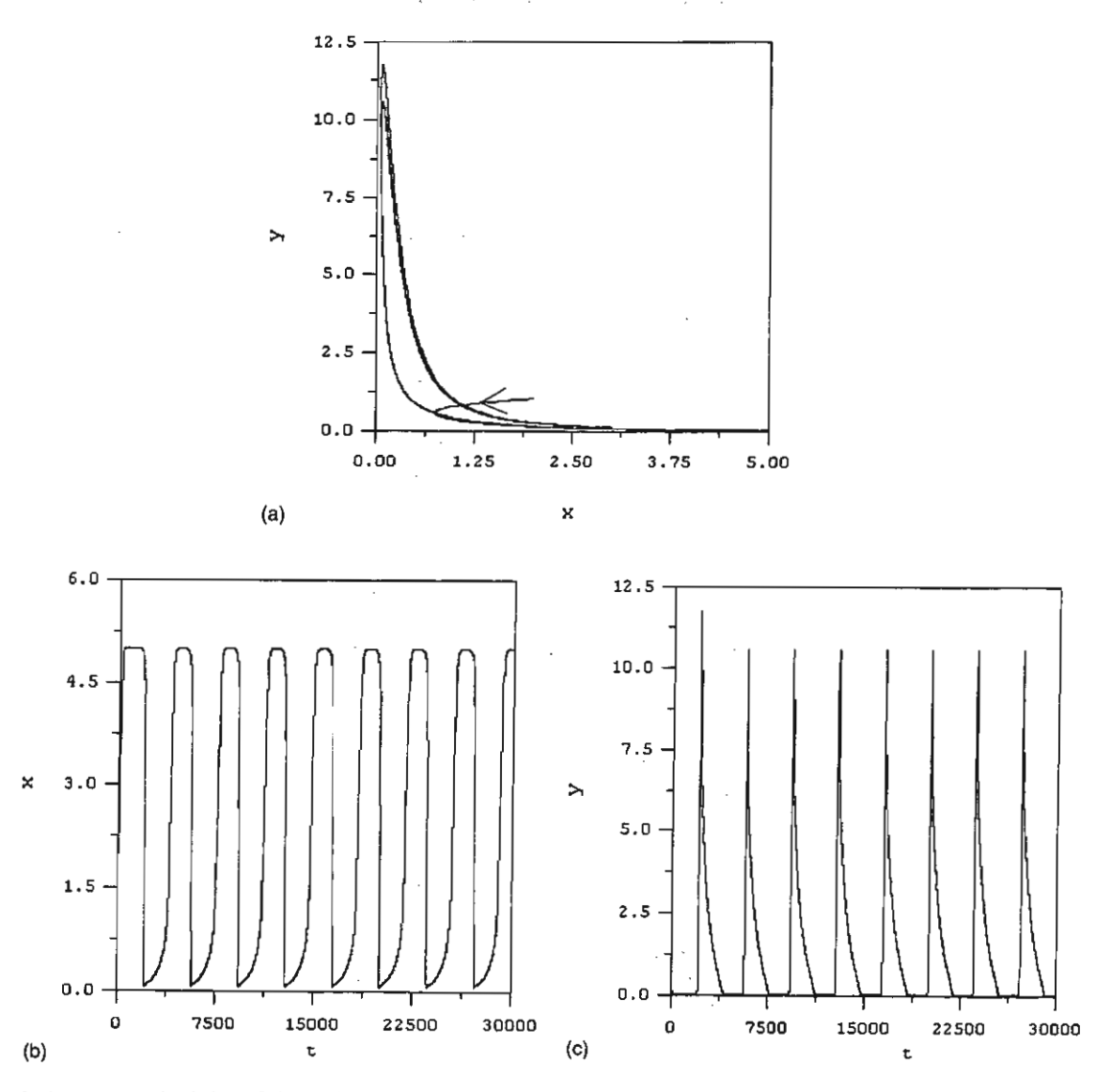


Fig. 3. A computer simulation of the model systems (4)–(6) with  $\varepsilon = 0.1$ ,  $\delta = 0.9$ ,  $a_1 = 0.05$ ,  $a_2 = 0.009$ ,  $a_3 = 0.675$ ,  $a_4 = 0.01$ ,  $a_5 = 0.005$ ,  $b_1 = 0.1$ ,  $b_2 = 0.3$ ,  $b_3 = 0.01$ ,  $k_1 = 0.1$ ,  $k_2 = 0.5$ ,  $k_3 = 0.025$ ,  $k_3 = 0.025$ ,  $k_4 = 0.025$ ,  $k_5 = 0.025$ ,  $k_6 = 0.025$ ,  $k_8 = 0.025$ ,  $k_8$ 

Thus, our model admits chaotic dynamics of PTH secretion, conforming to the clinical evidence in the above-mentioned reports which suggests a new interpretation of osteoporosis and hyperparathyroidism as dynamic diseases (Prank et al., 1994), associated with the loss of an adaptive hormonal rhythm.

# 7. Responses to PTH/estrogen therapy

We further illustrate how the characteristics of nonlinear diversified time responses inherent to the system modeled by Eqs. (4)–(6) can give rise to different surprising dynamic behavior which might seem puzzling when observed in clinical data.

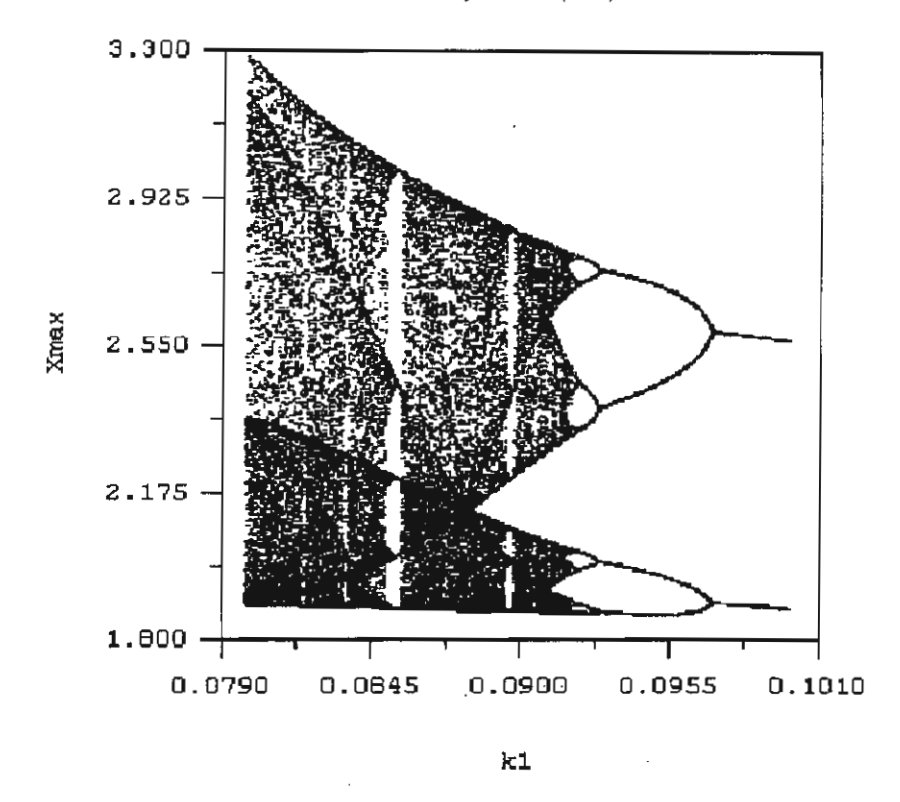


Fig. 4. Bifurcation diagram for the model systems (4)-(6) with  $\varepsilon = 0.8$ ,  $\delta = 0.1$ ,  $a_1 = 0.0900$ ,  $a_2 = 0.01125$ ,  $a_3 = 1.3750$ ,  $a_4 = 0.1125$ ,  $a_5 = 0.0625$ ,  $b_1 = 0.1500$ ,  $b_2 = 0.4375$ ,  $b_3 = 0.1250$ ,  $k_2 = 1.5000$ ,  $k_3 = 0.0250$ , and  $0.08 < k_1 < 0.1$ . Plots are of  $x_{\text{max}}$  against  $k_1$ .

#### 7.1. Responses to PTH administration

We investigate the action of PTH, administered continuously and intermittently, by first incorporating a term  $k_p > 0$  into the rate Eq. (4) to represent continuous administration of the PTH. The result of a computer simulation of the modified model system:

$$\frac{\mathrm{d}x}{\mathrm{d}t} = \frac{c_1}{k_1 + y} - b_1 x + k_p \tag{35}$$

$$\frac{\mathrm{d}y}{\mathrm{d}t} = \varepsilon \left[ \frac{(a_2 + a_3 x)yz}{k_2 + x^2} - b_2 y \right]$$
 (36)

$$\frac{\mathrm{d}z}{\mathrm{d}t} = \varepsilon \delta \left( a_4 x - \frac{a_5 x z}{k_3 + x} - b_3 z \right) \tag{37}$$

is shown in Fig. 6a. Here,  $k_p = 0.5$  and administration starts at  $t = t_0 = 10,000$ . We observe that oscillatory behavior in the active osteoblastic population ceases and the level tends toward a steady level higher than the peak levels attainable prior to the administration.

However, the active osteoclastic population shows an exponential increase, and hence a net bone loss can, therefore, be expected. Looking closely at the positions of the three equilibrium manifolds in Fig. 2, we can see that the addition of  $k_p > 0$  means a re-location of the manifold  $\{F = 0\}$  which results in the violation of the necessary condition for limit cycle behavior and the solution trajectory is forced to follow the curve on the manifold  $\{F = 0\}$  while  $x \to 0$ , and y increases without bound.

However, if we add the term  $k_p > 0$  only in pulses or intermittently, a different dynamic behavior is obtained, although the same value of  $k_p = 0.5$  is used. Fig. 6b shows the simulation result of daily administration of PTH which lasts for 6h at a time (using the time scale estimate mentioned at the end of Section 5). Although the active osteoblastic population still oscillates about a mean which is close to that prior to the start of the protocol, the active osteoclastic population now oscillates around a lower mean value

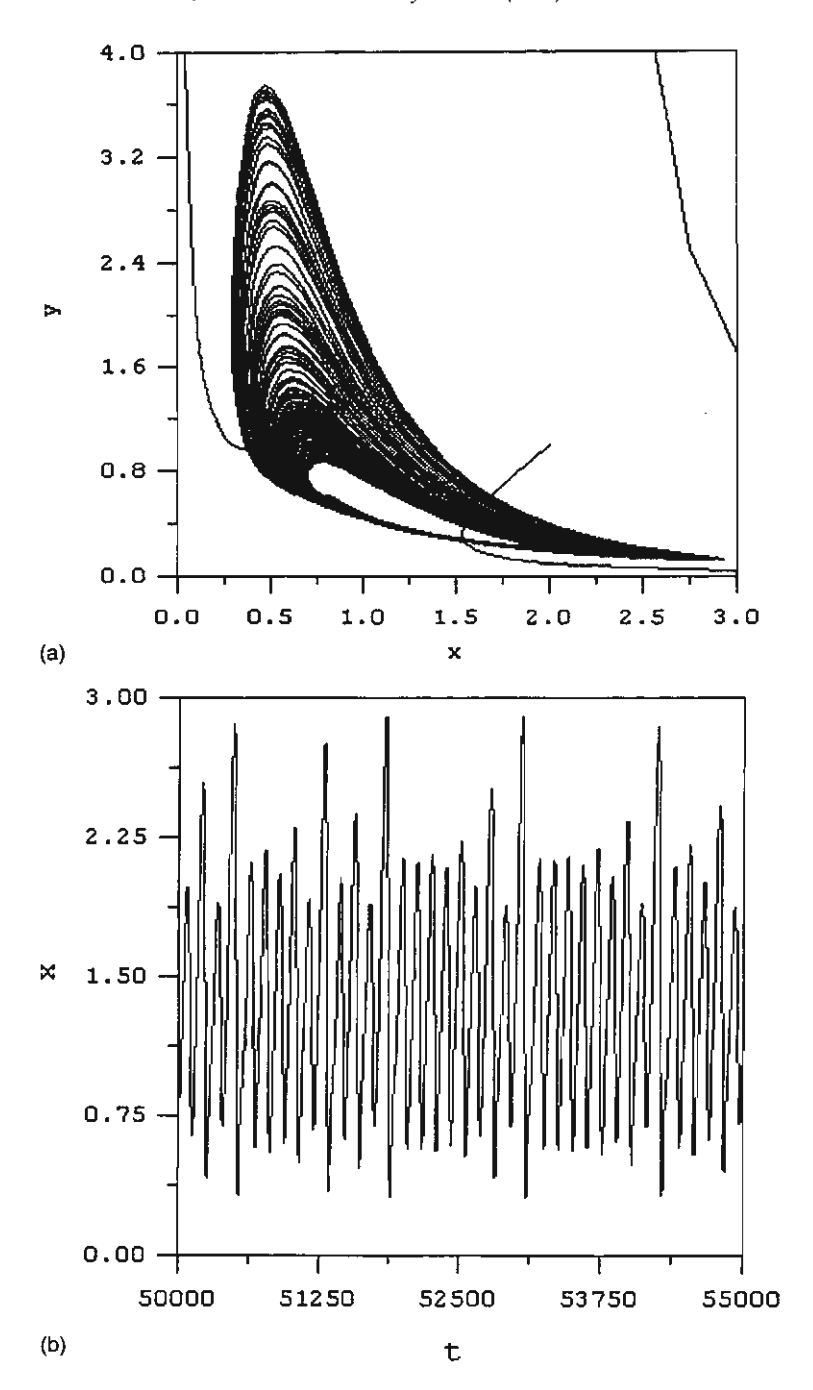


Fig. 5. A computer simulation of the model systems (4)–(6) with  $\varepsilon = 0.8$ ,  $\delta = 0.1$ ,  $a_1 = 0.0900$ ,  $a_2 = 0.01125$ ,  $a_3 = 1.3750$ ,  $a_4 = 0.1125$ ,  $a_5 = 0.0625$ ,  $b_1 = 0.1500$ ,  $b_2 = 0.4375$ ,  $b_3 = 0.1250$ ,  $b_2 = 1.5000$ ,  $b_3 = 0.0250$ , and  $b_4 = 0.087$  in the chaotic range, showing a strange attractor projected onto the (x, y)-plane in (a). The corresponding time series of PTH (x) is shown in (b).

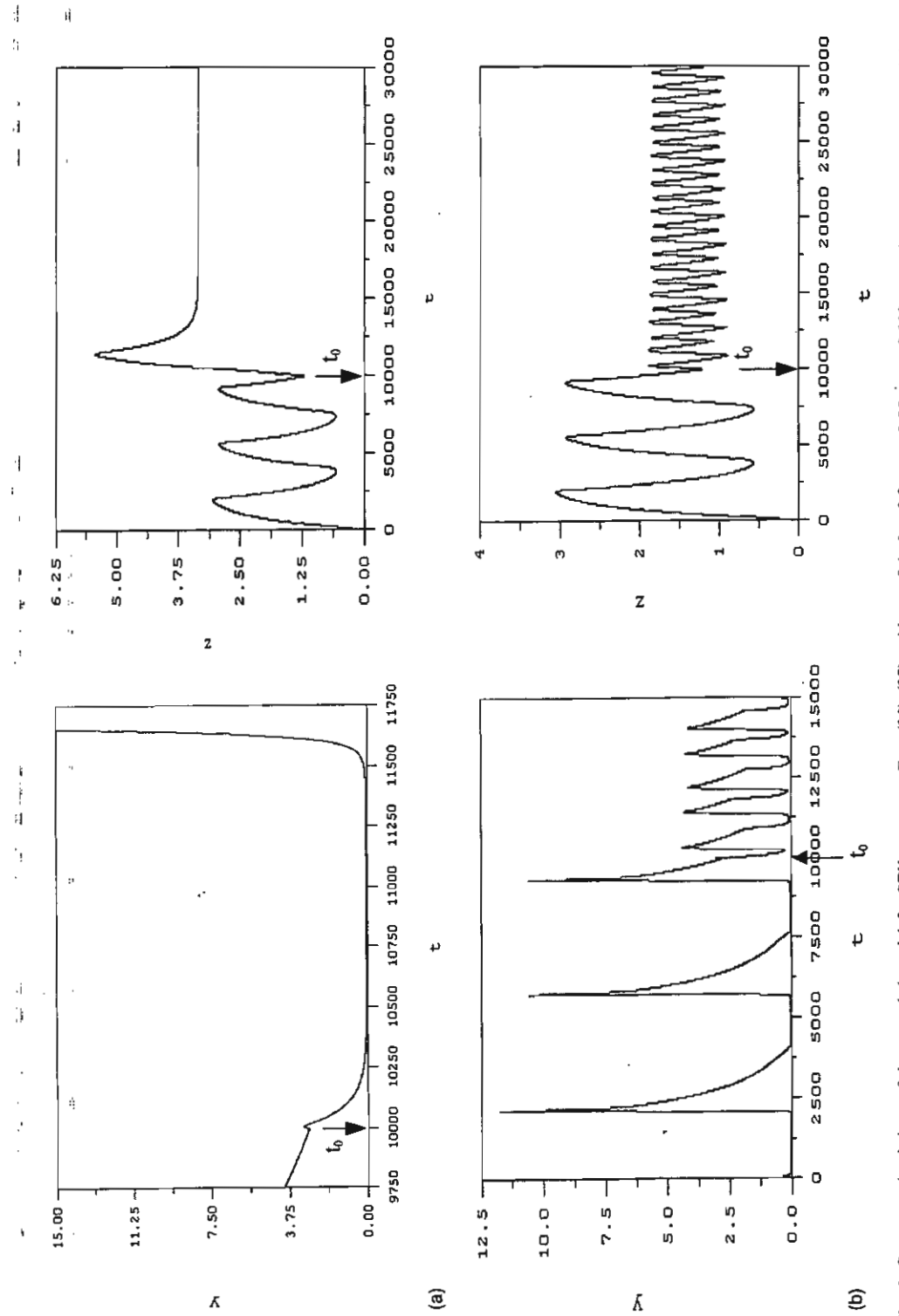


Fig. 6. Computer simulations of the extended model for PTH treatment, Eqs. (35)–(37), with e = 0.1,  $\delta = 0.9$ ,  $a_1 = 0.05$ ,  $a_2 = 0.009$ ,  $a_3 = 0.675$ ,  $a_4 = 0.01$ ,  $a_5 = 0.005$ ,  $b_1 = 0.1$ ,  $b_2 = 0.3$ ,  $b_3 = 0.01$ ,  $b_1 = 0.1$ ,  $b_2 = 0.3$ , and  $b_3 = 0.01$ ,  $b_3 = 0.025$ . PTH treatment, initiated at the time  $b_0 = 10,000$ , is continuous in (a) and for 6h daily in (b), with  $b_1 = 0.5$ .

and peaks at a much lower level. This results in apparent net bone formation, which is in agreement with the reports from several researchers (Kroll, 2000; Tam et al., 1982; Hock and Gera, 1992) that daily injection of the hormone caused an increase in the bone apposition rate, accompanied by an increase in the formation surface without an increase in the resorption surface. Continuous infusion, on the other hand, resulted in an increased apposition, increases in both formation and resorption surfaces, and a net decrease in bone volume.

Studying the three equilibrium manifolds more closely, we understand that the addition of  $k_p$  increases the rate of change of PTH in an episodic manner. The x-component (PTH) now has even faster dynamics and changes very quickly with time. Thus, C does not have time to reach a high peak, because it is pulled back down as the PTH level starts to rise very early and quickly, and similarly for the osteoblastic population. But since the effect only lasts 6 h at a time, the system returns to its oscillatory patterns in a short space of time. Thus, it appears that the behavior clinically observed is one of the manifestations of the nonlinearity property of the system together with the fact that the process is characterized by highly diversified dynamics. If PTH therapy is to develop into a viable alternative to estrogen treatment against osteoporosis, possibilities of such nonlinear or dissipative effects admitted by the system must be more closely scrutinized.

# 7.2. Responses to estrogen administration

On the other hand, realizing that long-term treatment of estrogen poses risks of side effects, we also attempted to better understand the action of estrogen on bone remodeling by again incorporating an extra term into the second rate Eq. (5) for the active osteoclastic population. According to Whitfield et al. (1998), in a young woman, a normal premenopausal estrogen concentration may limit the size of the preosteoclast population by stimulating apoptosis. But as her estrogen level declines with menopause, so does the estrogen receptor-mediated signaling; osteoclast precursors may thus live longer. Thus, to simulate the effect of daily intake to supplementary estrogen, we increase the removal rate of C by subtracting the term  $k_C y$ ,  $k_C > 0$ , from the rate Eq. (5) for a duration  $\Delta T$ of every interval of p days.

In so doing, we are assuming that estrogen is more stable than PTH and remains effective in the human body accumulatively over a long enough period so that daily intake of estrogen can be taken as equivalent to continuous application of the steroid, all through the time period  $\Delta T$ , during which time the model equations then become

$$\frac{\mathrm{d}x}{\mathrm{d}t} = \frac{a_1}{k_1 + y} - b_1 x \tag{38}$$

$$\frac{\mathrm{d}y}{\mathrm{d}t} = \varepsilon \left[ \frac{(a_2 + a_3 x)yz}{k_2 + x^2} - b_2 y - k_C y \right] \tag{39}$$

$$\frac{\mathrm{d}z}{\mathrm{d}t} = \varepsilon \delta \left( a_4 x - \frac{a_5 x z}{k_3 + x} - b_3 z \right) \tag{40}$$

Fig. 7 shows the results of computer simulations in two different cases. In Fig. 7a, the term  $-k_C y$  is kept in Eq. (39) for a duration of  $\Delta T = 12$  days, every interval of p = 28 days. We observe that when the administration period  $\Delta T$  is over, the effect still lasts for quite some time before the system recovers itself and there is a resetting of oscillatory behavior in the active osteoblastic population. The "plateau" is much wider than  $\Delta T$ . This is again a result of the diversified time responses of the three components in this nonlinear system. Since B is the very slow variable, it takes a long time to respond to the change in the proliferation rate of C. In particular, the plateau width is inversely proportional to  $\varepsilon$  and  $\delta$ . We also found, upon experimenting with different values, that different dosage (or  $k_C$ ) will yield different plateau width.

In Fig. 7b,  $\Delta T=21$  days, and p=28 days. We see that there is no longer any resetting of oscillatory behavior. Even though estrogen has already been cut off, the dissipative effect still lasts long enough to overlap with the next application of estrogen. This seems to suggest that with appropriate choices of  $\Delta T$ , p, and the prescribed dosage, administration may not necessarily be kept on for the entire time, while a net bone surface formation can still be expected.

#### 7.3. Investigating estrogen action in monthly bursts

In several clinical data, such as those mentioned in Muse et al.'s report (1986), estrogen level was

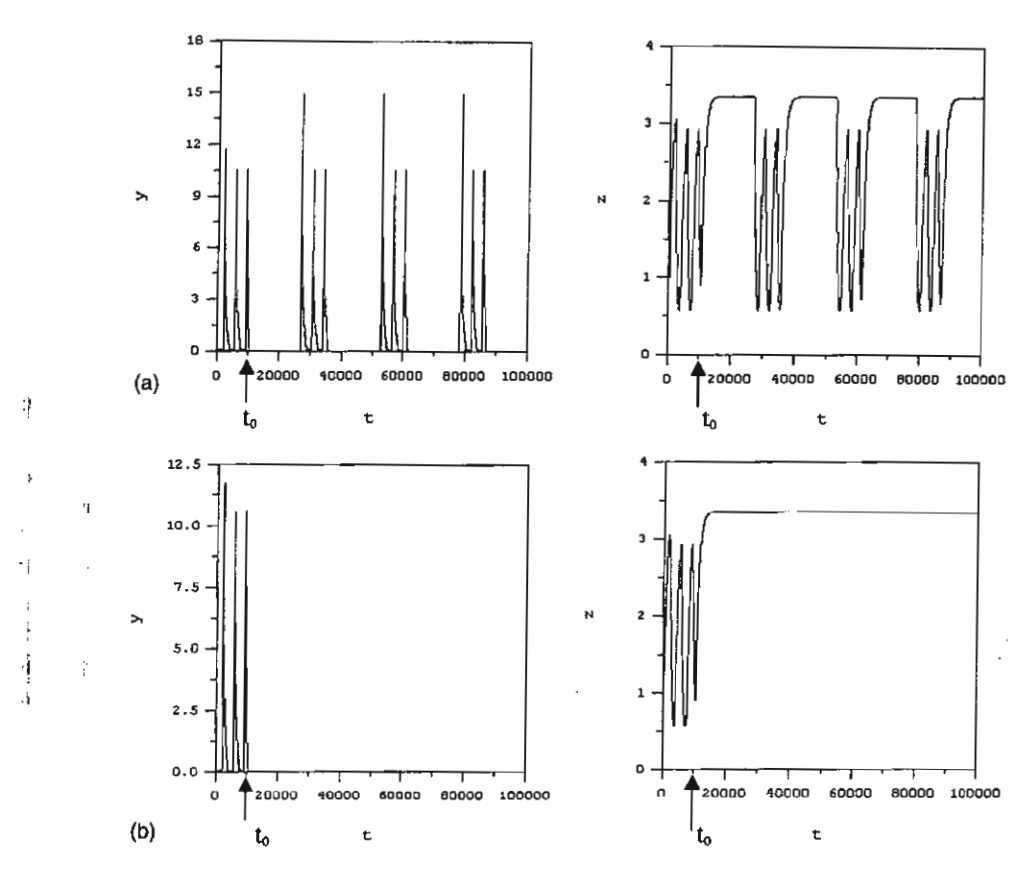


Fig. 7. Computer simulations of the extended model for estrogen treatment, Eqs. (38)–(40), with  $\varepsilon = 0.1$ ,  $\delta = 0.9$ ,  $a_1 = 0.05$ ,  $a_2 = 0.009$ ,  $a_3 = 0.675$ ,  $a_4 = 0.01$ ,  $a_5 = 0.005$ ,  $b_1 = 0.1$ ,  $b_2 = 0.3$ ,  $b_3 = 0.01$ ,  $k_1 = 0.1$ ,  $k_2 = 0.5$ , and  $k_3 = 0.025$ . The duration of estrogen treatment, initiated at the time  $t_0 = 10,000$ , is (a) 12 days, (b) 21 days, with  $k_C = 0.2$ .

observed to peak for a short period just a couple of days prior to menstruation across a woman's menstrual cycle. This may lead us to wonder whether such monthly bursts in estrogen secretion could play an important role in the controlling mechanism by which estrogen takes part in the regulation of bone mass balance in the premenopausal women. We investigate theoretically whether administration of estrogen in monthly (equivalently every 28 days) bursts to a postmenopausal subject could effect some observable change in the dynamics of the bone remodeling process which may compensate for the functional role of estrogen secretion in the premenopausal period. This is done by taking the system of Eqs. (38)-(40) to the limit as  $\Delta T \rightarrow 0$ , while p = 28 days, such that the single-bursts of estrogen across the menstrual cycle can be modeled by the original system Eqs. (4)-(6)

with the additional resetting conditions:

$$x(m+) = x(m-) \tag{41}$$

$$y(m+) = (1 - k_C)y(m-)$$
(42)

$$z(m+) = z(m-) \tag{43}$$

where m = pn, n = 0, 1, 2, ... and  $k_C$  represents the amplitude of the estrogen bursts. We can carry out an analysis of the dynamics of solutions to the system of Eqs. (4)-(6) with resetting conditions (41)-(43) by following the technique described by Robert and Kao (1998) in their work on the dynamics of infectious diseases with birth pulses.

If (x(t), y(t), z(t)) is a solution of (4)–(6) for  $t \in (0, p)$ , and boundary conditions

$$x(0) = x(p) \tag{44}$$

$$y(0) = (1 - k_C)y(p)$$
 (45)

$$z(0) = z(p) \tag{46}$$

then Eqs. (4)-(6) with (41)-(43) have a periodic solution defined by

$$(x_p(t), y_p(t), z_p(t)) = (x(t), y(t), z(t))$$
  
for  $t \in (0, p)$ 

and

$$(x_p(t+p), y_p(t+p), z_p(t+p))$$
  
=  $(x_p(t), y_p(t), z_p(t))$ 

for all non-integer t (Robert and Kao, 1998; Heesterbeek and Robert, 1995).

The local stability of the period 1 solution  $(x_p(t),$  $y_p(t)$ ,  $z_p(t)$ ) of (4)–(6) with (41)–(43) may be determined by considering the behavior of small-amplitude perturbations of the solution. Defining

$$(x(t), y(t), z(t)) = (x_p(t) + \chi(t), y_p(t) + \eta(t), z_p(t) + \xi(t))$$

these may be written as

$$\begin{pmatrix} \chi(t) \\ \eta(t) \\ \xi(t) \end{pmatrix} = \Phi(t) \begin{pmatrix} \chi(0) \\ \eta(0) \\ \xi(0) \end{pmatrix}$$

where  $\Phi(t)$  satisfies

$$\frac{\mathrm{d}\Phi(t)}{\mathrm{d}t} = J_1 \bigg|_{(x_n, y_n, z_n)} \Phi(t)$$

while 
$$J_{1} = \begin{pmatrix} -b_{1} & -\frac{a_{1}}{(k_{1}+y)^{2}} & 0\\ \varepsilon \left[ \frac{a_{3}k_{2} - 2a_{2}x - a_{3}x^{2}}{(k_{2}+x^{2})^{2}} \right] yz & \varepsilon \left[ \frac{(a_{2}+a_{3}x)z}{k_{2}+x^{2}} - b_{2} \right] & \varepsilon \left[ \frac{(a_{2}+a_{3}x)y}{k_{2}+x^{2}} \right]\\ \varepsilon \delta \left[ a_{4} - a_{5}z \left( \frac{k_{3}}{(k_{3}+x)^{2}} \right) \right] & 0 & \varepsilon \delta \left( -\frac{a_{5}x}{k_{3}+x} - b_{3} \right) \end{pmatrix}$$

with  $\Phi(0) = I$ , the identity matrix. The resetting conditions (41)-(43) become

$$\begin{pmatrix} \chi(m+) \\ \eta(m+) \\ \xi(m+) \end{pmatrix} = J_2 \begin{pmatrix} \chi(m-) \\ \eta(m-) \\ \xi(m-) \end{pmatrix}$$

where

$$J_2 = \begin{pmatrix} 1 & 0 & 0 \\ 0 & 1 - k_C & 0 \\ 0 & 0 & 1 \end{pmatrix}$$

Hence, if all three eigenvalues of

$$M = \begin{pmatrix} 1 & 0 & 0 \\ 0 & 1 - k_C & 0 \\ 0 & 0 & 1 \end{pmatrix} \Phi(1)$$

have absolute values less than one, then the period 1 solution is locally stable (Heesterbeek and Robert, 1995).

Now, through some straightforward manipulations, it can be found, for small-amplitude solutions about the steady state  $(x_1, 0, z_3)$ , that the conditions for the absolute values of the three eigenvalues of M to be less than one will be assured if those conditions for the eigenvalues of  $J_1(x_1, 0, z_3)$  to have negative real parts are satisfied. To be precise, the stability conditions for the eigenvalues of M to have absolute values less than one are that

$$\frac{(a_2 + a_3 x_1) z_3}{k_2 + x_1^2} < b_2 \tag{47}$$

$$1 - k_C < \exp\left[\varepsilon \left(b_2 - \frac{(a_2 + a_3 x_1) z_3}{k_2 + x_1^2}\right)\right]$$
 (48)

if all parametric values are assumed positive. However, if (47) holds then (48) is automatically satisfied. But, (47) is the required condition for the eigenvalues of  $J_1(x_1, 0, z_3)$  to have negative real parts.

$$\begin{bmatrix}
\varepsilon \left[ \frac{(a_2 + a_3 x)y}{k_2 + x^2} \right] \\
\varepsilon \delta \left( -\frac{a_5 x}{k_3 + x} - b_3 \right)
\end{bmatrix}$$

This means that if the steady state  $(x_1, 0, z_3)$  is stable before the application of estrogen in monthly bursts, it will remain stable afterwards, apart from the spikes appearing every period of 28 days in the osteoclasts time series due to external estrogen administration.

The analysis of small perturbations about a different solution, other than  $(x_1, 0, z_3)$ , is not so straightforward, however, and we resorted to carrying out numerical experiments instead. As a result, we found not so surprisingly that estrogen applications in monthly bursts do not appear to effect any change in the dynamic behavior of the solution to the system model in all the cases that we attempted, irrespective of the magnitude of  $k_C$ , discounting the appearance of spikes due to external estrogen each menstrual cycle. Noticeable affect is only observed if the hormone application lasts for a significant duration  $\Delta T$ , as has been noted in Section 7.2. This is, in fact, in agreement with the conclusion made by Muse et al. (1986), from their investigation, that the alterations in calcium-regulating hormones and bone mass that occur during menopause, and several amenorrhea states, appear to occur when perturbations of gonadal steroids are of greater magnitude and duration than those in the normal menstrual cycle. We note, however, that clinical reports are still contradictory and the mechanisms behind this steroid's action remain unclear. Further careful study and investigation need to be carried out before any definite conclusions can be made.

# 8. Conclusion

We have demonstrated, through the construction and analysis of a core model for the bone formation and resorption process mediated by PTH, that several nonlinear dynamic behavior can be deduced which closely simulates clinical data. Even though the model is kept relatively simple, it incorporates the nonlinearity property of the system as well as the way the state variables possess highly diversified time responses. The model can then elucidate certain aspects of the underlying mechanisms. Apart from yielding valuable insights, such investigation, taken with great care, can suggest new possibilities, new interpretations, or a different approach in dealing with this complexed remodeling process.

Moreover, it has been proposed (Prank et al., 1995; Prank et al., 1994) that in simple organisms, the detection of nonlinear behavior in information transfer is in fact associated with differentiation and proliferation. Modulation of the amplitude and/or the frequency of the hormone pulses in higher organisms can modify

intracellular signaling pathways, gene expression, cell proliferation, and cellular function (Goldbeter and Li, 1989). Further studies on the effects of pulsatile hormone secretion on the regulation of cell and organ function and structure can be found in the work of Veldhuis (2000) and that of Brabant et al. (1992). More recently, Hock et al. (2002) also gave a very clear outline of the actions of PTH, focusing on the physiological and cellular effects of PTH on the skeleton but also considering the kidney and the cardiovascular system, the latter being a recently recognized target of PTH action. This line to investigation, therefore, deserves closer attention and further study, since it could help explain the physiological linkage between functional and genetic programs of the living organisms.

#### Acknowledgements

This work is supported by the Thailand Research Fund with a senior researcher grant (contract number RTA/02/2542) and a scholarship of the Royal Golden Jubilee Ph.D. Program (contract number PHD/0016/2543, 3 M.MU/43/A.1).

#### References

Albright, F., Smith, P.H., Richardson, A.M., 1941. Postmenopausal osteoporosis. JAMA 116, 2465-2474.

Albright, J.A., Sauders, M., 1990. The Scientific Basis of Orthopaedics. Appleton & Lange, Norwalk, CT.

Brabant, G., Prank, K., Schofl, C., 1992. Pulsatile patterns in hormone secretion. Trends Endocrinol. Metab. 3, 183-190.

Brown, E.M., 1991. Extracellular Ca<sup>2+</sup> sensing, regulation of parathyroid cell function, and role of Ca<sup>2+</sup> and other ions as extracellular (first) messengers. Physiol. Rev. 71, 371-411.

Burgess, T.L., Qian, Y., Kaufman, S., Ring, B.D., Van, G., Capparelli, C., Kelly, M., Hsu, H., Boyle, W.J., Dunstan, C.R., Hu, S., Lacey, D.L., 1999. The ligand for osteoprotegerin (OPGL) directly activates mature osteoclasts. J. Cell Biol. 145, 527-538.

DeCherney, A., 1993. Physiologic and pharmacologic effects of estrogen and progestins on bone. J. Reprod. Med. 38 (Suppl. 12), 1007-1014.

Dempster, D.W., Cosman, F., Parisisen, M., Shen, V., Linsay, R., 1993. Anabolic actions of parathyroid hormone on bone. Endocr. Rev. 14, 690-709.

Eckhaus, W., 1979. Asymptotic analysis of singular perturbation. North-Holland, Amsterdam.

Goldbeter, A., Li, Y.X., 1989. In: Goldbeter, A. (Ed.), Cell to Cell Signalling: From Experiments to Theoretical Models. Academic Press, London.

- Harms, H.M., Kaptaina, U., Kulpmann, W.R., Brabant, G., Hesch, R.D., 1989. Pulse amplitude and frequency modulation of parathyroid hormone in plasma. J. Clin. Endocrinol. Metab. 69 (4), 843-851.
- Heersche, J.N.M., Cherk, S., 1989. Metabolic Bone Disease: Cellular and Tissue Mechanisms. CRC Press, Boca Raton.
- Heesterbeek, J.A.P., Robert, M.G., 1995. Threshold quantities for helminth infections. J. Math. Biol. 33 (4), 415-434.
- Hock, J.M., Gera, I., 1992. Effects of continuous and intermittent administration and inhibition of resorption on the anabolic response of bone to parathyroid hormone. J. Bone Miner. Res. 7 (1), 65-72.
- Hock, J.M., Fitzpatrick, L.A., Bilezikian, J.P., 2002. Principle of Bone Biology, vol. 1, 2nd ed. Academic Press, London.
- Isogai, Y.T., Akatsu, T., Ishizuya, T., Yamaguchi, A., Hori, M., Tokahashi, N., Suda, T., 1996. Parathyroid hormone regulates osteoblast differentiation positively or negatively depending on differentiation stages. J. Bone Miner. Res. 11, 1384-1393.
- Jones, C.K.R.T., 1994. Geometric singular perturbation theory. Dyn. Syst. Montecatibi Terme Lect. Notes Math. 1609, 44-118.
- Kaper, T.J., 1999. An introduction to geometric methods and dynamical systems theory for singular perturbation problems. Analyzing multiscale phenomena using singular perturbation methods. In: Cronin, J., O'Malley Jr., R.E. (Eds.), Proceedings of the Symposia on Applied Mathematics, vol. 56. American Mathematical Society.
- Kong, Y.Y., Yoshida, H., Sarosi, I., Tan, H.L., Timms, E., Capparelli, C., Morony, S., Santos, A., Van, G., Itie, A., Khoo, W., Wakeham, A., Dunstan, C., Lacey, D., Mak, T., Boyle, W., Penninger, J., 1999. OPGL is a key regulator of osteoclastogenesis, lymphocyte development and lymph-node organogenesis. Nature 397, 315-323.
- Kroll, M.H., 2000. Parathyroid hormone temporal effects on bone formation and resorption. Bull. Math. Bio. 62, 163-188.
- Leah, E.K., 1988. Mathematical Models in Biology. Random House, New York.
- Lenbury, Y., Kumnungkit, K., Novaprateep, B., 1997. Detection of slow-fast limit cycles in a model for electrical activity in the pancreatic β-cell. IMA. J. Maths. Appl. Med. Biol. 133 (1), 49-97.
- Marcus, R., 1994. Osteoporosis. Blackwell Scientific Publication, Oxford.
- Momsen, G., Schwarz, P., 1997. A mathematical/physiological model of parathyroid hormone secretion in response to blood-ionized calcium lowering in vivo. Scand. J. Clin. Lab. Invest. 57, 381-394.
- Moon, L.Y., Wakley, G.K., Turner, R.T., 1991. Dose-dependent effects of tamoxifen on long bones in growing rats: influence of ovarain status. Endocrinology 129, 1568-1574.
- Muratori, S., Rinaldi, S., 1992. Low- and high-frequency oscillations in three-dimensional food chain systems. Siam. J. Appl. Math. 52, 1688–1706.

- Muse, K.N., Manolagas, S.C., Deftos, L.J., Alexander, N., Yen, S.S.C., 1986. Calcium-regulating hormones across the menstrual cycle. J. Clin. Endocrinol. Metab. 62 (2), 1313– 1315.
- O'Malley Jr., R.E., 1974. Introduction to Singular Perturbations. Academic Press, London.
- Osipove, A.V., Soderbacka, G., Eirold, T., 1986. On the existence of positive periodic solutions in a dynamical system of two predator-one prey type. Viniti Deponent No. 4305-B4386 (in Russian).
- Prank, K., Harms, H., Dammig, M., Brabant, G., Mitschke, F., Hesch, R.D., 1994. Is there is low-dimensional chaos in pulsatile secretion of parathyroid hormone in normal human subjects? Am. J. Physiol. 266, E653–E658.
- Prank, K., Harms, H., Brabant, G., Hesch, R.D., 1995. Nonlinear dynamics in pulsatile secretion of parathyroid hormone in normal human subjects. Chaos 5, 76-81.
- Prestwood, K.M., Pilbeam, C.C., Burleson, J.A., Woodiel, F.N., Delmas, P.D., Deftos, L.J., Raisz, L.G., 1994. The short-term effects of conjugated estrogen on bone turnover in older women. J. Clin. Endocrinol. Metab. 79, 366-371.
- Robert, M.G., Kao, R.R., 1998. The dynamics of an infectious disease in a population with birth pulses. Math. Biosci. 149, 23-36.
- Schecter, S., 1985. Persistence unstable equilibria and closed orbits of a singularly perturbed equation. J. Diff. Equas. 60, 131– 141.
- Schmitt, C.P., Schaefer, F., Bruch, A., Veldhuis, J.D., Gayk, H.S., Stein, G., Ritz, E., Mehls, O., 1996. Control of pulsatile and tonic parathyroid hormone secretion by ionized calcium. J. Clin. Endocrinol. Metab. 81, 4236–4243.
- Takahashi, N., Udagawa, N., Suda, T., 1999. A new member of tumor necrosis factor ligand family, ODF/OPGL/TRANCE/ RANKL, regulates osteoclast differentiation and function. Biochem. Biophys. Res. Commun. 256, 449-455.
- Tam, C.S., Heersche, J.N.M., Murray, T.M., Parsons, J.A., 1982. Parathyroid hormone stimulates the bone apposition rate independently of its resorptive action: differential effects of intermittent and continuous administration. Endocrinology 110 (2), 506-512.
- Turner, R.T., Lawrence, B.R., Thomas, C.S., 1994. Skeletal effects of estrogen. Endocr. Rev. 15 (3), 275-300.
- Veldhuis, J.D., 2000. Nature of altered pulsatile hormone release and neuroendocrine network signaling in human ageing: clinical studies of the somatotropic, gonadotropic, corticotropic and insulin axes. Novartis Found. Symp. 227, 163– 189.
- Weryha, G., Leclere, J., 1995. Paracrine regulation of bone remodeling. Horm. Res. 43, 69-75.
- Whitfield, J.F., Morley, P., Willick, G.E., 1998. The parathyroid hormone: an unexpected bone builder for treating osteoporosis. Landes Bioscience Company, Austin, Tex.

# A delay-differential equation model of the feedback-controlled hypothalamus-pituitary-adrenal cortex hormone secretion system in humans

YONGWIMON LENBURY\*and PORNSARP PORNSAWAD

Department of Mathematics, Faculty of Science, Mahidol University,

Rama 6 Road, Bangkok 10400, Thailand

September 30, 2004

The present work develops and analyzes a model system of delay-differential equations which describes the core dynamics of the stress-responsive hypothalamus-pituitary-adrenal axis. This neuroendocrine ensemble exhibits prominent pulsatile secretory patterns governed by nonlinear and time-delayed feedforward and feedback signal interchanges. Formulation and subsequent bifurcation analysis of the model provide qualitative and mathematical frame work for better understanding of the delayed responsive mechanisms as well as the dynamic variations in different pathological situations.

Keywords: cortisol secretion; delay-feedback controlled system; Hopf bifurcation; nonlinear model.

## 1 Introduction

The hypothalamus-pituitary-adrenal axis is a critical stress-responsive component which initiates life sustaining adaptive reactions to internal stresses, such as disease, and external stresses, such as hard work or lack of sleep. Signals may originate from either outside or inside the body and are mediated by the central nervous system. Thus, many changes in the environment ultimately can stimulate the secretion of releasing hormones, which produce effects in the body in order to adapt to the change.

<sup>\*</sup>Corresponding author

Neurons synthesize and package releasing hormone precursors in their cell bodies, and these products are transported down the length of their axons to the nerve endings, where a signal is awaited for secretion (Norman & Litwack, 1997). Since most of the cell bodies of these neurons are found in different areas of the hypothalamus, signals for secretion come from higher levels, usually from aminergic or cholinergic neurons in various parts of the brain. The hippocampus of the limbic system may signal the neurons to release the hormone by changing the firing rate of electric signals or by chemical interneuronal contacts (Norman & Litwack, 1997). The response of the hypothalamus to signals from the limbic system is the secretion of the corticotropin-releasing hormone, CRH. CRH is released from specific cells in the hypothalamus into a closed portal circulation intimately connected with the anterior pituitary. Releasing hormones act at cognate plasma membrane receptor levels either to cause an increase in cyclic AMP or to stimulate the phosphatidylinositol cycle, leading to the stimulation of protein kinase C and an increase in cytoplasmic calcium ion concentration. The increased level of cyclic AMP stimulates protein kinase A leading to ACTH release from the corticotroph of the anterior pituitary. Vasopressin also increases the secretion of ACTH, although the main role of vasopressin appears to be one of helping CRH in this activity. Also, according to Engler et al. (1999) the nanopeptide vasopressin is a weak ACTH secretagog in rat and in man, although it appears to be potent in the bovine species. Therefore, we shall not consider its direct stimulatory effect in this work.

Following the secretion of ACTH into the blood circulation after stimulation by CRH from the hypothalamus, ACTH molecules bind to a specific receptor on the outer cell membranes of all three layers of cells of the adrenal cortex, the zona glomerulosa, the zona fasciculata, and the zona reticularis. Cortisol is the main product of ACTH stimulation of the zona fasciculate and reticularis cells of the human adrenal cortex. A glucocorticoid essential to life, cortisol acts on different cells in different ways. Without the secretion of cortisol during stress, a human could not survive. When cortisol is overproduced, often by a pituitary tumor causing high level of circulating ACTH, the resulting disease is known as Cushing's disease. When cortisol is underproduced, the resulting disease is known as Addison's disease, which is most frequently the result of adrenal destruction.

When cortisol is produced in response to ACTH, it has negative feedback effects on various elements of the hormonal cascade system, schematically described in Fig 1. Malfunctions in this negative feedback mechanisms can lead to several complications. Lowered cortisol levels or enlarged output of ACTH by the anterior pituitary, due to reduced negative feedback, results in adrenal hyperplasia and hypersecretion, which, together with adrenal testosterone, can lead to masculinization of female babies. Precocious puberty in males can also result from this condition (Norman & Litwack, 1997).

It is therefore crucial that a better biomathematical description of such a process be attempted to provide more solid framework for the study and assessment of dynamic interfaces in health and disease. Such studies are necessary especially since a recent report by Ilias *et al.* (2002) on the complexity of cortisol seems to

A delay-differential equation model of the feedback-controlled hypothalamus-pituitary-adrenal cortex3

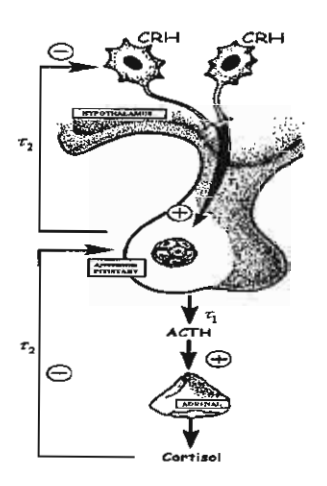


Figure 1: A schematic representation of feedforward-feedback model of plasma CRH, ACTH, and cortisol.

confirm that cortisol secretion operates under non-regular dynamics. Its fractal dimension after sleep deprivation (a weakened state) is lower than that measured before sleep deprivation (healthier state). In the past, basal cortisol secretion has been proposed to arise via linear mechanisms. Then, in 1991 Lenbury and Pacheenburawana presented a mathematical model in which cortisol secretion was described by nonlinear differential equations with exponential feedback terms. However, Ilias et al. (2002) were the first, to our knowledge, to utilize nonlinear/fractal analysis in the experimental study of the complex mechanisms underlying the circadian secretion of cortisol.

Complexity and nonlinear methods have become one of the most versatile and promising new research tools for the study and characterization of circadian rhythmicity in humans. Episodic secretion of cortisol has been clinically observed and reported in several research works (Carnes et al., 1991; Carnes et al., 1989; Krieger et al., 1971; Weitzman et al., 1971) as early as that of Weitzman et al. (1971) which reported on twenty-four hour patterns of episodic cortisol secretion in normal subjects. Their data seriously challenged the concept that a "steady state" or "basal level" of cortisol is present during any extended time compartment of the 24-hour cycle. In a different report in the same year, Krieger et al. (1971) attempted to delineate more precisely the time course of adrenal secretory activity in the normal human and patients with Cushing's syndrome. Later, Moore-Ede et al. (1983) pointed out several advances in characterization of the properties of hypothalamic circadian pacemakers and the implications of such rhythmicity for medical diagnosis. It was not until very recently, however, that an attempt was made by Ilias et

al. (2002) to use mathematical methods based on nonlinear/fractal analysis in the experimental study of the underlying complex mechanisms. Their conclusion, that post-sleep deprivation changes the fractal dimensions of cortisol, supports Lenbury and Pacheenburawana's (1991) suggestion that nonlinear dynamics analysis may be a viable tool in our attempts to delineate pulsatile secretory patterns in health and disease.

Lenbury and Pacheenburawana's (1991) nonlinear model did not, however, account for the delays associated with the time interval needed before an action in response to the stimulating signal can be taken by the release of the appropriate hormones. Several studies have presented clinical evidence of such delayed responses in the hypothalamus-pituitary-adrenal cortex (Norman, 1997; Posener et al., 1997; Won et al., 1986). Specifically, Posener et al. reported in 1997 that cortisol exerted a feedback effect by significantly decreasing plasma ACTH levels with a time delay of approximately 60 min. An earlier study by Hermus et al. (1984) reported a 30 min. delay in the positive feedforward effects of CRH on plasma ACTH levels, the increase of which was followed by a rise in the cortisol level with time delay of an extra 30 minutes.

To our knowledge, mathematical modelling and analysis of hormonal secretion systems with delays have up to date been the subject of few published reports in humans. In 2001, Keenan et al. presented a biostatistical model which incorporated expected within axis physiological linkages via time-delayed, nonlinear, dose-responsive, rate-sensitive, and integral feedforward and feedback controls. Although the model appeared to generate realistic pulsatile secretory patterns, it contributed little towards the illumination of the underlying mechanism of the secretion network or the crucial role which the delayed responses might play in this important feedback controlled system. Because of its nonlinear structure, the introduction of a time delay in feedback loops can alter the stability and dynamic properties of the hormonal cascade yielding insightful clinical implications.

We propose, therefore, to incorporate such time delays into the earlier model by Lenbury and Pacheenburawana (1991) and subsequently analyze the model by Hopf bifurcation in order to find the critical time delay, beyond which the model system may exhibit periodic dynamics. With the set of parameters appropriately chosen through such analysis, we shall construct a bifurcation diagram in order to identify the ranges of the system's parametric values for which chaotic secretory patterns are permitted by our time-delay differential equation model. The simulated solution in such a case appears to compare well with clinical data which consistently showed multifactorical frequency structure (Carnes et al., 1991).

# 2 A Feedforward-Feedback Delay Model

In formulating our mathematical model of the negative feedback regulation of cortisol secretion, the following events are considered. CRH (R) is secreted from the hypothalamus and stimulates the secretion of ACTH (A) from the anterior pitu-

itary with a delay of  $\tau_1$  in time. ACTH then stimulates the cortisol (C) secretion from the adrenal gland with the same time delay  $\tau_1$  as that in the short loop feedforward effect of CRH on ACTH secretion. Thus, we assume equal delays in both short feedforward loops in the cascade, following the clinical evidence reported by Hermus et al. (1984) mentioned above. We also take into account the negative feedback effects of cortisol on ACTH, incorporating a time delay of  $\tau_2$ , supported by the clinical evidence already mentioned above (Moore-Ede et al., 1983). The investigation by Posener et al. (1998) also utilized a covariance analysis which suggested that the inhibition effects of ACTH on CRH were not due to the rise in cortisol caused by the rise in ACTH itself. Thus, we shall ignore the long-loop negative feedback effect of cortisol on CRH and only consider the short-loop feedback effect of ACTH on CRH not mediated by cortisol, which is then assumed to occur with a delay time of  $\tau_2$  as well.

These assumptions on delay are made here in order to carry out a theoretical analysis to investigate the stability and the possibility of periodic solutions of the system comparable to clinically observed behavior. In the later section, the time lags in the feedforward or feedback loops are allowed to be different in our numerical experiment to investigate the possibility of chaotic dynamics

In 1986, Won et al. investigated the mechanisms responsible for glucocorticoid feedback on nonstress induced ACTH secretion in normal subjects and reported a linear relationship between the degree of inhibition of ACTH ( $\Delta$ ACTH) levels after cortisol administration. The degree of inhibition was measured as the reduction in ACTH as percentages of the mean baseline level. They found that "A linear correlation between the degree of inhibition of ACTH level and the corresponding cortisol concentrations does exist at 60 min. after administration (r=0.95, P<0.05)". From such clinical evidence, we see that the specific rate of change of ACTH at time t,  $A_t$ , due to the negative feedback effect of high cortisol concentration at time  $t-\tau_2$ ,  $C(t-\tau_2)$ , may be described by the following equation

$$\frac{1}{A_t} \frac{d}{dC(t - \tau_2)} A_t = -kC(t - \tau_2)$$
 (2.1)

where k is some positive constant of variation. Integrating (2.1) yields  $k_2e^{\gamma(C_0^2-C^2(t-\tau_2))}$  for the rate  $A_t$ , where  $\gamma=\frac{k}{2}$  and  $k_2$  corresponds to the rate  $A_t$  when  $C=C_0$ . Thus,  $C_0$  is the critical value of A, which means that if C falls below  $C_0$  then the secretion rate of A should rise above  $k_2$ . If C rises above  $C_0$ , on the other hand, the secretion rate of A should be reduced in magnitude below  $k_2$ , with a time delay of  $\tau_2$ . Similar arguments can be applied to the rate of change  $R_t$ . However, the rate of change of ACTH should also vary in direct proportion to plasma CRH concentration at time  $t-\tau_1$ ,  $R(t-\tau_1)$ . This concentration-dependent effects of CRH on ACTH was investigated by Engler et al. (1999), who reported clinical data showing ACTH release (not its level) increasing exponentially as the log of CRH. This means, in fact, that ACTH secretion rate may be assumed to depend in a linear fashion on CRH level, at least to the first order. It is reasonable to

also assume the same linear dependence between the secretion rate of cortisol and ACTH level. Therefore, the three component hormonal cascade can be described by the following system of nonlinear differential equations:

$$\frac{dR(t)}{dt} = -\delta_1 R(t) + k_1 e^{\alpha (A_0^2 - A^2(t - \tau_2))}$$
(2.2)

$$\frac{dA(t)}{dt} = -\delta_2 A(t) + k_2 R(t - \tau_1) e^{\gamma (C_0^2 - C_0^2 (t - \tau_2))}$$
(2.3)

$$\frac{dC(t)}{dt} = -\delta_3 C(t) + k_3 A(t - \tau_1) \tag{2.4}$$

where R(t) is the concentration of CRH at any time t; A(t) and C(t) are the concentrations of ACTH and cortisol, respectively, above their respective residual levels, while  $k_1, k_2$ , and  $k_3$  the respective secretion rate constants of R, A, and C, while  $\alpha$  and  $\gamma$  are the feedback potency constants.  $\delta_1, \delta_2$ , and  $\delta_3$  are the removal rates of R, A, and C, respectively. It is assumed that each of these hormones is cleared from the blood stream according to the first-order kinetics. In order to arrive at the above mathematically tractable model, we have assumed that the stimulating/inhibitory effects of other known factors are relatively weak and thus negligible. More detail of the derivation of the model can been seen in the paper by Lenbury and Pacheenburawana (1991).

We associate the initial values of the form:

$$R(t) = \phi_1(t)$$
 for  $-\tau_1 \le t \le 0$ ,  
 $C(t) = \phi_2(t)$  for  $-\tau_2 \le t \le 0$ ,  
 $A(t) = \phi_3(t)$  for  $-\tau_3 \le t \le 0$ , (2.5)

where  $\tau_3 = max(\tau_1, \tau_2), \ \phi_i \in C([-\tau_i, 0], \Re^+) \ \text{and} \ \phi_i(0) > 0, \ i = 1, 2, 3.$ 

We now introduce dimensionless variables by letting  $x=\frac{R}{R_0},\ y=\frac{A}{A_0},\ z=\frac{C}{C_0},\ K_1=\frac{k_1}{R_0},\ K_2=\frac{k_2}{A_0}R_0,\ \beta_1=\alpha A_0^2,\ \beta_2=\gamma C_0^2,\ \text{and}\ K_3=\frac{k_3}{C_0}A_0,\ \text{where}\ R_0,A_0,\ \text{and}\ C_0$  are the critical values of R,A, and C, respectively. We are then led to

$$\dot{x}(t) = -\delta_1 x(t) + K_1 e^{\beta_1 (1 - y^2 (t - \tau_2))}$$
(2.6)

$$\dot{y}(t) = -\delta_2 y(t) + K_2 x(t - \tau_1) e^{\beta_2 (1 - z^2(t - \tau_2))}$$
(2.7)

$$\dot{z}(t) = -\delta_3 z(t) + K_3 y(t - \tau_1). \tag{2.8}$$

So that the steady state values of R, A, and C are  $R_0$ ,  $A_0$ , and  $C_0$ , respectively, at which point the 3 state variables should be stationary, we see that we need to put  $K_1 = \delta_1$ ,  $K_2 = \delta_2$ , and  $K_3 = \delta_3$  in (2.6)-(2.8). We also note further that  $\alpha$  and  $\gamma$  represent the strength of the negative feedback effect of ACTH on CRH and that of cortisol on ACTH, respectively. Since ACTH and cortisol are secreted at noticeably different orders of magnitude  $\alpha$  and  $\gamma$  may be different. However, after

A delay-differential equation model of the feedback-controlled hypothalamus-pituitary-adrenal cortex?

rescaling by  $A_0$  and  $C_0$ , the corresponding feedback potency constant  $\beta_1$  should be comparable to  $\beta_2$ . Therefore to carry out our bifurcation analysis, we first put  $\beta = \beta_1 = \beta_2$ , but will allow them to be different in our later investigation. We now arrive at the following core model equations:

$$\dot{x}(t) = -\delta_1 x(t) + \delta_1 e^{\beta(1 - y^2(t - \tau_2))}$$
(2.9)

$$\dot{y}(t) = -\delta_2 y(t) + \delta_2 x(t - \tau_1) e^{\beta(1 - z^2(t - \tau_2))}$$
(2.10)

$$\dot{z}(t) = -\delta_3 z(t) + \delta_3 y(t - \tau_1). \tag{2.11}$$

## 3 Bifurcation Analysis

The model system (2.9)-(2.11) has one positive steady state  $(x_0, y_0, z_0)$ , that is,  $(x_0, y_0, z_0) = (1, 1, 1)$ .

Letting  $X = x - x_0$ ,  $Y = y - y_0$ , and  $Z = z - z_0$ , we are led to the following linearized system of (2.9)-(2.11) at  $(x_0, y_0, z_0)$ .

$$\begin{pmatrix} \dot{X} \\ \dot{Y} \\ \dot{Z} \end{pmatrix} = \begin{pmatrix} -\delta_1 & -2\beta\delta_1 e^{-\lambda\tau_2} & 0 \\ \delta_2 e^{-\lambda\tau_1} & -\delta_2 & -2\beta\delta_2 e^{-\lambda\tau_2} \\ 0 & \delta_3 e^{-\lambda\tau_1} & -\delta_3 \end{pmatrix} \begin{pmatrix} X \\ Y \\ Z \end{pmatrix}$$
(3.21)

The associated characteristic equation of the model system (2.9)-(2.11) is then

$$F(\lambda) \equiv \lambda^3 + a\lambda^2 + b\lambda + c + (d_1\lambda + d_2)e^{-\lambda(\tau_1 + \tau_2)} = 0$$
(3.13)

where

$$a = \delta_1 + \delta_2 + \delta_3 \tag{3.14}$$

$$b = \delta_1 \delta_2 + \delta_1 \delta_3 + \delta_2 \delta_3 \tag{3.15}$$

$$c = \delta_1 \delta_2 \delta_3 \tag{3.16}$$

$$d_1 = 2\beta \delta_2 [\delta_1 + \delta_3] \tag{3.17}$$

$$d_2 = 4\beta \delta_1 \delta_2 \delta_3 \tag{3.18}$$

using the steady state relations that  $\dot{x} = \dot{y} = \dot{z} = 0$  at the point (x, y, z) = (1, 1, 1). We let  $\tau = \tau_1 + \tau_2$  be the composite lag-time and first consider equation (3.13) when  $\tau = 0$ . That is,

$$\lambda^{3} + a\lambda^{2} + (b + d_{1})\lambda + (c + d_{2}) = 0.$$
(3.19)

Using (3.14)-(3.18), it is easily shown that a > 0,  $c + d_2 > 0$ , and  $a(b + d_1) - c - d_2 > 0$ , for all positive parametric values. Thus, by the Routh-Hurwitz condition, all roots of equation (3.19) have negative real parts. Therefore, the steady state (1,1,1) is stable when  $\tau = 0$ .

If we let  $\lambda(\tau) = \alpha(\tau) + i\omega(\tau)$ , where  $\alpha$  and  $\omega$  are real, then we have  $\alpha(0) < 0$ , by the above reason. By continuity, we know that  $\alpha(\tau) < 0$  for positive value of  $\tau$  which is sufficiently small. Thus, the steady state shall remain stable for values of  $\tau$  such that  $0 \le \tau < \tau_0$  for some  $\tau_0 > 0$ .

Suppose  $\alpha(\tau_0) = 0$  for some  $\tau_0 > 0$ , and  $\alpha(\tau) < 0$  for  $0 \le \tau < \tau_0$ , then the stability of (1, 1, 1) is lost at  $\tau = \tau_0$ , at which point  $\lambda = i\omega(\tau_0)$ .

Now,  $i\omega$  is a root of (3.13) iff

$$-i\omega^3 - a\omega^2 + ib\omega + c + (id_1\omega + d_2)(\cos\omega\tau - i\sin\omega\tau) = 0.$$
 (3.20)

Equating real and imaginary parts of both sides of (3.20), we obtain

$$-\omega^3 + b\omega + d_1\omega\cos\omega\tau - d_2\sin\omega\tau = 0 \tag{3.21}$$

$$-a\omega^2 + c + d_1\omega\sin\omega\tau + d_2\cos\omega\tau = 0. \tag{3.22}$$

Adding up the squares of (3.21) and (3.22), one obtains

$$f(\omega) \equiv \omega^6 + (a^2 - 2b)\omega^4 + (b^2 - 2ac - d_1^2)\omega^2 + c^2 - d_2^2 = 0.$$
 (3.23)

If we let  $s = \omega^2$ ,  $p = a^2 - 2b$ ,  $q = b^2 - 2ac - d_1^2$ , and  $r = c^2 - d_2^2$ , then equation (3.23) becomes

$$h(s) \equiv s^3 + ps^2 + qs + r = 0. (2.24)$$

We can consequently write down the following result.

**Lemma 1.** Suppose  $s_1 = \frac{-p + \sqrt{p^2 - 3q}}{3}$ .

(i) Equation (3.24) has a positive root if either

$$(a) r < 0 (3.25)$$

or

(b) 
$$r \ge 0,$$
 (3.26)

$$p^2 - 3q > 0, (3.27)$$

$$s_1 > 0, \tag{3.28}$$

and 
$$h(s_1) < 0.$$
 (3.29)

(ii) Equation (3.24) has no positive real roots if

$$r \ge 0$$
 and 
$$p^2 - 3q < 0.$$

A delay-differential equation model of the feedback-controlled hypothalamus-pituitary-adrenal cortex9

#### Proof.

- (i) Suppose r < 0, then h(0) < 0. Since  $\lim_{s \to \infty} h(s) = \infty$ , equation (3.24) must have a positive root where h = 0, by the intermediate value theorem. Suppose  $r \ge 0$ , on the other hand, and  $p^2 3q > 0$ , then  $s_1 = \frac{-p + \sqrt{p^2 3q}}{3}$  is the stationary point of h(s) located on the positive x-axis if  $s_1 > 0$ . Thus, if  $h(s_1) < 0$  while  $h(0) = r \ge 0$ , by the intermediate value theorem, h must vanish somewhere between 0 and  $s_1$ .
- (ii) If  $r \ge 0$  while h'(s) > 0, h is then an increasing function and does not vanish anywhere along the positive x-axis  $\square$ .

If conditions in Lemma 1(ii) hold, then all roots of the characteristic equation (3.13) have negative real parts for all  $\tau \geq 0$ . Thus, the steady state (1,1,1) is always stable in this case.

If, on the other hand, conditions in Lemma 1(i) hold, then equation (3.24) has a positive root. Without loss of generality, we may denote the three positive roots of (3.24) by  $s_1$ ,  $s_2$ , and  $s_3$ . Then, equation (3.23) has three positive roots

$$\omega_k = \sqrt{s_k}, \quad k = 1, 2, 3.$$

Now, let  $\tau_0 > 0$  be the smallest of such  $\tau$  for which  $\alpha(\tau_0) = 0$ . Substituting  $\omega_k$  into equations (3.21)-(3.22) and solving for  $\tau$ , one obtains

$$\tau_k^{(j)} = \frac{1}{w_k} \arcsin\left[\frac{(ad_1 - d_2)\omega_k^3 + (bd_2 - cd_1)\omega_k}{d_2^2 + d_1^2\omega_k^2}\right] + \frac{2\pi(j-1)}{\omega_k}$$
(3.30)

where k = 1, 2, 3, and j = 1, 2, ...

Thus,

$$\tau_0 = \tau_{k_0}^{(j_0)} = \min_{1 < k < 3, j > 1} \left\{ \tau_k^{(j)} \right\} \tag{3.31}$$

and

$$\omega_0 = \omega_{k_0} \tag{3.32}$$

Now, for our model system (2.9)-(2.11), the following result can be shown.

**Lemma 2.**  $s_1 < 0$  if

$$\beta < \beta_0 \equiv \sqrt{\frac{\delta_1^2 \delta_2^2 + \delta_1^2 \delta_3^2 + \delta_2^2 \delta_3^2}{4\delta_2^2 (\delta_1 + \delta_3)^2}}$$
 (3.33)

10

**Proof.** From (3.14)-(3.17), we find that

$$q = \delta_1^2 \delta_2^2 + \delta_1^2 \delta_3^2 + \delta_2^2 \delta_3^2 - 4\beta^2 \delta_2^2 (\delta_1 + \delta_3)^2$$

which is positive if (3.33) holds. We will then have

$$p^2 - 3q < p^2$$

and

$$p = \delta_1^2 + \delta_2^2 + \delta_3^2 > 0.$$

Hence,

$$s_1 = \frac{-p + \sqrt{p^2 - 3q}}{3} < 0.$$

We now make the claim that  $i\omega_0$  is a simple root of equation (3.13), provided (3.33) holds.

Lemma 3. If (3.33) holds, then

$$\frac{dF}{d\lambda}(i\omega_0) \neq 0$$

**Proof.** Suppose, by contradiction, that  $\frac{dF}{d\lambda}(i\omega_0) = 0$ , while  $F(i\omega_0) = 0$ , then after some lengthy manipulations, it can be shown that

$$\frac{d}{d\omega}f(\omega_0) = 0$$

However,

$$\frac{df}{d\omega}(\omega_0) = 2\omega_0 \frac{dh}{ds}(s_0)$$

where  $s_0 = \omega_0^2$ . Since  $\omega_0 > 0$ , we would have  $\frac{dh}{ds}(s_0) = 0$  also. However, the solution of  $h'(s_0) = 0$  would be

$$s_0 = \frac{1}{3} \left[ -p \pm \sqrt{p^2 - 3q} \, \right] = s_1.$$

But,  $s_1<0$  when (3.33) is satisfied, by Lemma 2. This would mean that  $s_0<0$  which contradicts its definition. Therefore,  $h'(s_0)\neq 0$  and so  $\frac{dF}{d\lambda}(i\omega_0)\neq 0$  as claimed

This then leads us to conclude that  $i\omega_0$  is a simple root of equation (3.13) which implies that

 $A\ delay-differential\ equation\ model\ of\ the\ feedback-controlled\ hypothalamus-pituitary-adrenal\ cortex 11$ 

$$\frac{d}{d\tau} \operatorname{Re} \lambda(\tau) \bigg|_{\tau = \tau_0} \neq 0. \tag{3.34}$$

Thus, the steady state (1,1,1,) shall lose its stability and Hopf bifurcation will occur as  $\tau$  increases past the critical value  $\tau_0$ , provided the conditions in Lemma 1(ia) and (3.33) are satisfied.

Summarizing the above analysis, we have the following theorem.

**Theorem 1.** For the composite lag-time  $\tau = \tau_1 + \tau_2$ , let the critical composite lag-time  $\tau_0$  be defined as in (3.31), then the system of delay differential equations (2.9)-(2.11) exhibits the Hopf bifurcation at  $(x_0, y_0, z_0) = (1, 1, 1)$  if  $\frac{1}{4} < \beta < \beta_0$ , when  $\beta_0$  is as defined in (3.33). That is, there exists  $\epsilon > 0$  such that the system (2.9)-(2.11) will have periodic solutions for  $\tau \in (\tau_0, \tau_0 + \epsilon)$ .

**Proof.** It remains only to note that if  $\beta > \frac{1}{4}$  then, considering equations (3.16) and (3.18), we would have r < 0 which is condition (ia) in Lemma 1. Thus, the condition  $\beta > \frac{1}{4}$  ensures that there is a  $\tau_0 > 0$  such that the steady-state (1,1,1) loses its stability at the point  $\tau = \tau_0$ . The condition  $\beta < \beta_0$ , by Lemma 2, ensures that (3.34), which is a necessary condition for Hopf bifurcation, is satisfied  $\square$ .

#### 4 Numerical Results

Fig. 2 shows a computer simulation of equations (2.9)-(2.11) with parametric values chosen to satisfy the requirements for Hopf bifurcation set out in the previous section (Theorem 1). The solution trajectory, projected onto the (y,z) plane, tends to a limit cycle as theoretically predicted. The corresponding time courses of CRH and ACTH are shown respectively in Fig. 2b) and 2c) where they become periodic as time passes.

Since there has been evidence (Carnes et al., 1991; Carnes et al., 1989; Ilias et al., 2002; Krieger et al., 1971) of low-dimensional chaos in pulsatile secretion of plasma adrenocorticotropin mentioned in the introduction, we carried out a numerical investigation to discover whether chaotic behavior may occur in our delay feedback controlled model of the hormonal secretion cascade. To this end, a bifurcation diagram was constructed by using parametric values that would lead to cycling in the three state variables, guided by our work in the previous section. Then the system of equations (2.6)-(2.8) was allowed to run for  $10^5$  time steps. We retained only the last  $2\times10^4$  time steps to eliminate transient behavior, using values of  $\beta_2$  between 3.75245 and 3.7538 and changing  $\beta_2$  in steps of  $10^{-5}$ . The relative maximum values of x (CRH) were collected during the last  $2\times10^4$  time steps and plotted as a function of  $\beta_2$  as shown in Fig. 3.

We discover in this bifurcation diagram a period doubling route to chaotic dynamics which can be expected for values of  $\beta_2$  beyond 3.7532. We observe that

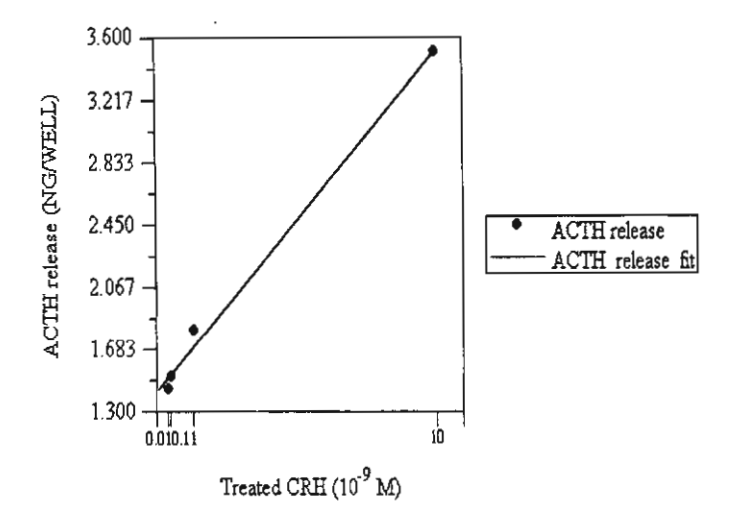


Figure 2: Computer simulation of equation (2.9)-(2.11) with  $\delta_1 = 0.5, \delta_2 = 0.38, \delta_3 = 0.6, \beta = 1.091, \tau_0 = 1.22, \tau_1 = 0.5$  and  $\tau_2 = 0.77$ .

periodic orbits can be found for values of  $\beta_2$  in the range  $0.25 < \beta_2 < 3.7528$  suggesting that chaotic mode of secretion is adopted when the negative feedback effects are relatively strong. When the feedback signals are weak, a more regular episodic secretory patterns are exhibited.

Fig. 4 shows a computer simulation of the model system (2.6)-(2.8) using the parametric values in the chaotic range, with  $\beta_2 = 3.75346$ . The strange attractor is seen in Fig. 4a) projected onto the (y,z)-plane, while the corresponding time series of CRH (x), ACTH (y), and cortisol (z) are shown in Fig. 4b)-4d), respectively.

Characteristic of such chaotic dynamics is the sensitivity to initial conditions. We illustrate this sensitivity by simulating our model system, using the parametric values in the chaotic range employed in Fig. 4, starting from two initial conditions which are different only by  $10^{-9}$  in x(0), while y(0) and z(0) are the same in the two simulations. The two time courses follow the same path only for a short time initially, but diverge to drastically different paths as time progresses as seen in Fig. 5. This clearly demonstrates the sensitivity to initial conditions of the system under nonlinear dynamics which, for this reason, makes any attempts at system control an extremely difficult task to tackle.

A delay-differential equation model of the feedback-controlled hypothalamus-pituitary-adrenal cortex13

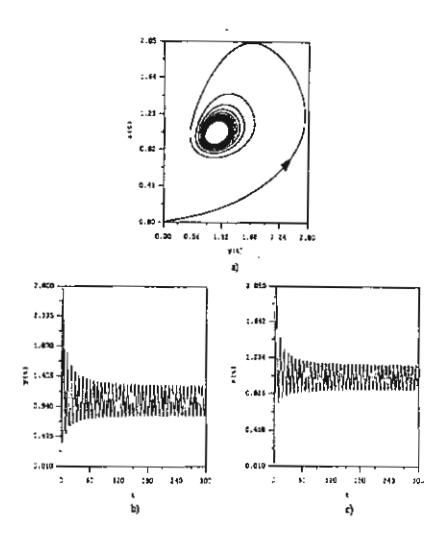


Figure 3: Bifurcation diagram of equations (2.6)-(2.8) with  $\delta_1=0.47, \delta_2=0.401, \delta_3=0.422, K_1=0.477, K_2=0.422, K_3=0.411, \beta_1=0.001, \tau_0=0.522,$  and  $\tau=10$ .

### 5 Discussion and Conclusion

We present in Fig. 6a) some clinical data partly adapted from the report by Engler  $et\ al.$  (1999) on the review of the evidence for the existence of inhibitory as well as stimulatory hypophysiotropic regulation of adrenocorticotropin secretion and biosynthesis. The figure shows pituitary venous concentrations of CRH in two mares given naloxone at a low dose rate at the arrow. In Fig. 6b), actual data of plasma ACTH concentration in a rat sampled every 2 min. is shown, taken from Carnes  $et\ al.$ 's (1989) earlier work. The time series exhibits irregular characteristics in agreement with those simulated from our model, an example of which is shown in Fig. 4, where we need to recall that the state variables x,y, and z plotted in Fig. 4 are ratios of the three hormones over their respective critical levels.

However, there are at least three factors that complicate the interpretation, if not the measurement, of CRH concentration, as cautioned by David N. Orths (1992) in his work on CRH in humans. First, like other hypothalamic releasing factors, the concentration of CRH, presumed to be present in the hypothalamic hypophysial portal venous blood, is hugely diluted by the time it reaches the peripheral veins. Secondly, CRH is produced and presumably secreted by many extrahypothalamic tissues, even though we have assumed this to be of relatively small and thus negligible amount in our model. Finally, there are specific high-affinity, high-capacity CRH-binding proteins present in human plasma. Thus, even

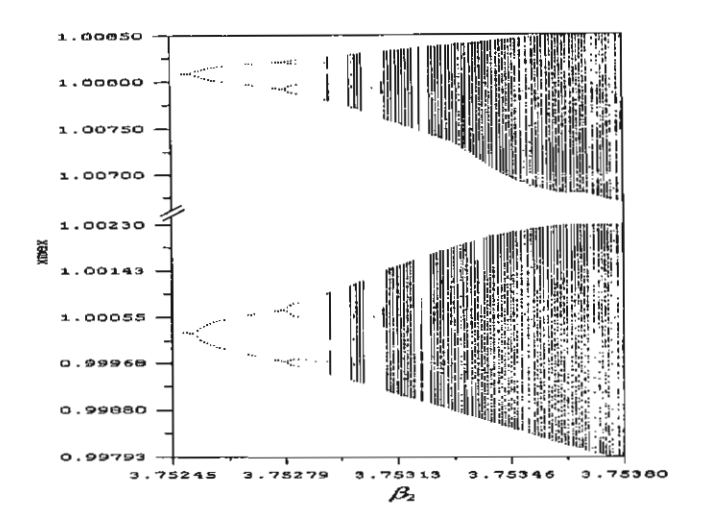


Figure 4: Computer simulation of equations (2.6)-(2.8) with  $\delta_1 = 0.47, \delta_2 = 0.401, \delta_3 = 0.422, K_1 = 0.477, K_2 = 0.422, K_3 = 0.411, \beta_1 = 0.001, \beta_2 = 3.75346, \tau_0 = 0.522, \text{ and } \tau = 10.$ 

though it is possible to measure immunoreactive CRH in peripheral plasma, the absolute peripheral plasma CRH concentration at any moment may not accurately reflect hypothalamic CRH secretion, and thus should be considered with caution.

ACTH measurement also poses problems associated with its bioassays at low plasma concentration. Detection of primary abnormal functioning at the pituitary level is made easier only by the availability of the releasing hormones that make evocater tests possible. In cases of inadequate availability of a pituitary hormone, such as ACTH supply, the target gland hormone (cortisol) is supplied instead (Norman & Litwack, 1997).

In spite of such cautionary notes, our model still provides a viable means by which the complexity and non-linear dynamics of diurnal hormone secretory patterns can be analyzed and qualitative description can be made of this complex delay feedback controlled systems. Our analysis yielded, for each set of physical parameters, a critical composite time delay  $\tau_0$  beyond which value the system exhibits episodic secretory pattern if  $\beta > \frac{1}{4}$ . As the feedback response factor  $\beta$  increases further, more irregular secretory patterns may be expected. Low dimensional chaotic dynamics would appear if  $\beta_2$  increased beyond a certain critical value  $\beta_c$  identified in the bifurcation diagram. This seems to suggest, considering Ilias *et al.*'s (2002) result from their nonlinear analysis of cortisol secretory patterns before and after sleep deprivation, that if the negative feedback effects are too weak, a diseased state is the reasonable diagnosis which then corresponds to the more regular secretory

 $A\ delay-differential\ equation\ model\ of\ the\ feedback-controlled\ hypothalamus-pituitary-adrenal\ cortex 15$ 

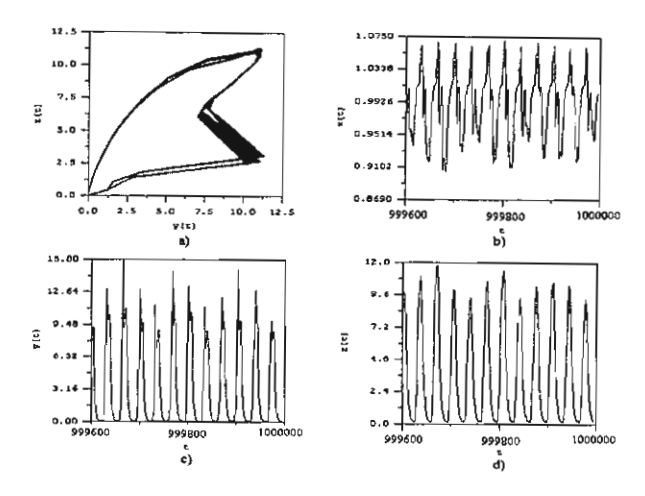


Figure 5: Divergence of time courses, when  $\beta_2 = 3.75346$  in the chaotic range, initiating from two different initial conditions only by  $10^{-9}$  in the initial value of x.

patterns. A relatively strong negative feedback mechanism for larger  $\beta$  leads to a more irregular pattern characteristic of a higher dimensional chaotic dynamics associated then with health. When  $\beta_2$  increases further, becoming greater than approximately 3.87549, the feedback mechanism is now faulty and the system returns to more regular periodic behavior which appears to be the mode of secretion in a diseased state.

Also, there is a critical composite time-delay  $\tau_0$  below which all state variables tend asymptotically to the respective steady-state levels as  $t \to \infty$ . We observe that it is the value of the composite time-delay  $\tau$  which delineates different dynamic behavior in the Hopf bifurcation analysis, not each of the feedforward delay  $\tau_1$  or the feedback delay  $\tau_2$  in our model. We may deduce from this that, in the human body, the feedforward and feedback response processes may be operating in a complimentary fashion. In health, an over zealous response in the feedforward loop can be compensated for by a late response in the feedback loop, and vise versa, resulting in an optimal turn-around time for all components in the whole cascade. When this complimentary mechanism is not functioning properly, a diseased state may be expected. In Fig. 4, where the apparently irregular secretion pattern is shown, comparable to the data presented in Fig. 6, the critical composite time-delay is  $\tau_0 = 0.522$  in the unit in which t is measured. We also observe that in Fig. 6b) ACTH peaks approximately 3 times during a 4 hour period in a rat. Comparing this with the corresponding simulated ACTH level in Fig. 4 where 3

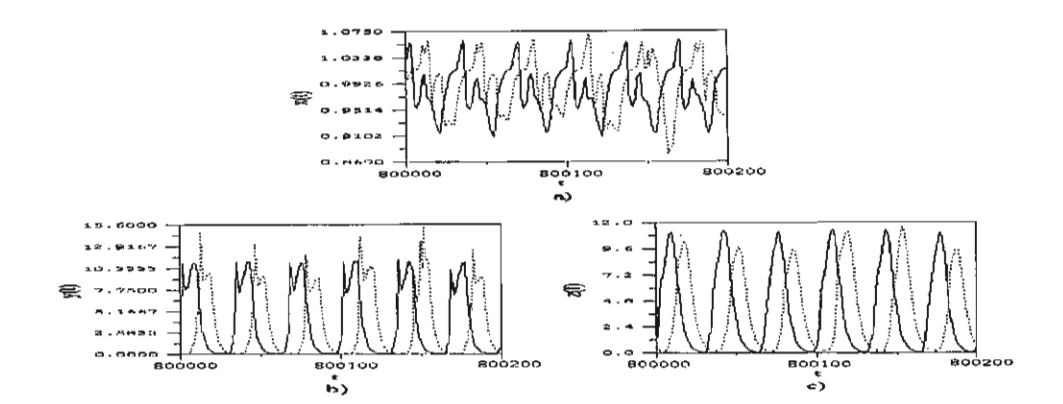


Figure 6: a) Pituitary venous concentrations of CRH in two mares ( $\blacksquare$ , marel;  $\bullet$ , mare2) given naloxone (adapted from the work of Engler *et al.*'s (1999)). b) Plasma ACTH concentration in a rat (taken from the work of Carnes *et al.*'s (1989)).

peaks are observed in 100 units of time t, we may then scale accordingly by taking t to be measured in the unit of 24 min., so that t=100 is equivalent to 4 hours. Then, the critical composite time-delay may be estimated as

$$\tau_0 \approx 0.522 \times \frac{240}{100} \approx 1.25 \text{ min.}$$

in a rat, and the composite time-delay may be estimated as

$$au pprox 10 imes rac{240}{100} = 24 ext{ min.}$$

based on the parametric values used in the simulation shown in Fig. 4. Unfortunately, similar estimates cannot be arrived at for humans, since frequent enough hormone measurements cannot be made and less peaks may then appear in the time series than there actually are. However, from the reports by Posener et al. (1997) and Hermus et al. (1984) mentioned earlier, in humans the delay in the short feedforward loop was observed to be around 30 min., while that in the short feedback loop was around 60 min.

From the above observation, we are also led to conclude that the role of individual time lag  $(\tau_1 \text{ or } \tau_2)$  in each of the responsive mechanisms is apparently not as significant to the well being of the cascade as the potency  $\beta$  of each feedback responsive signal. As seen in the bifurcation diagram shown in Fig. 3,  $\beta_2$  was found to be the bifurcation parameter which delineates different dynamical behavior and identifies the interfaces between sickness and health.

Although more intensive experimental/theoretical studies are necessary before definite conclusions can be made, such nonlinear approaches promise to offer sig-

 $A\ delay-differential\ equation\ model\ of\ the\ feedback-controlled\ hypothalamus-pituitary-adrenal\ cortex 17$ 

nificant contributions in our attempts to give a more qualitative description of the diurnal variations of hormone secretion in order to better understand the dynamic interfaces among different pathological situations.

#### Acknowledgment

Y.L. and P.P. would like to extend their deepest appreciation to the Thailand Research Fund for the financial support.

#### REFERENCES

- Berson, S. A., and Yalow, R. S. 1968 Radioimmunoassay of ACTH in plasma. J. Clin Invest. 47, 2725–2750.
- Carnes, M., Goodman, B. M., and Lent, S. J. 1991 High resolution spectral analysis of plasma adrenocorticotropin reveals a multifactorial frequency structure. Endocrinology 128, 902-910.
- Carnes, M., Lent, S., Feyzi, J., and Hazel, D. 1989 Plasma adrenocorticotropic hormone in the rat demonstrates three different rhythms within 24 h. Neuroendocrinology 50, 17-25.
- Engler, D., Redei, E., and Kola, I. 1999 The corticotropin-release inhibitory factor hypothesis: A review of the evidence for the existence of inhibitory as well as stimulatory hypophysiotropic regulation of adrenocorticotropin secretion and biosynthesis. *Endocr. Rev.* 20(4), 460–500.
- Hermus, A.R.M.M., Pieters, G.F.F.M, Smals, A.G.H., Benraad, T.J., Kloppenborg, P.W.C. 1984 Plasma adrenocorticotropin, cortisol, and aldosterone responses to corticotropin-releasing factor: modulatory effect of basal cortisol levels. J. Clin. Endocr. and Metab. 58 (1), 187-191.
- Ilias, I., Vgontzas, A. N., Provata, A., and Mastorakos, G. 2000 Complexity and non-linear description of diurnal cortisol and growth hormone secretory patterns before and after deprivation. *Endocrine Regulations* **36**, 63–72.
- Keenan, D. M., Licinio, J., and Veldhuis, J. D. 2001 A feedback-controlled ensemble model of the stress-responsive hypothalamo-pituitary-adrenal axis. *Proc Natl Acad Sci.*, 98 (7), 4028–4033.
- Krieger, D. T., Allen, W., Rizzo, F., and Khieger, H. P. 1971 Characterization of the normal temporal pattern of plasma corticosteroid levels. J Clin Endocrinol Metab 32, 266-284.
- Lenbury, Y. and Pacheenburawana, P. 1991 Modelling fluctuation phenomena in the plasma cortisol secretion system in normal man. *Biosystems* 26, 117–125.

- Moore-Ede, M. C., Czeisler, C. A., and Richardson, G. S. 1983 Circadian time-keeping in health and disease Part 2. Clinical implications of circadian rhythmicity. The New England Journal of Medicine 309 (9), 530-534.
- Norman, W. A., and Litwack G. 1997 *Hormones*. 2nd ed. London: Academic Press.
- Orth, D. N. 1992 Corticotropin-releasing hormone in humans. *Endocr. Rev.* 13 (2) 164-191.
- Posener, J. A., Schildkraut, J. J., Williams, G. H., and Schatzbarg, A. F. 1997 Cortisol feedback effects on plasma corticotropin levels in healthy subjects. *Psychoneuroendocrinology* 22 (3) 169-176.
- Posener, J. A., Schildkraut, J. J., Williams, G. H., and Schatzbarg, A. F. 1998 Late feedback effects of hypothalamic-pituitary-adrenal axis hormone in healthy subjects. it Psychoneuroendocrinology 23 (4) 371–383.
- Weitzman, E. D., Fukushima, D., Nogeire, C., Roffwarg, H., Gallagher, T. F., and Hellman, L. 1971 Twenty-four hour pattern of the episodic secretion of cortisol in normal subjects. J. Clin. Endocr. 33 14-22.
- Won, G.S.., Jap, T. S., Chang, S. C., Ching, K. N., and Chiang, C. N. 1986 Evidence for a delayed, integral, and proportional phase of glucocorticoid feedback on ACTH secretion in normal human volunteers. *Metabolism* 35 (3) 254-259.

Pure Appl. Chem., Vol. 74, No. 6, pp. 881–890, 2002. © 2002 IUPAC

# Cascade mechanism in a self-regulatory endocrine system. Modeling pulsatile hormone secretion\*

Thongchai Dumrongpokaphan and Yongwimon Lenbury<sup>‡</sup>

Department of Mathematics, Faculty of Science, Mahidol University, Thailand

Abstract: Many endocrine systems have been found to incorporate some form of cascade mechanism into their operation. Such a mechanism involves an amplification system where an initial reaction gives rise to the generation of multiple second reactions, each of which sets off multiple third reactions, and so on. Examples will be presented, with special attention paid to the hypothalamus-pituitary-testicular axis. The production and secretion of luteinizing hormone (LH) is governed by the medial-basal region of the hypothalamus. It is well known that the release of LH is a highly regulated process determined by negative and positive feedback, as well as neural components. The presence of gonadatropin-releasing hormone (GnRH) on specific adenohypophyseal cell membrane receptors results in the release of LH, which is then transported systemically to the Leydig cells of the testes. All the factors governing the release of these hormones, as well as a biochemical description of their actions, have not been completely elucidated, nor is the mechanism behind the pulsatile fashion in which the decapeptide GnRH and LH are released clearly explained. We describe how such a cascade mechanism in a self-regulatory system may be modeled and analyzed by a singular perturbation approach, identifying conditions that give rise to episodic hormone secretion or activity. Insightful and valuable interpretations can be made from such analysis of the cascade system.

#### INTRODUCTION

In recent years, there has been a great surge of interest in the study of how information is represented and transmitted in biological systems, specifically in the new field of bioinformatics. In nerve cells, information is transmitted through electrical impulses, which are sometimes generated as high-frequency bursts, followed by periods of quiescence. These impulses also cause muscles to contract and endocrine cells to secrete hormones. Quite often, bursting or episodic activities are observed in biological systems, particularly in endocrine cells. Attempts to model and simulate such mechanisms most frequently lead to nonlinear differential equations. This presents us with quite a challenge to develop nonlinear systems theory and analytical techniques to qualitatively and quantitatively unravel the intrinsic mechanisms that generate such behavior in these complex systems.

The study of endrocrinology over the past century has been mainly dependent upon the scientific methodologies available to probe the various endocrine systems. Thus, endocrinology has developed from being largely pursued at the physiological level into a biochemical era, which began in approximately 1955–1960 [1] and extends to the present time. Advances in chemical methodology, such as chromatography, mass spectrometry, nuclear magnetic resonance spectroscopy (NMR), and X-ray crystallography, have and continue to permit the detection and chemical characterization of minute quantities (nanograms or picograms) of new hormones and the characterization of the many receptors.

<sup>\*</sup>Plenary lecture presented at the International Conference on Bioinformatics 2002: North-South Networking, Bangkok, Thailand, 6-8 February 2002. Other presentations are presented in this issue, pp. 881-914.

<sup>&</sup>lt;sup>‡</sup>Corresponding author

#### T. DUMRONGPOKAPHAN AND Y. LENBURY

With the invention of scanning electron microscopes and confocal microscopy, which allows realtime imaging of living cells, the science of endocrinology is advancing rapidly. Scientists have been busily active in categorizing and defining the scope of influence and molecular mode of action of different hormones, as well as the mechanisms in their secretion.

Many endocrine systems incorporate some form of cascade mechanism into their operation [1]. A system with a cascade mechanism is an amplification process where an initial reaction results in the generation of multiple second reactions, each of which sets off multiple third reactions, and so on.

In this paper, we first discuss two examples of such cascade systems and explain how modeling and analysis of the system may be carried out based on singular perturbation principles. The method utilizes simple geometric arguments based on the assumption of highly diversified dynamics inherent to the cascade system. Application of the technique is done on the hypothalamus—pituitary—testicular axis involved in the biosynthesis and secretion of testosterone in response to blood levels of luteinizing hormone (LH). Episodic release of LH is triggered by the presence of the gonadotropin-releasing hormone (GnRH), secreted from the hypothalamus in a pulsatile fashion [1,2], which we attempt to explain through modeling and analysis. The analysis will then be extended to encompass higher-dimensional systems, which involve a multitude of components or species.

#### **CASCADE HORMONE SYSTEMS**

In the following, we describe two examples of systems with cascade mechanism. One classical biochemical cascade mechanism, at the cellular and molecular level, is generated by the action of a hormone, such as the action of glucagon at the cell membrane to produce an increase in cyclic AMP. Figure 1 shows a schematic description of a mechanism leading from the cell surface hormonal signal to the cellular metabolic response: glucagon and glycogenolysis. The cascade may be visualized in terms of alter-

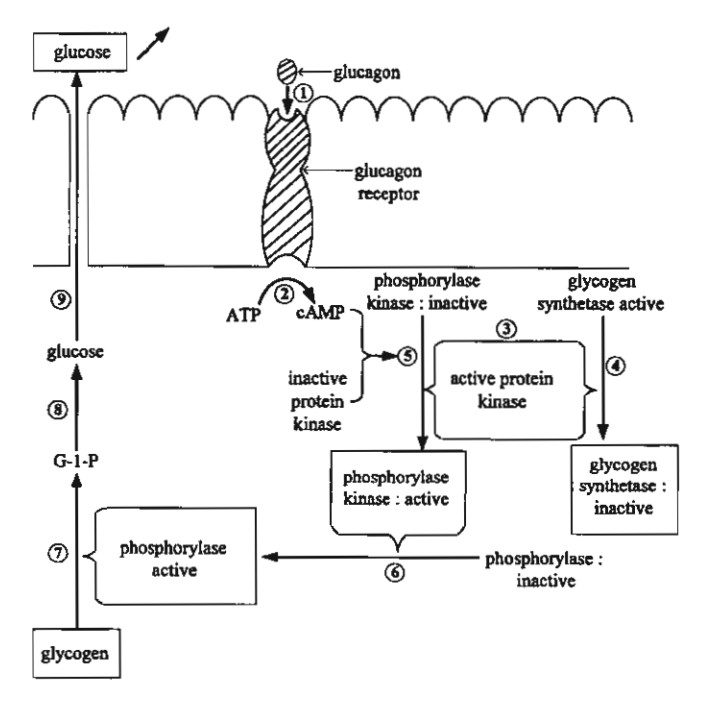


Fig. 1 A schematic description of a mechanism leading from the cell surface hormonal signal to the cellular metabolic response: glucagon and glycogenolysis.

ations of cellular response, stimulation of glycogenolysis to generate glucose for export to the extracellular space, and the general circulating system [1].

As so clearly elucidated by Norman and Litwack [1], the cascade begins with glucagon combining with its cell membrane receptor, marked (1) in Fig. 1. This then stimulates the activity of adenylate cyclase, possibly mediated by a transducing element, on the cytoplasmic side of the membrane, marked (2) in Fig. 1. As a result, the level of cyclic AMP increases, which activates a protein kinase (3), while the protein kinase subunits catalyze the phosphorylation of inactive phosphorylase kinase in reaction (5), as well as the active glycogen synthetase (4), to produce the phosphorylated inactive form, a step marked (6) in Fig. 1. The resulting phosphorylated inactive form consequently stimulates glycogenolysis in step (7) to form glucose 1-phosphate, which is further metabolized to glucose (8). Finally, glucose is transported to the extracellular space and into the general circulation (9). More detailed discussion of each step in the above-described cascade may be found in the work by Norman and Litwack [1]. The system is considered a cascade system due to the fact that each step following hormone binding is mediated by an enzyme that can turn over multiple substrate molecules.

Another system, which also incorporates the cascade mechanism, involves the central nervous system (CNS), the hypothalamus, pituitary, and the distal hormone secretion glands.

As explained by Norman and Litwack in their seminal work on hormones [1], the cascade effect may be produced by a single event or signal in the external or internal environment. A signal can be sent by either electrical or chemical transmission to the limbic system and then to the hypothalamus. This results in the secretion of a releasing hormone into the closed portal system connecting the hypothalamus and anterior pituitary shown in Fig. 2. It has been documented that releasing hormones may be secreted in nanogram amounts and half-lives of about 3–7 min. The releasing hormone consequently

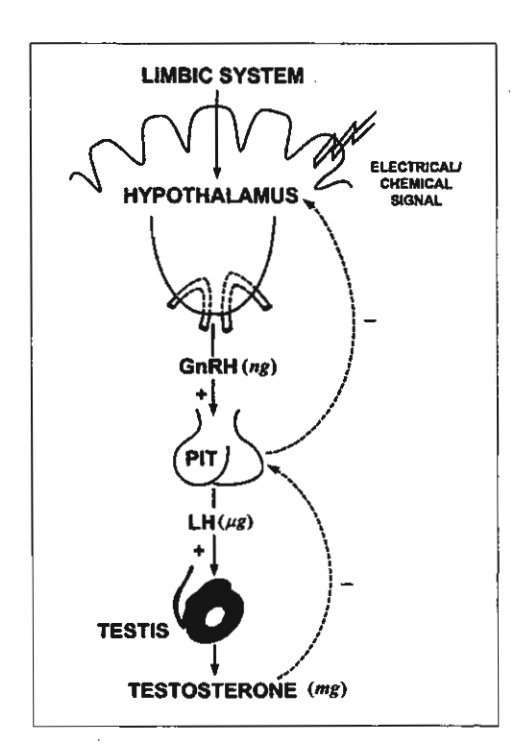


Fig. 2 Diagram showing the cascade hormonal system, the hypothalamus-pituitary-testicular axis, on proceeding down the cascade from the releasing hormone to the terminal hormone, there are increasing masses of the hormones released.

© 2002 IUPAC, Pure and Applied Chemistry 74, 881-890

#### T. DUMRONGPOKAPHAN AND Y. LENBURY

signals the release of the specific anterior pituitary hormones, which may be secreted in microgram amounts with half-lives on the order of 20 min or longer. The anterior pituitary in turns signals the release of the ultimate hormone, which may be secreted in many micrograms or milligram amounts and can be quite stable.

Thus, amplification of a single event at the outset could prove to be a factor of thousands to a millionfold, as hormone stability and the amounts of hormones increase as we proceed down the cascade.

#### Three-component cascade system

Letting x(t), y(t), and z(t) represent the densities or levels of the three components at anytime t in the cascade system described above, their rates of production will form a model consisting of the following system of differential equations

$$\dot{x} = f(x, y, z) \tag{1}$$

$$\dot{y} = \varepsilon g(x, y, z) \tag{2}$$

$$\dot{z} = \varepsilon \delta h(x, y, z) \tag{3}$$

where  $\varepsilon$  and  $\delta$  are small positive parameters. Thus, when the quantities on the right sides of eqs. 1-3 are finite and different from zero,  $|\dot{y}|$  is of the order  $\varepsilon$  and  $|\dot{z}|$  is of the order  $\varepsilon$   $\delta$ . Thus, x is assumed to possess the fastest dynamics, y an intermediate time response, while z possesses the slowest dynamics of the three components.

It is well known that the system (1-3) with small  $\varepsilon$  and  $\delta$  can be analyzed with the singular perturbation method [3], which under suitable regularity conditions, allows the approximation of the solution of the system (1-3) with a sequence of simple dynamic transitions occurring at different speeds.

Given an initial condition  $(x_0, y_0, z_0)$ , the slow z and intermediate (y) variables are frozen, and the system will develop according to the "fast system".

$$\dot{x}(\tau_1) = f[x(\tau_1), y_0, z_0]$$
 ,  $\tau_1 = \frac{t}{\varepsilon \delta}$ 

Thus,  $x(\tau_1)$  eventually tends toward a stable equilibrium  $\overline{x}(x_0, y_0, z_0)$  of the fast system. Then, as z is still frozen at  $z_0$ , the transitions will develop at intermediate speed according to the "intermediate system"

$$\dot{y}(\tau_2) = g\{\bar{x}[x_0, y(\tau_2), z_0], y(\tau_2), z_0\}$$
,  $\tau_2 = \frac{t}{\varepsilon}$ 

until an equilibrium  $\overline{y}(x_0, y_0, z_0)$  of the intermediate system is reached. A third transition then develops at low speed along the curve f = g = 0 to end at an equilibrium or form a closed cycle, depending on the stability properties of the three equilibrium manifolds f = 0, g = 0, and h = 0.

The sequence of these transitions thus constructed then approximates the solution of the system, in the sense that the real trajectory is contained in a tube around the traced transitions, and that the radius of the tube goes to zero with  $\varepsilon$  and  $\delta$ . More detail of the main aspects of the method can be found in the work by Muratori and Rinaldi [3], while examples of applications to nonlinear systems in biology and medicine are available in the works of Lenbury et al. [4,5].

#### Application in modeling pulsatile secretion of LH

The hypothalamus-pituitary-testicular axis is diagrammed schematically in Fig. 2. The release of LH is a highly regulated process determined by (a) negative feedback, (b) positive feedback, and (c) neural components.

Table 1 Relevant information on testosterone.

Biochemical aspects	Data
Plasma concentration (ng/100 ml)	300–1100
Testes secretion rate	5000
Metabolic clearance rate (litre/day)	980
Site of production	Leydig cells of testes
Structure	OH OH
Principal biological function	Maintenance of functional male repro- ductive system and secondary male sex characteristics

The decapeptide GnRH is released from the hypothalamus in a pulsatile fashion with short latency and initiates the episodic secretion of LH. The LH is then transported systemically to the Leydig cells of the testes. LH-mediated stimulation of testosterone synthesis and secretion by the Leydig cells is initiated by the binding of LH to hormone-specific receptors on the outer membranes of the Leydig cell. The rate of biosynthesis and secretion of testosterone, whose structure is shown in Table 1, is positively correlated with the blood levels of LH, while the secretion of the gonadotropin can be diminished by increasing blood concentrations of testosterone, which facilitates their binding to steroid receptors in both the hypothalamus and pituitary. This is called "suppressive negative feedback". The precise details of the feedback mechanism in this self-regulatory system are not yet clear. Nevertheless, close study of the process has led Liu and Deng [6] to propose a model consisting of the following equations.

$$\frac{dR}{dt} = \frac{a_1 + a_2 R + a_3 R^2}{1 + \alpha_4 T + \alpha_5 T^2 + a_6 R + a_7 R^2} - a_8 R \tag{4}$$

$$\frac{dL}{dt} = \frac{a_9 + a_{10}R}{1 + a_{11}T + a_{12}R} - \alpha_{13}L \tag{5}$$

$$\frac{dT}{dt} = a_{14} + \alpha_{15}L + \frac{\alpha_{16}L + \alpha_{17}L^2}{1 + \alpha_{18}L + \alpha_{19}L^2 + \alpha_{20}RT + \alpha_{21}RLT} - \alpha_{22}T$$
(6)

where R, L, and T are concentrations of GnRH, LH (above the basal level), and testosterone, respectively. The first term in eq. 4 accounts for the autoregulatory effect of GnRH and T on GnRH secretion. The second term represents the removal of GnRH proportional to the amount present, and similarly for all the last terms in eqs. 4–6.

The factor  $a_{10}R$  in eq. 5 accounts for the stimulating effect of GnRH on the release of LH, while  $a_9$  accounts for the autonomous secretion of LH independent of GnRH. The term  $\alpha_{15}L$  in eq. 6 accounts for the stimulating effect of LH on testosterone secretion, while  $a_{14}$  is the secretion rate of T independent of LH. The factors in the denominators of the positive terms in the 3 equations account for autoregulation on the rates of secretion of all 3 hormones.

Taking into account the cascade effect of the system described earlier, we can assume that the time responses of the three components in the above system are quite diversified, and scale the dynamics of the cascade by means of two small dimensionless positive parameters  $\varepsilon$  and  $\delta$  as follows. Letting

#### T. DUMRONGPOKAPHAN AND Y. LENBURY

$$x = R, y = \varepsilon L, z = \varepsilon \delta T, \ a_4 = \frac{\alpha_4}{\varepsilon \delta}, \ a_5 = \frac{\alpha_5}{\varepsilon^2 \delta^2}, \ a_{11} = \frac{\alpha_{11}}{\varepsilon \delta}, \ a_{13} = \frac{\alpha_{13}}{\varepsilon}, \ a_{15} = \frac{\alpha_{15}}{\varepsilon}, \ a_{16} = \frac{\alpha_{16}}{\varepsilon}, \ a_{17} = \frac{\alpha_{17}}{\varepsilon^2}, \ a_{18} = \frac{\alpha_{18}}{\varepsilon}, \ a_{19} = \frac{\alpha_{19}}{\varepsilon^2}, \ a_{20} = \frac{\alpha_{20}}{\varepsilon \delta}, \ a_{21} = \frac{\alpha_{21}}{\varepsilon^2 \delta}, \ \text{and} \ a_{22} = \frac{\alpha_{22}}{\varepsilon \delta}, \ \text{we are led to the following system.}$$

$$\frac{dx}{dt} = \frac{a_1 + a_2 x + a_3 x^2}{1 + a_4 z + a_5 z^2 + a_6 x + a_7 x^2} - a_8 x \equiv f(x, y, z)$$
 (7)

$$\frac{dy}{dt} = \varepsilon \left[ \frac{a_9 + a_{10}x}{1 + a_{11}z + a_{12}x} - a_{13}y \right] \equiv \varepsilon g(x, y, z)$$
(8)

$$\frac{dz}{dt} = \varepsilon \delta \left[ a_{14} + a_{15}y + \frac{a_{16}y + a_{17}y^2}{1 + a_{18}y + a_{19}y^2 + a_{20}xz + a_{21}xyz} - a_{22}z \right] = \varepsilon \delta h(x, y, z)$$
(9)

We are able to show that the relative positions of the 3 equilibrium manifolds f = 0, g = 0 and h = 0 will be as depicted in Fig. 3 if the following conditions hold:

$$a_8 < a_2 \tag{10}$$

$$a_6 a_8 - a_3 < 0 ag{11}$$

$$a_{15}a_{18}^2 + a_{17}a_{18} + 2a_{15}a_{19} > a_{16}a_{19}$$
 (12)

$$27q^2 + 4p^3 < 0 ag{13}$$

$$4u^3 + 27v^2 > 0 ag{14}$$

$$y_1 < y_m \text{ and } y_M < y_2$$
 (15)

where

$$p = \frac{s^2}{3} \tag{16}$$

$$q = t + \frac{2s^3}{27} \tag{17}$$

$$s = \frac{a_6 a_8 - a_3}{2 a_7 a_8} \tag{18}$$

$$t = \frac{a_1}{2a_7 a_8} \tag{19}$$

$$u = c_2 - \frac{c_1^2}{3} \tag{20}$$

$$v = c_3 - \frac{c_1 c_2}{3} + \frac{2c_1^3}{27} \tag{21}$$

$$c_1 = \frac{a_6 a_8 - a_3}{a_7 a_8} \tag{22}$$

887

Cascade mechanism in a self-regulatory endocrine system

$$c_2 = \frac{a_8 - a_2}{a_7 a_8} \tag{23}$$

$$c_3 = -\frac{a_1}{a_7 a_8} \tag{24}$$

while  $y_1$ ,  $y_2$  are the y-coordinates of the minimum and maximum points, respectively, on the f = g = 0 curve, and  $y_m$ ,  $y_M$  are those of the f = h = 0 curve, as seen in Fig. 3. Specifically, inequality (15) is the separation condition which ensures that the slow manifold h = 0 separates the two stable branches of the curve f = g = 0 for y in a certain interval containing the point where f = g = h = 0.

The system, initially at a generic point, say point A of Fig. 3, will make a fast O(1) transition, indicated by three arrows, to the stable portion of the slow manifold f = 0 (point B in Fig. 3). As point B is approached, y has slowly become active. An O( $\varepsilon$ ) transition at intermediate speed, indicated by two arrows, is made along f = 0 in the direction of decreasing y, since g > 0 here, to point C on the stable part of the curve f = g = 0. From point C, a slow O( $\varepsilon\delta$ ) transition, indicated by a single arrow, is then made along this curve in the direction of increasing z, since h > 0 here below the surface h = 0.

Once point D is reached, the stability of the manifold is lost. The O(1) time-scale becomes dominant once again. Hence, the orbit follows a path close to the curve y = constant, z = constant, at high speed, bringing the system to point E on the other stable branch of the manifold f = 0. This is followed by a motion at intermediate speed on f = 0 to point F on the curve f = g = 0 Consequently, the system will slowly develop along this line in the direction of decreasing z, since h is now negative.

At point G on this curve, the stability will again be lost and a fast transition will bring the system back to point H on the stable portion of f = 0, followed by a motion at intermediate speed to point I on the curve f = g = 0, before repeating the same previously described path, thereby forming a closed cycle IDEFGHI. Thus, the existence of a limit cycle in the system for  $\varepsilon$  and  $\delta$  sufficiently small is assured. The exact solution trajectory of the system will be contained in a tube about this closed curve, the radius of which tends to zero with  $\varepsilon$  and  $\delta$ .

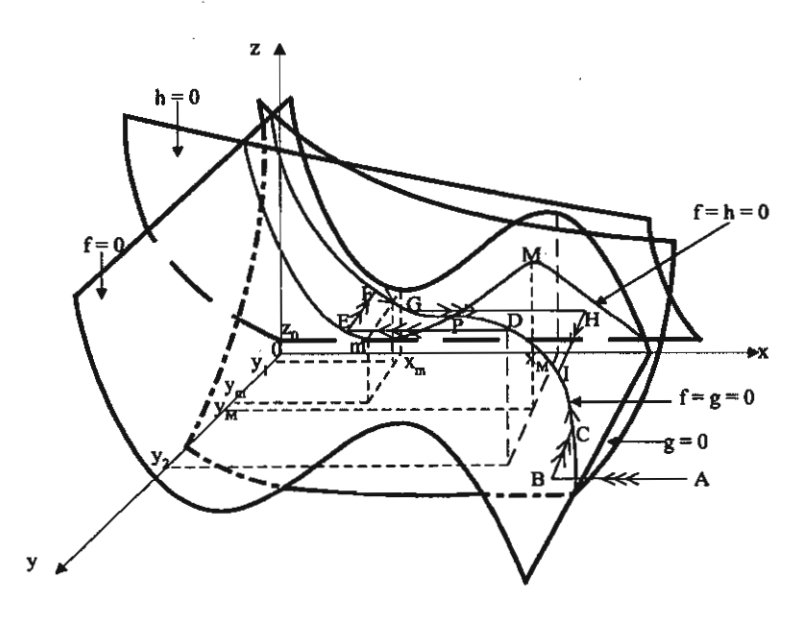


Fig. 3 Shapes and relative positions of the equilibrium manifolds in the case where a limit cycle exists. Here, three arrows indicate fast transitions, two arrows indicate transitions at intermediate speed, and a single arrow indicates slow transitions.

© 2002 IUPAC, Pure and Applied Chemistry 74, 881-890

#### T. DUMRONGPOKAPHAN AND Y. LENBURY

A computer simulation of eqs. 7-9 is presented in Fig. 4 with parametric values chosen to satisfy the inequalities (10-15). The solution trajectory, projected onto the (y, x)-plane, is seen in Fig. 4a to tend to a limit cycle as theoretically predicted. The corresponding periodic time series of LH is shown in Fig. 4b.

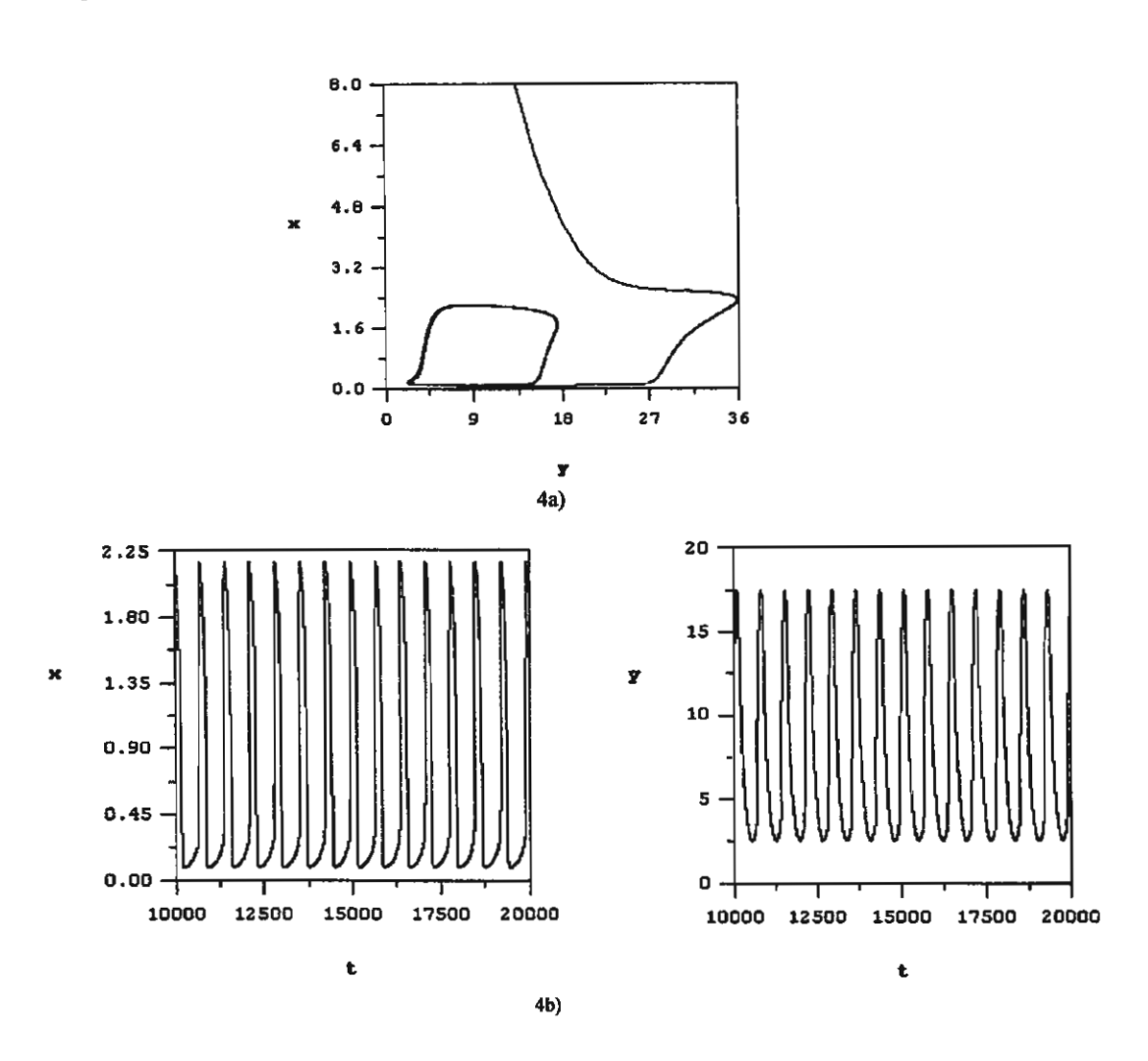


Fig. 4 A computer simulation of the model system of eqs. 7–9 with parametric values chosen to satisfy the conditions identified in the text for which periodic solutions exist. The solution trajectory, projected onto the (y,x)-plane, is seen in (a) to tend toward a stable limit cycle as theoretically predicted. The corresponding time series of GnRH (x) and LH (y) are shown in (b). Here,  $\varepsilon = 0.8$ ,  $\delta = 0.05$ ,  $a_1 = 0.2$ ,  $a_2 = 0.1$ ,  $a_3 = 3$ ,  $a_4 = 0.1$ ,  $a_5 = 0.01$ ,  $a_6 = 0.5$ ,  $a_7 = 2$ ,  $a_8 = 0.5$ ,  $a_9 = 0.05$ .  $a_{10} = 1.5$ ,  $a_{11} = 1.0$ ,  $a_{12} = 0.2$ ,  $a_{13} = 0.01$ ,  $a_{14} = 0.2$ ,  $a_{15} = 0.1$ ,  $a_{16} = 0.1$ ,  $a_{17} = 0.1$ ,  $a_{18} = 0.2$ ,  $a_{19} = 0.2$ ,  $a_{20} = 0.1$ ,  $a_{21} = 0.1$ , and  $a_{22} = 0.1$ .

#### Extension to higher-dimensional systems

In order to extend the above concept to higher dimensional systems, let us consider a system of n + 3 differential equations which may be written in the form

© 2002 IUPAC, Pure and Applied Chemistry 74, 881-890

Cascade mechanism in a self-regulatory endocrine system 889

$$\dot{x} = F(x, y, z, w; \alpha) \tag{25}$$

$$y = \varepsilon G(x, y, z, w; \alpha)$$
 (26)

$$\dot{y} = \varepsilon \delta H(x, y, z, w; \alpha) \tag{27}$$

$$\dot{w} = \varepsilon \delta \eta \, K(x, y, z, w; \alpha) \tag{28}$$

where  $\varepsilon$ ,  $\delta$ , and  $\eta$  are small positive constants,  $\alpha \in \Re^N$  is the N-dimensional vector of system parameters,

while 
$$\begin{bmatrix} x \\ y \\ z \end{bmatrix} \in \Re^3$$
 and

$$w = \begin{bmatrix} w_1 \\ w_2 \\ \vdots \\ w_n \end{bmatrix} \in \Re^N$$

are the n + 3 state variables, and

$$K = \begin{bmatrix} K_{I}(x, y, z, w; \alpha) \\ K_{2}(x, y, z, w; \alpha) \\ \vdots \\ K_{n}(x, y, z, w; \alpha) \end{bmatrix}$$

Hence, x is the fast variable, y the intermediate, z the slow, and  $w_i$ , i = 1, 2, ..., n, the very slow components of the system.

Employing the same line of arguments as above, we first assume that w is varying extremely slowly in comparison to the first three components x, y, and z. Then, we may initially assume that w is kept frozen at a constant value w(0) while x, y, and z vary according to the three-dimensional system

$$\dot{x} = F[x, y, z, w(0); \alpha] = f(x, y, z) \tag{29}$$

$$\dot{\mathbf{y}} = \varepsilon G[\mathbf{x}, \mathbf{y}, \mathbf{z}, \mathbf{w}(0); \alpha] = \varepsilon g(\mathbf{x}, \mathbf{y}, \mathbf{z}) \tag{30}$$

$$\dot{y} = \varepsilon \delta H[x, y, z, w(0); \alpha] = \varepsilon \delta h(x, y, z) \tag{31}$$

Thus, if, for suitable parametric values  $\alpha$ , the relative positions of the three equilibrium manifolds of the system (29–31) are the same as those three shown in Fig. 3, then trajectories will develop as described earlier. However, as w varies with time, though very slowly, the shapes and positions of the three manifolds shift slowly as time passes. The coordinates of the points m, M, and O are, in this case,  $[x_{\rm m}(w;\alpha),y_{\rm m}(w;\alpha),z_{\rm m}(w;\alpha),y_{\rm m}(w;\alpha),y_{\rm m}(w;\alpha),z_{\rm m}(w;\alpha)]$ , and  $[x_{\rm o}(w;\alpha),y_{\rm o}(w;\alpha),z_{\rm o}(w;\alpha)]$  respectively, since F, G, and G are all functions of G.

Moreover, if we further assume that each of the equations

$$K_i(x, y, z, w; \alpha) = 0, \quad i = 1, 2, ..., n,$$
 (32)

can be solved for z as an explicit function of the other components:

$$z = Z_i(x, y, w; \alpha), \quad i = 1, 2, ..., n,$$
 (33)

#### T. DUMRONGPOKAPHAN AND Y. LENBURY

then separation conditions are needed to ensure that the manifold H = 0, as well as those described by the equations in (33) are positioned in between the two stable branches of the curve F = G = 0, in order that a limit cycle exists. These conditions are stated in the following theorem, under all the assumptions mentioned above.

**Theorem:** Suppose that the functions  $F(x, y, z, w; \alpha)$ ,  $G(x, y, z, w; \alpha)$ ,  $H(x, y, z, w; \alpha)$ , and  $K(x, y, z, w; \alpha)$ , are continuous, and that the functions  $x_{\mathbf{M}}(w; \alpha), z_{\mathbf{M}}(w; \alpha), x_{\mathbf{m}}(w; \alpha), z_{\mathbf{m}}(w; \alpha), x_{\mathbf{O}}(w; \alpha), z_{\mathbf{O}}(w; \alpha)$ , and  $Z_i$ , i = 1, 2, ..., n, are continuous and bounded. If, for some permissible value of  $\alpha$ , and each fixed value of w, there exists a unique equilibrium point O, where F = G = H = 0, and K = 0, such that

$$\sup_{w} x_{\mathrm{m}}(w;\alpha) < \inf_{w} x_{\mathrm{O}}(w;\alpha) \tag{34}$$

$$\sup x_O(w;\alpha) < \inf_w x_M(w;\alpha) \tag{35}$$

$$\sup_{i} z_{\mathrm{m}}(w;\alpha) < \min_{i} \inf_{\Lambda} Z_{i} \tag{36}$$

$$\max_{i} \sup_{\Delta_{i}} Z_{i} < \inf_{w} Z_{M}(w; \alpha)$$
(37)

where the supremum and infemum of  $Z_i$  are taken over its domain  $\Delta_i$  which is a subset of  $\Re^{n+2}$ , then a limit cycle exists for the system of eqs. 25-28, provided that  $\varepsilon$ ,  $\delta$ , and  $\eta$ , are sufficiently small.

#### CONCLUSION

Analysis of a self-regulatory endocrine system that incorporates a cascade mechanism has been elucidated through modeling and arguments based on the singular perturbation principles that have exploited the highly diversified dynamics of the cascade system. The method decomposes the system into fast, intermediate, and slow components. The slow-motion trajectories lie on the equilibrium manifold of the fast component. The existence of limit cycles characterized by fast transitions between stable equilibria gives rise to periodic solutions. Thus, the temporal secretion patterns often observed in clinical data [1,2] appear to be the effect of the inherent cascade mechanism combined with the mixture of negative and positive feedback autoregulation process, giving rise to a natural frequency in the pulsatile mode of secretion. When this is interfered with by signals from the neural components or other external factors, irregular secretion patterns may result which have been frequently observed clinically [1,2].

The above analysis provides an example of how episodic activities in a cascade system may be modeled and explained. The technique has then been extended to higher-dimensional systems in order to be capable of coping with multiple-component cascades.

#### **ACKNOWLEDGMENT**

Appreciation is extended to the Thailand Research Fund for the financial support that made this research project possible (contract number RTA/02/2542 and PHD/0029/254).

#### REFERENCES

- 1. L. L. Ewing and B. Zirkin. Recent Prog. Hormone Res. 39, 599-632 (1983).
- 2. R. V. Gallo. Biol. Reprod. 24, 771-777 (1981).
- 3. S. Muratori and S. Rinaldi. Siam. J. Appl. Math. 52, 1688-1706 (1992).
- 4. Y. Lenbury, K. Kamnungkit, B. Novaprateep. IMA J. Math. Applied Med. Biol. 13, 1-21(1996).
- 5. Y. Lenbury, R. Ouncharoen, N. Tumrasvin. IMA J. Math. Applied Med. Biol. 17, 243-261(2000).
- 6. B.-Z. Liu and G.-M. Deng. J. Theor. Biol. 150, 51-58 (1991).

Mathematical Medicine and Biology (2005) 22, 99-112 doi:10.1093/imammb/dqh023

# Mathematical models for pressure controlled ventilation of oleic acid-injured pigs

P. S. CROOKET

Biomathematics Study Group, Department of Mathematics, Vanderbilt University, Nashville, TN 37240, USA

K. KONGKUL AND Y. LENBURY

Department of Mathematics, Mahidol University, Bangkok, Thailand

AND

A. B. ADAMS, C. S. CARTER, J. J. MARINI AND J. R. HOTCHKISS

Pulmonary and Critical Care Medicine, Regions Hospital and University of Minnesota,

St. Paul, MN 55101, USA

[Received on 31 January 2003; accepted on 1 December 2003]

One-compartment, mathematical models for pressure controlled ventilation, incorporating volume dependent compliances, linear and nonlinear resistances, are constructed and compared with data obtained from healthy and (oleic acid) lung-injured pigs. Experimental data are used to find parameters in the mathematical models and were collected in two forms. Firstly, the  $P_e$ -V curves for healthy and lung injured pigs were constructed; these data are used to compute compliance functions for each animal. Secondly, dynamic data from pressure controlled ventilation for a variety of applied pressures are used to estimate resistance parameters in the models. The models were then compared against the collected dynamic data. The best mathematical models are ones with compliance functions of the form C(V) = a + bV where a and b are constants obtained from the  $P_e$ -V curves and the resistive pressures during inspiration change from a linear relation  $P_r = RQ$  to a nonlinear relation  $P_r = RQ^\epsilon$  where Q is the flow into the one-compartment lung and  $\epsilon$  is a positive number. The form of the resistance terms in the mathematical models indicate the possible presence of gas-liquid foams in the experimental data.

Keywords: oleic acid injury; mathematical model; variable compliance.

#### 1. Introduction

Oleic acid-injured animal models are used to test a wide variety of physiologic approaches and adjunctive therapies in mechanical ventilation (Bowton & Kong, 1989; Hernandez et al., 1990; Wilson et al., 2001). Using animal models of lung injury and disease, researchers have probed acute physiologic and therapeutic techniques ranging from liquid ventilation (Sawada et al., 2002), splanchnic perfusion and oxygenation (Jedlinska et al., 2001), ventilatory support (Martynowicz et al., 2001; Mutch et al., 2000; Nam et al., 2000; Neumann et al., 2000; Neumann & Hedenstierna, 2001) to tracheal gas insufflation or TGI (Carter et al., 2002; Cereda et al., 1999; Zhan et al., 2001). One of the more important uses of oleic acid-injury models is to evaluate the efficacy of recruitment manoeuvres (Cakar et al., 2000; Crott et al., 2001; Martynowicz et al., 2001; Pelosi et al., 2001; Van der Kloot et al., 2000). In this paper we report on

Corresponding Author. Email: philip.s.crooke@vanderbilt.edu

data collected from pigs that were subjected to mechanical ventilation before and after oleic acid injury. Using these data, robust mathematical models of prevailing lung mechanics are constructed that capture the differences in pre- and post-injury physiology of the animals. Such accurate mathematical models allow prediction of key outcome variables of mechanical ventilation: tidal volume, average volume, end-expiratory pressure, mean alveolar pressure, and ventilator power. The physiologic parameters of the animals, compliance and resistance (both inspiratory and expiratory), must be identified so that these quantities can be used in the dynamic mathematical models. Using the static elastic pressure-volume  $(P_e-V)$  curves, compliance functions are constructed for each animal and the dynamic data are used to estimate inspiratory and expiratory resistance constants.

The experimental protocol was approved by the Animal Care and Use Committee of Region Hospital; all animals were managed according to NIH standards. In these animal studies, pigs were anesthetized with pentobarbital, paralyzed, and tracheally intubated. Mechanical ventilation was initiated using pressure controlled ventilation with applied pressure ( $P_{set}$ ) of 10 cm H<sub>2</sub>O during inspiration, positive end-expiratory pressure (PEEP) of 5 cm H<sub>2</sub>O, FIO<sub>2</sub> of 0·6, and duty cycles of either 1/3, 1/2, or 2/3. Continuous IV general anesthesia and paralysis (pentobarbital and pancuronium) was provided.  $P_e-V$  curves were then collected for each animal. The pigs were ventilated using different combinations of duty cycles and applied airway pressures during inspiration ( $P_{set}$ ) and expiration ( $P_{peep}$ ); the time, airway pressure, and flow were measured over several cycles of the ventilator. Lung injury was then induced by oleic infusion using a standard protocol and static  $P_e-V$  curves again measured. Using the same ventilator settings that were employed before injury, data were again collected for time, airway pressure, and flow.

The mathematical models used to analyse the experimental data are based on a unicompartmental model that permits the compliance of the respiratory system to vary with lung volume: i.e. elastic pressure,  $P_e$ , is given by  $P_e = F(V)$  where V is the lung volume at any instant of time above its rest volume and F is a function that can be calculated from the  $P_e-V$  curves during inspiration and expiration. Furthermore, the models permit the resistive pressure  $P_r$  to depend on the flow  $Q = |\dot{V}|$  in a nonlinear fashion.

The paper is structured as follows. A brief overview of variable compliance is presented in Section 2, showing that the compliance of the respiratory system can be approximated by continuous linear functions of the volume V. In Section 3, a mathematical model for pressure controlled ventilation with variable compliance, linear and nonlinear resistances is then constructed. In the clinical setting, the clinician sets the levels of applied airway pressures ( $P_{set}$  and  $P_{peep}$ ), frequency of breathing (f), and the inspiratory time fraction or duty cycle (D) while the compliance (C) and resistances ( $R_i$  and  $R_e$ ) are uncontrolled variables. The key outcome variables of the ventilation are the tidal volume ( $V_T$ ), minute ventilation ( $\dot{V}_E$ ), end-expiratory pressure ( $P_{ex}$ ), mean alveolar pressure ( $P_m$ ), and power ( $\dot{W}_m$ ). These quantities are computable from the mathematical model.

Data for the validation of the mathematical models were sampled from data collected in other studies at Region Hospital. Although the database included several animals, in this paper we restrict our discussions to three pigs (labelled A, B, C). The ideas presented here were tested on other animals and found to be consistent with the data sets from the three pigs. For brevity, we do not include the extra data.

TABLE 1 One-segment compliance function parameters for inspiration and expiration, pre- and post-injury, for a particular animal (Pig A)

	Pre-injury		Pre-injury Post-injury	
Parameter	Inspiration	Expiration	Inspiration	Expiration
aj	0.0419	0.0952	0.0121	0.103
$b_j$	-0.00272	-0.0388	0.0241	-0.0449

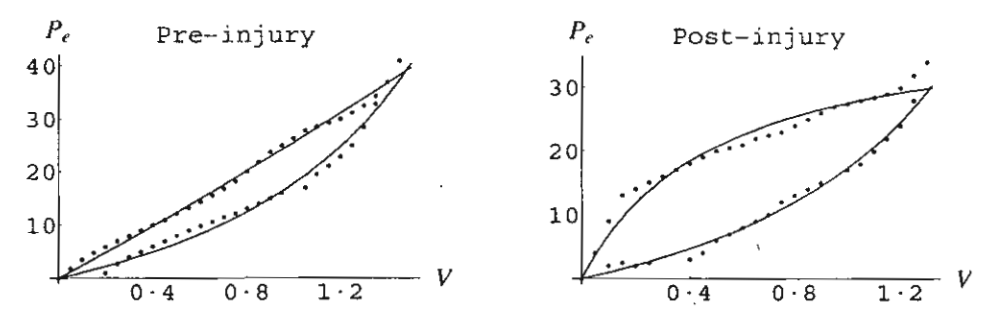


Fig. 1.  $P_e$ -V data for a particular animal (Pig A) approximated by a one-segment compliance function.

#### 2. A variable compliance model for the $P_e-V$ curves

In Crooke et al. (2002), a variable compliance model was proposed for pressure controlled ventilation. In its simplest form, it assumes that the elastic pressure in the lungs is of the form

$$P_e = \frac{V}{a+bV} \tag{2.1}$$

where  $P_e$  denotes the elastic pressure in the one-compartment lung, V is the volume of the compartment above its rest volume, and the parameters, a and b, are obtained from experimental data. In the collection of the elastic pressure-volume data, it is assumed that the end-expiratory pressure of the lung is zero. In other words, these data were collected without applied PEEP after a protracted exhalation minimizing auto-PEEP.

We call the linear function, C(V) = a + bV, the compliance function of the model. Since, in fact,  $C = \frac{dV}{dP}$ , the approximation C(V) = a + bV is only accurate provided  $\frac{bV}{a} \ll 1$ . If C varies too quickly with V, the physical data for the compliance function may deviate significantly from the linear approximation a + bV. The parameters, a and b, of the compliance function during inspiration may be different from those during expiration. That is, there is hysteresis. During passive ventilation, C represents the compliance of the total respiratory system, lungs and chest cavity. Because during these experiments, the animals were pharmacologically paralyzed, this is an appropriate assumption. In Fig. 1, each  $P_e - V$  curve (inspiration/expiration and pre/post-injury) for a particular animal (Pig A) is approximated by functions of the form  $P_e = V/(a + bV)$  with a and b chosen to give the best least squares fit. The constants for this data set are listed in Table 1. As can be seen in Fig. 1, we obtain a reasonable fit of the experimental data, although there is some error at the extremes of the curves. However, as will be seen in later sections, our model is found to uniformly produce good approximations to experimental data.

#### 3. Models for pressure controlled ventilation

Along with the  $P_e-V$  data collected for each animal in this study, pressure controlled ventilation data was collected for a variety of  $P_{set}$  and  $P_{peep}$  combinations using breaths of 6 s in length and an inspiratory time fraction or duty cycle of either 1/3, 1/2, or 2/3. In this section we attempt to match the data with a variety of mathematical models for controlled preset ventilation.

Several mathematical models for pressure controlled ventilation of a single compartment lung were examined. It is assumed that breaths are identical and are of duration  $t_{tot}$ . Each breath is subdivided into an inspiratory phase of length  $t_i$  and expiratory phase of length  $t_e$  so that  $t_{tot} = t_i + t_e$ . At any instant of time in  $[0, t_{tot}]$ , there is a pressure balance between applied pressures or ventilatory pressures  $(P_{vent})$ , pressures due to elastic forces  $(P_e)$ , pressures due to resistive losses  $(P_r)$ , and the end-expiratory pressure  $(P_{ex})$ :

$$P_r + P_e + P_{ex} = P_{vent}$$

In this model, the symbol V(t) represents the volume above the volume of the lung at the end of the previous breath. Hence, V(t) is referenced to a constant volume  $V_{ex}$  which is explained below. Assuming breaths of uniform length  $(t_{tot})$ , V(t) is zero at the beginning and ending of each breath. We define the end-expiratory volume  $(V_{ex})$  to be the volume of the lung above its rest volume due to  $P_{ex}$ ; that is,  $P_{ex} = V_{ex}/C(V_{ex})$ . We denote by  $V_i(t)$  the volume of the compartment above  $V_{ex}$  during inspiration and by  $V_e(t)$  the compartmental volume above  $V_{ex}$  during expiration. We assume that  $V_i(0) = V_e(t_{tot}) = 0$ .  $V_T$  denotes the tidal volume and it is assumed that  $V_T = V_i(t_i) = V_e(t_i)$ . For the elastic pressure, we assume that  $P_e = V/C(V)$  where C(V) is the compliance function discussed in the previous section. For the resistive pressure, we assume that  $P_r = RQ^e$  where Q is the flow into or out of the lung, i.e. Q = |dV/dt|, R is a constant, and e is a positive parameter. We allow R, e, and e obtained by the during inspiration and expiration. In addition, during inspiration, a constant pressure e is maintained until the start of the next breath, e and during expiration, a constant pressure e is maintained until the start of the next breath, e is an addition.

Inspiration:

$$R_i \left(\frac{\mathrm{d}V_i}{\mathrm{d}t}\right)^{\epsilon_i} + \frac{V_i}{C_i(V_i)} + P_{ex} = P_{set}, \ 0 \leqslant t \leqslant t_i$$
 (3.1)

Expiration:

$$-R_e \left( \left| \frac{\mathrm{d}V_e}{\mathrm{d}t} \right| \right)^{\epsilon_e} + \frac{V_e}{C_e(V_e)} + P_{ex} = P_{peep}, \ t_i < t \leqslant t_{tot}. \tag{3.2}$$

Differential equation (3.1) has the initial condition  $V_i(0) = 0$  and (3.2) requires  $V_e(t_i) = V_T$ . The constant  $P_{ex}$  (end-expiratory pressure) is determined by the boundary condition  $V_e(t_{tot}) = 0$ . The relationship between  $P_{ex}$  and  $V_{ex}$  is given by  $P_{ex} = V_{ex}/C_e(V_{ex})$ .

Special cases of the above model have been treated in the literature. In the case when  $\epsilon_i = \epsilon_e = 1$  and  $C_i(V) = C_e(V) \equiv C$ , analytical solutions of the system of differential equations can be found (see e.g. Burke *et al.*, 1993; Marini & Crooke, 1993); for  $\epsilon_i = \epsilon_e = 1/2$  or 2 and  $C_i(V) = C_e(V) \equiv C$ , see Crooke & Marini (1993); and when  $\epsilon_i = \epsilon_e = 1$  and  $C_i(V)$  are piecewise linear functions of V, see Crooke *et al.* (2002).

Data collected for the pre- and post-injury experiments are composed of ventilator delivered and retrieved volume, flow, and airway pressure, sampled every 0.025 s. Various combinations of applied

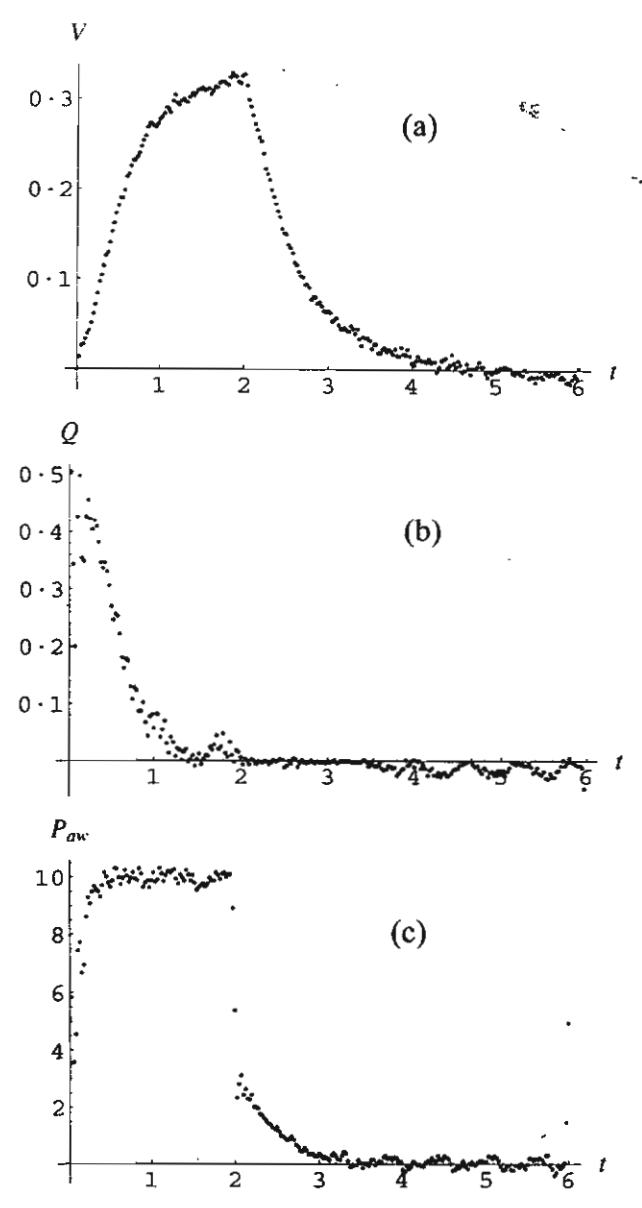


Fig. 2. Experimental data for a pre-injury pig (Pig B) with  $P_{set} = 10 \text{ cm H}_2\text{O}$ ,  $P_{peep} = 0 \text{ cm H}_2\text{O}$ ,  $t_{tot} = 6 \text{ s}$ , D = 1/3. The collected data for volume, flow, and airway pressure are presented in (a), (b), and (c), respectively.

pressures ( $P_{set}$  and  $P_{peep}$ ) and inspiratory time fraction ( $D = t_i/t_{tot}$ ) were used for ventilator settings. A sample of the collected data (volume, flow, and airway pressure) is pictured in Fig. 2.

If we assume that the dynamic behaviour of the physical system is modelled by the differential equations (3.1) and (3.2), then the unknown resistances,  $R_i$  and  $R_e$ , in theory, can be obtained from the

experimental data. For example, if we assume that the resistive pressure,  $P_r$ , is directly proportional to an exponential power of the flow during inspiration or expiration, then

$$P_r^{(i)} = R_i Q_i^{\epsilon_i} = P_{set} - P_{ex} - \frac{V_i}{C_i(V_i)}$$
 (3.3)

$$P_r^{(e)} = R_e Q_e^{\epsilon_r} = -P_{peep} + P_{ex} + \frac{V_e}{C_e(V_e)}$$
 (3.4)

where  $V_i$ ,  $V_e$ ,  $Q_i$  and  $Q_e$  are lung volumes and the flows in and out of the lung during inspiration and expiration, respectively. In (3.3) and (3.4), we assume that  $P_{ex} \approx P_{peep}$  and the compliance functions are obtained from the  $P_e$ -V data. The resistive pressure can then be plotted *versus* the flow and volume and a nonlinear regression algorithm used to estimate  $R_i$ ,  $R_e$ ,  $\epsilon_i$ , and  $\epsilon_e$ . Significant variability in the data can occur for a particular animal and among the various data sets. This is primarily a problem in the expiratory data since the flow levels are small and subject to experimental error. Furthermore, the resistive pressure dependence on the flow must be checked for different dynamic settings:  $P_{set}$ ,  $P_{peep}$ , and D.

Various models (i.e. different combinations for  $\epsilon_i$  and  $\epsilon_e$ ) were investigated. The accuracy of (3.2) with  $\epsilon_e = 1$  was universally good over the various data sets. The accuracy of (3.1) with  $\epsilon_i = 1$  in some cases seem to deteriorate at a particular point in the time during inspiration, which we denote by  $t_{i_1}$ . We speculated that a new and different dynamics is in control for  $t_{i_1} \leq t \leq t_i$ . The difference was assumed to reside solely in the resistive pressure behaviour during inspiration. This led us to a new hybrid model which is defined by the differential equations (3.5)–(3.7). In particular, the model assumes that there is a change in the resistance law during inspiration from  $P_r = RQ^{\epsilon_{i_1}}$  to  $P_r = RQ^{\epsilon_{i_2}}$ . The change-over time,  $t_{i_1}$ , was found from the experimental data. The initial conditions for each differential equation are  $V_{i_1}(0) = 0$ ,  $V_{i_2}(t_{i_1}) = V_{i_1}(t_{i_1})$ , and  $V_e(t_i) = V_{i_2}(t_i)$ . In particular, we have

Inspiration:

$$R_{i_1} \left( \left| \frac{dV_{i_1}}{dt} \right| \right)^{\epsilon_{i_1}} + \frac{V_{i_1}}{C_i(V_{i_1} + V_{ex})} + P_{ex} = P_{set}, \ 0 \le t \le t_{i_1}$$
 (3.5)

$$R_{i_2} \left( \left| \frac{dV_{i_2}}{dt} \right| \right)^{\epsilon_{i_2}} + \frac{V_{i_2}}{C_i(V_{i_2} + V_{ex})} + P_{ex} = P_{set}, \ t_{i_1} < t \le t_i$$
 (3.6)

Expiration:

$$-R_e \left( \left| \frac{\mathrm{d}V_e}{\mathrm{d}t} \right| \right)^{\epsilon_e} + \frac{V_e}{C_e(V_e + V_{ex})} + P_{ex} = P_{peep}, \ t_i < t \leqslant t_{tot}. \tag{3.7}$$

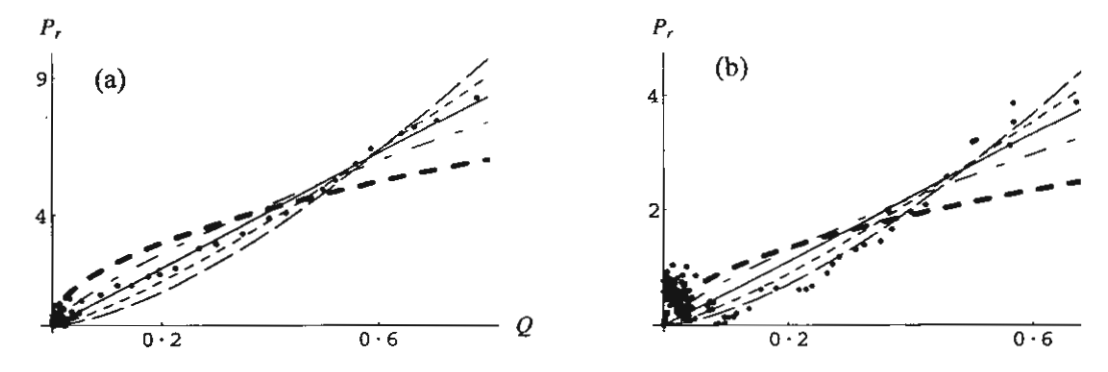
The values of  $\epsilon_{i_1}$ ,  $\epsilon_{i_2}$ ,  $\epsilon_e$ , together with  $R_{i_1}$ ,  $R_{i_2}$ , and  $R_e$ , were found by nonlinear regression of resistive pressure—flow data. The value of the change-over time  $t_{i_1}$  was taken also from observed data to be the time at which an abrupt change in the slope of the resistive pressure—flow curve occurs. If this change is not observed in the data, which is the case for most of our pre-injury data, then the change-over time  $t_{i_1}$  is set equal to  $t_i$ .

In Fig. 3, we present an example of the regression fit of  $P_r-Q$  curves of both inspiration and expiration periods for a pre-injury data set, showing curves using five different values of  $\epsilon$ . For this particular animal (Pig C), we found  $t_{i_1} = t_i = 2$  s in the pre-injury data, so that the inspiration period consists of only one part, namely  $0 \le t \le t_i$ , in which  $\epsilon_{i_1} = 1$  and  $R_{i_1} = 10.3615$  yielded the least sum

TABLE 2 The values of respiratory resistances,  $R_i$  and  $R_e$ , obtained for five different values of the flow exponents ( $\epsilon$ ) for inspiratory period and expiratory period of a particular pre-injury pig (Pig B). The Sum of Squares and Mean Square are from the Mathematica ANOVA table used in the nonlinear regression

		Inspiration		
$\varepsilon_{i_1}$	$R_{i_1}$	Sum of Squares	Mean Square	
0-50	6-68892	45.7886	0-6024820	
0.75	8-70176	10.9364	0.1439000	
1.00	10-3615	4.77519	0-0628315	
1.25	11-9432	7-54956	0.0993364	
1.50	13-5367	13-9685	0.1837960	
		Expiration		
εe	Re	Sum of Squares	Mean Square	
0.50	3.00691	34-3241	0.220026	

		LAPITATION	
$\epsilon_e$	Re	Sum of Squares	Mean Square
0.50	3.00691	34-3241	0.220026
0.75	4.33729	26.0255	0.166830
1.00	5-52216	25-5054	0.163496
1-25	6.68317	26.9782	0-172937
1.50	7.90083	28-8444	0.184900



of squares, compared with the other values of  $\epsilon_{i_1}$  tried, as can be seen in Table 2. During the expiration period for this pre-injury case (Fig. 3),  $\epsilon_e = 1$  and  $R_e = 5.52216$  yielded the least sum of squares, as can be seen in Table 2, as well.

In Fig. 4, we present an example of the nonlinear regression fit of  $P_r-Q$  curves of inspiration and expiration periods for a post-injury data set, showing curves using five different values of  $\epsilon$ . Here, we found  $t_{i_1} = 0.525$  with  $t_i = 4$ , so that the inspiration period is split into two parts; one during  $0 \le t \le t_{i_1}$  and the other during  $t_{i_1} < t \le t_i$ . During the first part, we found  $\epsilon_{i_1} = 1$  and  $R_{i_1} = 17.3134$ , while

TABLE 3 The values of respiratory resistances.  $R_{i_1}$ , and  $R_e$ , obtained for five different values of the flow exponents  $(\epsilon)$  for the first part of inspiration,  $0 \le t \le t_{i_1}$ , second part of inspiration,  $t_{i_1} < t \le t_i$ , and the expiration period,  $t_i < t \le t_{tot}$  of a particular post-injury pig (Pig C)

		Inspiration		
		$0 \leqslant t \leqslant t_{i_1} = 0.525$		
$\varepsilon_{i_1}$	$R_{i_1}$	Sum of Squares	Mean Square	
0.50	16-9763	170-854	8-54272	
0.75	17-4100	41.5195	2.07597	
1.00	17.3134	21.0766	1.05383	
1.25	16.8154	79.8231	3.99116	
1.50	16-0472	189-879	9-49393	
		$0.525 < t \leqslant t_i = 4$		
$\epsilon_{i_2}$	$R_{i_2}$	Sum of Squares	Mean Square	
0.05	4.20541	516-723	3.717430	
0-25	8.85992	225.081	1-619290	
0.50	18-3022	72-1459	0.519035	
0.75	29.4639	251-702	1.810800	
1.00	37-5697	664-919	4.783590	
		Expiration		
		$t_i < t \leqslant t_{tot} = 6$		
$\varepsilon_e$	$R_e$	Sum of Squares	Mean Square	
0-50	3.17990	22.1118	0-2871660	
0-75	3-54351	6-62740	0.0860701	
1.00	3-66977	5-44785	0.0707512	
1.25	3.65902	10.7329	0.1393890	
1.50	3.56458	19-1001	0.2480530	

in the second part,  $\epsilon_{i_2} = 0.5$  and  $R_{i_2} = 18.3022$  are the best choice, as shown in Table 3. During the expiration period of this post-injury case (Pig C),  $\epsilon_e = 1$  and  $R_e = 3.6698$  gave the best fit.

We carried out the fitting of  $P_r - Q$  curves from several other animals, apart from the ones shown here, and found that using different data sets still yielded the resistive pressure exponent values close to those found for the data set of Pig C shown in Figs. 3 and 4. In other words, the resistive pressure exponent  $\epsilon$ , in each separate part of the breathing cycle, is not extremely sensitive to variations of different data sets, not changing very much from one animal to another that exhibit similar modes of gas exchange. Thus, it appears that the resistive pressure exponent  $\epsilon$  is a constant characteristic to a specific flow dynamics and does not mirror the varying of physical data sets, while the nonlinear resistance R is the system parameter which reflects such variations through the process of least squares fitting.

In all our experiments, constant pressure ventilation was used. That is, the applied pressure to the airway is constant during inspiration. In the airway pressure data, the measurement of the applied airway pressure by sensors is for a sudden zero pressure to  $P_{set}$  at the beginning of inspiration and then a sudden return in zero pressure at the end of inspiration. Although a slight variation from constant pressure at the beginning and ending of inspiration is usually encountered, this was in fact found to have no significant effect on the resistive pressure exponent  $\epsilon$ . This is indeed borne out by the observations made by some

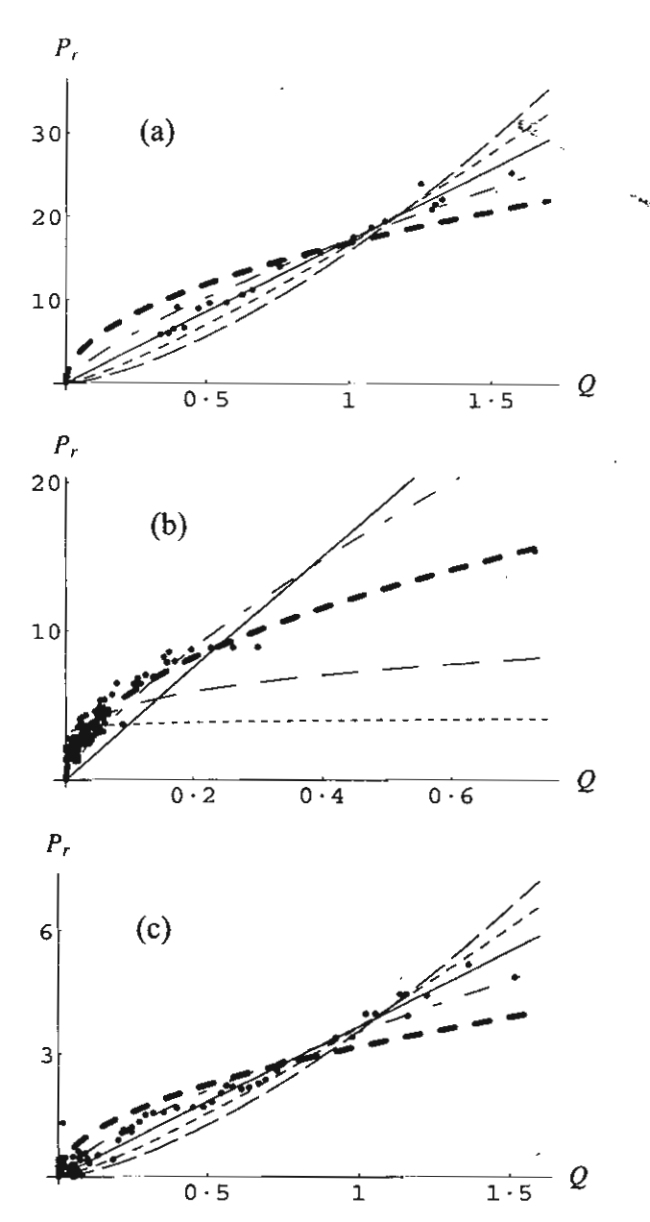


FIG. 4. Curve fitting of resistive pressures during the first part of inspiration (a), second part of inspiration (b) and expiration (c) for post-injury case with different values of parameters  $(R_{i_1}, R_{i_2}, R_{\epsilon}, \text{ and } \epsilon)$  given in Table 3. Here,  $P_{set} = 25 \text{ cm H}_2\text{O}$ ,  $P_{peep} = 5 \text{ cm H}_2\text{O}$ ,  $t_{tot} = 6 \text{ s}$ , and D = 2/3, while  $t_{i_1} \neq t_i$ . For (a), (b), and (c);  $- - \epsilon = 1.5$ ,  $- - \epsilon = 1.25$ ,  $- - \epsilon = 0.75$ ,  $- - - \epsilon = 0.5$ ,  $- - - \epsilon = 0.5$ ,  $- - - \epsilon = 0.5$ , and  $- \epsilon = 0.5$ 



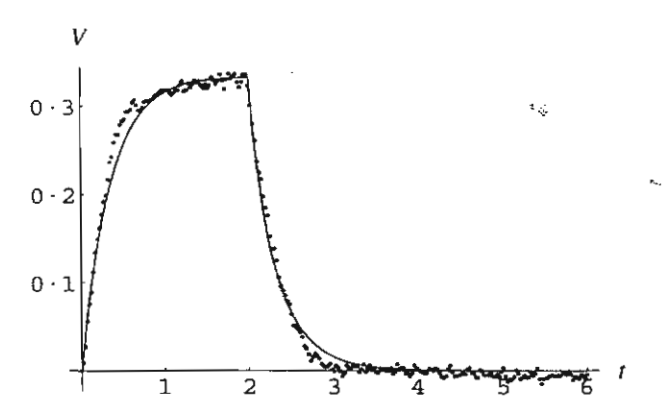


Fig. 5. Comparison of model simulation and experimental data for a particular pre-injury pig (Pig C) of Fig. 3. Here,  $t_{i_1} = t_i = 2$  s,  $R_{i_1} = 10.3615$  cm H<sub>2</sub>O/l/s,  $R_e = 5.52216$  cm H<sub>2</sub>O/l/s, and  $\epsilon_{i_1} = \epsilon_e = 1$  (see Table 2). The solid line corresponds to the model prediction of the lung volume, while the dots are data obtained from the experiment over one breathing cycle.

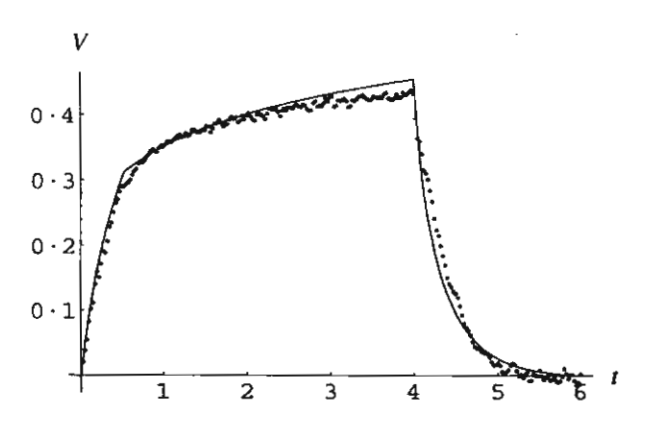


FIG. 6. Comparison of model simulation and experimental data for a particular post-injury pig of Fig. 4 (Pig C). Here,  $t_{i_1} = 0.525$  s,  $t_i = 4$  s,  $R_{i_1} = 17.3134$  cm  $H_2O/l/s$ ,  $R_{i_2} = 18.3022$  cm  $H_2O/l/s$ ,  $R_e = 3.66977$  cm  $H_2O/l/s$ ,  $\epsilon_{i_1} = \epsilon_e = 1$ , and  $\epsilon_{i_2} = 0.5$  (see Table 3). The solid line corresponds to the model prediction of the lung volume, while the dots are data obtained from the experiment over one breathing cycle.

earlier researchers mentioned by Smith et al. (1991) that there was no convincing physiologic evidence of an advantage on gas exchange derived from a given inspiration gas flow pattern. According to these researchers, there were no significant differences in gas exchange or dynamics between various air flow waveforms. In view of this and our earlier discussion on the sensitivity of the resistive pressure exponent, which appears to be characteristic of a specific flow structure, our assumption of a square wave form, and the slight variation thereof, were found to have little effect on the exponent, as expected.

The model (3.5)–(3.7), with  $\epsilon$  and R found as described above, was then used to compare with preinjury and post-injury data of volume versus time. These comparisons with the experimental data are shown in Figs. 5 and 6, respectively. The hybrid model was used for other sets of experimental data and uniformly produced accurate approximations. Thus, this defines a class of models that is mathematically tractable and capable of accurate simulations of mechanical ventilation of normal and diseased lungs.

TABLE 4 Theoretical tidal volumes, end-expiratory pressures, mean alveolar pressures, and average lung volumes for different levels of applied PEEP using the hybrid model of Figs. 3 and 4 for both pre-and post-injury cases of a particular animal (Pig C)

		Pre-i	njury		Post-injury			
PEEP	$V_T$	$P_{ex}$	$P_m$	Vave	$v_T$	$P_{ex}$	$P_m$	$V_{ave}$
0.0	0-66529	0.00473	6-13007	0.55141	0-62441	0.15164	13-22760	0.49562
1.0	0.63207	1.00310	6.82353	0.52392	0.58600	1.10617	13.71900	0.51424
2.0	0.59884	2.00203	7-51701	0-49641	0-54978	2.07399	14-20520	0-44356
3.0	0.56559	3.00132	8-21049	0.46889	0.51569	3.05139	14.68590	0.41915
4-0	0.53233	4.00086	8.90398	0.44136	0.48361	4-03561	15-16080	0.39581
5.0	0.49907	5.00056	9.59747	0.41381	0.45340	5.02464	15.63000	0.37606

Having mathematical expressions for  $V_i(t)$  and  $V_e(t)$  permits the calculation of tidal volume  $V_T$ , average volume  $V_{ave}$ , minute ventilation  $\dot{V}_E$ , end-expiratory pressure  $P_{ex}$ , and mean alveolar pressure  $P_m$ . In particular,  $V_T = V_i(t_i)$ ,  $P_{ex}$  is determined from solving  $V_e(t_{tot}) = 0$ , and the other two outcomes are defined by

$$V_{ave} = \frac{1}{t_i} \int_0^{t_i} V_i(t) \, \mathrm{d}t$$

and

$$P_m = \frac{D}{t_i} \int_0^{t_i} \frac{V_i(t)}{C_i(V_i(t) + V_{ex})} dt + \frac{1 - D}{t_e} \int_{t_i}^{t_{tot}} \frac{V_e(t)}{C_e(V_e(t) + V_{ex})} dt + P_{ex}.$$

In Table 4, theoretical values for these quantities using the hybrid model simulations shown in Figs. 3 and 4, before and after injury, are shown. As one can see, there are substantial reductions in the tidal and average volumes at different PEEP levels. At each level of PEEP, the reductions in tidal and average volumes are approximately 5%. However, approximately 75% of the beginning (PEEP = 0) tidal and average volumes still remains at the last level of PEEP (PEEP = 5 cm  $H_2O$ ). One possible explanation of the drop-off in volumes from pre- to post-injury is the large resistance,  $R_{i_2}$ , in the post-injury simulations. Although we do not show the calculation in this paper, it is possible to investigate changes in the key outcome variables as functions of f and D. This could give the clinician insights into the optimal choice of f and D to ventilate at a given  $P_{set}$  and  $P_{peep}$ .

#### 4. Discussion and conclusion

An interesting speculation about the physiology during this mechanical ventilation (pre- and post-injury) comes from the use of nonlinear resistive pressure  $P_r = RQ^{\epsilon}$ . It was shown in Deshpande & Barigou (2000) that the flow of gas-liquid foams in vertical pipes follows the rheological relationship

$$\Delta P = k \frac{16LQ_F^n}{\pi \rho^4}$$

where  $\Delta P$  is the pressure drop along the pipe,  $\rho$  is the radius of the circular pipe, L is its length, k is a constant, and  $Q_F$  is the steady flow of the foam-liquid. The parameter n is a number in the interval [0.4, 0.9] with its exact value depending on the foam structure, liquid viscosity, and concentration. The hybrid model fits the experimental data quite well in the inspiratory time interval  $[t_{i_1}, t_i]$ , especially for the post-injury data sets, perhaps because the airways of the lungs of the pigs are filled with gas-liquid

foam due to edema (the lung failure condition caused by the accumulation of the fluid in the lungs). The magnitude of  $R_{i_2}$  can then be used to indicate the severity of the edema which is a result of the oleic injury and/or the ventilator induced injury. This hypothesis may have important clinical implication since the model seems to agree well with experimental data (Hubmayr, 2002).

Our curve fitting in the pre-injury case invariably yielded  $t_{i_1} = t_i$  and  $\epsilon_i = \epsilon_{i_1} = 1$  during the inspiration period, with the exception of only a few cases where  $t_{i_1}$  was found to be a little less than  $t_i$ . In such a case then  $\epsilon_{i_1} = 1$  and  $\epsilon_{i_2} = 0.5$ , or very close to it. We speculate that, although this is a pre-injury data set, a short period of liquid-foam flow may have resulted from an injury induced by prolonged ventilation with too high an applied pressure, before being subjected to oleic acid injury. As Scarpelli (2003) has asserted in his discussion of the physiology of the alveolar surface network (ASN) that ASN is the totally fluid continuum circulating through ultrathin molecular conduits formed by appositions of unit bubbles of alveolar gas. In fact, ASN is the analogue of foam in vitro, and operates in all regions of the lung, at all lung volumes, beginning at birth and continuing throughout life. The characteristics of alveolar flooding are then explained by the ASN conformation. According to Scarpelli (2003), they are analogous to liquid-overloading of an established foam in vitro to produce 'froth', in which the ratio of continuous phase (liquid) to dispersed phase (gas in unit bubbles) is significantly increased.

In fact, one function of the pulmonary surfactant system is stabilization of the fluid balance in the lung and protection against lung edema. However, it has been shown that mechanical ventilation can damage the lungs when a mode of ventilation that allows high inspiration lung volumes and low levels of positive PEEP is applied (Vazquez de Anda & Lachmann, 2001), leading to loss of surfactant from the airways and eventually pulmonary edema.

The present work presents one-compartment mathematical models of respiratory systems, incorporating variable compliances and nonlinear resistances. The predictions of the hybrid model were compared against experimental data and were found to uniformly produce accurate approximations. Desired outcomes of mechanical ventilation are a minute ventilation  $\dot{V}_E$  that is adequate to protect the systemic pH (via removal of CO<sub>2</sub>) and a mean alveolar pressure which is sufficient to maintain lung volume and support adequate oxygenation. In Table 4, the tidal volume  $V_T$ , end-expiratory pressure  $P_{ex}$ , mean alveolar pressure  $P_{mi}$ , and average lung volume  $V_{ave}$ , are shown for different levels of PEEP, using  $P_{set} = 20$  cm  $H_2O$ ,  $t_{tot} = 6$  s, and  $t_i = 2$  s in pre-injury case and  $P_{set} = 25$  cm  $H_2O$ ,  $t_{tot} = 6$  s, and  $t_i = 4$  s in post-injury case. These calculations demonstrate the usefulness of a mathematical model as a means to experiment with the ventilation parameters to achieve the desired levels for the outcome variables. The increase in applied PEEP is observed here to lower the tidal volume and the average lung volume in both the pre-injury and post-injury cases. However, the magnitude of this change varies with the injury.

It is worth nothing that incorporating a variable compliance and the nonlinear resistance was critical to obtain models that accurately portrayed the experimental data. With all the caveats of using a one-compartment model for a complex physical system, the mathematical model may indicate important physiologic processes that are present in injured lungs. For example, is the value of  $t_{i_1}$  in the interval  $[0, t_i]$  and/or the magnitude of  $R_{i_2}$  an indication of the level of injury? Alternatively, are shifts in the parameters,  $a_j$  and  $b_j$ , of the compliance function indicative of injury and if so, what is the level of injury?

We have developed a hybrid model, depicted in (3.5)–(3.7), which is very robust, mathematically tractable, and capable of accurate simulations of mechanical ventilation of normal and injured lungs. The model will be used to study effects of clinical-set inputs on the key ventilation outcome variables.

An example of why such approaches may be useful is the controversy concerning appropriate treatment of ARDS patients in ARDSNet studies (Stewart, 2002). The National Institute of Health

has recently stopped these trials involving 20 medical institutions because it is difficult to determine if the patients in the control group were receiving inferior treatment. An outcome based analysis of the ARDSNet trails, along with four other independent studies, raised questions about the effectiveness of low tidal volume ventilation on patient mortality (Eichacker et al., 2002). There is great variation from patient to patient and treatment to treatment between studies. Accounting for this variability is difficult and making judgements of the effectiveness of low tidal volume ventilation by this top-down approach to the data is problematical. If it was possible to measure, non-invasively and instantaneously, physiologic parameters whose values indicate the level of lung injury during mechanical ventilation, then some of the uncertainty of the treatment could be resolved. Furthermore, having the resistance and compliance parameters permits calculation of important lung pressure variables such as the peak and mean alveolar pressure, key predictors of lung injury.

#### Acknowledgements

Kongkul was supported by Ministry of University Affairs, Thailand. Lenbury was supported by The Thailand Research Fund. Marini was supported in part by Health Partners Research Foundation and Hotchkiss is a Scientist Development Grantee of the American Heart Association.

#### REFERENCES

- BOWTON, D. L. & KONG, D. L. (1989) High tidal volume ventilation produces increased lung water in oleic acid-injured rabbit lungs. Crit. Care Med., 17, 908-911.
- BURKE, W. C., CROOKE, P. S. et al. (1993) Comparison of mathematical and mechanical models of pressurecontrolled ventilation. J. Appl. Physiol., 74, 922-933.
- CAKAR, N., VAN DER KLOOT, T. et al. (2000) Oxygenation response to recruitment maneuver during supine and prone positions in an oleic acid-induced lung injury model. Am. J. Respir. Crit. Care Med., 161, 1949–1956.
- CARTER, C. S., ADAMS, A. B. et al. (2002) Tracheal gas insufflation during late exhalation reduces PaCO<sub>2</sub> in experimental acute lung injury. Inten. Care Med., 28, 504-508.
- CEREDA, M. F., SPARACINO, M. E. et al. (1999) Efficacy of tracheal gas insufflation in spontaneously breathing sheep with lung injury. Am. J. Respir. Crit. Care Med., 159, 845-850.
- CROOKE, P. S. & MARINI, J. J. (1993) A nonlinear mathematical model of pressure preset ventilation: description and limiting values for key outcome variables. *Math. Mod. Meth. Appl. Sci.*, 3, 839-859.
- CROOKE, P. S., MARINI, J. J. & HOTCHKISS, J. R. (2002) Modeling recruitment maneuvers with a variable compliance model for pressure controlled ventilation. J. Theor. Med., 4, 197–207.
- CROTT, S., MASCHERONI, D. et al. (2001) Recruitment and decruitment during acute respiratory failure-A clinical study. Am. J. Respir. Crit. Care Med., 164, 131-140.
- DESHPANDE, N. S. & BARIGOU, M. (2000) The flowof gas-liquid foams in vertical pipes. Chem. Eng. Sci., 55, 4297-4309.
- EICHACKER, P. Q., GERSTENBERGER, E. P. et al. (2002) Meta-analysis of acute lung injury and acute respiratory distress syndrome trials testing low tidal volume. Am. J. Respir. Crit. Care Med., 166, 1510-1514.
- HERNANDEZ, L. A. et al. (1990) Mechanical ventilation increases microvascular permeability in oleic acid-injured lungs. J. Appl. Physiol., 69, 2057–2061.
- HUBMAYR, R. D. (2002) Perspective on lung injury and recruitment: a skeptical look at the opening and collapse story. Am. J. Respir. Crit. Care Med., 165, 1647-1653.
- JEDLINSKA, B., MELLSTROM, A. et al. (2001) Evaluation of splanchnic perfusion and oxygenation during positive end-expiratory pressure ventilation in relation to subcutaneous tissue gases and pH-An experimental study in pigs with oleic acid-induced injury. Eurp. Surg. Res., 33, 237-244.

- MARINI, J. J., CROOKE, P. S. et al. (1989) Determinants and limits of pressure-preset ventilation: a mathematical model of pressure control. J. Appl. Physiol., 67, 1081-1092.
- MARINI, J. J. & CROOKE, P. S. (1993) A general mathematical model for respiratory dynamics relevant to the clinical setting. Am. Rev. Respir. Dis., 147, 14-24.
- MARTYNOWICZ, M. A. et al. (2001) Mechanisms of recruitment in oleic acid-injured lungs. J. Appl. Physiol., 90, 1744–1753.
- MUTCH, W. A. C., HARMS, S. et al. (2000) Biologically variable ventilation increases arterial oxygenation over that seen with positive end-expiratory pressure alone in a porcine model of acute respiratory distress syndrome. Crit. Care Med., 28, 2457–2464.
- NAM, A. J., BROWER, R. G. et al. (2000) Biologically variability in mechanical ventilation rate and tidal volume does not improve oxygenation or lung mechanics in canine oleic acid lung injury. Am. J. Respir. Crit. Care Med., 161, 1797-1840.
- NEUMANN, P., BERGLUND, J. E. et al. (2000) Effects of inverse ratio ventilation and positive end-expiratory pressure in oleic acid-induced injury. Am. J. Respir. Crit. Care Med., 161, 1537-1545.
- NEUMANN, P. & HEDENSTIERNA, G. (2001) Ventilatory support by continuous positive airway pressure breathing improves gas exchange as compared with partial ventilatory support with airway pressure release ventilation. *Anesth. Analgesia*, **92**, 950-958.
- PELOSI, P., GOLDNER, M. et al. (2001) Recruitment and derecruitment during acute respiratory failure-An experimental study. Am. J. Respir. Crit. Care Med., 164, 122-130.
- SAWADA, S., MATSUDA, K. et al. (2002) Effects of partial liquid ventilation on unilateral lung injury in dogs. Chest, 121, 566-572.
- SCARPELLI, E. M. (2003) Review physiology of the alveolar surface network. Com. Bioc. Physiol., 135, 39-104.
- SMITH, R. A., RASANEN, J. O. & DOWNS, J. B. (1991) Flow, pressure, and time modifications. *Contemporary Management in Critical Care: Mechanical Ventilation and Assisted Respiration*, Vol. 1. (A. Grenvik & J. B. Downs, eds). New York: Churchill Livingstone, pp. 15-28.
- STEWART, T. E. (2002) Controversies around lung protective mechanical ventilation (editorial). Am. J. Respir. Crit. Care Med., 166, 1421-1422.
- VAN DER KLOOT, T. E., BLANCH, L. et al. (2000) Recruitment maneuvers in three experimental models of acute lung injury-Effect on lung volume and gas exchange. Am. J. Respir. Crit. Care Med., 161, 1485-1494.
- VAZQUEZ DE ANDA, G. F. & LACHMANN, B. (2001) Review article treatment and prevention of acute respiratory failure: physiological basis. Arch. Med. Res., 32, 91-101.
- WILSON, T. A. et al. (2001) Mechanical of edematous lungs. J. Appl. Physiol., 90, 2088-2098.
- ZHAN, Q. Y., WANG, C. et al. (2001) Efficacy of continuous tracheal gas insufflation in spontaneously breathing canine with acute lung injury. Chin Med. J., 144, 658-660.



Craphs With Small Corounference and Connected Complements

# A NUMERICAL STUDY OF BLOOD FLOW PATTERNS IN CORONARY ARTERY BYPASS GRAFTS\*

D. POLTEM †, B. WIWATANAPATAPHEE †, P. RUENGSAKULRACH <sup>‡</sup>, Y. LENBURY †, M. PUNPOCHA <sup>‡</sup>, AND Y.H WU <sup>¶</sup>

Abstract. The control of flow pattern of blood through the grated coronary artery is essential for the success of a bypass surgery. Over the last few decades, extensive studies have been carried out to model many sapects of the coronary artery bypass grafting (CABG). However, due to the complexity of the problem, some physiological and mechanical aspects have still not been fully understood. In this paper, we develop a finite element based on numerical model for the almulation of the flow of blood through the grafted coronary artery and then use the model to study the flow behavior of blood in the right coronary artery for the cases with and without a bypass graft. The effects of bypass graft angle on flow pattern are presented.

1. Introduction. It has been reported that cardiovascular disease is the leading cause of death in developed countries [7, 15]. In recent years, surgical treatments of cardiovascular diseases have been developed rapidly, and coronary artery bypass grafting (CABG) has been widely used for patients with serve coronary artery bypass grafting (CABG) has been widely used for patients with serve coronary artery bypass. A large number of bypass grafts are implanted worldwide each year. However, up to 25% of the grafts fail in one year and up to 50% fail in ten years [16]. Several reasons have been proposed to explain why these grafts clog up or fail [1, 19]. Typical reasons include: (1) improper anastomosis techniques and configuration resulting in an inadequate or overflow of blood through the grafted coronary artery, (2) progression of atheroxclerotic disease of the native coronary artery related to intimal hyperplassis, wall shear stress and progressive risk factors [2, 22]. One of the most important determinants if r a successful bypass surgery is the proper bypass geometry and flow distribution in the neighborhood of the anastomosis.

To understand the flow behavior, extensive studies have been conducted to study the flow patterns of blood through the graft and the native coronary artery. Various flow quantification techniques such as intravacular ultrasound (IVUS) [6], haser Doppler anemometry (LDA) [13], ultrasound Doppler (US) [12]and magnetic resonance imaging (MRI) [14] are commonly used to study arterial hymodynamics. Nowedsys, computational fluid dynamics (CFD) algorithms coupled to realistic 3-D model of such vessel make these data accessible [3]. A number of numerical studies of the blood flow patterns in CABG have also been carried out [8, 9, 10, 11, 18, 20].

The purpose of this paper is to develop a CFD based finite element technique [23] for simulating blood flow in coronary arteries and then uses the technique to study the

<sup>4</sup>Department of Mathematics. Curtin University of Technology, Perth, Australia.

Bangkok 10800, Thalland.

<sup>&</sup>quot;This work was supported by the Thalland Research Fund (TRF) and by the Division of Cardiac Surgery, Heart Institute Saint Louis Hospital and Foundation.

Surgery, Heart Institute Saint Louis Hospital and Foundation. <sup>†</sup>Department of Mathematics, Faculty of Science, Mahidol University, Bangkok 10400, Thalland (acbur**tnah**idol.ac.th).

<sup>&</sup>lt;sup>‡</sup>The Division of Cardisc Surgery, Heart Institute, Saint Louis Hospital, Bangkok 10120, Thaid.

<sup>‡</sup>Department of Mathematics, Faculty of Science, King Mongkut's Institute of Technology,

flow behavior of blood through the bypass graft and the coronary artery. The effects of varying the anastomesis graft angle on the llow behavior in the native coronary artery are investigated. 2. The Underlying Boundary Value Problem. The blood is assumed as an incompressible Newtonian fluid. The governing equations consist of the continuity equation and the Navier-Stokes equations, which can be expressed in index notation

$$0 = \int_{\mathcal{U}_{i}} \left( u_{i,j} + u_{j} u_{i,j} \right) + p_{i,l} - (\mu(u_{i,j} + u_{j,l}))_{i,j} = 0$$

(2.2)

constitute a system of four partial differential equations in terms of four coordinate tively pressure and density of blood;  $\mu$  is the viscosity of blood. Equations (2.1)-(2.2) where it, denotes the velocity component in the x, direction, p and p denote respecdependent unknown functions  $(u_1, u_2, u_3 \text{ and } p)$  for three dimension cases To completely define the flow problem, boundary conditions for the velocity and pressure fields must be specified. For a typical CABG system as shown in Figure 1, the boundary of the computation region consists of four parts, namely the inflow SHIFINCES Of the native artery Io and the bypass graft In, the artery wall In and the outflow boundaries Lexit.

On the inflow surfaces  $\Gamma_0$  and  $\Gamma_n$ , velocity is set to mean velocity, namely  $U_{nn}$ . No-slip condition is applied to the artery wall. The outflow boundaries, I ezes, correspond to

$$-p + \left(\frac{1}{R_e} \frac{\partial H}{\partial H}\right) = 0$$

ber delined by  $Re = \frac{eUd}{u}$ , U and d denote the average velocity and the diameter of where n is the unit normal vector to the outlet section and Re is the Reynold numinvestigation, respectively.

In summary, the fluid flow problem in CABG is governed by the following boundary

BVP: Find u1, u2, u3 and p such that the field equations (2.1) and (2.2) are satisfied in  $\Omega$  and all boundary condition are satisfied. 3. A Numerical Algorithm Based on the Finite Element Method. To solve the BVP problem, firstly, the penalty function method is used to weaken the continuity requirement (2.1) by the following equation

$$u_{i,i} = -\delta p_i$$

where 6 is a small positive number. Thus, we obtain the following alternative boundary value problem.

Find  $u_{i,i} = 1, 2, 3$  and  $p \in H^1(\Omega)$  such that for all  $\xi^i$  and  $\zeta \in H^1_0$ , all the Dirichlet boundary conditions are satisfied and

# A NUMERICAL STUDY OF BLOOD FLOW PAITTERNS

(3.1) 
$$(u_{i,i},\varsigma) = (-\delta p,\varsigma),$$

(3.2) 
$$\left(\frac{\partial u_i}{\partial t}, \xi^i\right) + \left(u_j u_{i,j}, \xi^i\right) - \left(\left(\frac{\mu}{\rho} \left(u_{i,j} + u_{j,i}\right)_{,j}\right), \xi^i\right) + \frac{1}{\rho} \left(p_{,i}, \xi^i\right) = 0$$

where  $(\cdot,\cdot)$  denotes the inner product on the square integrable function space  $L^2(\Omega), H^1(\Omega)$  is the Sobolev space  $W^{1,2}(\Omega)$  with norm  $\|\cdot\|_{1,2,\Omega}$  and  $H^1_0(\Omega) = \{v \in H^1(\Omega)|v=0 \text{ on the Dirichlet type boundary}\}.$ 

lem into a finit, dimension subspace. Firstly, we choose an N-dimensional subspace  $H_h \subset H^1(\Omega)$  for  $u_i$  and the corresponding test function. Let  $\{\phi_i\}_{i=1}^N$  be the basis To find the Galerkin numerical solution of the above problem, we pose the probfunctions of  $H_h$ , then we have

(3.3) 
$$u_j(x,t) \approx (u_j)_h = \sum_{i=1}^N (u_j)_i(t)\phi_i(x)_i$$

$$\xi' \cong \xi_i' = \sum_{i=1}^N \phi_i(x)\xi_i'$$

Secondly, we choose an M-dimensional subspace  $H_{eta}\subset H^1(\Omega)$  for p and  $\varsigma$ . Let  $\{\psi_i\}_{i=1}^N$ be the basis function of  $H_{\beta}$ , then we have

(3.5) 
$$p(x,t) = \sum_{i=1}^{M} (p_i)(t)\psi_i(x),$$

(3.6) 
$$\zeta = \sum_{i=1}^{M} \psi_i(x) \zeta_i.$$

In principle,  $H_{\beta}$  can be chosen to be the same as  $H_{\lambda}$ . However, our numerical experiments have shown that it is necessary to choose  $H_{\beta}$  to be different from  $H_{\Lambda}$  to By substituting (3.3)-(3.6) and noting that \$\xi^4\$ and \$\xi\$ are arbitrary and using Green's ensure the convergence of the solution to our problem.

 $(\psi_k,\phi_{j,k})u_{ji}=(\delta\psi_k,\psi_l)p_l,$ formula, we have (3.7)

$$(\phi_k,\phi_l)_{il(l)} + \{(\phi_k,u_j\phi_{l,j}) + (v\phi_{k,j},\phi_{l,i})\} u_{li} - \frac{1}{\rho} + \left\{(\phi_{k,l},\psi_l) - \int\limits_{\Gamma \in \mathcal{I}(l)} \phi_k \psi_l n_i d\Gamma\right\}_{p_l}$$

$$(3.8)$$

A NUMERICAL STUDY OF BLOOD FLOW PATTERNS

where  $\nu=\frac{\mu}{\rho},$   $u_R$  represents the value of  $v_R$  at the tkh node of the linite element mesh. The system of equations (3.7) and (3.8) can be written in matrix form as follows

$$(3.9) C^T U = -\delta M_p P,$$

(3.10) 
$$M\dot{U} + (\dot{A} + B)U - CP = 0,$$

From (3.10), we have

11) 
$$P = -\frac{1}{\delta}M_p^{-1}C^TU$$

which is then used to eliminate the pressure in the momentum equations, and thus

$$(3.12) M\dot{\mathbf{U}} + D\mathbf{U} =$$

where  $D = A + B + \frac{1}{3}CM_p^{-1}C^T$ 

Using the backward Euler differentiation scheme for a typical time step (t, -th+1), we have from system (3.12) that

$$\left(\frac{M}{\Delta t_n} + D\right) U_{n+1} = \frac{M}{\Delta t_n} U_n$$

which is nonlinear because D depends on  $U_{n+1}$ . To deal with this nonlinearity for an iterative solution of (3.13), we use the iterative update

$$\left(\frac{M}{\Delta t_n} + D_{n+1}^i\right) U_{n+1}^i = \frac{M}{\Delta t_n} U_n$$

where the superscript i denotes evaluation at the ith iteration step. Therefore, in a typical time step  $(t_n \to t_{n+1})$ , starting from  $U_{n+1}^0 = U_n$ , we determine  $U_{n+1}$  by solving system (3.14) repeatedly until  $||U_{n+1}^{l+1} - U_{n+1}^{l}|| < T$  olerance. By repeatedly using above procedure for n=0,1,2,, we can determine the state U of the system at  $t_0,t_1,t_2,...$  If the norm  $\|U_{n+1}-U_{n+1}\|$  is sufficiently small, then the system approaches the so-called steady state.

shown in Figure 2, represents the 50% stenosed right coronary artery. Diameter of the native artery varies from 0.125 cm to 0.384 cm and the length of investigation is 10,525 cm. Using the flow rate Q(t) reported by Bertolotii et.al (2001) [5] as shown Flow simulations were conducted under a typical physiological condition: a heart fate of 84 beat per minute. The fluid properties are typical of human blood with a viscosity  $3 \times 10^{-2} \text{ gcm}^{-1}\text{s}^{-1}$  and a density of 1.06 gcm<sup>-3</sup> [21]. The computation region, as in Figure 3, the mean flow rate is estimated by the following formula

(3.15) 
$$Q_{\alpha\nu\rho} = \frac{1}{T_c} \int_0^{T_c} Q(t) dt$$

where  $T_o$  is the period of each cycle of 0.714 s, Qavg and Q(t) denote respectively the mean flow rate and the translent flow rate. The mean flow velocity can be approximated as 20.13 cm/s. Various angles of bypass graft were used to investigate the effect of graft angles on blood flow patterns in native coronary artery. We simulate the blood flow through the bypassed right coronary artery in twodimension. The mesh as shown in Figure 4 consists of 8257 nodes and 15006 elements. To get flow patterns in successive cycles, we consider 1.4 cycles in the computation and each cycle is divided into 200 time steps with step size 3.57 ms.

tomosis leads to higher velocity in the neighborhood of the proximal and immediate distal parts in comparison to the one with higher degree anastomosis. Figure 6 shows that there exists turbulent retrograde flow along the vessel wall in the neighborhood of the heel and toe parts. The velocity of the recirculating flow tands to decrease with the increase of the anastomosis angles. Compared with other angles, the configuration with a 10 degree angle of anastomosis produces the highest flow velocity at the far The results as shown in Figure 5 indicate that the bypass grafting with a  $10^{
m o}$  anasdistal part of the native artery as abown in Figure 7.

the mean flow in the far distal coronary artery has a quadratic relationship with the right coronary artery bypass grafting is presented based on the Bubnov-Galerkin Finite Element formulation. The two-dimensional regional flow is calculated. As the blood flows from a graft into the native coronary artery, it hits the jet flow from the native artery. The results indicate that the residual flow issued from the stenosed artery creates a jet flow, which intends to decrease after bypass operation. The study shows that for a graft with the same diameter as the native artery, the mean flow velocity in the neighborhood of the far distal part of the native artery is larger than that in the proximal part of the native artery. The recirculation zone occurs in the neighborhood of the toe and heel of the graft for all graft angles. It is also found that graft angless. Proper choice of the diameter of the graft might improve the balance of inflow and outflow in the coronary artery. It shall be addressed that to improve the accuracy of results, the two-dimensional blood flow study has to be extended to 4. Conclusions. A numerical model of blood flow patterns in the half stenowed pulsatile inflow, three-dimensional realistic domain.

Acknowledgments. The authors are grateful to the Thailand Research Fund (TRF) for the support of this research and also wish to thank the Division of Cardinc Surgery, Heart Institute Saint Louis Hospital and Foundation for the information.

### REFERENCES

[1] H.B. Barner, Techniques of myocardial revuscularization, In: Edmunds LH Jr (vd) Cardine surgery in the adult. McGrnw Hill, New York, (1997), pp.

# POLTEM, WIWATANAPATAPHEE, RUENGMAKULRAGH, LENBURY, PUNPOGHA AND WU

.\_

- II.S -BASSIOUNY, WHITE S, GLAGOV S, CHOI E, GIDDENS DP, ZAILINS CK, Anastomotic intimal hyperplasia and medial thickening in autogenous vein graft, Sugery, 15(1992), pp. 708-17.
  - BERTHIER, R. BOUZERAR, C. LEGALLAIS, Blood flow pattern in an anatomicully realistic coronary vessel: influence of three different reconstruction methods, J Biomech, 35(2002), pp. 1347-56. Ė E
- BERTOLOTTI, V. DEPLANO, Three-dimensional numerical simulations of flow through a stenosed coronary bypass, J Blomech, 33(2002), pp. 1011-22. j
- BERTOLOTTI, DEPLANO V, FUSERI J, DUPOUY P, Numerical and experimental models of post-operative realistic flows in stenosed coronary bypasses, J Biomech, 45(2001), pp. 1049-64. : ::
  - ments in humans. Feasibility, reproducibility, and hemodynamic flow versus C.R., WIJNS, W., Simultaneous coronary artery presure and flow measure-BRUYNE, B., BARTUNEK, J., SYS, S.U., PIJLS, N.H.J., HEYNDRICKX, presure stope index, and fractional flow reserve, Circulation, 94(1996), pp. Ö :=.
- (7) CARO, C.G., FITZ-GERALD, J.M., SCLIROTER, R.C, Atheroma and arterial wall shear; observation, correlation and proposal of a shear dependent mass transfer mechanism for stherogenesis, Proc. Roy. Soc. B, 177(1971), pp. 109-
- S. CHAKRAVARTY, P.K. MANDAL, Two-dimensional blood flow through tapered arteries under stenotic conditions, Internat. J. Non-lineur Mech, 35(2000), 2
- 191 TU CHENG, MICHEL DEVILLE, Pulsatile flow of non-Newtonian fluid through arterial stenosis, J Biomech, 29(1996), pp. 899-908.
- 10 J.S. Cole, J.K. Warrenson, M.J.G. O'Reilly, Numerical investigation of heamodynamics at a palched arterial bypass anastomosis, Medical Engineerия & Physics. 24(2002), pp. 393-401.
  - D.Y. FEI, J.D. THOMAS, S.E. RITTGERS, The effect of angle and flow rate upon hemodynamics in distal vascular graft anastomoses: a numerical model study, J Biomech Eng, 116(1994), pp. 331-6. ---
    - [12] L. ILATLE, B.P. ANGELSEN, Doppler Ultrasound in Cardiology, Lea and Felbiger, Philadelphia, PA. 1985.
- 13 D. LEUPHECHT S. MORAVEC, Pubaille flow of non-Newtonian fluid in distensible models of human arteries, Biorheology, 21(1984), pp. 571-86.
- [14] G.L. NAYLER, D.N. FIRMIN, D.B. LONGMORE, Blood flow imaging by cine magnetic resonance imaging, Journal of Computer Assisted Tomography,
- [15] Organisation Mondiale de la Sante (OMS). Annual Report, 1999. [16] Y. Papahanilaou, D.J. Doorly, S.J. Shenwin, The influence of out-of plane geometry on pulsatile flow within a distal end-to-side anastomosis, J Biomech 35(2002), pp. 1255-39.
- RENE, R. GERHARD, B.S. MARKUS, L. DIETER, P. KARL, B. PETER; Hemodynamics in the carotid artery bifurcation: a comparison between numerical simulations and in vitro MRI measurements, J Biomech, 33(2002). m 17]
  - 18, C. Ross Etheir, D.A. Steinman, X. Zhang, S.R. Karpik, M. Ojha, Flow waveform effects on end-to-side anastomotic flow patterns, J Biomech, 31(1998), pp.

## A NUMERICAL STUDY OF BLOOD FLOW PATTERNS

- T. SEKI, KITAMURA S KAWACHI K, A quantitative study of postoperative luminal narrowing of the internal thoracic artery graft in the coronary bypass surgery, J Thorne Cardiovase Surg, 104(1992), pp. 1532. 13
  - [20] M.H SONG, MASARU SATO, YUICHI UEDA, Three-dimensional Simulation of coronary artery bypass grafting with the use of computational fluid dynamics
    - [21] D. TANG, C. YANG, S. KOBAYASHI, KU DIN, Steady flow and wall compres-Surgery Today, 30(2002), pp. 993-98.
      - sion in stenotic arteries: a three-dimensional thick-wall model with fluid-wall interactions, J Biomech Eng, 123(2001), pp. 548-57. [22]
        - K.C. WATTS, A.E. MARBLE, S.N. SARWAL, C.E. KINLEY, J. WATTON, M.A. MASON, Simulation of coronary artery revascularization, J Biomech, 19(1986), pp. 491-99.
- B. WIWATANAPATAPHEE, Mathematical modeling of fluid flow and heat transfer the continuous steel casting, Ph.D Thesis. (1998), pp. 107-131 [23]

## A COMPARISON OF THE AGE DISTRIBUTIONS IN THE DENGUE HEMORRHAGIC FEVER EPIDEMICS IN SANTIAGO DE CUBA (1997) AND THAILAND (1998)

P Pongsumpun<sup>1</sup>, S Yoksan<sup>2</sup> and IM Tang<sup>2,3</sup>

<sup>1</sup>Department of Mathematics; <sup>3</sup>Department of Physics, Faculty of Science, Mahidol University, Bangkok 10400, Thailand; <sup>2</sup>Center for Vaccine Development, Institute of Science and Technology for Research and Development, Mahidol University, Nakhon Pathom 71730, Thailand

Abstract. The age profiles of the infected populations of two dengue hemorrhagic fever (DHF) epidemics, the 1997 epidemic, in Santiago de Cuba and the 1998 epidemic in Thailand, are compared. Using an age-structured model of disease transmission, the dependence of the forces of infection on age was determined for each epidemic. The difference in the behavior of the two epidemics and the role of primary and secondary infection in the development of DHF are discussed.

#### INTRODUCTION

Dengue hemorrhagic fever (DHF) is an emerging viral disease that is spreading throughout the tropics. Since its first appearance, in the Philippines in 1953, DHF has become the most important arthropod-borne viral disease of humans (WHO, 1997). It has been estimated that there are between 50 and 100 million cases of dengué fever (DF) a year; more than 250,000 annual cases of dengue hemorrhagic fever (DHF) result in some 10,000 infant deaths. Classic dengue fever is a disease of older children and adults; DHF, on the other hand, is primarily a disease of children under the age ... 15 (Gubler, 1998). DHF differs from DF: plasma leakage is seen in DHF. Both diseases are caused by one of four serotypes of the dengue virus, (DEN1, DEN2, DEN3, and DEN4) which belongs to the genus Flavivirus, family Flaviviridae.

Because two of the mosquito vectors, Aedes aegypti and Aedes albopictus, exist in the Americas, DF has become endemic in the New World (Pan American Health Organization, 1994). The first severe outbreak of DHF

Correspondence: IM Tang, Department of Physics, Faculty of Science, Mahidol University, Bangkok 10400, Thailand.

E-mail: scimt@mahidol.ac.th

in the Americas occurred in 1981 in Cuba (Guzman et al. 1990) and gave rise to 334,203 DF cases, 10,313 documented DHF cases, and 158 deaths. The serotype responsible for the epidemic was DEN2. An earlier epidemic of mild classic dengue fever, which occurred between 1977 and 1979, was caused by a different strain (DEN1). During this epidemic, the sera of 44.5% of a random sample of 2,000 people contained DEN1 virus antibodies (HI; hemagglutination inhibition). Strict infection control measures adopted after the 1981 epidemic lead to the disappearance of DHF from Cuba for the next sixteen years. A localized outbreak of DHF occurred in Santiago de Cuba in 1997 (Kouri et al. 1998; Guzman et al, 2000). The culprit was the DEN2 virus.

To get a better understanding of the transmission of this disease, we compared the DHF epidemic that occurred in Santiago de Cuba in 1997 with the one that occurred in Thailand in 1998. We were interested in the age distribution of those infected during the two epidemics. Most literature on DHF mentions that the disease affects mainly those under the age of 16; Guzman et al (1997) noted that almost no-one under the age of 17 became sick with DHF (Fig 1a). This is quite different from the age pattern seen in epidemics, which occur in countries in which the disease is fully established. Fig 1b shows the age distribution in

one province of Thailand during the 1998 epidemic (Ministry of Public Health, 1998).

#### MATERIALS AND METHODS

Before a discussion of the differences between the two distributions can be held, the age distribution of the forces of infection in the 1997 DHF epidemic in Santiago de Cuba must be determined. The force of the DHF infection in Thailand during the 1998 epidemic has already been established. Pongsumpun and Tang (2001) who showed that the percentage of infected people (I) in the i-th age cohort (I) is

$$I_{i} = \frac{\alpha}{\alpha + r + \mu_{h}} I_{i-1} + \frac{\beta^{h} i I_{v}}{\alpha + r + \mu_{h}} S_{i}$$

for i = 2,...N-1 (i)

with

$$I_{l} = \frac{\beta^{h} II_{v}}{\alpha + r + \mu_{h}} S_{l}$$
 (ii)

$$S_i = \frac{\alpha}{\beta^h i I_v + \alpha + \lambda} S_{i-1}$$
 (iii)

and

$$S_{i} = \frac{\lambda}{\beta^{h} II_{v} + \alpha + \lambda}$$
 (iv)

In the above,  $\beta_i^h$  is the transition rate for the virus to be transmitted to humans by mosquitos (the force of infection);  $\alpha$  is the rate at which one cohort age into the next; r is the recovery rate;  $\lambda$  is the birth rate;  $\mu_h$  is the death rate of the human population; and  $I_{\nu}$  is the number of infected mosquitos divided by their total number.

#### RESULTS AND DISCUSSION

The forces of the DHF infections can be determined by fitting the incidence rates given

in Fig 1a to equations (i) to (iv) by varying the values of  $\beta^h$ ; this yields the values of  $\beta^h$ ; that are shown in Fig 2. The behaviors of the forces of infection in the two epidemics look the same, ie, an initial increase followed by a drop to a nearly constant force of infection, except that the initial increase is shifted 16 years in the case of the Santiago de Cuba epidemic.

To understand why this happens and why the age distributions shown in Figs 1a and 1b are as they are, two theories of the pathogenesis of dengue hemorrhagic fever must be considered. The first, more commonly accepted theory, is the immune enhancement or secondary-infection hypothesis (Halstead, 1988). According to this hypothesis, the pre-existing heterologous dengue antibody in an infected person recognizes a novel dengue virus and forms an antigen-antibody complex, which then bonds the virus to the membrane of a leukocyte. Because the antibody is heterologous. the virus is not neutralized and remains free to replicate inside the leukocyte. These infected cells then produce and secrete vasoactive mediators in response to the infection; these mediators cause an increase in vascular permeability, leading to hypovolemia and shock.

In the second theory, the dengue virus mutates as it replicates in the human and/or the mosquito. Some of these mutations lead to more virulent viruses: these viruses causing DHF. Because a pre-existing antibody is implicated in the first theory, the infection causing DHF must be a secondary one. In the second theory, no pre-existing antibody is required: primary dengue infection can cause DHF.

43

If the secondary-infection hypothesis is correct, the paucity of DHF-infected children in the 1997 epidemic in Cuba is under stand able: no-one under the age of 16 would have had pre-existing dengue virus antibodies in his blood because he would have been born after the 1981 epidemic. Of the individuals under the age of 16 years who were tested for dengue antibodies in Santiago de Cuba. only 2% had

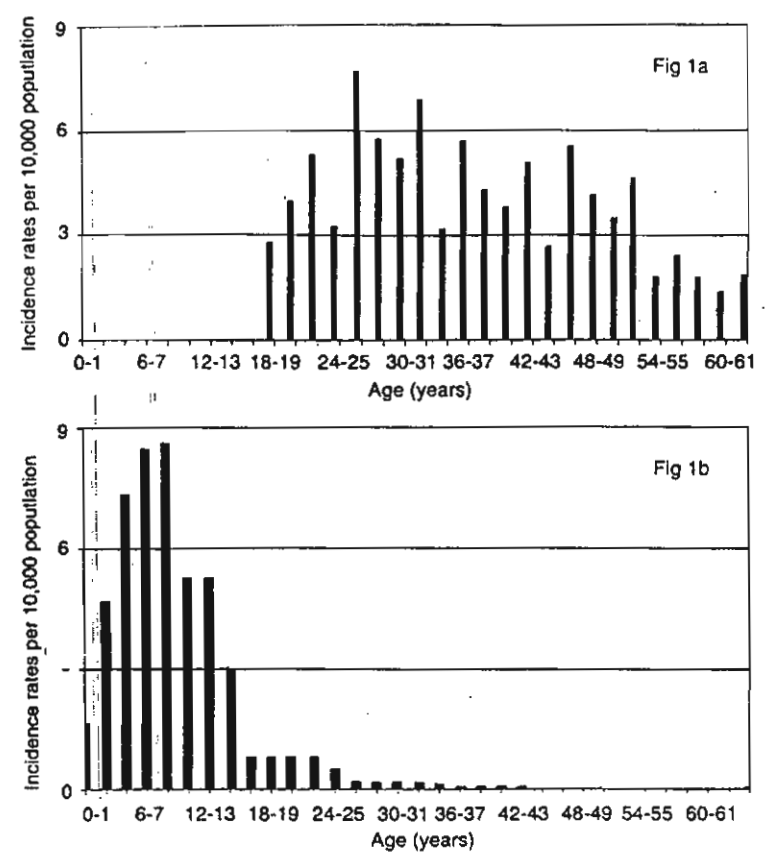


Fig 1-Age distribution of dengue hemorrhagic fever. (1a) Age distribution of the 1997 epidemic in Santiago de Cuba.

(Data from Guzman et al, 2000). (1b) Age distribution of the 1998 epidemic in Mukdahan Province, Thailand (Data from Ministry of Public Health, 1998).

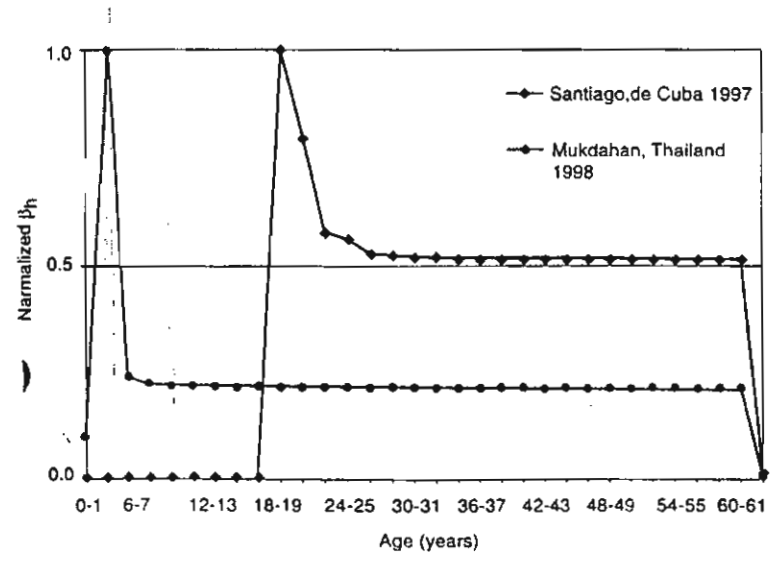


Fig 2-Forces of infection in the two epidemics. Forces of infection in Santiago de Cuba are denoted by (♠); forces of infections in Mukdahan Province, Thailand, are denoted by (♠). Values obtained by fitting equations (i) to (iv) to the incidence rates presented in Figs 1a and 1b.

the neutralizing antibodies to DEN2 and none had the antibodies to DEN1 (Guzman et al, 2000). Serological tests showed that the dengue infections in 98% of the DHF/DSS cases were secondary. In a study of the 1994 epidemic in Thailand (Vaughn et al, 1997) it was found that while 93% (56 of 60) of the children with DHF were experiencing a secondary infection, only 4% were experiencing a primary infection. Vaughn et al (1997) also showed that the viremia was correlated with the body temperature of the patient; they were able to isolate the virus in 59 of 60 DHF patients, who were in the early febrile stage.

However, not all the evidence supports the secondary-infection hypothesis. During the 1996-1997 epidemic in Belem, Brazil (Travassos de Rosa et al. 2000) none of the 24 individuals, in whom the DEN2 virus was isolated and who were previously infected with the DEN1 virus, developed DHF. tional evidence was obtained about the 1998 epidemic in Thailand from the serological records of the Department of Pediatrics, Siriraj Hospital (the largest hospital in Thailand). The pediatric ward at Siriraj Hospital admitted 316 children suffering from DHF in 1998. Hemagglutination inhibition assay (HAI) and IgM/IgG capture enzyme-linked immunosorbent assay were conducted for serum samples from all the patients. The dengue virus (49 DEN1, 29 DEN2, 41 DEN3, and 1 DEN4) was isolated in 120 of these patients.

We are interested in this subgroup. Vaughn et al (1997) have suggested that the following criteria be used to determine whether an infection is primary or secondary. Primary infection: HAI reciprocal titers ≤ 640; IgM to IgG ratio > 1.8. Secondary infection: HAI reciprocal titers > 1,280; IgM to IgG ratio < 1.8. Applying these criteria to the

serological results, 56 of the 120 DHF patients were experiencing a primary infection by the HAI criterion; 27 were experiencing a primary infection by the IgM/G criterion; and 13 satisfied both criteria. Among this group of 13 children, there were 7 cases in which the primary infection was due to DEN1 virus; 3 cases were due to DEN2 virus, and 3 were due to the DEN3 virus. This would appear to contradict the findings from the 1994 Thai epidemic, in which only 4% of DHF cases were the results of primary infection. We examined the records of Siriraj Hospital for the year 1999. One hundred and thirty-seven children suffering from DHF were admitted to the pediatric ward that year. The dengue virus was isolated in 31 of these patients, none of whom ...d a primary infection based on both tests. It appears that the DHF epidemics in Thailand during 1994 and 1999 differed from the 1998 epidemic in terms of the primary/secondary cause of infection. The reason for this difference is not clear. It is interesting to note that epidemics in Thailand peak every three years (Hay et al, 2001): 1998 was a peak year, while 1994 and 1999 were not. We are now studying this phenomenon to see whether it is of relevance to the problem of primary/secondary infection.

#### **ACKNOWLEDGEMENTS**

P Pongsumpun would like to thank the Thailand Research Fund for a Royal Golden Jubilee PhD Scholarship (contract PHD 154/2543). The authors would like to thank the Serological Laboratory, Siriraj Hospital, and the Ministry of Public Health, Thailand for the data used in this study.

#### REFERENCES

- Gubler DJ. Dengue and dengue hemorrhagic fever. Clin Microbiol Rev 1998; 11: 480-91.
- Guzman MG, Kouri GP, Bravo J, et al. Dengue hemorrhagic fever in Cuba, 1981: A retrospective seroepidemiologic study. Am J Trop Med Hyg 1990; 42: 179-84.
- Guzman MG, Kouri GP, Valdes L, et al. Epidemiologic studies on dengue in Santiago de Cuba, 1997. Am J Epidemiol 2000; 152: 793-9.
- Halstead SB. Pathogenesis of dengue: challenges to molecular biology. Science 1988; 239: 476-81.
- Hay SI, Mymers MF, Burke DS, et al. Etiology of interepidemic periods of mosquito-borne disease. PNAS 2001; 97: 9335-9.
- Kouri G, Guzman MG, Aldes L, et al. Reemergence of dengue in Cuba: A 1997 epidemic in Santiago de Cuba. Emerg Infect Dis 1998; 4: 87-92.
- Ministry of Public Health, Thailand, Annual Epidemiological Surveillance Report (1992-8). Division of Epidemiology, Ministry of Public Health, Thailand, 1998.
- Pan American Health Organization. Dengue and dengue hemorrhagic fever in the Americas: guidelines for prevention and control. Washington DC: PAHO. 1994; 548.
- Pongsumpun P, Tang IM. A realistic age structured transmission model for dengue hemorrhagic fever in Thailand. Southeast Asian J Trop Med Public Health 2001; 32: 336-40.
- Travassos da Rosa APA, Vasconcelos PFC, Travassos da Rosa ES, et al. Dengue epidemic in Belem, Para, Brazil, 1996-97. Emerg Infect Dis 2000; 6: 298-301.
- Vaughn DW, Green S, Kalayanarooj S, et al. Dengue in the early febrile phase: Viremia and antibody responses. J Infect Dis 1997; 176: 322-30.
- World Health Organization. Dengue hemorrhagic fever: diagnosis, treatment, prevention and control, 2<sup>nd</sup> ed. 1997.

### AGE STRUCTURE IN A MODEL FOR THE TRANSMISSION OF DENGUE HAEMORRHAGIC FEVER IN THAILAND

P. Pongsumpun 1,a, Y.Lenbury land I.M.Tang 2,b

Department of Mathematics and <sup>2</sup> Department of Physics
Faculty of Science, Mahidol University, Rama 6 Rd., Bangkok 10400, Thailand

<sup>2</sup> Institute of Science & Technology for Research & Development Salaya Campus, Mahidol University, Nakorn Pathom 71730, Thailand

a g4236738@student.mahidol.ac.th and b scimt@mahidol.ac.th

#### Abstract

The influence of age structure in the human population in the Susceptible-Infected-Recovered (SIR) model used to describe the transmission of Dengue Haemorrhagic Fever (DHF) is studied. The human population is separated into an adult class and juvenile class with only the juveniles being susceptible to infection by the disease. A new expression for the basic reproduction rate is obtained. It is found that age structure reduces the periods of oscillations in the susceptible human population, infected human population and infected mosquito population and the tightness of the spiraling into the endemic equilibrium state.

Key words and phrases: Dengue haemorrhagic fever, Age structure, SIR model, Endemic equilibrium, Local stability.

#### 1 Introduction

Mathematical modeling of disease transmission has a long history. In 1911, an epidemiology model for malaria transmission was developed by Ross [1]. MacDonald [2] later added a layer of biological realism to the model by providing careful interpretation and estimation of the parameter, which should go into the model. McKenzie [3] has pointed out that the utility of a model depends not as much on how well a mathematical job has been accomplished but how on well a particular question has been translated. One is interested in disease transmission, it is imperative that the model describes as closely as possible the characteristics of the disease being transmitted. In this paper, we are interested in the transmission of dengue haemorrhagic fever (DHF).

Dengue Haemorrhagic fever is one of the emerging viral diseases spreading throughout the tropical regions of the world. From its first appearance in the Philippines in 1953, it has become the most important arthropod-borne viral disease of humans [4]. It has been estimated that there are between 50 and 100 million cases a year, with approximately 10,000 infant deaths due to this disease. Its emergence is associated with the rapid urbanization occurring in the developing countries. Because two of the transmitting vectors, the Aedes aegypti and Aedes albopictus mosquitoes, exist in the Americas, it has been possible for the disease and its rather benign precursor, dengue fever (DF), to become endemic in the New World [5]. The first

#### AGE STRUCTURE IN A MODEL FOR THE TRANSMISSION OF DENGUE

severe outbreak of DHF in the Americas occurred in 1981 in Cuba with 116,000 hospitalized patients, 34,000 documented DHF cases and 158 deaths. Important outbreaks of DHF have also occurred in Mexico[6].

In hopes of understanding the mechanics that allow the invasion and persistence of a serotype of the dengue virus in a region, Esteva and Vargas [7-9] introduced a mathematical model to provide a qualitative assessment for the problem. The model they used is based on the Susceptible Infected-Recovered (SIR) model often used to model the dynamics of transmission of some diseases. They showed that the endemic state was globally stable whenever a parameter  $R_0$  called the basic reproduction number is greater than one. Application of an ultra low volume (ULV) amount of insecticides (the standard method used to control the spread of dengue fever and other arthropod-borne disease) could reduce the value of  $R_0$  to below one. The value of  $R_0$  would return to the above one value once the application is stopped and since the endemic state is globally stable, the disease would return. Therefore the eradication program would have to be a continuing one.

In the SIR model used Esteva and Vargas, no age structure was incorporated into the models. While the lack of an age structure may be appropriate for describing the 1981 DHF epidemic in Cuba [10] and the DHF outbreak in Santiago de Cuba in 1997 [11], it is not appropriate for Thailand. Most DHF cases in Thailand occur in children less than 15 years old. In figure 1, we show the age distribution of the incidence rates in one province in Thailand during the 1998 DHF epidemic [12]. Feng and Velasco-Hernandez [13] pointed to the need of a model that incorporates age structure into the dengue population dynamics. It is the purpose of this paper to report on a DHF transmission model, which includes an age structure in the human population. Central to any discussion of any population growth is the basic reproduction rate or number. The basic reproduction rate or number. The basic reproduction is intrinsically capable of producing. The inclusion of an age structure leads to a new expression for this number. This is done in section 3.

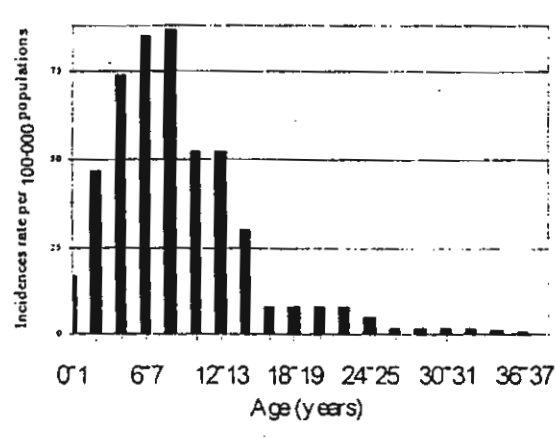


Figure 1. Age distribution of the 1998 Dengue Fever incidence rates in Mukdahan, a province in Central Thailand.

#### 2 Mathematical Model

The simplest way to incorporate an age structure into a disease in which only the children are susceptible to the disease is to divide up the human population into two categories,

transmission of the dengue virus to the mosquito from an infected juvenile.  $\beta_V$  is the transmission probability of dengue virus from an infected juvenile to the mosquito. Introducing the normalized parameters  $S = S'/N_T$ ,  $I = I'/N_T$ ,  $R = R'/N_T$ ,  $A = A'/N_T$ ,  $S_V = S_V'/(B/\mu_V)$  and  $I_V = I_V'/(B/\mu_V)$ , equations (1a) to (2b) reduce to

$$\frac{dS}{dt} = \lambda' - \gamma_h I_v S - (\mu_h + \delta) S \qquad , \qquad (3a)$$

$$\frac{dI}{dt} = \gamma_h SI_v - (\mu_h + \delta + r)I \qquad , \qquad (3b)$$

$$\frac{dR}{dt} = rI - (\mu_h + \delta)R \tag{3c}$$

anc

!

$$\frac{\mathrm{d}l_{\mathrm{V}}}{\mathrm{d}t} = \gamma_{\mathrm{V}} (1 - l_{\mathrm{V}}) l_{\mathrm{V}} - \mu_{\mathrm{V}} l_{\mathrm{V}} \tag{3d}$$

where

$$\gamma_h = \frac{b \beta_h (B / \mu_V)}{N_T + m} \tag{4a}$$

and

$$\gamma_{V} = \frac{b \beta_{V} N_{T}}{N_{T} + m} \tag{4b}$$

The dynamical equations for A and  $S_V$  are not needed since S + I + R + A = I and  $S_V + I_V = I$ . The requirement that  $N_T$  be a constant leads to the condition that the birth rate,  $\lambda$  is equal to the death rate,  $\mu_h$ .

#### 2.1 Equilibrium States

The equilibrium states are obtained by setting the RHS of equations (3a) to (3d) to zero. Doing this, we get two equilibrium states, the disease free equilibrium state,  $E_0 = (S, 0, 0, 0)$  where

$$S = \frac{\mu_h}{\mu_h + \delta} \tag{5}$$

and the endemic equilibrium state,  $E_1 = (S^{\bullet}, I^{\bullet}, R^{\bullet}, I_{V}^{\bullet})$  where

$$S = \frac{\gamma_h + \mu_h X_0}{X_0 (\gamma_h + \mu_h M)}$$
 (6a)

$$I \cdot = \frac{\mu_{V} \mu_{h} (X_{0} - M)}{\gamma_{V} (\gamma_{h} + \mu_{h} M)}$$
 (6b)

$$R = \frac{\mu_{V} \Gamma(X_{0} - M)}{\mu_{V} M(\mu_{D} + \mu_{D} M)}$$
 (6c)

and

$$I_{V} = \frac{\mu_{h} (X_{0} - M)}{(\gamma_{h} + \mu_{h} X_{0})}$$
 (6d)

with

$$M = \frac{\mu_h + \delta}{\mu_h} \tag{7a}$$

and

$$X_0 = \frac{\gamma_h \gamma_v}{\mu_v (\mu_h + \delta + r)} \tag{7b}$$

#### 2.2 Local Asymptotical Stability

The local stability of an equilibrium state is determined from the Jacobian (gradient) matrix of the RHS of the set of differential equations evaluated at the equilibrium state.

#### 2.2.1 Disease Free State

g

For the system defined by equations (3a) to (3d), the Jacobian matrix evaluated at  $E_0$  is the  $4 \times 4$  matrix given by

$$\begin{pmatrix}
-(\mu_{h} + \delta) & 0 & 0 & -\gamma_{h} / M \\
0 & -(\mu_{h} + \delta + r) & 0 & \gamma_{h} / M \\
0 & r & -(\mu_{h} + \delta) & 0 \\
0 & \gamma_{V} & 0 & -\mu_{V}
\end{pmatrix}$$
(8)

Diagonalizing this matrix, yields the following characteristic equation;

$$(\lambda + \mu_h + \delta)^2 \left\{ \lambda^2 + (M\mu_h + r + \mu_V)\lambda + \mu_V(M\mu_h + r) \left( 1 - \frac{X_0}{M} \right) \right\} = 0$$
 (9)

The eigenvalues are

$$\lambda_{1,2} = -(\mu_{\rm h} + \delta)$$

and

$$\lambda_{3,4} = \frac{-(\mu_h + \delta + r + \mu_v) \pm \sqrt{((M\mu_h + r) - \mu_v)^2 + 4\mu_v (M\mu_h + r) \frac{X_0}{M}}}{2}$$
(10)

For  $X_0 < M$ , the square root will be less than  $(\mu_h + \delta + r + \mu_V)$ . This means that all the eigenvalues will be negative; leading to the disease free state being locally asymptotically stable.

#### 2.2.2 Endemic Disease State

The characteristic equation for the Jacobian matrix evaluated at the endemic equilibrium state, given by equations (6a) - (6d), is

$$f(\lambda + \mu_H + \delta)(\lambda^3 + A\lambda^2 + B\lambda + C) = 0$$
 (11)

where

$$A = \frac{\mu_{v}(\gamma_{h} + \mu_{h}X_{0})}{\gamma_{h} + \mu_{h}M} + \frac{\mu_{h}X_{0}(\gamma_{h} + \mu_{h}M)}{\gamma_{h} + \mu_{h}X_{0}} + \frac{\gamma_{h}\gamma_{v}}{\mu_{v}X_{0}}, \qquad (12)$$

$$B = \frac{\mu_{h} \gamma_{v} \gamma_{h} (X_{0} - M)}{X_{0} (\gamma_{h} + \mu_{h} M)} + \frac{\mu_{h} (\gamma_{h} + \mu_{h} M) (\mu_{v}^{2} X_{0} + \gamma_{v} \gamma_{h})}{\mu_{v} (\gamma_{h} + \mu_{h} X_{0})} + \left(\frac{\mu_{h} X_{0} (\gamma_{h} + \mu_{h} M)}{(\gamma_{h} + \mu_{h} X_{0})}\right) \left(\frac{\mu_{h} \mu_{v} (X_{0} - M)}{(\gamma_{h} + \mu_{h} M)}\right)$$
(13)

and

$$C = \mu_h \gamma_h \gamma_v \left( 1 - \frac{M}{X_0} \right). \tag{14}$$

The real parts of the eigenvalues are negative when the coefficients A,B and C satisfy the Routh-Hurwitz criteria, [7] i.e.,

i. 
$$A > 0$$
ii.  $C > 0$  (15)

and

Looking at equations (12) to (14), we see that conditions i. is always satisfied. Conditions ii. and iii. are satisfied when  $X_0 > M$ . [To see that condition iii. is satisfied when  $X_0 > M$ , we note that the cross product AB will be the sum of positive terms. Given the sum of positive numbers is greater than any individual number, we have  $AB > \mu_h \{ \mu_v^2 X_0 + \gamma_h \gamma_v \}$  (this being the product of the first term in A and the second term in B). Dropping  $\mu_v^2 X_0$  in the bracket, we see that  $\mu_h \gamma_h \gamma_V$  is larger than  $\mu_h \gamma_h \gamma_V (1-M/X_0)$ , which is C. We thus have AB > C.] This shows that if  $X_0 > M$ , the real parts of all the eigenvalues of the Jacobian evaluated at the endemic state are negative. Thus the equilibrium state  $E_2(S^*, I^*, R^*, I_V)$  given by equations (6a) - (6d) is a locally asymptotically stable state.

#### 3 Discussion

#### 3.1 Basic Reproduction number

For a disease to be capable of invading and establishing itself in a host population, the basic reproduction number  $R_0$  must be greater than one. If  $R_0 < 1$ , then every successive generation will diminish in size until its number approaches zero. The basic reproduction number for a particular growth can be determined by direct observation of the growth pattern. If  $t_d$  is the first doubling time of the epidemic in a human population, then

$$R_0 = \left[ \frac{\ln 2}{(\mu + \delta)t_d} + 1 \right]$$

where  $\mu$  and  $\delta$  refer to the inverse life time and recovery time of the human. The average reproduction number for the 1990-91 dengue fever epidemic in twelve cities in Brazil was 2.03 [14]. This number means that each infective person infected 2.03 other people. Koopman et al.,[15] found the number to be 1.33 for the dengue fever epidemic in Mexico in the same year.

The different models for disease transmission have yielded expression for the basic reproduction number. These expressions have provided insights into the control of the various diseases. One of the first expressions obtained was

$$R_0 = \frac{b^2 \beta_h \beta_v m}{\mu \gamma}$$
 (16)

where m is the ratio between the mosquito population and the human population. Based on the epidemiological data, Molineaux and Gramiccia [16] estimated  $R_0$  to be 80 for the malaria epidemic in northern Nigeria. The implication of this (each infective person infects 80 other people) points to possible shortcoming of the model used model the transmission of malaria. We note that for dengue fever,  $R_0$  is close to 2. It was pointed out by MacDonald that the malaria transmission model did not take into account an incubation period during which the malaria parasite develops inside the mosquito and during which the mosquito is not infections. Taking this period into account, MacDonald obtained a new expression for the basic reproduction number

$$R_0 = \frac{b^2 \beta_h \beta_v m}{\mu \gamma} e^{-\mu r}$$
 (17)

where  $\mu$  and  $\tau$  are the inverse life time of the mosquito and the incubation period of the malaria parasite in the mosquito. Equation (17) points to the fact that if the incubation period is longer than the life expectancy of the mosquito, the disease will not be established since the mosquito will die before it becomes infectious. The appearance of an exponential factor containing the life expectancy of the mosquito has led to the changes in the strategy of control malaria, exterminate the mosquito during its adult state and not in it's the larva stage.

Looking at the conditions (given in sections 2.2.1 and 2.2.2), which made the disease free state or the endemic state, the stable equilibrium state, we obtain the following conditions

$$\frac{b^2 \beta_v \beta_h \mu_h N_T (B/\mu_v)}{\mu_v (N_T + m)^2 (\mu_h + \delta + r) (\mu_h + \delta)} < 1$$

for the equilibrium state to be the disease free state. If however,

$$\frac{b^{2}\beta_{V}\beta_{h}\mu_{h}N_{T}(B/\mu_{V})}{\mu_{V}(N_{T}+m)^{2}(\mu_{h}+\delta+\Gamma)(\mu_{h}+\delta)} > 1$$

then the endemic steady state is the equilibrium state. We can therefore identify the LHS of the two inequalities as being the basic reproduction number, i.e.,

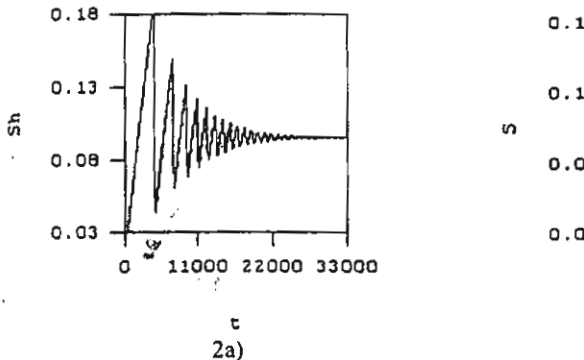
$$R_{0} = \frac{b^{2} \beta_{V} \beta_{h} \mu_{h} N_{T} (B / \mu_{V})}{\mu_{V} (N_{T} + m)^{2} (\mu_{h} + \delta + r) (\mu_{h} + \delta)}$$
(18)

If the susceptible humans are not divided up into juveniles and adults, there is no need for the parameter  $\delta$ , the rate at which juveniles mature into adults. Setting  $\delta = 0$ , expression (18) reduces to the expression for the basic reproduction rate obtained in [7]. The modification to R<sub>0</sub> we have introduced to taken into account the presence of an age structure is similar to the one introduced by Esteva and Vargas in [9] where they looked at the changes arising when both a vertical and horizontal mode of transmission of the dengue virus to the mosquitoes are possible.

#### 3.2 Numerical Studies

The main effect of introducing an age structure into the model is change the definition of the basic reproduction rate. Using the values of the parameters similar to those used by Esteva and Vargas ( $\mu_h = 0.0000457$ ,  $\mu_V = 0.25$ , b = 0.5,  $\beta_h = 0.75$ ,  $\beta_V = 1.0$ , m = 0.0, r = 0.1428,  $N_T = 10,000$ , A = 5,000), the value of the basic reproduction number defined in [7] would be 10.5. Numerically solving the set of equations given by Esteva and Vargas (equation (2) in [7]), we obtain the time development of the susceptible human as seen in Figure 2a). In figure 2b), we show the solution to equation (3a), the values of some of the parameters have been changed (i.e.,  $\delta$  = 0.000183, B = 200,  $\mu_h$  = 0.00003914,  $\mu_V$  = 0.0714 and r = 0.0714, with the others staying the same). Substituting these values in expression (18), we get  $R_0 = 1.8$ . In figure 3 and 4, we show the time development of the infected humans and infected mosquitoes for the case of no age structure and an age structure model. In Figure 5, we plot the number of infected humans versus the number of susceptible humans in both a no age structure population and an age structure population. The values of the parameters are such that for both populations, the equilibrium state is the endemic state. The endemic state is a stable spiral state. As we see, the period of fluctuations in the number of individuals in each class is much shorter in the absence of any age structure. The spiraling is much more severe in the absence of the age structure. The age structure appears to calm down the fluctuations.

#### P. PONGSUMPUN, Y.LENBURY and I.M.TANG



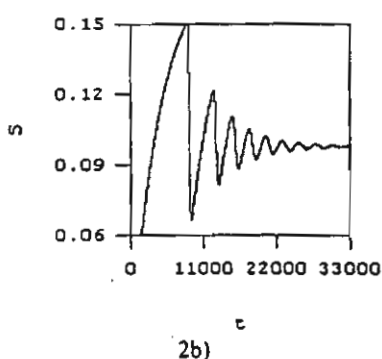
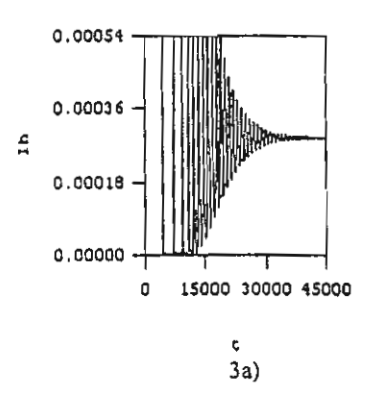


Figure 2. Number of susceptible humans as a function of time. 2a) Solution of equation (2) in [7] for a SIR model of dengue fever transmission with no age structure. 2b) Solution of equation (3a) of the present text for a SIR model having an age structure. The values of the parameters are given in the text.



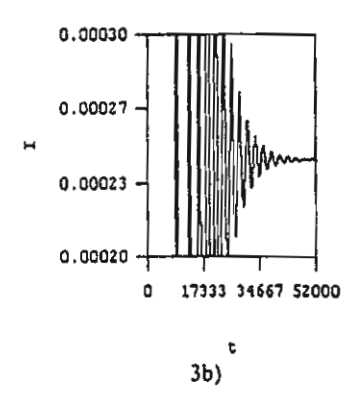
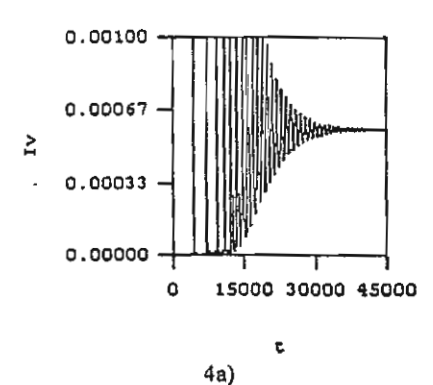
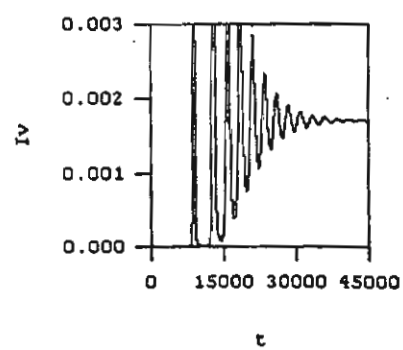


Figure 3. Number of infected humans as a function of time. 3a) Solution of equation (2) in [7] for a SIR model of dengue fever transmission with no age structure. 3b) Solution of equation (3b) of the present text for a SIR model having an age structure. The values of the parameters are given in the text.





4b)

'-55/

Figure 4. Number of infected mosquitoes as a function of time. 4a) Behavior in a non age structure SIR model. 4b) Behavior in an age structured model.

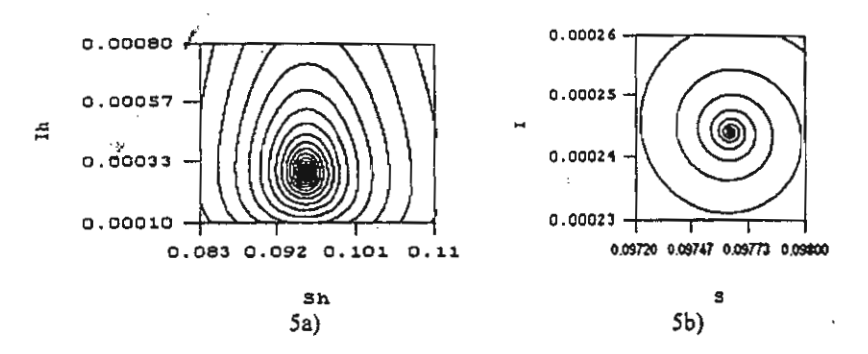


Figure 5. Plot of number of susceptible and infected humans. 5a) Behavior in a non age structured SIR model. 5b) Behavior in an age structured model.

#### 4 Acknowledgements

This work is supported by the Thailand Research Fund with the grant from the Golden Jubilee Ph.D. Program according to the contract number PHD/0154/2543, 3.M.MU/43/B.2.

#### References

- [1] R. Ross, The prevention of Malaria, 2nd Ed. Murray, London, 1911.
- [2] G. MacDonald, The epidemiology and control of Malaria, Oxford U.Press, London, 1957.
- [3] F.E. McKenzie, Why model Malaria?, Parasitology Today, 16 (2000), 511-516.
- [4] T.P. Monath, Dengue. The risk to developed and developing countries, Proc. Nat. Acad. Sci. USA, 91 (1994), 2395-2400.
- [5] Pan America Health Organization, "Dengue and dengue haemorrhagic fever in the Americas: guidelines for prevention and control", Washington DC: PAHO, 1994.
- [6] J. F. Mendez Galvan, R. M. Castellanos, "Manual para la viglancia epidemiology del dengue", Secretaria de Salud, DF. Mexico, 1994.
- [7] L. Esteva, C. Vargas, Analysis of a dengue disease transmission model, Math. BioSci., 150, (1998), 131-151.
- [8] L. Esteva, C. Vargas, A model for dengue disease with variable human population, J. Math. Bio., 38, (1999), 220-240.
- [9] L. Esteva, C. Vargas, Influence of vertical and mechanical transmission of the dynamics of dengue disease, Math. BioSci., 167,(2000), 51-64.
- [10] M.G. Guzman, G. P. Kouri, J. Bravo, M. Solet, S. Vasquez, M. Santos, R. Villaescusa, P. Basanta, G. Indan, J. M. Ballester., Dengue haemorrhagic fever in Cuba II. Clinical investigations, Trans.R.Soc.Trop.Med.Hyg., 78, (1984), 239-241.
- [11] M. G. Guzman, G.P. Kouri, L. Valdes, J. Bravo, M. Alvarez, S. Vasquez, I. Delgado, S.B. Halstead, *Epidemiologic Studies on Dengue in Santiago de Cuba*, 1997. Am. J. Epidemiol., 152, (2000), 793-799.

#### P. PONGSUMPUN, Y.LENBURY and I.M.TANG

- [12] Annual Epidemiological Surveillance Report, (1992-1998). Division of Epidemiology, Ministry of Public Health, Royal Thai Government.
- [13] Z. Feng, J. X. Velsco-Hernandez, Competitive exclusion in a vector-host model for the dengue fever, J.Math.Bio., 35, (1997), 523-544.
- [14] C. A. Marques, O. P. Forattini and E. Massad, The basic reproduction number for dengue fever in San Paulo state, Brazil: 1990-1991 Epidemic. Trans. R. Soc. Trop. Med. Hyg., 88, (1994), 58-59.
- [15] J. S. Koopman, D. R. Prevots, M. A. V. Marin, H. G. Dantes, M. L. Z Aquino, I. M. Logini, Jr. and Js. Amor., Determinants and predictors of dengue infection in Mexico, Am. J. Epidemiol., 133 (1991), 1168-1178.
- [16] L.Molineaux and G. Gramiccia, *The Garki Project*, World Health Organization, Gevena, (1980).

Computational Mathematics and Modeling, An International Conference, CMM2002, Bangkok.
Copyright © by East-West J. of Mathematics.
All rights of reproduction in any form reserved.

#### Transmission of Plasmodium Vivax Malaria

#### A. Kammanee<sup>†</sup>, Y. Lenbury<sup>‡</sup> and I. M. Tang<sup>\*</sup>

†‡ Department of Mathematics, Faculty of Science Mahidol University, Rama 6 Rd. Bangkok 10400, Thailand

\* Department of Physics Institute of Science & Technology for Research & Development Salaya Campus, Mahidol University, Nakorn Pathom 71730, Thailand

#### Abstract

In this paper, we look at the transmission of *Plasmodium vivax* malaria. We divide the host population into 3 categories containing susceptible, infected and dormant population as well as construct the nonlinear differential equations system. By using the basic dynamical method, we obtain the basic reproduction number  $R_0$ , which is considered by the steady state. If  $R_0 < 1$ , then the malaria becomes extinct; moreover, if  $R_0 > 1$  then the equilibrium point is asymptotically stable that endemic state occurs.

#### 1 Introduction

il.

1

Malaria is a serious disease endemic in many parts of Africa, Asia, the Middle East, Central and South America, Hispaniola, and Oceania [10]. There are more than 3 hundred million cases of malaria each year, with between 1 and 1.5 million death mostly among children [7]. Malaria in humans is due to 4 species of the intracrythrocytic protozoa of the genus Plasmodium, i.e., Plasmodium falciparum, Plasmodium vivax, Plasmodium malariae and Plasmodium ovale. Most of the death in childhood is due to P. falciparum. Recently P. vivax has become an enormous problem. In 1997 P. falciparum and P.vivax were found 36.7% and 48.9% of infected population in United states, respectively. In 1997, Luxemburger et al. showed that the transmission rate for P. vivax parasite is higher than that for the P. falciparum.

The mathematical model of malaria has a long history. Ronald Ross was the first person to created a mathematical model of malaria. His model consisted of 4 differential equations, describing changes in the densities of not only the susceptible and the infected host population but also the uninfected (susceptible) and infected mosquitoes [9]. In 2000, McKenzie described the advantages and shortcoming of modeling malaria. He stated that models help us to understand and analyze relationship among variables. Most mathematical model presented so for describe the dynamic of *P. falciparum* malaria infection [6]. Because of the increased incidence of *P. vivax* infection, we are faced with the need to model the dynamics of *P. vivax* infection.

The progression of *P. vivax* malaria differs from *P. falciparum* in that a patient can die from *P. falciparum* but does not die from *P. vivax* infection. Also a person who suffers from *P. falciparum* will recover from the disease (if he does not die from his

illness); a person who is ill with *P. vivax* infected will suffer relapses. The *P. vivax* is induced into blood circulation in the sporozoite form by the bite of an infected female mosquitoes of the genus *Anopheles*. The sporozoite will then migrate to the liver. The sporozoites separate themselves into 2 groups. The first group are the merozoites which invade the blood cell and produce the illness. The second group are the hynozoites which lay dormant in the liver. When the patient is weak, the hynozoites will transform themselves into the merozoites and reinvade the blood cell and reproduce the sickness. These relapse can occur up to five years after the first infection [2]. A mathematical model for *P. vivax* transmission should take this into account.

#### 2 The Mathematical Model

We begin the formulation of the model by dividing the host population (total  $N_h$ ) into 3 groups; susceptible  $(S_h')$ , infected  $(I_h')$  and dormant  $(D_h')$  population. The dormant population can move to either the infected or susceptible class. The latter occurs since malaria does not confer permanent immunity to further infection. We assume that a susceptible mosquitoes when biting a person in the dormant class will not reinfected the person. We also assume that the number of mosquitoes is constant  $(\frac{dN_v}{dt}=0)$ . The mosquitos' population (total  $N_v$ ) is separated into 2 sets; the uninfected (susceptible)  $(S_v')$  class and the infected  $(I_v')$  class.  $N_h = S_h' + I_h' + D_h'$  and  $N_v = S_v' + I_v'$  are, respectively, the total human and vector population at time t. The model is assumed that newborns in both population are uninfected.

The time rate of change of any state is equal to the number entering into the state minus the number leaving the state. The dynamic equation describing the density of host population are then

$$\frac{dS_{h}^{'}}{dt} = \lambda N_{h} + (1 - \alpha)r_{1}I_{h}^{'} + r_{3}D_{h}^{'} - (\gamma_{h}^{'}I_{v}^{'} + \mu_{h})S_{h}^{'}$$
 (1)

$$\frac{dI_{h}^{'}}{dt} = \gamma_{h}^{'} I_{v}^{'} S_{h}^{'} + r_{2} D_{h}^{'} - (r_{1} + \mu_{h}) I_{h}^{'}$$
(2)

$$\frac{dD'_{h}}{dt} = \alpha r_{1} I'_{h} - (r_{2} + r_{3} + \mu_{h}) D'_{h}$$
(3)

and 
$$\frac{dN_h'}{dt} = (\gamma_h - \mu_h)N_h \tag{4}$$

where all parameter in the model are assumed positive;  $\lambda$  is the natural birth rate of host population;  $\mu_h$  is the natural mortality rate of human population which will be the same for all classes;  $r_1^{-1}$  is the mean life time for the parasite to remain infectious in the human;  $\alpha$  is the percentage of individuals leaving the infected state and entering dormant state;  $r_2$  is the relapse rate;  $r_3$  is the recovery rate. The transmission rate for malaria is given by

$$\gamma_h' = b \frac{\beta_h}{N_h + p}$$

where b is the specie-dependent bitting rate of the mosquitoes; p is the population of other animals the the mosquitoes can fed on and  $\beta_h$  is the probability that the P. vivax is passed on by the mosquito to the human. If there is no the dormant state  $(D_h)$  and  $r_2 = 0$ , the model is reduced to the transmission model for P. falciparum.

The rate equations of mosquitoes' population are

$$\frac{dS'_{v}}{dt} = A - \gamma'_{v} I'_{h} S'_{v} - \mu_{v} S'_{v} \tag{5}$$

$$\frac{dI_{v}^{'}}{dt} = \gamma_{v}^{'} I_{h}^{'} S_{v}^{'} - \mu_{v} I_{v}^{'} \tag{6}$$

and 
$$\frac{dN_{v}^{'}}{dt} = A - \mu_{v}N_{v} \tag{7}$$

where A is the recruitment rate which is not related to the mosquito's birth rate  $\lambda_{v}$ . The mosquitoes lay eggs which give rise to the larvae stage of the mosquitoes. Only a small number of the larvae will grow into the adult stage. This number depend on the carrying capacity of the environment and not on the number of eggs laid at [2].

We assume that the total number of humans and mosquitoes are constant,  $N_h = S_h' + I_h' + D_h'$  and  $N_h = S_v' + I_v'$ . We now introduce the normalized variables  $S_h = \frac{S_h'}{N_h}$ ,  $I_h = \frac{I_h'}{N_h}$ ,  $D_h = \frac{D_h'}{N_h}$ ,  $S_v = \frac{S_v'}{N_v}$  and  $I_v = \frac{I_v'}{Nv}$ . The domain of acceptable solution is given by

$$\Omega = \{ (S_h, I_h, D_h, S_v, I_v) | 0 \le S_h, I_h, D_h, S_v, I_v \le 1 \}$$

The dynamic equations can now be rewritten as

띩

$$\frac{dS_h}{dt} = \lambda + (1 - \lambda)r_1I_h + r_3D_h - (\gamma_hI_v + \mu_h)S_h$$
 (8)

$$\frac{dI_h}{dt} = \gamma_h I_v S_h + r_2 D_h - (r_1 + \mu_h) I_h \tag{9}$$

$$\frac{dD_h}{dt} = \alpha r_1 I_h - (r_2 + r_3 + \mu_h) D_h \tag{10}$$

$$\frac{dS_v}{dt} = \mu_v - \gamma_v I_h S_v - \mu_v S_v \tag{11}$$

and 
$$\frac{dI_{v}}{dt} = \gamma_{v}I_{h}S_{v} - \mu_{v}I_{v}$$
 (12)

where  $\gamma_h = \gamma_h' \frac{\mu_h}{A}$  and  $\gamma_v = \gamma_v' N_h$ . We use  $S_h + I_h + D_h = 1$  and  $S_v + I_v = 1$  to reduce the number of differential equations from 5 to 3 since  $\frac{dS_h}{dt} = -(\frac{dI_h}{dt} + \frac{dD_h}{dt})$ 

280

and 
$$\frac{dS_v}{dt} = -\frac{dI_v}{dt}$$
. We thus have

$$\frac{dI_h}{dt} = \gamma_h I_v (1 - I_h - D_h) + r_2 D_h - (r_1 + \mu_h) I_h \tag{13}$$

$$\frac{dD_h}{dt} = \alpha r_1 I_h - (r_2 + r_3 + \mu_h) D_h$$
 (14)

and 
$$\frac{dI_v}{dt} = \gamma_v I_h (1 - I_v) - \mu_v I_v \tag{15}$$

#### 2.1 Equilibrium State

Setting the RHS of (13)-(14) to zero and solving for the 3 variables, we gain two equilibrium states; the disease free state  $E_0=(0,0,0)$  and the endemic state  $E_1=(I_h^*,D_h^*,I_v^*)$  where  $D_h^*=\frac{\alpha r_1}{r_1+r_3+\mu_h}I_h^*$ ;  $I_v^*=\frac{\gamma_v}{\gamma_vI_h^*+\mu_v}I_h^*$  and  $I_h^*=\frac{R_0-1}{R_0M}$  with  $M=1+\frac{r_1+\mu_h}{\gamma_h}+\frac{\alpha r_1(\gamma_h-r_2)}{\gamma_h(r_2+r_3+\mu_h)}$  and the basic reproduction number is found to be given by

$$R_0 = \frac{\gamma_h \gamma_v}{\mu_v (r_1 + \mu_h - \frac{\alpha r_1 r_2}{r_2 + r_3 + \mu_h})}$$
(16)

Examiniting the expressing above, we find that physical values of  $I_h^*$ ,  $D_h^*$  and  $I_v^*$  are possible when  $R_0 > 1$ . When  $R_0 < 1$ , the epidemic state is not possible. This leaves the disease free state as the only possibility.

#### 2.2 Locally Asymptotical Stability

The local stability of the equilibrium state is determined by the Jacobian (gradient) matrix evaluated at the equilibrim states. We find its eignvalues by solving the determinant equation det  $|J - \lambda I| = 0$  where

$$J(I_h^*, D_h^*, I_v^*) = \begin{pmatrix} -(r_1 + \mu_h + \gamma_h I_h^*) & r_2 - \gamma_h I_v^* & \gamma_h (1 - I_h^* - D_h^*) \\ \alpha r_1 & -(r_2 + r_3 + \mu_h) & 0 \\ \gamma_v (1 - I_v^*) & 0 & -(\gamma_v I_h^* - \mu_v) \end{pmatrix}$$

The equilibrium state is stable if the real parts of all the eigenvalus are negative. The trajectory of the state towards this equilibrium occurs when two of the eigenvalues are complex conjugates pairs.

#### 2.2.1 Disease Free State

The system equation (4), the gradient matrix at disease free state,  $E_0$ , is given by

$$J(0,0,0) = \begin{pmatrix} -(r_1 + \mu_h) & r_2 & \gamma_h \\ \alpha r_1 & -(r_2 + r_3 + \mu_h) & 0 \\ \gamma_v & 0 & -\mu_v \end{pmatrix}$$

The charectesistic equation is found that is  $\lambda^3 + a_1\lambda^2 + a_2\lambda + a_3 = 0$  where

$$a_1 = r_1 + r_2 + r_3 + 2\mu_h + \mu_v$$

$$a_2 = (r_1 + \mu_h)(r_2 + r_3 + \mu_h + \mu_v) + \mu_v(r_2 + r_3 + \mu_h) - \gamma_h\gamma_v - \alpha r_1 r_2$$

$$a_3 = \mu_v(r_1 + \mu_h)(r_2 + r_3 + \mu_h) - \gamma_h\gamma_v(r_2 + r_3 + \mu_h) - \alpha r_1 r_2 \mu_v$$

The real parts of eigenvalues will be negative if  $a_1 > 0$ . Two of the eigenvalues will be conjugate pairs if  $a_3 > 0$ . We see that this condition is satisfied if  $R_0 < 1$ .

#### 2.2.2 Endemic Disease State

The characteristic equation for the gradient matrix evaluated at the endemic disease state is given by

$$\lambda^3 + a_1 \lambda^2 + a_2 \lambda + a_3 = 0 \tag{17}$$

where

1

$$a_{1} = r_{1} + r_{2} + r_{3} + 2\mu_{h} + \mu_{v} + (\gamma_{h} + \gamma_{v})I_{h}'$$

$$a_{2} = (r_{1} + \mu_{h} + \gamma_{h}I_{h}')(r_{2} + r_{3} + \mu_{h}) + \gamma_{v}I_{h}' + \mu_{v}) + (r_{2} + r_{3} + \mu_{h})(\gamma_{v}I_{h}' + \mu_{v})$$

$$- \gamma_{v}\gamma_{h}(1 - I_{v}')(1 - I_{h}' - D_{h}') - \alpha r_{1}(r_{2} + \gamma_{h}I_{v}')$$

$$a_{3} = -det(J)$$

The root of equation (17) will have a negative real part when  $a_1 > 0$ . We find that this is always true if  $R_0 > 1$ . We have a stable spiral mode if  $a_2 > 0$ . When  $a_2 < 0$ , but  $a_1 > 0$ , the trajectory will be a stable star mode.

#### 3 Discussion

#### 3.1 The Basic Reproduction Number

The basic reproduction number  $R_0$ , is defined as the number of secondary infections produced by an initial infect [7]. MacDonald [5] defined  $R_0$  for P. falciparum malaria to be

$$R_0 = \frac{ma^2b_1b_2e^{-\mu T}}{\mu r} \tag{18}$$

where m is the ratio of mosquito to post population density;  $b_1$  is the transmission of the infectiousness from an infected human to a mosquito;  $b_2$  is the transmission of the infectiousness from an infected mosquito to a human;  $\mu$  is the daily death of the mosquito; T is the parasite's developmental period in the mosquito; r is the recovery rate in human and  $e^{-\mu T}$  is the probability that the mosquito survives the developmental period of the parasite from the initial infection to become infectious.

MacDonald concluded that changes in the mosquito death would have most effect on  $R_0$ . Here we are interested in the effects of the relapse on the transmission of P.vavix malaria. We find that  $R_0$  increase as the relapse rate increase.

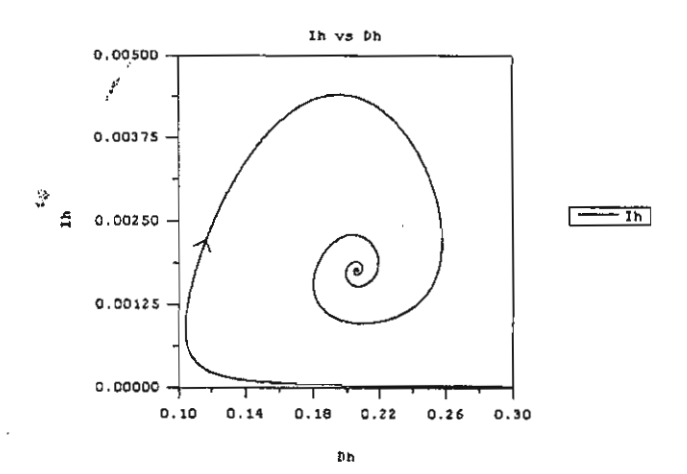


Fig 5. Initial behaviour of the proportions  $I_h$  and  $D_h$ . The parameters are the same as in Figure 3. There is a threshold parameter  $R_0$  and the disease can exist in the epidemic state if and only if  $R_0$  exceeds one. The disease-free equilibrium exists and is globally stable if  $R_0 \leq 1$ . The endemic equilibrium is a stable spiral state.

#### References

- [1] L. Esteva and C. Vargas, Analysis of Dengue Disease Transmission Model, Math BioSci, 150(1998) 131-161.
- [2] A. Kammanee, N. Kanyamee, I.M. Tang. Basic Reproduction Number for Transmission of Plasmodium Vivax Malaria, Southeast Asian J. Trop. Med. Public Health, 32(2001) 702-706.
- [3] C. Luxemburger, F. Ricci, F. Noten, D. Raimond and S. Bather, *The Epidemiology of Severe Malaria in an Area of Low Transmission in Thailand*, Transactions of The Royal Society of Tropical Medicine and Hygiene, **19**(1997) 105-111.
- [4] G. MacDonald, "The Epidemiology and Control of Malaria". Oxford Uni. Press, 1957.
- [5] D. P. Mason and F.E. Mckenzie, Blood-Stage Dynamics and clinical Implications of Mixed Plasmodium Vivax-Plasmodium Falciparum infections, The American Society of Tropical Medicine and Hygene, 603 (1999) 367-374.
- [6] F. E. McKenzie, Why Model Malaria?, Parasitology Today, 16(2000), 511-516.
- [7] G. A. Ngwa and W.S. Shu, A Mathematical Model for Endemic Malaria with Variable Human and Mosquito Populations, Mathematical and Computer Modelling, 32 (2000) 747-763.
- [8] R. Ross, "The Prevention of Malaria", 2nd ed., Murray, London, 1991.
- [9] R. M. Anderson and R. M. May, "Infectious Diseases of Humans: Dynamics and Control", Oxford Uni. Press, 1992.
- [10] http://www.cdc.gov/mmwr/preview/mmwrhtml/ss5005a1.htm

Computational Mathematics and modeling, An International Conference, CMM2002, Bangkok Copyright©by East-West J. of Mathematics.

All rights of reproduction in any form reserved.

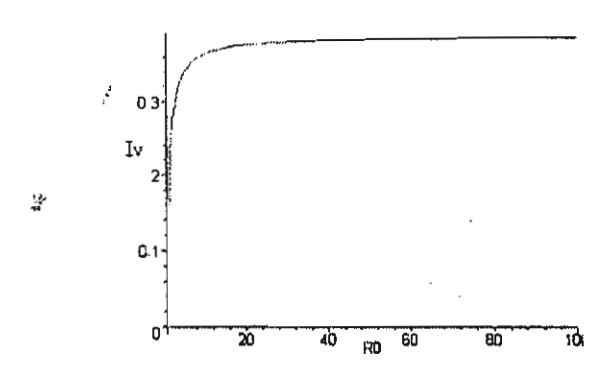


Fig 1. Diagram showing graph of  $R_0$  against  $I_v$  where  $\mu_h = \frac{1}{365 \times 60}$ ;  $r_1 = 0.76$ ;  $r_2 = 0.5$ ;  $r_3 = 0.001$ ;  $\alpha = 0.84$ ;  $\mu_v = 0.25$ ;  $\gamma_h = 0.1428$ ;  $\gamma_v = 0.5$ 

We plotted  $R_0$  again  $I_v^*$ . In figure 1,we can clearly see that the proportions of infected mosquitoes vary with the basic reproduction number. When  $R_0$  is below 50, a small change in  $R_0$  will lead to a large changes in  $I_v^*$ . However for high  $R_0$ , the increase is at a slower rate. Reducing the density of the mosquitos' population will not have a significant effect in the endemic regions where the basic reproduction number is large ( $R_0$  decline as the density of the mosquito decline)

#### 3.2 Simulation

We have numerically solved equations (8) - (12) using a computer. The program was run for different sets of initial conditions. The steady state solutions are the same. We have formed the endemic steady state solution to be unique and globally and asymptotically stable. We have pick set of the values of the variable appearing in the expressions for the equilibrium states to be  $I_h = 0.5$ ,  $D_h = 0.25$  and  $I_v = 0.00001$ . For case of  $R_0 > 1$ , we formed that the endemic equilibrium would be locally and asymptotically stable. Numerical simulation confirmed this result.

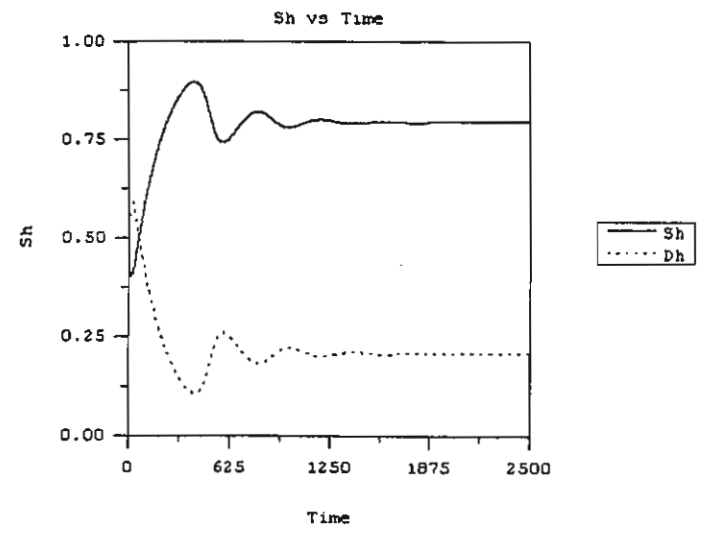


Fig 2. Initial behavior of the proportions  $S_v$  and  $D_v$  with time (days). The parameters are  $r_2 = 0.000007$ ;  $\alpha = 0.65$ ;  $r_3 = 0.005$ ;  $r_1 := 0.91$ ;  $\mu_v := 0.25$ ;  $\gamma_h := 1.95$ ; and  $\gamma_v := 0.25$ ;

#### A. KAMMANEE, Y. LENBURY AND I. M. TANG

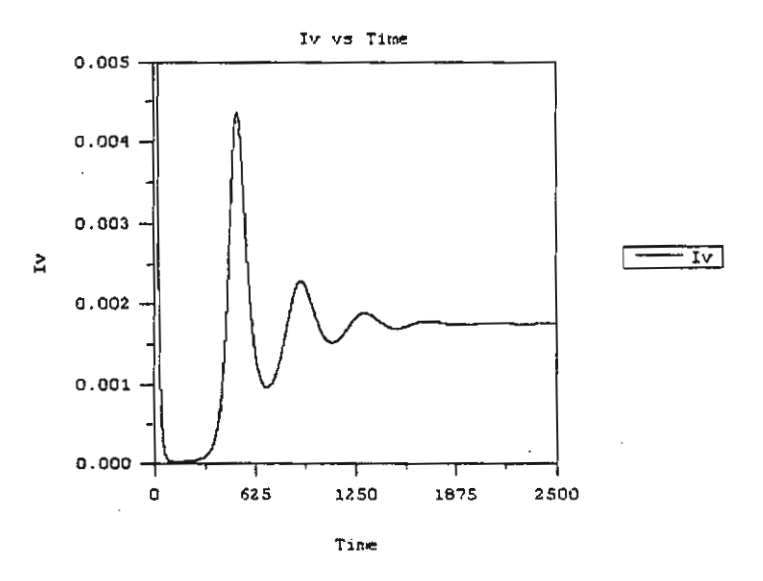


Fig 3. Initial behaviour of the proportions  $I_v$  with time (days). The parameters are the same as Figure 2

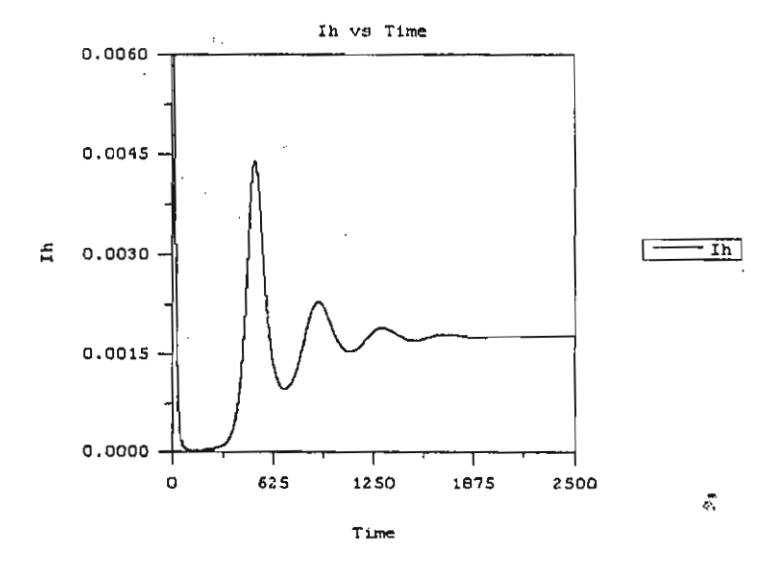


Fig 4. Initial behaviour of the proportions  $I_h$  with time (days). The parameters are the same as in Figure 2

#### THE EFFECT OF MIGRANT WORKERS ON THE TRANSMISSION OF MALARIA

N. Kanyamee<sup>†</sup>, Y. Lenbury<sup>‡</sup> and I. M. Tang<sup>\*</sup>

†‡ Department of Mathematics and \* Department of Physics Faculty of Science, Mahidol University, Rama 6 Rd. Bangkok 10400, Thailand \*Institute of Science & Technology for Research & Development Salaya Campus, Mahidol University, Nakorn Pathom 71730. Thailand

#### Abstract

In this research, we model the transmission of malaria in the movement of population by considering a system of nonlinear differential equations in the Susceptible-Infected-Susceptible (SIS) model. The human population is divided into a host population (in community) class and a migrant workers class. We analyze the behavior of our system. The conditions for equilibrium are obtained by looking at the conditions for zeros in a third degree polynomial. By considering the standard dynamical method, the percentage of infectious migrant worker is used as an adjustable parameter. Numerical simulations are used to illustrate the results for supporting our theoretical data.

#### 1 Introduction

Malaria is a serious acute and chronic relapsing infection to human [14]. It is transmitted to human by biting of mosquitoes in genus Anopheles. Four types of protozoa species (strain) belonging to the genus Plasmodium, namely P. falciparum, P. vivax, P.malariae and P. ovale, cause an infection. The World Health Organization estimated that there are over one million child deaths per year in sub-Saharan Africa, 300-500 million cases of malaria per year and more than two billion people are at risk throughout the world [13].

The first person who attempts to construct a mathematical model of the dynamics of malaria transmission was Ronald Ross[9]. His model consisted of a few differential equations to describe changes in the densities of susceptible and infected people and mosquitoes. He found that for any given set of malariological circumstances some minimum number of mosquitoes, above zero, was needed to keep transmission going. If number fell below, the disease becomes extinct. After Ross demonstrated that malaria are transmitted by mosquitoes, he stated [8] that To say that a disease depends upon certain factors is not to say much, until we can also form an estimate as to how largely each factor influences the whole result. Recently, McKenzie[8] had pointed out that models can be powerful tools for integrating information from different disciplines. In 1950, Macdonald [6], extended the model by introduced a layer

of biological realism (infection rate) to the model. He studies the influences of the mosquito malaria-infection rate. The Ross-Macdonald model is used to analyze equilibrium state for malaria in term of the influence of the mosquito malaria-infection rate on the human infection rate and of the human infection rate on the mosquito infection rate. Other advance models about malaria transmission have been introduced. In 2000, A. Kammanee, N. Kanyamee and I.M. Tang[3] have introduced a new model for the transmission of *P.vivax* malaria. The population is divided into 4 classes by considering the possibility of relapse. In the present work, we use some parameter and introduce a migration factor from this model.

The incidences of malaria have increased in many regions in the world and in area which people thought was disease free [7]. One of the important factor that leads to the malaria transmission is the movement of migrant worker due to the poverty. The spread of disease is enhanced when population move from that place to the others. In Luxemburger[5] study, a town located on the western border of Thailand, reported that in the area adjacent to Burma there are significant population movements. This movement was thought to be a major factor in the regional spread of multi-drug resistance. There are many evidences in other regions in the world supporting this idea [13]. At the beginning of the 1960's malaria had been eradicated from Tajikistan, but it reappeared an endemic in the 1990's in the area bordering Afghanistan. Laboratoryconfirmed malaria cases increased from 175 in 1990 to 2400 in 1994, mainly from the southern border areas. The appearance of malaria in the United Kingdom was due to the infection being brought in from abroad. Of the 1,887 malaria cases in the United Kingdom, 704 occurred in people who, while living in the UK, traveled to visit family in their country of origin. In Cambodia, about 2.5 million people have malaria. 26% of the population is considered to live in areas at risk of malaria transmission. The most intense transmission occurs in the forested areas along the Thai border and in the northeastern part of the country. In this study we are interested in the effect of migration in the malaria transmission. The identification and understanding of the influence of those population movements can improve the prevention measures and malaria control programs.

#### 2 The Mathematical Model

In our study, we construct a simple model for malaria transmission. We assume that the human population and mosquito population  $(N_V)$  are constants; resulting birth and death rates are the same. The total population is divided into two populations, a host population  $(N_T)$  with a total population of a migrant worker population  $(N_W)$ . The host population is divided into two subclasses, susceptible (S') and infected (I') host population. The migrant population is also divided into two subclasses that are susceptible  $(S'_w)$  and infected  $(I'_w)$  worker population. In the standard transmission model for P. vivax [3], the model has 4 subclasses with no migration term. We consider the effect of migrant workers by adding the migration term into the model. The mosquito (vector) population is also divided into two subclasses, uninfected (susceptible)  $(S'_v)$  and infected  $(I'_v)$  mosquito population. Since malaria does not give a

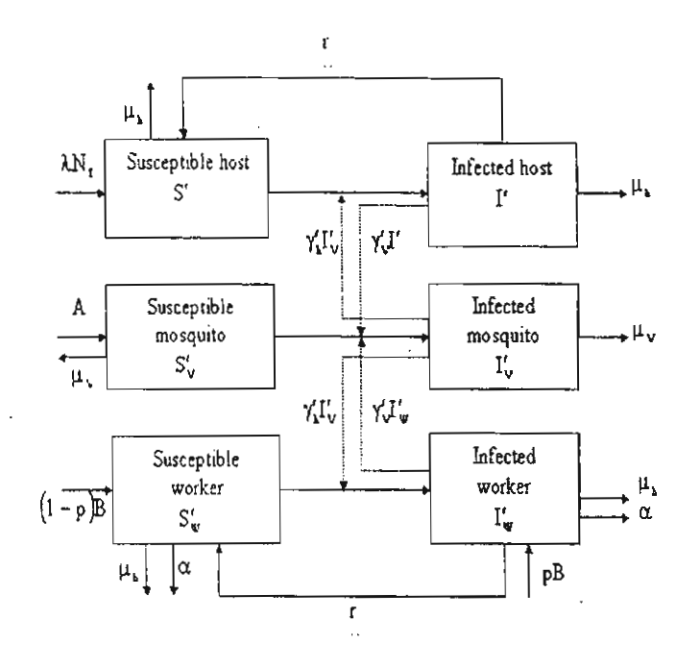
•

3

ŝ

permanent immunity to further infection, we allow the individual in an infected class to reenter into the susceptible class, with rate r, the rate at which they loss their immunity.

The flowchart of the disease is shown in the figure below. We assume that the workers migrate in and out at constant rates. The infectious migrant workers enter the country with percentage p. The time rate of change of any class is equal to the number entering into the class minus the number leaving the class. The migrant worker population moves out rom country with rate  $\alpha$ , the reciprocal of the time migrant workers stay in the country. A is the recruitment rate of mosquitoes. B is the recruitment rate of migrant workers.  $\lambda$  is the birth rate among host population. We assume that the migrant worker population stays long enough to reproduce.  $\mu_h$  is the natural death rate of human and  $\mu_v$  is the natural death rate of moquitoes.



The dynamic equations for this SIS model with migration is described by the flowchart are

$$\frac{dS'}{dt} = \lambda N_T + rI' - \gamma'_h I'_v S' - \mu_h S' \tag{1}$$

$$\frac{dI'}{dt} = \gamma_h' I_v' S' - (\mu_h + r) I' \tag{2}$$

$$\frac{dS'_{w}}{dt} = (1-p)B + rI'_{w} - \gamma'_{h}I'_{v}S_{w}' - (\mu_{h} + \alpha)S_{w}'$$
(3)

and 
$$\frac{dI_{w'}}{dt} = pB + \gamma'_{h}I'_{v}S_{w'} - (\mu_{h} + \alpha + r)I'_{w}$$
 (4)

For vector (mosquito) transmitted disease,  $\gamma_h^{'}$  is the unrenormalized rate of trans-

mission of malaria parasite from mosquitoes to humans as shown by Esteva and Vargas [2] and [3]

$$\gamma_h' = \frac{b\beta_h}{N_T + N_w + m} \tag{5}$$

where species-dependent biting rate b of mosquitoes is the average number of bites per mosquito per day; m denote the number of other animals available as blood sources and  $\beta_h$  is the transmission probability that parasite passed from vector to human and continue to thrive in the human.

The time rates of changes of the mosquito population are given by

$$\frac{dS'_{v}}{dt} = A - \gamma'_{v}I'S'_{v} - \gamma'_{v}I'_{w}S'_{v} - \mu_{v}S'_{v}$$
(6)

and 
$$\frac{dI'_{v}}{dt} = \gamma'_{v}I'S'_{v} + \gamma'_{v}I'_{w}S'_{v} - \mu_{v}I'_{v}$$
 (7)

where  $\gamma_{v}$  is the unrenormalized rate at which the mosquito becomes infected with the malaria parasites once the mosquito has bitten an infected human and it is given[2]

$$\gamma_{v}^{'} = \frac{b\beta_{v}}{N_{v} + m} \tag{8}$$

where  $\beta_v$  is the transmission probability that parasite passed on an infection from human to vectors.

When the total population of each group is constant, we normalized the variables

by dividing by 
$$N_T$$
,  $N_w$  or  $N_v$  ( $N_w = \frac{B}{\mu_h + \alpha}$ ,  $N_v = \frac{A}{\mu_v}$ ), i.e., the proportions  $S = \frac{S'}{N_T}$ ,  $I = \frac{I'}{N_T}$ ,  $S_w = \frac{S'_w}{B/(\mu_h + \alpha)}$ ,  $I_w = \frac{I'_w}{B/(\mu_h + \alpha)}$ ,  $S_v = \frac{S'_v}{A/\mu_v}$ .  $I_v = \frac{I'_v}{A/\mu_v}$ . Since we have  $S + I = 1$ ,  $S_w + I_w = 1$ , and  $S_v + I_v = 1$ , only three of the six

variables will be independent. Picking the three to be I,  $I_w$ , and  $I_v$ , we have

$$\frac{dI}{dt} = \gamma_h I_v (1 - I) - (\mu_h + r)I \tag{9}$$

$$\frac{dI_w}{dt} = p(\mu_h + \alpha) + \gamma_h I_v (1 - I_w) - (\mu_h + \alpha + r) I_w \tag{10}$$

and 
$$\frac{dI_v}{dt} = \gamma_v I(1 - I_v) + \gamma_v (\frac{N_w}{N_T}) I_w (1 - I_v) - \mu_v I_v$$
 (11)

The domain region  $\Lambda$  of biological interest is given by

$$\Lambda = \{(S, I, S_w, I_w, S_v, I_v) | 0 \le S, I, S_w, I_w, S_v, I_v \le 1, 0 \le S + I \le 1,$$

$$0 \le S_w + I_w \le 1, 0 \le S_v + I_v \le 1 \}. \tag{12}$$

This domain is positively invariant under the flow induced by the six equations, as the vector field on the boundary does not point to the exterior.

301

#### 2.1 Equilibrium points of the model

We use the standard dynamical modelling methods to analyze our model. The equilibrium points of our system are obtained by setting the RHS of equations (9) to (11) to zero. The equilibrium points are given by:

$$I = \frac{\gamma_h I_v}{\gamma_h I_v + \mu_h + r} \tag{13}$$

$$I_{w} = \frac{p(\mu_{h} + \alpha) + \gamma_{h}I_{v}}{\gamma_{h}I_{v} + \mu_{h} + \alpha + r}$$

$$\tag{14}$$

and 
$$I_{v} = \frac{\gamma_{v}I + \gamma_{v}(\frac{N_{w}}{N_{T}})I_{w}}{\gamma_{v}I + \gamma_{v}(\frac{N_{w}}{N_{T}})I_{w} + \mu_{v}}$$
(15)

Substituting Eq.(13) and (14) into Eq. (15), Eq. (15) can be rearranged as a cubic equation in  $I_{\nu}$ , i.e.,

$$b_1 I_v^3 + b_2 I_v^2 + b_3 I_v + b_4 = 0 (16)$$

where

1

$$b_{1} = \gamma_{h}^{2} \gamma_{v} + \gamma_{h}^{2} \gamma_{v} \left(\frac{N_{w}}{N_{T}}\right) + \gamma_{h}^{2} \mu_{v}$$

$$b_{2} = \gamma_{h} \gamma_{v} (\mu_{h} + \alpha + r) + \gamma_{h} \gamma_{v} \left(\frac{N_{w}}{N_{T}}\right) p(\mu_{h} + \alpha) + \gamma_{h} \gamma_{v} \left(\frac{N_{w}}{N_{T}}\right) (\mu_{h} + r)$$

$$+ \gamma_{h} \mu_{v} (\mu_{h} + \alpha + r) + \gamma_{h} \mu_{v} (\mu_{h} + r) - \gamma_{h}^{2} \gamma_{v} - \gamma_{h}^{2} \gamma_{v} \left(\frac{N_{w}}{N_{T}}\right)$$

$$b_{3} = \gamma_{v} \left(\frac{N_{w}}{N_{T}}\right) p(\mu_{h} + \alpha) (\mu_{h} + r) + \mu_{v} (\mu_{h} + r) (\mu_{h} + \alpha + r)$$

$$- \gamma_{h} \gamma_{v} (\mu_{h} + \alpha + r) - \gamma_{h} \gamma_{v} \left(\frac{N_{w}}{N_{T}}\right) p(\mu_{h} + \alpha) - \gamma_{h} \gamma_{v} \left(\frac{N_{w}}{N_{T}}\right) (\mu_{h} + r)$$
and 
$$b_{4} = -\gamma_{v} \left(\frac{N_{w}}{N_{T}}\right) p(\mu_{h} + \alpha) (\mu_{h} + r)$$

$$(17)$$

Denoting  $I_v^*$  as the solutions of Eq. (16), we have a nonzero equilibrium state exists if at least one solution of Eq. (16) is real and positive. This will happen when either

(i) 
$$b_{2} < 0, b_{3} > 0$$
  $b_{2}^{2} > 3b_{1}b_{3}, and \Omega < 0$   
or (ii)  $b_{2} \ge 0, b_{3} < 0$  and  $\Omega < 0$   
or (iii)  $b_{2} > 0, b_{3} \ge 0, b_{2}^{2} > 3b_{1}b_{3}, and \Omega < 0$   
or (iv)  $(\frac{1}{54b_{1}^{3}}(9b_{1}b_{2}b_{3} - 27b_{1}^{2}b_{4} - 2b_{2}^{3}) + (\frac{\Omega}{4})^{\frac{1}{2}})^{\frac{1}{3}}$   
 $+ (\frac{1}{54b_{3}^{3}}(9b_{1}b_{2}b_{3} - 27b_{1}^{2}b_{4} - 2b_{2}^{3}) - (\frac{\Omega}{4})^{\frac{1}{2}})^{\frac{1}{3}} > \frac{b_{2}}{3b_{1}}, and \Omega > 0$  (18)

where

$$\Omega = \frac{4}{27}b_1b_3^3 - \frac{1}{27}b_2^2b_3^2 + \frac{4}{27}b_2^3b_4 - \frac{2}{3}b_1b_2b_3b_4 + b_1^2b_4^2.$$

Proof of these conditions is given in the appendix.

If any of the above conditions are met, then one of the solutions of Eq. (16) will  $\cdot \cdot$  be real and positive. Calling this solution  $I_v^*$ , the equilibrium state will be

$$E = (S^*, I^*, S_w^*, I_w^*, S_v^*, I_v^*)$$

where  $I_v^*$  is the solution of Eq.(16),

$$I^* = \frac{\gamma_h I_v^*}{\gamma_h I_v^* + \mu_h + r}, I_w^* = \frac{p(\mu_h + \alpha) + \gamma_h I_v^*}{\gamma_h I_v^* + \mu_h + \alpha + r}.$$
 (19)

 $S^* = 1 - I^*$ ,  $S_w^* = 1 - I_w^*$ , and  $S_v^* = 1 - I_v^*$  (Once it has been established that a positive real solutions of Eq.(16) exists, numerical method can be used to find it).

### 2.2 Stability of the equilibria

The local stability of the equilibrium points can be determined by linearizing the system (Eq.(9) to (11)) about the equilibrium point  $(I^*, I_w^*, I_v^*)$ . The eigenvalues are found by diagonalizing the Jacobian matrix or det  $|J - \lambda I| = 0$ . This gives the Jacobian matrix

$$J(I^*, I_w^*, I_v^*) = \begin{pmatrix} \gamma_h I_v^* - (\mu_h + r) & 0 & \gamma_h (1 - I^*) \\ 0 & -\gamma_h I_v^* - (\mu_h + \alpha + r) & \gamma_h (1 - I_w^*) \\ \gamma_v (1 - I_v^*) & \gamma_v (\frac{N_w}{N_T}) (1 - I_v^*) & -\gamma_v I^* - \gamma_v (\frac{N_w}{N_T}) I_w^* - \mu_v \end{pmatrix}$$

Computing this matrix and noting

$$\gamma_{h}I_{v}^{*} + (\mu_{h} + r) = \frac{\gamma_{h}I_{v}^{*}}{I^{*}}$$

$$\gamma_{h}I_{v}^{*} + (\mu_{h} + \alpha + r) = \frac{p(\mu_{h} + \alpha) + \gamma_{h}I_{v}^{*}}{I_{w}^{*}}$$
and
$$\gamma_{v}I^{*} + \gamma_{v}(\frac{N_{w}}{N_{T}})I_{w}^{*} + \mu_{v} = \frac{\gamma_{v}I^{*} + \gamma_{v}(\frac{N_{w}}{N_{T}})I_{w}^{*}}{I_{v}^{*}}, \tag{20}$$

303

we get the following characteristic equation

$$\lambda^3 + c_1 \lambda^2 + c_2 \lambda + c_3 = 0 \tag{21}$$

where

$$c_{1} = \frac{\gamma_{h}I_{v}^{*}}{I^{*}} + (\frac{p(\mu_{h} + \alpha) + \gamma_{h}I_{v}^{*}}{I_{w}^{*}}) + (\frac{\gamma_{v}I^{*} + \gamma_{v}\frac{N_{w}}{N_{T}}I_{w}^{*}}{I_{v}^{*}})$$

$$c_{2} = (\frac{p(\mu_{h} + \alpha) + \gamma_{h}I_{v}^{*}}{I_{w}^{*}})(\frac{\gamma_{v}I^{*} + \gamma_{v}\frac{N_{w}}{N_{T}}I_{w}^{*}}{I_{v}^{*}}) - \gamma_{h}\gamma_{v}(1 - I_{v}^{*})((1 - I^{*}) + \frac{N_{w}}{N_{T}}(1 - I_{w}^{*}))$$

$$- \frac{\gamma_{h}I_{v}^{*}}{I^{*}}(\frac{p(\mu_{h} + \alpha) + \gamma_{h}I_{v}^{*}}{I_{w}^{*}}) + \frac{\gamma_{v}I^{*} + \gamma_{v}\frac{N_{w}}{N_{T}}I_{w}^{*}}{I_{v}^{*}})$$

$$and * c_{3} = \frac{\gamma_{h}}{I^{*}}(\frac{p(\mu_{h} + \alpha) + \gamma_{h}I_{v}^{*}}{I_{w}^{*}})(\gamma_{v}I^{*} + \gamma_{v}\frac{N_{w}}{N_{T}}I_{w}^{*})$$

$$- \gamma_{h}\gamma_{v}(1 - I_{v}^{*})(\frac{\gamma_{h}I_{v}^{*}}{I^{*}}\frac{N_{w}}{N_{w}}(1 - I_{w}^{*}) + (1 - I^{*})(\frac{p(\mu_{h} + \alpha) + \gamma_{h}I_{v}^{*}}{I^{*}})). \tag{22}$$

The eigenvalues are the solutions of (21) will be negative real part when the coefficient  $c_1, c_2$ , and  $c_3$  satisfy the Routh-Hurwith criteria[1], i.e.

$$c_1 > 0 \tag{23}$$

$$c_3 > 0 \tag{24}$$

$$and \quad c_1c_2 > c_3 \tag{25}$$

We see that the first condition is always satisfied hence we only need to consider conditions (24) and (25) to establish whether the equilibrium point is locally and asymptotically stable.

## 3 Discussion

In this section, we performed some numerical simulations to illustrate the results of our model. The numerical values of the parameters were picked so that conditions (23) to (25) and (18) are satisfied. The numerical program was written in Fortran to solve the set of Eq. (9)to (11). Using the parametric values in unit of year,  $\gamma_h = 0.27$ ,  $\gamma_v = 0.7$ ,  $\mu_h = 1/60$ ,  $\mu_v = 15.0$ , r = 0.16,  $\alpha = 0.2$ ,  $N_T = 100,000$ ,  $N_w = 50,000$ , and  $N_v = 2,000,000$ . At time t = 0, the following initial conditions were used as I(0) = 0.45,  $I_w(0) = 0.6$ , and  $I_v(0) = 0.5$  where the other variables are obtained from S = 1 - I,  $S_w = 1 - I_w$ , and  $S_v = 1 - I_v$ .

The general behavior of the model is shown in figures 1 to 5 where the numerical results are plotted in time (year) versus the normalized populations. Figures 1 to 4 show the initial and long time behavior of human populations plotted on the same graph

when p increases from 0.00005 to 0.5 and 0.95 respectively. The equilibrium point is given by  $E = (S^*, I^*, S_w^*, I_w^*, S_v^*, I_v^*)$  are (0.999999, 0.00000125, 0.999971, 0.00002929. 0.999999,  $7.35882 \times 10^{-7}$ ), (0.989033, 0.0109673, 0.708703, 0.291297, 0.992744, 0.0072557), and (0.979614, 0.0203857, 0.550844, 0.986384, 0.0136164) when p increases from 0.00005 to 0.5 and 0.95 respectively. In Figure 1, we see that when infected workers first introduced into the community for small values of p the susceptible worker population is rapidly rising to 0.999971 and infected worker population is declining to 0.708703. In Figure 2 where p is set to be 0.5, the susceptible worker population keep on increasing but at a rate smaller than previously. When p is 0.95, we see in Figure 3 that the normalized infected worker population is higher than the normalized susceptible worker population whereas the normalized host population has the same behavior with a smaller change. Figure 4 represents the long-term behavior of the normalized human population. At first, they change but as time changed they become stable for a long time period (year). Figure 5 represents the behavior of the normalized mosquito population. It appears not to change as we increase p but it actually does. In conclusion, the higher percentage of infected workers affects high level of infected population and small level of susceptible population.

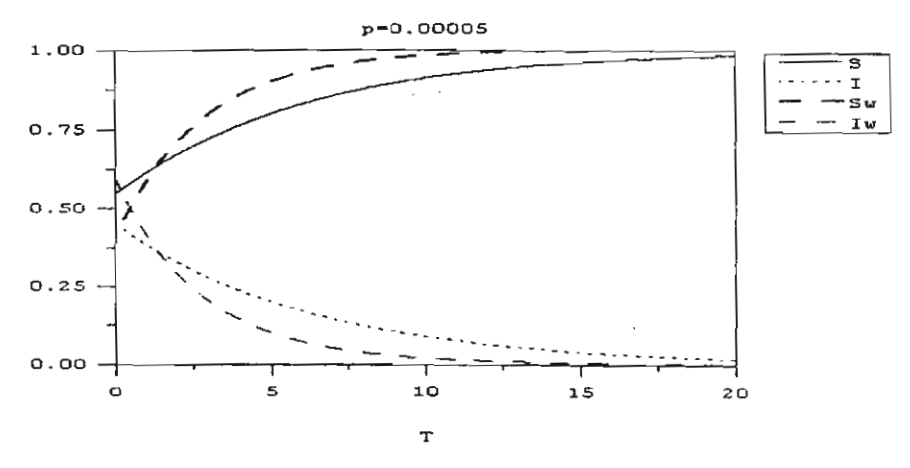


Fig 1. Initial behaviour of the human proportions  $S, I, S_w$  and  $I_w$  with time (years) when p is 0.00005.

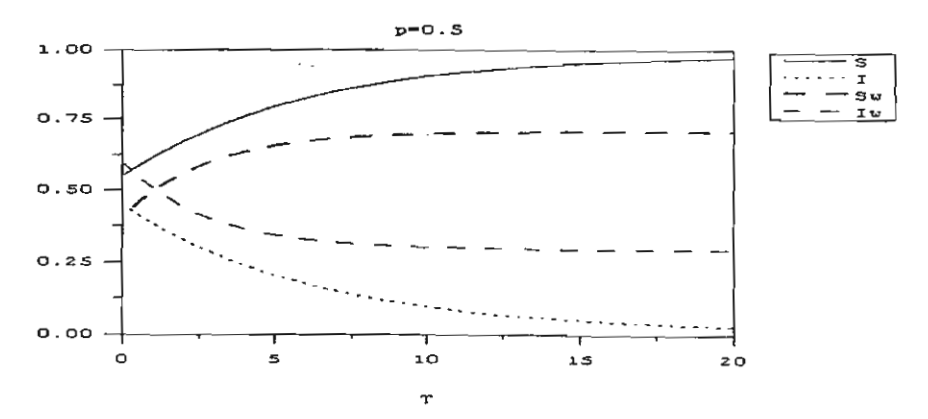


Fig 2. Initial behaviour of the human proportions  $S, I, S_w$  and  $I_w$  with time (years) when p is 0.5.

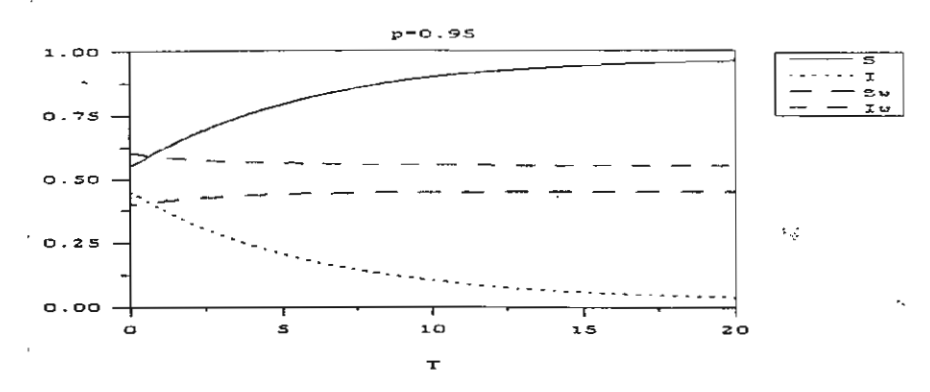


Fig 3. Initial behaviour of the human proportions  $S, I, S_w$  and  $I_w$  with time (years) when p is 0.95.

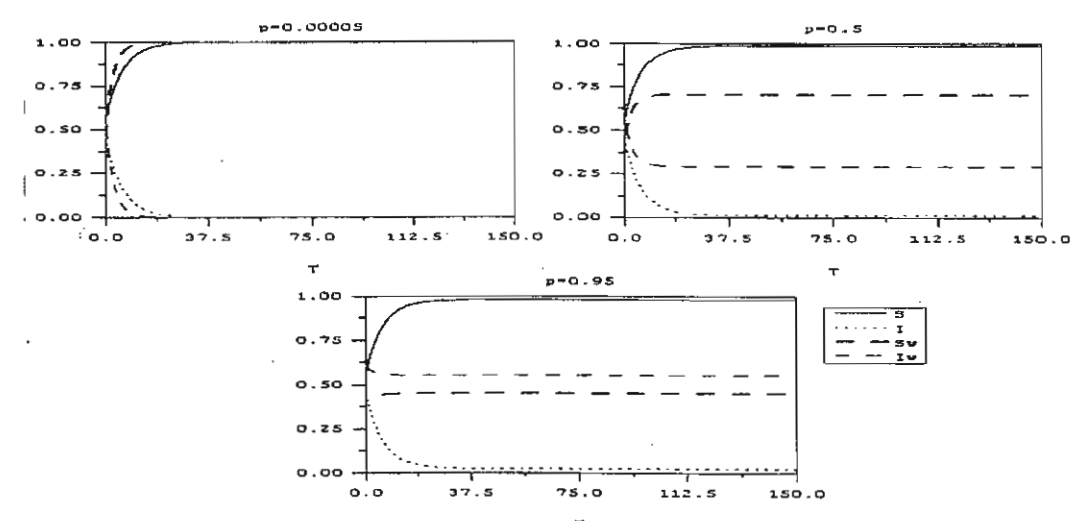


Fig 4. Long-term behaviour of the human proportions  $S, I, S_w$  and  $I_w$  with time (years) when p increases from 0.00005 to 0.5 and 0.95 respectively.

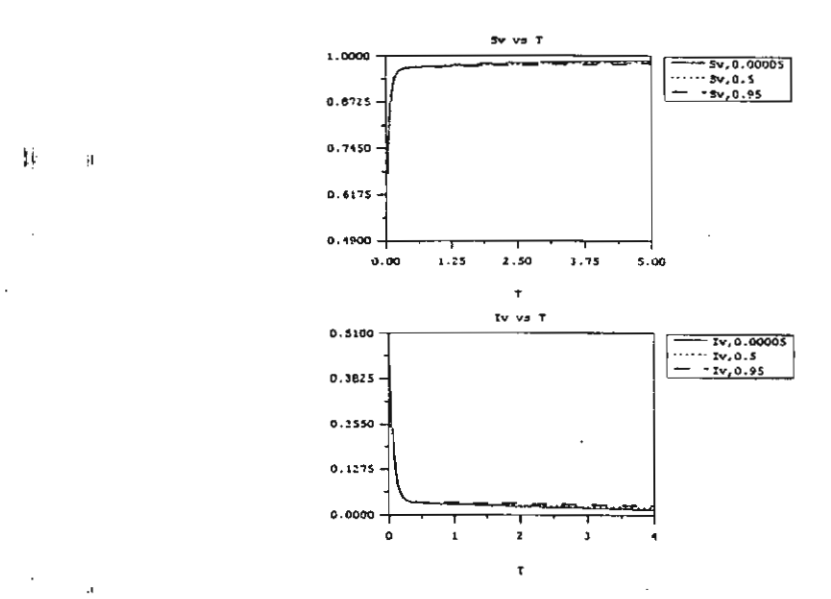


Fig 5. The behaviour of the mosquito proportions  $S_{\nu}$  and  $I_{\nu}$  with time (years) when p increases from 0.00005 to 0.5 and 0.95, respectively.

306

## Appendix

Diving Eq.(16) by  $b_1$ , we get

$$f(I_v^*) = I_v^{*3} + a_1 I_v^{*2} + a_2 I_v^* + a_3$$

where  $a_1 = \frac{b_2}{b_1}$ ,  $a_2 = \frac{b_3}{b_1}$ , and  $a_3 = \frac{b_4}{b_1}$ . Since  $b_1 > 0$  and  $b_4 < 0$ ,  $a_3 < 0$ . We have [11]

$$\lim_{I_v^* \to \infty} f(I_v^*) = \infty \quad and \quad f(0) = a_3 < 0$$

Given the above, there is a cutting point  $I_{v,0}^* \in [0,\infty)$  at which  $f(I_{v,0}^*) = 0$ . We, however, require at least one positive real root for  $I_v^*$  in our domain,  $I_v^* \in [0,1]$ . For cubic equation, we have two possibility when  $f(I_v^*)$  is large where  $I_v^*$  is large  $(f(I_v^*) \to \infty \text{ as } I_v^* \to \infty)$ . We begin by differentiation  $f(I_v^*)$ . Doing this, we get

$$f'(I_n^*) = 3I_n^{*2} + 2a_1I_n^* + a_2$$

The zeros of this equation are located at the extrema of  $f(I_{\nu}^{*})$  and are at

$$I_{v}^{*} = \frac{-2a_{1} \pm \sqrt{4a_{1}^{2} - 12a_{2}}}{6} = -\frac{1}{3}a_{1} \pm \frac{1}{3}\sqrt{a_{1}^{2} - 3a_{2}}$$
i.e, 
$$I_{v,c_{1}}^{*} = -\frac{1}{3}a_{1} + \frac{1}{3}\sqrt{a_{1}^{2} - 3a_{2}} = -\frac{1}{3}a_{1} + \frac{1}{3}\sqrt{\Delta}$$
and 
$$I_{v,c_{2}}^{*} = -\frac{1}{3}a_{1} - \frac{1}{3}\sqrt{a_{1}^{2} - 3a_{2}} = -\frac{1}{3}a_{1} - \frac{1}{3}\sqrt{\Delta}$$

case 1: all roots are positive real

Since  $f(0) = a_3$ , all roots would not equal to zero. In this case, both turning points are positive real so we need

$$I_{v,c_2}^* = -\frac{1}{3}a_1 - \frac{1}{3}\sqrt{a_1^2 - 3a_2} > 0$$

$$a_1 < 0$$
 and  $-a_1 > \sqrt{a_1^2 - 3a_2}$  and  $\Delta > 0$   
 $a_1^2 > a_1^2 - 3a_2$   $a_1^2 > 3a_2$   
 $a_2 > 0$ 

The conditions for  $f(I_v^*)$  to have at least one positive real root are  $a_1 < 0, a_2 > 0$  and  $a_1^2 > 3a_2$ .

case 2: two negative and one positive real roots

In this case, we separate the behavior of turning points into 2 cases.

case 2.1: one turning point is negative and another one is positive. We need

$$\sqrt{a_1^2-3a_2}>-a_1$$
  $a_1\geq 0$  and  $-3a_2>0$   $a_2<0$ 

In this case,  $\Delta$  is always positive since  $a_2 < 0$ . The conditions for  $f(I_v^*)$  to have at least one positive real root are  $a_1 \ge 0$  and  $a_2 < 0$ .

case 2.2: one turning point is negative and another turning point is negative or zero. We need

$$a_1 > 0$$
 and  $a_1^2 \ge a_1^2 - 3a_2$  and  $\Delta > 0$   
 $a_2 \ge 0$   $a_1^2 > 3a_2$ 

The conditions for  $f(I_v^*)$  to have at least one positive real root are  $a_1 > 0, a_2 \ge 0$  and  $a_1^2 > 3a_2$ .

Moreover, [4] since  $f(I_{v,c_2}^*) > f(0) > 0$  and  $f(I_{v,c_1}^*) < 0$  so

$$\Omega^* = f(I_{v,c_1}^*)f(I_{v,c_2}^*) < 0$$

$$\Omega^* = \frac{4}{27}a_2^3 - \frac{1}{27}a_1^2a_2^2 + \frac{4}{27}a_1^3a_3 - \frac{2}{3}a_1a_2a_3 + a_3^2 < 0$$

By using 
$$a_1 = \frac{b_2}{b_1}$$
,  $a_2 = \frac{b_3}{b_1}$ , and  $a_3 = \frac{b_4}{b_1}$ ,  $\Omega^*$  becomes

$$\Omega = \frac{4}{27}b_1b_3^3 - \frac{1}{27}b_2^2b_3^2 + \frac{4}{27}b_2^3b_4 - \frac{2}{3}b_1b_2b_3b_4 + b_1^2b_4^2.$$

Conditions (i) to (iii) in (18) are proven.

For case (iv), complex case, the possibility to get at least one positive real root is only the case for one real and two complex conjugate roots. From mathematical handbook[12], let

$$Q = \frac{3a_2 - a_1^2}{9}, \qquad R = \frac{9a_1a_2 - 27a_3 - 2a_1^3}{54}$$
$$S = \sqrt[3]{R + \sqrt{Q^3 + R^2}}, \quad T = \sqrt[3]{R - \sqrt{Q^3 + R^2}}$$

The conditions for  $f(I_v^*)$  to have at least one positive real root are  $Q^3 + R^2 > 0$  and  $S + T > \frac{1}{3}a_1$ .

$$Q^{3} + R^{2} = \frac{1}{9^{3}} (27a_{2}^{3} - 27a_{1}^{2}a_{2}^{2} + 9a_{1}^{4}a_{2} - a_{1}^{6}) + \frac{1}{54^{2}} (81a_{1}^{2}a_{2}^{2} - 486a_{1}a_{2}a_{3} - 36a_{1}^{4}a_{2} + 27^{2}a_{3}^{2} + 108a_{1}^{3}a_{3} + 4a_{1}^{6}) > 0$$

$$Q^{3} + R^{2} = \frac{4}{27}a_{2}^{3} - \frac{1}{27}a_{1}^{2}a_{2}^{2} + \frac{4}{27}a_{1}^{3}a_{3} - \frac{2}{3}a_{1}a_{2}a_{3} + a_{3}^{2} > 0$$

this is the same as  $\Omega^*$ , so condition  $Q^3 + R^2 > 0$  is  $\Omega > 0$ . By substituing  $a_1 = \frac{b_2}{b_1}, a_2 = \frac{b_3}{b_1}$ , and  $a_3 = \frac{b_4}{b_1}$ , the condition  $S + T > \frac{1}{3}a_1$  becomes  $(\frac{1}{54b_1^3}(9b_1b_2b_3 - 27b_1^2b_4 - 2b_2^3) + (\frac{\Omega}{4})^{\frac{1}{2}})^{\frac{1}{3}} + (\frac{1}{54b_1^3}(9b_1b_2b_3 - 27b_1^2b_4 - 2b_2^3) - (\frac{\Omega}{4})^{\frac{\Omega}{2}})^{\frac{1}{3}} > \frac{b_2}{3b_1}$ 

### References

- [1] L. Edelstein-Keshet, "Mathematical models in biology", Random House Inc., New York, 1988, 233-234.
- [2] L. Esteva and C. Vargas, Analysis of Dengue Disease Transmission Model, Math. BioSci. 150(1998), 131-161.
- [3] A. Kammanee, N. Kanyamee and I.M. Tang, Basic Reproduction Number for Transmission of Plasmodium Vivax Malaria, Southeast Asian J. Trop. Med. Public Health32[4](2001), 702-706.
- [4] Q. J. A. Khan and D. Greenhalgh, Hopf bifurcation in epidemic models with a time delay, IMA J.Math.Appl.Med.Biol.16(1999), 113-142.
- [5] C. Luxemburger, M. V. Vugt, S. Jonathan, R. McGready, S. Looareesuwan, N. J. White and F. Nosten, Treatment of vivax malaria on the western border of Thailand, Trans. R. Soc. Trop. Med. Hyg. 93(1999), 433-438.
- [6] G. MacDonald, "The Epidemiology and Control of Malaria", Oxford Univ. Press, London, 1957.
- [7] P. Martents and L. Hall, Malaria on the move: Human population movement and malaria transmission, Emerging Infectious Disease 6[2](2000), 103-109.
- [8] F. E. McKenzie, Why Model Malaria?, Parasitology Today, 16[12](2000), 511-516.
- [9] R. Ross, "The Prevention of Malaria", 2nd ed., Murray, London, 1991.
- [10] R. M. Anderson and R. M. May, "Infectious diseases of humans: Dynamics and Control", Oxford Uni. Press, 1992, 375-428.
- [11] S. Ruan and J. Wei, On the zeros of a third degree exponential polynomial with applications to a delayed model for the control of testosterone secretion, IMA J.Math.Appl.Med.Biol.,18(2001), 41-52.
- [12] M. R. Spiegel, "Mathematical handbook of formulas and tables", McGraw-Hill Inc., 1990.
- [13] WHO, World malaria situation in 1994, Weekly Epidemiological Record, WHO 72[38], 1997, 285-292.
- [14] http: www.britannica.com/bcom/cb/article/310,5716,1092831+40,00.html, 2000.

Computational Mathematics and modeling, An International Conference, CMM2002, Bangkok Copyright©by East-West J. of Mathematics.

All rights of reproduction in any form reserved.



**PERGAMON** 

Mathematical and Computer Modelling 37 (2003) 949-961

MATHEMATICAL AND COMPUTER MODELLING

www.elsevier.nl/locate/mcm

# Transmission of Dengue Hemorrhagic Fever in an Age Structured Population

#### P. Pongsumpun

Department of Mathematics, Faculty of Science, Mahidol University Bangkok 10400, Thailand

I. M. TANG\*

Department of Physics, Faculty of Science, Mahidol University Bangkok 10400, Thailand

and

Institute of Science and Technology for Research and Development Salaya Campus, Mahidol University Nakorn Pathom 71730, Thailand scimt@mahidol.ac.th

(Received May 2001; revised and accepted December 2002)

Abstract—The influence of age structure in the human population in the susceptible-infected recovered (SIR) model used to describe the transmission of Dengue hemorrhagic fever (DHF) is studied. The human population is separated into an adult class and juvenile class with the transmission of the disease being different in the two classes. Two equilibrium states are found and the condition for stability of one of these states, the disease free state, is established. The stability of the endemic state of this model is discussed. A simplified version of the model, one in which no adults become sick, is introduced. The conditions for the stability of the endemic state of this latter model are determined. Numerical calculations show that age structure in the simplified model reduces the periods of oscillations in the susceptible human population, the infected human population, and the infected mosquito population and the tightness of the spiraling into the endemic equilibrium state. © 2003 Elsevier Science Ltd. All rights reserved.

Keywords---Disease transmission, Dengue hemorrhagic fever, Age structure, SIR model.

#### 1. INTRODUCTION

Mathematical modeling of disease transmission has a long history. In 1911, an epidemiology model for malaria transmission was developed by Ross [1]. MacDonald [2] later added a layer of biological realism to the model by providing careful interpretation and estimation of the parameter, which should go into the model. McKenzie [3] has pointed out that the utility of a model depends not as much on how well a mathematical job has been accomplished but on how well a particular question has been translated. If one is interested in disease transmission, it is imperative that

<sup>\*</sup>Author to whom all correspondence should be addressed.

Both authors would like to thank the Thailand Research Fund (TRF) for financial support. P. Pongsumpun would especially like to thank TRF for awarding her a Royal Golden Jubilee Ph.D. Scholarship.

<sup>0895-7177/03/\$ -</sup> see front matter © 2003 Elsevier Science Ltd. All rights reserved. Typeset by AMS-TEX PII: S0895-7177(03)00111-0

the model describes as closely as possible the characteristics of the disease being transmitted. In this paper, we are interested in the transmission of Dengue hemorrhagic fever (DHF).

Dengue hemorrhagic fever is one of the emerging viral diseases spreading throughout the tropical regions of the world. From its first appearance in the Philippines in 1953, it has become the most important arthropod-borne viral diseases of humans [4]. It has been estimated that there are between 50 and 100 million cases of Dengue fever (DF) a year, over 250,000 cases of Dengue hemorrhagic fever (DHF) with approximately 10,000 infant deaths due to the latter form of this disease. The classical Dengue fever is a disease of older children and adults. DHF on the other hand is primarily a disease of children under the age of 15, see [5]. DHF differs from DF by the manifestation of plasma leakage in DHF. DF and DHF are illnesses arising through an infection by any one of the four serotypes of a virus belonging to the genus Flavirus, in the family Flavicidae. Immunity to one serotype does not confer immunity to the others. Since two of the transmitting vectors, Aedes aegypti and Aedes albopictuus mosquitoes, exist in the Americas, it has been possible for DHF and its benign precursor, DF, to become endemic in the New World, see [6]. The first severe outbreak of DHF in the Americas occurred in 1981 in Cuba with 116,000 hospitalized patients, 34,000 documented DHF cases, and 158 deaths. Important outbreaks of DHF have also occurred in Mexico, see [7].

In hopes of understanding the mechanisms that allow the invasion and persistence of a serotype of the Dengue virus in a region, Esteva and Vargas [8–10] introduced a mathematical model to provide a qualitative assessment for the problem. The model they used is based on the susceptible-infected-recovered (SIR) model often used to model the dynamics of transmission of some diseases. They showed that the endemic state was globally stable whenever a parameter  $R_o$  called the basic reproduction number is greater than one. Application of an ultra low volume (ULV) amount of insecticides (the standard method used to control the spread of Dengue fever and other arthroped-borne disease) could reduce the value of  $R_o$  to below one. The value of  $R_o$  would return to the above one value once the application is stopped and since the endemic state is globally stable, the disease would return. Therefore, the eradication program would have to be a continuing one.

In the SIR model used by Esteva and Vargas, no age structure was incorporated into the models. While the lack of an age structure may be appropriate for describing the 1981 DHF epidemic in Cuba [11] and the DHF outbreak in Santiago de Cuba in 1997 [12], it is not appropriate for Thailand. Most DHF cases in Thailand occur in children less than 15 years old, in agreement with the remark made by Gubler [5]. Feng and Velasco-Hernandez [13] have pointed to the need for a model that incorporates age structure into the Dengue population dynamics. It is the purpose of this paper to report on a DHF transmission model, which includes an age structure in the human population. In our model, the human population is divided into two classes, a juvenile class and an adult class. In Section 2, we introduce a mathematical model describing the transmission of DHF in a two class age structure of the human population. A mathematical analysis of this model is done in Section 3. In Section 4, we perform a complete analysis of a simplified model, one in which no further infection occurs in the adult population. Numerical solutions of the simplified model are presented in Section 5.

#### 2. MATHEMATICAL MODEL

The simplest way to incorporate an age structure into a disease model is to divide up the human population into two classes, juveniles (J) and adults (A). Another way is to divide the population into N cohorts and then divide up the cohorts into the three subcategories, susceptible, infected, and recovered. This latter approach (leading to what is known as a realistic age structure (RAS) approach) would make an analytical analysis difficult and one would have to resort to simulations [14]. We have chosen the first method since it allows us to establish the conditions leading to the disease free state and the endemic state. We have allowed infection to occur in both classes but with rate of infection in the adult class being much lower than that in

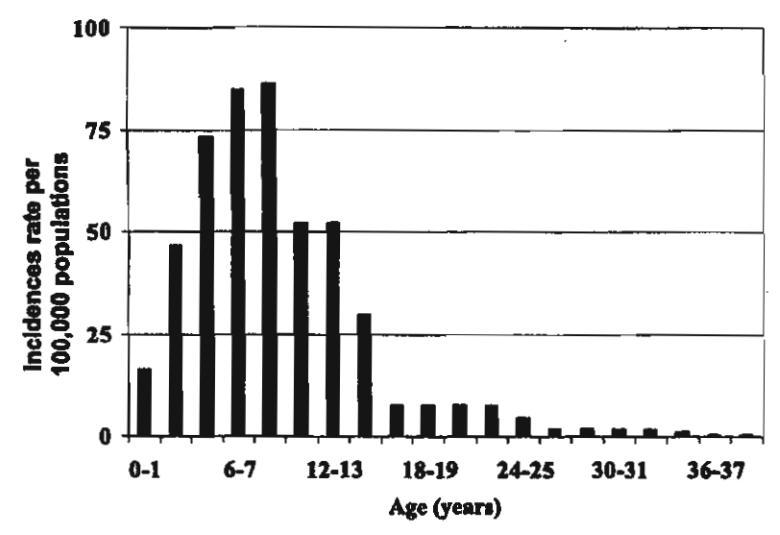


Figure 1. Age distribution of the 1998 Dengue fever incidence rates in Mukdahan, a province in central Thailand.

the juvenile class. In Figure 1, we show the age distribution of the incidence rates in one province in Thailand during the 1998 DHF epidemic [15]. As we see, most cases occur in children under the age of 15. However, a small number of cases do occur in older people. Similar distributions are seen in the other provinces in the country.

Most adults in the population have been exposed to the infection even though they are not aware of it. Burke et al. [16] reported that 87% of the infected children in his study (done in Bangkok, Thailand in 1980–1981) were either asymptomatic or minimally symptomatic. Antibodies against the virus will still develop in these infected children. This silent population will enter into adulthood, immune to further infections. The adult population will then be composed of people who are known to have been infected, members of the silent population and people who were never infected as a juvenile. We have initially classified all the adults as susceptible adults  $S_A$ , because of the uncertainty of which group the adult comes from. Treating all adults as being the same leads to the rate of transmission of the virus from a mosquito to a susceptible adult to be the average of the transmission rates to the different subclasses the adults came from. This leads the transmission rates of the virus to a (average) susceptible adult to be much lower than that to a susceptible juvenile.

In our SIR model with age structure, the dynamics of each component of the human is given by

$$\frac{dS'_J}{dt} = \lambda' N_T - \frac{b\beta_J}{N_T + m} S'_J I'_v - (\mu_h + \delta) S'_J, \tag{1a}$$

$$\frac{dR'_{J}}{dt} = rI'_{J} - (\mu_{h} + \delta)R'_{J}\frac{dI'_{J}}{dt} = \frac{b\beta_{J}}{N_{m} + m}S'_{J}I'_{v} - (\mu_{h} + \delta + r)I'_{J},\tag{1b}$$

$$\frac{dS'_A}{dt} = \delta(S'_J + I'_J + R'_J) - \varepsilon \beta_J \frac{b}{N_T + m} S'_A I'_v - \mu_h S'_A, \tag{1c}$$

$$\frac{dR_A'}{dt} = rI_A' - \mu_h R_A',\tag{1d}$$

and

١,٩

şį

$$\frac{dI_A'}{dt} = \epsilon \beta_J \frac{b}{N_T + m} S_A' I_v' - (\mu_h + r) I_A', \tag{1e}$$

where  $S'_{J(A)}$ ,  $I'_{J(A)}$ , and  $R'_{J(A)}$  are the numbers of susceptible juveniles (adults), infected juveniles (adults), and recovered juveniles (adults), respectively;  $N_T$ , the total population (taken to be constant); m, the number of other animals the mosquitoes can bite; b, the average number of

bites a mosquito takes per day;  $\lambda'$ , the birth rate;  $\mu_h$ , the death rate (assumed to be the same for all categories);  $\delta$ , the rate at which the juveniles pass into adulthood, and r is the rate at which the infected juveniles recover.  $I'_{\nu}$  is the number of infected mosquitoes;  $\beta_J$ , the probability of the virus surviving in the juvenile after being bitten by an infected mosquito [8], and  $\varepsilon\beta_J$  is the probability of the virus surviving in a susceptible adult after being bitten by an infected mosquito.  $\varepsilon$  is the ratio between the probability that an adult becomes infected and the probability that a juvenile becomes infected by the bite of an infected mosquito and is assumed to be less than one.

If we add equations (1a)-(1f) together, we get

$$\frac{d(S'_J + I'_J + R'_J + S'_A + I'_A + R'_A)}{dt} = \lambda N_T - \mu_h \left( S'_J + I'_J + R'_J + S'_A + I'_A + R'_A \right). \tag{2a}$$

For the total human population to be constant, i.e.,  $\frac{dN_T}{dt} = 0$ , the birth rate would have to be equal to the death rate,  $\lambda = \mu_h$ . If we now add only equations (1a)-(1c) together, we get

$$\frac{dN_J}{dt} = \lambda N_T - (\mu_h + \delta)N_J, \tag{2b}$$

where  $N_J (= S_J' + I_J' + R_J')$  is the total number of juveniles. Assuming that the total number of juveniles is also constant, equation (2b) would give us the ratio between the number of adults and the number of juveniles, i.e.,

$$\frac{N_A}{N_J} = \frac{\delta}{\mu_b},$$

where  $N_A$  is the total number of adults and is equal to  $S'_A + I'_A + R'_A$ .

The dynamics of the mosquitoes is described by

$$\frac{dS'_{v}}{dt} = A - \frac{b\beta_{v}}{N_{T} + m} S'_{v} (I'_{J} + I'_{A}) - \mu_{v} S'_{v}$$
(3a)

and

$$\frac{dI'_{v}}{dt} = \frac{b\beta_{v}}{N_{T} + m} S'_{v} (I'_{J} + I'_{A}) - \mu_{v} I'_{v}, \tag{3b}$$

where  $S'_v$  and  $I'_v$  the number of susceptible and infected mosquitoes, respectively;  $\mu_v$ , the death rate of the mosquitoes; A, the carrying capacity of the environment (for the mosquitoes) and  $\beta_v$  is the probability that a Dengue virus transmitted to the mosquito from an infected human, be it a juvenile or adult. If we add equations (3a) and (3b) together, we get

$$\frac{d(S_v' + I_v')}{dt} = A - \mu_v N_v, \tag{3c}$$

where  $N_v$  is the number of mosquitoes and is equal to  $S'_v + I'_v$ . If the number of mosquitoes is also constant, equation (3c) gives  $N_v = A/\mu_v$ .

Introducing the normalized parameters  $S_{J(A)} = S_{J(A)'}/N_{J(A)}$ ,  $I_{J(A)} = I'_{J(A)}/N_{J(A)}$ ,  $R_{J(A)} = R'_{J(A)}/N_{J(A)}$ , and  $I_v = I'_v/(A/\mu_v)$ , we find that equations (1a)–(1f) and equation (3b) can be rewritten as

$$\frac{dS_J}{dt} = (\mu_h + \delta)(1 - S_J) - \gamma_h S_J I_v, \tag{48}$$

$$\frac{dI_J}{dt} = \gamma_h S_J I_v - (\mu_h + \delta + r) I_J, \tag{4b}$$

$$\frac{dS_A}{dt} = \mu_h - \varepsilon \gamma_h S_A I_v - \mu_h S_A, \tag{4c}$$

$$\frac{dI_A}{dt} = \varepsilon \gamma_h S_A I_v - (\mu_h + r) I_A, \tag{4d}$$

Transmission of Dengue Hemorrhagic Fever

953

and

$$\frac{dI_{v}}{dt} = \gamma_{vJ}(1 - I_{v})I_{J} + \gamma_{vA}(1 - I_{v})I_{A} - \mu_{v}I_{v}, \tag{4e}$$

where

$$\gamma_h = \frac{b\beta_J(A/\mu_v)}{N_T + m} \tag{5a}$$

and

1

$$\gamma_{vJ(A)} = \frac{b\beta_v N_{J(A)}}{N_T + m}. (5b)$$

The dynamical equations for  $R_{J(A)}$  and  $S_v$  are not needed, since  $S_{J(A)} + I_{J(A)} + R_{J(A)} = 1$  and  $S_v + I_v = 1$ .

#### 3. MATHEMATICAL ANALYSIS

#### 3.a. Equilibrium States

The equilibrium states  $(S_J, I_J, S_A, I_A, I_v)$  are obtained by setting the RHS of equations (4a)–(4e) to zero. Doing this, we get two equilibrium states, the disease free state  $E_o = (1, 0, 1, 0, 0)$  and the endemic state  $E_1 = (S_J*, I_J*, S_A*, I_A*, I_v*)$  where

$$S_{J^*} = \frac{1}{1 + (\gamma_h/(\mu_h + \delta))I_{v^*}},$$
 (6a)

$$I_{J}* = \frac{b\beta_{J}(A/\mu_{v})}{(N_{T} + m)(\mu_{h} + r)}S_{J}*I_{v}*, \tag{6b}$$

$$S_A * = \frac{1}{1 + \varepsilon (b\beta_J(A/\mu_v))/(\mu_h(N_T + m))} I_v *, \tag{6c}$$

and

$$I_{A}* = \varepsilon \frac{b\beta_{J}(A/\mu_{v})}{(\mu_{h} + r)(N_{T} + m)} S_{A} * I_{v}*, \tag{6d}$$

with  $I_v^*$  being the solution of

$$A_1(I_{\nu}^*)^2 + A_2I_{\nu}^* + A_3 = 0, \tag{7a}$$

with

$$A_1 = \varepsilon \gamma_h^2 \left[ \frac{\gamma_{vJ}}{\mu_h(\mu_h + r + \delta)} + \frac{\gamma_{vA}}{(\mu_h + r)(\mu_h + \delta)} + \frac{\mu_v}{\mu_h(\mu_h + \delta)} \right], \tag{7b}$$

$$A_{2} = \frac{\gamma_{h}\gamma_{vJ}}{\mu_{h} + r + \delta} + \frac{\gamma_{h}\mu_{v}}{\mu_{h} + \delta} + \varepsilon\gamma_{J} \left[ \frac{\mu_{v}}{\mu_{h}} + \frac{\gamma_{vA}}{\mu_{h} + r} - \frac{\gamma_{h}\gamma_{vJ}}{\mu_{h}(\mu_{h} + r + \delta)} - \frac{\gamma_{h}\gamma_{vA}}{(\mu_{h} + r)(\mu_{h} + \delta)} \right], \tag{7c}$$

and

.1

į

$$A_3 = \mu_h - \gamma_h \left[ \frac{\gamma_{vJ}}{\mu_h + r + \delta} + \varepsilon \frac{\gamma_{vA}}{\mu_h + r} \right], \tag{7d}$$

with  $\gamma_h$ ,  $\gamma_{vA}$ , and  $\gamma_{vJ}$  defined by equations (5a) and (5b).

#### 3.b. Local Asymptotical Stability

E The local stability of an equilibrium state is determined from the Jacobian (gradient) matrix of the RHS of the above set of differential equations evaluated at the equilibrium state.

#### 3.b.1. Disease free state

For the system defined by equation (4a)-(4e), the Jacobian matrix evaluated at  $E_o$  is the  $5 \times 5$ matrix given by

$$\begin{vmatrix}
-(\mu_{h} + \delta) & 0 & 0 & 0 & -\gamma_{h} \\
0 & -(\mu_{h} + r + \delta) & 0 & 0 & \gamma_{h} \\
0 & 0 & -\mu_{h} & 0 & -\varepsilon\gamma_{h} \\
0 & 0 & 0 & -(\mu_{h} + r) & \varepsilon\gamma_{h} \\
0 & \gamma_{vJ} & 0 & \gamma_{vA} & -\mu_{v}
\end{vmatrix}.$$
(8)

The eigenvalues are obtained by solving the matrix equation,  $\det |\lambda I - J| = 0$ . Using the program MATHEMATICA, (Wolfram Research, Champaign, IL) to evaluate the determinant, we get the following characteristic equation:

$$(\lambda + \mu_h + \delta)(\lambda + \mu_h)(\lambda^3 + A\lambda^2 + B\lambda + C) = 0, \tag{9}$$

where

$$A = (\mu_h + r) + (\mu_h + r + \delta) + \mu_v, \tag{10}$$

$$B = (\mu_h + r)(\mu_h + r + \delta) + \mu_v(\mu_h + r + \delta)(1 - R_1) + \mu_v(\mu_h + r)(1 - \varepsilon R_2), \tag{11}$$

and

$$C = \mu_{\nu}(\mu_h + r)(\mu_h + r + \delta)(1 - R_o'), \tag{12}$$

with

$$R_1 = rac{b^2 eta_v eta_J N_J (A/\mu_v)}{\mu_v (N_T + m)^2 (\mu_h + r + \delta)},$$
 $R_2 = rac{b^2 eta_v eta_J N_A (A/\mu_v)}{\mu_v (N_T + m)^2 (\mu_h + r)},$ 

and

(iii)

$$R_o' = R_1 + \varepsilon R_2. \tag{13}$$

Looking at the characteristic equation, equation (9), we see that two of the eigenvalues are

$$\lambda_1 = -(\mu_h + \delta) \quad \text{and} \quad \lambda_2 = -(\mu_h + r + \delta). \tag{14}$$

Both of these are negative. The signs of the other three eigenvalues can be ascertained by the use of the Routh-Hurwitz conditions [18]

(i) 
$$A > 0$$
,  
(ii)  $C > 0$ , and (15)  
(iii)  $AB > C$ .

Looking at equation (10), we see that Condition (i) is always satisfied. Condition (ii) is satisfied if  $R'_{o} < 1$ . To see when Condition (iii) is satisfied, we note that the cross product AB will be the sum of positive terms if  $R_1 < 1$  and  $R_2 < 1$ . Given that the sum of positive numbers is greater than any individual number, we have  $AB > \mu_v(\mu_h + r)(\mu_h + r + \delta)(2 - R_o')$  (this being the sum of the product of the first term in A and the second term in B and the product of the second term in A and the third term in B).  $\mu_v(\mu_h + r)(\mu_h + r + \delta)(2 - R'_o) > C$ . We therefore have AB > C. From the definition of  $R'_o$ ,  $R'_o < 1$  implies  $R_1 < 1$  and  $R_2 < 1$ . Thus, the real parts of the three eigenvalues determined from

$$\lambda^3 + A\lambda^2 + B\lambda + C = 0$$

will be negative. Combining this with the signs of the first two eigenvalues, equation (14), we see that all the real parts of all eigenvalues are negative. Thus, the disease free state will be a locally asymptotically stable state when  $R_o < 1$ .

#### 3.b.2. Endemic state

1.

The stability of the epidemic state,  $E_1$ , like that of  $E_0$ , is determined by looking at the eigenvalues of the Jacobian evaluated at  $E_1$ . The Jacobian for this state is

$$\begin{vmatrix}
-(\mu_{h} + \delta) - \gamma_{h} I_{v} * & 0 & 0 & 0 & -\gamma_{h} S_{J} * \\
\gamma_{h} I_{v} * & -(\mu_{h} + r + \delta) & 0 & 0 & \gamma_{h} S_{J} * \\
0 & 0 & -\mu_{h} - \varepsilon \gamma_{h} I_{v} * & 0 & \varepsilon \gamma_{h} S_{J} * \\
0 & 0 & \varepsilon \gamma_{h} I_{v} * & -(\mu_{h} + r) & -\varepsilon \gamma_{h} S_{J} * \\
0 & \gamma_{vJ} (1 - I_{v} *) & 0 & \gamma_{vA} (1 - I_{v} *) -\mu_{v} - \gamma_{vA} I_{A} * -\gamma_{vJ} I_{J} *
\end{vmatrix}, (16)$$

where  $S_{J^*}$ ,  $I_{J^*}$ ,  $S_{A^*}$ ,  $I_{A^*}$ , and  $I_{v^*}$  are given by equation (5a)–(5d) and equation (6). The 5 × 5 matrix equation, det  $|\lambda I - J| = 0$ , can again be solved by MATHEMATICA. MATHEMATICA can also diagonalize the above Jacobian. The characteristic equation will be a fifth-order polynomial in  $\lambda$  and the expressions for the eigenvalues will be very long and complicated, preventing an easy analysis. We find out that an easy analysis can be made if we make a further simplifying assumption, no adults become sick with DHF.

#### 4. SIMPLIFIED MODEL

Looking at the medical records of Department of Pediatrics, Siriraj Hospital, the largest health care hospital in Bangkok, Thailand, out of the 318 patients with confirmed DHF who were admitted in 1998, only two were above the age of 15; of the 137 patients admitted in 1999, only one was above 15 years old; out of 84 patients admitted in 2000, again only one was above 15 years old and out of 332 patients admitted in 2001, none were above 15 years old. From these records, it appears that in Bangkok, the adults have only a small or no chance of becoming sick with DHF. To overcome the untractable mathematical nature of the analysis of the epidemic state encountered in our original model, we have looked at a model in which adults do not become sick with the disease. Such a model can be obtained by setting  $\varepsilon$  to be zero. Doing this, the 5 × 5 Jacobian matrix given by equation (16) takes on a much simplified form. But before we find the eigenvalues of the new Jacobian, let us review some additional modifications we will have made.

We now assume that the reason for the adults not becoming sick with DHF is that they are immune to the infections. The categories  $I'_A$  and  $R'_A$  would no longer exist and all the adults fit into one category,  $S'_A$ . The dynamics of the human population is given by

$$\frac{dS'_J}{dt} = \lambda' N_T - \frac{b\beta_J}{N_T + m} S'_J I'_v - (\mu_h + \delta) S'_J, \tag{17a}$$

$$\frac{dI_J'}{dt} = \frac{b\beta_J}{N_T + m} S_J' I_v' - (\mu_h + \delta + r) I_J', \tag{17b}$$

$$\frac{dR'_J}{dt} = rI'_J - (\mu_h + \delta)R'_J,\tag{17c}$$

and

4.

$$\frac{dS'_{A}}{dt} = \delta(S'_{J} + I'_{J} + R'_{J}) - \mu_{h}S'_{A}. \tag{17d}$$

In the absence of infected adults, the dynamics of the mosquitoes are now given by

$$\frac{dS_v'}{dt} = A - \frac{b\beta_v}{N_T + m} S_v' I_J' - \mu_v S_v'$$
(18a)

and

$$\frac{dI_v'}{dt} = \frac{b\beta_v}{N_T + m} S_v' I_J' - \mu_v I_v'. \tag{18b}$$

Introducing the new set of normalized parameters  $S = S'_J/N_T$ ,  $I = I'_J/N_T$ ,  $R = R'_J/N_T$ ,  $S_A = S'_A/N_T$ , and  $I_v = I'_v/(A/\mu_v)$ , equations (17a)–(18b) reduce to

$$\frac{dS}{dt} = \lambda - \gamma_h I_v S - (\mu_h + \delta) S, \tag{19a}$$

$$\frac{dI}{dt} = \gamma_h S I_v - (\mu_h + r + \delta) I, \tag{19b}$$

$$\frac{dR}{dt} = rI - (\mu_h + \delta)R,\tag{19c}$$

and

$$\frac{dI_{v}}{dt} = \gamma_{v}(1 - I_{v})I - \mu_{v}I_{v}, \qquad (19d)$$

$$\gamma_{\rm v} = \frac{b\beta_{\rm v}N_T}{(N_T + m)}.\tag{19e}$$

It should be noted that  $\gamma_v$  differs from  $\gamma_{vJ}$  in that it has an  $N_T$  instead in the numerator. The dynamical equations for  $S_A$  and  $S_v$  are not needed since  $S+I+R+S_A=1$  and  $S_v+I_v=1$ . The requirement that  $N_T$  be a constant leads to the condition that the birth rate,  $\lambda$  is equal to the death rate,  $\mu_h$ .

#### 4.a. Endemic Equilibrium States

Setting the RHS of equations (19a)-(19d), we obtain endemic equilibrium state  $E_1 = (S*, I*, R*, I*_V)$ , where

$$S* = \frac{\beta + M}{((\mu_h + \delta)/\mu_h)(\beta + MX_o)}, \tag{20a}$$

$$I* = \frac{(X_o - 1)}{\beta + MX_o},\tag{20b}$$

$$R* = \left(\frac{r}{\mu_h + \delta}\right) \left(\frac{X_o - 1}{\beta + MX_o}\right),\tag{20c}$$

and

$$I_{v}^{*} = \beta \left( \frac{X_{o} - 1}{X_{o}[M + \beta]} \right), \tag{20d}$$

where

$$X_o = \frac{\mu_h \gamma_h \gamma_v}{\mu_v (\mu_h + \delta)(\mu_h + \delta + r)},$$
 (21a)

$$M = \frac{\mu_h + \delta + r}{\mu_h},\tag{21b}$$

and

$$\beta = \frac{\gamma_v}{\mu_v}.\tag{21c}$$

For the endemic state to be meaningful,  $X_o > 1$ . Equations (20a), (20b), and (20d) have the same form as those in Esteva and Vargas's paper [8] except for the definitions of  $X_o$  (the basic reproduction number  $(R_o)$  in [8]) M and the presence of some prefactors. In the limit,  $\delta$  goes to zero and there is no differentiation between adults and juveniles, they are the same.

#### 4.b. Local Asymptotical Stability

For the system defined by equation (19a)-(19d), the Jacobian matrix evaluated at  $E_1$  is the  $4 \times 4$  matrix given by

$$\begin{vmatrix}
-(\mu_{h} + \delta) - \gamma_{h} I_{v} * & 0 & 0 & -\gamma_{h} S * \\
0 & -(\mu_{h} + \delta + r) & 0 & \gamma_{h} S * \\
0 & r & -(\mu_{h} + \delta) & 0 \\
0 & \gamma_{v} (1 - I_{v} *) & 0 & -\mu_{v} - \gamma_{h} I *
\end{vmatrix}.$$
(22)

Using MATHEMATICA to diagonalize this matrix, we obtain the following characteristic equation;

$$(\lambda + \mu_h + \delta) \left( \lambda^3 + A\lambda^2 + B\lambda + C \right) = 0, \tag{23}$$

where

$$A = (\mu_h + \delta) \left( \frac{\beta + MX_0}{\beta + M} \right) + \mu_h M + \mu_v X_0 \left( \frac{\beta + M}{\beta + MX_0} \right), \tag{24}$$

$$B = \mu_h(\mu_h + \delta)M\left(\frac{\beta + MX_0}{\beta + M}\right) + \mu_v(\mu_h + \delta)X_0 + \mu_v\mu_h M\beta\left(\frac{X_0 - 1}{\beta + MX_0}\right),\tag{25}$$

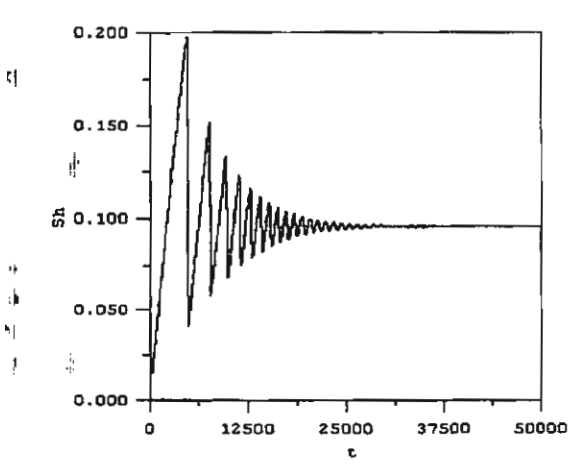
and

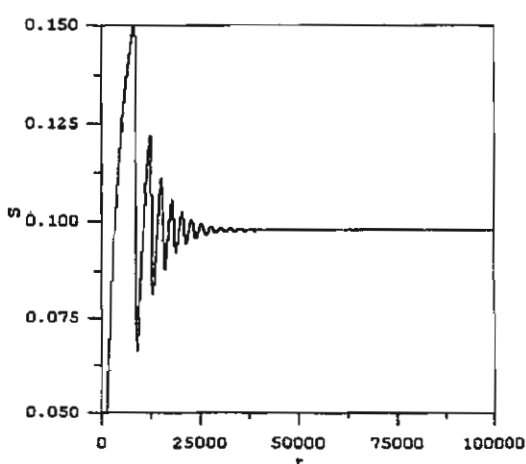
+

$$C = \mu_{\nu}(\mu_h + r)(\mu_h + r + \delta)(X_o - 1), \tag{26}$$

where  $X_0$ , M, and  $\beta$  are given by equations (21a)-(21c). The real parts of the eigenvalues are negative when the coefficients A, B, and C satisfy the Routh-Hurwitz condition given by equation (15). Looking at equation (23), we see that Condition (i) is always satisfied. Conditions (ii) and (iii) are satisfied when  $X_0 > 1$ . (To see that Condition (iii) is satisfied when  $X_0 > 1$ , we note that the cross product  $AB > \mu_v \mu_h (\mu_h + \delta) M X_o$  (this being the product of the second terms in A and B). This term is larger than C. We thus have AB > C.)

This shows that if  $X_0 > 1$ , the real parts of all the eigenvalues of the Jacobian evaluated at the endemic state are negative. Thus, the equilibrium state  $E_1(S*, I*, R*, I_v*)$  given by equations (20a)–(20d) is a locally asymptotically stable state. Since the simplified model is obtained

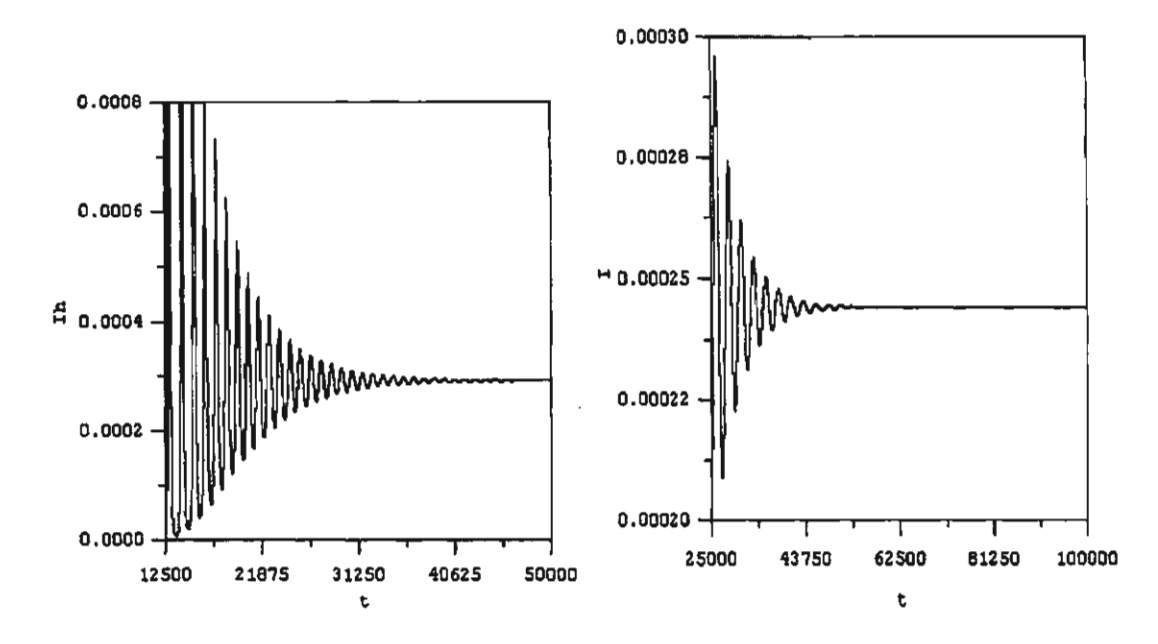




(a) Solution of equation (2) in [7] for an SIR model of Dengue fever transmission with no age structure.

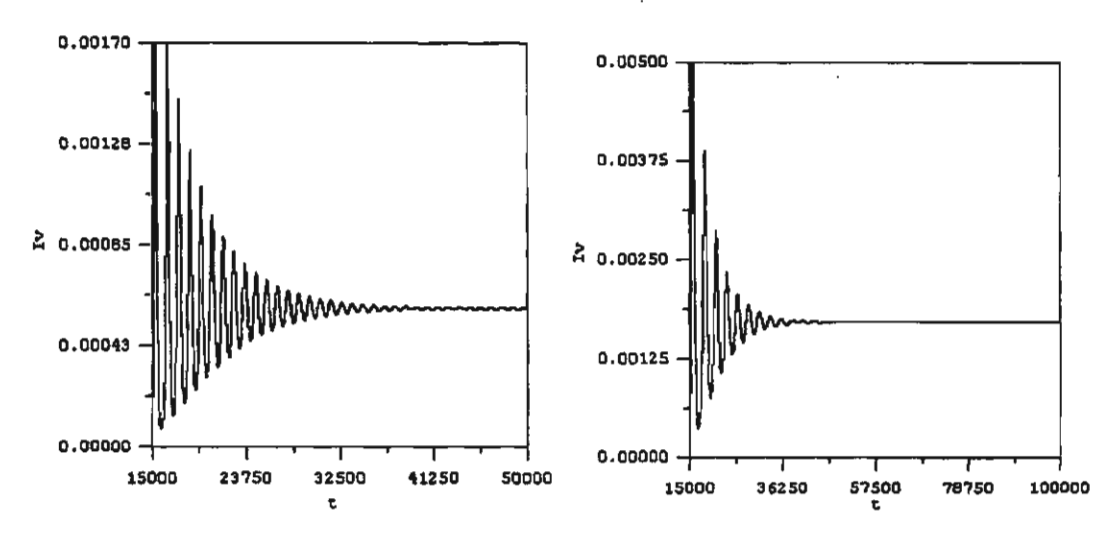
(b) Solution of equation (3a) of the present text for a SIR model having an age structure. The values of the parameters are given in the text.

Figure 2. Number of susceptible humans as a function of time.



- (a) Solution of equation (2) in [7].
- (b) Solution of equation (3b) for a SIR model having an age structure.

Figure 3. Number of infected humans as a function of time.



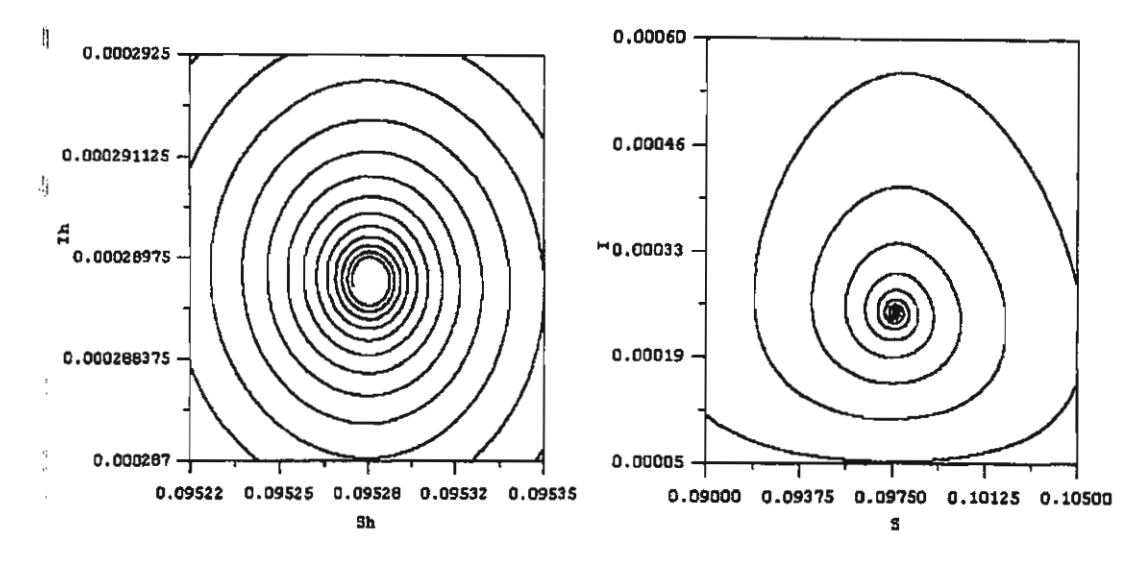
- (a) Behavior in a nonage structured SIR model.
- (b) Behavior in an age structured model.

Figure 4. Number of infected mosquitoes as a function of time.

from equations (1a)-(1f) by setting  $\varepsilon$  to zero and dropping the categories  $I_A$ ,  $R_A$ , one would expect that an analysis similar to the one done in Section 3.b.1 would yield the same results (except that  $\varepsilon$  would be equal to 0). When  $\varepsilon$  in  $R_0'$  is set to zero, we find that  $R_0' = R_1$ , which is the same as  $X_0$  after  $N_J$  has been replaced by  $\mu_h N_T/(\mu_h + \delta)$  (this being what  $N_J$  is equal to) in the definition of  $R_1$ . We can therefore conclude that when  $X_0 < 1$ , the equilibrium state is the disease free state and that this state is locally asymptotically stable.

#### 4.c. Numerical Studies

The main effect of introducing an age structure into the model is to change the definition of the basic reproduction rate. Using the values of the parameters similar to those used by Esteva and Vargas ( $\mu_h = 0.0000456$ ,  $\mu_v = 0.23$ , b = 0.3,  $\beta_h = 0.75$ ,  $\beta_v = 1.0$ , m = 0.0, r = 0.343,  $N_T =$ 



(a) Behavior in a nonage structured SIR model.

4

k.

(b) Behavior in an age structured model. The equilibrium states in both cases are stable spiral nodes.

Figure 5. Plot of number of susceptible and infected humans.

10,000, A=5000), the value of the basic reproduction number defined in [8] would be 10.3. Numerically solving the set of equations given by Esteva and Vargas [8, equation (2)], we obtain the time development of the susceptible humans as seen in Figure 2a. In Figure 2b, we show the solution to equation (3a). The values of some of the parameters have been changed (i.e.,  $\delta=0.000283$ , A=200, and  $\tau=0.0713$ , with the others staying the same). Substituting these values into equation (16), we get  $R_0=1.8$ . In Figures 3 and 4, we show the time development of the infected humans and infected mosquitoes for the case of no age structure and an age structure model. In Figure 5, we plot the number of infected humans versus the number of susceptible humans in both a nonage structure population and age structure population. The values of the parameters are such that for both populations, the equilibrium state is the endemic state. The endemic state is the stable spiral state. As we see, the periods of fluctuations in the number of individuals in each class are much shorter in the absence of any age structure. The spiraling in is much more severe in the absence of the age structure. The age structure appears to calm down the fluctuations.

#### 5. DISCUSSION

The square of the basic reproduction number is the number of secondary infections, which can result from one primary infection. For a disease to be capable of invading and establishing itself in a host population, this must be greater than one. If the number is less than one, then every successive generation will diminish in size until its number approaches zero. To determine what this number is, we note that an infected juvenile (adult) will be bitten by

$$\frac{b(A/\mu_v)}{(N_T+m)(\mu_h+r+\delta)} \left( \frac{b(A/\mu_v)}{(N_T+m)(\mu_h+r)} \right) \tag{27}$$

mosquitoes during the time juvenile (adult) is infectious. Of these mosquitoes, a portion of them will become infected (the above numbers multiplied by  $\beta_v$ ). One of these infected mosquitoes will in turn bite

 $\frac{bN_J}{(N_T+m)\mu_v}$  juveniles and  $\frac{bN_A}{(N_T+m)\mu_v}$  adults .

during its lifetime. Multiplying the first number by  $\beta_J$  and the second by  $\epsilon\beta_J$ , we get the number of juveniles and adults infected by an infectious mosquito. Multiplying the number of juveniles

infected by the number of mosquitoes infected during the lifetime of the infectious juvenile, we get

$$\frac{\mu_h b^2 \beta_v \beta_J N_J (A/\mu_v)}{\mu_v (N_T + m)^2 (\mu_h + \delta + r)}.$$
 (28)

If we multiply the number of infectious adults infected by the number of mosquitoes infected during the lifetime of the infectious adults, we get

$$\varepsilon \frac{\mu_h b^2 \beta_v \beta_h N_A (A/\mu_v)}{\mu_v (N_T + m)^2 (\mu_h + r)}.$$
 (29)

Adding these two numbers together, we obtain the basic reproduction number. The sum of equation (28) and (29) is the  $R'_0$  given by equation (21).

The different models for disease transmission have yielded expressions for the basic reproduction number. These expressions have provided insights into the control of the various diseases. One of the first expressions obtained was the basic reproduction number for the spread of malaria. It is given by

$$R_o = \frac{b^2 \beta_v \beta_h m}{\mu_v (\mu_h + r)},\tag{30}$$

where m is the ratio between the mosquito population and the human population. Based on the epidemiological data, Molineaux and Gramiccia [18] estimated  $R_0$  to be 80 for the malaria epidemic in northern Nigeria. The implication of this (each infective person infects 80 other people) points to possible shortcoming of the model. It was pointed out by MacDonald that the malaria transmission model did not take into account an incubation period during which mosquito is not infectious. Taking this period into account, MacDonald obtained a new expression for the basic reproduction number

$$R_o = \frac{b^2 \beta_v \beta_h m}{\mu_v (\mu_h + r)} e^{-\mu_v \tau}, \tag{31}$$

where  $\tau$  is the incubation period of the malaria parasite in the mosquito [19]. Equation (31) points to the fact that if the incubation period is longer than the life expectancy of the mosquito, the disease will not be established since the mosquito will die before it becomes infectious. The appearance of an exponential factor containing the life expectancy of the mosquito has led to the changes in the strategy for controlling malaria, exterminate the mosquito during its adult state and not in its larva stage.

#### REFERENCES

- 1. R. Ross, The Prevention of Malaria, Second Edition, Murray, London, (1911).
- 2. G. MacDonald, The Epidemiology and Control of Malaria, Oxford University Press, London, (1957).
- 3. F.E. McKenzie, Why model malaria?, Parasitology Today 16, 511-516, (2000).
- T.P. Monath, Dengue. The risk to developed and developing countries, Proc. Nat. Acad. Sci. USA 91, 2395-2400, (1994).
- 5. D.J. Gubler, Dengue and dengue hemorrhagic fever, Clin. Mirobiol. Rev. 11, 480-491, (1998).
- Pan American Health Organization, Dengue and Dengue hemorrhagic fever in the Americas: Guidelines for prevention and control, Washington DC, PAHO, Scientific Publication #548, (1994).
- J.F. Mendez Galvan and R.M. Castellanos, Manual para la viglancia epideniologica del Dengue, Secretaria de Salud, DF, Mexico, (1994).
- L. Esteva and C. Vargas, Analysis of a dengue disease transmission model, Math. BioSci. 150, 131-151, (1998).
- Esteva and C. Vargas, A model for dengue disease with variable human population, J. Math. Bio. 38, 220-240, (1999).
- L. Esteva and C. Vargas, Influence of vertical and mechanical transmission on the dynamics of Dengue disease, Math. Biosci. 167, 51-64, (2000).
- M.G. Guzman, G.P. Kouri, J. Bravo, M. Solet, S. Vasquez, M. Santos, R. Villaescusa, P. Basanta, G. Indan and J.M. Ballester, Dengue hemorrhagic fever in Cuba. II. Clinical investigations, Trans. R. Soc. Trop. Med. Hyg. 78, 239-241, (1984).

- M.G. Guzman, G.P. Kouri, L. Valdes, J. Bravo, M. Alvarez, S. Vasquez, I. Delgado and S.B. Halstead, Epidemiologic studies on dengue in Santiago de Cuba, 1997, Am. J. Epidemiol. 152, 793-799, (2000).
- Z. Feng and J.X. Velsco-Hernandez, Competitive exclusion in a vector-host model for the Dengue fever, J. Math. Bio. 35, 523-544, (1997).
- D.A. Focks, E. Daniels, D.G. Haile and J.E. Kleesling, A simulation model of the epidemiology of urban dengue: Literature analysis, model development, preliminary validation and samples of simulation results, Am. J. Trop. Mede. Hyg. 53 (5), 489-506, (1995).
- Annual Epidemiological Surveillance Report, 1992–1998, Division of Epidemiology, Ministry of Public Health, Royal Thai Government.
- D.S. Burke, A. Nisalak, D.E. Johnson and R.M. Scott, A prospective study of dengue infections in Bangkok, Am. J. Trop. Mede. Hyg. 38 (1), 172-180, (1988).
- J.E. Marsden and M. McCracken, The Hopf Bifurcation and Its Applications, Springer-Verlag, New York, (1976).
- 18. L. Molineaux and G. Gramiccia, The Garks Project, World Health Organization, Geneva, (1980).
- 19. R.M. Anderson and R.M. May, Infectious Diseases of Humans, Oxford University, Oxford, (1992).



Available online at www.sciencedirect.com



ECOLOGICAL MODELLING

Ecological Modelling 167 (2003) 213-220

www.elsevier.com/locate/ecolmodel

## Cannibalism in an age-structured predator-prey system

C. Kaewmanee a, I.M. Tang b,\*

<sup>a</sup> Department of Mathematics, Faculty of Science, Mahidol University, Bangkok 10400, Thailand
<sup>b</sup> Department of Physics and Center for Nanoscience, Faculty of Science, Mahidol University, Bangkok 10400, Thailand

Received 18 April 2001; received in revised form 29 May 2002; accepted 11 October 2002

#### Abstract

The effect of cannibalism on an age-structured predator-prey system is studied. Three stable equilibrium states are found. Using a Hopf bifurcation analysis, it is found that the non washout steady state looses its stability as the cannibalism attack rate increases past a bifurcation point  $S_c$ . The dependence of the bifurcation point on the other parameters in the model is found. It is shown that the trajectory of the solution spirals in for attack rates  $S < S_c$  and exhibits limit cycle behavior for  $S > S_c$ . © 2003 Elsevier B.V. All rights reserved.

Keywords: Predator-prey; Cannibalism; Hopf bifurcation; Limit cycle

#### 1. Introduction

Under what circumstances is cannibalism adaptive? For evolutionary games being played on a small part of nature's stage, one could measure the rewards of the games in terms of expected future reproductive success, i.e. by seeing whether the species goes extinct or not. To win the game, one looks for an evolutionary stable strategy (ESS) (Maynard-Smith, 1982). An ESS is a population strategy that yields a higher reward than any other feasible mutant strategies. The nature of the strategy depends on the values of the ecological parameters, which are present at the time. Change the time and the ESS may be different, e.g. it may be one of the mutant strategies or it could be a completely new one.

An intuitive belief of biologists is that evolution should favor behaviors with the lowest cost to the

that of BSE. Cannibalism, thus leads to a higher mor-

species practicing them (Mesterton-Gibbons and

Adams, 1998). Because it costs energy to breed and

E-mail address: scimt@mahidol.ac.th (I.M. Tang).

0304-3800/\$ - see front matter © 2003 Elsevier B.V. All rights reserved. doi:10.1016/S0304-3800(03)00190-X

because cannibalism would waste this energy, evolution would not select cannibalism as a desirable trait. Another reason is that intraspecific feeding facilitates the spread of prion proteins (abnormal protein growth in the brain and other internal organs) among the individuals within the species. The presence of these proteins in the brains leads to fatal diseases such as bovine spongiform encephalopathy (BSE) in cows, trans-missible spongiform encephalopathy (TSE) in sheep and kuru in the Fore people of New Guinea. The first two diseases are not due to cannibalism per se, but are the result of eating feed meal made from ground up diseased animals of the same species. The much dreaded disease vCJD (variant Creutzfeldt--Jakob disease) is due to the interspecific transmission of bovine prion proteins from the cow to the human. Because the bovine prion is foreign to humans, the efficacy of the transmission would be much less than that of intraspecific transmission. This is one of the reasons for the incidence of vCJD not being as wide spread as

<sup>\*</sup> Corresponding author. Present address: Institute of Science & Technology for Research & Development, Mahidol University, Nakorn Pathom 71730, Thailand.

tality rate and animals that practice it would then be at a competitive disadvantage with those who do not.

Having said the above, it was surprising when two recent mathematical studies of cannibalism showed that cannibalism could stabilize a predator-prey system. Kohlmeier and Ebenhöh (1995) found that the cannibalism of the predator could lead to an increase of the standing stocks of both the prey and predator. The authors were surprised by this result since as they pointed out, it is contrary to intuitive expectation. Van den Bosch and Gabriel (1997) have pointed out that in the absence of cannibalism, the system of equations used in by Kohlmeier and Ebenhöh (KE) has for certain parameter combinations an unstable internal steady state. For these parameter combinations, predator-prey cycles occur. Cannibalism suppresses these cycles since increasing cannibalism attack rates causes the internal steady state to change from being unstable to being stable. We would like to point out that the model of KE employs a Holling type II functional response. This means that they are using a model that contains predatory switching. The reason for pointing this out is that several studies (see for instance, Pelletier, 2000) have shown that prey switching has a strong stabilizing effect on a multi-species ecosystem.

In their paper, Van der Bosch and Gabriel went on to improve the predator-prey model by incorporating an age structure in the predator population. It was reasoned that cannibalism usually involves larger (adult) predators eating smaller (juvenile) predators and so an age structure would be required to properly describe the predator-prey relation. The predator-prey cycles in their study are generated by the age structure while the cycles seen in KE's study are due to the interaction between the logistic prey growth and the hyperbolic functional response. Increasing the cannibalism attack rate would diminish the effects of the age structure. The fluctuations (cycles) would, therefore, be suppressed implying that cannibalism stabilized the predator-prey system.

Recently, Magnusson (1999) has reexamined the effects of cannibalism on the predator-prey system. He found that cannibalism has a destabilizing effect. For the case of large prey carrying capacity of the environment, Magnusson finds that as the cannibalism attack rate is increased, the non washout equilibrium point (a stable spiral point) becomes unstable via a Hopf

bifurcation. He goes on to state that the loss of stability is not possible without a high juvenile mortality rate and a low adult recruitment rate. We have studied cannibalism in an age-structured predator—prey system described by the same set of basic equations as those used by Magnusson but with a different set of scaling parameters. The new set of equations allows us to follow the loss of stability for all values of the parameters in the model (not just those for large carrying capacity, high juvenile mortality rates and low adult recruitment rate) as the cannibalism attack rate is changed continuously. Like Magnusson, we use an analysis based on the Hopf bifurcation theory. We have found the dependence of the bifurcation point on the values of the other parameters in the system.

In this study, we have ignored any structure, which may occur in the juvenile population. In their study, Van den Bosch and Gabriel proposed that only juveniles of an age within the "cannibalism window" would be vulnerable to cannibalism by adults. Juveniles of age below this window would be too small to satisfy the hunger of the adults or would be protected by their mothers. Older juveniles would be active enough to get away from the adults. This brings up the question of whether the old juveniles should be reclassified as young (immature) adults. In this type of population structure, it is not the age, which counts, but the size. The population model should, therefore, be called a size-structured population model (Cushing, 1992).

A true age-structured population model is achieved when the juvenile population or, the adult population or the whole population is divided into discrete age groups regardless of other distinctions. The division of the juvenile population is often done in the study of the transmission of childhood diseases (Anderson and May, 1992). These studies are often referred to as being realistic age-structured population model studies. The division of the adult population has been used in a study of fishery management (Allen and Miranda, 1998). The erratic recruitment of a specie of fish (crappie) year to year has caused difficulties in the development of management strategies of this fish. Allen and Miranda divided the adult population into cohorts of fishes entering into the population each year and followed the progression of each cohort as they are subjected to various life and death factors. Many population studies (Roughgarden, 1979) divide

up the whole population into different age groups and see what the age distribution would be under different circumstances.

It has been noted that cannibalism in certain species are often directed at the egg or larvae of the specie. This would necessitate the division of the juveniles into different developmental stages. Yang et al. (1997) divided the citrus rust mite population into four populations: egg, protonymph, deutonymph and adults in their studies of the population dynamics of fruit mite-fungal pathogen system. Krivan and Havelka (2000) divided the gall-midge juvenile population into three sub populations: egg, larvae and pupae, in their study of the use of gall-midge for biological control of pests. This type of division leads to what would be better called a stage-structured population model.

Having pointed out that "juvenile" (nonadult) population often has an internal structure, we will nevertheless assume that the juvenile population is a single group. Cushing (1991) remarked that even a simple two-age class population model with appropriate negative and positive feedbacks due to cannibalism can account for several important phenomena concerning cannibalistic populations. Cushing's study differs from ours in that it uses discrete time, while this work is based on a continuous time development. In Section 2, we introduce the model and obtain the equilibrium states, while in Section 3, we perform a stability analyses of both washout and non washout equilibrium states. In Section 4, we study the effects of cannibalism on the stability of the non washout state. We present the numerical solutions, which show the transition from a steady state behavior to a limit cycle behavior as the attack rate increases past the critical attack rate. In Section 5, we present some conclusions.

#### 2. The model

The ecosystem in our model consists of a single predator species, a prey population and the vegetation. The predator population is divided into juvenile predators (denoted by Y) and adult predators (denoted by X). The prey population may consist of several herbivore species, but since we use only one set of parameters to describe their interaction with each other and the rest of the ecosystem, the prey population is treated as being a single species (denoted by Z). We assume that

the prey population is subjected to a logistic growth condition. Magnusson makes the implicit assumption that there is a second prey species present. The second species is required since Magnusson allows for the possibility that the predator population can exist when the primary prey species becomes extinct. The equations describing their ecosystem do not contain any reference to the second prey population. The second species would, therefore, be invisible to the predator species, meaning that the predators could not feed on them when the primary prey species becomes extinct. The fourth steady state  $(x_0, y_0, 0)$  obtained by Magnusson would, therefore, be impossible. In our ecosystem, the different species interact via some sort of mass action inaction. This leads to the time rate of change of the prey population density to be given by

$$\frac{\mathrm{d}Z}{\mathrm{d}t} = (T - UZ)Z - VZX \tag{1}$$

where T is the net rate of growth; T/U, the prey carrying capacity and VX is the increase in the prey's mortality rate due to predation by the adult predator. As we have pointed out, Kohlmeier and Ebenhöh use a Holling type II functional response to describe the predation. Its use means that the predation will change depending on whether the population density of the prey or predator is high or low. This is probably a better description of the actual predation seen in nature. Since we are interested in this paper on the effects of cannibalism, we have used the simplest description, i.e. predation is described by a constant value. In writing Eq. (1), we have assumed that juvenile predators do not eat any prey. They obtain their subsistence from their parents.

The time rates of change of the predator populations are given by

$$\frac{\mathrm{d}X}{\mathrm{d}t} = AY - \mu_{a}X + \gamma SXY + CXZ \tag{2}$$

and

$$\frac{\mathrm{d}Y}{\mathrm{d}t} = \lambda X - AY - \mu_{\mathrm{j}}Y - SXY \tag{3}$$

where A is the recruitment rate (rate at which juveniles mature into adults);  $\mu_a$  ( $\mu_j$ ), mortality rate of the adult (juvenile) predator; S, the cannibalism attack rate;  $\gamma SY$  and CZ, the increases in the adult mortality rate due to being better fed through eating juveniles and prey, respectively, and  $\lambda$  is the birth rate of the predators.

Looking at Eqs. (2) and (3), we see that there are five (plus the two mortality rates) parameters whose values have to be assigned. There are three additional parameters in Eq. (1). We can reduce the number of parameters by making the following change of variables (a rescaling):

$$x = \frac{V}{\mu_a}X$$
,  $z = \frac{C}{\mu_a}Z$ ,  $y = \frac{VA}{\mu_a}Y$ 

and

$$\tau = \mu_a T. \tag{4}$$

Making these changes, Eqs. (1)–(3) assume the much simpler form

$$\frac{dx}{d\tau} = y - x + xz + \gamma' sxy, \quad \frac{dy}{d\tau} = rx - my - sxy$$

and

$$\frac{\mathrm{d}z}{\mathrm{d}z} = (t - uz - x)z\tag{5}$$

where s = S/V,  $\gamma' = \gamma \mu_a/A$ ,  $t = T/\mu_a$ ,  $r = RA/\mu_a^2$ , u = U/C and  $m = (A + \mu_j)/\mu_a$ . The rescaling here is different from those introduced by Magnusson. We believe that they are better since they allow for the role of the cannibalism attack rate to be followed more closely (s is directly proportional to the cannibalism attack rate).

The equilibrium (or steady state) points are obtained by setting the LHS of Eq. (5) to zero. Doing this, we get the following equilibrium points E(x,y,z);

$$E_1 = (0, 0, 0), \tag{6a}$$

$$E_2 = \left(0, 0, \frac{t}{u}\right) \tag{6b}$$

and

$$E_3 = (x^*, y^*, z^*)$$
 (6c)

where

$$x^* = \frac{\delta + \sqrt{\delta^2 - 4s(mu - ru - tm)}}{2s},\tag{7a}$$

$$y^* = \frac{rx^*}{m + sx^*} \tag{7b}$$

and

$$z^* = \frac{t - x^*}{u} \tag{7c}$$

with  $\delta = st - su - m + \gamma' sru$ . It can be shown that the term appearing in the square root in Eq. (7a) is always positive. The requirement that  $x^* > 0$ , places certain restrictions on the values of the parameters. Their values must be such that  $st - su - m + \gamma' sru > 0$  and mu - ru - tm < 0. We will discuss the stability of the three equilibrium points in the next section. We do not find a fourth equilibrium point  $E_4$ . As we have mentioned, the existence of the equilibrium point at  $(x_0, y_0, 0)$  would imply that it would be possible for the predators to exist in the absence of food to eat.

#### 3. Stability analysis

The stability of the equilibrium points is determined by first linearizing the system of first-order differential equations and then assuming that the solutions vary as  $\exp \{\lambda t\}$  where the  $\lambda s$  are the eigenvalues of the Jacobian matrix evaluated at the equilibrium point. The equilibrium point is a stable point if all the eigenvalues are real and negative; unstable point if they are real and positive and is a saddle point if two of them are real and of opposite signs. If the eigenvalues are complex, the equilibrium points are stable spiral points or unstable spiral points if the real parts of the eigenvalues are negative or positive.

#### 3.1. Predator washout states (0, 0, 0) and (0, 0, t/u)

The Jacobian matrix for the present set of differential equations is

$$\begin{pmatrix} -1 + z' + \gamma' s y' & 1 + \gamma' s x' & x' \\ r - s y' & -m - s x' & 0 \\ -z' & 0 & t - x' - 2uz' \end{pmatrix}$$
(8)

where x', y' mad z' are the values of rescaled variables at the equilibrium point. For the first predator washout state, the diagonalization of the Jacobian matrix yields the following characteristic equation

$$(\lambda - t)(\lambda^2 + (m+1)\lambda + (m-r)) = 0. \tag{9}$$

The eigenvalues for the washout state (0, 0, 0) are

$$\lambda_1 = t > 0$$

and

$$\lambda_{2.3} = \frac{-(m+1) \pm \sqrt{(m+1)^2 - 4(m-r)}}{2}.$$
 (10)

For m > r and m > -1,  $\lambda_{2,3}$  are both negative. Therefore, the washout equilibrium state is a saddle point.

Evaluating the Jacobian matrix at the second washout point (0, 0, t/u), we find that the eigenvalues for this equilibrium point are

$$\lambda_{1} = -t$$
and
$$-(1 + m - (t/u))$$

$$\lambda_{2,3} = \frac{\pm \sqrt{(1+m-(t/u))^{2}-4(m-r-(t/u)m)}}{2}$$
.

It can be shown that all of these eigenvalues will be negative if

$$1 - \frac{t}{u} > \frac{r}{m}.\tag{12}$$

If the values are the parameters satisfy condition (11), then (0, 0, t/u) is a stable equilibrium. If the opposite is true, then (0, 0, t/u) will be an unstable saddle point.

The eigenvalues of the Jacobian evaluated at the non washout equilibrium point are the roots of the following cubic equation

$$\lambda^3 + a_2 \lambda^2 + a_1 \lambda + a_0 = 0 \tag{13}$$

where

$$\begin{split} a_0 &= z^* \left[ mu \left( z^* + \frac{r}{m} - 1 \right) + x^* (m + sx^*) \right], \\ a_1 &= uz^* \left( \frac{y^*}{x^*} + r \frac{x^*}{y^*} \right) + x^* z^* - m \left( 1 - z^* - \frac{r}{m} \right) \end{split}$$

and

$$a_2 = \frac{y^*}{x^*} + r \frac{x^*}{y^*} + uz^* \tag{14}$$

where  $x^*$ ,  $y^*$  and  $z^*$  are given by Eqs. (7a)–(7c). Given  $a_0$ ,  $a_1$  and  $a_2$ , we now define

$$q = \frac{1}{3}a_1 - \frac{1}{9}a_2^3, \quad r = \frac{1}{6}(a_1a_2 - 3a_0) - \frac{1}{27}a_2^3.$$

$$S_{1,2} = [r \pm (q^3 + r^2)^{1/2}]^{1/3}.$$
(15)

If  $q^3 + r^2 > 0$ ,  $\lambda_1$  and  $\lambda_2$  would be the complex conjugate of each other and  $\lambda_3$  would be real.

In terms of the above constants, the three eigenvalues of the Jacobian matrix are

$$\lambda_{1,2} = -\frac{1}{2}(S_1 + S_2) - \frac{a_3}{3} \pm i \frac{\sqrt{3}}{2}(S_1 - S_2)$$

and

$$\lambda_3 = (S_1 + S_2) = \frac{a_2}{3}. (16)$$

Now if the values of the parameters are such that

$$\frac{-2a_2}{3} < S_1 + S_2 < \frac{a_2}{3},$$

the real parts of all three eigenvalues would be negative and the non washout state  $E_3$  would be stable.

## 4. Effect of cannibalism on stability of non washout state

#### 4.1. Bifurcation point

A Hopf bifurcation occurs (see Marsden and Mc-Cracken, 1976) when for some critical value of the bifurcation parameter (which we take in this study to be the cannibalism attack rate), the following are true

- (a)  $Re \lambda_{1,2}(s^*) = 0$
- (b)  $Re \lambda'_{1,2}(s^*) \neq 0$
- (c)  $Im \lambda_{1,2}(s^*) \neq 0$
- (d) The real parts of all other eigenvalues of the Jacobian evaluated at the steady state point negative.

From the above conditions, it can be shown that for Hopf bifurcation to occur, we need

$$a_0 > 0$$
,  $a_1 a_2 < a_0$ 

with

$$a_2 < 0$$
.

If we define  $s_1^*$  as the critical value where  $a_1(s_1^*)a_2(s_1^*)$ =  $a_0(s_1^*)$ , we get

$$s > s_1^* \equiv \frac{r}{y^*} \left( 1 + \frac{ru}{y^*} \right) + \frac{1}{z^* (x^*)^2} \times \left[ a \left( \frac{rx^*}{y^*} + \frac{y^*}{x^*} \right) + z^* (b + cxc^* + y^*) \right]$$
(17)

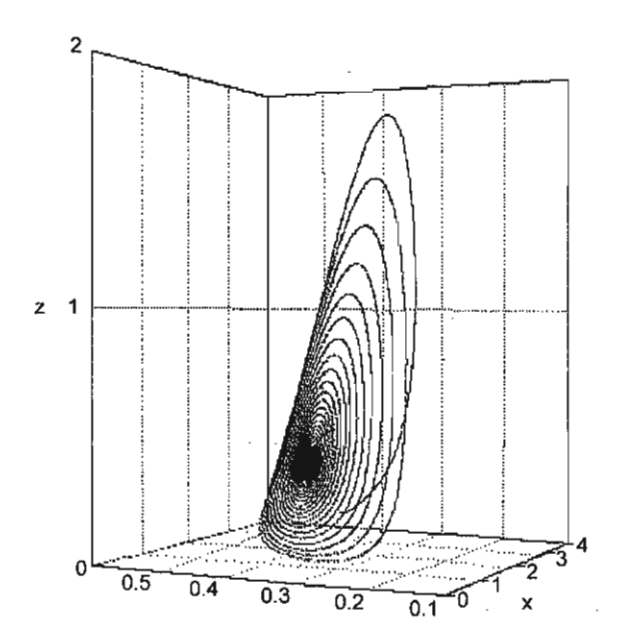


Fig. 1. Trajectory of the solution of Eq. (5) for values of the parameters lying in region II. X denotes the adult predator, Y, the juvenile predator and Z, the prey. The non washout steady state point is a stable spiral point. The values of the parameters are s = 0.9, m = 1,  $\gamma' = 1.5$ , r/m = 0.5 and u = 0.1.

where

$$a = m(z^* - 1) + (uz^*)^2 + r, \quad b = 2ru + \frac{u(y^*)^2}{(x^*)^2}$$

and

$$c = uz^* - m.$$

Next we define another critical value  $s_2^*$  as the value where  $a_0(s_2^*) = 0$ . This give us

$$s > s_2^* \equiv \frac{mu}{(x^*)^2} \left[ 1 - \frac{r}{m} - z^* - \frac{x^*}{u} \right].$$
 (18)

Since  $s > s_1^* > s_2^*$ , we can pick the bifurcation point  $s^*$  to be  $s_1^*$ .

#### 4.2. Description of parametric space

To study the effect of increasing the (rescaled) cannibalism attack rate 's', we introduce a hyperspace  $\Omega$  in which each point is designated by the values of s, r, m, t, u and  $\gamma'$ , i.e.  $(s', r', m', t', u', \gamma'')$ . In this hyperspace, there are families of hypersurfaces on which

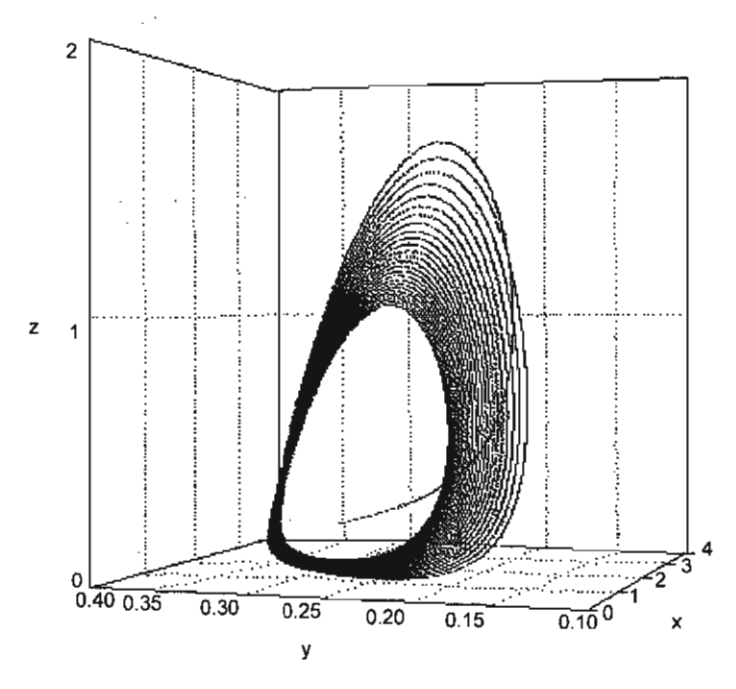


Fig. 2. Trajectory of the solution of Eq. (5) when s is changed to 1.0 which is greater than the critical bifurcation point  $s^* = 0.98$ . X denotes the adult predator; Y, the juvenile predator and Z, the prey. The values of all other parameters are the same as those used for Fig. 1. The bifurcation is a supercritical one.

the parameters have the values satisfying the relationship  $a_2 > 0$ . Each of the hypersurfaces are divided into three regions by the hypercurves  $a_0 = 0$  and  $a_1a_2 = a_0$ . In region I of the hypersurface, the values of the parameters are such that  $a_0 < 0$  and  $a_1a_2 >$  $a_0$ ; in region II, the values are such that  $a_0 > 0$  and  $a_1a_2 > a_0$ ; while in region III, the values are such that  $a_0 > 0$  and  $a_1 a_2 < a_0$ . Only the two washout states (0, 0, 0) and (0, 0, t/u) would be possible for values of the parameters in region I. The first would be a saddle point while the second would be a stable or unstable point depending on the initial conditions. The values of the parameters in region II would produce a phase solution trajectory which would spiral into the non washout steady state  $(x^*, y^*, z^*)$  given by Eqs. (7a)-(7c). For values of parameters in region III, the non washout steady state would lose its stability and the trajectory of the solution in phase space would jump to a limit cycle behavior.

#### 4.3. Numerical solutions

Given Eq. (14), we can calculate the value of the bifurcation point. Picking m = 1, y' = 1, r/m = 0.5 and t = 1.3, we have calculated  $s^*$  to be 0.98. Picking s = 0.9, we have a set of parameters belonging to region II. Numerically solving Eq. (5), we obtain the three-dimensional trajectory shown in Fig. 1. As we see, the trajectory spirals into the stable point  $(x^*, y^*, z^*)$ . If we change s (only) to 1.0, we would then be in region III. Now solving, Eq. (5), we get the limit cycle behavior seen in Fig. 2. Further increasing the value of s, yields limit cycle trajectories. All the bifurcations appear to be supercritical.

#### 5. Conclusion

Our numerical studies show that the predator non washout steady state solution of a predator-prey system looses its stability as the cannibalism attack rate increases beyond a critical value  $s^*$ . Whether or not this is adaptive depends on whether or not the predator species becomes extinct. Passage into a limit cycle behavior means that during some time in its life cycle, the predator will experience harshness in its life. This would cause nature to select those traits that would allow future descendants to have the ability to adapt to

changes in the environment. Many species who have reached the pinnacle of their food chain have become over specialized and have become extinct when nature changed; witness of the fate of the dinosaurs.

Magnusson has obtained results similar to ours. However, he restricts his conclusions to the case where there is high juvenile mortality and/or low recruitment rate and high conversion efficiency. One of the reasons for this is the nature of the rescaling he introduced. The only parameter appearing in his equations that depends on the cannibalism attack rate, depends on the inverse of attack rate. As the attack rate increases, its influence on the dynamics would decrease. Also, he assumes that the carrying capacity for the prey is high. This allows him to drop a very important factor in his predator—prey model (limitations due to logistic growth of the prey).

The appearance of oscillations in the populations in certain cannibalistic ecosystems has also been explained by Diekmann et al. (1986). Their approach is somewhat different from the one used in this study. They used integrodifferential equations to model their predator—prey interaction. Cushing (1991) has used difference equations to study the predator prey system. He finds that if the environmental resources are low and the net reproductive number is below replacement, then cannibalism might insure the survival of the species. All of this shows that the predicted outcome of cannibalism on a predator—prey system depends on the model used to model the system.

#### Acknowledgements

Two of the authors, Y.L. and I.M.T., would like to thank the Thailand Research Fund for financial support while doing this study.

#### References

Allen, M.S., Miranda, L.E., 1998. An age-structured model for erratic crappie fisheries. Ecol. Mod. 107, 289-303.

Anderson, R.M., May, R.M., 1992. Infectious Diseases of Humans, Dynamics and Control. Oxford University Press, Oxford.

Cushing, J.M., 1991. A simple model of cannibalism. Math. Biosci. 107, 47–71.

Cushing, J.M., 1992. A size-structured model for cannibalism. Theory Pop. Biol. 42, 347–361.

- Diekmann, O., Nisbet, R.M., Gurney, W.S.C., van den Bosch, F., 1986. Simple mathematical models for cannibalism: a critique and a new approach. Math. Biosci. 76, 21-46.
- Kohlmeier, C., Ebenhöh, W., 1995. The stabilizing role of cannibalism in a predator-prey system. Bull. Math. Biol. 57, 401-411.
- Krivan, K., Havelka, J., 2000. Leslie model for predatory gall-midge population. Ecol. Mod. 126, 73-77.
- Magnusson, K.G., 1999. Destablizing effect on cannibalism on a structured predator-prey system. Math. Biosci. 155, 61-75.
- Marsden, J.E., McCracken, M., 1976. The Hopf Bifurcation and Its Application. Springer-Verlag, New York.
- Maynard-Smith, J., 1982. Evolution and the Theory of Games. Cambridge University Press, Cambridge.

- Mesterton-Gibbons, M., Adams, E.S., 1998. Animal contests as evolutionary games. Am. Sci. 86, 334-341.
- Pelletier, J.D., 2000. Are large complex ecosystems more unstable?

  A theoretical reassessment with predator switching. Math.

  Biosci. 162, 91-96.
- Roughgarden, J., 1979. Theory of Population Genetics and Evolutionary Ecology: An Introduction. Macmillan, New York.
- Van den Bosch, F., Gabriel, W., 1997. Cannibalism in an age structured predator-prey System. Bull. Math. Biol. 59, 551-567.
- Yang, Y., Allen, J.C., Knapp, J.L., Stansly., , 1997. An age-structured population model of citrus rust mite: a fruit-mite-fungal pathogen system. Ecol. Mod. 104, 71-85.

# Dengue Haemorrhagic Fever in Thailand, 1998-2003: Primary or Secondary Infection

by

M Sriprom\*, P Pongsumpun\*, S Yoksan\*\*, P Barbazan\*\*\*,
J P Gonzalez\*\* and I M Tang\*\*

\*Department of Mathematics, Faculty of Science, Mahidol University, Bangkok 10400, Thailand

\*\*Department of Physics, Faculty of Science, Mahidol University, Bangkok 10400, Thailand

\*\*Center for Vaccine Development, Institute of Science and Technology for Research and Development,

Mahidol University, Nakhon Pathom 73170, Thailand

\*Research Center of Emerging Viral Diseases IRD, Institute of Science and Technology for Research and Development, Mahidol University, Nakhon Pathom 73170, Thailand

#### \* Abstract

The pathogenesis of dengue haemorrhagic fever (DIHF) is tooked for in the serological records of DHF patients (mainly children) petween the ages of one month and 15 years) at Sirina Hospital in Thalland over a six-year period beginning 1998 (covering two three-year cycles) Based on the primary and secondary infections by both the haemagglutination inhibition assay (HI) test and the IgM capture enzyme linked unmunosorbent assay (ELISA) test, it was found that in 1998, 14 of the cases (g) which paired sera specimens were tested using both HI and ELISA (or 9.6% of 146 cases) had resulted from primary infections. In 1999, 2000, 2001, 2002, and the first half of 2003, three out of 57 cases (5.3%), six out of 48 cases (12.5%), 85 out of 293 cases (29%), 23 out of 90 cases (25.6%), and 16 out of 56 cases (28.6%), respectively, resulted from primary infections. The percentages of primary infections during the last three years are well above 14.0% reported for cases occurring in Bangkok between 1988 and 2003.

Keywords: Dengue haemomhagic fever, serological tests, primary secondary infection

#### Introduction

Dengue fever (DF) is a rather benign febrile disease, afflicting mainly older children and adults<sup>(1)</sup> and often remaining unapparent in young children<sup>(2)</sup>. The sudden onset of fever and a variety of non-specific signs and

symptoms characterize DF. The high fever lasts for two or three days, followed by additional symptoms. Its clinical presentations are similar to those of several other diseases, meaning thereby that many of the reported cases of DF could be due to other febrile illnesses and also that many

<sup>\*</sup> For correspondence: scimt@mahidol.ac.th

dengue infections are not recognized. During the 1977 epidemic in Santiago de Cuba<sup>(3)</sup>, only 3,012 out of 9,747 people who developed febrile illnesses and whose sera were tested, turned out to be infected with dengue fever. DF is caused by the dengue virus which belongs to the genus, *Flavivirus*, in the *Flaviviridae* family. There are four serotypes of this virus known as DEN-1, DEN-2, DEN-3 and DEN-4. Infection by any of the four serotypes causes similar clinical presentations, and confers permanent immunity to that particular serotype, but only a temporary one to the others.

The dengue virus is transmitted by the Aedes mosquitoes, i.e. Aedes aegypti and Aedes albopictus, in countries of South-East Asia. Introduction of the dengue virus by just one individual into a susceptible population residing in a locality where the above mosquitoes are prevalent can quickly lead to an epidemic. In many tropical countries, DF has now emerged as a major public health problem<sup>(4)</sup>.

The pathogenesis of dengue haemorrhagic fever (DHF) is still a matter of controversy. According to one school of thought<sup>(5)</sup>, pre-existing heterologous dengue antibodies recognize the infecting virus and form an antigen-antibody complex, which then binds the virus to the cell membrane of some leukocyctes. Since the antibodies are heterologous, the virus neutralized and is free to replicate once inside the cell. It is then thought that these mediators cells secrete vasoactive response to dengue infection. mediators cause an increased vascular permeability, which leads to hypovolemia and shock. Since the antibodies have to be pre-existing, this hypothesis terms it as the secondary infection or immune enhancement.

A cautionary note should be added here. It appears that the occurrence of DHF after a second infection depends on the strain of the serotype. During the 1996-1997 dengue epidemic in Belem Para, Brazil, none of the 24 patients who had been previously infected by the DEN-1 virus developed DHF after they had been reinfected by the DEN-2 virus(6). Watts et al(7) observed the same pattern during the 1995 epidemic in Iquitos, Peru. No cases of DHF/DSS were reported even though it was expected that between 887 to 10,247 cases would have occurred. The DEN-2 isolates were found to be of the American genotype (strain). Kochel et al(8), attributed the nonoccurrence of DHF/DSS to the presence of common envelope epitopes in both the American strain of the DEN-2 virus and the DEN-1 virus and the absence of these epitopes in the Asian strain of the DEN-2 virus. The common epitopes could have been acquired through the recombination between the American DEN-2 and the DEN-1 virus co-circulating in the Americas or through genetic drift (mutation).

The other school of thought<sup>(5)</sup> maintains that the mutation of the viruses could have produced viruses with greater virulence and therefore greater epidemic potential. DHF would then be due to the appearance of these mutant strains among the circulating virus. This second hypothesis does not presuppose the presence of pre-existing antibodies and so the DHF/DSS infection would be the result of a primary infection. In an attempt to contribute to this debate, we

reviewed the serological status of children suffering from DHF who were admitted to the Paediatrics ward of Siriraj Hospital (a tertiary-care medical centre with a 300-bed facility in Bangkok, Thailand) between 1998 and mid-2003. A similar review of children admitted to the Department of Paediatrics, Chulalongkorn Hospital, Bangkok, between 1985 and 1995 was made recently<sup>(9)</sup>.

definition of WHO<sup>(4)</sup>. Serological tests, i.e. haemagglutination inhibition (HI) assay<sup>(10)</sup> and IgM/IgG enzyme-linked immunosorbent assay (ELISA)<sup>(11)</sup>, were used to determine whether the patients had dengue virus infection. Attempts were made to isolate the virus on *Toxorhynchites* mosquito to identify the serotype of the virus responsible for the illness.

#### Materials and methods

## Criteria for primary and secondary infections

The World Health Organization (WHO)(4) has established a set of criteria to determine whether a case of dengue fever is due to primary or a secondary infection. The determination is based on the results of either HI tests or ELISA tests or both, done on a paired set of sera taken at least seven days apart, one in the acute phase and the other in the convalescence phase. The criteria for primary infection are that, for a paired set of sera specimens there should be a fourfold increase in the IgM antibody response and HI titers of any of the DEN serotypes and the IgM/IgG ratio should be HL ≥1.8 and/or the titers convalescence phase should be <1,280. The criteria for determining secondary infection are that the IgM/IgG ratio should be <1.8 and/or the HI titers in the convalescence phase should be ≥2,560.

#### **Patients**

Admission to the ward was based on the clinical presentation of DHF as per the case

#### Results

The results of the laboratory survey are given in the Table. Of the 1,183 patients admitted, the serological tests established that 1,082 of them were confirmed as of DHF. A total of 214 patients were determined to be due to primary infections, 291 due to secondary infection and 577 remained undetermined. One hundred and one patients turned out not to be sick with DHF. The virus responsible for the infection was isolated in 373 cases. The predominant virus was DEN-1 (162), followed by DEN-2 (121), DEN-3 (70) and DEN-4 (17). Multiple viruses were found in three patients (not included in the table). On the basis of the serological tests and using the WHO criteria for primary and secondary infections, our study found that in 1998, 14 of the cases for which paired sera specimens were tested by both tests (or 9.6% of 146 cases) had resulted from primary infection. In 1999, 2000, 2001, 2002 and the first half of 2003, three out of 57 cases (5.3%), six out of 48 cases (12.5%), 85 out of 293 cases (29%), 23 out of 90 cases (25.6%) and 16 out of 56 cases (28.6%), respectively, had resulted from primary infection.

Table. Summary of the serological records of DHF patients admitted to Siriraj Hospital, 1998-2003

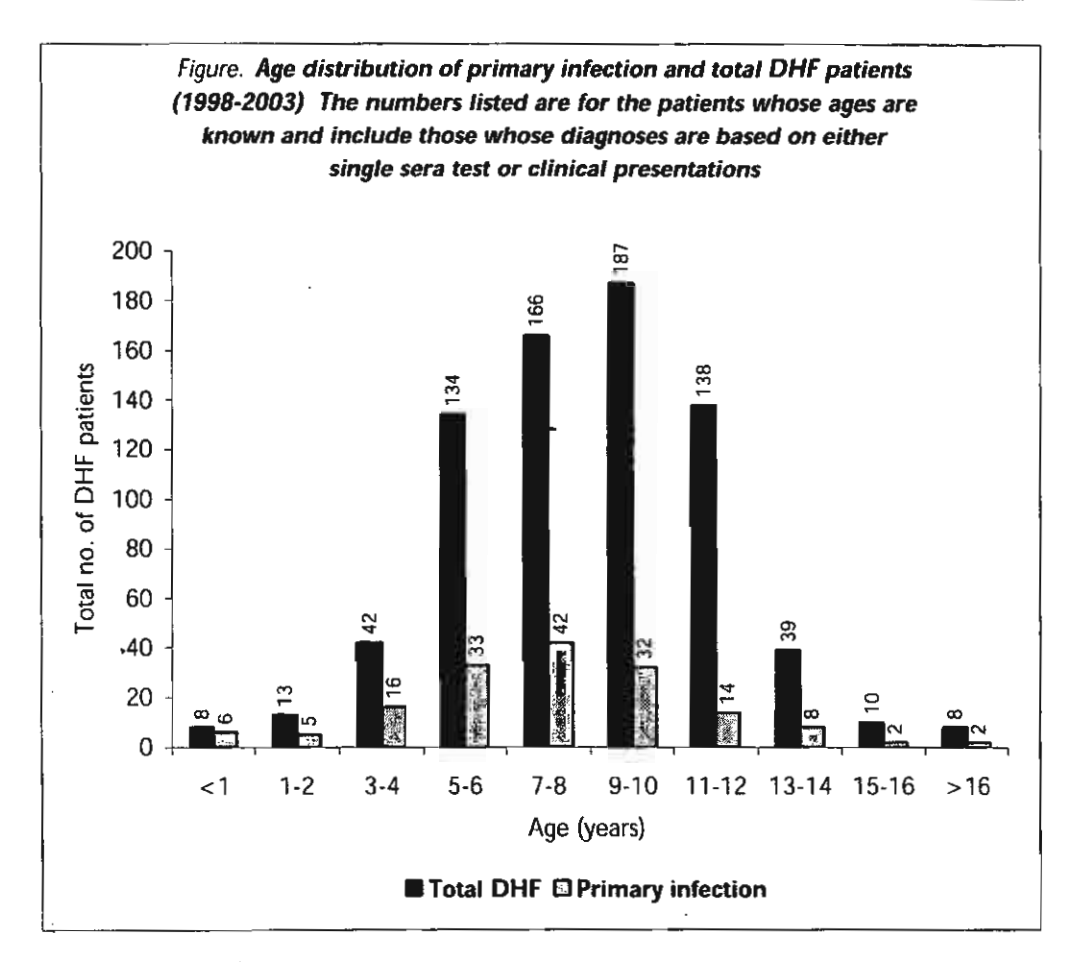
Year	Number of patients 4 admitted	Number sick with DHF	Number of cases where virus				
			DEN-1	DEN-2	DEN-3	DEN-41	Total
1998	318	281	51	28	41	1	121
1999	137	112	9	13	3	4	29
2000	84	71	13	13	5	0	31
2001	334	334	49	36	17	8	110
2002	186	186	23	22	4	1	50
2003	121	121	17	9	0	3	29

<sup>\*</sup>From January - June 2003

Regarding the results of virus isolation, of the 121 cases where virus was isolated in 1998, 40.0% were of DEN-1, 24.2% were of DEN-2, 34.2% were of DEN-3 and 1.7% were DEN-4. In 1999, the respective percentages were 31.0, 44.8, 10.3 and 13.8. In 2000, the percentages changed to 42, 42, 16.1 and 0, respectively. In 2001, they were 44.5, 32.7, 15.5 and 14.1. In 2002, they were 46.0, 44.0, 8.0 and 2.0 respectively. For the first half of 2003, the percentages were 31.0, 0 and 10.3 respectively. Comparing the percentages year by year, we can quantify the relative amount of the virus in circulation during that year. The relative abundance of DEN-1 virus appears to be increasing year after year, while that of DEN-3 appears to be decreasing. Overall, DEN-2 appeared to be the second-most abundant serotype in circulation throughout the study period.

The age distribution of the patients suffering from DHF is given in the Figure.

This looks similar to the one of the DHF/DSS patients admitted to Yangon Children's Hospital, Myanmar, between 1995 and 1996, but is different from that of the children admitted to the Children's Hospital in Bangkok between 1995 and 1998(12). The age distribution pattern for the latter hospital shows a bimodal distribution, with the second maximum in infants below the age of one year. Haistead et al(12) proposed that this group should be the one to study for understanding primary infections. found that infants with DHF/DSS constituted 4.9% of the patients in their study group. Only eight infants were recorded in our study group. A similarly small number of infants was seen in the study group of Pancharoen et al<sup>(9)</sup>. Also shown in the Figure is the age distribution of the DHF cases resulting from primary infection. In all the three studies, DHF infections in infants were primary infections.



#### Discussion

The period covered in the present study spans two complete three-year cycles in the month of incidence of DHF in Bangkok, Thailand, between January 1998 and June 2003. Hays et al<sup>(13)</sup> carried out a spectral density analysis of the data and found an annual variation and a super-annual variation (of three years). The 1998 epidemic was one of the peak years in the annual occurrence of DHF in Thailand. Based on this, Hays predicted during a dengue fever conference held in December

2000 in Chiang Mai that 2001 would be a peak year for DHF. This was borne out by the increase observed in the incidence of DHF in Bangkok in that year. Many of us also made similar predictions<sup>(14)</sup>. As observed in this study, the incidence of DHF peaked in 1998 and then decreased in 1999 and again went down in 2000. It rose sharply in 2001 (a peak year in the three-year cycle) and then dropped in 2002. The decrease appeared to be continuing in 2003. Based on the previous trends, it is expected that there will be a rise in the incidence of DHF in 2004.

In the present study, dengue virus was isolated only in 34.5% of the 1,082 DHF confirmed serological patients by This is far below examinations. percentage isolated by Vaughn et al(15), who were able to isolate the virus in 98% of their patients. Their study was done in 1994. The difference in the percentages is due to the fact that Vaughn et al carried out their isolation within three days of the beginning of the high fever. Using similar criteria for differentiating between primary secondary infections as the cause of the DHF illness, Vaughn et al established that only 8% of the acute dengue illnesses were due to primary infections (92% were due to secondary infections).

The relative abundance of the four serotypes observed by Vaughn et al, in 1994 was DEN-1 (20.3%), DEN-2 (28.8%), DEN-3 (16.9%) and DEN-4 (33.9%). Combining these numbers with the relative abundance observed in our study and in 1960<sup>(16)</sup>, we observed that there was permanent

circulation of the four serotypes in Thailand. This is likely to be the cause of the short intervals between the high epidemic peaks, compared to what is observed, for example, Polynesia mono-serotype where epidemics occur at an interval of at least sixto-seven years(17). Looking at the relative abundance of all the four serotypes on a year-to-year basis, we found that the relative abundance of DEN-4 was fluctuating the most, followed by DEN-3. No significant (p < 0.05)differences observed were between confirmed primary and secondary infections for any serotype during any year.

The percentages of primary infections during the last three years are well above 14.0 reported for cases occurring in Bangkok between 1988 and 1995<sup>(S)</sup>. This raises the question: Does the fact that the percentages of DHF/DSS arising from primary infections have almost doubled during the last three years signify that the dengue viruses have become more virulent or are there other factors at play?

#### References

- Gubler DJ. Dengue and dengue haemorrhagic fever. Clin Microbiol Rev, 1998, 11(3): 480-496.
- Burke DS, Nisalak A, Johnson DE and Scott RM. A prospective study of dengue infections in Thailand. Am J Trop Med Hyg, 1988, 38(1): 172-180.
- Guzman MG, Kouri G, Valdes L, Bravo J, Alvarez M, Vazques S, Delgado I and Halstead SB. Epidemiologic studies on dengue in Santigo de Cuba, 1997. Am J Epidemiol, 2000, 152(9): 793-799.
- World Health Organization, Dengue haemorrhagic fever: Diagnosis, treatment, prevention and control (2<sup>nd</sup> ed). WHO (Geneva), 1997.

- Halstead SB. The pathogenesis of dengue. Molecular-epidemiology in infectious disease. Am J Epidemiol, 1981, 114: 632-648.
- Travassos da Rosa APA, Vasconcelos PFC, Travassos da Rosa ES, Rodrigues SG, Mondet B, Cruz ACR, Sousa MR and Travassos da Rosa JFS. Dengue epidemic in Belem Para, Brazil, 1996-97. Emerg Inf Dis, 2000, 6(3): 298-301.
- Watts DM, Porter KR, Putvatana P, Vasquez B, Calampa C, Hayes CG and Halstead SB. Failure of secondary infection with American genotype dengue 2 to cause dengue haemorrhagic fever. The Lancet, 1999, 354: 1431-1434.

- Kochel TJ, Watts DM, Halstead SB, Hayes CG, Espinoza A, Felices V. Caceda R, Bautista CT, Montoya Y, Douglas S, Russell KL. Effect of dengue-1 antibodies on American dengue-2 viral infection and dengue haemorrhagic fever. The Lancet, 2002, 360: 310-312.
- Pancharoen C, Mekmullica J and Thisyakorn U. Primary dengue infection: What are the clinical distinctions from secondary infections? Southeast Asian J Trop Med Public Health, 2001, 32(3): 476-480.
- Clarke CW and Casals J. Techniques of hemagglutination and hemagglutination inhibition with arthropod viruses. Am J Trop Med Hyg, 1958, 7: 561-573.
- Innis BL, Nisalak A, Nimmanitya S, Kusalerdchariys S, Chongswarsdi V, Suntayakorn S, Puttisri P. Hoke CH. An enzyme-linked immunosobent assay to characterize dengue infections where dengue and Japanese encephalitis co-circulate. Am J Trop Med Hyg, 1989, 40: 418-427.
- Halstead SB, Lan NT, Myint TT, Shwe TN, Nisalak A, Kalyanarooj S, Nimmannitya S, Soegijanto, Vaughn DW and Endy TP. Dengue hemorrhagic fever in infants: Research opportunities ignored. Emerg Inf Dis, 2002, 8(12): 1474-1479.

- Hay SI, Myers MF, Burke DS, Vaughn DW, Endy T. Ananda N, Shanks GD, Snow RW, and Rogers DJ. Etiology of interepidemic periods of mosquitoborne diseases. PNAS, 2000, 97(16): 9335-9339.
- Barbazan P, Yoksan S and Gonzalez JP. Dengue hemorrhagic fever epidemiology in Thailand: Description and forecast of epidemics. Microbes and Infections, 2002, 4(7): 699-705.
- Vaughn DW, Green S, Kalayanarooj S, Innis BL, Nimmannitya S, Suntayakorn S, Rothman AL, Ennis FA and Nisalak A. Dengue in the early febrile phase: Viremia and antibody responses. J Infect Dis, 1997, 176: 322-330.
- Hammon VM and Sather GE. Virological findings in the 1960 hemorrhagic fever epidemic (dengue) in Thailand. Am J Trop Med Hyg. 1964, 13: 629-641.
- Deparis X, Chungue E, Pauck S, Roche C, Murgue B and Gleize. Surveillance epidemiologique de la dengue: Methode et interet lors de l'epidmic de dengue 2 en Polnesie francaise en 1996. Trop Med and Inti Health, 1998, 3: 566-570.

š

H.Nishiura et al. / Journal of Medical Safety 1(1) 2003 (Details explanation by authors)

The impact of initial attack size on SARS epidemic for SARS free countries: Possible reason for Japan without a domestic transmission.

Hiroshi Nishiura abd\*, I. Ming Tang bc, Masayuki Kakehashi d

Bangkok School of Tropical Medicine, Mahidol University, Bangkok, Thailand
 Department of Mathematics, Faculty of Science, Mahidol University, Bangkok, Thailand
 Institute of Science & Technology for Research & Development, Mahidol University, Bangkok, Thailand
 Institute of Health Science, Faculty of Medicine, Hiroshima University, Hiroshima, Japan

**Background:** The newly identified coronavirus has caused an epidemic of severe acute respiratory syndrome (SARS) to appear worldwide, particularly in parts of Asia. Although Japan has experienced the entry of a SARS-CoV infected person, the virus has so far not succeeded in invading the community.

Method: A mathematical model based on Kermack & McKendrick epidemic model, was recently developed to be used, is applied for evaluating the effect of interventions such as quarantine and isolation. An analysis centered on initial attack size has been done to estimate the conditions needed for the successful invasion of SARS.

Results: The possible trajectories of SARS epidemics are obtained for different initial attack sizes, i.e., the number of infectious persons who are first introduced into a specific community having a susceptible population. It was demonstrated that the successful invasion of SARS would largely dependent on the initial attack size under certain assumptions. Mathematical analyses were performed to prove that the maximum number of susceptible humans who would be infected could be estimated on the basis of the initial attack size, using simple formulas.

Conclusion: The initial attack size is one of the most important determinants of whether a SARS epidemic can occur or not. Under an effective quarantine (which would lead to  $R_0 < 1$ ) regime, it would be difficult to generate secondary cases through the entry of only a few infectious individuals into large populace. The method was considered to also be useful when we estimate the degree of quarantine required.

Keywords: Severe Acute Respiratory Syndrome (SARS); Mathematical Model; Initial Attack Size; Japan

This work was presented at the SARS e-Conference by World Health Risk Management Center, October 2003, Tokyo, Japan.

\* Corresponding author.

Tel: +66-(0)2-246-1381 fax: +66-(0)2-246-1381

E-mail address: Nishiurah@aol.com (H. Nishiura)

#### 1. Introduction

Since November 2002, SARS (Severe Acute Respiratory Syndrome)-associated coronavirus (SARS -CoV) has caused outbreaks of an atypical pneumonia worldwide, particularly in parts of Asia<sup>1)</sup>. Since the average overall case-fatality rate for all countries has ranged from 10.4 to 14.7 %<sup>2)</sup>, growing fears for SARS among public as well as health-care workers have spread dramatically. The spread of SARS stopped when public health measures such as quarantine and

isolation were imposed on the public. Riley et al<sup>3)</sup> believed that the reduction in the contact rate between the infectious individual and the rest of the susceptible population was the main reason for the end of the SARS crisis. By the time of the last report of someone becoming sick with SARS, 8457 individuals had been afflicted with the illness, 813 of who died<sup>4)</sup>.

From the beginning of the epidemics, SARS has been a worry to Japan because of its close proximity to Hong Kong and other SARS affected Southeast-Asian countries<sup>5</sup>. Many Japanese and foreign travelers have traveled to these countries and have returned to Japan after their visits. The Japanese government has therefore drawn up contingency plans for the possibility of SARS-infected individuals entering into Japan. Medical doctors of national hospitals have been dispatched to each airport quarantine office around the country. In addition, thermometers has been put in place, and all passengers from countries where SARS infections are presently occurring have been subject to a temperature check upon their arrival at each airport. Although strengthened quarantine has been carried out at each international airport, Japan has experienced the entry of a SARS-CoV (SARS associated coronavirus) infected person in mid May, 2003. He traveled to western Japan for a vacation and was later confirmed to be suffering from SARS6). Fortunately, Japan with its highly concentrated population has so far not experienced a domestic spread of SARS.

One of the greatest concerns and questions, among Japanese experts as well as public, is why SARS epidemic or domestic transmission has not occurred in Japan. Recently, we proposed possible reasons, through the use of mathematical model, for why 'the introduction of only a few cases into the communities in Japan can not easily lead to an epidemic<sup>7)1</sup>. Here we present further mathematical analysis centered on the impact of initial attack size on SARS epidemic in order to clarify the reason and to determine the optimal level of quarantine that can break the transmission cycle of SARS-CoV.

#### 2. Materials and Methods

Here, we employ a mathematical model for SARS

epidemic to determine properties of disease invasion, spread and persistence of the disease. The model is based on a simple modification of the Kermack & McKendrick epidemic model<sup>8)</sup>. The new model is a SEIR (Susceptible-Exposed-Infectious-Recovered (or Dead) type model<sup>9)</sup>) and is described by a set of ordinal differential equations. Fig. 1 illustrates the simple flow diagram about our model. We incorporated the effects of quarantine and isolation into our model. It is assumed those who were quarantined and isolated would not contribute to the spread of SARS-CoV. Detailed descriptions of model structure and parameter assumptions are beyond the scope of this paper, and are given elsewhere<sup>7)</sup>. The equations describing the new model is given by the following approximately parameterized set of differential equations:

$$\frac{dS}{dt} = -\zeta (q - \beta(q + \kappa - 1))SI + \sigma T$$

$$\frac{dT}{dt} = (1 - \beta)q\zeta SI - \sigma T$$

$$\frac{dEq}{dt} = \beta q(1 - \kappa)\zeta SI - \phi Eq$$

$$\frac{dE}{dt} = \beta(1 - q)(1 - \kappa)\zeta SI - \phi E$$

$$\frac{dQ}{dt} = \phi Eq - (\gamma_2 + \delta)Q$$

$$\frac{dI}{dt} = \phi E - (\gamma_1 + \delta)I$$

$$\frac{dIq}{dt} = \delta(I + Q) - \gamma_1 Iq$$

$$\frac{dR}{dt} = \gamma_1 (I + Iq) + \gamma_2 Q$$

The basic reproductive number,  $R_0$  is given by:

$$R_0 = \frac{1}{\delta + \gamma_1} \zeta \beta (1 - q)(1 - \kappa) N \quad [2]$$

Here,  $I/(\delta+\gamma_1)$  is the mean duration of infectious period.  $\zeta\beta$  represents the infection rate because  $\zeta$  and  $\beta$  are the probability of transmission per contact and the daily number of contacts per capita, respectively. The fraction of those who undertook 100% effective precaution and those whose contacts were traced and removed would be described by  $\kappa$  and q respectively. Both  $\kappa$  and q are the function of precaution and quarantine. N is the size of the population in which the

epidemic occurs.

The values of the biological variables for Japan will be assumed to be not much different from those for Hong Kong<sup>10)</sup>, although this is clearly a rough assumption. We have used the values given in the epidemiologic reports<sup>11)</sup> and analyses<sup>(2)(3)</sup> of the epidemics in Hong Kong in our analyses. Secondly, we have assumed that there is homogenous mixing among the infectious and susceptible, so that every infectious person would transmit the virus to exactly  $R_0$  susceptible individuals within an infectious period. This means that the cases of "super-spreading" events 4 (SSEs), those arising from individuals who generate much more than the average number of secondary cases, and which has been described as a rare heterogenous events 13)14), are not taken consideration. This is done since the purpose of this report is to understand the role of initial attack size and interventions with the commonest transmission route as a possible scenario in Japan. The degree of quarantine is assumed to be 75%, the number for the epidemic occurring case in Hong Kong. This is a pessimistic values given that the Japanese government has traced approximately 2500 persons among 2600 suspected contacts. Further description of the principal parameters in the model and of their assigned value is presented elsewhere<sup>7)</sup>.

In this study, two important analyses are performed. First, simulations have been done using different basic

reproductive numbers. We then perform a linear regression analyses to establish the linear correlation that can be approximated by a simple mathematical formula. Secondly, further mathematical analyses were carried out in order to investigate the role of initial attack size in SARS epidemic. The model has been programmed using Turbo Pascal Version 1.5 (Borland International Inc. Scotts Valley, CA, USA) working on Microsoft WindowsTM® platform. All data from the program were analyzed using Microsoft Excel 2000 (Microsoft Corporation, Redmond, WA, USA) except regression analysis performed using Epi Info 2002 (Centers for Disease Control and Prevention, Atlanta, GA, USA).

#### 3. Results

Fig. 2 shows the model generated maximum number of newly infected generated over the time period examined for different values for  $R_0$ . Linear correlations between the initial attack size and the maximum number of infected are seen when the values of  $R_0$  are less than 1 because of the level of public health interventions. Based on this finding, we propose that the coefficient of initial attack size could be represented as the function of basic reproductive number by:

$$(E(t) + Eq(t))_{\text{max}} = (\frac{R_0}{2} - 0.167)I(0)$$
 [3]

This result was found in the previous study<sup>7)</sup>. It should

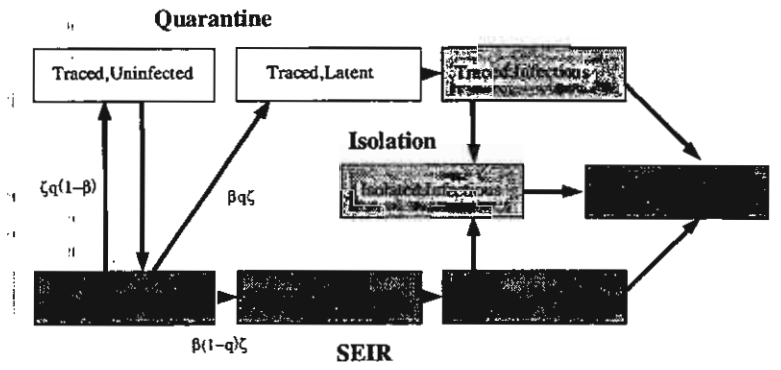


Figure 1. The transmission dynamics of the SARS taking into account the impact of precautionary measures and quarantine system. The new infection would be quarantined or not with a proportion q. A proportion,  $\kappa$ , of the potentially infected contacts is protected.

be noted that the simulations were done under the condition that the initial attack size is small compared to the susceptible population. When the susceptible population is small in comparison to the 'traced and uninfected' population, equations [1] can be simply described (for the purpose of analysis) to

$$\frac{dS}{dt} = -\zeta \beta(\kappa - 1)SI$$

$$\frac{dE}{dt} = \beta(1 - q)(1 - \kappa)\zeta SI - \phi E \qquad [4]$$

$$\frac{dI}{dt} = \phi E - (\gamma_1 + \delta)I$$

According to analyses by Kendall who applied phase portrait into simple epidemic model<sup>15)</sup>, there should be an equilibrium point at which the number of susceptible at infinite time is given by

$$\lim_{t\to\infty} S(t) = S(+\infty) \quad [5]$$

and I(t) and E(t) are zero. The epidemic curve would always start at an unstable equilibrium point and end up at the stable equilibrium point described above. It can be shown that the function given by

$$V(S, E, I) = S^{\frac{\gamma_i + \delta}{\beta \zeta (1 - \kappa)}} e^{\left[(1 - q)S + E + I\right]}$$
 [6-1]

would be constant for every S, E, and I (see Appendix 1). V is called as Liapunov function that would always give us the constant solutions. Taking the time  $t = t_{max}$ , to be one at which

$$\frac{dE}{dt} = \frac{dI}{dt} = 0 \quad [6-2]$$

we can obtain  $E_{max}$  and  $I_{max}$ , the values of E and I at

Figure 2. Maximum number of newly infected SARS cases according to different basic reproductive numbers,  $R_0$ . The linear correlation can be seen for whole values drawn here.

the peak of epidemic curve. The value of  $S_{max}$  is given by

$$S_{\text{max}} = S(t_{\text{max}}) = \frac{\gamma_1 + \delta}{\zeta \beta (1 - \kappa)(1 - q)}$$
 [7]

 $S_{max}$  is often denoted as  $N_{cr}$ , a proportionality constant, whose inverse would be the sum of all the biological, social, and environmental aspects of transmission. Independent from the time after onset of epidemic, V would be constant due to equation [6]. Hence

$$V(S_{\text{max}}, E_{\text{max}}, I_{\text{max}}) = V(S_0, E_0, I_0)$$
 [8]

Performing a logarithmic manipulation in expression [8] gives

$$-\frac{\gamma_1 + \delta}{\beta \zeta (1 - \kappa)} \log S_0 + (1 - q)S_0 + E_0 + I_0$$

$$= -\frac{\gamma_1 + \delta}{\beta \zeta (1 - \kappa)} \log S_{\text{max}} + (1 - q)S_{\text{max}} + E_{\text{max}} + I_{\text{max}}$$
[9]

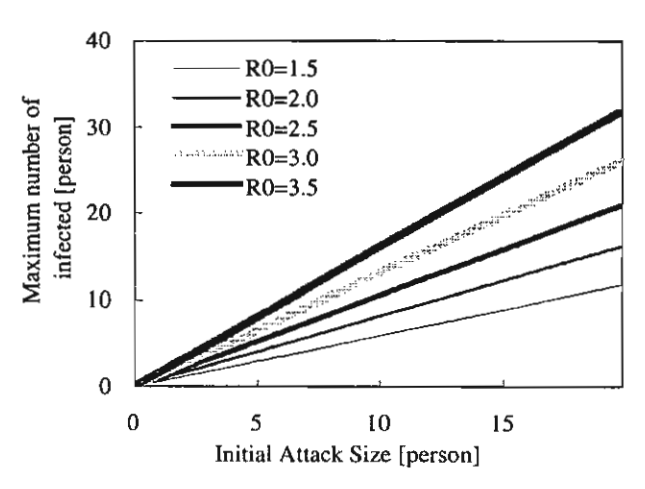
Substituting  $E_{max}$  by  $I_{max}$  since  $E_{max} = \frac{\gamma_1 + \delta}{\phi} I_{max}$ 

we get

$$(\frac{\gamma_1 + \delta}{\phi} + 1)I_{\text{max}}$$

$$= (1 - q)(S_0 - S_{\text{max}}) + E_0 + I_0 + (1 - q)S_{\text{max}} \log \frac{S_{\text{max}}}{S_0}$$
[10]

Therefore,  $I_{max}$  can be seen as being a function of initial attack size under the assumptions used in our model. Clearly, one could obtain the same result for the maximum number of infected, using an analysis similar to one given above.



#### 4. Discussion

It has been demonstrated that the maximum number of newly infected, or the crude size of epidemic, could be estimated on the basis on initial attack size in the presence or in the absence of any public health interventions. In this study, we provided both a mathematical analyses and numerical solutions of the equations describing the model. Our analysis shows that it would be possible to predict the fate of epidemic whenever SARS infected persons enter into any communities having approximately the same transmissibility and employing the same control strategy. In spite of the fact that our theoretical framework did not take into account stochastic effects and that conditions such as such as I(0)N < 1 does not exist in real situations, we obtained a simple formula which showed that the introduction of only a few cases into a given community would not necessarily lead to an a epidemic. The fact that number of infected individuals entering into Japan is below the number to succeed invasion might be one of the reasons for Japan not experiencing the SARS epdemic so far. In addition, by taking into account the initial attack size and transmission potential of pathogen, the formula might be generalized for it to estimating the degree of quarantine required.

Homogenous mixing may not be a correct depiction actual population interactions of SARS transmission. Although we are still presented with many unknowns including the role of SSEs, the small number of transmissions in most of the countries that experienced SARS occurrences suggests that the daily contact among the populace is not sufficient for transmission did not occur<sup>16)</sup>. For instance, an index case, not a SSEs, caused the epidemic in one hospital in Toronto<sup>(7)</sup>. Secondly, the fact that 76% of the infections in Singapore were acquired in a health-care facility<sup>14)</sup> points to the easy spread of SARS in only certain settings. Therefore, it is too optimistic to apply the assumption that every infected person will pass the disease to exactly  $R_0$  susceptible individuals to the real world. It would be necessary to incorporate probability theory and contact patterns into the research since the epidemic threshold parameters based

approximating the infection process during its initial stages as a branching process<sup>18)</sup>. It should be possible to apply network theory when it comes to the story of SARS, since the thesis of transmission dynamics on scale-free networks is well fitted to several epeidemiologic findings of SARS. Complex systems of transmission dynamics of SARS are not based upon random networks as has been thought for the last 40 years, but are governed by power laws, and that only a few hubs dominate the whole network<sup>19)</sup>. We must apply these thoughts by considering models, which are most realistic, as well as ones that include variance in reproductive number.

One approach to overcome the problem of risk management is to model the potential episodes with mathematical modeling. SARS is believed to recur in this winter because of the viral ecology<sup>20</sup>. In order to prepare the possible recurrence of SARS, much more studies in ecological aspects are required as well.

#### Acknowledgements

This work was mainly carried out while HN was staying in Thailand. The authors are grateful to Dr. Pratap Singhasivanon and the other members of Department of Tropical Hygiene, Mahidol University for their coordination in our research. We furthermore sincerely thank Dr. Minato Nakazawa at Yamaguchi Prefectural University for his technical advice and comments.

#### Referrences

- 1. Tsang KW, Ho PL, Ooi GC, Yee WK, Wang T, Chan-Yeung M, et al. A cluster of cases of severe acute respiratory syndrome in Hong Kong. N Eng J Med 2003; 348: 1977-85.
- 2. Galvani AP, Lei X, Jewell NP. Severe acute respiratory syndrome: temporal stability and geographic variation in case-fatality rates and doubling times. *Emerg Infect Dis* 2003; 8: 991-5.
- 3. Riley S, Fraser C, Donnelly CA, Ghani AC, Abu-Raddad LJ, Hedley AJ, et al. Transmission dynamics of the etiological agent of SARS in Hong

Kong: Impact of public health interventions. Science. 2003; 300: 1961-6.

- 4. World Health Organization. Cumulative number of reported cases (SARS) since March 17, 2003. Geneva: World Health Organization, 2003. Available at <a href="http://www.who.int/csr/sarscountry/en/">http://www.who.int/csr/sarscountry/en/</a>
- 5. The Ministry of Foreign Affairs of Japan. Severe Acute Respiratory Syndrome (SARS) (Current Situation in Japan and Measures taken by the Government of Japan). Tokyo: The Ministry of Foreign Affairs of Japan, 2003.
- Anonyms. Taiwan tourist diagnosed with SARS in Japan. Canadian Press. June 19, 2003. Available at: <a href="http://cnews.canoe.ca/CNEWS/World/2003/06/26/119">http://cnews.canoe.ca/CNEWS/World/2003/06/26/119</a>
   688-ap.html
- 7. Nishiura H, Patanarapelert K, Sriprom M, Sarakorn W, Sriyab S, Tang I.M. Modeling potential responses to severe acute respiratory syndrome (SARS) in Japan: the role of initial attack size, precaution and quarantine. *J Epidemiol Com Health*. 2003; 58: 186-91.
- 8. Kermack WO, McKendrick AG. Contributions to the mathematical theory of epidemics I. *Proc R Soc* 1927; 115A: 700-21. (Reprinted *Bull Math Biol* 1991; 53: 33-55.)
- Anderson RM, May RM. Infectious Diseases of Humans: Dynamics and Control. Oxford: Oxford University Press. 1991.
- 10. Tsang KW, Ho PL, Ooi GC, Yee WK, Wang T, Chan-Yeung M, et al. A cluster of cases of severe acute respiratory syndrome in Hong Kong. *N Eng J Med* 2003; 348: 1977-85.
- 11. Donnelly CA, Ghani AC, Leung GM, Hedley AJ, Fraser C, Riley S, et al. Epidemiological determinants of spread of casual agent of severe acute respiratory syndrome in Hong Kong. *Lancet* 2003; 361: 1761-6.
- 12. Lipsitch M, Cohen T, Cooper B, Robins JM, Ma S, James L, et al. Transmission dynamics and control of Severe Acute Respiratory Syndrome. *Science*. 2003; 300: 1966-70.
- 13. Lee N, Hui D, Wu A, Chan P, Cameron P, Joynt GM, et al. A major outbreak of Severe Acute Respiratory Syndrome in Hong Kong. N Eng J Med. 2003; 348: 1986-94.
- 14. Center for Disease Control and Prevention. Severe

- Acute Respiratory Syndrome-Singapore, 2003. *MMWR* 2003; 52: 405-11.
- 15. Kendall DG. Deterministic and stochastic epidemics in closed populations. Proceedings of the Third Berkeley Symposium on Mathematical Statistics and Probability. Neyman J Eds., Vol VI, California University Press: 149-65.
- 16. Arita I, Kojima K, Nakane M. Transmission of Severe Acute Respiratory Syndrome. *Emerg Infect Dis* 2003; 9: 1183-4.
- 17. Dwosh HA, Hong HHL, Austgarden D, Herman S, & Schabas R. Identification and containment of an outbreak of SARS in a community hospital. *Can Med Assoc J* 2003; 168: 1415-20.
- 18. Becker NG, Dietz K. The effect of household distribution on transmission and control of highly infectious disease. *Math Biosci* 1995; 127: 207-19.
- 19. May RM, Lloyd AL. Infection dynamics on scale-free networks. *Phys Rev E* 2001; 64: 1-4.
- 20. Abdullah ASM. Will the Severe Acute Respiratory Syndrome (SARS) epidemic recur? *J Epidem Com Health*. 2003; In Press.

#### Appendix 1.

Let us look for a V that will always be a constant. We begin by considering the ordinary differential equation

of 
$$VO\left(\frac{dV}{dt}=0\right)$$
. That is, we start by considering

$$\frac{dV}{dt} = \frac{\partial V}{\partial S} \frac{dS}{dt} + \frac{\partial V}{\partial E} \frac{dE}{dt} + \frac{\partial V}{\partial I} \frac{dI}{dt}$$

Here, each solution can be written as follows:

$$\frac{\partial V}{\partial S} \frac{dS}{dt} = -\beta \zeta (1 - \kappa) S I \begin{bmatrix} -\frac{\gamma_1 + \delta}{\beta \zeta (1 - \kappa)} S^{-\frac{\gamma_1 + \delta}{\beta \zeta (1 - \kappa)}} e^{\left[(1 - q)S + E + I\right]} \\ +(1 - q) S^{-\frac{\gamma_1 + \delta}{\beta \zeta (1 - \kappa)}} e^{\left[(1 - q)S + E + I\right]} \end{bmatrix}$$

$$\frac{\partial V}{\partial E}\frac{dE}{dt} = S^{-\frac{N+\delta}{\beta\zeta(1-\kappa)}}e^{\left[(1-q)S+E+I\right]}(\beta\zeta(1-\kappa)(1-q)SI - \phi E)$$

$$\frac{\partial V}{\partial I}\frac{dI}{dt} = S^{-\frac{\gamma_1+\delta}{\beta\zeta(1-\kappa)}}e^{\left[(1-q)S+E+I\right]}\left[\phi E - (\gamma_1+\delta)I\right]$$

Putting everything together, we have

$$\frac{dV}{dt} = 0$$

This completes the proof.

# INFECTION RISK TO TRAVELERS GOING TO DENGUE FEVER ENDEMIC REGIONS

by

P. Pongsumpun, <sup>a</sup> K. Patanarapelert, <sup>a</sup> M. Sriprom, <sup>a</sup> S. Varamit, <sup>b</sup> I.M. Tang, <sup>b#</sup>

Department of Mathematics and <sup>b</sup>Department of Physics, Faculty of Science

and

b Institute of Science & Technology for Research & Development, Salaya Campus Mahidol University, Bangkok 10400, Thailand

## Abstract:

ij

The risk of dengue virus infection to travelers visiting dengue fever endemic regions is studied through the use of mathematical modelling. A Susceptible-Infected-Recovered (SIR) model is used to describe the transmission of Dengue Fever (DF) in an endemic region into which tourists enter. The dynamics of a new class of humans, the travelers, is incorporated into the systems of first order differential equations in the SIR describing the dynamics of the transmission in the host region. Using standard dynamic analysis methods, the numbers of travelers who become infected with the dengue virus are calculated as a function of the length of time the tourist stays in the region.

Keywords: Disease Transmission, Dengue Fever, SIR Model, and Foreign Travel.

<sup>\*</sup>Corresponding author: email address scimt@mahidol.ac.th.

## I. Introduction.

Dengue fever (DF) is an illness that is characterized by a moderately high fever, extreme pain in and stiffness in the joints, a rash and a reduction in the white blood cells (Gubler 1998). These symptoms are caused by the toxins produced by one of the four serotypes of a virus belonging to the genus *Flavivirus*, in the family *Flaviviridae*. In many cases, the illness is asymptomatic and an infection can only be determined through serologic tests. It has been estimated that there are between 50 and 100 million cases of dengue fever (DF) a year. Some 40% of the world's population live in the endemic areas of this disease. Areas which are potential endemic region for this disease are those in which the transmitting vectors *Aedes aegypti* and *Ae. albopictuus* mosquitoes thrive and where the climate is right for the development of the virus. In 1990, almost 30% of the world population lived in regions where the risk of dengue transmission was greater than 50% (Hales *et al.*, 2002).

As air travel becomes less expensive, people from non-endemic countries in Europe and the United States are increasingly traveling to countries where the disease is endemic. The travelers (tourists) should be aware of the risk of dengue virus infection and so many governmental health organization (such as Center for Disease Control and Prevention (CDC), 2003) issue out travel warnings. Dengue infections are the second most common infections (after malaria) among travelers who go aboard (Schwartz et al., 1996). Because there are no prophylaxis or vaccine against the dengue virus, the travelers to the dengue-endemic regions are at special risk. The only defense is not to be bitten by the mosquitoes. Awareness of the risk then becomes the best defense.

Recently there have been reports of increased number of travelers to Thailand who are being infected with the dengue virus. A special report issued by the surveillance net TropNetEurop (2002) point out that during 2002, 61.4% of the 68 reported cases (among German or Swiss tourists) had become infected while they were visiting Ko Phangan and Ko Samui, two islands in the Gulf of Thailand. During the previous three years, only 20.4%

of the imported dengue cases among this group of tourists originated in Thailand. In a study of Swedish tourists (Lindback *et al.*, 2003), 71% of the imported dengue cases during 1998-99 were infected in Thailand. A similar preponderance was seen among Israeli tourists during 1994-1995, i.e., 14/18 confirmed infections originated on the island of Ko-Pangan (Schwartz *et al.*, 1996). The average duration of the visits in these three studies was three to four weeks. A prospective study of Israeli travelers to tropical countries who stay a long time (at least three months) indicate that the incident rate of dengue infection for these travelers may be as high as 600 per 100,000 travelers (Potasman *et al.*, 1999).

To study the risk of travelers (tourists) becoming infected while they are visiting an endemic area, we have set up a mathematical model to describe the transmission of the dengue virus in a host population in which B numbers of travelers visit per unit time and stay for a length of time,  $\tau_1$ . We are interested in this study on what the risk increases with the time spent in the endemic area. It is assumed that the conditions are such that the disease is endemic in the host population and that none of the travelers carry the virus when they enter into the country. In Section II. we introduce the mathematical model. The results of dynamical analyses of the system of equations are presented in Section III. In Section IV. we present the results of our numerical solutions of the equations and discuss their implications.

## II. Mathematical Model.

To formulate a mathematical model for the transmission of dengue virus in the system of interest, we need to introduce different population groups. The time rate of change in the number of subjects in each group is equal to the number of subjects entering into the group minus the number leaving the group. For our system, we have two human populations, host and travelers, and one mosquito population. Each human population is divided into three classes, susceptible, infected and recovered, i.e., S'h, I'h and R'h (S't, I't and R't), respectively. The mosquito population is divided into two classes, S'v and I'v. To see how

the rate of change of the numbers in each population, let us consider in detail the rate of change of the number of susceptible travelers, i.e.,

$$\frac{dS'_{t}}{dt} = B - \frac{b\beta_{h}'}{N_{T} + c} S'_{t} I'_{v} - (\mu_{h} + (1/\tau_{l})) S'_{t}$$
(1)

where  $N_T$  is the total host population (taken to be constant);  $\mu_h$ , the death rate (assumed to be the same for all categories); b, the biting rate of the mosquito; c, the total number of other animals which can also be bitten by the mosquito and  $\beta_h$  is the probability that the dengue virus will survive in the human after it is transmitted from the mosquito. The first term on the RHS is the number of travelers entering into the region. The next term is the number of travelers lost by them becoming infected. To get this term, we note that bl'<sub>v</sub> is the total number of bites, which could transmit the virus.  $S'_t/(N_T+c)$  is the fraction of the bites which are delivered to susceptible travelers and  $\beta_h$  is the probability that these virus transmitted by the bite survive in the human and begin to reproduce there. The next two terms are the losses due to natural death and to the traveler leaving the region. The other equations are obtained by similar considerations (Esteva and Vargas, 1998).

The number of equations we need to consider would be reduced to five if we assume that the total numbers of host, travelers and mosquitoes remain constant. It can be easily established the total number of travelers is  $B/(\mu_h + (1/\tau_1))$  and the total mosquito population is  $A/\mu_v$ , where A is the recruitment rate of the mosquitoes and  $\mu_v$  is the death rate of the mosquitoes. Dividing  $S'_h$ ,  $I'_h$ , and  $R'_h$  by  $N_T$ ;  $S'_t$ ,  $I'_t$  and  $R'_t$  by the total number of travelers and  $S'_v$  and  $I'_v$  by the total number of mosquitoes, we obtain the population densities and the conditions  $S_h + I_h + R_h = 1$ ,  $S_t + I_t + R_t = 1$  and  $S_v + I_v = 1$ . The differential equations for the time rate of change of the population densities are

$$\frac{dS_t}{dt} = \mu_h + (1/\tau_1) - \gamma_h S_t I_v - (\mu_h + (1/\tau_1)) S_t$$
(2a)

$$\frac{dS_h}{dt} = \lambda - \gamma_h S_h I_v - \mu_h S_h$$
(2b)

$$\frac{dI_h}{dt} = \gamma_h S_h I_v - (\mu_h + r) I_h$$

, (2c)

$$\frac{dI_{t}}{dt} = \gamma_{h} S_{t} I_{v} - (\mu_{h} + (1/\tau_{1}) + r) I_{t}$$

(2d)

(2e)

and

$$\frac{dI_{v}}{dt} = \gamma_{v,h} S_{v} I_{h} + \gamma_{v,t} I_{t} - \mu_{v} I_{v}$$

with

$$\gamma_h = b\beta_h m$$
, (3a)

$$\gamma_{v,t} = b\beta_h m_o$$

, (3b)

and

$$\gamma_{\mathbf{v}, \mathbf{h}} = \mathbf{b} \boldsymbol{\beta}_{\mathbf{v}}$$
 (3c)

where  $\beta_V$  is the probability that the virus after it is transmitted to the mosquito will survive; r, the rate at which the infected recover; m and  $m_0$  are the ratios between the total number of mosquitoes and total number of host humans and between the total number of travelers and total number of host humans. Eqn. (2a) is obtained by dividing eqn. (1) by  $B/(\mu_h+)1/\tau_1$ ), the total number of visitors. We have also assumed that  $N_T >> B/(\mu_h+)1/\tau_1$ ), i.e., the number of people permanently living in the area is greater than the number of visitors.

## III. Analytical Results.

## III.a Equilibrium States.

The equilibrium states are obtained by setting the RHS of eqns. (2a) to (2e) to zero. Doing this, we get two equilibrium states, the disease free state,  $E_0 = (1, 0, 1, 0, 0)$  and the endemic equilibrium state,  $E_1 = (S_h^*, I_h^*, S_t^*, I_t^*, I_v^*)$  where

(4c)

$$S_h^* = \frac{1}{1 + \beta_1 I_v^*}$$
, (4a)  
 $I_h^* = \frac{\beta_2 I_v^*}{1 + \beta_1 I_v^*}$ 

$$S_t^* = \frac{1}{1 + \beta_3 I_V^*}$$
 (4b)

$$I_{t}^{*} = \frac{\beta_{4}I_{v}^{*}}{1 + \beta_{3}I_{v}^{*}}$$
(4d)

with  $\beta_1 = \gamma_h/\mu_h$ ,  $\beta_2 = \gamma_h/(\mu_h + r)$ ,  $\beta_3 = \gamma_h/(\mu_h + (1/\tau_1))$ ,  $\beta_4 = \gamma_h/(\mu_h + (1/\tau_1) + r)$  and  $I_v^*$  is the positive solution of a quadratic equation obtained by substituting eqns. (4a) to (4d) into the RHS of eqn. (2e) and setting it equal to zero. The algebraic expression for  $I_v^*$  is quite complicated and therefore will not be written down.

## III.b Local Asymptotical Stability.

The local stability of an equilibrium state is determined from the Jacobian (gradient) matrix of the RHS of the set of differential equations evaluated at the equilibrium state. If all the eigenvalues (obtained by diagonalizing the Jacobian matrix) have negative real parts, then the equilibrium state in question is locally asymptotically stable. Performing the necessary calculations for the *disease free state*, we find that the characteristic equation is a product of three polynomials, two of order one and the remaining of order three. The eigenvalues given by the two polynomials of order one are negative. Using the Routh-Horwitz criterion (May, 1973) for the eigenvalues determined by a third order characteristic equation to have negative real parts, we find that the conditions would be satisfied if  $R_{0,1} < 1$  and  $R_{0,2} < 1$  where  $R_{0,1}$  and  $R_{0,2}$  are defined as

$$R_{0,1} = \frac{b^2 \beta_{v} \beta_{h} m}{\mu_{v} (\mu_{h} + r)} \quad \text{and} \quad R_{0,2} = \frac{b^2 \beta_{v} \beta_{h} m m_{o}}{\mu_{v} (\mu_{h} + r) (\mu_{h} + (1/\tau_{1}))}$$
(5)

The disease free state will occur since the basic reproduction number  $R_0 = R_{0.1} < 1$ , and since  $m_0 << 1$ , the second condition will also be met. The disease free state will arise whenever the number of mosquitoes falls below  $\mu_v(\mu_h + r)/b^2\beta_h\beta_v$ .

The determination of the stability of the endemic state is more difficult. This is due to the fact that the Jacobian matrix evaluated at endemic equilibrium state E<sub>1</sub> is much more complicated than that for the disease free state. Diagonalizing this 5×5 matrix is quite difficult and so we have used the computer program MATHEMATICA<sup>TM</sup> to perform this task. The program yields a fifth order characteristic equation of the form

$$\lambda^{5} + K_{4}\lambda^{4} + K_{3}\lambda^{3} + K_{2}\lambda^{2} + K_{1}\lambda + K_{0} = 0$$
 (6)

where the coefficients  $K_0$ ,  $K_1$ ,  $K_2$ ,  $K_3$  and  $K_4$  are extremely complicated expressions. In some cases, they have up to 45 terms. The Routh-Hurwitz stability criterion for fifth orders polynomials to use to determine whether all the eigenvalues determined from eqn. (6) have negative real parts. Again, this is done by MATHEMATICA<sup>TM</sup>. The program shows that the Routh-Hurwitz criterions are met when  $R_{0,1} > 1$  and  $R_{0,2} < 1$ . The endemic equilibrium state  $E_1 = (S_h^*, I_h^*, S_l^*, I_l^*, I_v^*)$  will therefore be locally asymptotically stable when these two conditions are met. In the next section, we show numerically that this is indeed true.

#### III. Numerical Results and Discussion.

1

In this paper, we are interested in the transmission of the dengue virus, not whether a person is sick or not. Therefore, we should only be interested in whether a person has immunity to the virus or not and whether the person is infectious or not. A susceptible person is one who is both not immune and not infectious. An infected person should be one who is infectious. This occurs only during the period of viremia which last for approximately three days. After that, the infected person still suffers from the presence of the toxins produced by the virus and is classified as still being sick. He has immunity to new infections during both stages of the illness. Once the toxin disappears, the person

becomes well and is classified as being recovered. For dengue infection, he keeps his immunity after he has recovered. For the purpose of transmission, there is no difference between the infected person after the viremia stage and a recovered person (provided we do not consider the presence of more than one strain of the dengue virus) since both will have immunity to the virus and not be infectious. This means that the recovery rate r should be 1/3 per day.

The values of the other parameters used are:  $\mu_h = 0.0000456$  per day, corresponding to a life expectancy of 70 years;  $\mu_v = 0.071$  per day, corresponding to a mean life of 14 days: b = 0.33, one bite providing enough bloodmeal for three days;  $\beta_h$  = 0.5,  $\beta_v$  = 0.75, which are arbitrarily chosen; r = 0.33, the reciprocal of the viremia period. The length of stay is varied from one week to three months while the two ratios m and mo are adjusted to have R<sub>0,1</sub> and R<sub>0.2</sub> have the values for the endemic state to be locally asymptotically stable and were taken to be 0.17 and 0.0007. These values yielded a  $R_{0.1}$  equal to 2.48 and  $R_{0.2}$  less than one. This means that the trajectory of the solutions in phase space should be that of a stable spiral node. Numerically solving eqns. (2a) to (2e) and plotting  $I_h$  versus  $S_h$  for the case of  $\tau_1 = 90$ days on Figure 1a, we do indeed see a stable spiral node. In Figure 1b, we plot the time development of the infected travelers for this case. In Figure 2, we plot the equilibrium values of the infected travelers as a function of  $\tau_1$ . As we see, the incidence rates (proportional to I<sub>t</sub>) increase (but not linearly) as the tourists stay longer in the endemic region. The risk appears to level off, as the tourists stay longer. This appears reasonable since the risk of infection to the tourists should approach the risk to the host population if they stay long enough

To see whether there is evidence for the risk to infection to increase with the duration of stay, we consider another group of travelers, U.S. soldiers. While not tourists, American military personnel have spent time in various dengue fever endemic regions around the world. They are ideal candidates for this type of determination since their medical care are

well documented. They are taken to medical facilities almost as soon as they come down with a febrile illness. Among the 30,000 U.S. troops who participated in Operation Restore Hope in Somalia during 1992-1993, 59 out of 289 febrile cases were confirmed as being due to the dengue virus (Sharp et al., 1996). The average length of time spent in Somalia before they become sick was four weeks. Given the number of troops, this indicates an incidence rate for dengue infection of 195 per 100,000 troops (visitors). In another operation, Operation Uphold Democracy, Haiti, 1994 (CDC, 1994), where 20,000 U.S. soldiers participated, the onset of the febrile illness among the soldiers showed a peak in the fourth week after the soldiers' arrival. 24 out of the 106 cases of febrile illness showed clinical symptoms of dengue fever. This gives an incidence rate of 120 per 100,000 troops (visitors). These incidence rates should be compared to those of the Israeli travelers (600 per 100,000 travelers) who stayed a much longer (three months vs. one month for the U.S. soldiers). Even though we have not given the values of basic reproduction rates for the different endemic regions that the visitors went to so that real comparisons can be made, it does appear that the incidence of dengue fever increases as the travelers (visitors) extend their stays in an epidemic area in keeping with our predictions.

## Acknowledgement.

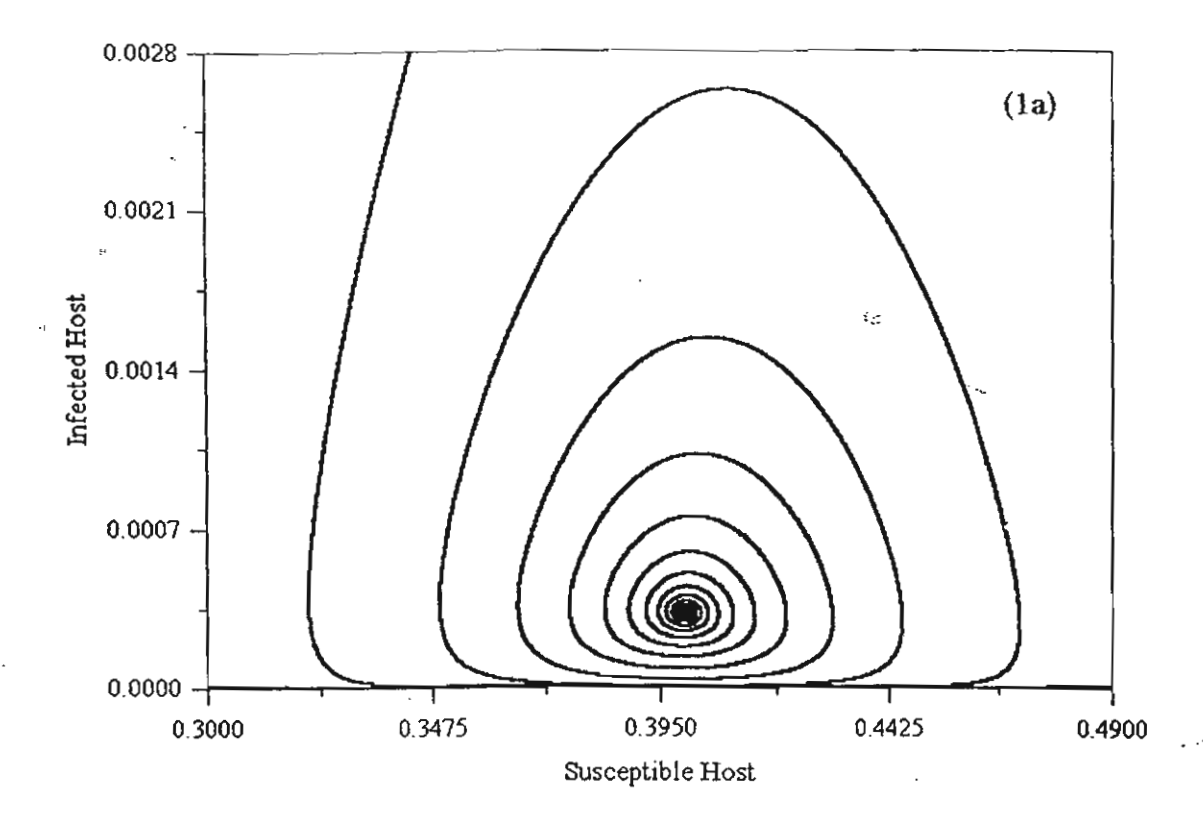
Two of the authors (YL and IMT) would like to thank the Thailand Research Fund (TRF) for financial support. PP would like to thank TRF for awarding her a Royal Golden Jubilee Ph.D. Scholarship. MS would like to thank the Ministry of Education, Royal Thai Government for a Staff Development Scholarship (Ph.D. level).

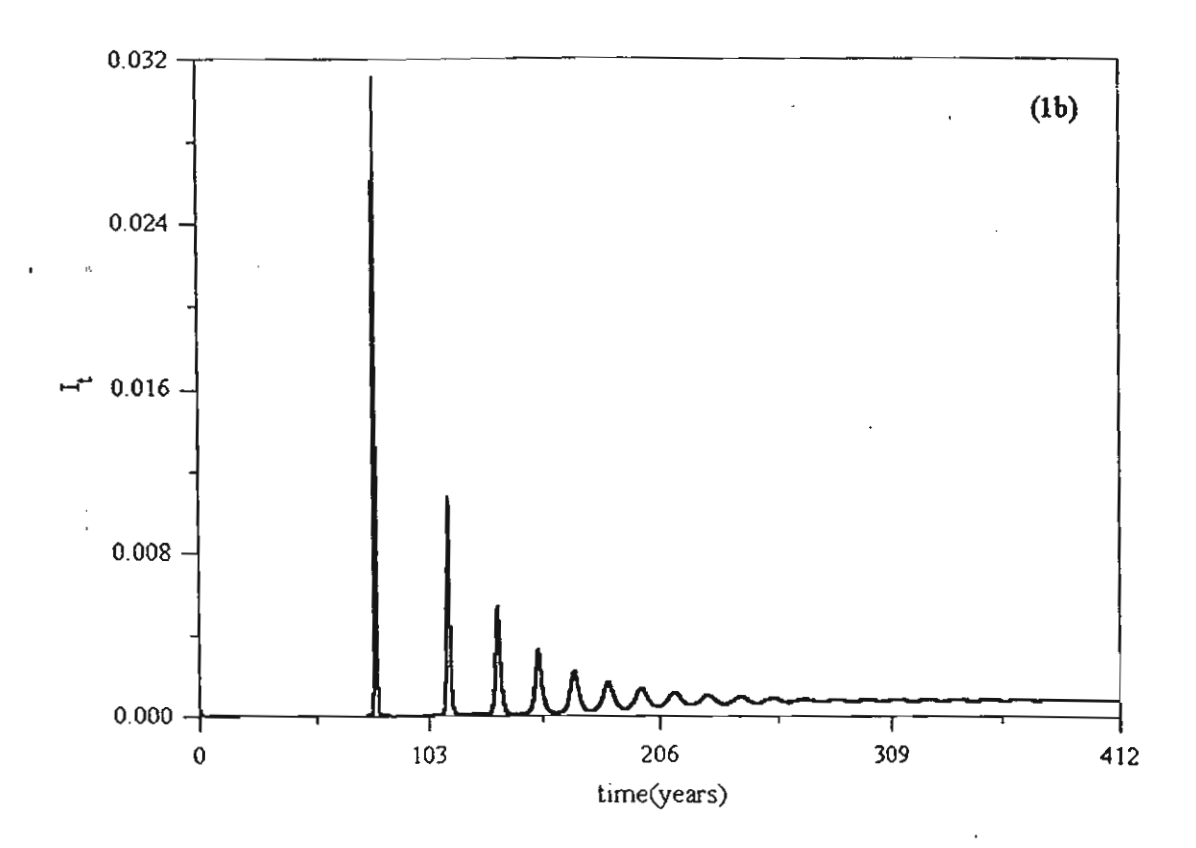
#### References.

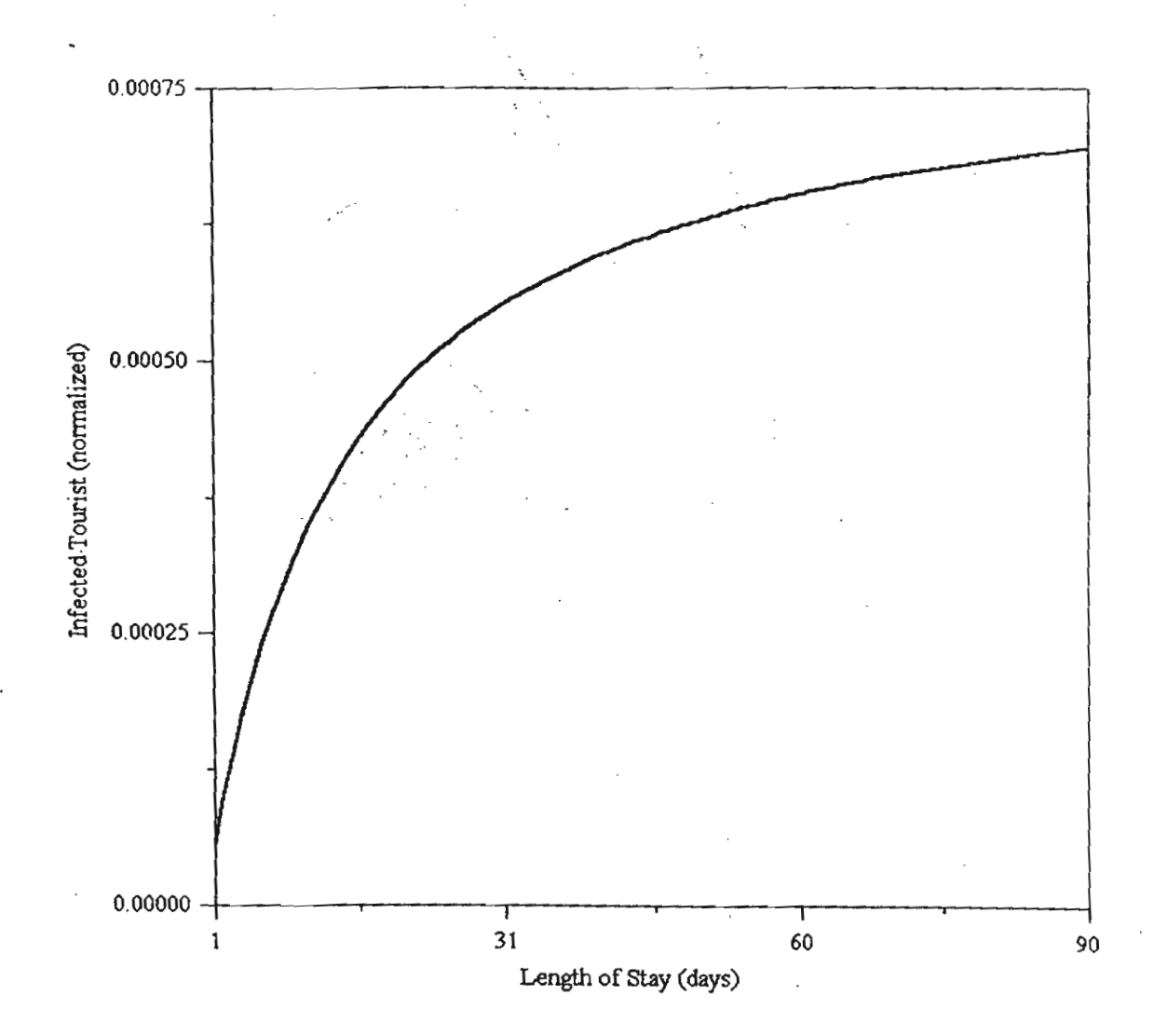
- CDC, 2003. Web site: http/www.cdc.gov/travel
- CDC, 1994. Epidemiologic Notes and Reports, Dengue Fever among U.S. Military Personnel-Hati. Spetember 19-November 4, 1994, MMWR 43(46): 845-848.
- Esteva L, Vargas C, 1998. Analysis of a dengue disease transmission model. *Math. BioSci.* 150: 131-151 (1998).
- Gubler DJ., Dengue and Dengue Hemorrhagic Fever, Clin. Mirobiol. Rev. 1998, 11:480-91.
- Hales S, de Wiet N, Maindonald J, Woodward A, 2002. Potential effect of population and climate changes on global distribution of dengue fever: an empirical model. *The Lancet* 360: 830-34.
- Lindback H, Lindback J, Tegnell A, Janzon R, Vene S, Ekdahl, 2003. Dengue fever in travelers to the tropics, 1998 and 1999. Emerg Infect Dis [serial online] 2003 Apr[date cited] 8. Available from URL:http//www.cdc.gov/ncidod/EID/vol9no4/02-0267.htm
- May MM., Stability and Complexity in Model Ecosystems. Princeton U. Press (Princeton, N.J.) 1973.
- Potasman I, Srugo I, Schwartz E, 1999, Dengue seroconversion amoug Israeli travelers to tropical countries. *Emer. Inf. Dis.* 5: 824-82713.
- Schwartz E, Mendelsen E, Sidi Y, 1996, Dengue fever amoug travelers. Am. J. Med. 101: 516-20.
- Sharp TW, Wallace MR, Hayes CG, Sanchez JL, DeFraites RF, Arthur RR, et al., 1996,
   Dengue fever in U.S. troops during Operation Restore Hope, Somalia, 1992-1993. Am. J.
   Trop. Med. Hyg. 53: 89-94.
- TropNetEurop Sentinel Surveillance, 2002. Dengue fever in 2002. Special Report 23.06.02

## Figure Caption.

- Figure 1. Numerical Solutions of Eqns. (2a) to (2e). (1a) Phase space trajectory of  $I_h$   $S_h$  for the case of  $\tau_1$  = 90 days. (1b) Time development of the infected travelers for this case. Values of other parameters given in the text.
- Figure 2. Equilibrium values of infected travelers population as a function of the time they stay in an endemic area..







# Effect of bird-to-bird transmission of the West Nile virus on the dynamics of the transmission of this disease

by

Surapol Naowarat and I Ming Tang 2,3

Department of Mathematics and <sup>2</sup>Department of Physics
Faculty of Science, Mahidol University, Bangkok, Thailand

<sup>3</sup>Institute of Science and Technology for Research and Development Salaya Campus, Mahidol University, Nakorn Pathom, Thailand

and

Abstract. Two recent publications (Komar et al, 2003, and Glaser et al, 2003) report that direct bird-to-bird transmission of West Nile virus is possible. The effect of a bird-to-bird transmission on the transmission dynamics of this virus is studied through mathematical modeling. The model still treats the bird-to-mosquito-to-bird as the main transmission route. The results of numerical calculations show that there are changes in the dynamics of the transmission of West Nile fever in humans when the non-mosquito transmission route becomes more important.

(Keywords: West Nile virus, disease transmission, mathematical modeling, atypical transmission route)

running title: Bird-to-bird transmission of the WN virus

## Correspondence:

I Ming Tang, Department of Physics, Faculty of Science, Mahidol University, Bangkok 10400, Thailand. Tel. +66 (0) 246-1381

E-mail address: scimt@mahidol.ac.th

# Effect of bird-to-bird transmission of the West Nile virus on the dynamics of the transmission of this disease

by

Surapol Naowarat and I Ming Tang<sup>2,3</sup>

Department of Mathematics and Department of Physics
Faculty of Science, Mahidol University, Bangkok, Thailand

and

<sup>3</sup>Institute of Science and Technology for Research and Development Salaya Campus, Mahidol University, Nakorn Pathom, Thailand

Abstract. Two recent publications (Komar et al, 2003, and Glaser et al, 2003) report that direct bird-to-bird transmission of West Nile virus is possible. The effect of a bird-to-bird transmission on the transmission dynamics of this virus is studied through mathematical modeling. The model still treats the bird-to-mosquito-to-bird as the main transmission route. The results of numerical calculations show that there are changes in the dynamics of the transmission of West Nile fever in humans when the non-mosquito transmission route becomes more important.

(Keywords: West Nile virus, disease transmission, mathematical modeling, atypical transmission route)

running title: Bird-to-bird transmission of the WN virus

## Correspondence:

I Ming Tang, Department of Physics, Faculty of Science, Mahidol University, Bangkok 10400, Thailand. Tel. +66 (0) 246-1381

E-mail address: scimt@mahidol.ac.th

## Introduction

The spread of diseases knows no international borders, witness the recent spread of severe acute respiratory syndrome (SARS) (WHO, 2003) and West Nile fever (WNF) (CDC, 2003). The first was spread by the international travel of infected persons from Hong Kong, while the second is believed to be spread by the migration of birds. WNF has been of particular concern to the American public health community because the disease, as was pointed out at the 69<sup>th</sup> annual meeting of the American Mosquito Control Association (Minnaepolis, and Minn, 2003), is a foretaste of possible newly emerging diseases that can be brought into the USA. Unlike SARS where the spread of the disease to uninfected countries can be controlled by the strict quarantine of the persons exposed to the SARS virus, the WN virus is spread to uninfected areas by the migration of birds (Rappole *et al*, 2000) that can not be controlled.

The spread of WN virus to the Western Hemisphere was preceded by its appearance in Romania in 1996-97. Hubalek and Halouzka, (1999) warned of the possible appearance of WNF epidemics in the temperate countries of Western Europe in the years following the Romanian outbreak. Instead, the migration of birds brought the epidemic to New York City (Bernard et al, 2000). From there, it spread to the rest of the Americas (again through the migration of birds' (Rappole et al, 2000)). Any regions in the world having the right conditions and are along the flight patterns of the migration of particular birds become candidates for future WNF epidemics. WNF is therefore a potential public health threat to Asia since one of the major bird migration paths in the world is along the West Coast of North America, over the Bering Sea and into North-eastern Asia. The case-fatality rate of this disease has been reported to be

as high as 10% in some regions (CDC, 20003; Hubalek and Halouzka, 1999) of the World, which have experienced the epidemic. WNF would therefore be of a great threat to countries that do not have a well-developed public health infrastructure. Also in countries having warmer climates, the transmission of West Nile virus can be year round (CDC, 2003).

A full understanding of the transmission dynamics of the WN virus is still being developed. In 2002, it was reported that human-to-human transmission of the WN virus was possible by 1) blood transfusion, 2) organ transplantation, 3) transplacental transfer, and 4) breast-feeding. Very recently, WN viral infection among turkey farm workers was reported (Glaser et al, 2003). Turkeys belong to one of the bird species that do not develop enough viremia to infect the mosquitoes that bite them. The authors suggested that the transmission was accomplished by some less typical routes, e.g., exposure of broken skin or mucous to infected turkey feces or exposure to aerosolized infected turkey feces. The last route is believed to be the means by which the 280 people at the Amoy Gardens Apartment Complex in Hong Kong became infected with the SARS (WHO, 2003). Komar et al. (2003) have found WN virus in the feces of 71% of the 24 species of (infected) birds they studied and that the American Crow was one of them.

One of the best ways to study the effects of non-typical routes of infections or specific public heath measures is through mathematical modeling. During the early stages of the WNF epidemic in New York City, Thomas and Urena, (2001) introduced a mathematical model to describe the evolution of West Nile-like encephalitis in New York City. Their model was based on several assumptions, which have subsequently turned out to be wrong. This report is concerned with the effects of non-mosquito transmission (through inhalation of aerosolized

In the above,  $S_{b(h)}$  is the density of the susceptible bird (human) population and  $I_{b(m(h))}$  is the density of the infected bird (mosquito(human)) population. We have assumed that the total populations of the three groups are constant and so  $S_b + I_b + R_b = 1$ ,  $S_m + I_m = 1$  and  $S_h + I_h + R_h = 1$  (where R represents the density of the recovered in each group). The total bird population is denoted by  $N_b$ , which we take to be a constant. This occurs if we assume that the no additional deaths are caused disease. This is an approximation given that many dead birds are seen during the epidemic.  $d_b$ ,  $\mu_b$  and  $r_b$  are the rates at which the birds are introduced in the location, died of natural causes and recover from the virus, respectively. The birth rate, the death rate and the recovery rates of the human population are denoted as  $\lambda_b$ ,  $\mu_b$  and  $r_b$ .  $\mu_m$  is the death rate of the mosquitoes.  $\gamma_b$ ,  $\gamma_m$  and  $\gamma_h$  are the rates at which the WN virus is transmitted to a bird by a bite of the mosquito. Because the viremia in an infected human is not high enough for the virus to be transmitted to a susceptible mosquito, the transmission rate  $r_{b \to m}$  is zero.

The factor

$$\left[\frac{aI_b}{b+I_b}\right] \tag{2}$$

is a Holling type II response function. It goes to zero as  $I_b \to 0$  and goes to a non-zero constant as  $I_b$  becomes large. Its presence means that the direction transmission of the WN virus only occurs when the density of the birds is large, i.e., during the flocking of the birds. In normal situations, the birds are spread out and so the mosquitoes are needed in order to maintain the virus in the bird population. What determines whether the density is small or large is the constant b, whether  $I_b < b$  or > b.

## Results

## Numerical Solutions

We have numerically solved eqns (1a) to (1e) for different values of a, a measure of the contribution of the bird-to-bird route to the transmission of the West Nile virus among the birds belonging the *Corvidae* family. B was chosen so that calculated density of birds varied from being a high density and a low density during different periods in the transmission cycle.

Table 1

Other parameters used in the calculations

Rate at which birds are introduced	d <sub>b</sub>	1/2,920	days
Death rate of the birds	μь		**
Recovery rate of infected birds	гь	1/3	days
Birth rate of humans	λ <sub>h</sub>	1/21,90	0 days
Death rate of humans	μդ		**
Recovery rate of infected humans	r <sub>h</sub>	1/30	days
Death rates of mosquitoes	$\mu_{m}$	1/25	days
Transmission probability from			
an infected mosquito to a bird	γь	0.95	
Transmission probability from			
an infected bird to a mosquito	γm	0.0792	
Transmission probability from			
an infected mosquito to a human	γh	0.275	
		l	•

In Figure 1, we show the trajectory of the human population densities in the  $I_h$ - $I_b$  phase space for increasing contributions of the bird-to-bird route to the transmission

of the West Nile virus. B is set to 0.001. The value of a is changed from 0 (Fig 1a) to 0.475 (Fig 1b), to 0.95 (Fig 1c) and to 1.9 (Fig 1d). Fig 1a, shows that the trajectory spirals into its equilibrium state. As the contribution of the bird-to-bird route begins to increase, Fig 1b shows that the trajectory is spiraling into a tight limit cycle. As the contribution is further increases, the trajectories exhibit more complicated limit cycles behavior (Fig 1c and 1d).

In Figure 2, we show the trajectories for the case b = 0.0025. The values of a are now; 0.475 (Fig 2a), 0.95 (Fig 2b), 1.9 (Fig 2c) and 2.85 (Fig 2d). Comparing Fig 1b and Fig 2a, we see for the same values of 'a' (measure of the contribution of the bird-to-bid route to the transmission dynamics, an increase in the parameter 'b' delays the transition of the trajectory into a limit cycle. As we mentioned before, 'b' is a parameter that determines at what density the new transmission route makes a difference to the dynamics of the spread of the disease.

## Discussion

The present study shows that the presence of bird-to-bird transmission can play an important role in the transmission of West Nile Fever. Bird-to-bird transmission of WN virus has been shown to be possible when the density of birds (including some belonging to the *corvidae* family) is high. We have used a Holling type II response function to represent the existence of two contact rates for this route of infection. Our results indicate that a limit cycle trajectory can be prevented by keeping the density of the birds lower, which can be done by preventing the birds from flocking together before the beginning of the mosquito scason.

## Acknowledgements

Surapol Naowarat would like to thank the Secondary Education Quality Improvement Project, Ministry of Education, Thailand for financial support.

## References

- Bernard KA, Maffei JG, Jones SA, et al. West Nile Virus Infection in Birds and Mosquitoes, New York State, 2000. Emerg Infect Dis 2000; 7: 679-85.
- Centers for Disease Control and Prevention. Epidemic/Epizootic West Nile Virus in the United States: Guidelines for Surveillance, Prevention, and Control. 3<sup>rd</sup> Revision, 2003.
- Glaser LC, Wegner MV, Davis JP. West Nile Virus Infection Among Turkey Breeder Fram Workers-Wisconsin, 2002. MMWR 2003; 52:1017-9.
- Hubalek Z, Halouzka J. West Nile Fever-a Reemerging Mosquito-Borne Viral disease in Europe. Emerg Infect Dis 1999; 5: 643-50.
- 5. In Questions and Answers. October 23, 2003. Available at <a href="http://www.cdc.gov/nicdod/bivbid/westnile/index.htm">http://www.cdc.gov/nicdod/bivbid/westnile/index.htm</a>.
- In Vertebrate Ecology. July 2, 2003. Available at http://www.cdc.gov/nicdod/bivbid/westnile/index.htm.
- Komar N, Langevin S, Hinten S, et al. Experimental Infection of North American Birds with the New York 1999 Strain of West Nile Virus. Emerg Infect Dis 2003; 9: 311-22.
- American Mosquito Control Association. The 69 th annual meeting. Minneapolis, Minnesota, March 1-6, 2003.
- Nasci RS, Savage HM, White DJ, et al. West Nile Virus in Overwintering Culex Mosquitoes, New York City, 2000. Emerg. Infect. Dis. 2000; 7: 1-3.
- Rappole JH, Derrickson SR, Hubalek Z. Migratory Birds and Spread of West Nile Virus in the Western Hemisphere. Emerg Infect Dis 2000; 6: 319-28.

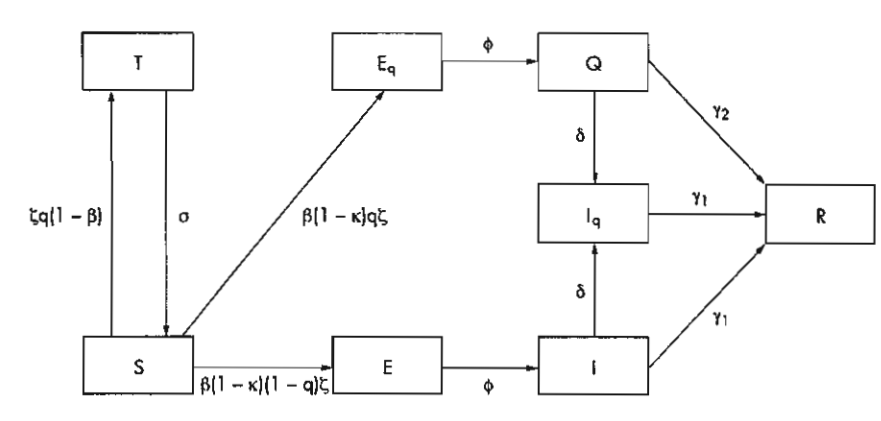


Figure 1 Transmission dynamics of the SARS taking into account the impact of precautionary measures and quarantine system. The subscript a denotes whether the new infections are quarantined or not with a proportion q. When 100% effective precautionary measures are implemented, a proportion, κ, of the potentially infected contacts is protected. S and I represent the proportion of the population susceptible and infectious; E, the proportion of untraced latent persons; Eq the proportion of traced latent contacts; T, the proportion of traced uninfected contacts; Q the proportion of infectious in guarantine; la the proportion of infectious isolated, R the proportion of recovered and death.

biological and intervention assumptions about the transmission dynamics of SARS (fig 1). An SARS-CoV infection of the susceptible population (S) results first in a non-infectious incubation period, which constitute the latency period (E). A proportion of the exposed persons, who had taken effective precautionary measures, would not be infected.19 The others become infectious, often being symptomatic with fever followed by rapidly progressive respiratory compromise (these being labelled (1)) and, then slowly recover or die (R).1 While infectious, they transmit the disease to susceptible persons at a rate dependent on the basic reproductive rate, Ro. Two of the public health interventions for interrupting the transmission are quarantining the people who are known to have been exposed and therefore may be infected but are not yet ill (denoted by the compartments T and  $E_{qr}$  which does each refer to "traced but not infected" and "traced and infected" in fig 1) and moving infectious people into isolation  $(I_a)^{20}$  We assume each susceptible makes  $\zeta$  contacts per day with the infectious person. Among the known contacts (in S), some would be infected with the probability of  $\beta$  per contacts (and enter into Eq) and  $(1-\beta)$  remains uninfected (and enter into T). These processes can be modelled using an approximately parameterised set of differential equations(1) as follows:

$$\frac{dS}{dt} = \zeta(q - \beta(q + \kappa - 1))SI + \sigma T$$

$$\frac{dT}{dt} = (1 - \beta)q\zeta SI - \sigma T$$

$$\frac{dEq}{dt} = \beta q(1 - \kappa)\zeta SI - \phi E_q$$

$$\frac{dE}{dt} = \beta(1 - q)(1 - \kappa)\zeta SI - \phi E$$

$$\frac{dQ}{dt} = \phi Eq - (\gamma_2 + \delta)Q$$

$$\frac{dI}{dt} = \phi E - (\gamma_1 + \delta)I$$

$$\frac{dIq}{dt} = \delta(I + Q) - \gamma_1 I_q$$

$$\frac{dR}{dt} = \gamma_1 (I + Iq) + \gamma_2 Q$$
(1)

Given that our model is based on the Kermack and McKendrick epidemic model,21 the situation just before the entrance of infectious persons into the community is given by (S(t), E(t), I(t), R(t)) = (N, 0, 0, 0) and its subsequent development by:

$$\frac{dI(t)}{dt} = (\beta(1-q)(1-\kappa)\zeta N - (\gamma_1 + \delta))I(t)$$
(2)

where N is the size of the population in which the epidemic occurs. As the condition that SARS becomes possible to invade the community is  $\beta(1-q)(1-\kappa)\zeta N - (\zeta+\gamma_1) > 0$ , the basic reproductive rate, Ro, is given by:

$$R_0 = \frac{\beta(1-q)(1-\kappa)\zeta N}{\delta + \gamma_1} \tag{3}$$

A description of the other principal parameters in the model and of their assigned value is presented below.

### Parameter values

Table 1 contains the parameter values for our base case. Assuming that the biological variables for Japan do not differ much from those of Hong Kong because of similar population densities and lifestyles (this clearly being a rough assumption), we use the values given in the epidemic modelling of Hong Kong14 for those parameters whose values are not available for Japan. The infection rate β ζ is chosen so that  $R_0 = 3$ , which is the mean value on the order of 2 to 4 estimated in the previous studies done in similar ways.14 15 22 We assume that the pattern of contact is linearly related to the population size so that  $\zeta N$  denotes the daily number of contacts in the population. We varied Ro while doing sensitivity analyses with regards to q and  $\kappa$ . We assume that an attack of 10 initial cases entered into a population of 287 000 persons, supposedly Shinjuku, Tokyo, as our baseline case but vary the attack size between 0 and 20 cases in our sensitivity analysis. It is somewhat unrealistic to expect that the population at risk would be at the national or prefectural level as it would not be possible to have 100% of this population come into possible direct or indirect contact with the disease within the short time period of concern. We have instead considered the epidemic within a city or ward sized population level, such as Shinjuku. Here, Shinjuku is assumed because of its similar population density to Hong Kong in addition to its population size.

We first estimate the number of newly infected (secondary) cases that results in a failed invasion in certain community for different initial attack size. We defined "failed invasion" as there being no secondary cases within incubation period after contacts with infectious people. We then performed a linear regression analysis to establish the linear correlation using a simple mathematical formula.

Parameters	Description	Baseline values	Reference
β,	the probability of transmission per contacts	0.0666667 person/day	14
9	the daily rate at which latent individuals are traced	0.75	14, see text
κ	the proportion of exposed person who performed effective precaution	0	See text
φ	the average rate at which latent individuals become infectious	0.2/day	27
σ	the rate at which the traced uninfected contacts released into the community	0.2/day	29
ζ	the daily number of contacts per capita	9/person/day	14
δ	the mean daily rate at which infectious cases are isolated	0.0333333/day	14
Υı	the percapita rate for recovery and death	0.1666667/day	27
$(\gamma_2)^{-1}$	the mean duration for quarantine	10 days	29

Additional assumptions are that no transmission occurs from those people who are quarantined, isolated, dead, and recovered. As for the precautionary measures, we would like to point out that it may be too optimistic to assume that the measures are 100% effective so that there are no spreads of the disease among the people coming in contact with the infected. An analysis on the impact of isolation is not covered in this paper because it has already been well analysed.<sup>14</sup>

In this study, the total number of people in the population is taken to be constant during the epidemic. The background mortality rate is assumed to be negligible over the time periods examined. As the cases of "super-spread" events (SSEs), where a person may generate much more than the average number of secondary cases, has been described as a rare heterogeneous event,8 23 we did not take this mode of transmission into consideration as the known values  $R_0$  for SARS were calculated with certain adjustments of the number of secondary infections in this phenomenon and our aim is not to estimate the exact value of the basic reproductive rate but to understand, as a possible scenario in Japan, the role of initial attack size and interventions for the commonest transmission route. We assume that there is homogenous mixing among the infectious and susceptible, so that every infected person will pass the disease to exactly  $R_0$ susceptible persons simultaneously within an infectious period of  $(\gamma_t)^{-1}$  days. Simulations were performed with a time step of 0.1 days. The model has been programmed using Turbo Pascal Version 1.5 (Borland International, Scotts Valley, CA, USA) working on Microsoft Windows platform. All data from the program were analysed using Microsoft Excel 2000 (Microsoft Corporation, Redmond, WA, USA) except regression analysis performed using Epi Info 2002

(Centers for Disease Control and Prevention, Atlanta, GA, USA).

#### **RESULTS**

The results of a simple scenario analysis show the probable dynamics of the SARS epidemics under different conditions (fig 2). The results in the analyses are given for up to 50 days after the onset of epidemic in the figure. It is unrealistic to estimate for longer time periods as one should not expect the health policy and control strategies as well as social reactions to remain static over longer periods. In figure 2A, four possible trajectories are shown for different initial attack sizes-that is, how many infectious persons were first introduced into a specific community having a susceptible population. The number of newly infected cases quickly rises, peaks, and then falls when more than five initial number of infectious  $(1(0)N \ge 5)$  are introduced while dramatic increase is not seen with one initial infectious (I(0)N < I). Even though the control strategy remains the same, a more steep increase and more prolonged epidemic would be caused by bigger initial attack size. Figure 2B shows the model generated maximum number of newly infected as well as cumulative incidence over the time period examined. The maximum number of newly infected denotes the number of newly infected at the peak of the curve in figure 2A. It was found that there exists a linear correlation (coefficient of determination,  $r^2 = 0.998$ ) between the maximum number and the initial attack size. The cumulative incidence, on the other hand, looks like a power two dependence on the initial attack size that is mathematically expected as the cumulative incidence is the area between the curves and x axis in figure 2A. From a regression analysis, the relation between

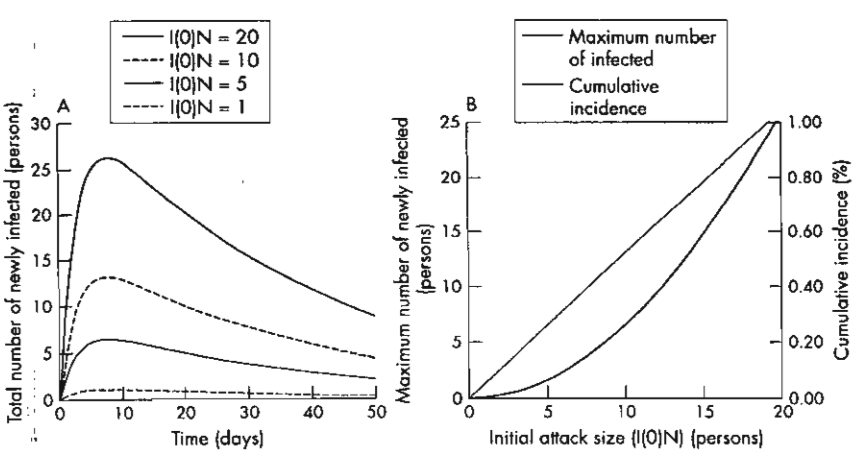


Figure 2 Dynamics of a SARS attack with the basic reproductive rate  $R_0 = 3$ . Effectiveness of the quarantine denoted by, q = 0.75, and of the precautionary measures,  $\kappa = 0$ . (A) Number of newly infected SARS cases according to initial number of infectious population. (B) Maximum number of newly infected SARS cases and the cumulative incidence as a function of the initial attack size (number of people initially infected).

www.jech.com

ĝ

the proportion of initial attack size (I(0)) and the proportion of maximum number of newly infected persons  $((E(t)+Eq(t))_{MAX})$  among total number of population, was found to be (under the assumptions leading to the epidemic)

$$(E(t) + Eq(t))_{MAX} = 1.295 \times 10^{-9} + 1.311I(0)$$
(4)

where  $1.295 \times 10^{-9}$  and 1.311 are the regression coefficient of intercept and slope, respectively. Here,  $1.295 \times 10^{-9}$  can be ignored as it does not lead to a large affect even though it is multiplied by total population N. Performing regression analysis by varying  $R_0$ , the correlation was found to be represented by:

$$(E(t) + Eq(t))_{MAX} = \left(\frac{R_0}{2} - 0.167\right)I(0)$$
 (5)

when  $R_0 < I$  because of public health interventions  $(r^2 = 0.977)$ . When we consider the maximum number of newly infected (denoted by m, where  $m = N(E(t) + Eq(t))_{MAX}$ ), we found that it was possible to relate this value with  $R_0$  and I(0) through:

$$I(0)N = \frac{m}{\frac{R_0}{2} - 0.167} \tag{6}$$

Next, we found the condition that would result in failed invasion (no secondary transmission) for each of the specific communities with population (N), is m < 1 in equation (6). Based on this, theoretically, at least 0.750 persons infected with SARS must be introduced into the population to produce secondary cases in our baseline simulation.

Figure 3A shows the number of newly infected SARS cases for various values of  $\kappa$  (the proportion of susceptible people who have undertaken the precautionary public health measures) and when no quarantine was carried out. Four possible trajectories are shown. Less effective precautionary measures ( $\kappa = 0.30$ ) lead to an exponential growth of SARS. Even with relatively high proportion of people undertaking precautionary measures ( $\kappa = 0.60$ ), a gradual increase in the number of new SARS cases is seen. When effective precautionary measures are taken by a higher proportion of the susceptible persons, one sees qualitative reductions in the number of cases. This occurs even in the absence of quarantine. The effect of a quarantine system is shown by the linear correlation with  $R_0$  in figure 3B. It is seen that in the absence of any precautionary measures, one needs to quarantine at least 66.7% of the susceptible people who had contacts into compartment Eq and T in order for the epidemic to die down. Other information can be gained from the formula of basic reproductive rate, by noting that by interchangeable variables and q in figures 3A and 3B, we would be looking at the effects of changing the values of q with no precautionary measures being taken. Hence, the

## Key points

- Initial attack size is one of the determinants of whether SARS can successfully invade or not.
- It is seen that the introduction of only a few cases into certain communities would not lead easily to an epidemic.

condition to break the chain in person to person transmission of SARS can be described as:

$$(1-q)(1-\kappa) < \frac{1}{R_0} \tag{7}$$

This relation is shown in figure 3C. The curve shows the cut off points for  $R_0$  to be 1. Figure 3D shows the changing pattern of  $R_0$  for different combination of quarantine coverage and precautionary measure coverage in a three dimensional illustration. For the baseline simulation where  $R_0 = 3$ , the left form of equation (7) should be less than 0.33 in order to control SARS effectively.

#### **DISCUSSION**

Two important conclusions can be drawn from our analyses on the assessment of the role of initial attack size, and of the impact of interventions on possible SARS epidemic in Japan. Firstly, it is shown that the maximum number of newly infected, or the crude size of epidemic, could be roughly estimated based on initial attack size under certain public health interventions. In other words, it would be possible to predict the fate of an epidemic when SARS infected persons enter each community having approximately the same transmissibility and using the same control strategy. Secondly, the possible trajectories of a SARS epidemic depends on the levels of public health interventions as quarantine and precautionary measures greatly affect the transmissibility. There exist threshold levels of interventions to cause the SARS epidemic to settle down, and improved effective interventions can lead to dramatic decreases in its incidence.

Despite problems with the accuracy and uncertainty with the data released by WHO,24 a simple dynamical model still gives reasonable simulations of the SARS dynamics. Except for the crucial parameter for the transmissibility,  $\beta \zeta$ , it was determined that the initial attack size is one of the most important factors to determine the course of the epidemic. It should be pointed out the cumulative incidence follows a power two law dependence on the initial attack size while the maximum number has a linear correlation with the size. Thus, a larger epidemic would be experienced if the initial attack size grows. The contribution of initial attack size to a SARS outbreak can be transliterated into equation (6). Although it is obtained within a theoretical framework based on certain assumptions without taking stochastic effect into account, and though the condition such as I(0)N<1 might not be practical in the real situation, we showed that the introduction of a few cases into a given community would not necessarily lead to an epidemic using this formula-that is, successful invasion is hard to be achieved with a few initial cases. It might be possible to say that the introduction of only a few infectious persons into Japan was one of the reasons for Japan not experiencing the SARS epidemic so far. Although the fate of epidemic is determined by threshold theorem, that is,  $R_0 > 1$  or not, successful or failed invasion itself can be considered using generalised formula such as ours under the condition when  $R_0 < 1$ . The formula could be reasonably applied to other countries.

One must be cautious about its application, however, because the formula is based on mathematical assumptions that might sometimes not be true. As each compartment, denotes the proportion of total population, it could give us the value of real number of persons to be smaller than 1. This may not be practical findings, but theoretically this notion becomes important in analyses such as ours. It should be also noted that it is based on several simple assumptions that may not be the same for all countries. The pattern of contacts between people differs from country to country. Lipsitch et al



Nishiura, Patanarapelert, Sriprom, et al

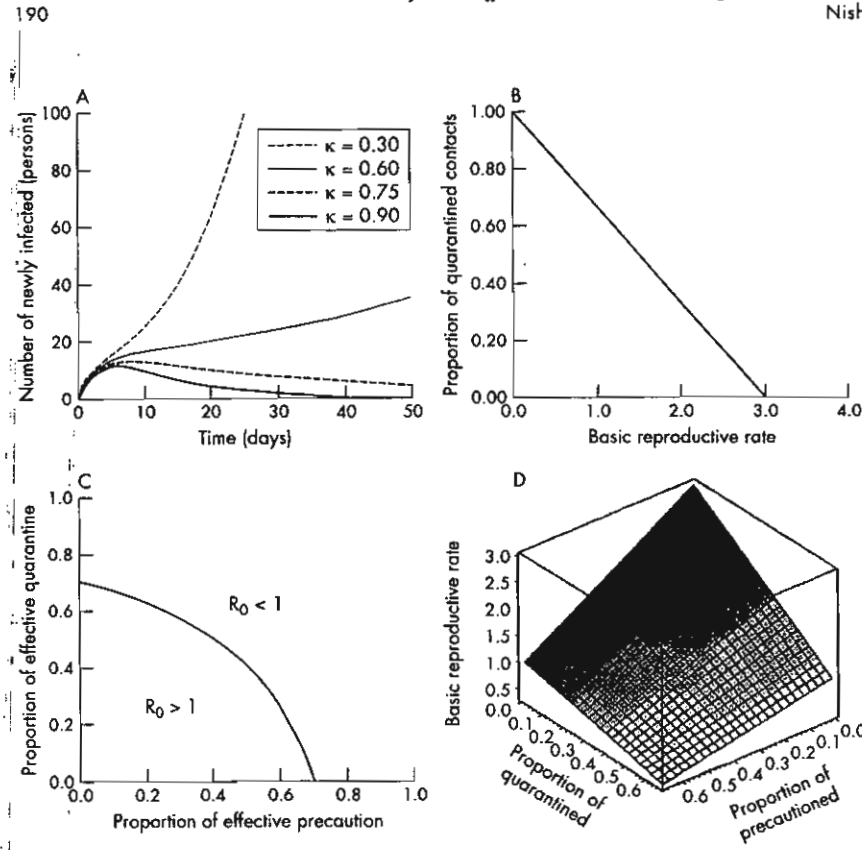


Figure 3 (A) Number of newly infected SARS cases for different proportion of susceptible persons who performed 100% effective precautionary measures for the case of  $R_0 = 3$ , and q = 0. (B) and (C) Sensitivity analysis for model parameters whose values are unknown. Basic reproductive rate,  $R_0$ , versus (B) the proportion of quarantined contacts, (C) both the proportion of quarantined contacts and the proportion of exposed persons who took effective precautionary measures. (D) The necessary condition to have the basic reproduction ratio lower than 1 for different values of q and  $\kappa$ .

described an outbreak of SARS through the use of probability theory of non-extinction of a branching process. Such a probability theory should be taken into account when it comes to describe the possibility of a SARS epidemic. It also should be noted that the size of the epidemic does not always depend on the initial attack size. This is clearly evident when we note that 76% of the infections in Singapore were acquired in a healthcare facility. SARS can easily be spread by direct personal contact in the hospital setting. As is well known, air borne transmission is not through the droplet nuclei but is instead through the large droplets, themselves. The wearing of a surgical mask can stop this.

Another example of why the initial attack size may not be the important factor is seen in Hong Kong. There we see that clusters have played an important part in the course of the epidemic in that city." The role of close and casual contacts<sup>26</sup> and the possibility of other routes of transmission such as through touching contaminated objects or other unknown way should be incorporated into the model.

There has been an intensive assessment of the different public health interventions that contributed substantially to the eventual curtailing of the epidemic in Hong Kong.<sup>27</sup> It is well known that an effective strategy requires aggressive public health measures in combination with stringent

## Policy implications

- There exist threshold levels of interventions at which the SARS epidemic settles down.
- Two of the most effective policy procedures to prevent new infections would be to apply stringent precautionary measures and to impose quicker and more effective quarantine of the exposed populace.

hospital infection control practices that meet the recommendations of World Health Organisation. 39 30 The SARS pandemic has shown that governments and public health officials need to consider the use of quarantine as a public health tool to prevent the spread of infectious diseases, particularly when other preventive interventions (for example, vaccines and antibiotics) are unavailable." From our study, it is shown that either 100% effective precautionary measures or quarantine would lead to decline in the incidence. Both of them reduce Ro in a linear way unlike the practice of isolation. The importance in the coverage should be therefore emphasised. Although recent studies with modelling14 15 provided us with dynamics of SARS including transmissibility as well as the impact of quarantine and isolation, the role of precautionary steps was not taken into consideration. Precautionary measures themselves are quite important especially in hospital settings because a high proportion of the SARS patients were healthcare workers as was pointed out.23 26

The increased amount of world travel increases the likelihood of this disease spreading faster than past worldwide epidemics. It is therefore critically important to prepare for the possible introduction of SARS into the country by introducing specific public health measures now. Two of the most effective procedures would to introduce stringent precautionary measures and to impose better and quicker quarantine of those exposed. This would reduce the number of people who get a secondary infection from contacts with infectious persons. The important challenge is that some of the most important public health measures have to be taken outside the health sector."2 These measures include maintenance in a healthy and hygienic environment such as penalties for spitting and closely monitoring the integrity of sewage disposal systems.12 33 The government distributing free surgical masks and showing how they can be used effectively can overcome the strong fear among the general

population about this disease. In addition to infection control measures, it should be noted that case detection, reporting, clear and timely dissemination of information would play important parts in the fight against SARS."

Our study has several limitations, however. Firstly, one of the major problems, which the world must confront, is the absence of knowledge on SARS. In particular, it would be hard to predict the possible trajectories in Japan as the country has no experience with this epidemic. We believe that one approach to overcome the problem of risk management is to model the potential episodes with mathematical modelling. This study was conducted with only a few known parameter values. Although we used a single value of  $R_0$ throughout an epidemic, Ro is likely to decrease after the onset of an epidemic is detected and announced. The qualitative and quantitative patterns of diminishing Ro, because of behavioural change (that is, if people reduce the frequency of going out), should be incorporated in further studies. We here performed sensitivity analyses of  $R_0$  for parameters whose values are not known. Secondly, we made a simple assumption that either the precautionary measures or the quarantine were perfectly effective (an optimistic assumption) or not. Thirdly, although possible outcomes were determined for a certain population sizes, for example, that of Shinjuku, Tokyo, one should not expect the same outcome for cities of the same size because of regional variances in the age distribution, behaviour, and contact pattern. Intercommunity transportation, migration, should also be taken into account. Further research is therefore necessary. It would be important to incorporate probability theory and contact patterns into the research as the epidemic threshold parameters should be considered based on approximating the infection process, during its initial stages, by a branching process.14 The mathematical model might be modified so that the effects of changing staffing policy for the healthcare facilities could be simulated. Finally, incorporating quarantine of visitors from overseas might give us more practical simulation.

#### **ACKNOWLEDGEMENTS**

This work was mainly carried out while HN was staying in Thailand. The authors are grateful to Dr Pratap Singhasivanon and the other members of Department of Tropical Hygiene, Mahidol University for their coordination in our research. We furthermore sincerely thank Professor Edward Kaplan at Yale School of Management and Professor Masayuki Kakehashi at Institute of Health Sciences, Hiroshima University School of Medicine for their technical advice and comments.

## Authors' affiliations

H Nishiura, Bangkok School of Tropical Medicine, Mahidol University,

H Nishiura, K Patanarapelert, M Sriprom, W Sarakom, 5 Sriyab, I Ming Tang, Department of Mathematics, Faculty of Science, Mahidol

I Ming Tang, Institute of Science and Technology for Research and Development, Mahidol University

Funding: none.

Conflicts of interest: none declared.

This work was presented in part at the SARS e-Conference by World Health Risk Management Center, October 2003 held on internet.

#### REFERENCES

Tsang KW, Ho PL, Ooi GC, et al. A cluster of cases of severe acute respiratory syndrome in Hong Kong. N Engl J Med 2003;348:1977–85.

- 2 World Health Organisation. Cumulative number of reported cases (SARS) since March 17, 2003. Geneva: World Health Organisation, 2003. (http://www.who.int/csr/sarscountry/en/).
- www.wno.inr/csr/sarscountry/en/).

  World Health Organisation. Case definitions for surveillance of severe acute respiratory syndrome (SARS). Geneva: World Health Organisation, 2003, [http://www.who.int/csr/sars/casedefinition/en].

  Galvani AP, Lei X, Jewell NP. Severe acute respiratory syndrome: temporal stability and geographic variation in case-fatality rates and doubling times.

  Emerg Infect Dis 2003;8:991-5.

  Gentheriting II. Ensist but four enough? Personalize the acide in the content of the
- Emerg Intect Dis 2003;8991-5.

  Gerberding JL Faster...but fast enough? Responding to the epidemic of Severe Acute Respiratory Syndrome. N Engl J Med 2003;348:2030-1.

  Poutanen SM, Low DE, Henry B, et al. Identification of severe acute respiratory syndrome in Canada. N Engl J Med 2003;348:1995-2005.

  Drazen IM. Case clusters of the severe acute respiratory syndrome. N Engl J Med 2003;348:e6-7.

- N Engl J Med 2003;348:e6-7.

  8 Lee N, Hui D, Wu A, et al. A major outbreak of severe acute respiratory syndrome in Hong Kang. N Engl J Med 2003;348:1986-94.

  9 World Health Organisation. Update 96—Taiwan, China: SARS transmission interrupted in lost outbreak area. Geneva: World Health Organisation, 2003. (http://www.who.int/csr/don/2003\_07\_05/en/print.html).

  10 The Ministry of Foreign Affairs of Japan. Severe acute respiratory syndrome (SARS) (Current situation in Japan and Measures taken by the government of Japan). Tokyo: The Ministry of Foreign Affairs of Japan, 2003.

  11 Anonymous. Taiwan tourist diagnosed with SARS in Japan. Canadian Press 2003;19 Jun. (http://cnews.canae.co/CNEWS/World/2003/06/26/
- 19 Jun. (http://cnews.canoe.ca/CNEWS/World/2003/06/26/ 119688-ap.html).

- 119488-ap.html).

  Ananymous. Japan SARS-free thanks to luck.and hand-washing. Reuters Health 2003;15 Apr. [http://asia.reuters.com/newsArticle.jhtml?type=healthNews&storyID=2570826).

  Abdullah ASM. Virus pathogens suggest an autumn return. J Epidemial Community Health 2003;57:770-1.

  Lipsitch M, Cohen T, Cooper B, et al. Transmission dynamics and control of severe acute respiratory syndrome. Science 2003;300:1966-70.

  Riley S, Fraser C, Donnelly CA, et al. Transmission dynamics of the etiological agent of SARS in Hong Kong: impact of public health interventions. Science 2003:300:1961-6. agent of SAKS III 1. 2003;300:1961-6.
- Chai BCK, Pak AWP. A simple approximate mathematical model to predict the number of SARS cases and deaths. J Epidemiol Community Health
- 2003;37:831-5.

  Blower SM, Medley GF. Epidemiology, HIV and drugs: mathematical models and data. Br J Addiction 1992;87:31-9.

  Anderson RM, May RM. Infectious diseases of humans: dynamics and control. Oxford: Oxford University Press, 1992.

  Seto WH, Tsang D, Yung RWH, et al. Effectiveness of precautions against
- droplets and contact in prevention of nosocomial transmission of severe acute respiratory syndrome (SARS). Lancet 2003;361:1519-20.

  Center for Disease Control and Prevention. Fact sheet: severe acute
- respiratory syndrome—isolation and quarantine. Atlanta, GA: Centers for Disease Control and Prevention, 2003.

  Kermack WO, McKendrick AG. Contributions to the mathematical theory epidemics-1. Proc R Soc 1927;115A:700-21, (Reprinted Bull Math Biol 2003, 22-25). 1991:53:33-55
- Dye C, Gay N. Modeling the SARS epidemic. Science 2003;300:1884-5.
  Centers for Disease Control and Prevention. Severe acute respiratory
- syndrome—Singapore, 2003. MMWR 2003;52:405–11.

  Rainer TH, Cameron PA, Smit DV, et al. Evaluation of WHO criteria for identifying patients with severe acute respiratory syndrome out of hospital: prospective observational study. BMJ 2003;326:1354–8.
- Giesecke J. Modern infectious disease epidemiology. 2nd edn. London: Arnold, 2002.
- Dwosh HA, Hong HHL, Austgarden D, et al. Identification and containment of an outbreak of SARS in a community hospital. Can Med Assoc J 2003;168:1415-20.
- Donnelly CA, Ghani AC, Leung GM, et al. Epidemiological determinants of spread of casual agent of severe acute respiratory syndrome in Hong Kong. Lancet 2003;361:1761-6.

  Song B, Castillo-Chaves C, Aparicia JP. Tuberculosis models with fast and
- dynamics: the role of close and casual contacts. Math Biosci 2002:180:187-205.
- World Health Organisation. Severe acute respiratory syndrome (SARS): Status of the outbreak and lessans for the immediate future. Geneva: World
- Status of the outbreak and tessans for the immediate luture. Seneral Propagation, 2003.

  Twu SJ, Chen TJ, Chen CJ, et al. Control measures for severe acute respiratory syndrome (SARS) in Taiwan. Emerg Infect Dis (http://www.cdc.gov/ncidod/EID/vol9no6/03-0283.htm)
- Centers for Disease Control and Prevention. Use of quarantine to prevent transmission of severe acute respiratory syndrome—Taiwan, 2003 MMWR 2003:52:680-3
- Lee A, Abdullah ASM. Severe acute respiratory syndrome: a challenge for public health practice in Hong Kong. *J Epidemiol Community Health* 2003;57:655–8.
- 33 Abdullah ASM, Tomlinson B, Cockram CS, et al. Lessons from the severe acute respiratory syndrome outbreak in Hong Kong. Emerg Infect Dis 2003;9:1042-5.
- Diekmann O, Heesterbeek JAP. Mothematical epidemiology of infectious diseases. Model building, analysis and inerpretation. New York: Wiley,

## Original Article

Modeling for a Smallpox-vaccination Policy against Possible Bioterrorism in Japan: The Impact of Long-lasting Vaccinal Immunity

Hiroshi Nishiura,1.2 and I. Ming Tang.2.3

BACKGROUND: There has been concern that variola virus might be held clandestinely elsewhere. Through constructing mathematical model based on the detailed epidemiologic data, we focused on simulating the various possible scenarios arising from a bioterrorist attack whereby smallpox virus was introduced into Japan, and sought to develop the most effective way of nationwide vaccination policy based on the theory of residual immunity.

METHOD: The analysis is based on a deterministic mathematical model which predicted the epidemiologic outcome while simultaneously evaluating the effect of any specified control strategy of the smallpox epidemic. To clarify the required amount of vaccines, we performed mathematical analysis for hypothetical population to acquire herd immunity based on long-lasting vaccinal immunity.

RESULTS: It is demonstrated that the crude size of the potential epidemic could be greatly affected by possible level of residual immunity. The results also suggest the possibility to develop optimal distribution of nationwide vaccination according to the immune status. The prevalence at 50th day among population without immunity in our simulation would be approximately 405 times greater than expected population with residual immunity, and required amount of vaccines for equal distribution would be 3.13 times more than optimal distribution.

CONCLUSION: The mathematical model formulated could determine the vaccination priority based on the real status of immunity which required much less amount of vaccinations than would be calculated using an equal distribution program. It is therefore crucial to determine the real immunity status of the population via epidemiologic studies.

J Epidemiol 2004;14:41-50.

Key words: smallpox; bioterrorism; models, mathematical; vaccination; immunity.

Bioterrorism is the intentional use of micro-organisms, or their products, to cause harm, and may be used to target humans, animals or crops. Variola virus, which causes smallpox, is one of the most dangerous bioterrorism agents to be worried about. If used as a biological weapon, it poses a serious threat to the civilian populations because of its case fatality proportion of 30% or more among the unvaccinated persons and the absence of specific therapy. Furthermore, because the World Health Organization (WHO) announced the total eradication of the smallpox in 1979, routine vaccination gradually ceased worldwide, leaving the younger age individuals today who have never been vaccinated, and are thus extremely susceptible to smallpox infection. There is

concern that the virus might be held clandestinely and less securely elsewhere. In the aftermath of the September 11 terrorist attacks in 2001, the United States, after receiving direct threats, began stockpiling 286 million doses of smallpox vaccine, and the Centers for Disease Control and Prevention (CDC) interim response plan calling for targeted vaccination and quarantine. Disaster plans for managing a biological attack must be developed in detail and realistic training provided to ensure effective response to an actual terrorist event.

Japan should not feel that it is exempt from the various terrorist threats. It has been said that if Japan were to become a key ally in a United States-led military campaign against terrorism in Asia,

Received November 5, 2003, and accepted February 11, 2004.

Bangkok School of Tropical Medicine, Mahidol University, Thailand.

<sup>&</sup>lt;sup>2</sup> Department of Mathematics, Faculty of Science, Mahidol University, Thailand.

Institute of Science & Technology for Research and Development, Mahidol University, Thailand.

Addréss for correspondence: Dr. Hiroshi Nishiura, The Research Institute of Tuberculosis, Matsuyama 3-1-24, Kiyose, Tokyo 204-18533, Japan.

both Japan and Japanese living abroad would become terrorist targets.7 In response to the mailborne anthrax terrorist attacks in the United States, the Ministry of Health, Labor and Welfare of the Japanese government has formed a working group on protection against bioterrorism in December 2001, and has started preparing mass production of vaccine against smallpox for 10 million civilian persons using less neuropathogenic tissue culture freeze-dried vaccine with LC16m8 strain.9 The Ministry has also begun to prepare vaccines for first-line health care workers in case of smallpox bioterrorism. The Self Defense Force personnel who are serving in peace-keeping operations in the Middle Eastern countries have already been vaccinated. Although the Ministry has announced a contingency plan for a possible outbreak of smallpox in Japan,10 detailed information and guidelines are still lacking when compared to the ones produced by the CDC. Although the Japanese government prepared its plan using much from the CDC, unlike CDC, it has neither given the scientific justification in their policy for amount of the vaccines necessary, nor provided the reason why post-exposure vaccination should be carried out within the four days after exposure. Because the Japanese government has not made it clear to the public its policy and intention regarding the smallpox vaccination, the public until date remains ignorant and thus unprepared.

In the face of many unknowns, several mathematical epidemiologists have challenged the presently used models for assessing public health interventions including the vaccination policy regarding the survival and spread of smallpox, "LIZLIAM or for estimating its transmissibility using past epidemiologic records. 15.16 Models may be conceptualized as thought experiments, and are extremely useful tools when physical experiments are impossible

to perform due to time, monetary, practical, or ethical constraints." The purposes of this study are to simulate the possible scenarios which could arise from a bioterrorist attack of introducing smallpox into Japan, and to describe the possible outcome of different nationwide vaccination policies based on the hypothesis on residual immunity in the population. This would allow the Japanese government to impose its original vaccination policy, and determine what new epidemiologic study is needed.

#### **METHODS**

#### Mathematical Model

The analysis presented in this paper is based on a deterministic mathematical model for epidemic which could predict the epidemiologic outcome while simultaneously evaluating the effect of any specified control strategy on smallpox. The model is a modification of the SEIJR model,18 which separates the population into the classes of people who are susceptible (S), exposed (E), infectious (I), diagnosed (J), and recovered (R). The model is described by a set of ordinal differential equations which are based upon specific biological and intervention assumptions about the transmission dynamics of smallpox (Figure 1). We first separate the susceptible population (S) into three age groups according to the expected immunity:19 (Group A) represents those who have never been vaccinated (Sa) i.e., born after 1977, and who constitute the proportion (1-x-y) of the total population, (Group B) represents those who received only primary vaccination (SB) i.e., born between 1969-1977, and is denoted as xN, and (Group C) represents those who have received both primary and revaccination (Sc) i.e., born before 1969, and is denoted as yN. A

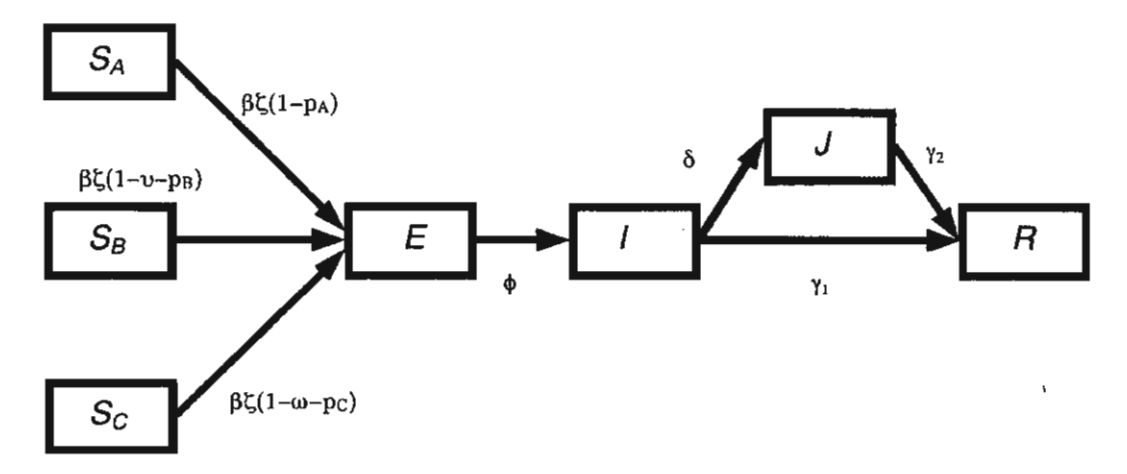


Figure 1. The transmission dynamics of the smallpox taking into account the impact of different residual immunity and interventions.

Here: SA, SB and SC represents the proportion of population susceptible among Groups A (born after 1977), B (born in 1969-1977), and C (born before 1969), respectively; E represents the proportion of untraced latent individuals; I the proportion of the population infectious; J the proportion of infectious isolated; R the proportion of recovered and death.

certain proportion from each population groups (A, B, and C) are assumed to be effectively protected by present vaccination strategy, and denoted as ps. ps , and pc. A smallpox infection among the susceptible population (SA, SB, and Sc) firstly begins with a non-infectious incubation period (E), which constitute the latency period. It would be followed by prodrome with non-specific symptoms, and by an overtly infectious (I) and symptomatic stage, characterized by a pustular rash. By this time, most of infections would be apparent and be diagnosed (J). The patients would then either slowly recover or die (R).20 While infectious, the infected patients can transmit the disease to other susceptible individuals at a rate dependent on the basic reproduction number, Ro.21 There are currently three possible public health interventions for interrupting the transmission of the virus. These are (1) vaccinating those who are at risk or may have already been exposed, (2) quarantining certain proportion of those who are known to have been exposed and therefore may be infected but are not yet ill (see Appendix), and (3) moving infectious individuals (1) into isolation after being diagnosed (J). We assume that each susceptible makes  $\zeta$  contacts per day with an infectious person. Among the known contacts (in SA, SB, and Sc), some would be infected with the probability of  $\beta$  per contacts (and enter into E) and  $(I - \beta)$ remains uninfected and susceptible. Untraced infectious persons would recover or die after ( y 1)" days. Apparent infectious person would be diagnosed and isolated with the mean daily rate  $\delta$ (and enter into J), and recover or die  $(y_2)^{-1}$  days after isolation. Because isolation can never be perfect, we estimate that those who are isolated also contribute to the generation of newly infected cases. Therefore, relative measure of reduced risk among those isolated ( $\pi$ ) is multiplied to J. These processes can be modeled using an approximately parameterized set of differential equations [1] as given by:

$$\frac{dS_A}{dt} = -\zeta \beta (1 - p_A) S_A (I + \pi J)$$

$$\frac{dS_B}{dt} = -\zeta \beta (1 - \nu - p_B) S_B (I + \pi J)$$

$$\frac{dS_C}{dt} = -\zeta \beta (1 - \omega - p_C) S_C (I + \pi J)$$

$$\frac{dE}{dt} = -\beta \zeta \left\{ (1 - p_A) S_A + (1 - \nu - p_B) S_B + (1 - \omega - p_C) S_C \right\} (I + \pi J) - \phi E \quad [1]$$

$$\frac{dI}{dt} = \phi E - (\gamma_1 + \delta) I$$

$$\frac{dJ}{dt} = \delta I - \gamma_2 J$$

$$\frac{dR}{dt} = \gamma_1 I + \gamma_2 J$$

Because isolation measure is not usually undertaken in the early stage of the epidemic (the stage of which is given by  $S_A + S_B + S_C = N$  and (E(t), I(t), J(t)) = (0, 0, 0), where N is the size of the population in which the epidemic occurs), I(t) at the initial attack with-

out the effect of quarantine would be given by:

$$\frac{dE(t)}{dt} = \left[\beta\zeta\left\{(1-p_A)S_A(0) + (1-v-p_B)S_B(0) + (1-\omega-p_C)S_C(0)\right\} - \gamma_1\right]I(t) \quad [2]$$

Therefore, the growth of infectious person at initial stage will follow Malthusian model as follows:

$$I(t) = I(0)e^{\int \beta \zeta \{(1-\rho_A)S_A(0) + (1-\nu-\rho_B)S_B(0) + (1-\omega-\rho_C)S_C(0)\} - \gamma_1\}}$$
[3]

From the second generator approach,<sup>22</sup> we obtain the following expression for the basic reproduction number, Ro:

$$R_{0} = \zeta \beta N \left\{ (1 - p_{A}) (1 - x - y) + (1 - v - p_{B})x + (I - \omega - p_{C})y \right\} \times \left\{ \frac{1}{\delta + \gamma_{1}} + \frac{\delta \pi}{\gamma_{2}(\delta + \gamma_{1})} \right\}$$
[4]

A description of the other principal parameters in the model and of their assigned value is presented below.

#### Parameter Values

Table 1 contains the parameter values for our baseline case. Assuming that the biological variables do not differ much from those of past epidemics, we use the values given in previous epidemic modeling studies 12,13,15,66 for possible scenario analyses. The infection rate  $\beta \zeta$  is chosen and fixed so that  $R_0 = 6.87$ , which is derived from an estimate on the order of 4.52 to 10.1 estimated in the previous study that have involved calculation of Ro." Because our purposes here are to draw crude pictures of the possible smallpox bioterrorist attack and describe the impact of residual immunity, we performed an analysis based on a single value of Ro (although we have varied parameter assumption in sensitivity analysis for assumed residual immunity and initial attack size discussed below). These types of analyses on the impact of public health interventions are beyond the scope of this paper. Such studies have already been undertaken elsewhere. "" Therefore, our simulation itself in this paper excludes the effect of quarantine (see Appendix, where we formulated the model incorporating the effect of quarantine). We assume that the pattern of contact is linearly related to the population size so that every infectious person will pass the disease to exactly Ro susceptible individuals simultaneously within an incubation period of  $(\phi)^{-1}$  days. From this assumption,  $\zeta N$  denotes the daily number of contacts in the population. In addition, we use a single value of Ro throughout the epidemic that represents the post-detection scenario so as to estimate the natural course (without interventions) of the epidemic although the transmission rate is likely to decrease after the epidemic is detected and announced. Although homogenous (or free) mixing is not an accurate description of the actual population interactions, free mixing usually leads to larger epidemics than nonrandom mixing.23 In addition, we assumed homogenous mixing because smallpox infections as caused by a bioterrorist attack would not necessarily accumulate in a small number of limited locations. We start the bioterrorism scenario with an entry of 10 initial cases into a population of 1,000,000 people, with enough population density to give the more than necessary critical proportion of the population, as our baseline case. It is assumed that one million people with a certain population density is a typical representation of a population of one ward in an urban area in Japan (i.e., Setagaya ward of Tokyo has a population of 815,000). It is somewhat unrealistic to expect the population at the prefectural or national level to be at risk because it would not be possible to have 100% of this population to come into possible direct or indirect contact with the disease within the short time period of

concern. We have therefore considered a scenario of an epidemic in a city or ward sized population, such as the one of Setagaya.

We first simulate three possible scenarios for different proportion of people whose residual immunity still exist. In the first scenario, based on the hypothetical long-lasting immunity in Japan's estimated using latest study in India, we assume that approximately 30% of Group B and 90% of Group C (with population size of  $1.05 \times 10^6$  and  $6.01 \times 10^6$ , respectively) will still have protective immunity against smallpox. The proportion of people with immunity in Group B (v) and C ( $\omega$ ) would thus be set as 0.30

Table 1. Parameter values for transmission dynamics of smallpox.

Parameters	Description	Baseline Values	Referrence
β	The probability of transmission per contacts	$\beta \zeta = 4.26$	*a
ζ	The daily number of contacts per capita		*a
рл	The proportion of exposed person among Group A who was effectively protected by vaccination	0.00	*b
ps	The proportion of exposed person among Group B who was effectively protected by vaccination	0.00	*b
рc	The proportion of exposed person among Group C who was effectively protected by vaccination	0.00	*b
φ	The average rate at which latent individuals become infectious	0.0685 day <sup>.1</sup>	3
δ	The mean daily rate at which infectious cases are diagnosed and isolated	0.95 day <sup>-1</sup>	3
γι	The percapita rate for recovery and deth	0.116 day-1	27
у2	The percapita rate for recovery and deth after isolated	0.132 day-1	3,28
π	Relative measure of reduced risk among isolated cases	0.10	16,29
x	The proportion of Group B population	0.105	19
y	The proportion of Group C population	0.601	19
υ	The proportion of population with residual immunity among Group B estimated	0.30	19,24
ω	The proportion of population with residual immunity among Group C estimated	0.90	19

<sup>\*</sup>a: The infection rate  $\beta\zeta$  is chosen and fixed so that the basic reproduction number becomes 6.87.

<sup>\*</sup>b: Projected epidemic curves (baseline case) given by simulation ignored vaccination.

Discussion for these parameters are given in text.

and 0.90, respectively. Because Group A consists of only those who were born in 1977 and thereafter have never been vaccinated, no one in this group will have the protective immunity. For the second scenario, we assume that half of estimated population still possesses immunity (v = 0.15, w = 0.45). It is believed that loss of immune protection might contribute to the epidemic. For the third scenario, we assume that no person possess protective immunity (v = 0, w = 0). To make the differences between those three scenarios clearly visible, we assume that there is no public health intervention except isolation in all three scenarios.

"We then consider the impact of different levels of vaccine distributions for the three age groups (A, B, and C), which would become crucial if nationwide mass-vaccination is required (level III). By estimating the optimal condition in order to prioritize, we generalize the condition with simple mathematical formula so that it can be applied to other communities having different age distribution. Finally, we estimate the total amount of smallpox vaccines needed in Japan using a generalized formula. In this study, the total number of people in the population is assumed to be constant during the epidemic. The background mortality rate is assumed to be negligible over the time periods examined.

#### Sensitivity analysis

Because model parameters regarding the proportion of the population in Groups B and C with residual immunity (v,  $\omega$ ) and initial attack size (1(0)N) possess the most uncertainty, a sensitivity analysis comparing the reproduction number is performed for different settings of them. Firstly, we compare the sensitivity of the reproduction number for either v or  $\omega$ , and then varied both. In three of the comparisons, both v and  $\omega$  are varied from 0 to 1.0 separately. When we vary both of them, we multiplied the relative reliability, which we define as a variable from 0 to 1.0, to our assumed immune proportion ( v = 0.30 or  $\omega = 0.90$ ). As for the initial attack size, we analyzed the reproduction number by varying I(0)N from 10 to 100,000 cases. A hundred thousand is selected as the maximum number of initial cases because it would be 10% of the total population. Whatever the way of introduction would be, we consider it is unrealistic to assume much more number of initial cases in our assumed ward-sized community.

#### **RESULTS**

The result of a simple scenario analysis is seen in Figure 2. It shows the probable dynamics of the smallpox epidemics under different conditions of residual immunity. The results are given for up to 50 days after the onset of epidemic. It is unrealistic to estimate for longer period of time because one would not expect the health policy and control strategies as well as social reactions to remain static over longer periods. Without any public health interventions and protective immunity, exponential growth of daily number of new cases would occur. The point prevalence (here denoted as the number of infectious individuals) would exceed 500 persons by the 33rd day after onset of epidemic. If the

half of estimated immune population in Groups B and C still possesses immunity, the incidence rate (=rapidity) of smallpox will be lessened, but the trend of exponential growth would not cease without any interventions. On the other hand, the daily number of new cases would be in relatively controllable number if parts of the Groups B and C were perfectly immune as hypothesized. It is notable that trend of increase would still be observed without interventions. The difference in the prevalence between a population which had no immunity and the one which had the expected immunity at 50th day would be approximately 405 folds.

If a proportion p of the population is successfully immunized, the critical proportion of the population to be immunized ( $p_{cri}$ ), which is needed to attain the eradication,<sup>21</sup> is given simply by:

$$p_{cri} = 1 - \frac{1}{R_0}$$
 [5]

Approximate estimate of the vaccination coverage (the degree of herd immunity) needed to eradicate smallpox is known to be in the order of 70 to 80%. Here, we separate the susceptible into three age groups based on their possible residual immunity. Based on this assumption, the condition to break the chain in the person-

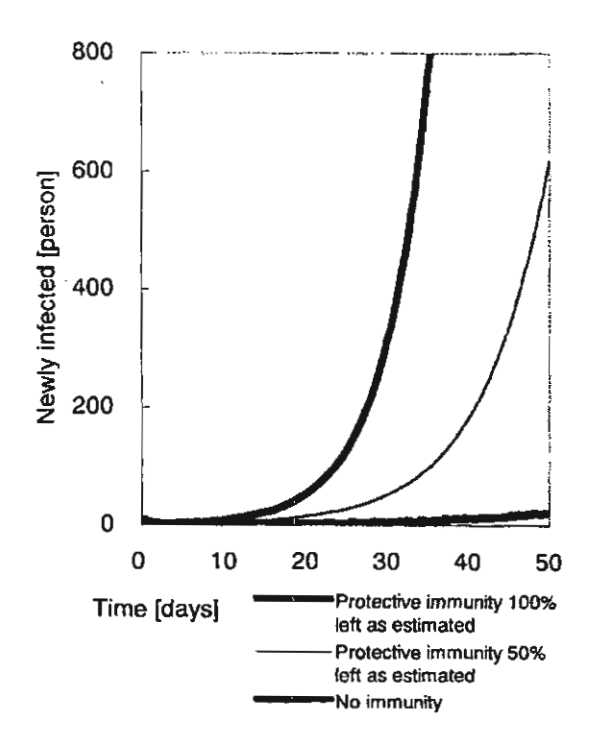


Figure 2. Dynamics of a smallpox attack with the basic reproduction number Ra = 6.87.

The number of infectious smallpox cases according to the protective (residual) immunity in Groups B (born in 1969-1977) and C (born before 1969), v and  $\omega$ . Simulations were performed with a time-step of 0.1 days.

to-person transmission of smallpox is given by the equation [4]:

$$(1-p_A) \left(1-x-y\right) + (1-v-p_B) x + (1-\omega-pc)y < \frac{1}{R_0} \qquad [6]$$

where x and y are the proportion of Groups B and C in susceptible population, respectively. Population of the Group A can be represented as (1-x-y)N. If the hypothesized level of immunity were perfectly realistic (such as our baseline case, v = 0.30 and w = 0.90 described in Table 1), the prioritization in order to achieve the most effective vaccine intervention can be calculated by:

$$f(p) = (1 - x - y) p_A + xp_B + yp_C$$
  
= 0.294 $p_A$  + 0.105 $p_B$  + 0.601 $p_C$  [7]

According to Arita's assumptions, <sup>19</sup> which he calculated from another study carried in India, <sup>24</sup> the optimal distribution of vaccine priority should be based on the population without immunity:

$$m_A: m_B: m_C = (1-x-y): (1-v) \times : (1-\omega) y$$
  
; 69:17:14

where mA, mB, and mc are the ratio of the population who have not been immune based on residual immunity by Group A, B, and C. When we assume that the total amount of vaccines would be constant (for the purpose of comparison of immune population to be covered), we can transform these conditions into the ratio of proportion in need of vaccination by adjusting for the number in

each population as,

$$p_A: p_B: p_C; 86:9:5$$
 [9]

The conditions here are expressed as the proportion of people who needs to be vaccinated in each age group. Based on the equation [6], the optimal distribution of vaccine priority (the amount of vaccines) should be:

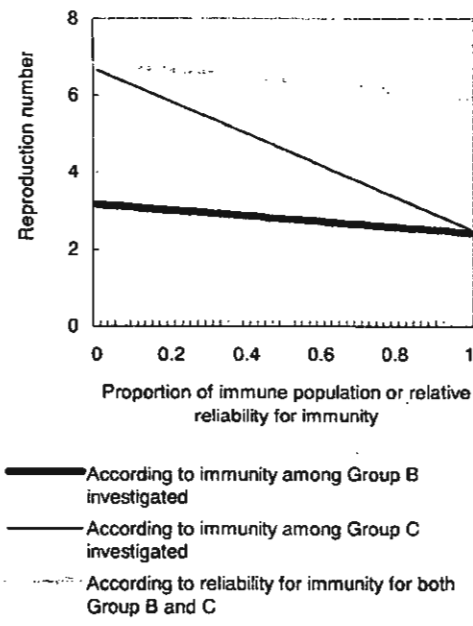
$$v_A: v_B: v_C; 84:4:12$$
 [10]

where  $v_A$ ,  $v_B$ , and  $v_C$  are the amount of vaccines needed by Group A, B, and C. Because we have set  $R_0 = 6.87$ , into eqn. [6] and [7], the minimum coverage and amount required to cause the small-pox epidemic to settle down in each age group is,

$$p_A \ge 74.21\%$$
  $v_A \ge 218,169$   
 $p_B \ge 2.65\%$   $v_B \ge 2,783$  [11]  
 $p_C \ge 8.59\%$   $v_C \ge 51,605$ 

The total amount of vaccination (V) should cover at least vA+vB+vC=272,557 persons in this scenario analysis. This can be calculated from:

$$V \ge v_A + v_B + v_C = \{ p_A (1 - x - y) + p_B x + p_C y \} N$$
 [12]



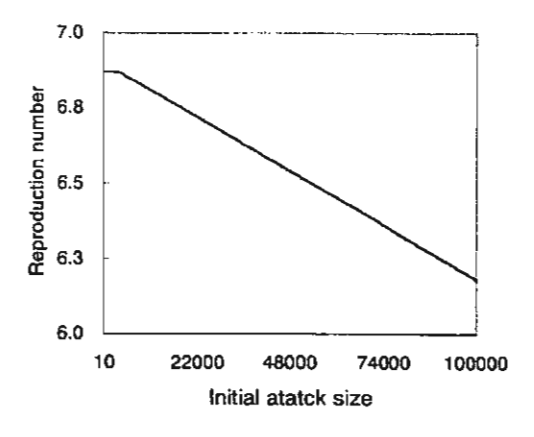


Figure 3. Sensitivity analysis for uncertain parameters.

The reproduction number under (a) varied proportion of the population with residual protective immunity as well as relative reliability for immunity among the population in Groups B (born in 1969-1977) and C (born before 1969), (b) different initial attack sizes from 10 to 100,000. The total population size was fixed at 10<sup>6</sup>.

Approximate coverage should be more than 27.3% of total population in our scenario analysis, while it would be necessary to cover 85.4% if we do not take immunity into account. If it becomes necessary to carry out nationwide mass-vaccination, we would need vaccines for between 27.3 and 85.4 million people depending on the different policies. Because the number does not take efficacy of the vaccine into account, the actual coverage might be greater than is given here.

Figure 3 shows the results of sensitivity analysis. The reproduction number changes linearly related to v,  $\omega$  and I(0)N. Comparing the proportion of the population possessing residual immunity between Group B and C, the reproduction number by varying Group B is more sensitive than C to the proportion of the immune population. Although the reproduction number increases as the relative reliability declines for both v and  $\omega$ , its increase seems rather small compared to drastic change in  $\omega$ . The reproduction number will also decline when initial attack size increases. However, compared to the change of the reproduction number on the order of 2.4 to 6.9 in Figure 3 (a), the varying interval in Figure 3 (b) is limited such as from 6.1 to 6.9

#### DISCUSSION

Two important conclusions can be drawn from our assessments of the impact of immunity on possible smallpox epidemic in Japan. First, it demonstrates that the crude size of the potential epidemic could be greatly affected by the possible residual immunity within the population. Depending on the actual protective immunity, huge differences in smallpox incidence among the various population groups might be observed. Secondly, it is possible to determine how the optimal levels of vaccination should be when a nationwide vaccination becomes necessary, which is based on the immune status of the individuals. Therefore, if we could formulate a prioritization scheme for vaccination, which is based on the immunity of the individual, the total amount of vaccines could turn out to be much lower than the estimate given by the equal distribution policy.

Despite the problems of uncertainty with the real epidemiologic data of bioterrorism, a simple dynamic model still gave reasonable simulations of the smallpox dynamics. Because transmission potential varies from community to community, we performed a sensitivity analysis according to the residual immunity and initial attack size for determined Ro, which was within the range of precise estimate. Because initial attack size itself does not largely affect the transmission potential, the size of epidemic would be linearly increase according to the initial attack size in further simulations based on our assumption (mostly it originates from assuming homogenous mixing). Although the results of a longlasting protective effects of smallpox vaccination is still based on theoretical analysis25 with certain assumptions, the impact of residual immunity on the size of epidemic can clearly be demonstrated when we examine the natural course of epidemic (without any interventions). Because mass-vaccination measures greatly

affect the transmissibility, the rapidity with which the smallpox epidemic spread would largely be lessened by the presence of the residual immunity. The national policy to achieve optimal distribution of vaccination should therefore be formulated on the basis of residual immunity among its population. This might affect the longevity of the epidemic as well as how fast it spreads. The contribution of residual immunity to the probability of controlling smallpox outbreak can be described by equation [6]. It might be possible to estimate the total amount of vaccines needed (equation [12]) when smallpox begins to spread into each community. The model has also been generalized so that it can be used to achieve the estimation for other communities. The minimum amount of vaccines that needs to be stocked in order to obtain herd immunity (or eradicate) against smallpox would be 3.13 times lesser than the amount needed when no immunity exists. According to sensitivity analysis, the possible trajectories would be sensitive to the proportion of immune population in Group C. It is considered to be due to the large number of the population in Group C. The overall number of vaccine doses would be an underestimate because efficacy of the vaccine must also be taken into account if a mass-vaccination was to take place.

Although our study demonstrates the large impact of residual immunity on the epidemic, the real percentage and duration of immunity are unknown. Our study is based on certain assumptions. It is therefore critically important to know the status of immunity in the real population from epidemiologic studies. In this study, we considered the impact of varying residual immunity in each age group by looking at the sensitivity of associated parameters ( v and  $\omega$  being the most critical). Such sensitivity analyses can help estimating the variability in the size of epidemic and the reproduction number. One should also note that mass vaccination before a bioterrorist attack actually takes place is not practicable in the real settings. Although we focused on the impact of residual immunity and its application for calculating required stock for vaccination as a possible implication, vaccination would start after an identification of the attack. There would be a race of time between implementing of vaccination and the spread of transmission. 12.26 For the purpose of practical planning or simulation, it would be necessary to consider these important aspects.

Our study has several limitations, however. Much needs to be overcome in order to increase model realism. First, one of the major problems, which the world must confront, is the uncertainty and lack of knowledge on smallpox bioterrorism. We believe that one approach to overcome the problem of risk management is to model the potential episodes with mathematical modeling. This study was conducted with only a few known parameter values, and our method assumed a closed population with crude results (in addition, simulations without quarantine). Although we assumed the introduction of smallpox into an urban community, epidemic could be different between urban and rural communities because population density as well as many of the socio-demographic and behavioral characteristics vary. Thus there are many uncertainties. It should be noted that many other variables could

affect the course of epidemic in real world bioterrorism such as the pattern of contacts. Although we assumed homogenous mixing within the community, the spread in scale-free networks should further be considered, and intercommunity migration should also be taken into account. Secondly, the estimation of total amount of vaccine needed is based on optimistic assumption. We do not know the actual percentage of residual immunity and the vaccine efficacy. We need further epidemiologic studies on immunity as well as on vaccine trials for smallpox. Finally, although possible outcomes were determined for a certain population size, one should not expect the same outcome for cities of the same size because of regional variances in the age distribution. Since the formula for the total amount of vaccination needed has been generalized, each community should be able to calculate the requirements based on their own epidemiologic records and age distributions. In order to prepare the various communities, including ours, for future possible bioterrorist attacks as well as to facilitate the use of mathematical models in policy formulation, we open ourselves to criticisms, comments and suggestions for collaborations with others academic who share the same concern.

#### **ACKNOWLEDGEMENTS**

This work was mainly carried out while HN was staying in Thailand. Thanks are due to Professor Masayuki Kakehashi at Institute of Health Sciences, Hiroshima University for his technical advice and comments. Thanks are also due to Dr Isao Arita at Agency for Cooperation in International Health for his suggestions and critical opinions. We are grateful to Ms. Lisa Imadzu, Dr Hideki Yanai (both at The Research Institute of Tuberculosis, Japan), and reviewers of editorial board for their critical review and suggestion for improvement. HN is also grateful to the Showa Ikeda Memorial Foundation for supporting his stay in Thailand.

#### REFERENCES

- Hughes JM. The emerging threat of bioterrorism. Emerg Infect Dis 1999;5:494-5.
- Henderson DA, Inglesby TV, Bartlett JG, Ascher MS, Eitzen E, Jahrling PB et al. Smallpox as a biological weapon: medical and public health management. Working Group on Civilian Biodefense. JAMA 1999;281:2127-37.
- Fenner F, Henderson DA, Arita I, Jezek Z, Ladnyi ID. Smallpox and its eradication. World Health Organization, Geneva, 1988 (Available at: http://www.who.int/emc/diseases/smallpox/Smallpoxeradication.html).
- Anonymus. US sounds alarm over smallpox weapon threat. Nature 1999;399:628.
- Centers for Disease Control. CDC Interim Smallpox Response Plan and Guidelines. Centers for Disease Control, Atlanta, 2002.
- Holloway HC, Norwood AE, Fullerton CS, Engel CC, Jr., Ursano RJ. The threat of biological weapons. Prophylaxis

- and mitigation of psychological and social consequences. JAMA 1997;278:425-7.
- Council on Foreign Relations. Terrorism Q&A: Japan. Council on Foreigin Relations, New York, 2002.
- Jernigan JA, Stephens DS, Ashford DA, Omenaca C, Topiel MS, Galbraith M, et al. Bioterrorism-related inhalational anthrax: the first 10 cases reported in the United States. Emerg Infect Dis 2001;7:933-44.
- Anonymus. Domestic production of smallpox vaccines; developed 20 years ago. Kyodo Press. 28th July. (In Japanese), 2003.
- Ministry of Health, Labor and Welfare. Response plan for domestic biological warfare. Ministry of Health, Labor and Welfare, Tokyo, 2003. (In Japanese)
- Meltzer MI, Damon I, LeDuc JW, Millar JD. Modeling potential responses to smallpox as a bioterrorist weapon. Emerg Infect Dis 2001;7:959-69.
- Kaplan EH, Craft DL, Wein LM. Emergency response to a smallpox attack: the case for mass vaccination. Proc Natl Acad Sci U S A 2002;99:10935-40.
- Bozzette SA, Boer R, Bhatnagar V, Brower JL, Keeler EB, Morton SC, et al. A model for a smallpox-vaccination policy. N Eng J Med 2003;348:416-25.
- Eichner M. Case isolation and contact tracing can prevent the spread of smallpox. Am J Epidemiol 2003;158:118-28.
- Gani R, Leach S. Transmission potential of smallpox in contemporary populations. Nature 2001;414:748-51.
- Eichner M, Dietz K. Transmission potential of smallpox: estimates based on detailed data from an outbreak. Am J Epidemiol 2003;158:110-7.
- Blower SM, Medley GF. Epidemiology, HIV and drugs: mathematical models and data. Br J Addict 1992;87:371-9.
- Banks T, Castillo-Chavez C. Mathematical and Modeling Approaches in Homeland Security. SIAM's, Frontiers in Applied Mathematics, New York, 2003.
- Arita I. Duration of immunity after smallpox vaccination: a study on vaccination policy against smallpox bioterrorism in Japan. Jpn J Infect Dis 2002; 55: 112-6.
- Henderson DA, Moss B. Smallpox and vaccinia. In Plotkin SA, Orenstein WA, Offit PA, eds. Vaccines, 4th eds. Elsevier Science, New York. 2003: Chapter 6 (3rd eds available at http://www.ncbi.nlm.nih.gov/books/bv.fcgi?call=bv.View..Sh owSection&r id=vacc.chapter.3)
- Anderson RM, May RM. Infectious Diseases of Humans: Dynamics and Control. Oxford University Press, Oxford, 1991.
- Diekmann O, Heesterbeek JAP. Mathematical Epidemiology of Infectious Diseases: Model Building, Analysis and Interpretation. Wiley, New York, 2000.
- Kaplan EH. Mean-max bounds for worst-case endemic mixing models. Math Biosci 1991;105:97-109.
- 24. Rao AR. Smallpox. Kothari Book Dept., Bombay, 1972.
- 25. Eichner M. Analysis of historical data suggests long-lasting

H, et al. 49

protective effects of smallpox vaccination. Am J Epidemiol 2003;158:717-23.

- Ferguson NM, Keeling MJ, Edmunds WJ, Gani R, Grenfell BT, Anderson RM, et al. Planning for smallpox outbreaks. Nature 2003;425:681-5.
- Gelfand HM, Posch J. The recent outbreak of smallpox in Meschede, West Germany. Am J Epidemiol 1971;94:234-7.
- 28. Mack TM. Smallpox in Europe, 1950-1971. J Infect Dis 1972;125:161-9.
- Chowell G, Fenimore PW, Castillo-Garsow MA, Castillo-Chavez C. SARS outbreaks in Ontario, Hong Kong and Singapore: the role of diagnosis and isolation as a control mechanism. J Theor Biol 2003;224:1-8.
- 30. Iwasaki M, Otani T, Ohta A, Yosiaki S, Kuroiwa M, Suzuki S. Rural-urban differences in sociodemographic, social network and lifestyle factors related to mortality of middle-aged Japanese men from the Komo-Ise cohort study. J Epidemiol 2002;12:93-104.

#### **APPENDIX**

For the purpose of further realistic simulation, here we consider the effect of quarantine onto our model (using additional five compartments, Figure 4). We suppose the fraction q, of those who are known to have been exposed and therefore may be infected but are not yet ill, would be quarantined (denoted by the compartment  $E_q$ ). Those who are in  $E_q$  will become infectious after the latency period (and enter into  $I_q$ ). Some of them would be diagnosed and moved into isolation with the mean daily rate  $\delta$  (and enter into J). The other of infectious and traced individuals are assumed to recover or die after ( $\gamma$ ) days of quarantine. In addition to quarantining the infected individuals, we need to consider uninfected and traced individuals. Among uninfected,  $(I-q)(I-\beta)$  remains susceptible and  $q(I-\beta)$  would be traced and enters into

Qs, Qg and Qc: which represent those who are traced but uninfected for each age group. Those who were traced but uninfected would finish quarantine (released into community again and enter the susceptible population)  $\sigma^{-1}$  days after their known contact. Since we should assume the quarantine can never be perfect to protect an additional transmission, relative measure of reduced risk among those quarantined ( $\theta$ ) is multiplied to  $I_q$ . Incorporating these assumptions onto equations [1], the transmission dynamics with the modification of quarantine system can be described to

$$\frac{dS_A}{dt} = -\zeta (1 - p_A) \{q + \beta (1 - q)\} S_A (I + \theta I_q + \pi J) + \sigma Q_A$$

$$\frac{dS_B}{dt} = -\zeta (1 - v - p_B) \{q + \beta (1 - q)\} S_B (I + \theta I_q + \pi J) + \sigma Q_B$$

$$\frac{dS_C}{dt} = -\zeta (1 - v - p_C) \{q + \beta (1 - q)\} S_C (I + \theta I_q + \pi J) + \sigma Q_C$$

$$\frac{dQ_A}{dt} = (1 - p_A) (1 - \beta) \zeta qS_A (I + \theta I_q + \pi J) - \sigma Q_A$$

$$\frac{dQ_B}{dt} = (1 - v - p_B) (1 - \beta) \zeta qS_B (I + \theta I_q + \pi J) - \sigma Q_B$$

$$\frac{dQ_C}{dt} = (1 - \omega - p_C) (1 - \beta) \zeta qS_C (I + \theta I_q + \pi J) - \sigma Q_C$$

$$\frac{dE_q}{dt} = \beta \zeta q \{(1 - p_A)S_A + (1 - v - p_B)S_B + (1 - \omega - p_C)S_C\} (I + \theta I_q + \pi J) - \phi E_q$$

$$\frac{dE}{dt} = \beta \zeta (1 - q) \{(1 - p_A)S_A + (1 - v - p_B)S_B + (1 - \omega - p_C)S_C\} (I + \theta I_q + \pi J) - \phi E_q$$

$$\frac{dI_q}{dt} = \phi E_q - (\gamma_3 + \delta)I_q$$

$$\frac{dI_q}{dt} = \phi E - (\gamma_1 + \delta)I$$

$$\frac{dJ}{dt} = \delta (I + I_q) - \gamma_2 J$$

$$\frac{dR}{dt} = \gamma_1 I + \gamma_2 J - \gamma_3 I_q$$

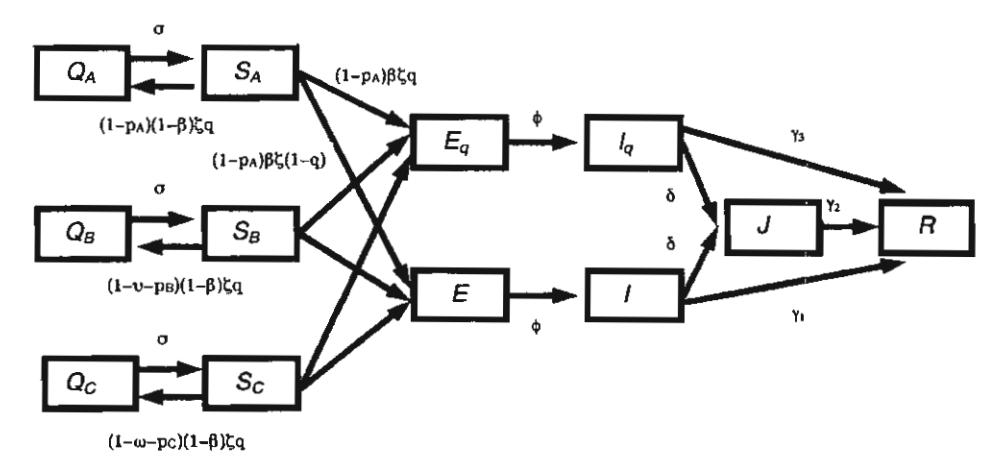


Figure 4. The transmission dynamics of the smallpox incorporating the effect of quarantine.

Additional compartments:  $E_q$  represents the proportion of traced latent contacts;  $Q_A$ ,  $Q_B$  and  $Q_C$ , the proportion of traced uninfected contacts from Groups A (born after 1977), B (born in 1969-1977), and C (born before 1969);  $I_q$  the proportion of infectious in quarantine.

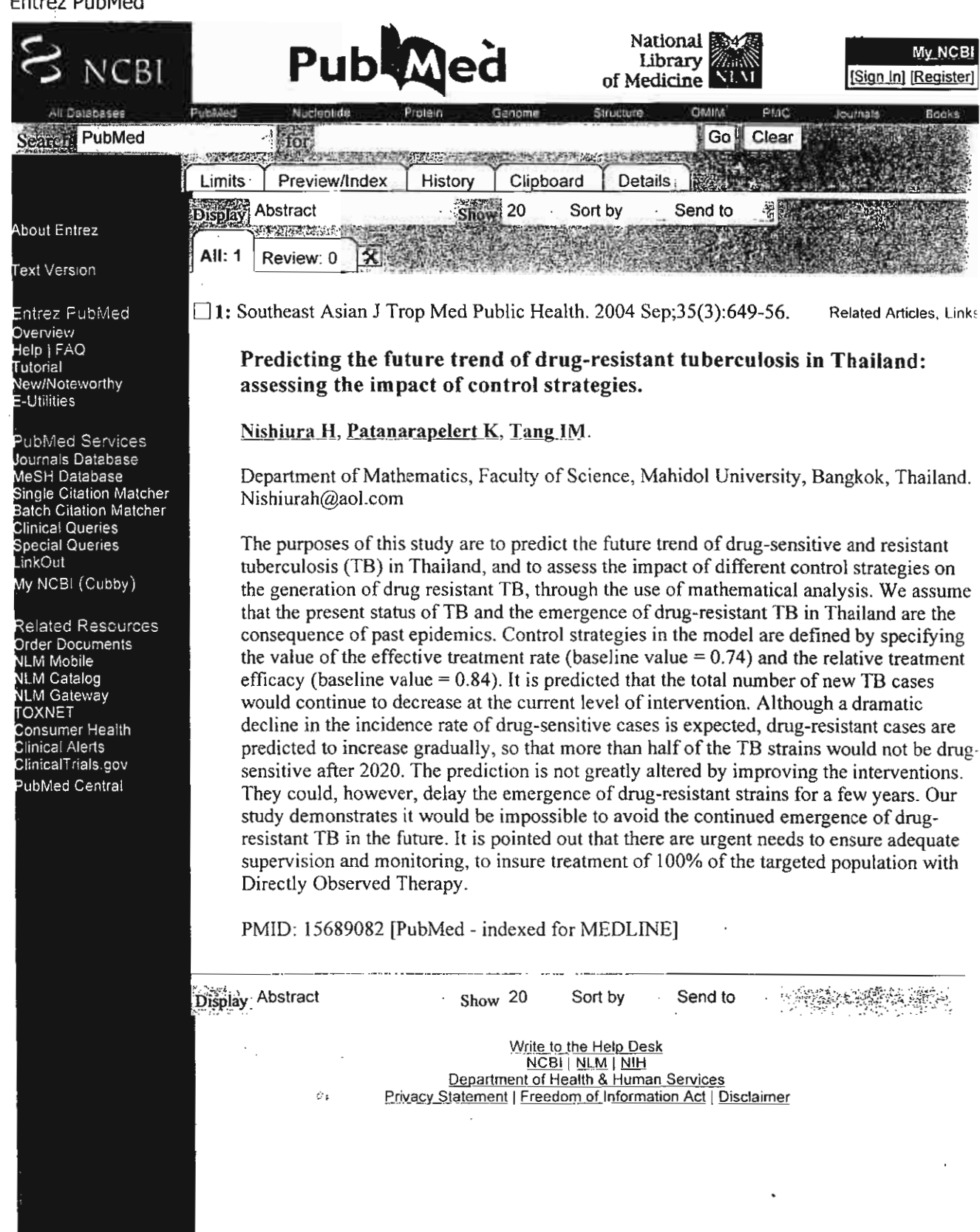
In this case, the basic reproduction number would be given by

$$R_{0} = \zeta \beta (1-q) N \{ (1-p_{A}) (1-x-y) + (1-v-p_{B})x + (1+\omega-p_{C})y \}$$

$$\times \left\{ \frac{1}{\delta + \gamma_{1}} + \frac{\theta}{\delta + \gamma_{3}} + \frac{\delta \pi}{\gamma_{2}(\delta + \gamma_{1})} \right\}$$
[2']

This would allow to increase the realism for simulation.

#### Entrez PubMed





ą

ScienceAsia 31 (2005): 193-199

### Limit Cycle in a Herbivore-Plant-Bee Model Containing a Time Delay

Charoen Kaewpradit, Wannapong Triampob and I-Ming Tangbe.

- Openation of Mathematics
- Department of Physics and Capability Building Unit in NanoScience & NanoTechnology Faculty of Science, Mahido! University, Bangkok 10400, Thailand
- c Institute of Science & Technology for Research & Development Mahidol University, Nakhon Pathorn 73170, Thalland
- \*Corresponding author: e-mail address scimt@mahidol.ac.th

Received 28 Jul 2004 Accepted 23 Mar 2005

**ABSTRACT:** The dynamical behavior of time delay herbivore-plant-pollinator ecosystem is studied. The time delay arises from the fact that it takes time for a pollinated flower to develop into a new plant. A dynamical analysis is used to show that a stable steady state undergoes a Hopf bifurcation to a limit cycle behavior as the delay time crosses a critical value. This prediction is verified by numerically solving the set of first order differential equations. One finds that the trajectory which is spiraling into the steady state point when  $\tau < \tau_o$  becomes a trajectory into a limit cycle about the state when  $\tau > \tau_c$ .

KEYWORDS: Herbivore-plant-pollinator ecosystem, time delay, Hopf Bifurcation.

#### INTRODUCTION

Very recently, Bandyopadhyay, Bhattacharyya and Mukopadhyay (BBM)1, studied the dynamics of an autotroph-herbivore ecosystem with nutrient recycling. They considered both the case where there is no time delay and the case where there is a delay. For the former case, they found that when the rate of increase of the nutrients attained a certain threshold value, the system became stable. The autotroph and herbivore populations would oscillate about an interior steady state point. Below the threshold value, the system became unstable. Note that in the absence of nutrient replenishing, the nutrients would eventually disappear from the soil and the autotrophic state would go to zero. For the latter case, BBM found that a sufficiently large delay in the time needed to convert dead organic matter into the nutrients, would cause the stable state to become unstable. Using Hopf Bifurcation analysis<sup>2</sup>, they established the conditions for the switching of the stability.

Jang<sup>3</sup> has studied the dynamics of a herbivore-plant-pollinator ecosystem. Jang's model is somewhat different from that of BBM. He looked at the roles of the energetic rewards of the interactions between the plant and the pollinator and of the specificity of the pollinator to the plant. Jang was particularly interested in how the reduction of the visitation rate of the bee to the plant caused by the action of the herbivore affected

the ecosystem. A Hopf Bifurcation analysis was again used to determine the stability of the steady states. Jang did not include any time delay<sup>4,5</sup> into his model.

The purpose of the present paper is to determine the effects of a time delay in Jang's model. Unlike the BBM model, where the time delay should be inserted is obvious, it is not in Jang's model. We believe that it should be inserted into the term describing the birth rate of the plant;

$$\frac{k_1 \sigma \mu XY}{1 + \sigma \phi \mu^2 Y} \tag{1}$$

where X and Y are the bee and plant populations, respectively;  $k_1$ , number of ovules fertilized per visit of the bee;  $\sigma$ , the probability of an encounter between the flower and the bee;  $\phi$ , reciprocal of the time it takes the bee to extract the nectar (or pollen); and  $\mu$ , the energetic reward to the bee when it encounters the flower. This gives the number of flowers fertilized at time t. It then takes time for the fertilized ovules to develop into seeds and fall to the ground. The number of new plants that will begin to flower at time t will depend on the number of ovules that were fertilized at time t- $\tau$ , where  $\tau$  is the time delay. In Section II, we introduce the Jang model and present some of his results. We put the time delay into the model in Section III, and carry out a Hopf Bifurcation analysis. In Section IV, we present our

numerical solution. In Section V, we present an extension of our model and discuss how it can be used to provide quantitative predictions for the farmers.

#### II. Jang's Model.

The herbivore-plant-pollinator ecosystem considered by Jang consists of three first order differential equations;

$$X = bX(K - X) + \frac{g(Z)k_2\sigma\mu^2XY}{1 + \phi\sigma\mu^2Y}$$
(2a)  

$$Y = \frac{k_1\sigma\mu g(Z)XY}{1 + \phi\sigma\mu^2Y} - \gamma Y - \frac{m_1YZ}{a + Y}$$
(2b)

$$\dot{Y} = \frac{h_1 \sigma \mu g(Z) X Y}{1 + 4 \sigma \mu^2 Y} - \gamma Y - \frac{m_1 Y Z}{n + Y}$$
 (2b)

and

$$\dot{Z} = \frac{m_2 YZ}{a + Y} - \delta Z \tag{2c}$$

where Z denotes the herbivore population; g(z) represents the loss in attractiveness of the flower to the bee due to the damage caused by the herbivore;

$$\frac{m_2 Y}{a + Y} \tag{3}$$

is the visitation rate of the herbivore to the plant; m, and m, the maximal ingestion rate and the leafhopper maximal growth rate with 0 < m, ≤ m, respectively; 'a', the half - saturation constant;  $\delta_1$ , the maximum per capita birth rate of the bees;  $\lambda$  and  $\delta$ , the death rate of the bees and herbivore, respectively; 'b', the density dependent regulation constant of bee, and K is the measure of the diversity of bee to the plant  $(K=(\delta_1-\lambda)/$ b). In the present model, the flower on the plant becomes pollinated and after awhile, the plant dies. The life cycle begins again when the seed developed from the pollinated flower falls off the plant and germinates in the soil. All of the population classes must be positive at all times, i.e.,

$$X(t), Y(t), Z(t)^3 \ge 0$$
.

Setting the RHS of eqns. (2a) - (2c) to zero, we obtained

m, 
$$\overline{x} = K + \frac{g(\overline{z})k_1\mu^2\sigma\overline{y}}{b(1+\phi\sigma\mu^2\overline{y})}$$
 (4a)

$$\overline{y} = \frac{a\delta}{m - \delta}, m_2 > \delta$$
 (4b)

$$\bar{z} = \frac{a + \bar{y}}{m_1} \left[ \frac{k_1 k_2 \mu^3 o^2 \bar{y}}{b(1 + \phi o \mu^2 \bar{y})^2} g(\bar{z})^2 + \frac{k_1 \mu o K}{1 + \phi o \mu^2 \bar{y}} g(\bar{z}) - \gamma l (4c) \right]$$

at one of the steady states  $(\bar{x}, \bar{y}, \bar{z})$ . To determine when the state is stable or not, we first diagonalize the Jacobian of eqns. (2a) to (2c) at the steady state. We then check to see if all the eigenvalues have negative real parts. When this happens, the state is stable. Diagonalizing the Jacobian, we obtain the following characteristic equation

$$\lambda^{3} + (p_{1} - s_{1})\lambda^{2} + (p_{2} - s_{2})\lambda + (p_{3} - s_{3}) = 0$$
 (5)

$$p_1 = \gamma + \delta - bK + 2b\overline{x} - m_2h(\overline{y}) - k_2\mu f(\overline{y})g(\overline{z}) + m_1\overline{z}h'(\overline{y}),$$

$$\begin{split} p_2 &= \gamma \delta - b K \delta - b K \gamma + 2 b \gamma \overline{x} + b K h(\overline{y}) m_1 - \gamma h(\overline{y}) m_2 - 2 b h(\overline{y}) \overline{x} m_2 \\ &+ 2 b \delta \overline{x} - \gamma f(\overline{y}) k_2 \mu g(\overline{z}) - \delta f(\overline{y}) k_2 \mu g(\overline{z}) + f(\overline{y}) h(\overline{y}) k_2 m_2 \mu g(\overline{z}) \\ &- b K \overline{z} m_1 h'(\overline{y}) + \delta \overline{z} m_1 h'(\overline{y}) + 2 b \overline{x} \overline{z} m_1 h'(\overline{y}) - f(\overline{y}) \overline{z} \ k_2 m_1 \mu g(\overline{z}) h'(\overline{y}), \end{split}$$

$$\begin{split} p_3 &= 2b\gamma\delta\overline{\mathbf{x}} - bK\gamma\delta + bK\gamma h(\overline{\mathbf{y}}) m_{\gamma} - 2b\gamma h(\overline{\mathbf{y}})\overline{\mathbf{x}} m_{\gamma} - \gamma\delta h(\overline{\mathbf{y}})k_{\gamma}\mu g(\overline{\mathbf{z}}) \\ &+ \gamma f(\overline{\mathbf{y}})h(\overline{\mathbf{y}})k_{\gamma}m_{\gamma}\mu g(\overline{\mathbf{z}}) - bK\delta\overline{\mathbf{z}} m_{\gamma}h'(\overline{\mathbf{y}}) + 2b\delta \quad \overline{\mathbf{x}}\overline{\mathbf{z}} m_{\gamma}h'(\overline{\mathbf{y}}) \\ &- \delta f(\overline{\mathbf{y}})\overline{\mathbf{z}}k_{\gamma}m_{\gamma}\mu g(\overline{\mathbf{z}})h'(\overline{\mathbf{y}}), \end{split}$$

 $s_1 = g(\overline{z})\overline{x} k_1 f'(\overline{y}),$ 

$$s_1 = -bKg(\overline{z})\overline{x}k_1f'(\overline{y}) + \delta g(\overline{z})\overline{x} k_1f'(\overline{y}) + 2bg(\overline{z})\overline{x}^2k_1f'(\overline{y})$$
  
$$-g(\overline{z})h(\overline{y})\overline{x} k_1m_1f'(\overline{y}) + f(\overline{y})\overline{x} \overline{z}k_1m_2g'(\overline{z})h'(\overline{y})$$

$$\begin{split} s_3 &= 2b\delta g(\overline{z})\overline{x}'k_1f'(\overline{y}) - bK\delta g(\overline{z})\overline{x}k_1f'(\overline{y}) + 2b\ f(\overline{y})\ \overline{x}^2\ \overline{z}\ k_1m_2g'(\overline{z})\ h'(\overline{y}) \\ &+ bK\ g(\overline{z})\ h(\overline{y})\ \overline{x}\ k_1m_2\ f(\overline{y}) - 2b\ g(\overline{z})\ h(\overline{y})\ \overline{x}^2k_1m_2\ f'(\overline{y}) \\ &- bK\ f(\overline{y})\ \overline{x}\ \overline{z}\ k_1m_2\ g'(\overline{z})\ h'(\overline{y}) \end{split} \tag{6}$$

Equation (5) has negative real roots if and only if (Theorem 1, Appendix)

$$P_1-S_1>0$$
,  $P_3-S_3>0$  and  $(P_1-S_1)(P_2-S_2)-(P_3-S_3)>0$ . (7)

When the above conditions are satisfied  $(\bar{x}, \bar{y}, \bar{z})$ , the steady state will be stable.

#### III.Effect of Time Delay. Illa. The Stability of $\overline{E} = (\overline{x}, \overline{y}, \overline{z})$ with Time Delay.

A time delay in the herbivore-plant-pollinator system arises because a new flower only arrives after the pollinated flower develops into a seed, falls off the plant, germinates into a new plant and then grows into the flowering stage of the new plant. To include the effects of the time delay, we need to replace eqn. (2b)

$$\dot{y} = \frac{k_1 \mu \sigma g(z(t-\tau))x(t-\tau)y(t-\tau)}{1+\phi \sigma \mu^2 y(t-\tau)} \quad \gamma y \quad \frac{m_1 yz}{a+y} \quad (2b')$$

The Jacobian matrix for eqns. (2a), (2b') and 2c) evaluated at the steady state point  $\overline{E} = (\overline{x}, \overline{y}, \overline{z})$  is

$$\begin{pmatrix} bK - 2b\bar{x} + k_2 \ \mu g(\bar{z} \ ) \ f(\bar{y}) & k_2 \ \mu g(\bar{z}) \ f'(\bar{y}) \ \bar{x} \\ k_1 \ g(\bar{z}) \ f(\bar{y}) \ e^{-\omega \tau} & -\gamma - m_1 \ \bar{z} & h'(\bar{y}) + k_1 \ g(\bar{z}) \ \bar{x} \ f'(\bar{y}) \ e^{-\omega \tau} \\ 0 & m_2 \ \bar{z} & h'(\bar{y}) \end{pmatrix}$$

$$\begin{array}{c} k_{2}\mu g'\left(\overline{z}\right)f(\overline{y})\,\overline{x}\\ -m_{1}\,h(\overline{y}\,\,)+k_{1}\,g'(\overline{z}\,\,)\,\overline{x}\,\,f(\overline{y}\,\,)\,e^{-\omega\tau}\\ m_{2}\,\,h(\overline{y})-\delta \end{array} \right) \end{(8)}$$

Diagonalizing the above matrix, we obtain the following characteristic equation<sup>5</sup>

$$\omega^3 + p_1 \omega^2 + p_2 \omega + p_3 = e^{-\omega \tau} (s_1 \omega^2 + s_2 \omega + s_3)$$
 (9)

We now suppose that two of the eigenvalues of eqn. (9) are a pair of complex conjugates

i.e.,  $\omega_{\pm} = u(\tau) \pm iv(\tau)$ . Substituting  $\omega_{+}$  into eqn. (9) and separating the real and imaginary parts, we get

$$u^{3} - 3uv^{2} + p_{1}u^{2} - p_{1}v^{2} + p_{2}u + p_{3}$$

$$= e^{-u\tau} \{s_{1}u^{2}\cos(v\tau) - s_{1}v^{2}\cos(v\tau) + s_{2}u\cos(v\tau) + s_{3}\cos(v\tau)\}$$

$$+2s_{1}uv\sin(v\tau) + s_{2}v\sin(v\tau)$$
(10)

and

3

4

$$3u^{2}v - v^{3} + 2p_{1}uv + p_{2}v$$

$$\stackrel{\parallel}{=} e^{-u\tau} \{2s_{1}uv \cos(v\tau) + s_{2}v \cos(v\tau) - s_{1}u^{2} \sin(v\tau) + s_{1}v^{2} \sin(v\tau) - s_{2}u \sin(v\tau) - s_{3}\sin(v\tau)\}$$
(11)

where  $\tau$  is chosen to be the Hopf bifurcation parameter.

For a Hopf bifurcation to occur, three conditions must be met at the critical value  $(\tau_o)$ ;  $(1)u(\tau_o) = 0$ ,  $(2)v(\tau_o) \neq 0$  and  $(3)u'(\tau_o) > 0$  (Theorem 2, Appendix). To see if the eigenvalues of the Jacobian evaluated at the steady state point  $\overline{E} = (\overline{x}, \overline{y}, \overline{z})$  satisfy these conditions, we first assume that the critical value defined by  $u(\tau_o) = 0$  exist. However, we do not use this condition to find  $\tau_o$ . Instead we substitute the condition into eqns. (10) and (11) and see whether a non-zero value of  $v(\tau_o)$  exist. To do this, we set  $u(\tau_o) = u^* = 0$  into the two equations to get

$$-p_1 v^{*2} + p_3 = (s_3 - s_1 v^{*2}) \cos(v^* \tau_0) + s_2 v^* \sin(v^* \tau_0)$$
(12)

$$-v^{*3} + p_2 v^* = s_2 v^* \cos(v^* \tau_0) - (s_3 - s_1 v^{*2}) \sin(v^* \tau_0)$$
 (13)

Squaring the two equations and adding the squares together, we obtain

$$v^{*6} + (p_1^2 - 2p_2 - s_1^2)v^{*4} + (p_2^2 - 2p_1p_3 - s_2^2 + 2s_1s_3)v^{*2} + (p_3^2 - s_3^2) = 0$$
(14)

Letting  $v^{2}$ ,  $\eta$  eqn. (14) becomes the following cubic equation

$$S(\eta) = \eta^3 + d_1 \eta^2 + d_2 \eta + d_3 = 0$$
 (15)

where

$$d_1 = p_1^2 - 2p_2 - s_1^2 (16a)$$

$$d_2 = p_2^2 - 2p_1p_3 - s_2^2 + 2s_1s_3 \qquad (16b)$$

$$d_3 = p_3^2 - s_3^2 \tag{16c}$$

For  $v(\tau_n)$  to exist, the roots of eqn. (15) must be real and

positive. This can be determined by using the results of the lemma stated in the Appendix. We now assume that a set of values for the parameters can be found which satisfies the conditions of Lemma 1.

Next we need to show that for the present  $u(\tau)$ , the following is true

$$\frac{\mathrm{d}\mathbf{u}}{\mathrm{d}\tau}\bigg|_{\tau=\tau_0} > 0 \tag{17}$$

This is done by differentiating eqns. (10) and (11) with respect to  $\tau$  and then set  $\tau = \tau$ . Doing this, we get

$$B\frac{\mathrm{d}u}{\mathrm{d}\tau}\Big|_{\tau=\tau_0} + C\frac{\mathrm{d}v}{\mathrm{d}\tau}\Big|_{\tau=\tau_0} = D \qquad (18a)$$

$$-C\frac{\mathrm{d}u}{\mathrm{d}\tau}\Big|_{\tau=\tau_0} + B\frac{\mathrm{d}v}{\mathrm{d}\tau}\Big|_{\tau=\tau_0} = E \qquad (18b)$$

where

$$B = \begin{bmatrix} -3v_0^2 + p_2 - s_2\cos(v_0\tau_0) - 2s_1v_0\sin(v_0\tau_0) + s_3\tau_0\cos(v_0\tau_0) \\ -s_1v_0^2\tau_0\cos(v_0\tau_0) + s_2v_0\tau_0\sin(v_0\tau_0) \end{bmatrix}$$

$$C = \left[ -2p_1 v_0 + 2s_1 v_0 \cos(v_0 t_0) + s_3 \tau_0 \sin(v_0 t_0) - s_1 v_0^2 \tau_0 \sin(v_0 \tau_0) - s_2 \sin(v_0 \tau_0) - s_2 v_0 t_0 \cos(v_0 \tau_0) \right]$$

$$D = (s_1 v_0^3 - s_3 v_0) \sin(v_0 \tau_0) + s_2 v_0^2 \cos(v_0 \tau_0)$$
and

$$E = (s_1 v_0^3 - s_3 v_0) \cos(v_0 \tau_0) - s_2 v_0^2 \sin(v_0 \tau_0)$$
 (19)

Solving for 
$$\frac{du}{d\tau}\Big|_{\tau=\tau_0}$$
 we get
$$\frac{du}{d\tau}\Big|_{\tau=\tau_0} = \frac{BD - EC}{B^2 + C^2}$$
 (20)

where

BD-EC = 
$$v_0^2 [3v_0^4 + 2v_0^2(p_1^2 - 2p_2 - s_1^2) + (p_2^2 - 2p_1p_3 - s_2^2 + 2s_1s_3)]$$
(21)

Therefore, we have

$$\frac{du}{d\tau}\bigg|_{\tau=\tau_0} = \frac{v_0^2}{g^2 + C^2} \{3v_0^4 + 2v_0^2(p_1^2 - 2p_2 - s_1^2) + (p_2^2 - 2p_1p_3 - s_2^2 + 2s_1s_3)\}$$
Noting that

$$\frac{dS}{d\eta} = 3\eta^2 + 2(p_1^2 - 2p_2 - s_1^2)\eta + (p_2^2 - 2p_1p_3 - s_2^2 + 2s_1s_3)$$

where S is defined by eqn. (15), eqn. (22) can be written as

$$\frac{du}{d\tau}\Big|_{\tau=\tau_0} = \frac{v_0^2}{B^2 + C^2} \frac{dS}{d\eta}\Big|_{\eta=v_0^2}$$
 (24)

The condition  $\Delta < 0$  in part A of Lemma I requires the two turning points of  $S(\eta)$  not be a positive real root of  $S(\eta)$ , otherwise  $\Delta$  would be equal to zero. The two turning points of  $S(\eta)$ ,  $\varepsilon_1$  and  $\varepsilon_2$  (eqn. A2), are the zeros of eqn. (23). Since  $v_0^2 \neq {}^1 \varepsilon_{12}$ , the following must be true

$$\frac{dS}{d\eta}\Big|_{\eta=v_0^2} \neq 0 \tag{25}$$

Thus

$$\frac{du}{d\tau}\Big|_{\tau=\tau_0} = \frac{v_0^2}{B^2 + C^2} \frac{dS}{d\eta}\Big|_{\eta=v_0^2}$$
 (26)

and condition 3 of the Hopf bifurcation theory is satisfied. Therefore the system undergoes a Hopf bifurcation.

#### IIIb.Critical Time Delay.

The critical delay time can be found by using the method introduced by Tam.<sup>6</sup> We rewrite eqns (12) and (13) as

$$M\cos(v * \tau_0) + N\sin(v * \tau_0) = P$$
 (27a)

$$N\cos(v * \tau_0) - M\sin(v * \tau_0) = Q \qquad (27b)$$

where

$$M = S_3 - S_1 V^{*2} (28a)$$

$$N = S_2 V^* \tag{28b}$$

$$P = -P_1 V^{*2} + P_3 (28c)^{*}$$

and

$$Q = -V^{*3} + P_2 V^*$$
 (28d)

Eqns. (27a) and (27b) leads to

$$M^2 + N^2 = P^2 + Q^2 = G^2$$
, where  $G > 0$ . (29)

M and N can be rewritten as

$$M = G \cos \theta$$

$$N = G \sin \theta$$
 (30)

This allows us to determine  $a\theta \in [0, 2\pi)$  uniquely. With this value of  $\theta$ , eqns. (27a) and (28b) become

$$G\cos(\tau_0 v^*)\cos\theta + G\sin(\tau_0 v)\sin\theta = P$$
 (31)

$$G\cos(\tau_0 v *)\sin\theta - G\sin(\tau_0 v *)\cos\theta = Q \qquad (32)$$

or

$$G\cos(\tau_{o}v * - \theta) = P$$
 (33a)

$$G\sin(\tau_0 \mathbf{v} * - \theta) = Q \tag{33b}$$

From this we get as the critical value

$$\tau_0 = \frac{1}{v} \{ \tan^{-1}(\frac{Q}{P}) + \theta \}$$
 (34)

#### IV. Numerical Solution.

#### IVa. Numerical Parameters.

The numerical values of the parameters in the herbivore-plant-pollinator ecosystem for a given plant are scarce. One has to guess at them since many of them will depend on which plant we are interested in, what is the locality (or country) or what time of the year it is. To gain ideas of the range of values the parameters can take, we look at the Mango tree, even though the present model is not an appropriate model for this plant. The model is developed for a flowering plant which after becoming pollinated, dies. Most Mango trees exhibit biannual flowering, once between May and June and again in December-January. This flowering is repeated every year for many years. Nevertheless, we have used the data available for the Mango trees to be typical of most plants.

Jamjanya<sup>7</sup> has looked at the increase in leafhopper population in two varieties of mango trees, On-som and Na thub. He found that leafhopper infestation on the Na-thub mango tree increased by 270% in a day, while the leafhoppers infestation on the On-sorn mango tree increased 63% in a day. This implies that m, can vary between 0.63 - 2.7 day-1 depending on the type of Mango tree. Boongird8 has measured the probability that a bee will visit a Nam dok mai mango tree in Thailand. He found  $\sigma$  to be 79.55%. In Trinidad, the probability that a bee will visit the mango is about 21%.9 We take  $\sigma$ , the probability of encounter to be in the range 0.21 - 1.0. The extraction rate of the nectar by the bee range between 0.3 μl/sec in grove and 2.0 μl/sec in pool.10 φ, which is reciprocally related to the speed of nectar extraction, is set to be in the range  $1.93 \times 10^{-5} - 3.86 \times 10^{-5}$ 10-5 (µl/day)-1. Other studies find that a bee will visit 8 -10 flowers per visit.11 Since only about 5-75 % of the flowers are perfect, the number of ovules fertilized per visit,  $k_1$ , will be in the range of 0.4 - 7.5 flowers per visit.

The normal death rate of the bees has been changing. The French National Bee Surveillance Unit  $^{12}$  has stated that the death of the bees during the winter months was one out of ten in previous years. Now, the death rate is six out of ten. This means that  $\lambda$  is in the range 0.001 - 0.006. For the birth rate of the bees,  $\delta_1$ , we assume that the queen bee lays about 1200 - 2000 eggs/day. For a typical small hive containing perhaps 20,000 bees,  $^{9,13}$  the birth rate of the bees would be in the range, 0.06-0.1 day  $^{1}$ . The estimated values of the parameters are listed in Table I.

#### IVb. Numerical Solutions.

For the purpose of getting an idea of what might occur, we have set the values of the parameters at: a =500, b = 1/8,  $\lambda$  = 0.0035,  $k_1$  = 3.95,  $k_2$  = 0.00005,  $m_1$  = 7.5,  $m_2$  = 1.6,  $\phi$  = 0.0000386,  $\sigma$  = 0.25,  $\gamma$  = 0.0111,  $\mu$  = 23 and  $\delta$  = 0.05. Substituting the above values into eqns. (4a)-(4c), we get the steady state

Table 1. Parameter values

Parame	ters Units	parameter range		
a	no. of flower	500		
Ъ	1/(bee day)	1/8		
ķΚ	no. of bee	$\frac{\delta_1 - \lambda}{b}$		
ιk,	mango/(bee visit)	0.4 - 7.5		
jμ	microliter/visit	. 22.72-63.63		
ŀφ	(microliter/day)-1	1.93x10-5 - 3.86x10-5		
.;σ	-	0.21 - 1.0		
∄δ,	day- <sup>1</sup>	0.06 - 0.1		
σ  δ <sub>ι</sub>  λ	day-1	0.001 - 0.006		
Įk,	microliter <sup>-1</sup>	>1.48x10 <sup>-6</sup>		
" Y	day-1	0.0111		
.lm,	mango/day	10.93-910.75		
; m,	day¹	0.63 - 2.7		
δ	day-1	0.01-0.05		

 $\overline{E}(0.637873, 16.129, 29.4689)$ . (35) Substituting the values of  $(\overline{x}, \overline{y}, \overline{z})$  given by eqns. (4a)-(4c) and the values of the parameters into eqn. (7), we find that the Routh-Hurwitz conditions are met and the steady state is stable. Substituting the same values in eqn. (34), we find that the critical value is

$$\tau_{o} = 1.13 \text{ days}$$
 . (36)

As τ crosses this value, the steady state should become unstable. To see if this happens, we have solved eqns. (2a), (2b') and (2c) (for a delay time of 1 day) using the values of the parameters given above. In Figure 1, we see the trajectory of the solution spiral into the equilibrium state, eqn. (35). This would be expected since  $\tau < \tau_0$ . We then changed the value of the time delay to be 1.13 days. The trajectory is now a limit cycle (See Figure 2). As we have pointed out, the conditions for the system to undergo a Hopf bifurcation to a limit cycle are met with the values of the parameters used. Finally, we pick  $\tau = 10$  days. In Figure 3, we see the trajectory spiraling away from the steady state E(0.637873, 16.129, 29.4689). The trajectory initially starts at the left face of the cube, heads towards the steady state and then spirals away from the steady stater. This implies that the steady state has become unstable.

To understand why this happens, let us look at the biology. A nonzero steady state with  $\vec{y} \neq 0$  would be possible if a new plant would begin to flower while some of the original flowers are still present. This would require that a flower, pollinated at the beginning of the flowering season, would quickly develop into a seed. The seed must then fall to the ground and germinate into a plant that develops new flowers before the original flowers dry up and die. This does not usually happen in nature. Each step in the developmental stage of the plant takes time. Since the new plants do not usually arrive until the next year, the delay time appearing in eqn. (2b') would be one year. Between the period the time the last flowers of the season die and the new ones arrive, there would be no flowering plants present.

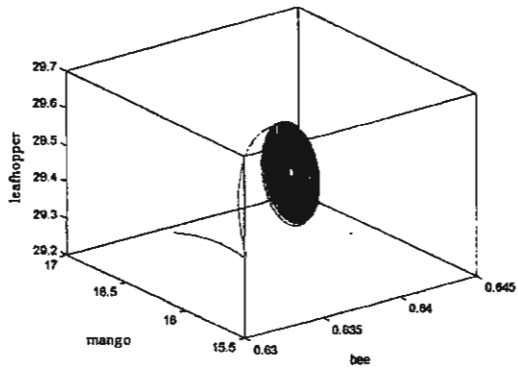


Fig 1. Numerical solution of equations (2a), (2b') and (2c) for a time delay of t=1 ( $t< t_0$ ). The graph shows the trajectory in the 3-D phase plane. The motion spirals toward the steady state solution  $\overline{R}(0.637873, 16.129, 29.4689)$ . The parameters used are: a=500, b=1/8, d<sub>1</sub>=0.08, l=0.0035, k<sub>1</sub>=3.95, k<sub>2</sub>=0.00005, m<sub>1</sub>=7.5, m<sub>2</sub>=1.6, j=0.0000386, s=0.25, g=0.0111, m=23, d=0.05

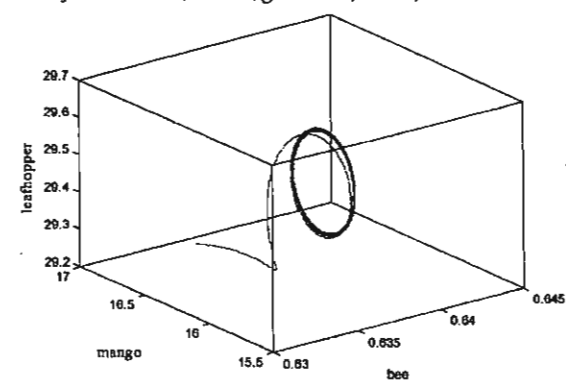


Fig 2. Numerical solution of equations (2a), (2b') and (2c) at the critical time delay  $t_o$ = 1.13 days. The parameters used are: the same as used for Figures 1. The trajectory projected on 3- dimensional phase plane. The motion is a limit cycle.

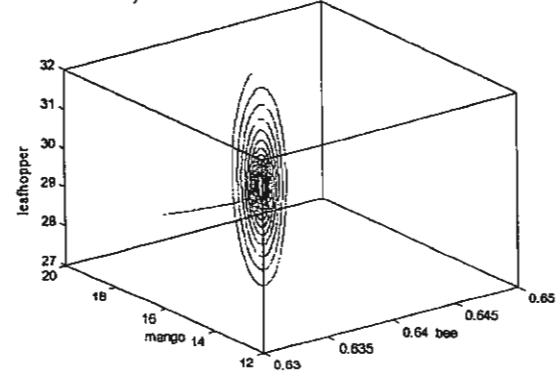


Fig 3. Numerical solution of equations (2a), (2b') and (2c) for a time delay of t=10 (15t<sub>0</sub>) days. The graph shows the trajectory in the 3-D phase plane. The trajectory moves away from the steady state solution. The parameters used are the same as those used to obtain Figs. 1 and 2.

This would happen if the time delays are greater than the lifetime of the flower, which we have taken to be nine days.

#### IVc. Real Applications.

To see how the present model might be of use to the farmers, we have modified the model to more accurately describe the production of mangos. We have inserted into eqn. (2b'), the added term  $\Phi\delta(t-t_a)$  to represent the appearance of non pollinated flowers on the tree at time t.  $\Phi$  is the number of flowers that appear on day t. We have assumed that the time delay is six months which is greater than the critical delay time. Therefore there will be no contribution from the term given by eqn. (1) in eqn. (2b'). We now look to see what would happen if the farmer has more bees on his farm. To see this, we have solved eqns. (2a), (2b') and (2c) using K values of 1000, 1,500 and 2000. The values of the other parameters are given on the figure captions. In Figure 4, we plot the number of flowers on a single tree that get pollinated each day after day to, the day the flowers began to bloom. The initial conditions for the starting day of the computer simulation, are Y(0) = 0, and X(0) and Y(0) are arbitrary. As the time passes, the number of bees begins to increase until it reaches the saturation value K. On the 100th, the flowers bloom. The figure shows that only for a short period do pollinated flowers get produced. The reason for this is that only during these nine days are the non pollinated flowers present. After this period, the flowers dried up and died. This  $\overline{lead}$  sto y = 0. We also see that the number of flowers that get pollinated increases as the number of bee increases. The three plots provide a quantitative measure of how much more mangoes can be obtained by increasing the number of bees

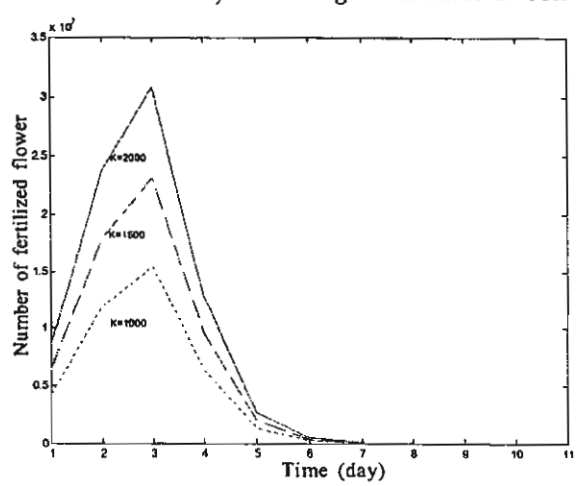


Fig 4. Number of flowers pollinated per day per tree for K equal to 1,000, 1,500 and 2,000. The number of flowers appearing on day t<sub>o</sub> is F=10,500,000. The values of the other parameters are the same as used to obtain figs. 1, 2 and 3.

available.

Another practice that can be carried out by the farmer is to decrease the number of leafhoppers. Spraying insecticides or introducing biological pests of the leafhoppers to kill them would accomplish this. The first method would however also decrease the number of bees unless the insecticide is of a type that only affects the leafhoppers and not the bees. We simulate the effects of employing an insecticide of this type or using the second method by increasing the value of the leafhopper's death rate. We have solved eqns. (2a), (2b') and (2c) for three values of the death rate  $\delta$  (0.05, 0.07 and 0.09). In Figure 5, we see that more flowers would be pollinated if the life time (inversely proportional to the death rate) of the leashopper were shorten. The time axis is changed so that it starts at day 100. We see that the flowers are only pollinated over a nine day period (i.e., during the period

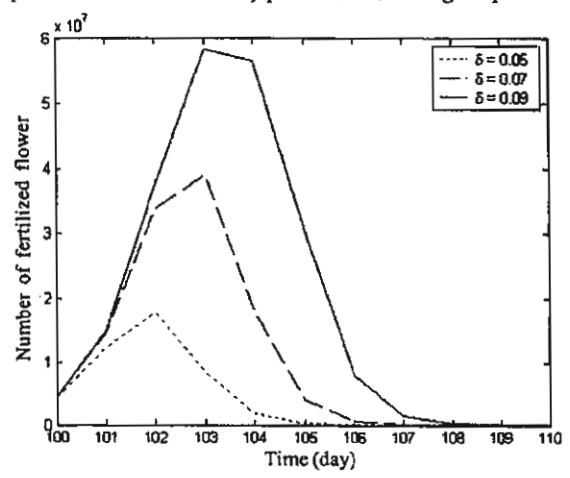


Fig 5.A graph shows the number of fertilized flower per day per tree for the death rate of leafhopper, d, equal to 0.05, 0.07 and 0.09. The number of flowers appearing on day  $t_0$  is F=10,500,000. The values of the parameters are: a=500,  $d_1$ =0.08, l=0.0035,  $k_1$ =3.95,  $k_2$ =0.00005,  $m_1$ =7.5,  $m_2$ =1.6, f=0.0000386, s=0.25, g=0.0111, m=23, b=  $d_1$ -1, K=1000

the flowers are present on the tree).

Another way for the number of pollinated flowers to be increased is to increase the number of flowers on the tree. This could be done by having the rain arrive at the right time and or having a new variety of mango plants that have more flowers. These are however beyond the control of the farmer.

#### REFERENCES

- Bandyopadhyay M, Bhattacharyya R, Mukhopadhyay B, (2004). Dynamics of an autotroph-herbivore ecosytem with nutrient recycling. Ecological Modelling 176, 201-9.
- 2. Marsden JE, McCracken M, (1976). The Hopf Bifurcation and

and

and

Its Application. Springer Verlag. New York.

 Jang SR, (2002). Dynamics of herbivore-plant-pollinator models. J. Math. Biol. 44, 129-49.

- Khan QJA, Greenhalgh D, (1999), Hopf bifurcation in epidemic models with a time delay in vaccination. IMA J. Math. Appl. Med. Biol. 16, 113-42.
- Xiao Y, Chen L, (2001). Modeling and analysis of a predatorprey model with disease in the prey. Math. Bioscience 171, # 59-82.
- Tam J. (1999). Delay effect in a model for virus replication. IMA J. Math. Appl. Med. Biol. 16, 29-37.
- Jamjanya T, Siri N, Kamarsa R. The mango leafhopper. (Homoptera. Dicadellidae) October 17, 2003. Available at http://www.agserver.kku.ac.th/kaenkaset/esearch/htm/perter/16-ok.ok.htm
- Boongird S, Bees and Honey Bees. (Funny Publishing, Bangkok (2001))
- Wangnai W, The Mango (Srisombat Publishing, Bangkok (1995)).
- In Plant-Pollinators Introduction, November 13, 2003.
   Available at http://www.d.umn.edu/~teraig/doevd/doevp-ollinators.htm
- Wongsiri S. Bee-keeping in Thailand, (Funny Publishing, Bangkok (1985))
- Laurenson J, Plight of France's honey bee, October 14, 2003.
   Available at http://www.news.bbc.co.uk/1/ni/world/europe/3173400.stm
- In Question and Answers. November 1, 2003. Available at http://www.nakhonsawan.go.th/q.bee.htm

#### APPENDIX

## Lemma 1. Conditions for the Existence of Positive Real Roots of a Cubic Equation.

Consider the following cubic equation

$$S(\eta) = \eta^3 + d_1 \eta^2 + d_2 \eta + d_3 = 0$$
 (A1)

**A.** If either (i)  $d_1 < 0$ ,  $d_2^3 = 0$  and  $d_1^2 > 3d_2$ , or (ii)  $d_2 < 0$ : and  $\Delta < 0$ , then eqn. (A1) has positive simple roots.

where

5

$$\Delta = S(\varepsilon_1)S(\varepsilon_2) = \frac{4}{27}d_2^3 - \frac{1}{27}d_1^2d_2^2 - \frac{2}{3}d_1d_2d_3 + \frac{4}{27}d_1^3d_3 + d_3^2$$
(A2)

with  $\varepsilon$ , and  $\varepsilon$ , being the two turning points of  $S(\eta)$  given by

$$\varepsilon_1 = \frac{-d_1 - \sqrt{d_1^2 - 3d_2}}{3}, \varepsilon_2 = \frac{-d_1 + \sqrt{d_1^2 - 3d_2}}{3}$$
 (A3)

**B.** If  $d_3 \ge 0$ , the necessary condition for eqn. (A1) to have no positive

real roots are either

(i) 
$$d_1^2 < 3d_2$$

(ii) 
$$d_1^2 = 3d_2$$

(iii) 
$$d_1^2 - 3d_2 > 0$$
 and  $\Delta > 0$ , or

(iv) 
$$d_1^2 - 3d_2 > 0$$
 and  $\Delta < 0$ ,  $d_1 > 0$  and  $d_2 > 0$ 

Proof of this lemma is found in Khan and Greenhalgh [4]. Theorem 1. (Routh-Hurwitz Criteria). Let x be an equilibrium point of eqn. (A4), and J be the Jacobian evaluated at the equilibrium point. Suppose the diagonalization of J yields the following characteristic equation

$$\lambda^3 + A\lambda^2 + B\lambda + C = 0 . \quad (A6)$$

The equilibrium state x\* will be local asymptotically stable if the coefficients A,B and C satisfy the following conditions:

**Theorem II. (Hopf Bifurcation).** Suppose the functions  $F_i(\{x\})$  depends on parameter  $\tau \in \mathbb{R}$ . The Jacobian will now depend on the parameter  $\tau$ , i.e.,

$$J(\tau) = D_{\mathbf{x}} F(\mathbf{x}^*, \tau) = \frac{\partial F_{\mathbf{i}}}{\partial \mathbf{x}_{\mathbf{j}}} (\mathbf{x}^*, \tau) \qquad i, \quad j = 1, 2, ..., n$$

If  $J(\tau)$  has a pair of complex eigenvalues,  $\lambda(\tau a) = u(\tau) \pm iv(\tau)$  such that

i. 
$$u(\tau_o) = 0$$
,  
ii.  $v(\tau_o) = v^* > 0$   
iii.  $\frac{du}{da}(\tau_o) \neq 0$  (A8)

where  $\tau_a$  is called a critical value of the bifurcation parameter ' $\tau$ ', and no other eigenvalues with zero real part exist, the system will undergo a transition to a limit cycle about the point ( $\mathbf{x}^*$ ,  $\tau_a$ ).

Proofs of this theorem can be found in various textbooks.<sup>2</sup>

JOURNAL OF BIOSCIENCE AND BIOENGINEERING Vol. 98, No. 3, 182–186, 2004

\*\*\*

1

ri

ıİ

# Effects of Static Magnetic Field on Growth of Leptospire, Leptospira interrogans serovar canicola: Immunoreactivity and Cell Division

WANNAPONG TRIAMPO, 1.4\* GALAYANEE DOUNGCHAWEE, 2 DARAPOND TRIAMPO, 3 JIRASAK WONG-EKKABUT, 1 AND I-MING TANG 1.4

Department of Physics, Faculty of Science, Mahidol University, Bangkok 10400, Thailand, Department of Pathobiology, Faculty of Science, Mahidol University, Bangkok 10400, Thailand, Department of Chemistry, Faculty of Science, Mahidol University, Bangkok 10400, Thailand, and Capability Building Unit in Nanoscience and Nanotechnology, Faculty of Science, Mahidol University, Bangkok 10400, Thailand

Received 4 March 2004/Accepted 14 June 2004

The effects of the exposure of the bacterium, Leptospira interrogans serovar canicola to a constant magnetic field with magnetic flux density from a permanent ferrite magnet=140±5 mT were studied. Changes in Leptospira cells after their exposure to the field were determined on the basis of changes in their growth behavior and agglutination immunoreactivity with a homologous antiserum using dark-field microscopy together with visual imaging. The data showed that the exposed Leptospira cells have lower densities and lower agglutination immunoreactivity than the unexposed control group. Interestingly, some of the exposed Leptospira cells showed abnormal morphologies such as large lengths. We discussed some of the possible reasons for these observations.

[Key words: leptospirosis, Leptospira interrogans, magnetic field, dark-field microscopy, immunoreactivity, cell division]

Leptospirosis is an acute febrile illness caused by pathogenic spirochete bacteria of the genus Leptospira (1, 2). This disease has emerged as an important public health problem worldwide. The symptoms of this disease can range from mild-flu-like symptoms to severe (often fatal) complications such as renal and/or liver failure and hemorrhage (referred to as Weil's syndrome) (3). Most outbreaks tend to be seasonal in nature and are often associated with environmental factors, animals, and agricultural and occupational cycles such as rice cultivation in marshy lands. Mammals such as rats and cattle are commonly involved in the transmission of this disease to humans via direct or indirect exposure to contaminated tissues or urine (1, 2, 4). Out-breaks of leptospirosis occur mainly after flood, making it an occupational hazard for sanitary and agricultural workers, as well as a recreational hazard for humans (5). Some pathogenic Leptospira species have also been found to be associated with domesticated animals. For example, serovar canicola (Leptospira canicola) has adapted itself to canines; therefore, it has become common in many human communities. Although there has been no report of leptospirosis in canines in Thailand, there is a great potential for the transmission of the disease between humans and dogs kept as household pets, unless one is aware of the disease.

\* Corresponding author. e-mail: scwtr@mahidol.ac.th; wtriampo@yahoo.com phone: +66-2-889-2337 fax: +66-2-354-7159

L. canicola cells used in our study are motile aerobes that are very thin, flexible and spiral-shaped of about 0.1 µm width and 6-20 μm length. Leptospira cells are difficult to observe under a light microscope. They can, however, be observed by dark-field microscopy using wet samples. This allows for the determination of agglutination immunoreactivity to be determined. The Leptospira outer membrane or surface antigens can be detected through its agglutination with a homologous (antiserum). The optimal conditions for its growth and as well, its biology are well documented in the literature (1, 2). Moist environments with a neutral pH are suitable conditions for the survival of Leptospira outside the host. The optimal cultivation temperature is approximately 20-32°C. In general, Leptospira species are highly susceptible to adverse environmental conditions such as exposure to dry air, chemicals such as chlorine or iodine in detergents, unfavorable pH (>8.0 or <6.5), strong electromagnetic fields and high temperatures (above 40°C).

Magnetic fields (MFs) also affect various biological functions of living organisms, for example, DNA synthesis and transcription (6), as well as ion transportation through cell membranes (7). Almost all living organisms are exposed to magnetic fields from various sources. The geomagnetic field on the surface of the earth is approximately 0.50–0.75 gauss in strength. There have been several studies on the effects of exposure to MFs and several of these have given rise to controversies over the past decades. The growth rate of the Burgundy wine yeast has been shown to decrease when an ex-

tremely low magnetic flux density (MFD) of 4 gauss is applied (8). The growth of *Trichomonas vaginalis* is accelerated when it is exposed to 460–1200 gauss (9). The growth rate of *Bacillus subtilis* increases when exposed to 150 gauss and decreases when exposed to more than 300 gauss (10). Similar results were reported for *Chlorella*; an exposure of less than 400 gauss increases the growth, while exposure to 580 gauss decreases the growth rate (11). Several studies point to the MF as a factor influencing the growth and survival of living organisms, which vary at different MFDs (12–15). Other researchers have studied the effects of MFs on bacteria at the enzyme (16) or genetic (17) level.

To study the efficacy of using magnetic field to control or prevent the growth of leptospire, we applied MF on selected *Leptospira* cells at various intensities and exposure duration levels. We then determined the agglutinating activity of experimental bacteria using dark field microscopy.

#### **MATERIALS AND METHODS**

Pathogenic Leptospira interrogans, serovar canicola was used in this study. Bacterial cells were grown in the Ellinghausen and McCullough modified by Johnson and Harris (EMJH) liquid medium (2). The bacterial cells were grown at a temperature of  $27\pm1^{\circ}\text{C}$  in the dark.

A cylindrical permanent ferrite magnet 5 cm in diameter was placed beside 15 ml culture glass tube (less than 1 ml apart) containing 1 ml of a suspension of newly subcultured Leptospira cells in the EMJH liquid medium. MF and homogeneity of 140±5 mT (northpole) were checked using a teslameter (Hall effect Teslameter digital, order no. 13610.93; Phywe Systeme, Göttingen, Germany). The intensity of static magnetic field used in our experiments was chosen on the basis of Genkov et al. (9) findings. Genkov et al. had used more or less this intensity of a constant MF to induce the growth and development of Trichomanas vaginalis. For this type of exposure, no shielding against the natural variations of terrestrial MF was required, the value of approximately 0.050 mT is negligible with respect to the MF intensities applied. An experiment using cells not exposed to MF was simultaneously performed as the control, which was placed at a distance of about 100 cm from the exposed group.

In the absence of magnets, MFD was 0.05±0.01 mT. All bacterial samples were exposed to MF for different durations, that is, 0 (control sample), 1, 2, 3, 4, 5, and 6 d. After MF exposure, individual samples were further incubated for 7 d. Immediately after 7 d of incubation, dark-field micrographs were taken using a CCD camera to observe cell development. The growth and agglutination properties using the microscopy agglutination test (MAT) with a homologous antiserum and immunoreactivity were scored as follows:

- 4+ = 100% absence of Leptospira cells from the field
- 3+=75% absence of *Leptospira* cells from the field
- 2+=50% absence of *Leptospira* cells from the field
- 1+ = 25% absence of Leptospira cells from the field

MAT has been commonly used as a diagnostic tool for leptospirosis. This may not be the most reliable test. It, however, is arguably the most appropriate test for this study. The same set of conditions and specimens were used in the experiments, which were repeated twice.

Atomic force microscopy (AFM) and sample preparation Scanning probe microscopy (SPM) (Digital Instruments Veeco Metrology Group, NY, USA) was used for AFM surface morphol-

Metrology Group, NY, USA) was used for AFM surface morphology imaging. Images were acquired in the contact mode showing height contours that highlight the spiral shape and fine surface

morphology of *Leptospira* cells. An AFM scanner with hardware correction for the nonlinearities of the piezoelectric element was used. The scanner has a maximum xy range of 125 by 125  $\mu m$  and a Z range of 6  $\mu m$ . The cantilevers of  $Si_3N_4$ , 125  $\mu m$  long and 35  $\mu m$  wide with a spring constant of 0.58 Nm $^{-1}$  were used. To locate the area of interest in the samples and identify any bacteria, we used a built-in long-range on-axis microscope, capable of a 5:1 zoom and  $\times 3500$  magnification. Imaging was carried out at scan speeds between 1 and 50  $\mu m/s$ . Images were acquired at 256  $\times 256$  pixels. A typical imaging session began using a built-in optical microscope and by moving the x-y table to search for bacterial cells. The AFM cantilever was then moved forward to the surface close to the chosen bacterial cell.

Each sample was prepared using the method described above. It was then dropped on a microscope glass slide and dried in air.

#### RESULTS

Figure 1 shows the AFM picture of an *L. interrogans* serovar *canicola* cell taken with a Digital Instrument Nanoscope IIIa (Digital Instruments Veeco Metrology Group) in the contact mode. The image shows a normal morphology of *L. interrogans* serovar *canicola*, that is, the spiral shape. It is worth noting that AFM usually reveals the actual roughness of the surface of the bacterial envelope. Other types of microscopy frequently show the surface to be relatively smooth. This technique was also used to observe the surface morphology of bacterial cells before and after the exposure to MF. It should be noted that this image does not demonstrate the rough envelope very clearly. However, it does show the normal bacterial morphology.

Figure 2 shows some representative dark field micrographs of *L. interrogans* serovar *canicola* taken at the logarithmic growth phase (at 1:10 dilution of culture samples) and for different durations of MF exposure, that is, 0, 2, 3, and 6 d. After 7 d of incubation, the samples were observed

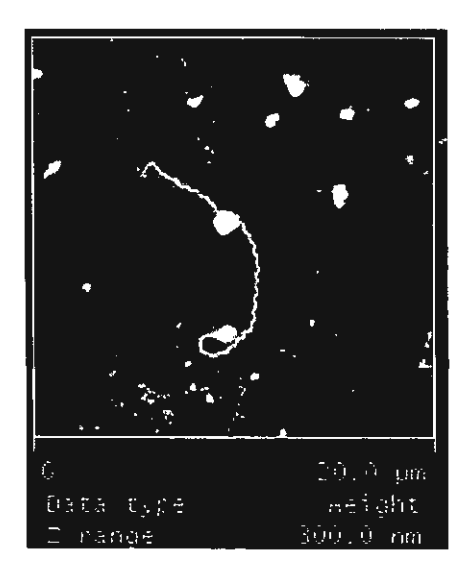


FIG. 1. Atomic force micrograph (AFM) of Leptospira interogans serovar canicola taken using Digital Instrument NanoScope IIIa in the contact mode under control conditions, that is, without MF exposure. Scan size was 20  $\mu m$  and scan rate was 1 Hz. It shows a spiral-shaped leptospire of approximately  $10{-}20~\mu m$ .

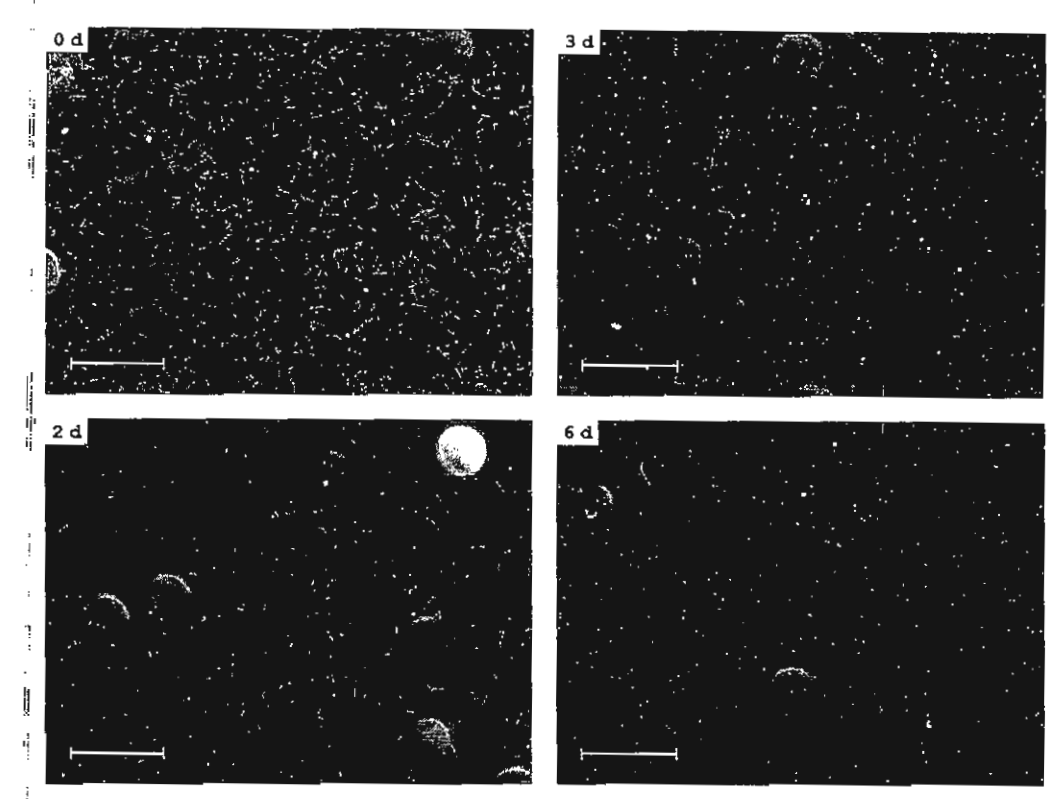


FIG. 2. Dark field micrographs of *L. interrogans* serovar canicola exposed to MF for different durations. The images were taken at the log phase of each experimental culture sample (diluted 1:10 of original). Bars: 100 μm.

under a dark field microscope and images were taken using a CCD camera. Even though there are some noises in the images, the inhibition of cell growth could be observed. The implications of these observations are significant given the results of other studies (6–17). From Fig. 2A to 2D, one can clearly observe that cell density decreased with exposure time, particularly after more than 3 d. This indicates the decrease in growth rate resulting in the decrease in the number of bacterial cells. This is one of the factors that explain the lower agglutination immunoreactivity, which indicates fewer

remaining living bacterial cells to agglutinate.

Figure 3 shows the dark field micrographs of agglutinated bacterial cells after reacting with the specific antiserum; Fig. 3A shows a complete agglutination (100% immuno) and Fig. 3B shows 50% agglutination (with only one half of free-living bacterial cells present).

On the basis of the criteria mentioned at the end of the previous section, the agglutination reactivities of the *L. interrogans* serovar *canicola* exposed to different intensities of MF are listed in Table 1 (with longer exposure time, the

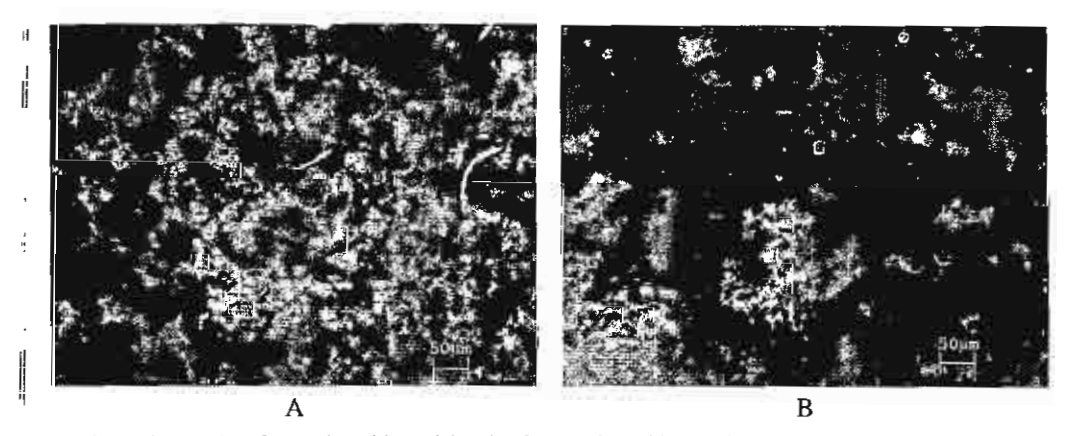


FIG. 3. Dark field micrographs of agglutinated bacterial cells after reacting with homologous antiserum, showing complete agglutination (100% reactivity; A) and 50% agglutination with one-half of free-living bacterial cells remaining (B).

TABLE 1. Agglutination characteristics of leptospires after magnetic field exposure for various durations

Exposure duration (d)	1:50 dilution	l:100 dilution	1:200 dilution	1:400 dilution	1:800 dilution	1:1600 dilution	1:3200 dilution
Oa	4+	3+	2+	2+	2+	2+	1+
1	3+	2+	<b>i</b> +	-	_	_	_
2	3+	2+	1+	_	_	_	_
3	2+		_	_	_	_	_
4	2+	_	_	_	_	_	_
5	1+		_	_	_	_	_
6	NA	_	-	_	_	_	_

<sup>&</sup>lt;sup>a</sup> Representive sample of control unexposed leptospires showing a higher MAT titer (1:1600) than exposed samples for various durations. NA indicates no agglutination occurred.

#### Agglutination immunoreactivity

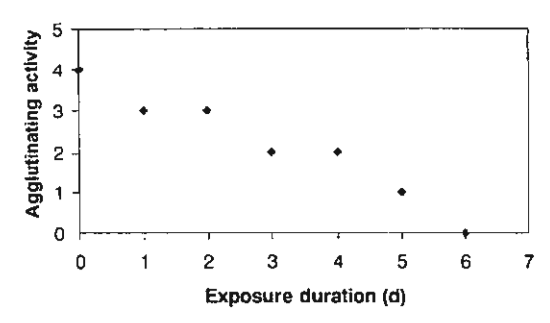


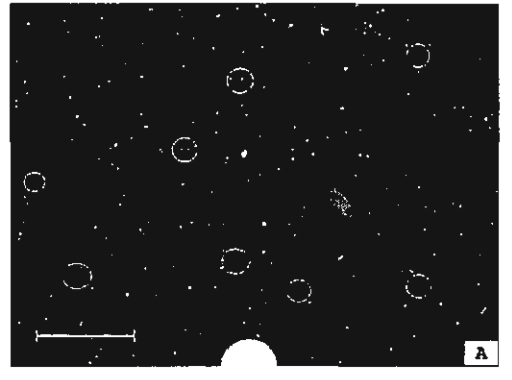
FIG. 4. Plots of data shown in Table 1.

Leptospira bacterial cells demonstrated a lower agglutination immunoreactivity than that of the reference antiserum tested. The end point of reactivity was 50% agglutination [2+]). The agglutination immunoreactivity score decreased with exposure time of Leptospira cells as shown in Fig. 4. Comparing the MAT results of control Leptospira cells (0 d exposure) and those of bacterial cells after exposed to MF, we found that the latter groups (particularly those with longer exposure) showed lower agglutination reactivies. These findings may indicate the presence of a lower amount of agglutinin or number (density) of Leptospira cells in the exposed samples than in the control samples. It should be emphasized that the same set of conditions and specimens were

used in the experiments that were repeated twice, and the experiments yields exactly the same (semiquantitative) results. The scoring data therefore did not show an error. Once again, in each experimental setup, it has one control (non-exposed) group and six exposed groups with different durations of exposure.

Besides the decrease in the number of Leptospira cells as the cause of the decrease in agglutination immunoreactivity as mentioned above, the "denaturing effect" of the antigenantibody reaction may be an other contributing factor to this phenomenon, which can be explained as follows: Typically, antibodies are large soluble protein molecules known as immunoglobins and are produced by B-cells. They bind to specific antigens in a lock-and-key fashion (lock = antibody; key = antigen) (18). Their shape should, therefore, be specific to particular antigens. When a specific antibody encounters an antigen, it will form an antigen-antibody complex through some noncovalent forces such as electrostatic force, hydrogen bond, van der Waal force or hydrophobic force. When a change in what of a single atom occurs, the complex can become unbound. This specificity could be the underlying factor for the denaturation of the antigen-antibody reaction. Under the conditions used in the study, the motion or transfer of any electrons or ions onto the cell membrane could induce an electric current. This current may perturb the other charge particle motion in the cell thus resulting in the loss of binding (19).

Surprisingly, we observed that some Leptospira cells exposed for three or more days were longer than the control



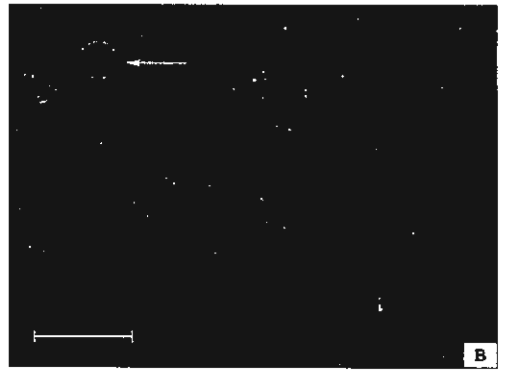


FIG. 5. Dark-field micrographs of *L. interrogans* serovar *canicola* taken at the same magnification ( $\times$ 200). Control sample unexposed to magnetic field; the leptospires have an approximate length of  $10-20~\mu m$  (A) compared with magnetic field-exposed leptospires (B) with some cells longer than others. Circles indicate individual bacterial cells. Bars:  $100~\mu m$ .

TRIAMPO ET AL.

J. BIOSCI, BIOENG.

bacterial cells (see Fig. 5). This preliminary finding probably indicates that there is some disturbance in cell division. More experiments must be carried out to examine and determine the exact mechanism underlying these observed phenomena. Our present explanation for this abnormality in cell division is based on the following: Like most bacteria and archaea, Leptospira cells divide symmetrically possibly via the formation of a septum in the middle of the cell (we consider that binary fission is less likely). For the time being, we use AFM in the investigation of division-related morphologies. Recent evidence indicates that synthesized proteins dedicated to cell division are assembled between segregated chromosomes at an appropriate time (20). The key to this assembly is the filamentous temperature exposure sensitive (Ftsz structural) analogue of tubulin (21). DNA damage caused by MF exposure induces mutation, resulting in the abnormal synthesis of FtsZ, which in turn could interfere or stop cell division. Similar to previous studies of Escherichia coli, FtsZ appears to induce the earliest (known) step in cell division. E. coli cells with a mutation of ftsz caused by exposure to certain conditions do not divide. This result in the formation of long filamentous cells that can replicate and segregate their chromosomes (22).

Our finding is at least the first step toward a grater understanding of the development of diagnostics, treatment, and prevention schemes for bacterium and leptospirosis. We hope that further studies of leptospirosis will lead to this disease in the near future.

#### ACKNOWLEDGMENTS

This research was supported in part by the Thailand Research Fund, TRG4580090 and RTA4580005 and MTEC Young Research Group funding MT-NS-45-POL-14-06-G. The support of the Royal Golden Jubilee Ph.D. Program (PHD/0240/2545) to Jirasak Wong-Ekkabut and I-Ming Tang is also acknowledged.

#### REFERENCES

- 1. Faine, S. (ed.): Guideline for control of leptospirosis, vol. 67,
- p. 129. World Health Organization, Geneva (1982).
  Faine, S., Adler, B., Bolin, C., and Perolat, P.: Leptospira and Leptospirosis, 2nd ed., p. 272. MediSci Ed, Melbourne
- 3. Sherris, J. C.: An introduction to infectious disease, 2nd ed., o. 432-435. Elsevier, New York (1990).
- Turner, L. H.: Leptospirosis I. Trans. R. Soc. Trop. Med. Hyg., 61, 842-855 (1967).
- 5. Benenson, A.S.: Leptospirosis, p. 293-296. In Chin, J. E. (ed.). Control of communicable diseases manual, American

- Public Health Association, Washington, D.C. (2000).
- Phillips, J. L., Haggren, W., Thomas, W. J., Ishida-Jones, T., and Adey, W. R.: Magnetic field-induced changes in specific gene transcription. Biochim. Biophys. Acta, 112, 140-144 (1992)
- 7. Liburdy, R. P., Callahan, D. E., Harland, J., Dunham, E., Sloma, T. R., and Yaswen, P.: Experimental evidence for 60 Hz magnetic fields operating through the signal transduction cascade: effects on calcium influx and c-MYC mRNA induction. FEBS Lett., 334, 301-308 (1993).
- Kimball, G. K.: The growth of yeast in a magnetic field. J. Bacteriol., 35, 109-122 (1938).
- Genkov, D., Cvetkova, A., and Atmadzov, P.: The effect of the constant magnetic field upon the growth and development of T. vaginallis. Folia Medica, 16, 95-99 (1974).
- 10. Moore, R. L.: Biological effects of magnetic fields: studies with microorganisms. Can. J. Microbiol., 25, 1145-1151 (1979)
- Takahashi, F. and Kamezaki, T.: Effect of magnetism of growth of Chlorella. Hakkokogaku, 63, 71-74 (1985)
- Yamaoka, Y., Takimura, O., Fuse, H., and Kamimura, K.: Effect of magnetism on growth of *Dunaliella salina*. Res. Photosynth., 3, 87-90 (1992).

  13. Singh, S. S., Tiwari, S. P., Abraham, J., Rai, S., and Rai,
- A. K.: Magnetobiological effects on a cyanobacterium, Anabena
- doliolum. Electro- Magnetobiol., 13, 227-235 (1994).

  Tsuchiya, K., Nakamura, K., Okuno, K., Ano, T., and Shoda, M.: Effect of homogeneous and inhomogeneous high magnetic fields on the growth of Escherichia coli. J. Ferment. Bioeng., 81, 343-346 (1996).
- Piatti, E., Albertini, M. C., Baffone, W., Fraternale, D., Citterio, B., Piacentini, M. P., Dacha, M., Vetrano, F., and Accorsi, A.: Antibacterial effect of a magnetic field on Serratia marcescens and related virulence to Hordeum vulgare and Rubus fruticosus callus cells. Comp. Biochem. Physiol. B. Biochem. Mol. Biol., 132, 359-365 (2002).
- Utsunomiya, T., Yamane, Y., Watanabe, M., and Sasaki, K.: Stimulation of porphyrin production by application of an external magnetic field to a photosynthetic bacteria, Rhodo-
- bacter sphaeroides. J. Biosci. Bioeng., 95, 401-404 (2003). Horiuchi, S., Ishizaki, Y., Okuno, K., Ano, T., and Shoda, M.: Drastic high magnetic field effect on suppression of Escherichia coli death. Bioelectrochemistry, 53, 149-153 (2001)
- Boyd, R. F.: Basic medical microbiology, 5th ed. Little, Brown and Co., Boston (1995).
- Jackson, J. D.: Classical electrodynamics, 3rd ed. Wiley Text Books, New York (1998).
- Rothfield, L., Justice, S., and Garcia-Lara, J.: Bacteria cell division. Annu. Rev. Genet., 33, 423-448 (1999).
- Lutkenhaus, J.: Ftsz ring in bacterial cytokinesis. Mol. Microbiol., 9, 403-410 (1993).
- Hale, C. A. and de Boer, P. A. J.: Direct binding of FtsZ to ZipA, an essential component of the septal ring structure that mediates cell division in E. coli. Cell, 88, 175-185 (1997).

Journal of the Korean Physical Society, Vol. 46, No. 4, April 2005, pp. 0~0

П

Ľ

į.

||-

# A Lattice Boltzmann Method for Modeling the Dynamic Pole-to-Pole Oscillations of Min Proteins for Determining the Position of the Midcell Division Plane

Waipot NGAMSAAD, Wannapong TRIAMPO,\* Paisan KANTHANG,
I-Ming TANG, Narin NUTTAWUT and Charin MODJUNG

Department of Physics and Capability Building Unit in Nanoscience and Nanotechnology,
Faculty of Science, Mahidol University, Bangkok 10400, Thailand

Yongwimon LENBURY

Department of Mathematics, Faculty of Science, Mahidol University, Bangkok 10400, Thailand

(Received 14 September 2004)

Determining the middle of the bacteria cell and the proper placement of the septum is essential to the division of the bacterial cell. In E. coli, this process depends on the proteins MinC, MinD, and MinE. Here, the lattice Boltzmann method (LBM) is used to study the dynamics of the oscillations of the min proteins from pole to pole. This determines the midcell division plane at the cellular level. The LBM is applied to the set of deterministic reaction diffusion equations proposed by Howard et al. to describe the dynamics of the Min proteins. The LBM results are in good agreement with those of Howard et al. and agree qualitatively with the experimental results. Our good results indicate that the LBM can be an alternative computational tool for simulating problems dealing with complex biological systems that can be described by using the reaction-diffusion equations

PACS numbers: 87.15.Aa

Keywords: Lattice Boltzmann method, Bacteria, E.coli, Cell division, Min proteins, MinCDE oscillation

#### I. INTRODUCTION

Cell division or cytokinesis is the process by which a cell separates into two after its DNA has been duplicated and distributed into the two regions that will become the future daughter cells. For a successful cell division to take place, the cell has to determine the optimal location of the cell separation and the time to start the cell cleavage. This involves the identification of the midpoint of the cell where the septum or cleavage furrow will form. For Escherichia coli and other rod-like bacteria, evidence accumulated over the past few years indicate that the separation into two daughter cells is achieved by forming a septum perpendicular to their long axes. To induce the separation, the FtsZ ring (Z ring), a tubulin-like GT-Pase, is believed to initiate and guide the septa growth by contraction [1]. The Z ring is usually positioned close to the center, but it can also form in the vicinity of the cell poles. Two processes are known to regulate the placement of the division site: nucleoid occlusion [2] and the action of the min proteins [3]. Both processes interfere with the formation of the Z ring, which is believed to

determine the division site. Nucleoid occlusion is based on cytological evidence that indicates that the Z ring assembles preferentially on those portions of the membrane that do not directly surround the dense nucleoid mass [4].

The min proteins that control the placement of the division site are the MinC, MinD, and MinE proteins [3]. Experiments involving the use of modified proteins show that MinC is able to inhibit the formation of the FtsZ-ring [5]. MinD is an ATPase that is connected peripherally with the cytoplasmic membrane. It can bind to MinC and activate the function of MinC [6,7]. Recent studies show that MinD recruits MinC to the membrane. This suggests that MinD stimulates MinC by concentrating it near its presumed site of activation [8, 9]. That MinE is required to give site specificity to the division inhibitor suggests that MinE acts as a topological specificity protein, capable of recognizing the midcell site and preventing the MinC division inhibitor from acting at that site [10]. Its expression results in a sitespecific suppression of the MinC/MinD action so that the FtsZ assembly is allowed at the middle of the cell, but is blocked at other sites [3]. In the absence of MinE, the MinC/MinD is distributed homogeneously over the entire membrane. This results in a complete blockage

<sup>\*</sup>E-mail: wtriampo@yahoo.com; Fax: 662-201-5843

of the Z-ring formation and the subsequent formation of a long filamentous cell which that will fail to divide 18, 9,11,12]. By fluorescent labeling, MinE was shown to attach to the cell wall only in the presence of MinD [13, 14]. Because MinD interacts with MinC, it is likely that they oscillate together. This results in a concentration of the division inhibitor at the membrane on either cell end, alternating between being high or low every other 20 seconds, so that the period of oscillation is about 40 seconds per cycle [8,9]. MinE is not only required for the MinC/MinD oscillation, it is also involved in setting the frequency of the oscillation cycle [11]. Several lines of evidence indicate that the MinE localization cycle is tightly coupled to the oscillation cycle of MinD. Recently, microscopy of fluorescently labeled proteins involved in the regulation of E.coli division uncovered coherent and stable spatial and temporal oscillations of these three proteins [15]. The proteins oscillate from one end of the bacterium to the other and move between the cytoplasmic membrane and the cytoplasm. The detailed mechanism by which these proteins determine the correct position of the division plane is currently unknown, but the observed pole-to-pole oscillations of the corresponding distribution are thought to be of functional importance.

## II. LATTICE BOLTZMANN METHOD AND MODEL DESCRIPTION

The Lattice Boltzmann method (LBM) is a numerical scheme evolved from the lattice gas model (LGM) in order to overcome the difficulties encountered with that model [16, 17]. The LGM or lattice gas automata is a method to determine the kinetics of particles by utilizing a discrete lattice and discrete time. It has provided insights into the underlying microscopic dynamics of the physical system whereas most other approaches focus only on the solution to the macroscopic equation. However, the LGM, in which the particles obey an exclusion principle, has microscopic collision rules. These rules are very complicated and require many random numbers. These random numbers create noise or fluctuations. An ensemble averaging is then required to smooth out the noise in order to obtain the macroscopic dynamics which are the results of the collective behavior of the many microscopic particles in the system and which are not sensitive to the underlying details at the microscopic level. The averaging requires a long time, which leads to an increase in the amount of computational storage required and which in turn leads to a reduction in the computational speed. For these reasons, the LBM is used only when one is interested in the evolution of averaged quantities and not in the influence of the fluctuations. The LBM gives a correct average description on the macroscopic level of a fluid. The LBM can also be viewed as a special finite difference scheme for the kinetic equation of the discrete-velocity distribution function. The simplicity and the kinetic nature of the LBM are among its appealing features.

The LBM consists of simple arithmetic calculations and is, therefore, easy to program. In the LBM, the space is divided into a regular Cartesian lattice grid as a consequence of the symmetry of the discrete velocity set. Each lattice point has an assigned set of velocity vectors with specified magnitudes and directions connecting the lattice point to its neighboring lattice points. The total velocity and particle density are defined by specifying the number of particles associated with each of the velocity vectors. The microscopic particle distribution function, which is the only unknown, evolves at each time step through a two-step procedure: convection and collision. The first step, convection (or streaming), simply advances the particles from one lattice site to another lattice site along the directions of motion according to their velocities. This feature is borrowed from kinetic theory. The second step or collision is models various interactions among particles by allowing for the relaxation of a distribution towards an equilibrium distribution through a linear relaxation parameter. The averaging process uses information based on the whole velocity phase space.

Most research reported in the literature is limited to the LBM for the Navier-Stokes equations [18,19]. The LBM scheme has been particularly successful in simulating fluid-flow applications for a broad variety of complex physical systems and has found application in different areas, such as hydrodynamic systems [17,20], multiphase and multi-component fluids [21], advection-dispersion [22] and blood flow [23–25]. Application to complex biological systems at the cellular and the molecular biological levels has been rare.

In the present paper, we propose a LBM to study the partitioning of the bacterial cell during cell division. This provides an alternative method to investigate quantitatively the division of the cell. We compare our results with those obtained by numerically solving a set of deterministic coarse-grained coupled reaction-diffusion equations [26] to demonstrate the validity of the proposed LBM.

#### 1. Reaction-diffusion Equation Model

We focus on the  $E.\ coli$  bacteria, a commonly studied rod shaped bacteria of approximately  $2-6\ \mu m$  in length and around  $1-1.5\ \mu m$  in diameter. Each  $E.\ coli$  bacteria divides roughly every hour via cytokinesis. We adopted the dynamic model of the compartmentization in the bacterial cell division process proposed by Howard  $et\ al.$  In the Howard model, dynamics at the mean-field level are given by a set of coarse-grained non-linear reaction-diffusion equations. The reaction-diffusion equations to model self-organization and pattern formation [27].

Our starting point is the set of one-dimensional deterministic coupled reaction-diffusion equations used to describe the dynamics of the interactions between the local densities of MinD and MinE proteins given by Howard et al [26]. They describe the time rates of change of the densities due to the diffusions of MinD and MinE and to the mass transfer between the cell membrane and the cytoplasm. Based on the experimental results given in Ref. 9, which showed that the MinC dynamics are similar to those of MinD, we have not written out the equations for MinC. In dimensionless form, the dynamics are written as in the start of 
$$\frac{\partial n_D}{\partial t} - D_D \frac{\partial^2 n_D}{\partial x^2} = R_D = -\frac{\sigma_1 n_D}{1 + \sigma_1' n_e} + \sigma_2 n_e n_d \quad (1)$$

$$\frac{\partial n_d}{\partial t} = D_d \frac{\partial^2 n_d}{\partial x^2} = -R_D = \frac{\sigma_1 n_D}{1 + \sigma_1' n_e} - \sigma_2 n_e n_d \qquad (2)$$

$$\frac{\partial n_E}{\partial t} - D_E \frac{\partial^2 n_E}{\partial x^2} = R_E = \frac{\sigma_4 n_e}{1 + \sigma_4' n_D} - \sigma_3 n_D n_E \quad (3)$$

$$\frac{\partial n_c}{\partial t} - D_e \frac{\partial^2 n_c}{\partial x^2} = -R_E = -\frac{\sigma_4 n_e}{1 + \sigma_4' n_D} + \sigma_3 n_D n_E \tag{4}$$

where  $n_s$  is the mass density of particle of species  $s = \{D, d, E, e\}$  at time t and position x. The first equation is for the cytoplasmic MinD density  $n_D$ . The second is for the membrane-bound MinD density  $n_d$ . The third is for the cytoplasmic MinE density  $n_E$ , and the last is for the membrane-bound MinE density  $n_e$ .  $R_s$  is the reaction term and depends on the density of the species  $n_s$  and on the densities of the other species that react with species  $s.D_s$  is the diffusion coefficient. In this paper, we assume that  $D_s$  is isotropic and independent of x. The constant  $\sigma_1$  represents the association of MinD to the membrane [12].  $\sigma_1$  corresponds to the membranebound MinE suppressing the recruitment of MinD from the cytoplasm.  $\sigma_2$  reflects the rate that MinE on the membrane drives the MinD on the membrane into the cytoplasm. Based on the evidence of the cytoplasmic interaction between MinD and MinE [7], we let  $\sigma_3$  be the rate that cytoplasmic MinD recruits cytoplasmic MinE for the membrane while  $\sigma_4$  corresponds to the rate of dissociation of MinE from the membrane to the cytoplasm. Finally,  $\sigma_4$  corresponds to the cytoplasmic MinD suppressing the release of the membrane-bound MinE. The time scale of the diffusion on the membrane is much slower than that in cytoplasm. It seems, therefore, reasonable to set  $D_d$  and  $D_e$  to zero. In this dynamics, we allow for the Min protein to bind/unbind from the membrane, but not for it to be degraded in the process. Thus, the total amount of each type of Min protein is conserved. The zero-flux boundary condition will be imposed. This boundary condition gives a closed system with reflecting or hard-wall boundary conditions.

#### 2. Lattice Boltzmann Equation

The dynamics determined by Eqs. (1)-(4) can be simulated using a Lattice-Boltzmann method having three one-dimensional velocities. Let  $f_s(\vec{x},i,t)$  be the one-particle distribution function of species s with velocity  $\vec{e_i}$  at some dimensionless time t and dimensionless position  $\vec{x}$ . The coordinate  $\vec{x}$  only takes on a discrete value: the nodes of the chosen lattice. The nearest neighbor vectors are defined as

$$\vec{e_i} = \begin{cases} \vec{0} & i = 0\\ \hat{x} & i = 1\\ -\hat{x} & i = 2 \end{cases}$$
 (5)

where  $\hat{x}$  is a unit vector along the x direction. For each lattice site, we have three states for each species. Following Ref. 28, the lattice Boltzmann equation for  $f_s(\vec{x}, i, t)$  can be written as

$$f_s(\vec{x} + \vec{e_i}, i, t + 1) - f_s(\vec{x}, i, t) = \Omega_s(\vec{x}, i, t)$$
 (6)

where  $\Omega_s$  is the collision operator for the species s and depends on the distribution function  $f_s$ . The collision operator  $\Omega_s$  can be separated into two parts [29], a non-reactive term  $(\Omega_s^{NR})$  and a reactive term  $(\Omega_s^R)$ , i.e.,

$$\Omega_{\varepsilon} = \Omega_{\varepsilon}^{NR} + \Omega_{\varepsilon}^{R} \tag{7}$$

In order to relate the results obtained by solving Eq. (6) with the solutions of Eqs. (1)-(4), we need to derive the evolution equations for the moments of the function  $f_s$ . The zeroth moment of  $f_s$ , the total number of particles of species s at time t and position x, is defined as

$$n_s(\vec{x}, t) \equiv \sum_i f_s(\vec{x}, i, t) = \sum_i f_s^{eq}(\vec{x}, i, t)$$
 (8)

For the nonreactive term,  $\Omega_s^{NR}$  we use the Bhatnagar-Gross-Krook (BGK) approximation with a single relaxation time  $\tau_s$  [30]:

$$\Omega_s^{NR} = -\frac{1}{\tau} [f_s(\vec{x}, i, t) - f_s^{eq}(\vec{x}, i, t)]$$
 (9)

where the equilibrium distribution function of the species  $f_s^{eq}(\vec{x},i,t)$  depends on  $\vec{x}$  and t through the local density and velocity. Here, we use the simple equilibrium distribution function corresponding to a system with zero mean flow as follow:

$$f_s^{eq} = w_{s,i} n_s \tag{10}$$

where the weights  $w_{s,i}$  depend on the lattice symmetry [31]. We can write

$$w_{s,i} = \begin{cases} z_s & i = 0\\ (1 - z_s)/2 & i = 1, 2, \end{cases}$$
 (11)

where  $z_s$  denotes the fraction of particles at rest and can be different for different species. For the reactive term  $\Omega_s^R$ , we use the simple isotropic form [31]

$$\Omega_s^R = w_{s,i}R_s, \tag{12}$$

where  $R_s$  is a non-linear reaction term and depends on the densities of the reacting species. Thus, it couples the Boltzmann equations for the different species. The choice given in Eq. (12) is the simplest choice that can provide the right macroscopic solution when using the LBM (as we shall see later).

To show that the lattice Boltzmann equation is valid for a reacting system, we employ a procedure called the Chapmann-Enskog expansion [17]. We first expand the left-hand side of Eq. 6 via a Taylor series:

$$f_{s}(\vec{x} + \vec{e_{i}}, i, t + 1) - f_{s}(\vec{x}, i, t),$$

$$\cong \frac{\partial f_{s}(\vec{x}, i, t)}{\partial t} + e_{i} \frac{\partial f_{s}(\vec{x}, i, t)}{\partial x} + \frac{1}{2} e_{i}^{2} \frac{\partial^{2} f_{s}(\vec{x}, i, t)}{\partial x^{2}},$$

$$= \Omega_{s}.$$
(13)

We then expand  $f_s$  about the equilibrium distribution function in terms of the parameter  $\varepsilon$ :

$$f_s \cong f_s^{eq} + \varepsilon f_s^{(1)} \tag{14}$$

We now assume [29]

$$\frac{\partial}{\partial x} \to \varepsilon \frac{\partial}{\partial x} \tag{15}$$

$$\frac{\partial}{\partial t} \to \varepsilon^2 \frac{\partial}{\partial t}$$
 (16)

$$R_s \to \varepsilon^2 R_s$$
 (17)

Substituting Eqs. (15), (16), and (17) into Eq. (13),

$$e_i \frac{\partial f_s^{eq}(\vec{x}, i, t)}{\partial x} = -\frac{f_s^{(1)}(\vec{x}, i, t)}{\tau_s}$$
 (18)

to order  $\varepsilon^1$  and

$$\frac{\partial f_s^{eq}(\vec{x}, i, t)}{\partial t} + e_i \frac{\partial f_s^{(1)}(\vec{x}, i, t)}{\partial x} + \frac{1}{2} e_i^2 \frac{\partial^2 f_s^{eq}(\vec{x}, i, t)}{\partial x^2} = w_{s,i} R_s$$
(19)

to order  $\varepsilon^2$ . From Eq. (18), we immediately obtain

$$f_s^{(1)}(\vec{x}, i, t) = -\tau_s w_{s,i} e_i \frac{\partial_s}{\partial_{\tau}}$$
 (20)

Inserting Eq. (20) to Eq. (19) and doing some simple algebra, we have, to order  $\varepsilon^2$ ,

$$\frac{\partial n_s}{\partial t} - (\tau_s - \frac{1}{2})e_i^2 \frac{\partial^2 n_s}{\partial x^2} = R_s \tag{21}$$

Eliminating the  $e_i^2$  term by carrying out an averaging with weight  $w_{s,i}$ , we get

$$\frac{\partial n_s}{\partial t} - (1 - Z_s)(\tau_s - \frac{1}{2})\frac{\partial^2 n_s}{\partial x^2} = R_s \tag{22}$$

which is the dimensionless version of the initial reaction-diffusion equation.

To summarize, we will now implement the numerical evaluation in two steps

· Collision step: 
$$\widetilde{f_s}(\vec{x},i,t+1) = f_s(\vec{x},i,t) - \frac{1}{\tau_s}[f_s - f_s^{eq}] + w_{s,i}R_s$$
 ,

Streaming step: 
$$f_s(\vec{x} + \vec{e_i}, i, t+1) = \tilde{f_s}(\vec{x}, i, t+1)$$

The boundary treatment is an important issue in the LBM simulation and advancement are still being made [32,33]. Here, we use the impermeable boundary suggested by Zhang et al. [34].

### III. NUMERICAL RESULTS AND DISCUSSION

To demonstrate the validity of the proposed LBM applied to the Howard dynamic model for determining the partition of E.~coli mediated by min proteins, we implemented the LBM as given in the previous section on a PC using C programming. In the simulation, we use the parameters given by Howard et~al. The 2-micronlong bacterium is divided into 250 grids. The discrete space steps are, therefore,  $dx=0.008~\mu\mathrm{m}$ . A time step of  $dt=6.410^{-5}$  s is chosen. The dimensionless param-

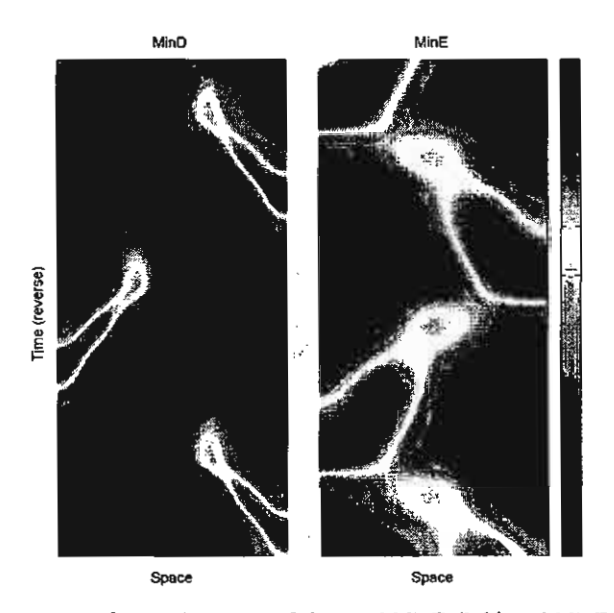


Fig. 1. Space-time plots of the total MinD (left) and MinE (right) densities. The color scale runs from the lowest (blue) to the highest (red). The MinD depletion from midcell and the MinE enhancement at midcell are immediately evident. Times increase from top to bottom, and the pattern repeats indefinitely as time increases. The vertical scale spans a time of 1000 second. The horizontal scale spans the bacteria's length (2  $\mu$ m).

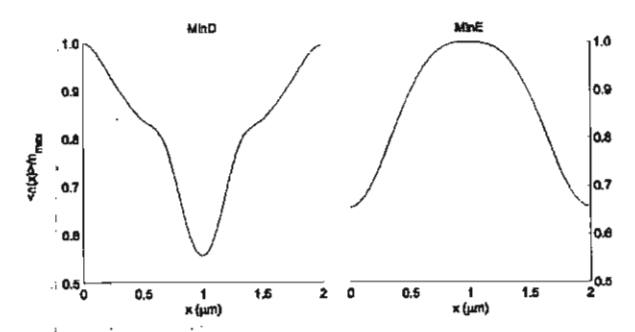


Fig. 2. Time-average MinD (left) and MinE (right) densities,  $< n(\chi) > /n_{max}$ , relative to their respective time-average maxima as functions of the position  $\chi$  (in  $\mu$ m) along the bacterium.

eters are  $D_D=0.28, D_E=0.6, D_d=D_e=0, \sigma_1=1.28\times 10^{-3}, \sigma_4=5.12\times 10^{-5}, \sigma_2=4.032\times 10^{-7}, \sigma_3=2.56\times 10^{-6}, \sigma_1=0.028,$  and  $\sigma_4=0.027.$  The relaxation time is calculated by using Eq. (22) and is given as  $\tau_s=D_s/(1-Z_s)+0.5.$  The initial number of MinD and MinE is randomly initialized as 3000 for  $n_D$  and 170 for  $n_E$ . Each simulation takes 156,250,000 iterations for  $10^4$  s of the time division of the bacterium. We test the system with two possible sets of the rest particle fraction,  $z_s=1/3$  and 2/3, for all species. We found that  $z_s=2/3$  gave the more accurate result. We now present some results to show the validity and the accuracy of our LBM and compare them with the results obtained from the deterministic reaction-diffusion equations.

In Fig. 1, the space-time plots of the MinD and the MinE concentrations for a cell of length 2  $\mu$ m are shown. They are in qualitative agreement with the simulation obtained by Howard et al. [26] and are in agreement with the experimental results. The MinE forms a line up in the middle of the cell and then sweeps towards a cell pole, displacing the MinD, which then reforms at the opposite pole. In Fig. 2, we plot the time-averaged MinD and MinE densities as functions of position. These are again in excellent agreement with those given by Howard et al. [26]. The results in both works are also in excellent agreement with the experimental data of Hale et al. [15]. The MinE concentration peaks at mid cell and has minimum at the cell rims, with MinD being virtually out of phase with MinE.

#### IV. CONCLUDING REMARKS

In this paper, we have proposed a new LBM approach to investigate the dynamic pole-to-pole oscillations of *min* proteins used to determine the middle of bacterial cell division. We have developed a numerical scheme based on the LBM to simulate the coarse-grained coupled reaction-diffusion equations model used to describe the MinD/MinE interaction. It is found that our results

are in good agreement with those given by Howard et al. The results, in particular the oscillatory pattern of min proteins, are also in qualitative agreement with experimental results [35]. The LBM approach provides an alternative fast computational tool to study protein oscillation. We believe that the LBM is a useful scheme for simulating at the cellular level those biological system governed by the reaction-diffusion equations. In a future work, we will generalize the current LBM so that it can be used to study the effects of the inhomogeniety in the intracellular space and the possibility of asymmetrical cell division.

#### ACKNOWLEDGMENTS

We thank M. Howard, J. Wong-ekkabut, and M. Chooduang for their useful comments and suggestions. This research is supported in part by the Thailand Research Fund through grant numbers TRG4580090 and RTA4580005. The IRPUS Program 2547 assistance to Charin Modjung and W. Triampo is acknowledged. The support of the Development and Promotion of Science and Technology Talents program given to W. Ngamsaad is acknowledged. And The Office of Commission for Higher Education is also acknowledged.

#### REFERENCES

- J. Lutkenhaus, Mol. Microbiol. 9, 403 (1993).
- [2] C. L. Woldringh, E. Mulder, P. G. Huls and N. Vischer, Res. Microbiol. 142, 309 (1991).
- [3] P. A. J. de Boer, R. E. Crossley and L. I. Rothfield, Cell 56, 641 (1989).
- [4] E. Mulder and C. L. Woldingh, J. Bacteriol. 171, 4303 (1989).
- [5] P. A. J. de Boer, R. E. Crossley and L. I. Rothfield, Proc. Natl. Acad. Sci. (USA) 87, 1129 (1990).
- [6] P. A. J. de Boer, R. E. Crossley, A. R. Hand and L. I. Rothfield, EMBO J. 10, 4371 (1991).
- [7] J. Huang, C. Cao and J. Lutkenhaus J. Bacteriol. 178, 5080 (1996).
- [8] Z. Hu and J. Lutkenhaus, Mol. Microbiol. 34, 82 (1999).
- [9] D. M. Raskin and P. A. J. de Boer, J. Bacteriol. 181, 6419 (1999).
- [10] X. Fu, Y-L. Shih, Y. Zhang and L. I. Rothfield, Proc. Natl. Acad. Sci. (USA) 98, 980 (2001).
- [11] D. M. Raskin and P. A. J. de Boer, Proc. Natl. Acad. Sci. (USA) 96, 4971 (1999).
- [12] S. L. Rowland, X. Fu, M. A. Sayed, Y. Zhang, W. R. Cook and L. I. Rothfield, J. Bacteriol. 182, 613 (2000).
- [13] K. C. Huang, Y. Meir and N. S. Wingreen, Proc. Natl. Acad. Sci. (USA) 100, 12724 (2003).
- [14] D. M. Raskin and P. A. J. de Boer, Cell 91 685 (1997).
- [15] C. A. Hale, H. Meinhardt and P. A. J. de Boer, EMBO J. 20, 1563 (2001).
- [16] R. Benzi, S. Succi and M. Vergassola, Phys. Rep. 222, 145 (1992).

- [17] S. Chen and G. D. Doolen, Ann. Rev. Fluid Mech. 30, 329 (1998).
- [18] Y. H. Qian, D. d'Humieres and P. A. Lallemand, Europhys. Lett. 17, 479 (1992).
- [19] H. Chen and S. Chen and W. H. Matthaeus, Phys. Rev. A 45, R5339 (1992).
- [20] N. S. Martys and H. D. Chen, Phys. Rev. E 53, 743 (1996).
- [21] G. D. Doolen, Lattice Gas Methods: Theory, Applications and Hardware, 2nd ed. (MIT, Cambridge, MA, 1991).
- [22] R. G. M. van der Sman and M. H. Ernst, J. Comput. Phys. 60, 766 (2000).
- [23] C. Migliorini, Y. H. Qian, H. Chen, E. Brown, R. Jainand and L. Munn, Biophys. J. 84, 1834 (2002).
- [24] C. H. Sun, C. Migliorini and L. Munn, Biophys. J. 85, 208 (2003).
- [25] M. Hirabayashi, M. Ohta, D. A. Rufenacht and B. Chopard, Future Gen. Comp. Sys. 20, 925 (2004).
- [26] M. Howard, A. D. Rutenberg and S. de Vet, Phys. Rev.

- Lett. 87, 278102 (2001).
- [27] G. Nicolis and I. Prigogine, Self Organization in Nonlinear Systems (Wiley, New York, 1977).
- [28] G. McNamara and G. Zanetti, Phys. Rev. Lett. 61, 2332 (1988).
- [29] S. P. Dawson, S. Chen and G. D. Doolen, J. Chem. Phys. 98, 1514 (1993).
- [30] P. L. Bhatnagar, E. P. Gross and M. Krook, Phys. Rev. 94, 511 (1954).
- [31] R. Blaak and P. M. Sloot, Comp. Phys. Comm. 129, 256 (2000).
- [32] S. Chen, D. O. Martinez and R. Mei, Phys. Fluids 8, 2527 (1996).
- [33] Q. Zou and X. He, Phys. Fluids 9, 6202 (1997).
- [34] X. Zhang, J. W. Crawford, A. G. Bengough and I. M. Young, Adv. Water Resour. 25, 601 (2002).
- [35] H. Meinhardt and P. A. J. de Boer, Proc. Natl. Acad. Sci. (USA) 98, 14202 (2001).

įį.

ij

ij

## Modeling of the Dynamic Pole-to-Pole Oscillations of the Min Proteins in Bacterial Cell Division: the Effect of an External Field

Charin Modchang, Paisan Kanthang, Wannapong Triampo,\*
Waipot Ngamsaad, Narin Nuttawut and I-Ming Tang
Department of Physics and Capability Building Unit in Nanoscience and Nanotechnology,
Faculty of Science, Mahidol University, Bangkok 10400, Thailand

Suchitra Sanguansin, Ankana Boondirek and Yongwimol Lenbury

Department of Mathematics, Faculty of Science, Mahidol University, Bangkok 10400, Thailand

(Received 18 November 2004)

One of the most important steps in the developmental process of the bacteria cells at the cellular level is the determination of the middle of the cell and the proper placement of the septum, these being essential to the division of the cell. In E. coli, this step depends on the proteins MinC, MinD, and MinE. Exposure to a constant electric field may cause the bacteria's cell-division mechanism to change, resulting in an abnormal cytokinesis. To see the effects of an external field e.g., an electric or magnetic field on this process, we have solved a set of deterministic reaction diffusion equations, which incorporate the influence of an electric field. We have found some changes in the dynamics of the oscillations of the min proteins from pole to pole. The numerical results show some interesting effects, which are qualitatively in good agreement with some experimental results.

PACS numbers: 87.15.Aa, 87.17.Aa Keywords: External fields, Bacteria, E. coli, Cell division, Min proteins, MinCDE oscillation

#### I. INTRODUCTION

Cell division is the process by which a cell separates into two new cells after its DNA has been duplicated and distributed into the two regions that will later become the future daughter cells. For a successful cell division to take place, the cell has to determine the optimal location of the cell separation and the time to start the cell cleavage. This involves the identification of the midpoint of the cell where the septum or cleavage furrow will form. For Escherichia coli (E. coli) and other rod-like bacteria, evidence has accumulated over the past few years which indicates that the separation into two daughter cells is achieved by forming a septum perpendicular to parent cell's long axis. To induce the separation, the FtsZ ring (Z ring), a tubulin-like GTPase, is believed to initiate and guide the septa growth by a process called contraction [1]. The Z ring is usually positioned close to the center, but it can also form in the vicinity of the cell poles. Two processes are known to regulate the placement of the division site: nucleoid occlusion [2] and the action of the min proteins [3]. Both processes interfere with the formation of the Z ring that determines the division site. Nucleoid occlusion is based on cytological evidence that indicates that the Z ring assembles preferentially on those portions of the membrane that do not directly surround the dense nucleoid mass [4].

The min proteins that control the placement of the division site are the MinC, the MinD, and the MinE proteins [3]. Experiments, involving the use of modified proteins show that inC is able to inhibit the formation of the FtsZ-ring [5]. MinD is an ATPase that is connected peripherally to the cytoplasmic membrane. It can bind to the MinC and activate the function of the MinC [6,7]. Recent studies show that MinD can also recruit MinC to the membrane. This suggests that MinD stimulates MinC by concentrating MinC near to its presumed site of activation [8,9]. MinE provides topological specificity to the division inhibitor [10]. Its expression results in a site-specific suppression of the MinC/MinD action so that FtsZ assembly is allowed at the middle of the cell, but is blocked at other sites [3]. In the absence of MinE, MinC/MinD is distributed homogeneously over the entire membrane. This results in a complete blockage of Z-ring formation. The long filamentous cells that are subsequently formed are not be able divide [8,9,11,12]. With fluorescent labeling, MinE was shown to attach to the cell wall only in the presence of MinD [13, 14]. As MinD dictates the location of MinC, the latter will oscillate by itself. This will result in a concentration of the division inhibitor at the membrane on either cell end, al-

<sup>\*</sup>E-mail: wtriampo@yahoo.com; Fax: 662-201-5843

ternating between being high or very low every other 20 s or so [8,9]. The presence of MinE is not only required for the MinC/MinD oscillation but also involved in setting the frequency of the oscillation cycle [11]. Several sets of evidence indicate that the MinE localization cycle is tightly coupled to the oscillation cycle of MinD.

Recent microscopy of the fluorescent labeled proteins involved in the regulation of *E. coli* division has uncovered stable and coherent oscillations (both spatial and temporal) of these three proteins [15]. The proteins oscillate from one end to the other end of the bacterium, moving between the cytoplasmic membrane and cytoplasm. The detail mechanism by which these proteins determine the correct position of the division plane is currently unknown, but the observed pole-to-pole oscillations of the corresponding distribution are thought to be of functional importance. Under different culture conditions and/or environment changes, *e.g.* pH, light, and external field, changes in the pole-to-pole oscillations can affect the growth of the bacteria. Here, we discuss only the effects of an electric field.

In the present work, we use a mathematical approach to investigate the influence of an external constant external field on cytokinesis mediated by pole-to-pole oscillations of the *min* protein. We propose a mathematical model and then solve it numerically to see how the *min* protein oscillation mechanism for bacteria cell division may change. We also present some comments about the connection between our mathematical approach and real-world experimental results.

#### II. MODEL

Sets of reaction-diffusion equations have often been used in biological applications to model self-organization and pattern formation [16]. These mathematical equations have two components. The first component is the diffusion term that describes diffusion of the chemical species. At the molecular level, the diffusion term often results in a net flow of chemical species from regions of high concentration to regions of lower concentration. The second component is the reaction term that describes the self-organization of the biological systems.

We have adopted the dynamic model of compartmentization in the bacterial cell division process proposed by Howard [17] by adding an extra term that depends on the external electric field. The dynamics of bacteria in the presence of an external field is described by a set of four non-linear coupled reaction-diffusion equations. We focus on the  $E.\ coli$  bacteria, which are commonly studied rod-shaped bacteria of approximately  $2-6\ \mu m$  in length and around  $1-1.5\ \mu m$  in diameter.  $E.\ coli$  divides roughly every hour via cytokinesis. Our starting point is the set of one dimensional deterministic coupled reaction-diffusion equations describing the dynamics of the interactions between the local concentrations of the

MinD and the MinE proteins. The equations describe the time rates of change of the concentrations due to the diffusion of the MinD and the MinE and to transfer between the cell membrane and the cytoplasm. The dynamics of these *min* proteins in the presence of an external field, are described by

$$\frac{\partial \rho_D}{\partial t} = D_D \frac{\partial^2 \rho_D}{\partial x^2} + J_D \frac{\partial \rho_D}{\partial x} - \frac{\sigma_1 \rho_D}{1 + \sigma_1' \rho_e} + \sigma_2 \rho_e \rho_d, (1)$$

$$\frac{\partial \rho_d}{\partial t} = D_d \frac{\partial^2 \rho_d}{\partial x^2} + J_d \frac{\partial \rho_d}{\partial x} - \frac{\sigma_1 \rho_D}{1 + \sigma_1' \rho_e} - \sigma_2 \rho_e \rho_d, \quad (2)$$

$$\frac{\partial \rho_E}{\partial t} = D_E \frac{\partial^2 \rho_E}{\partial x^2} + J_E \frac{\partial \rho_E}{\partial x} - \sigma_3 \rho_D \rho_E - \frac{\sigma_4 \rho_e}{1 + \sigma_4' \rho_D} (3)$$

and

$$\frac{\partial \rho_e}{\partial t} = D_e \frac{\partial^2 \rho_e}{\partial x^2} + J_e \frac{\partial \rho_e}{\partial x} + \sigma_3 \rho_D \rho_E - \frac{\sigma_4 \rho_e}{1 + \sigma_4' \rho_D} \tag{4}$$

where  $\rho_D$  and  $\rho_E$  are the concentrations of the MinD and the MinE proteins in the cytoplasm, respectively, and  $\rho_d$  and  $\rho_e$  are the concentrations of the MinD and the MinE proteins on the cytoplasmic membrane. The first equation describes the time rate of change of the concentration of MinD  $(\rho_D)$  in the cytoplasm. The second is for the change in the MinD concentration  $(\rho_d)$  on the cytoplasmic membrane. The third is for the change of the concentration of MinE  $(\rho_E)$  in the cytoplasm. The last one is for the change in the MinE concentration  $(\rho_e)$  on the cytoplasmic membrane. Since the experimental results given Ref. 9, show that the MinC dynamics simply follows that of the MinD protein, we have not written out the equations for the MinC explicitly.

The important feature of our model is the second terms on the right-hand sides of the equations. They represent the effect of the external field in the reaction-diffusion equation [18,19] controlled by the external field parameter. We assume that a chemical substance moving in the region of an external field will experience a force that is proportional to the external field parameter J times the gradient of the concentration of that substance. In general,  $J = \mu E$ , where E is the field strength and  $\mu$ is the ionic mobility of the chemical substance.  $\mu$ , in general, will be proportional to the diffusion coefficient of the chemical substance and will depend on the total amount of free charge in that substance. In this model  $J_i = \mu_i E\{i = D, E, d, e\}$  is the external field parameter for each protein types. We assume that the diffusion coefficients  $\{D_D, D_E, D_d, D_e\}$  are isotropic and independent of x. The constant  $\sigma_1$  represents the association of MinD to the membrane wall [12].  $\sigma'_1$  corresponds to the membrane-bound MinE suppressing the recruitment of MinD from the cytoplasm.  $\sigma_2$  reflects the rate that the MinE on the membrane drives the MinD on the membrane into the cytoplasm. Based on evidence for the cytoplasmic interaction between MinD and MinE [7], we let  $\sigma_3$  be the rate that cytoplasmic MinD recruits cytoplasmic MinE to the membrane and  $\sigma_4$  be the rate of dissociation of MinE from the membrane to the cytoplasm. Finally,  $\sigma_4'$  corresponds to the cytoplasmic MinD suppressing the release of the membrane-bound MinE. Evidence points to most of the diffusion process occurring in the cytoplasm. It is, therefore, reasonable to set  $D_d$  and  $D_e$  to zero. It follows immediately that  $\mu_d = \mu_e = 0$  and  $J_d = J_e = 0$ 

In our model, we assume that the total number of each type of protein is conserved. We further assume that the *min* proteins can bind/unbind from the membrane and that the proteins do not degrade during the process. The zero-flux boundary conditions are imposed at both ends of the bacterium. The total amounts of MinD and MinE, obtained by integrating  $\rho_D + \rho_d$  and  $\rho_E + \rho_e$  over the length of the bacterium, are conserved.

## III. NUMERICAL RESULTS AND DISCUSSION

Since the bacterium length is very short, it is reasonable to assume that the applied electric field has a constant value throughout the bacterium length. We have numerically solved the set of four coupled reactiondiffusion equations, Eqs. (1)-(4), by using the explicit Euler method [20]. The length of the E. coli is taken to be 2  $\mu m$ . The total time needed for each simulation is approximately 104 s. In our simulations, we have discretized space and time; i.e., we have taken  $dx = 8 \times 10^{-3} \ \mu \text{m}$  and  $dt = 1 \times 10^{-5} \ \text{s}$ . The space covering the bacterium is divided into 251 grid points, and the time is divided into 109 times steps (109 iteration steps). Initially, we assume that MinD and MinE are mainly at the opposite ends of the bacterium with the number of min molecules in each cell being 3000 for the MinD population [6] and 170 for the MinE population [21]. Since the total amount of MinD and MinE in E. coli must be conserved, we set the flux of MinD and MinE to zero at both ends of the bacterium. Since there are no experimental values of  $\mu$  for either MinD and MinE, we work with the external field parameter J, which is proportional to E, instead of E explicitly. We also assume that  $\mu_D = \mu_E$  (we assume MinD and MinE have the same type of charges). It follows immediately that  $J_D=J_E\equiv J$ . The values of the other parameters are:  $D_D = 0.28 \ \mu\text{m}^2\text{s}^{-1}$ ,  $D_E = 0.6 \ \mu\text{m}^2\text{s}^{-1}$ ,  $\sigma_1 = 20 \ \text{s}^{-1}$ ,  $\sigma_1 = 0.028 \ \mu\text{m}$ ,  $\sigma_2 = 0.0063 \ \mu\text{m}^{-1}$ ,  $\sigma_3 = 0.04 \ \mu\text{m}^{-1}$ ,  $\sigma_4 = 0.8 \ \text{s}^{-1}$ , and  $\sigma_4 = 0.027 \ \mu\text{m}$ . In our analyses of the numerical results, we looked at the time-averaged values of the concentrations of MinD and MinE and at the patterns of the oscillations of MinD and MinE for various Jvalues.

In the absent of an external field, the numerical results [17] show that most of the MinD will be concentrated at the membrane and the MinE at mid cell. This results in

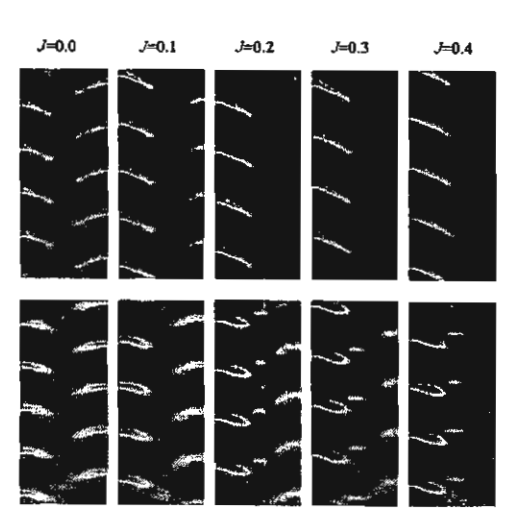


Fig. 1. Space-time plots of the total  $(\sigma_D + \sigma_d)$  MinD (above) and total  $(\sigma_E + \sigma_e)$  MinE (below) concentration for J=0.0 m/s to J=0.4 m/s. The color scale, running from blue to red, denotes an increase in the concentration from the lowest to the highest. The MinD depletion from mid cell and the MinE enhancement at the mid cell are immediately seen. The vertical scale spans time for 500 s. The times increase from bottom to top, and the oscillations pattern repeats infinitely as time increases. The horizontal scale spans the bacterial length  $(2~\mu m)$ . Note the increase in the MinD and MinE concentrations at the left end of the bacterium as J increases.

an accurate division at mid cell. In the presence of an external field, both MinD and MinE experience a force in the same direction. This force causes a shift of the time-averaged minimum of MinD. This shifts the division site from mid cell. Our numerical solutions show that the behavior of the Min system in the presence of an external field depends on the strength of the external field parameter J.

Figure 1 shows the oscillation patterns for  $J_E = J_D \equiv J = 0.0$  m/s to J = 0.4 m/s. It is seen that as J increase, both the MinD and the MinE concentrations in the left part of the E. coli become larger while the two concentrations in the right part become smaller as J is increased. This behavior is a reflection of the fact that the external force is acting in the left direction. These patterns show a shifting in the concentrations of the min proteins towards the left pole.

In Figure 2, we show the time-averaged concentrations of the MinD and the MinE proteins at different positions within the bacteria. In these curves, positive values of the external field parameter are used. From this Figure, we see that in the case of no external field ( $J=0.0~\rm m/s$ ), the time-averaged concentrations of MinD and MinE are symmetric about mid cell. MinD has a minimum at mid cell while MinE has a maximum. When an external field is applied, we see a shift in the minima of MinD and in the maxima of MinE. The time-averaged concentration

Journal of the Korean Physical Society, Vol. 46, No. 4, April 2005

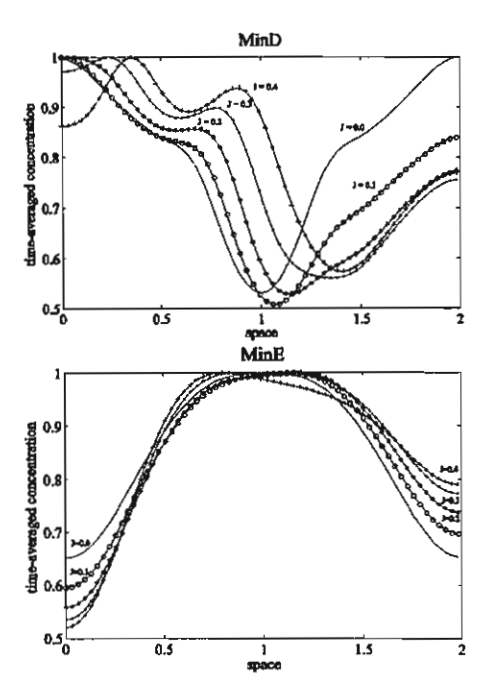


Fig. 2. Time-averaged concentration of MinD (above) and MinE (below) relative to their respective time-averaged maxima,  $\langle \sigma(x) \rangle / \sigma_{max}$ , as a function of the position x (in  $\mu$ m) along the bacterium axis under the influence of positive values of a static external field. The curves show a shift in the local minima of the MinD and the local maxima of the MinE from the mid cell that depends on the strength of the field.

curves are no longer symmetric about mid cell. In nature, the MinE protein looks like a ring structure that effectively positions the anti-MinCD activity [11,14]. MinCD inhibits the division process, so in nature, the bacterium divides at the site where the minimum MinD concentration occurs. The value of the MinE concentration is not maximum at the mid cell. The minimum of the MinD shifts to the right pole under the influence of positive J values.

We have measured the percent of shifting of the timeaveraged concentration in the local minima of MinD and the local maxima of MinE. This is shown in Fig. 3. The figure shows that the minimum of MinD is always shifted to the right pole. This is the result of the external force pulling MinD to the left. The maximum of MinE is not always shifted to the right. When J < 0.2 m/s, the maximum of MinE is shifted to the right, but when J > 0.2 m/s, it shifted to the left of mid cell. This difference arises because of the relative magnitudes of the forces acting on the two proteins. First of all, there is an internal force between the MinD and the MinE proteins. This force causes MinE to repel MinD. In the absence of any other forces, this explains why the location of the maximum of MinE is the location of the minimum of MinD. When an external field is applied (as expressed by a non-zero value of J), then one must take into account

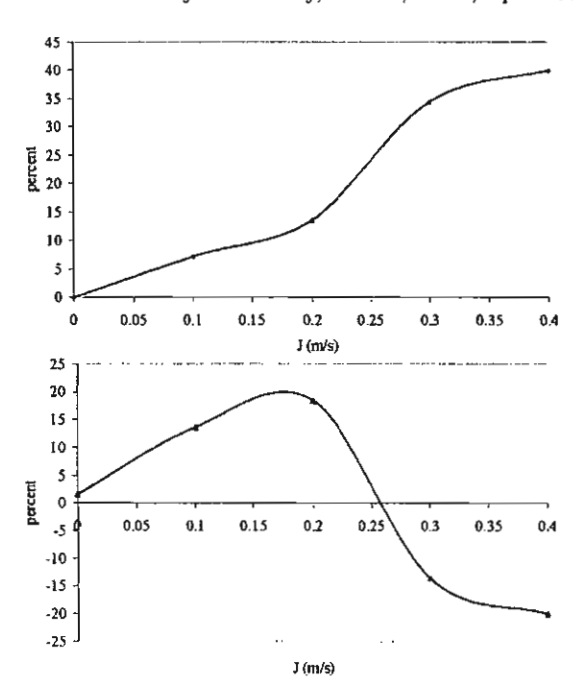


Fig. 3. Percents of the shifting of the local minima of MinD (above) and the local maxima of MinE (below) from mid cell for various values of J. Positive values denote a shift to the right pole and a negative value to the left pole.

the relative magnitudes of the two forces.

When J is large (larger than 2 m/s), the external force dominates the internal force between the MinD and the MinE proteins. The external force pulls MinD and MinE in the same direction, causing the location of the maximum of MinE to be no longer at the location of the minimum of MinD. If J is small (smaller than 0.2 m/s), the internal force between MinD and MinE dominates. This results in the two location (the maximum of MinE and the minimum of MinD) to be nearly the same. In Fig. 3, we also see that the shifts of the minimum of the MinD concentrations increase as the field parameter J increases. Since the division site will be the location where the MinD concentration is minimum, the shift in the minimum of MinD concentration to the right pole indicates that the division site must also shift to the right pole. When we let J be negative, the results are very similar to those for positive J values, as expected; the curves for the time averages of the concentrations of the min proteins shift in the mirror side about mid cell.

In Figs. 4(a) and 4(b), we show the concentrations of the MinD and the MinE proteins at the left end grid, the middle grid, and the right end grid versus time. In these figures, it is easy to see that when J = 0.0 m/s, the concentrations of MinD (or MinE) at the left end grid and the right end grid have the same patterns of oscillation with the same frequencies and amplitudes, but with a phase difference of 180°. At the mid cell grid, the frequency of the oscillation is two times greater than that

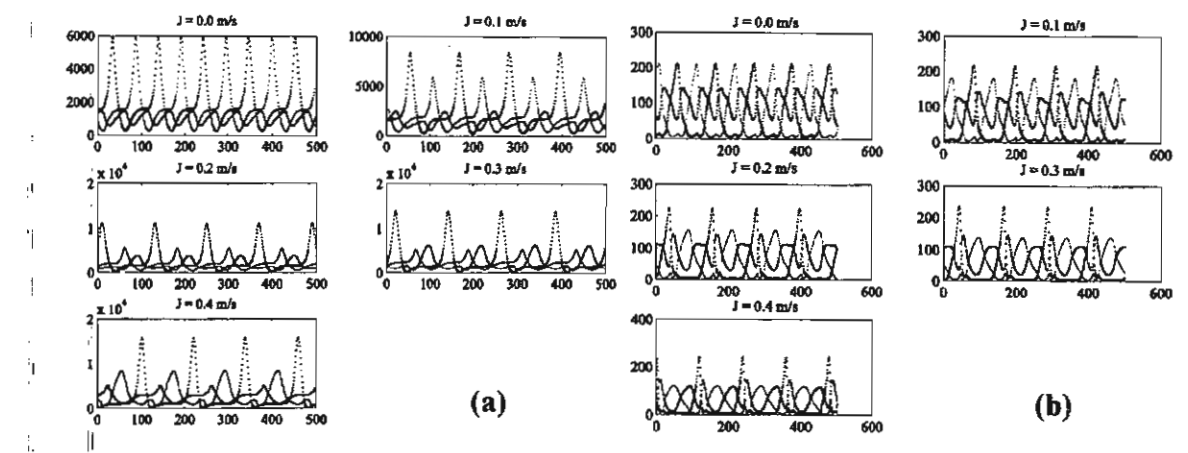


Fig. 4. (a) Plots of the concentration of MinD at the the left end grid (+), the middle grid (x), and the right end grid (·) versus time in seconds for J=0.0 m/s to J=0.4 m/s. The vertical scales denote concentration in molecules per meter. (b) Plots of the concentration of MinE at the left end grid (+), the middle grid (x), and the right end grid (·) as functions of time in seconds for J=0.0 m/s to J=0.4 m/s. The vertical scales denote concentration in molecules per meter.

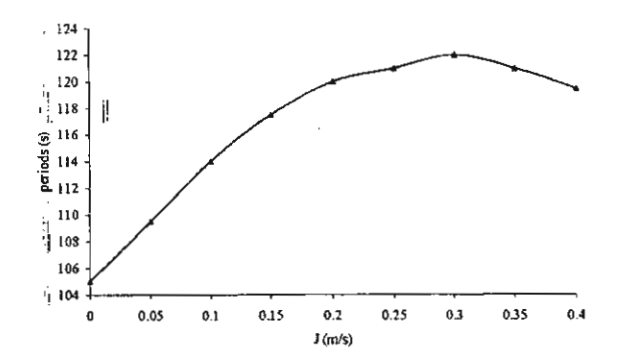


Fig. 5. Plots of the concentration of MinE at the left end grid (+), the middle grid (x), and the right end grid (·) as functions of time in seconds for J = 0.0 m/s to J = 0.4 m/s. The vertical scales denote concentration in molecules per meter.

of right end grid. When an external field is applied, the amplitudes of the oscillations at the two end grids are no longer equal, but the frequencies of the oscillations of the three grids become the same. As J is increased, the amplitude of the oscillation at the right end grid is seen to decrease while those of the left end and mid cell grids are seen to increase.

Figure 5 show the periods of oscillation for the MinD concentration at the left end grid for various value of J. In this figure, we see that for the case of no external field, the period of the oscillation is equal to 115 s, which is in good agreement with the experimental value. When an external field is applied, the period of the oscillation is seen to increase. When J is not too large (J < 0.3), the period of the oscillation increases as J is increased. The increase in the period of oscillation as an external field is applied indicates that in the presence of an external

field, the bacterium needs a longer time to divide.

#### IV. CONCLUDING REMARKS

Proper divisions of bacteria require accurate definition of the division site [3]. This accurate identification of the division site is determined by the rapid pole-to-pole oscillations of MinCDE [8,11,22]. Using a mathematical model to describe the dynamics of the *min* pole-to-pole oscillations, Howard *et al.* [17] found that the mid cell position in the *Escherichia coli* bacteria corresponded to the point where the time-averaged MinD and MinE concentrations were minimum and maximum, respectively. They also found that the concentrations of these two proteins were symmetric about the mid cell position.

To see the effect of exposing E. coli bacteria to an electric field, we have added some additional terms to the reaction-diffusion equations for the pole-to-pole oscillations proposed by Howard et al for the min proteins in the E. coli bacteria. The additional terms are the gradient terms appearing in Eqs.(1)-(4). These terms depend on the strength of the external field and the charge of the protein. We then used a numerical scheme to solve the resulting coarse-grained coupled reaction-diffusion equations. The results are shown in Figs. 1 to 5. Our results shows deviations from the results obtained by Howard et al., e.g.: the concentrations of MinD and MinE are no longer symmetric about the middle of the long axis, nor are the minimum and the maximum of the MinD and the MinE concentrations at the middle of the long axis. The shift in the minimum of the time-averaged concentration of MinD from mid cell should shift the division site. The shift of the minimum concentration of MinD from the midpoint appears to depend on the strength of the external field. This indicates that if the parent cell can divide under these condition, it must divide into two filamentous cells, providing the external field is strong enough. Since an external field can shift the minimum of the time-averaged concentration of MinD, an external electric field can interfere with the division process.

#### ACKNOWLEDGMENTS

We thank M. Howard, J. Wong-ekkabut, and M. Chooduang for their useful comments and suggestions. This research is supported in part by the Thailand Research Fund through grant numbers TRG4580090 and RTA4580005, and the Commission on Higher Education. The support of the Industrial and Research Projects for Undergraduate Students Program 2547 given to Charin Modchang and W. Triampo is acknowledged, as is the support of the Development and Promotion of Science and Technology Talents program given to Waipot Ngamsaad.

#### REFERENCES

- [1] J. Lutkenhaus, Mol. Microbiol. 9, 403 (1993).
- [2] C. L. Woldringh, E. Mulder, P. G. Huls and N. Vischer, Res. Microbiol. 142, 309 (1991).
- [3] P. A. J. de Boer, R. E. Crossley and L. I. Rothfield, Cell. 156, 4303 (1989).
- [4] E. Mulder and C. L. J. Woldingh, Bacteriol. 171, 4303 (1989).
- [5] P. A. J. de Boer, R. E. Crossley and L. I. Rothfield, Proc. Natl. Acad. Sci. USA 87, 1129 (1990).

- [6] P. A. J. de Boer, R. E. Crossley, A. R. Hand and L. I. Rothfield, EMBO J. 10, 4371 (1991).
- [7] J. Huang, C. Cao and J. Lutkenhaus, J. Bacteriol. 178, 5080 (1996).
- [8] Z. Hu and J. Lutkenhaus, J. Mol. Microbiol. 34, 82 (1999).
- [9] D. M. Raskin and P. A. J. de Boer, J. Bacteriol. 181, 6419 (1999).
- [10] X. Fu, Y-L. Shih, Y. Zhang and L. I. Rothfield, Proc. Natl. Acad. Sci. USA 98, 980 (2001).
- [11] D. M. Raskin and P. A. J. de Boer, Proc. Natl. Acad. Sci. USA 96, 4971 (1999).
- [12] S. L. Rowland, X. Fu, M. A. Sayed, Y. Zhang, W. R. Cook and L. I. Rothfield, J. Bacteriol. 182, 613 (2000).
- [13] K. C. Huang, Y. Meir and N. S. Wingreen, Proc. Natl. Acad. Sci. USA 100, 12724 (2003).
- [14] D. M. Raskin and P. A. J. de Boer, Cell. 91, 685 (1997).
- [15] C. A. Hale, H. Meinhardt and P. A. J. de Boer, EMBO J. 20, 1563 (2001).
- [16] G. Nicolis and I. Prigogine, Self Organization in Nonlinear Systems (Wiley, New York, 1977).
- [17] M. Howard, A. D. Rutenberg and S. de Vet, Phys. Rev. Lett. 87, 278102 (2001).
- [18] E. P. Zemskov, V. S. Zykov, K. Kassner and S. C. Müller, Physica D. 183, 117 (2003).
- [19] A. P. Munuzuri, V. A. Davydov, V. Perez-Munuzuri, M. Gomez-Gesteira and V. Perez-Villar, Chaos, Solitons & Fractals 7, 585 (1995).
- [20] W. H. Press, S. A. Teukolsky, W. T. Vetterling and B. P. Flannery Numerical Recipes in C++: The Art of Scientific Computing (Cambridge University Press, 2002).
- [21] C-R. Zhao, P. A. J. de Boer and L. I. Rothfield, Proc. Natl. Acad. Sci. USA. 92, 4313 (1995).
- [22] H. Meinhardt and P. A. J. de Boer, Proc. Natl. Acad. Sci. USA 98, 14202 (2001).

## A NOTE ON ASYMPTOTIC STABILITY CONDITIONS FOR DELAY DIFFERENCE EQUATIONS

T. KAEWONG, Y. LENBURY, AND P. NIAMSUP

Received 26 May 2004 and in revised form 27 February 2005

We obtain necessary and sufficient conditions for the asymptotic stability of the linear delay difference equation  $x_{n+1} + p \sum_{j=1}^{N} x_{n-k+(j-1)l} = 0$ , where n = 0, 1, 2, ..., p is a real number, and k, l, and N are positive integers such that k > (N-1)l.

#### 1. Introduction

In [4], the asymptotic stability condition of the linear delay difference equation

$$x_{n+1} - x_n + p \sum_{j=1}^{N} x_{n-k+(j-1)l} = 0,$$
 (1.1)

where  $n \in \mathbb{N}_0 = \mathbb{N} \cup \{0\}$ , p is a real number, and k, l, and N are positive integers with k > (N-1)l is given as follows.

THEOREM 1.1. Let k, l, and N be positive integers with k > (N-1)l. Then the zero solution of (1.1) is asymptotically stable if and only if

$$0 
(1.2)$$

where M = 2k + 1 - (N - 1)l.

Theorem 1.1 generalizes asymptotic stability conditions given in [1, page 87], [2, 3, 5], and [6, page 65]. In this paper, we are interested in the situation when (1.1) does not depend on  $x_n$ , namely we are interested in the asymptotic stability of the linear delay difference equation of the form

$$x_{n+1} + p \sum_{j=1}^{N} x_{n-k+(j-1)l} = 0, (1.3)$$

where  $n \in \mathbb{N}_0 = \mathbb{N} \cup \{0\}$ , p is a real number, and k, l, and N are positive integers with  $k \ge (N-1)l$ . Our main theorem is the following.

Copyright © 2005 Hindawi Publishing Corporation International Journal of Mathematics and Mathematical Sciences 2005:7 (2005) 1007–1013 DOI: 10.1155/IJMMS.2005.1007

#### 1008 A note on asymptotic stability conditions

THEOREM 1.2. Let k, l, and N be positive integers with  $k \ge (N-1)l$ . Then the zero solution of (1.3) is asymptotically stable if and only if

$$-\frac{1}{N}$$

where  $p_{min}$  is the smallest positive real value of p for which the characteristic equation of (1.3) has a root on the unit circle.

#### 2. Proof of theorem

The characteristic equation of (1.3) is given by

$$F(z) = z^{k+1} + p(z^{(N-1)l} + \dots + z^{l} + 1) = 0.$$
 (2.1)

For p = 0, F(z) has exactly one root at 0 of multiplicity k + 1. We first consider the location of the roots of (2.1) as p varies. Throughout the paper, we denote the unit circle by C and let M = 2k + 2 - (N - 1)l.

Proposition 2.1. Let z be a root of (2.1) which lies on C. Then the roots z and p are of the form

$$z = e^{w_{m}i}, (2.2)$$

$$p = (-1)^{m+1} \frac{\sin(lw_m/2)}{\sin(Nlw_m/2)} \equiv p_m \tag{2.3}$$

for some m = 0, 1, ..., M - 1, where  $w_m = (2m/M)\pi$ . Conversely, if p is given by (2.3), then  $z = e^{w_m i}$  is a root of (2.1).

Proof. Note that z=1 is a root of (2.1) if and only if p=-1/N, which agrees with (2.2) and (2.3) for  $w_m=0$ . We now consider the roots of (2.1) which lie on C except the root z=1. Suppose that the value z satisfies  $z^{Nl}=1$  and  $z^l\neq 1$ . Then  $z^{Nl}-1=(z^l-1)(z^{(N-1)l}+\cdots+z^l+1)=0$  which gives  $z^{(N-1)l}+\cdots+z^l+1=0$ , and hence z is not a root of (2.1). As a result, to determine the roots of (2.1) which lie on C, it suffices to consider only the value z such that  $z^{Nl}\neq 1$  or  $z^l=1$ . For these values of z, we may write (2.1) as

$$p = -\frac{z^{k+1}}{z^{(N-1)l} + \dots + z^l + 1}. (2.4)$$

Since p is real, we have

$$p = -\frac{\overline{z}^{k+1}}{\overline{z}^{(N-1)l} + \dots + \overline{z}^l + 1} = -\frac{z^{-k-1+(N-1)l}}{z^{(N-1)l} + \dots + z^l + 1},$$
 (2.5)

where  $\overline{z}$  denotes the conjugate of z. It follows from (2.4) and (2.5) that

$$z^{2k+2-(N-1)l} = 1 (2.6)$$

which implies that (2.2) is valid for m = 0, 1, ..., M - 1 except for those integers m such that  $e^{Nlw_m i} = 1$  and  $e^{lw_m i} \neq 1$ . We now show that p is of the form stated in (2.3). There are two cases to be considered as follows.

Case 1. z is of the form  $e^{w_m i}$  for some m = 1, 2, ..., M - 1 and  $z^{Nl} \neq 1$ . From (2.4), we have

$$p = -\frac{z^{k+1}(z^{l}-1)}{z^{Nl}-1} = -\frac{e^{(k+1)w_{m}i}(e^{lw_{m}i}-1)}{e^{Nlw_{m}i}-1}$$

$$= -\frac{e^{(k+1-(N-1)(l/2))w_{m}i}(e^{lw_{m}i/2}-e^{-lw_{m}i/2})}{e^{Nlw_{m}i/2}-e^{-Nlw_{m}i/2}}$$

$$= -e^{(k+1-(N-1)(l/2))w_{m}i}\frac{\sin(lw_{m}/2)}{\sin(Nlw_{m}/2)}$$

$$= -e^{m\pi i}\frac{\sin(lw_{m}/2)}{\sin(Nlw_{m}/2)} = (-1)^{m+1}\frac{\sin(lw_{m}/2)}{\sin(Nlw_{m}/2)} \equiv p_{m}.$$
(2.7)

Case 2. z is of the form  $e^{w_m i}$  for some m = 1, 2, ..., M - 1 and  $z^l = 1$ .

In this case, we have  $lw_m = 2q\pi$  for some positive integer q. Then taking the limit of  $p_m$  as  $lw_m \to 2q\pi$ , we obtain

$$p = -\frac{(-1)^{m+q(N-1)}}{N}. (2.8)$$

From these two cases, we conclude that p is of the form in (2.3) for m = 1, 2, ..., M - 1 except for those m such that  $e^{Nlw_m i} = 1$  and  $e^{lw_m i} \neq 1$ .

Conversely, if p is given by (2.3), then it is obvious that  $z = e^{w_m t}$  is a root of (2.1). This completes the proof of the proposition.

From Proposition 2.1, we may consider p as a holomorphic function of z in a neighborhood of each  $z_m$ . In other words, in a neighborhood of each  $z_m$ , we may consider p as a holomorphic function of z given by

$$p(z) = -\frac{z^{k+1}}{z^{(N-1)l} + \dots + z^l + 1}.$$
 (2.9)

Then we have

$$\frac{dp(z)}{dz} = -\frac{(k+1)z^k}{z^{(N-1)l} + \dots + z^l + 1} + \frac{z^k \{(N-1)lz^{(N-1)l} + \dots + lz^l\}}{\left(z^{(N-1)l} + \dots + z^l + 1\right)^2}.$$
 (2.10)

From this, we have the following lemma.

LEMMA 2.2.  $dp/dz|_{z=e^{mmi}} \neq 0$ . In particular, the roots of (2.1) which lie on C are simple.

*Proof.* Suppose on the contrary that  $dp/dz|_{z=e^{w_{mi}}}=0$ . We divide (2.10) by p(z)/z to obtain

$$k+1-\frac{l\{(N-1)z^{(N-1)l}+\cdots+z^l\}}{z^{(N-1)l}+\cdots+z^l+1}=0.$$
 (2.11)

Substituting z by  $1/\overline{z}$  in (2.10), we obtain

$$k+1-\frac{l\{(N-1)+(N-2)z^l+\cdots+z^{(N-2)l}\}}{z^{(N-1)l}+\cdots+z^l+1}=0.$$
 (2.12)

#### 1010 A note on asymptotic stability conditions

By adding (2.11) and (2.12), we obtain

$$2k + 2 - (N - 1)l = 0 (2.13)$$

which contradicts  $k \ge (N-1)l$ . This completes the proof.

From Lemma 2.2, there exists a neighborhood of  $z = e^{w_{m}i}$  such that the mapping p(z) is one to one and the inverse of p(z) exists locally. Now, let z be expressed as  $z = re^{i\theta}$ . Then we have

$$\frac{dz}{dp} = \frac{z}{r} \left\{ \frac{dr}{dp} + ir \frac{d\theta}{dp} \right\}$$
 (2.14)

which implies that

$$\frac{dr}{dp} = \text{Re}\left\{\frac{r}{z}\frac{dz}{dp}\right\} \tag{2.15}$$

as p varies and remains real. The following result describes the behavior of the roots of (2.1) as p varies.

PROPOSITION 2.3. The moduli of the roots of (2.1) at  $z = e^{w_m i}$  increase as |p| increases.

*Proof.* Let r be the modulus of z. Let  $z = e^{w_m i}$  be a root of (2.1) on C. To prove this proposition, it suffices to show that

$$\left. \frac{dr}{dp} \cdot p \right|_{z=e^{i\nu_{in}i}} > 0. \tag{2.16}$$

There are two cases to be considered.

Case 1  $(z^{NI} \neq 1)$ . In this case, we have

$$p(z) = -\frac{z^{k+1}(z^{l}-1)}{z^{Nl}-1} = -\frac{z^{k}f(z)}{z^{Nl}-1},$$
(2.17)

where  $f(z) = z(z^l - 1)$ . Then

$$\frac{dp}{dz} = -\frac{z^{k-1}g(z)}{(z^{NI}-1)^2},\tag{2.18}$$

where  $g(z) = (kf(z) + zf'(z))(z^{Nl} - 1) - Nlz^{Nl}f(z)$ . Letting  $w(z) = -(z^{Nl} - 1)^2/(z^kg(z))$ , we obtain

$$\frac{dr}{dp} = \operatorname{Re}\left(\frac{r}{z}\frac{dz}{dp}\right) = r\operatorname{Re}(w). \tag{2.19}$$

We now compute Re(w). We note that

$$f(\overline{z}) = -\frac{f(z)}{z^{l+2}}, \qquad f'(\overline{z}) = \frac{h(z)}{z^l},$$
 (2.20)

T. Kaewong et al. 1011

where  $h(z) = l + 1 - z^{l}$ . From the above equalities and as  $z^{M} = 1$ , we have

$$\overline{z}^{k}g(\overline{z}) = \frac{1}{z^{k}} \left\{ \left( kf(\overline{z}) + \frac{1}{z}f'(\overline{z}) \right) \left( \frac{1}{z^{Nl}} - 1 \right) - \frac{Nl}{z^{Nl}} f(\overline{z}) \right\} 
= \frac{\left( - kf(z) + zh(z) \right) \left( 1 - z^{Nl} \right) + Nlf(z)}{z^{Nl+l+2+k}} 
= \frac{\left( - kf(z) + zh(z) \right) \left( 1 - z^{Nl} \right) + Nlf(z)}{z^{2Nl-k}}.$$
(2.21)

It follows that

$$Re(w) = \frac{w + \overline{w}}{2}$$

$$= -\frac{1}{2} \left\{ \frac{(z^{Nl} - 1)^{2}}{z^{k} g(z)} + \frac{(\overline{z}^{Nl} - 1)^{2}}{\overline{z}^{k} g(\overline{z})} \right\}$$

$$= -\frac{1}{2} \left\{ \frac{\overline{z}^{k} g(\overline{z}) (z^{Nl} - 1)^{2} + z^{k} g(z) (\overline{z}^{Nl} - 1)^{2}}{|g(z)|^{2}} \right\}$$

$$= -\frac{1}{2 |g(z)|^{2}} \left\{ \frac{(-kf(z) + zh(z)) (1 - z^{Nl}) + Nlf(z)}{z^{2Nl - k}} \cdot (z^{Nl - 1})^{2} + z^{k} ((kf(z) + zf'(z)) (z^{Nl} - 1) - Nlz^{Nl} f(z)) (\frac{1}{z^{Nl}} - 1)^{2} \right\}$$

$$= -\frac{(z^{Nl} - 1)^{2} z^{k}}{2z^{2Nl} |g(z)|^{2}} \left\{ (kf(z) - zh(z)) (z^{Nl} - 1) + Nlf(z) + ((kf(z) + zf'(z)) (z^{Nl} - 1)) - Nlz^{Nl} f(z) \right\}$$

$$= -\frac{(z^{Nl} - 1)^{3} z^{k}}{2z^{2Nl} |g(z)|^{2}} \left\{ 2kf(z) + z(f'(z) - h(z)) - Nlf(z) \right\}. \tag{2.22}$$

Since

$$2kf(z) + z(f'(z) - h(z)) - Nlf(z) = Mf(z),$$
 (2.23)

we obtain

$$\operatorname{Re}(w) = \frac{(z^{Nl} - 1)^4 M}{2z^{2Nl} |g(z)|^2} \cdot \frac{-z^k f(z)}{z^{Nl} - 1} = \frac{(z^{Nl} - 1)^4 M p}{2z^{2Nl} |g(z)|^2}.$$
 (2.24)

The value of Re(w) at  $z = e^{iv_m i}$  is

$$Re(w) = \frac{(z^{Nl} - 1)^4}{z^{2Nl}} \cdot \frac{Mp}{2|g(z)|^2} = (2\cos Nlw_m - 2)^2 \cdot \frac{Mp}{2|g(z)|^2} > 0.$$
 (2.25)

#### 1012 A note on asymptotic stability conditions

Therefore,

$$\frac{dr}{dp} = \frac{2r(\cos Nlw_m - 1)^2 Mp}{|g(z)|^2}$$
 (2.26)

and it follows that (2.16) holds at  $z = e^{w_m i}$ .

Case 2 ( $z^l = 1$ ). With an argument similar to Case 1, we obtain

$$\frac{dr}{dp} = \frac{2rN^2Mp}{\left| (M+1)z - M + 1 \right|^2}$$
 (2.27)

which implies that (2.16) is valid for  $z = e^{i v_m i}$ .

This completes the proof.

We now determine the minimum of the absolute values of  $p_m$  given by (2.3). We have the following result.

PROPOSITION 2.4.  $|p_0| = \min\{|p_m| : m = 0, 1, ..., M-1\}$ .

To prove Proposition 2.4, we need the following lemma, which was proved in [4].

LEMMA 2.5. Let N be a positive integer, then

$$\left|\frac{\sin Nt}{\sin t}\right| \le N \tag{2.28}$$

holds for all  $t \in \mathbb{R}$ .

Proof of Proposition 2.4. From (2.3),  $p_m = (-1)^{m+1} (\sin(lw_m/2)/\sin(Nlw_m/2))$ . For m = 0, it follows from L'Hospital's rule that  $p_0 = -1/N$ . For m = 1, 2, ..., M-1, we have

$$|p_m| = \left| (-1)^{m+1} \frac{\sin(lw_m/2)}{\sin(Nlw_m/2)} \right| \ge \frac{1}{N}$$
 (2.29)

by Lemma 2.5. This completes the proof.

We are now ready to prove Theorem 1.2.

Proof of Theorem 1.2. Note that  $F(1) = 1 + Np \le 0$  if and only if  $p \le -1/N$ . Since  $\lim_{z \to +\infty} F(z) = +\infty$ , it follows that (2.1) has a positive root  $\alpha$  such that  $\alpha > 1$  when  $p \le -1/N$ . We claim that if |p| is sufficiently small, then all the roots of (2.1) are inside the unit disk. To this end, we note that when p = 0, (2.1) has exactly one root at 0 of multiplicity k + 1. By the continuity of the roots with respect to p, this implies that our claim is true. By Proposition 2.4,  $p_0 = -1/N$  and  $|p_m| \ge 1/N$  which implies that  $|p_0| = 1/N$  is the smallest positive value of p such that a root of (2.1) intersects the unit circle as |p| increases. Moreover, Proposition 2.3 implies that if  $p > p_{\min}$ , then there exists a root  $\alpha$  of (2.1) such that  $|\alpha| \ge 1$ , where  $p_{\min}$  is the smallest positive real value of p for which (2.1) has a root on C. We conclude that all the roots of (2.1) are inside the unit disk if and only if -1/N . In other words, the zero solution of <math>(1.3) is asymptotically stable if and only if condition (1.4) holds. This completes the proof.

### 3. Examples

Example 3.1. In (1.3), Let l and k be even positive integers, then we have

$$F(-1) = -1 + pN. (3.1)$$

Thus if p = 1/N, then F(-1) = 0 and we conclude that (1.3) is asymptotically stable if and only if -1/N .

Example 3.2. In (1.3), let N=3, l=3, and k=6. Then M=8 and we obtain  $p_0=-1/3$ ,  $p_1=\sin(3/8)\pi/\sin(9/8)\pi$ ,  $p_2=-\sin(3/4)\pi/\sin(9/4)\pi$ ,  $p_3=\sin(9/8)\pi/\sin(27/8)\pi$ ,  $p_4=-\sin(3/2)\pi/\sin(9/2)\pi$ ,  $p_5=\sin(15/8)\pi/\sin(45/8)\pi$ ,  $p_6=-\sin(9/4)\pi/\sin(27/4)\pi$ , and  $p_7=\sin(21/8)\pi/\sin(63/8)\pi$ . Thus,  $p_3=p_5=\sin(\pi/8)/\sin(3\pi/8)$  is the smallest positive real value of p such that (2.1) has a root on  $p_7=\sin(21/8)\pi/\sin(21/8)\pi$ . Thus,  $p_8=\pi/\sin(21/8)\pi/\sin(21/8)\pi$ .

### 4. Acknowledgments

This research is supported by the Thailand Research Fund Grant no. RTA458005 and RSA4780012. We would like to thank the referees for their valuable comments.

### References

٥

- [1] Y. Kuang, Delay Differential Equations with Applications in Population Dynamics, Mathematics in Science and Engineering, vol. 191, Academic Press, Massachusetts, 1993.
- [2] S. A. Kuruklis, The asymptotic stability of  $x_{n+1} ax_n + bx_{n-k} = 0$ , J. Math. Anal. Appl. 188 (1994), no. 3, 719–731.
- [3] S. A. Levin and R. M. May, A note on difference-delay equations, Theoret. Population Biology 9 (1976), no. 2, 178-187.
- [4] R. Ogita, H. Matsunaga, and T. Hara, Asymptotic stability condition for a class of linear delay difference equations of higher order, J. Math. Anal. Appl. 248 (2000), no. 1, 83–96.
- [5] V. G. Papanicolaou, On the asymptotic stability of a class of linear difference equations, Math. Mag. 69 (1996), no. 1, 34-43.
- [6] G. Stépán, Retarded Dynamical Systems: Stability and Characteristic Functions, Pitman Research Notes in Mathematics Series, vol. 210, Longman Scientific & Technical, Harlow, 1989.

T. Kaewong: Department of Mathematics, Faculty of Science, Chiang Mai University, Chiang Mai 50200, Thailand

E-mail address: theeradach@tsu.ac.th

Y. Lenbury: Department of Mathematics, Faculty of Science, Mahidol University, 272 Rama 6 Road, Bangkok 10400, Thailand

E-mail address: scylb@mahidol.ac.th

P. Niamsup: Department of Mathematics, Faculty of Science, Chiang Mai University, Chiang Mai 50200, Thailand

E-mail address: scipnmsp@chiangmai.ac.th

### ARTICLE IN PRESS



Available online at www.sciencedirect.com

APPLIED
MATHEMATICS
AND
COMPLITATION

ELSEVIER Applied Mathematics and Computation xxx (2005) xxx-xxx

www.elsevier.com/locate/amc

### Controllability and stability of the perturbed Chen chaotic dynamical system

Tidarut Plienpanich <sup>a</sup>, Piyapong Niamsup <sup>a,\*</sup>, Yongwimon Lenbury <sup>b</sup>

<sup>a</sup> Department of Mathematics, Faculty of Science, Chiang Mai University, Chiang Mai 50200, Thailand

### Abstract

In this paper, we study perturbed Chen chaotic dynamical system. Firstly, we study the sufficient conditions of parameters which guarantee that the equilibrium points of perturbed Chen chaotic dynamical system are asymptotically stable. Secondly, we study methods for controlling chaos such as feedback control and bounded feedback control that suppress the chaotic behavior to unstable equilibrium points. Finally, we present chaos synchronization of perturbed Chen chaotic dynamical system by using active control and adaptive control.

© 2005 Elsevier Inc. All rights reserved.

Keywords: Perturbed Chen chaotic dynamical system; Controlling chaos; Synchronization

0096-3003/\$ - see front matter © 2005 Elsevier Inc. All rights reserved. doi:10.1016/j.amc.2005.01.099

<sup>&</sup>lt;sup>b</sup> Department of Mathematics, Faculty of Science, Mahidol University, Bangkok 10400, Thailand

<sup>\*</sup> Corresponding author.

E-mail addresses: noynoy!111@hotmail.com (T. Plienpanich), piyapongniamsup@hotmail.com, seipnmsp@chiangmai.ac.th (P. Niamsup), scylb@mahidol.ac.th (Y. Lenbury).

### ARTICLE IN PRESS

T. Plienpanich et al. | Appl. Math. Comput. xxx (2005) xxx-xxx

### 1. Introduction

In the recent years, controlling chaos and synchronization of the dynamical systems have attracted many researchers. Controlling chaos and chaos synchronization have focused on the nonlinear systems such as Chen chaotic dynamical system. Various control algorithms have been proposed to control chaotic systems. The existing control algorithms can be classified mainly into two categories: feedback and nonfeedback. In this paper, we only focus on feedback control. Linear feedback control and bounded feedback control are proposed to control chaos of the system to the equilibrium points.

In [4], Yassen's studied the optimal control of Chen chaotic dynamical system presented by

$$\dot{x} = a(y - x),$$

$$\dot{y} = (c - a)x - xz + cy,$$

$$\dot{z} = xy - bz$$

where x, y, z are state variables and a, b, c are real positive constants.

In [1], Agiza's studied the different methods to control chaotic behavior of the coupled dynamos system, where the mathematical model equations for this system are

$$\dot{x} = \mu x + y(z + \alpha),$$
  

$$\dot{y} = \mu y + x(z - \alpha),$$
  

$$\dot{z} = 1 - xy,$$

where x, y, z are state variables and  $\mu$ ,  $\alpha$  are positive constants.

In [2], Agiza and Yassen's studied synchronization of Rossler and Chen chaotic dynamical systems using active control.

In [3], Wang, Guan and Wen's paper studied adaptive synchronization for Chen chaotic system with fully unknown parameters.

The objectives of this paper are as follows. Firstly, to give sufficient conditions of parameters that make equilibrium points of perturbed Chen chaotic dynamical system to be asymptotically stable. Secondly, to apply linear feedback control and bounded feedback control for controlling chaos of the perturbed Chen chaotic dynamical system, described by

$$\dot{x} = a(y - x), 
\dot{y} = (c - a)x - xz + cy, 
\dot{z} = xy - bz + dx^2,$$
(1.1)

where x, y, z are the state variables and a, b, c, d are positive real constants.

3

### 2. Stability of the perturbed Chen chaotic dynamical system

We will study the perturbed Chen chaotic dynamical system that is described by system of ordinary differential equations (1.1).

The equilibrium points of the system (1.1) are

$$E_1 = (0, 0, 0), \quad E_2 = (\beta, \beta, \gamma), \quad E_3 = (-\beta, -\beta, \gamma),$$

where 
$$\beta = \sqrt{\frac{b\gamma}{1+d}}$$
 and  $\gamma = 2c - a$ .

**Proposition 2.1.** The equilibrium point  $E_1 = (0,0,0)$  is

- (i) asymptotically stable if a > 2c and  $ac < b^2 < 2ac$ .
- (ii) unstable if 2c > a.

**Proof.** The Jacobian matrix of the system (1.1) at the equilibrium point  $E_1 = (0,0,0)$  is given by

$$J_1 = \begin{bmatrix} -a & a & 0 \\ c - a & c & 0 \\ 0 & 0 & -b \end{bmatrix}.$$

The characteristic equation of the Jacobian  $J_1$  has the form

$$\lambda^3 + a_1\lambda^2 + a_2\lambda + a_3 = 0,$$

where

$$a_1 = a + b - c,$$

$$a_2 = b(a-c) + a(a-2c),$$

$$a_3 = ab(a - 2c),$$

$$a_1a_2 - a_3 = (ab + a^2)(a - 2c) + a(b^2 - ac) + c(2ac - b^2) + bc^2$$
.

We see that  $a_1$  and  $a_1a_2 - a_3$  satisfy the Routh-Hurwitz criteria when a > 2c and  $ac < b^2 < 2ac$ , thus the equilibrium point  $E_1 = (0,0,0)$  is asymptotically stable.  $\square$ 

**Proposition 2.2.** The equilibrium point  $E_2 = (\beta, \beta, \gamma)$  is

- (i) asymptotically stable if  $\frac{3}{2}c < a < 2c$ , b > 6c and  $\frac{1}{3} < d < 1$ .
- (ii) unstable if b < c < a and  $a < \frac{4}{3}c$ .

**Proposition 2.3.** The equilibrium point  $E_3 = (-\beta, -\beta, \gamma)$  is

- (i) asymptotically stable if  $\frac{3}{2}c < a < 2c$ , b > 6c and  $\frac{1}{3} < d < 1$ .
- (ii) unstable if b < c < a and  $a < \frac{4}{3}c$ .

### 3. Controlling chaos

In this section, the chaos of system (1.1) is controlled to one of three equilibrium points of the system. Feedback and bounded feedback control are applied to achieve this goal. We shall study in the case when equilibrium points of (1.1) are unstable. For this purpose, we assume that b < c < a and  $a < \frac{4}{3}c$ .

### 3.1. Feedback control

The goal of linear feedback control is to control the chaotic behavior of the system (1.1) to one of three unstable equilibrium points  $(E_1, E_2 \text{ or } E_3)$ . We assume that the controlled system is given by

$$\dot{x} = a(y - x) + u_1,$$
  
 $\dot{y} = (c - a)x - xz + cy + u_2,$   
 $\dot{z} = xy - bz + dx^2 + u_3,$ 

where  $u_1$ ,  $u_2$  and  $u_3$  are controllers that satisfy the following control law

$$\dot{x} = a(y - x) - k_{11}(x - \bar{x}), 
\dot{y} = (c - a)x - xz + cy - k_{22}(y - \bar{y}), 
\dot{z} = xy - bz + dx^2 - k_{33}(z - \bar{z}),$$
(3.1)

where  $E = (\bar{x}, \bar{y}, \bar{z})$  is an equilibrium point of (1.1).

3.1.1. Stability of the equilibrium point  $E_I = (0,0,0)$ 

In this case  $E = E_1$  and the controlled system (3.1) is in the form of

$$\dot{x} = a(y - x) - k_{11}x, 
\dot{y} = (c - a)x - xz + cy - k_{22}y, 
\dot{z} = xy - bz + dx^2 - k_{33}z.$$
(3.2)

**Theorem 3.1.1.** The equilibrium point  $E_1 = (0,0,0)$  is asymptotically stable if  $k_{11} = 0$ ,  $k_{33} > 0$  and  $k_{22} > 3c$ .

3.1.2. Stability of the equilibrium point  $E_2 = (\beta, \beta, \gamma)$ 

In this case  $E = E_2$  and the controlled system (3.1) is in the form of

$$\dot{x} = a(y - x) - k_{11}(x - \beta), 
\dot{y} = (c - a)x - xz + cy - k_{22}(y - \beta), 
\dot{z} = xy - bz + dx^2 - k_{33}(z - \gamma).$$
(3.3)

**Theorem 3.1.2.** The equilibrium point  $E_2 = (\beta, \beta, \gamma)$  is asymptotically stable if  $k_{11}$ ,  $k_{33} > 0$  and  $k_{22} > 2c$ .

3.1.3. Stability of the equilibrium point  $E_3 = (-\beta, -\beta, \gamma)$ 

In this case  $E = E_3$  and the controlled system (3.1) is in the form of

$$\dot{x} = a(y - x) - k_{11}(x + \beta), 
\dot{y} = (c - a)x - xz + cy - k_{22}(y + \beta), 
\dot{z} = xy - bz + dx^2 - k_{33}(z - \gamma).$$
(3.4)

**Theorem 3.1.3.** The equilibrium point  $E_3 = (-\beta, -\beta, \gamma)$  is asymptotically stable if  $k_{11}$ ,  $k_{33} > 0$  and  $k_{22} > 2c$ .

### 3.1.4. Numerical simulation

Numerical experiments are carried out to investigate controlled systems by using fourth-order Runge-Kutta method with time step 0.001. The parameters a, b, c and d are chosen as a = 35, b = 3, c = 28 and d = 2 to ensure the existence of chaos in the absence of control. The initial states are taken as x = 0.1, y = 0.2 and z = 0.3. The control is active at t = 10. The equilibrium point  $E_1 = (0,0,0)$  of the system (1.1) is stabilized for  $k_{11} = 0$ ,  $k_{22} = 85$  and  $k_{33} = 5$ . Fig. 1 show the behavior of the states x, y and z of the controlled system (3.2) with time. The equilibrium point  $E_2 = (\sqrt{21}, \sqrt{21}, 21)$  of the system (1.1) is stabilized for  $k_{11} = 1$ ,  $k_{22} = 60$  and  $k_{33} = 5$ . Fig. 2 show the behavior of the states x, y and z of the controlled system (3.3) with time. The equilibrium point  $E_3 = (-\sqrt{21}, -\sqrt{21}, 21)$  of the system (1.1) is stabilized for  $k_{11} = 1$ ,  $k_{22} = 60$  and  $k_{33} = 5$ . Fig. 3 shows the behavior of the states x, y and z of the controlled system (3.4) with time.

### 3.2. Bounded feedback control

In this case, we control chaos with bounded controller that vanishes after the stabilization is achieved. T. Plienpanich et al. | Appl. Math. Comput. xxx (2005) xxx-xxx

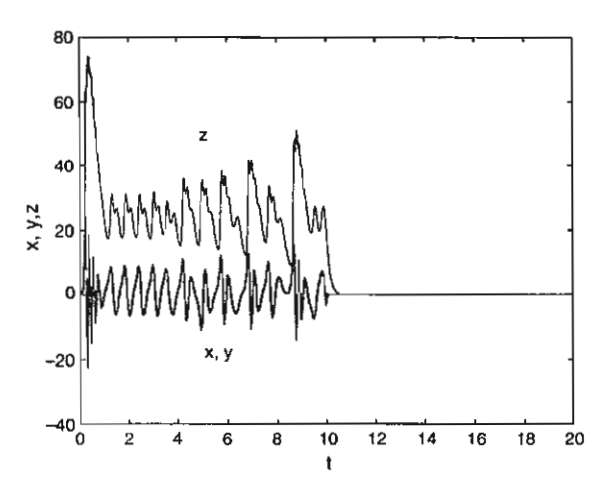


Fig. 1. The time responses for the states x, y and z of the controlled system (3.2) before and after control activation with time. The control is activated at t = 10,  $k_{11} = 0$ ,  $k_{22} = 85$  and  $k_{33} = 5$ .

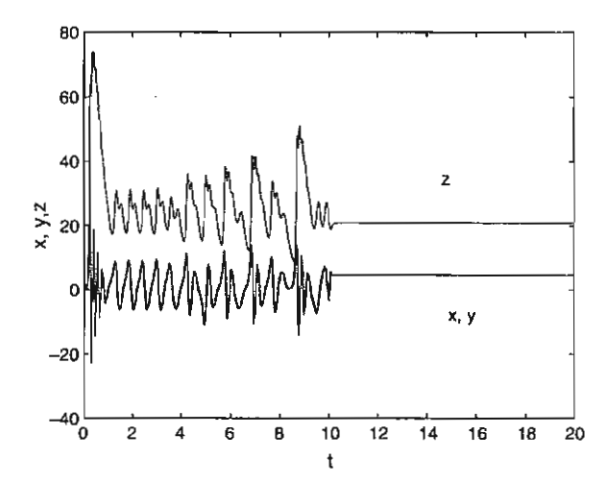


Fig. 2. The time responses for the states x, y and z of the controlled system (3.3) before and after control activation with time. The control is activated at t = 10,  $k_{11} = 1$ ,  $k_{22} = 60$  and  $k_{33} = 5$ .

### 3.2.1. Stability of the equilibrium point $E_1 = (0,0,0)$

In order to stabilize this equilibrium point by bounded feedback control, the control is chosen for system (1.1) as follows:

T. Plienpanich et al. 1 Appl. Math. Comput. xxx (2005) xxx-xxx

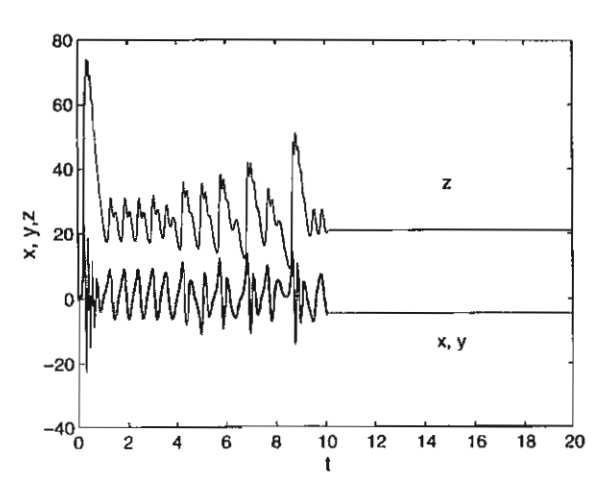


Fig. 3. The time responses for the states x, y and z of the controlled system (3.4) before and after control activation with time. The control is activated at t = 10,  $k_{11} = 1$ ,  $k_{22} = 60$  and  $k_{33} = 5$ .

$$\dot{x} = a(y - x),$$
  
 $\dot{y} = (c - a)x - xz + cy + u(t),$   
 $\dot{z} = xy - bz + dx^2,$ 
(3.5)

where u(t) = -k(a(x + y)), k > 0.

**Theorem 3.2.1.** The equilibrium point  $E_1 = (0,0,0)$  is asymptotically stable if  $k > \frac{2c}{a}$ .

### 3.2.2. Stability of the equilibrium point $E_2 = (\beta, \beta, \gamma)$

In order to stabilize this equilibrium point by bounded feedback control, the control is chosen for system (1.1) as follows:

$$\dot{x} = a(y - x),$$
  
 $\dot{y} = (c - a)x - xz + cy + u(t),$   
 $\dot{z} = xy - bz + dx^{2},$ 
(3.6)

where u(t) = -k(a(y - x)), k > 0.

**Theorem 3.2.2.** The equilibrium point  $E_2 = (\beta, \beta, \gamma)$  is asymptotically stable if  $k > \sqrt{2}$ .

\_

T. Plienpanich et al. | Appl. Math. Comput. xxx (2005) xxx-xxx

### 3.2.3. Stability of the equilibrium point $E_3 = (-\beta, -\beta, \gamma)$

In order to stabilize this equilibrium point by bounded feedback control, the control is chosen for system (1.1) as follows:

$$\dot{x} = a(y - x),$$
  
 $\dot{y} = (c - a)x - xz + cy + u(t),$   
 $\dot{z} = xy - bz + dx^2,$ 
(3.7)

where u(t) = -k(a(y - x)), k > 0.

**Theorem 3.2.3.** The equilibrium point  $E_3 = (-\beta, -\beta, \gamma)$  is asymptotically stable if  $k > \sqrt{2}$ .

### 3.2.4. Numerical simulation

We will show a series of numerical experiments by using the fourth-order Runge-Kutta method with step size 0.001. The parameters a, b, c and d are chosen as a = 35, b = 3, c = 28 and d = 2 to ensure the existence of chaos in the absence of control. The control is active at t = 10 for all simulations. In the first numerical experiment, we intend to control the chaos to equilibrium point  $E_1 = (0,0,0)$  of system (1.1). Figs. 4-6 show the time response of the states x, y and z of system (3.5) and the controller u(t) with time for k = 1.6. The initial condition are x = 0.1, y = 0.2 and z = 0.3. In the second numerical experiment, we intend to control the chaos to equilibrium point

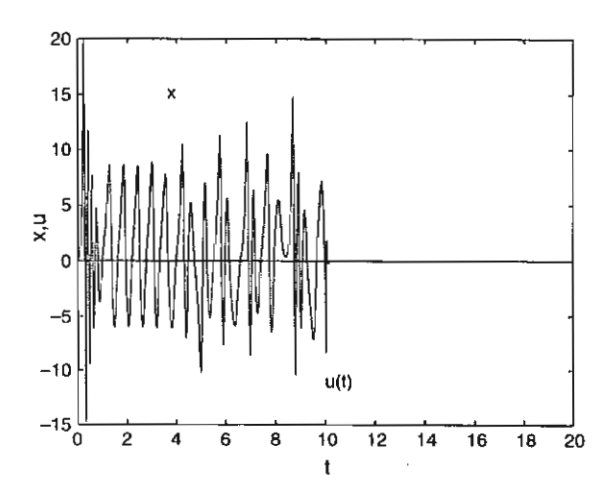


Fig. 4. The states x of the controlled system (3.5) and the control u(t) respond with time before and after control activation. The control is activated at t = 10, k = 1.6.

T. Plienpanich et al. | Appl. Math. Comput. xxx (2005) xxx-xxx

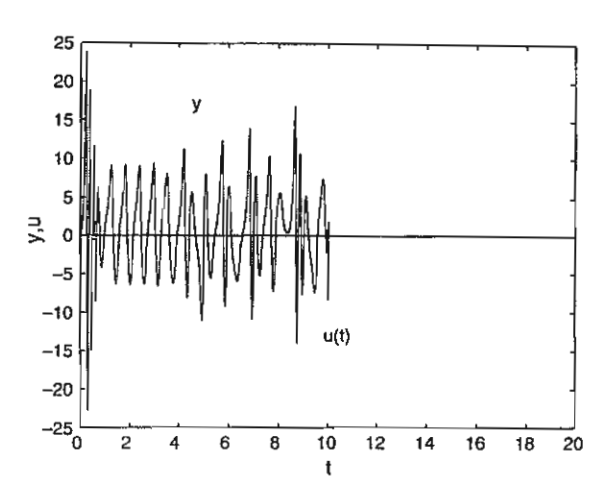


Fig. 5. The states y of the controlled system (3.5) and the control u(t) respond with time before and after control activation. The control is activated at t = 10, k = 1.6.

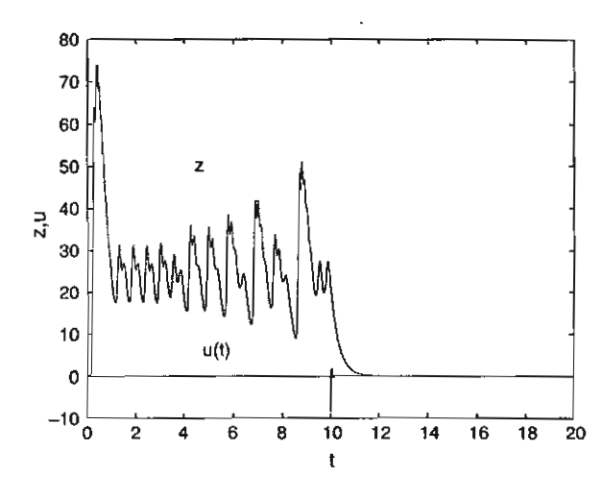


Fig. 6. The states z of the controlled system (3.5) and the control u(t) respond with time before and after control activation. The control is activated at t = 10, k = 1.6.

 $E_2 = (\sqrt{21}, \sqrt{21}, 21)$  of system (1.1). Figs. 7-9 show the time response of the states x, y and z of system (3.6) and the controller u(t) with time for k = 2. The initial condition are x = -2.5, y = -2.5 and z = 3. In the third numerical experiment, we intend to control the chaos to equilibrium point  $E_3 = (-\sqrt{21}, -\sqrt{21}, 21)$  of system (1.1). Fig. 10-12 show the time response of the states x, y and z of system (3.7) and the controller u(t) with time for k = 2. The initial condition are x = 2.5, y = 2.5 and z = 3.

T. Plienpanich et al. I Appl. Math. Comput. xxx (2005) xxx-xxx

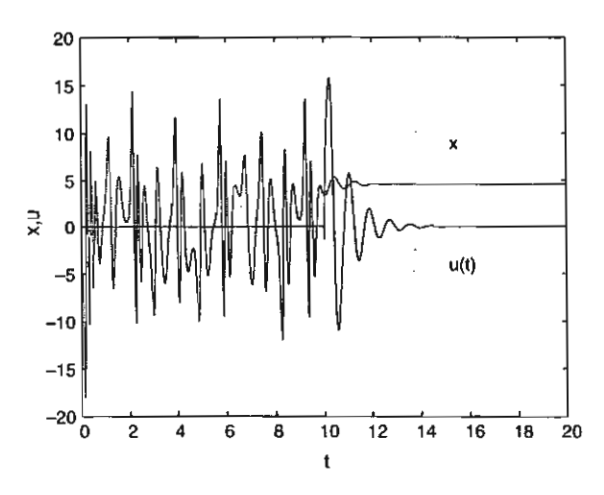


Fig. 7. The states x of the controlled system (3.6) and the control u(t) respond with time before and after control activation. The control is activated at t = 10, k = 2.

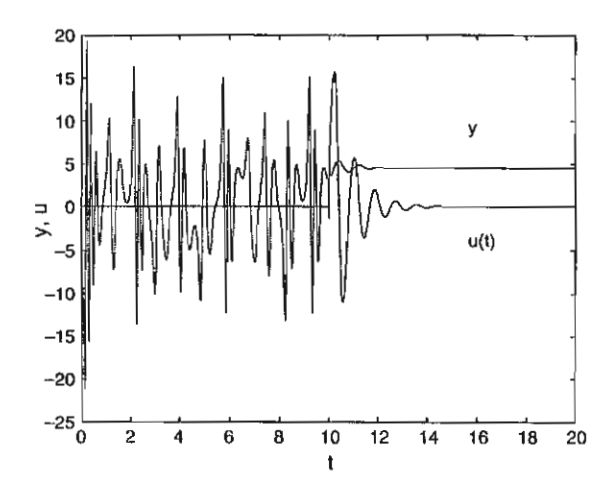


Fig. 8. The states y of the controlled system (3.6) and the control u(t) respond with time before and after control activation. The control is activated at t = 10, k = 2.

### 4. Synchronization

10

To begin with, the definition of chaos synchronization is given as follows. For two nonlinear chaotic system:

$$\dot{x} = f(t, x),\tag{4.1}$$

11

### T. Plienpanich et al. / Appl. Math. Comput. xxx (2005) xxx-xxx

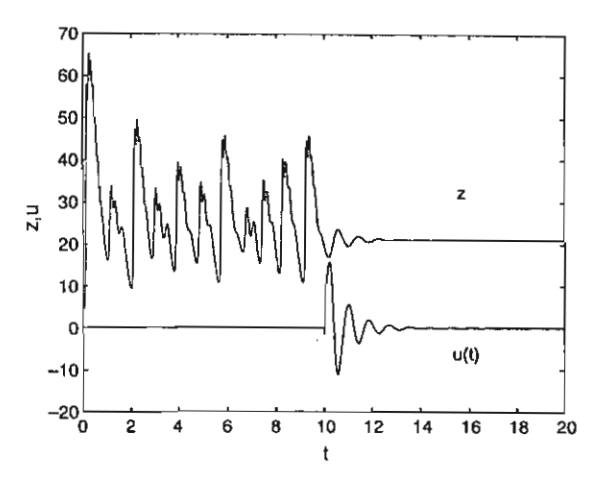


Fig. 9. The states z of the controlled system (3.6) and the control u(t) respond with time before and after control activation. The control is activated at t = 10, k = 2.

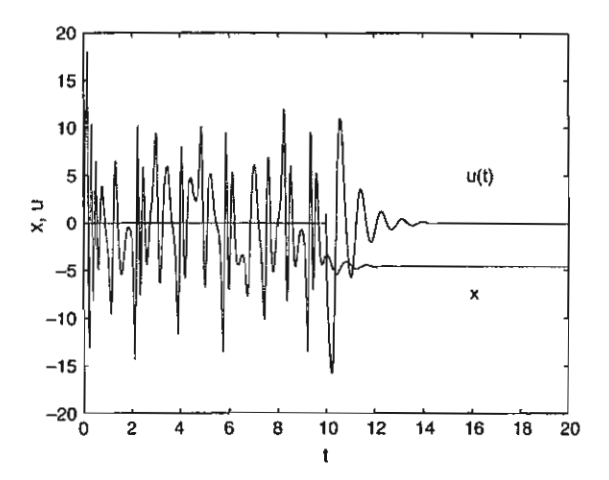


Fig. 10. The states x of the controlled system (3.7) and the control u(t) respond with time before and after control activation. The control is activated at t = 10, k = 2.

$$\dot{y} = g(t, y) + u(t, x, y),$$
 (4.2)

where  $x, y \in \mathbb{R}^n$ ,  $f, g \in C^r[\mathbb{R}^+ \times \mathbb{R}^n, \mathbb{R}^n]$ ,  $u \in C^r[\mathbb{R}^+ \times \mathbb{R}^n \times \mathbb{R}^n, \mathbb{R}^n]$ ,  $r \ge 1$ ,  $\mathbb{R}^+$  is the set of non-negative real numbers. Assume that (4.1) is the drive system, and (4.2) is the response system, u(t, x, y) is the control vector. Response system and drive system are said to be *synchronic* if for  $\forall x(t_0), y(t_0) \in \mathbb{R}^n$ ,

$$\lim_{t\to\infty}||x(t)-y(t)||=0.$$

### T. Plienpanich et al. / Appl. Math. Comput. xxx (2005) xxx-xxx

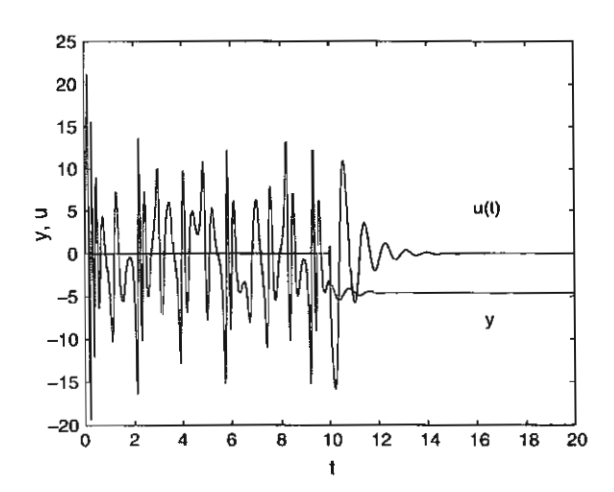


Fig. 11. The states y of the controlled system (3.7) and the control u(t) respond with time before and after control activation. The control is activated at t = 10, k = 2.

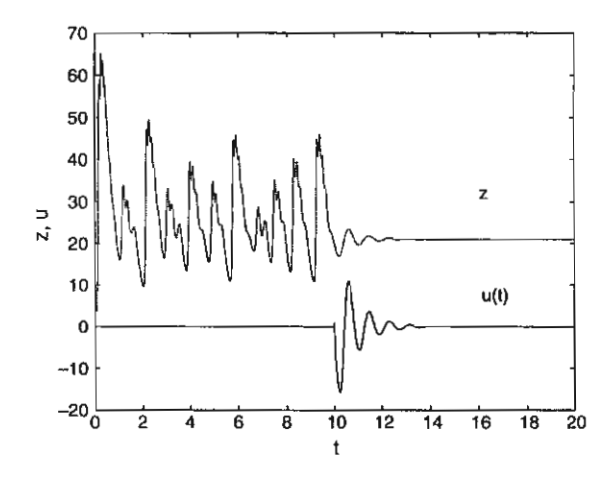


Fig. 12. The states z of the controlled system (3.7) and the control u(t) respond with time before and after control activation. The control is activated at t = 10, k = 2.

### 4.1. Active control

12

In this section, we will give some particular active control which ensures synchronization of drive system and response system of perturbed Chen chaotic dynamical system. System (1.1) has chaotic behavior at the parameters values

T. Plienpanich et al. / Appl. Math. Comput. xxx (2005) xxx-xxx 13

a = 35, b = 3, c = 28 and d = 2. Our aim is to make synchronization of system (1.1) by using active control. The drive system is defined as follows,

$$\dot{x}_1 = a(y_1 - x_1), 
\dot{y}_1 = (c - a)x_1 - x_1z_1 + cy_1, 
\dot{z}_1 = x_1y_1 - bz_1 + dx_1^2$$
(4.3)

and the response system is given by

$$\dot{x}_2 = a(y_2 - x_2) + \mu_1(t), 
\dot{y}_2 = (c - a)x_2 - x_2z_2 + cy_2 + \mu_2(t), 
\dot{z}_2 = x_2y_2 - bz_2 + dx_2^2 + \mu_3(t).$$
(4.4)

We have introduced three control functions  $\mu_1(t)$ ,  $\mu_2(t)$  and  $\mu_3(t)$  in (4.4). These functions are to be determined. Let the error states be

$$x_3 = x_2 - x_1,$$
  
 $y_3 = y_2 - y_1,$   
 $z_3 = z_2 - z_1.$ 

Using this notation, we obtain the error system.

$$\dot{x}_3 = a(y_3 - x_3) + \mu_1(t), 
\dot{y}_3 = (c - a)x_3 + cy_3 - x_2z_2 + x_1z_1 + \mu_2(t), 
\dot{z}_3 = -bz_3 - x_1y_1 + x_2y_2 + dx_2^2 - dx_1^2 + \mu_3(t).$$
(4.5)

We define the active control functions  $\mu_1(t)$ ,  $\mu_2(t)$  and  $\mu_3(t)$  as

$$\mu_{1}(t) = V_{1}(t),$$

$$\mu_{2}(t) = x_{2}z_{2} - x_{1}z_{1} + V_{2}(t),$$

$$\mu_{3}(t) = x_{1}y_{1} - x_{2}y_{2} - dx_{2}^{2} + dx_{1}^{2} + V_{3}(t).$$
(4.6)

Hence

$$\dot{x}_3 = a(y_3 - x_3) + V_1(t), 
\dot{y}_3 = (c - a)x_3 + cy_3 + V_2(t), 
\dot{z}_3 = -bz_3 + V_3(t).$$
(4.7)

The control inputs  $V_1(t)$ ,  $V_2(t)$  and  $V_3(t)$  are functions of  $x_3$ ,  $y_3$  and  $z_3$  and are chosen as

$$\begin{bmatrix} V_1(t) \\ V_2(t) \\ V_3(t) \end{bmatrix} = A \begin{bmatrix} x_3 \\ y_3 \\ z_3 \end{bmatrix}, \tag{4.8}$$

T. Plienpanich et al. / Appl. Math. Comput. xxx (2005) xxx-xxx

where the matrix A is given by

$$A = \begin{bmatrix} a-1 & -a & 0 \\ a-c & -(1+c) & 0 \\ 0 & 0 & b-1 \end{bmatrix}.$$

With this particular choice of A, (4.7) has eigenvalues which are found to be -1, -1 and -1. The choice will lead to the error states  $x_3$ ,  $y_3$  and  $z_3$  converge to zero as time t tends to infinity and this implies that the synchronization of perturbed Chen system is achieved.

### 4.1.1. Numerical simulation

Fourth-order Runge-Kutta method of differential equations (4.3) and (4.4) with time step size 0.001 are used in all numerical simulations.

The parameters are selected in (4.3) as follow: a = 35, b = 3, c = 28 and d = 2 to ensure the chaotic behavior of perturbed Chen system. The initial value of the drive system are  $x_1(0) = 0.5$ ,  $y_1(0) = 1$  and  $z_1(0) = 1$  and the initial value of the response system are  $x_2(0) = 10.5$ ,  $y_2(0) = 1$  and  $z_2(0) = 38$ . Then the initial value of the error system are  $x_3(0) = 10$ ,  $y_3(0) = 0$  and  $z_3(0) = 37$ .

Figs. 13–15 show the synchronization is occurred after applying active control at t = 5.

### 4.2. Adaptive control

This section considers adaptive synchronization of perturbed Chen system. This approach can synchronize the chaotic systems with fully unmatched

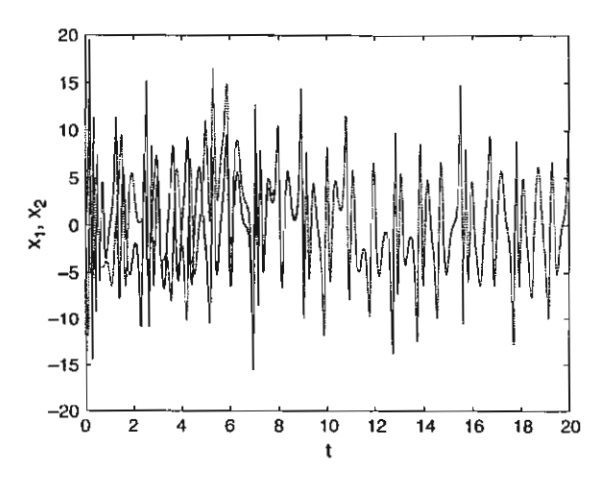


Fig. 13. The states  $x_1$ ,  $x_2$  of the coupled perturbed Chen system of equations with the active control activated.

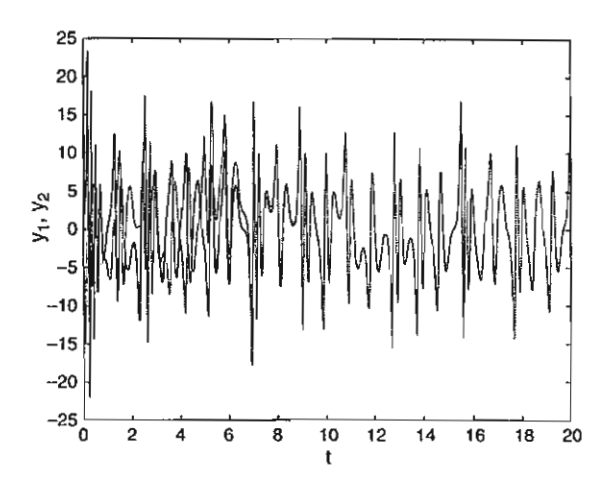


Fig. 14. The states  $y_1$ ,  $y_2$  of the coupled perturbed Chen system of equations with the active control activated.

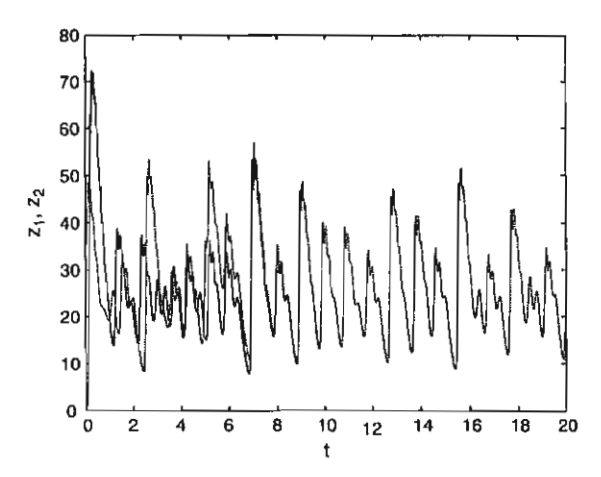


Fig. 15. The states  $z_1$ ,  $z_2$  of the coupled perturbed Chen system of equations with the active control activated.

parameters. The synchronization problem of perturbed Chen systems with fully unknown parameters will be studied in which the adaptive controller will be introduced.

Let system (1.1) be the drive system. Suppose that the parameters of the system (1.1) are unknown or uncertain, then the response system is given by

16 T. Plienpanich et al. | Appl. Math. Comput. xxx (2005) xxx-xxx

$$\dot{\tilde{x}} = \hat{a}(\tilde{y} - \tilde{x}) - u_1, 
\dot{\tilde{y}} = (\hat{c} - \hat{a})\tilde{x} - \tilde{x}\tilde{z} + \hat{c}\tilde{y} - u_2, 
\dot{\tilde{z}} = \tilde{x}\tilde{y} - \hat{b}\tilde{z} + \hat{d}\tilde{x}^2 - u_3,$$
(4.9)

where  $\hat{a}, \hat{b}, \hat{c}$  and  $\hat{d}$  are parameters of the response system which need to be estimated. Suppose that

$$u_1 = k_1 e_x,$$
  
 $u_2 = k_2 e_y,$   
 $u_3 = k_3 e_z + d\bar{x} e_x,$ 

$$(4.10)$$

where  $e_x = \bar{x} - x$ ,  $e_y = \tilde{y} - y$  and  $e_z = \tilde{z} - z$  and

$$\dot{\hat{a}} = f_a = -\gamma(\bar{y} - \bar{x})\rho e_x + \gamma \bar{x} e_y, 
\dot{\hat{b}} = f_b = \theta \tilde{z} e_z, 
\dot{\hat{c}} = f_c = -\beta(\bar{x} + \bar{y})e_y, 
\dot{\hat{d}} = f_d = -\delta \bar{x}^2 e_z,$$
(4.11)

where  $k_1, k_2, k_3 \ge 0$  and  $\rho, \gamma, \theta, \beta, \delta > 0$  are constants.

**Theorem 4.2.1.** Suppose that  $M_{C_x} > |x|, M_{C_y} > |y|, M_{C_z} > |z|, \rho, \gamma, \theta, \beta, \delta$  are positive constants. When  $k_1$ ,  $k_2$  and  $k_3 \ge 0$  are properly chosen such that the following matrix inequality holds,

$$P = \begin{bmatrix} \rho(k_1 + a) & -\frac{1}{2}(\rho a - a + c + M_{C_z}) & -\frac{1}{2}(M_{C_y} + dM_{C_x}) \\ -\frac{1}{2}(\rho a - a + c + M_{C_z}) & k_2 - c & 0 \\ -\frac{1}{2}(M_{C_y} + dM_{C_x}) & 0 & k_3 + b \end{bmatrix} > 0$$

$$(4.12)$$

or equivalently if k1, k2 and k3 are chosen so that the following inequalities hold:

(i) 
$$A = \rho(k_1 + a)(k_2 - c) - \frac{1}{4}(\rho a - a + c + M_{C_z})^2 > 0,$$
  
(ii)  $B = A(k_3 + b) - \frac{1}{4}(M_{C_y} + dM_{C_x})^2(k_2 - c) > 0$  (4.13)

then the two perturbed Chen systems (1.1) and (4.9) can be synchronized under the adaptive control of (4.10) and (4.11).

**Proof.** It is easy to see from (1.1) and (4.9) that the error dynamics can be obtained as follow

### ARTICLE IN PRESS

T. Plienpanich et al. | Appl. Math. Comput. xxx (2005) xxx-xxx 17

$$\dot{e}_{x} = \hat{a}(\tilde{y} - \tilde{x}) - a(y - x) - u_{1}, 
\dot{e}_{y} = -\hat{a}\tilde{x} + ax + \hat{c}\bar{x} - cx + \hat{c}\tilde{y} - cy - \tilde{x}\tilde{z} + xz - u_{2}, 
\dot{e}_{z} = -\hat{b}\bar{z} + bz + \tilde{x}\bar{y} - xy - u_{3}.$$
(4.14)

Let  $e_a = \hat{a} - a$ ,  $e_b = \hat{b} - b$ ,  $e_c = \hat{c} - c$ ,  $e_d = \hat{d} - d$ . Choose the following Lyapunov function:

$$V(e_x, e_y, e_z) = \frac{1}{2} \left( \rho e_x^2 + e_y^2 + e_z^2 + \frac{1}{\gamma} e_a^2 + \frac{1}{\theta} e_b^2 + \frac{1}{\beta} e_c^2 + \frac{1}{\delta} e_d^2 \right)$$
(4.15)

in which the differentiation of V along trajectories of (4.14) gives

$$\begin{split} \dot{V} &= \rho e_x \dot{e}_x + e_y \dot{e}_y + e_z \dot{e}_z + \frac{1}{\gamma} e_a \dot{e}_a + \frac{1}{\theta} e_a \dot{e}_a + \frac{1}{\beta} e_b \dot{e}_b + \frac{1}{\delta} e_d \dot{e}_d \\ &= \rho e_x [\hat{a}(\bar{y} - \bar{x}) - a(y - x) - u_1] + e_y [-\hat{a}\bar{x} + ax + \hat{c}\bar{x} - cx + \hat{c}\bar{y} - cy - \bar{x}\bar{z} + xz - u_2] \\ &+ e_z [-\hat{b}\bar{z} + bz + \bar{x}\bar{y} - xy - u_3] + \frac{1}{\gamma} e_a f_a + \frac{1}{\theta} e_b f_b + \frac{1}{\beta} e_c f_c + \frac{1}{\delta} e_d f_d \\ &= [\rho \hat{a}(\bar{y} - \bar{x}) - \rho a(\bar{y} - \bar{x}) + \rho a(\bar{y} - \bar{x}) - \rho a(y - x)] e_x - \rho u_1 e_x \\ &+ [-\hat{a}\bar{x} + a\bar{x} - a\bar{x} + ax] e_y + [-\bar{x}\bar{z} + \bar{x}z - \bar{x}z + xz] e_y - u_2 e_y \\ &+ [\hat{c}(\bar{x} + \bar{y}) - c(\bar{x} + \bar{y}) + c(\bar{x} + \bar{y}) - c(x + y)] e_z \\ &+ [-\hat{b}\bar{z} + b\bar{z} - b\bar{z} + bz] e_z + [\bar{x}\bar{y} - \bar{x}y + \bar{x}y - xy] e_z \\ &+ [\hat{d}\bar{x}^2 - d\bar{x}^2 + d\bar{x}^2 - dx^2] e_z - u_3 e_z + \frac{1}{\gamma} e_a f_a + \frac{1}{\theta} e_b f_b + \frac{1}{\beta} e_c f_c + \frac{1}{\delta} e_d f d \\ &= \rho(\bar{y} - \bar{x}) e_a e_x + \rho a(e_y - e_x) e_x - \rho u_1 e_x - \bar{x} e_a e_y - a e_x e_y - \bar{x} e_y e_z - z e_x e_y - u_2 e_y \\ &+ e_c e_y (\bar{x} + \bar{y}) + c(e_x + e_y) e_y - \bar{z} e_b e_z - b e_z^2 + \bar{x} e_y e_z + y e_x e_z \\ &+ \bar{x}^2 e_d e_z + de_x e_z (\bar{x} + x) - u_3 e_z + \frac{1}{\gamma} e_a f_a + \frac{1}{\theta} e_b f_b + \frac{1}{\beta} e_c f_c + \frac{1}{\delta} e_d f_d \\ &= \rho(\bar{y} - \bar{x}) e_a e_x + \rho a(e_y - e_x) e_x - \rho h_1 e_x^2 - \bar{x} e_a e_y - a e_x e_y - \bar{x} e_y e_z - z e_x e_y - k_2 e_y^2 \\ &+ e_c e_y (\bar{x} + \bar{y}) + c(e_x + e_y) e_y - \bar{z} e_b e_z - b e_z^2 + \bar{x} e_y e_z + y e_x e_z + \bar{x}^2 e_d e_z \\ &+ de_x e_z (\bar{x} + x) - (k_3 e_z + d\bar{x} e_x) e_z + \frac{1}{\gamma} e_a f_a + \frac{1}{\theta} e_b f_b + \frac{1}{\beta} e_c f_c + \frac{1}{\delta} e_d f_d \\ &= -\rho (k_1 + a) e_x^2 - (k_2 - c) e_y^2 - (k_3 + b) e_z^2 + (\rho a + c - a - z) e_x e_y + (y + x d) e_x e_z \\ &+ e_a \left[ \frac{1}{\gamma} f_a + (\bar{y} - \bar{x}) \rho e_x - \bar{x} e_y \right] + e_b \left[ \frac{1}{\theta} f_b - \bar{z} e_z \right] \\ &+ e_c \left[ \frac{1}{\beta} f_c + (\bar{x} + \bar{y}) e_y \right] e_d \left[ \frac{1}{\delta} f_d + \bar{x}^2 e_z \right] \\ &+ e_c \left[ \frac{1}{\theta} f_c - (h_1 + a) e_x^2 - (h_2 - c) e_y^2 - (h_3 + b) e_z^2 + (\rho a + c - a - M_C) e_x e_y \right] \\ &+ (M_C + M_C + M_C + e_z) e_z = e_z - e_z e_z - e_z e_z - e_z e_z - e_z e_z - e_z$$

T. Plienpanich et al. | Appl. Math. Comput. xxx (2005) xxx-xxx

18

where  $e = [|e_x| | |e_y| | |e_z|]^T$ , P is as in (4.12). Thus the differentiation of  $V(e_x, e_y, e_z)$  is negative definite, which implies that the origin of error system (4.14) is asymptotically stable. Therefore, the response system (4.9) is synchronizing with the drive system (1.1).  $\square$ 

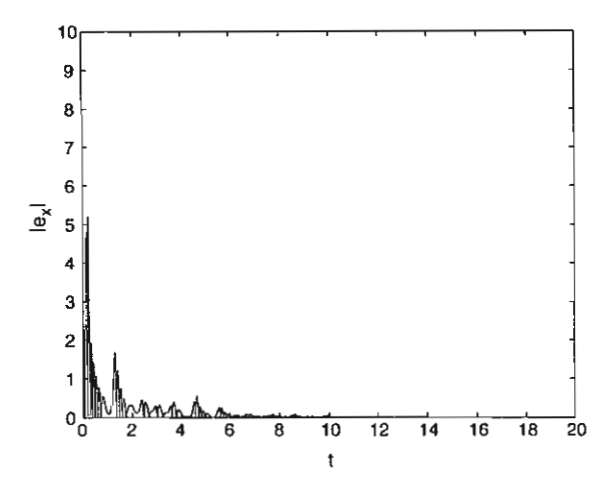


Fig. 16. Synchronization errors:  $|e_x|$ .

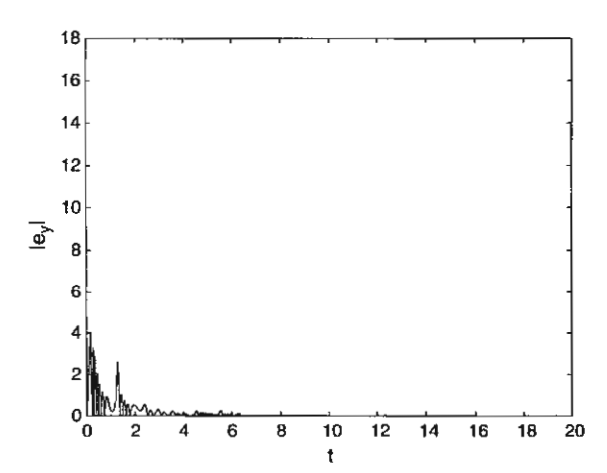


Fig. 17. Synchronization errors:  $|e_y|$ .

### 4.2.1. Numerical simulation

The numerical simulations are carried out using the fourth-order Runge-Kutta method. The initial conditions of the drive and response systems are (0.5, 1, 5) and (10.5, 20, 38). The parameters of the drive system are a = 35, b = 3, c = 28 and d = 2.

In order to choose the control parameters,  $M_{C_x} > |x|$ ,  $M_{C_y} > |y|$  and  $M_{C_z} > |z|$  must be estimated. Through simulations, we obtain  $M_{C_x} \approx 20$ ,

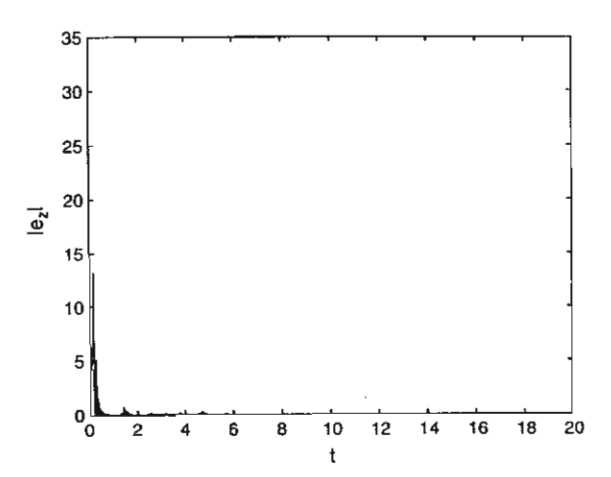


Fig. 18. Synchronization errors:  $|e_z|$ .

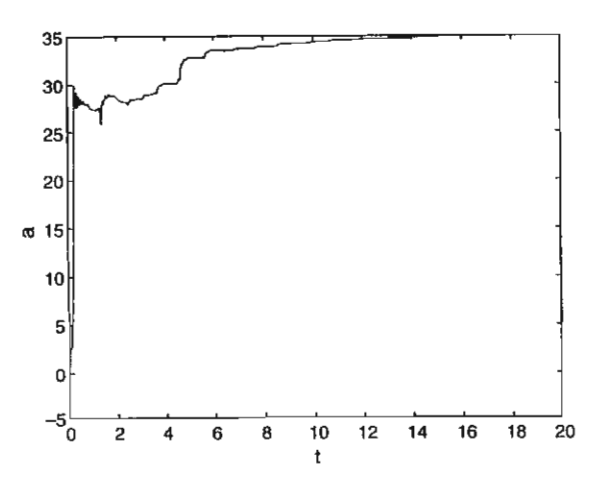


Fig. 19. Changing parameters: â.

T. Plienpanich et al. | Appl. Math. Comput. xxx (2005) xxx-xxx

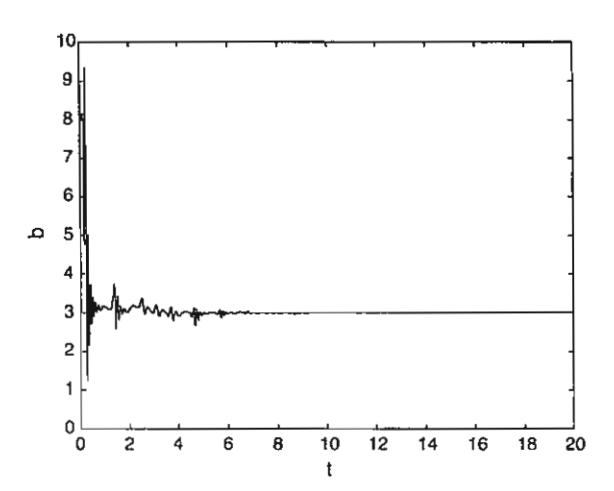


Fig. 20. Changing parameters:  $\hat{b}$ .

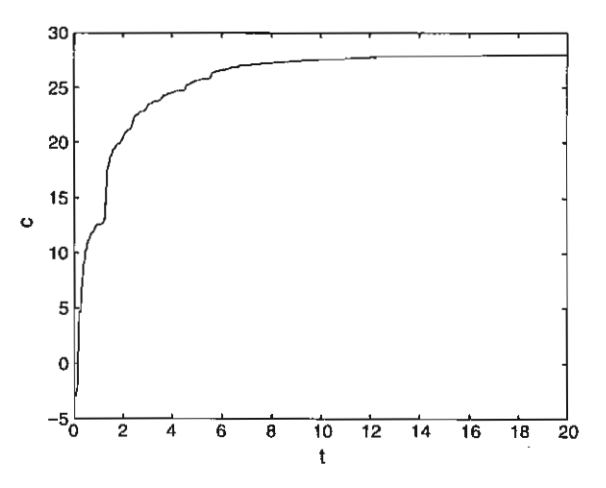


Fig. 21. Changing parameters: ĉ.

 $M_{C_y} \approx 25$  and  $M_{C_t} \approx 70$ . Then we firstly choose  $\rho = M_{C_y}^2/(ab)$ . Then choose  $\gamma = \theta = \beta = 1$  and then choose  $k_1 = 25$ ,  $k_2 = 88$ ,  $k_3 = 50$  which satisfy (4.13) and the initial values of the parameters  $\hat{a}, \hat{b}, \hat{c}$  and  $\hat{d}$  are all chosen to be 0, the response system synchronizes with the drive system as shown in Figs. 16–18 and the changing parameters of  $\hat{a}, \hat{b}, \hat{c}$  and  $\hat{d}$  are shown in Figs. 19–22.

T. Plienpanich et al. | Appl. Math. Comput. xxx (2005) xxx-xxx

21

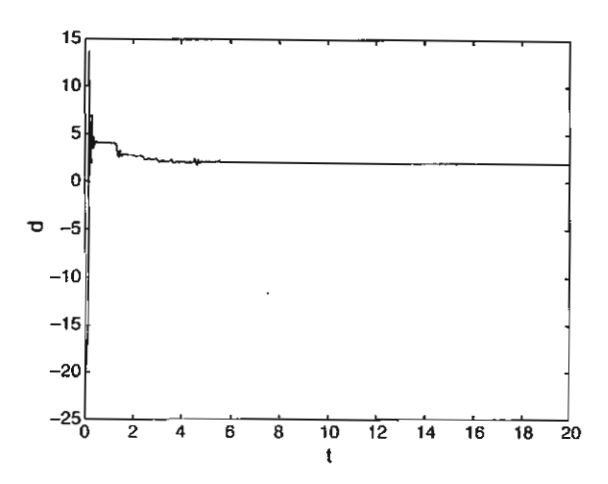


Fig. 22. Changing parameters:  $\hat{d}$ .

### References

- H.N. Agiza, Controlling chaos for the dynamical system of coupled dynamos, Chaos, Solitons and Fractals 13 (2002) 341-352.
- [2] H.N. Agiza, M.T. Yassen, Synchronization of Rossler and Chen chaotic dynamical system, Physic Letter A 278 (2001) 191-197.
- [3] Y. Wang, Z.H. Guan, X. Wen, Adaptive synchronization for Chen chaotic system with fully unknown parameters, Chaos, Solitons and Fractals 19 (2004) 899-903.
- [4] M.T. Yassen, The optimal control of Chen chaotic dynamical system, Applied Mathematics and Computation 131 (2002) 171-180.

Kyungpook Mathematical Journal Department of Mathematics College of Natural Sciences Kyungpook National University Daegu 702-701, Korea Telephone +82-53-950-5312 FAX +82-53-950-6306 E-mail: kmj@knu.ac.kr chnypark@knu.ac.kr URL: http://kmj.knu.ac.kr/

### REFEREE'S EVALUATION

Rec	comi	nendation:
	]	publication strongly recommended
	]	publication recommended
	V ]	revised required
	]	publication not recommended
Foi	rev	ised paper:
	]	recommended changed carried out satisfactorily
	1	recommended changed NOT carried out satisfactorily

### Evaluation report on KMJ #04103

### The asymptotic stability of ...

### P. Niamsup and Y. Lensury

I suggest few minor changes which might help the reader to better understand the present paper.

- 1. In the abstract, you just mention the topic paper but you do not describe its content. A few words might been added, e. g.
  - that the conditions are explicitly stated in terms of the coefficients of the given equation and
  - · a short remark about the methods of proof.
- 2. In the first line of the second page you announce that 'some properties of the Möbius transformation' will be used. However, neither the phrase 'Möbius transformation' does appear again at any other place in the paper nor could I find any place (notably in the proof of Lemma 2.5) where a property of Möbius transformations has been used. However, what I have found is that the paper heavily hings on arithmetic of complex numbers, polar coordinates and the (complex) sinus function.

Therefore, I suggest that

- either: if you make use of a property of a Möbius transformation you explicitly mention this in the prove at the place where you use it.
- or: you replace that sentence by a more accurate description of your methods of proof (should be consistent with the remark to be added in the abstract).

### 3. Overall evaluation:

- The result of the present paper is of interest.
- All the proofs required some lengthy calculations which locally are not difficult (at least not difficult to check) but at the whole it isn't trivial.
- The length is appropriate and all the necessary details of the proofs have been given. Any shortening might make it more difficult for any reader to understand the paper. No additions beside the above mentioned ones are needed.
- · Consequently, I do recommend the paper to be published at its full length.

### $M_r$ -FACTORS AND $Q_r$ -FACTORS FOR NEAR QUASINORM ON CERTAIN SEQUENCE SPACES

PIYAPONG NIAMSUP AND YONGWIMON LENBURY

Received 15 July 2004 and in revised form 20 June 2005

We study the multiplicativity factor and quadraticity factor for near quasinorm on certain sequence spaces of Maddox, namely, l(p) and  $l_{\infty}(p)$ , where  $p = (p_k)$  is a bounded sequence of positive real numbers.

We changed "p", "Q", and "M" from normal text to normal math. Please check such cases throughout.

"QUASI-NORM" in the title to

"QUASINORM."

We changed

Please check.

### 1. Introduction

.

Let X be an algebra over a field F (R or C). A quasinorm on X is a function  $|\cdot|: X \to R$  such that

- (i) |0| = 0,
- (ii)  $|x| \ge 0$ , for all  $x \in X$ ,
- (iii) |-x| = |x|, for all  $x \in X$ ,
- (iv)  $|x + y| \le |x| + |y|$ , for all  $x, y \in X$ ,
- (v) if  $t_k \in F$ ,  $|t_k t| \to 0$ , and  $x_k, x \in X$ ,  $|x_k x| \to 0$ , then  $|t_k x_k tx| \to 0$ .

If  $|\cdot|$  satisfies only properties (i) to (iv), then we call  $|\cdot|$  a near quasinorm. If the quasinorm satisfies |x| = 0 if and only if x = 0, then it is said to be total.

A quasinormed linear space (QNLS) is a pair  $(X, |\cdot|)$  where  $|\cdot|$  is a quasinorm on X. If  $(X, |\cdot|)$  is a quasinorm space, then the map  $|\cdot|: X \to R$  is continuous. For p > 0, a p-seminorm on X is a function  $||\cdot||: X \to R$  satisfying

- (i)  $||x|| \ge 0$ , for all  $x \in X$ ,
- (ii)  $||tx|| = |t|^p ||x||$ , for all  $t \in F$ , for all  $x \in X$ ,
- (iii)  $||x + y|| \le ||x|| + ||y||$ , for all  $x, y \in X$ .

A seminorm is called a norm if it satisfies the following condition:

(iv) ||x|| = 0 if and only if x = 0.

A p-seminormed linear space (p-semi-NLS) is a pair  $(X, \|\cdot\|)$  where  $\|\cdot\|$  is a seminorm on X. p-normed linear spaces (p-normed-LS) are defined similarly.

Copyright © 2005 Hindawi Publishing Corporation International Journal of Mathematics and Mathematical Sciences 2005:00 (2005) 1–6 DOI: 10.1155/IJMMS.2005.1

International Journal of Mathematics and Mathematical Sciences

In [1, 2], multiplicativity factors (or M-factors) and quadrativity factors (or Q-factors) for seminorms on an algebra X have been introduced and studied in detail. A number  $\mu > 0$  is said to be a multiplicativity factor for a seminorm S if and only if  $S(xy) \le \mu S(x)S(y)$ , for all  $x, y \in X$ . Similarly, a number  $\lambda > 0$  is said to be a quadrativity factor for S if and only if  $S(x^2) \le \lambda S(x)^2$ , for all  $x \in X$ . The necessary and sufficient conditions for existence of M-factor and Q-factor for S are answered in the following results.

THEOREM 1.1. Let X be an algebra and let  $S \neq 0$  be a seminorm on X. Then

(a) S has M-factors on X if and only if Ker S is an ideal in X and

$$\mu_{\inf} \equiv \sup \{ S(xy) : x, y \in X, \ S(x) = S(y) = 1 \} < +\infty,$$
 (1.1)

- (b) if S has M-factors on X and  $\mu_{inf} > 0$ , then  $\mu_{inf}$  is the best (least) M-factor for S,
- (c) if S has M-factors on X and  $\mu_{inf} = 0$ , then  $\mu$  is an M-factor for S if and only if  $\mu > 0$ .

THEOREM 1.2. Let X be an algebra and let  $S \neq 0$  be a seminorm on X. Then

(a) S has Q-factors on X if and only if KerS is closed under squaring (i.e.,  $(KerS)^2 \subset KerS$ ) and

$$\lambda_{\inf} \equiv \sup \{ S(x^2) : x \in X, S(x) = 1 \} < +\infty,$$
 (1.2)

- (b) if S has Q-factors on X and  $\lambda_{\inf} > 0$ , then  $\lambda_{\inf}$  is the best (least) Q-factor for S,
- (c) if S has Q-factors on X and  $\lambda_{\inf} = 0$ , then  $\lambda$  is a Q-factor for S if and only if  $\lambda > 0$ .

If S is a norm, then  $KerS = \{0\}$ . If in addition X is finite-dimensional, then a simple compactness argument shows that  $\mu_{inf}$  is finite. Therefore, by Theorem 1.1, norms on finite-dimensional algebras always have M-factors. If S is a seminorm on a finite-dimensional algebra X, then S has M-factors on X if and only if KerS is a (two-sided) ideal in X. In [1, 2] several examples of seminorms having M-factors and Q-factors are given. In [3], scalar multiplicativity factors for near quasinorms on certain sequence spaces of Maddox are studied. Motivated by these results we define  $M_r$ -factors and  $Q_r$ -factors for a near quasinorm q on an algebra X as follows.

A number  $\mu > 0$  is an  $M_r$ -factor for q if and only if  $q(txy) \le \mu |t|^r q(x)q(y)$ , there exists t > 0, for all  $t \in F$ , for all  $x, y \in X$ .

A number  $\lambda > 0$  is a  $Q_r$ -factor for q if and only if  $q(tx^2) \le \lambda |t|^r q(x)^2$ , there exists t > 0, for all  $t \in F$ , for all  $x \in X$ .

Let

$$\mu_{\inf} \equiv \sup \left\{ \frac{q(txy)}{|t|^r q(x)q(y)} : t \in F - \{0\}, \ x, y \in X - \operatorname{Ker} q \right\},$$

$$\lambda_{\inf} \equiv \sup \left\{ \frac{q(tx^2)}{|t|^r q(x)^2} : t \in F - \{0\}, \ x \in X - \operatorname{Ker} q \right\}.$$
(1.3)

### 2. $M_r$ -factors and $Q_r$ -factors for near quasinorms

In this section we will prove the following theorems.

We changed "\(\begin{align\*} \text{"} to \\ \text{"there exists" twice.} \\ Please check. \end{align\*}

THEOREM 2.1. Let X be an algebra over a field F(F = C or R). Let q be a near quasinorm on X. Then

- (a) q has  $M_r$ -factors on X if and only if Ker q is a (two-sided) ideal in X and  $\mu_{inf} < +\infty$ ,
- (b) if q has  $M_r$ -factors on X and  $\mu_{inf} > 0$ , then  $\mu_{inf}$  is the best (least)  $M_r$ -factor for q,
- (c) if q has  $M_r$ -factors on X and  $\mu_{inf} = 0$ , then  $\mu$  is an  $M_r$ -factor for q if and only if

We changed "factors" to "factor." Please check similar highlighted cases throughout.

THEOREM 2.2. Let X be an algebra over a field F (F = C or R). Let g be a near quasinorm on X. Then

- (a) q has  $Q_r$ -factors on X if and only if Ker q is closed under squaring (i.e.,  $x^2 \in \text{Ker } q$ , for all  $x \in \text{Ker } q$ ) and  $\lambda_{\inf} < +\infty$ ,
- (b) if q has  $Q_r$ -factors on X and  $\lambda_{\inf} > 0$ , then  $\lambda_{\inf}$  is the best (least)  $Q_r$ -factors for q,
- (c) if q has  $Q_r$ -factors on X and  $\lambda_{\inf} = 0$ , then  $\lambda$  is a  $Q_r$ -factors for q if and only if  $\lambda > 0$ .

Proof of Theorem 2.1. (a) Suppose that q has an  $M_r$ -factor  $\mu$  on X. Clearly, Ker q is a subspace of X. Now take any  $x \in \text{Ker } q$  and  $y \in X$ . Then  $q(xy) \le \mu q(x)q(y) = 0$  which implies that  $xy \in \text{Ker } q$ . Similarly,  $yx \in \text{Ker } q$ , so Ker q is a (two-sided) ideal in X. Now for  $t \in$  $F - \{0\}$  and  $x, y \in X - \text{Ker } q$ , we have  $q(txy) \le \mu |t|^r q(x)q(y)$  or  $q(txy)/|t|^r q(x)q(y) \le \mu$ which implies that  $\mu_{\inf} \leq \mu < +\infty$ . Conversely, suppose that Kerq is a (two-sided) ideal in X and  $\mu_{\inf} < +\infty$ . If t = 0,  $x \in \text{Ker } q$ , or  $y \in \text{Ker } q$ , then  $txy \in \text{Ker } q$ , so 0 = q(txy) = $\mu_{\inf}|t|^r q(x)q(y)$ . If  $t \neq 0$  and  $x, y \notin \text{Ker } q$ , then  $q(txy)/|t|^r q(x)q(y) \leq \mu_{\inf}$  or  $q(txy) \leq q$  $\mu_{\inf}|t|^r q(x)q(y)$ . Therefore,  $q(txy) \le \mu_{\inf}|t|^r q(x)q(y)$ , for all  $t \in F$  and for all  $x, y \in X$ which implies that q has  $M_r$ -factors on X.

- (b) Let  $\mu$  be an  $M_r$  factor for q on X and  $\mu_{\inf} > 0$ . Then  $q(txy) \le \mu |t|^r q(x)q(y)$  for all  $t \in F$  and for all  $x, y \in X$ . Therefore,  $q(txy)/|t|^r q(x)q(y) \le \mu$ , for all  $t \in F - \{0\}$  and for all  $x, y \in \text{Ker } q$ , so  $\mu_{\inf} \leq \mu$ .
  - (c) This part follows directly from definition of  $\mu_{inf}$  and  $M_r$ -factors for q on X.

*Proof of Theorem 2.2.* The proof of this theorem is a simple modification of the proof of Theorem 2.1 and will be omitted.

### 3. $M_r$ -factors and $Q_r$ -factors for near quasinorm on certain sequence spaces of Maddox

Let  $p = (p_k)$  be a bounded sequence of positive real numbers. The sequence spaces of Maddox  $l_{\infty}(p)$  and l(p) are defined as follows:

$$l_{\infty}(p) = \left\{ (x_k) : x_k \in C, \sup_{k} |x_k|^{p_k} < \infty \right\},$$

$$l(p) = \left\{ (x_k) : x_k \in C, \sum_{k} |x_k|^{p_k} < \infty \right\}.$$
(3.1)

### 4 M<sub>r</sub>-factors and Q<sub>r</sub>-factors

With the usual multiplication (i.e.,  $(x_k)(y_k) = (x_k y_k)$ ), both  $l_{\infty}(p)$  and l(p) are algebras over C. We define near quasinorms  $q_1$  on  $l_{\infty}(p)$  and  $q_2$  on l(p) as follows:

$$q_{1}((x_{k})) = \sup_{k} |x_{k}|^{p_{k}/M}, \quad (x_{k}) \in l_{\infty}(p),$$

$$q_{2}((x_{k})) = \left(\sum_{k} |x_{k}|^{p_{k}}\right)^{1/M}, \quad (x_{k}) \in l(p),$$
(3.2)

where  $M = \max\{1, \sup_k p_k\}$ . We observe that  $q_1$  and  $q_2$  may or may not be quasinorms. For example, when  $(p_k) = (1/k)$ , then  $q_1$  is a near quasinorm but not a quasinorm; if  $(p_k) = (1 - 1/(k+1))$ , then  $q_1$  is a quasinorm.

In this section we give necessary and sufficient conditions for sequence spaces  $l_{\infty}(p)$  and l(p) to have  $M_r$ -factors and  $Q_r$ -factors.

THEOREM 3.1. Let  $p = (p_k)$  and let M be defined as above. Then the following are equivalent

- (a)  $p_0 = p_k = p_{k+1}$  for all  $k \ge 0$  where  $p_0$  is a positive real number.
- (b)  $q_1$  has  $M_r$ -factors on  $l_{\infty}(p)$ .
- (c) q<sub>1</sub> has Q<sub>r</sub>-factors on l<sub>∞</sub>(p).
- (d)  $q_1$  is a  $p_0/M$ -seminorm on  $l_{\infty}(p)$ .

THEOREM 3.2. Let  $p = (p_k)$  and let M be defined as above. Then the following are equivalent.

- (a)  $p_0 = p_k = p_{k+1}$  for all  $k \ge 0$  where  $p_0$  is a positive real number.
- (b)  $q_2$  has  $M_r$ -factors on l(p).
- (c)  $q_2$  has  $Q_r$ -factors on l(p).
- (d)  $q_2$  is a  $p_0/M$ -seminorm on l(p).

Proof of Theorem 3.1. (a)  $\Rightarrow$  (b) If  $p_0 = p_k = p_{k+1}$  for all  $k \ge 1$ , then

$$q_1(txy) = \sup_{k} |txy|^{p_k/M} = \sup_{k} |txy|^{p_0/M} \le |t|^{p_0/M} q_1(x) q_1(y)$$
 (3.3)

for all  $x, y \in l_{\infty}(p)$ , so  $q_1$  has an  $M_r$ -factor on  $l_{\infty}(p)$ .

(b)  $\Rightarrow$  (a) Assume that  $q_1$  has  $M_r$ -factors on  $l_{\infty}(p)$ . This implies that

$$\mu_{\inf} = \sup \left\{ \frac{q_1(txy)}{|t|^r q_1(x)q_1(y)} : t \in F - \{0\}, \ x, y \in X - \operatorname{Ker} q_1 \right\} < +\infty.$$
 (3.4)

We shall show that  $r = \sup_k p_k/M = \inf_k p_k/M$  which implies that  $p_k = p_{k+1}$  for all  $k \ge 1$ . To this end we observe that

$$\mu_{\inf} = \sup \left\{ \frac{q_{1}(txy)}{|t|^{r}q_{1}(x)q_{1}(y)} : t \in F - \{0\}, x, y \in X - \operatorname{Ker} q_{1} \right\}$$

$$\geq \sup \left\{ \frac{q_{1}(txy)}{|t|^{r}q_{1}(x)q_{1}(y)} : t \in F - \{0\}, x, y = (1, 1, 1, ...) \right\}$$

$$\geq \sup \left\{ \frac{\sup_{k} |t|^{p_{k}/M}}{|t|^{r}} : t \in F, |t| \geq 1 \right\} = \sup \left\{ |t|^{\sup_{k} p_{k}/M} : t \in F, |t| \geq 1 \right\}$$
(3.5)

so that

$$\mu_{\inf} \ge \sup \left\{ \frac{|t|^{\sup_k p_k/M}}{|t|^r} : t \in F, |t| \ge 1 \right\}. \tag{3.6}$$

If  $r < \sup_k p_k/M$ , then  $\mu_{\inf} = +\infty$  which is a contradiction. Therefore,  $r \ge \sup_k p_k/M$ . Similarly, we can show that  $r \le \inf_k p_k/M$  from which it follows that  $r = \sup_k p_k/M = \inf_k p_k/M$  and the proof is complete.

- (a) $\Rightarrow$ (c) The same proof as (a) $\Rightarrow$ (b).
- $(c)\Rightarrow(a)$  The same proof as  $(b)\Rightarrow(a)$ .
- (d)⇒(b) This is obvious.
- (b) $\Rightarrow$ (d) Assume that  $q_1$  has  $M_r$ -factors. Then, by (a),  $p_0 = p_k = p_{k+1}$  for all  $k \ge 0$  where  $p_0$  is a positive real number. Moreover, we have

$$q_1(txy) = \sup_{t} |t \cdot (x_k)(y_k)|^{p_0/M} = |t|^{p_0/M} \sup_{t} |x_k y_k|^{p_0/M} = |t|^{p_0/M} q_1(xy)$$
(3.7)

for all  $x = (x_k)$ ,  $y = (y_k) \in l_{\infty}(p)$  and all  $t \in F$ . Putting y = (1, 1, 1...) we see that

$$q_1(tx) = |t|^{p_0/M} q_1(x) \tag{3.8}$$

and the proof is complete.

*Proof of Theorem 3.2.* The proof is almost the same as in Theorem 3.1 and will be omitted.

Remark 3.3. If the algebra X has an identity element  $x_0$  for multiplication and  $q \neq 0$  is a near-quasinorm on X which has an  $M_r$ -factor on X, then we obtain  $q(x_0) > 0$ ,  $\mu_{\inf} \geq 1/q(x_0)$  and

$$\frac{1}{q(x_0)\mu_{\inf}}|t|^r q(xy) \le q(txy) \le \mu_{\inf}|t|^r q(x)q(y)$$
 (3.9)

for all  $x, y \in X$  and all  $t \in F$ .

### References

[1] R. Arens and M. Goldberg, Multiplicativity factors for seminorms, J. Math. Anal. Appl. 146 (1990), no. 2, 469-481.

### 6 M<sub>r</sub>-factors and Q<sub>r</sub>-factors

- [2] \_\_\_\_\_, A class of seminorms on function algebras, J. Math. Anal. Appl. 162 (1991), no. 2, 592-609.
- [3] S. Suantai, Scalar multiplicative factors for near quasi-norms, Bull. Calcutta Math. Soc. 90 (1998), no. 3, 183-190.

Piyapong Niamsup: Department of Mathematics, Faculty of Science, Chiangmai University, Chiangmai 50200, Thailand

E-mail address: scipnmsp@chiangmai.ac.th

Yongwimon Lenbury: Department of Mathematics, Faculty of Science, Mahidol University, Bangkok 10400, Thailand

E-mail address: scylb@mahidol.ac.th

OU

### On estimation of a binomial proportion from a decision-theoretic point of view

by

Prof. Bimal Sinha

Department of Mathematics and Statistics,

University of Maryland Baltimore County, U.S.A.

Date: December 13, 2002

Time: 13.30

Location: Rm. M 302 M. Building, Faculty of Science, Mahidol University Host: Department of Mathematics, Faculty of Science, Mahidol University Rama 6 Rd., Bangkok 10400 Tel. 02-644-5419 Fax. 02-201-5343

on

## Mathematical Aspects of Geometric Modeling

þ

Prof. Charles A. Micchelli

Department of Mathematics

State University of New York, U.S.A.

Date: January 6, 2003

Time: 13.30

Host: Department of Mathematics, Faculty of Science, Mahidol University

Location: Rm. M 302 M. Building, Faculty of Science, Mahidol University

on

# Fluid Backflow Modeling for Drug Infusion into Brain Tissue

by

Assoc. Prof. Wayne Michael Lawton

Department of Mathematics

National University of Singapore

Date: January 9, 2003

Time: 13.30

Host: Department of Mathematics, Faculty of Science, Mahidol University

Location: Rm. M 302 M. Building, Faculty of Science, Mahidol University

on

## Elastic Modeling of Brain Tissue for Drug Infusion

by

Assoc. Prof. Wayne Michael Lawton

Department of Mathematics

National University of Singapore

Date : January 10, 2003

Time: 13.30

Location: Rm. M 304 M. Building, Faculty of Science, Mahidol University Host: Department of Mathematics, Faculty of Science, Mahidol University

on

# Fractal Analysis: A Morphometric Method for Life Science

by

Dr. Wannapong Triampo

Department of Physics

Faculty of Science, Mahidol University

Date: February 25, 2003

Time: 13.30

Host: Department of Mathematics, Faculty of Science, Mahidol University

Location: Rm. M 202 M. Building, Faculty of Science, Mahidol University

on

### Research in Algebraic Combinatorics

by

Dr. Matteo Mainetti

Sirindhorn International Institute of Technology

Thammasat University

Date: June 3, 2003

Time: 14.00

Host: Department of Mathematics, Faculty of Science, Mahidol University

Location: Rm. M 202 M. Building, Faculty of Science, Mahidol University

\*\*\*\* All\*interested-parties-are cordially invited-to-join-our-Special Seminar

on

# Surgical Modeling with Elasticity and Fluid Flow

2

Assoc. Prof. Dr. Wayne Michael Lawton

Department of Mathematics

National University of Singapore

Date: July 11, 2003

Time: 13.00

Host: Department of Mathematics, Faculty of Science, Mahidol University

Location: Rm. M 302 M. Building, Faculty of Science, Mahidol University Rama 6 Rd., Bangkok 10400 Tel. 02-644-5419 Fax. 02-201-5343

on

# Weighted Function Spaces and Harmonic Majorants

þ

Prof. Luis Manuel Tovar

Departamento de Mathematicas

Instituto Politecnico Nacional, Mexico

Date: July 25, 2003

Time: 13.30

Host: Department of Mathematics, Faculty of Science, Mahidol University

Location: Rm. M 305 M. Building, Faculty of Science, Mahidol University Rama 6 Rd., Bangkok 10400 Tel. 02-644-5419 Fax. 02-201-5343 All interested parties are cordially invited to join our

Special Seminar

OU

Interesting Problems in Soap Bubble Geometry and Discrete Geometry

þ

Dr. Wacharin Wichiramala

Departament of Mathematics

University of Illinois at Urbana-Champaign, U.S.A.

Date: August 1, 2003

Time: 13.30 - 14.30

Host: Department of Mathematics, Faculty of Science, Mahidol University

Location: Rm. M 305 M. Building, Faculty of Science, Mahidol University

on

# A New Model for Laser-induced Thermal Damage in the Retina

þ

Prof. George Rowlands

Department of Physics

University of Warwick, UK

Date: August 13, 2003

Time: 10.00 a.m.

Host: Department of Mathematics, Faculty of Science, Mahidol University

Location: Rm. M 304 M. Building, Faculty of Science, Mahidol University

Ľ

## Research in Delay Differential Equations

þ

Dr. Dang Vu Giang

Institute of Mathematics, Vietnam

Date: August 19, 2003

: August 27, 2003

Time: 10.00 - 12.00

Host: Department of Mathematics, Faculty of Science, Mahidol University

Location: Rm. M 302 M. Building, Faculty of Science, Mahidol University

on

## Generalized Lagrange Multiplier Conditions for DC-programs and Nonconvex Programs with DSL Upper Approximations

By

Assoc. Prof. Dr. Nguyen Dinh

Department of Mathematics-Informatics

Pedagogical Institute of Ho Chi Minh City, Vietnam

Date: August 25, 2003

Time: 13.00 - 15.00

Host: Department of Mathematics, Faculty of Science, Mahidol University

Location: Rm. M 202 M. Building, Faculty of Science, Mahidol University

on

# Sequential Lagrange Multiplier Conditions Characterizing Optimality

## for Cone-Convex Programs

 $\mathbf{B}\mathbf{y}$ 

Assoc. Prof. Dr. Nguyen Dinh

Department of Mathematics-Informatics

Pedagogical Institute of Ho Chi Minh City, Vietnam

Date: August 26, 2003

Time: 13.00 - 15.00

Host: Department of Mathematics, Faculty of Science, Mahidol University

Location: Rm. M 202 M. Building, Faculty of Science, Mahidol University

C

# Research in Delay Differential Equations

þ

Dr. Dang Vu Giang

Institute of Mathematics, Vietnam

Date: August 19, 2003

: August 27, 2003

Time: 10.00 - 12.00

Host: Department of Mathematics, Faculty of Science, Mahidol University

Location: Rm. M 302 M. Building, Faculty of Science, Mahidol University

ŭ

## Statistical Aspects of Social Network

By

Prof. Dr. Bikas K. Sinha

Indian Statistical Institute

Kolkata, India

Date: September 18, 2003

Time: 13.30 - 14.30

Host: Department of Mathematics, Faculty of Science, Mahidol University

Location: Rm. M 304 M. Building, Faculty of Science, Mahidol University

C

# Estimation of Variance Components in Linear mixed Models, a Review

By

Prof. Dr. Bimal K. Sinha

Department of Mathematics and Statistics

University of Maryland Baltimore County

Baltimore, USA

Date: September 18, 2003

Time: 14.30 - 15.30

Host: Department of Mathematics, Faculty of Science, Mahidol University

Location: Rm. M 304 M. Building, Faculty of Science, Mahidol University

## Introduction to Finite Population Samplings

and

## Statistical Methods in Assessing Agreement

 $\mathbf{R}^{\mathsf{A}}$ 

Prof. Dr. Bikas K. Sinha

Indian Statistical Institute

Kolkata, India

Date: September 19, 2003

Time: 10.00-12.00

Location: Rm. M 202 M. Building, Faculty of Science, Mahidol University Host: Department of Mathematics, Faculty of Science, Mahidol University

### **Compact Operators**

Date:

September 22, 2003

Time:

13.30-15.30

Location: Rm. M301 M. Building

### Schatten Class Operators

Date:

September 26, 2003

Time:

13.30-15.30

Location: Rm. K136 K. Building

### Schatten Class Operators

Date:

September 29, 2003

Time:

13.30-15.30

Location: Rm. M301 M. Building

### C\* - Algebras

Date:

October 3, 2003

Time:

13.30-15.30

Location: Rm. M301 M. Building

### C\* - Algebras

Date:

October 6, 2003

Time:

13.30-15.30

Location: Rm. M301 M. Building

### Vonn Neumann Algebras

Date:

October 10, 2003

Time:

13.30-15.30

Location: Rm. M202 M. Building

### By

Prof. Dr. Sing-Cheong Ong Central Michigan University, U.S.A.

Host: Department of Mathematics, Faculty of Science Mahidol University Tel. 02-644-5419 Fax. 02-201-5343

## Dynamic and Static Optimization

Dr. Dang Vu Giang

Institute of Mathematics, Vietnam

November 5, 12, 19, 2003 Date:

December 3, 24, 2003 January 7, 14, 21, 28, 2004 February 4, 11, 18, 25, 2004 Time: 9.00 - 12.00

Rm. K 128 Chalerm Prakiat Building Location:

Date:

November 26, 2003 December 17, 2003 Time: 9.00 - 12.00

Rm. M 302 M. Building Location: Host: Department of Mathematics, Faculty of Science, Mahidol University Rama 6 Rd., Bangkok 10400 Tel. 02-644-5419 Fax. 02-201-5343

c

## What is Voronoi Tessellation?

by

Mr. Kittisak Tiyapan

University of Manchester Institute of Science and Technology, U.K.

Date: November 28, 2003

Time: 9.00 - 10.00 a.m.

Location: Rm. M 301 M. Building, Faculty of Science, Mahidol University Host: Department of Mathematics, Faculty of Science, Mahidol University

IIO

# Bioinformatics: Some Challenging Statistical Problems

þ

Prof. Pranab Sen

Department of Biostatistics,

University of North Carolina at Chapel Hill, U.S.A.

Date: December 19, 2003

Time: 13.30-16.30

Location: Rm. M 304 M. Building, Faculty of Science, Mahidol University Host: Department of Mathematics, Faculty of Science, Mahidol University

on

## Shock Waves and Supersonic Flight

by

### Professor Dening Li

Department of Mathematics,

West Virginia University, USA.

Date: December 26, 2003

Time: 10.00 - 12.00

Location: Rm. M 304 M. Building, Faculty of Science, Mahidol University Host: Department of Mathematics, Faculty of Science, Mahidol University Rama 6 Rd., Bangkok 10400 Tel. 0 2644 5419 Fax. 0 2201 5343

C

## Wavelet Applications to the Petrov-Galerkin Method for Hammerstein Equations

þ

Professor Hideaki Kaneko

Department of Mathematics,

Oldominion University, U.S.A.

Date: January 5, 2004

Time: 10.30 - 12.00

Host: Department of Mathematics, Faculty of Science, Mahidol University

Location: Rm. M 302 M. Building, Faculty of Science, Mahidol University

on

## Discontinuous Galerkin Finite Element Method for Parabolic Problems

þ

Prof. Hideaki Kaneko

Department of Mathematics,

Oldominion University, U.S.A.

Date : January 6, 2004

Time: 9.00 - 10.30

Host: Department of Mathematics, Faculty of Science, Mahidol University

Location: Rm. M 306 M. Building, Faculty of Science, Mahidol University

On

# Convection in Smart Liquids Under Terrestrial or Micro-gravity

Situations

Вy

Prof. Dr. Pradeep G. Sidheshwar

UGC Centre for Advanced Studies in Fluid Mechanics

Department of Mathematics,
Bangalore University

Karnataka, India

Date: 29-30 April 2004

Time: 10.00-12.00

Location: Rm. M 302 M. Building, Faculty of Science, Mahidol University Host: Department of Mathematics, Faculty of Science, Mahidol University

## Robustness of t-statistic and t-test

Prof. Bimal K. Sinha

Prof. Bimal K. Sinha

Department of Mathematics and Statistics,

University of Maryland, Baltimore County, U.S.A.

Date: March 25, 2004 Time: 13.30-14.30

Location: Room M 202 M. Building, Faculty of Science, Mahidol University Host: Department of Mathematics, Faculty of Science, Mahidol University Rama 6 Rd., Bangkok 10400 Tel. 02-644-5419 Fax. 02-201-5343

on

## On The Modeling of Stochastic Systems With Time-Delayed Feedback

Ву

Dr. Till Daniel Frank

Department of Physics University of Münster Wilhelm-Klemm-Str. 9, 48149 Münster, Germany

Date: March 24, 2004

Time: 10.00-11.00

Location: Rm. M 304 M. Building, Faculty of Science, Mahidol University Host: Department of Mathematics, Faculty of Science, Mahidol University

### Modelling "Complex" Systems (an Introduction and a Few Comments)

Date: March 23, 2004 Time: 10.30-12.00

Location: Rm. M301 M. Building

### Modelling Systems in Ecology

Date: March 25, 2004 Time: 10.30-12.00

Location: Rm. M202 M. Building

### Modelling Systems in Epidemiology

Date: March 31, 2004 Time: 10.30-12.00

Location: Rm. M202 M. Building

By
Prof. Marc A. Dubois
Directeur du GDR 489 "ECOFIT"
Directeur du programme "MATECLID"
Service de Physique de l'Etat Condensé
CEA Saclay—Orme des Merisiers
(CEA Saclay—Orme des Merisiers
(OEA Saclay—Orme des Merisiers
(OEA Saclay—Orme des Merisiers
(OEA Saclay—Orme des Merisiers
(OEA Saclay—Orme des Merisiers)

Host: Department of Mathematics, Faculty of Science, Mahidol University

Tel. 02-644-5419 Fax. 02-201-5343

## ขอเชิญนักศึกษาและผู้สนใจเข้าฟังการบรรยายพิเศษ

<u>}</u>.

### ในหัวข้อเรื่อง

## Intra – class Models: Properties and Inference

โดย

Prof. Bimal K. sinha
Department of Mathematics and Statistics,
University of Maryland, Baltimore County, U.S.A.

วันที่ 22 **–** 24 มีนาคม 2547

เวลา 11.00 — 12.00 น.

ณ ห้อง M 202

Ç

000

## Data Mining and Text Classification

7

### Nick Cercone

### Dalhousie University

Date: March 15, 2004

Time: 13.00-16.00

Host: Department of Mathematics, Faculty of Science, Mahidol University

Location: Rm. M 202 M. Building, Faculty of Science, Mahidol University Rama 6 Rd., Bangkok 10400 Tel. 0 2644 5419 Fax. 0 2201 5343

on

Intelligent Interface

γď

Nick Cercone

Dalhousie University

Date: March 12, 2004

Time: 10.30-11.30

Host: Department of Mathematics, Faculty of Science, Mahidol University

Location: Rm. M 202 M. Building, Faculty of Science, Mahidol University

# Common Cyclic Vectors for Normal Operators

by
Professor Dr. Warren Wogen
University of North Carolina, U.S.A.

Date: February 9, 2004

Time: 10.00-12.00

Host: Department of Mathematics, Faculty of Science Mahidol University Location: Rm. M302 M. Building, Faculty of Science, Mahidol University Rama 6 Rd., Bangkok 10400 Tel. 02-644-5419 Fax. 02-201-5343

## Please note the change of schedule.\*

Special Seminar

on

# Some Asymptotic Problems for a Reaction/Diffusion System

by

Professor Thomas I. Seidman

Department of Mathematics and Statistics,

University of Maryland, Baltimore County, U.S.A.

Date : January 23, 2004\*

Time: 13.00 - 15.00

Host: Department of Mathematics, Faculty of Science, Mahidol University

Location: Rm. M 304\* M. Building, Faculty of Science, Mahidol University

 $^{\circ}$ 

# Hybrid Systems: Discontinuous Dynamics in a Continuous World

ф

Professor Thomas I. Seidman

Department of Mathematics and Statistics,

University of Maryland, Baltimore County, U.S.A.

Date: January 20, 2004

Time: 10.00 - 12.00

Host: Department of Mathematics, Faculty of Science, Mahidol University

Location: Rm. M 306 M. Building, Faculty of Science, Mahidol University Rama 6 Rd., Bangkok 10400 Tel. 0 2644 5419 Fax. 0 2201 5343

on

# Entitled Introduction to Learning Theory

δ

## Asst. Prof. Dr. Massimiliano Pontil

Department of Computer Science

University College London, U.K.

Date: January 12, 2004

Time: 11.00 - 12.00

Host: Department of Mathematics, Faculty of Science, Mahidol University

Location: Rm: M 303 M. Building, Faculty of Science, Mahidol University

\*

# xipuəddy / 61

on

# Symmetry and its Application to Mechanics

by

Assoc. Prof. Dr. Wayne Michael Lawton

Department of Mathematics,

National University of Singapore

Date: January 9, 2004

Time: 10.00 - 12.00

Host: Department of Mathematics, Faculty of Science, Mahidol University

Location: Rm. M 304 M. Building, Faculty of Science, Mahidol University Rama 6 Rd., Bangkok 10400 Tel. 0 2644 5419 Fax. 0 2201 5343

ב

# Reliability Estimation from Samples from an Exponential Population

β

Prof. Dr. Bikas K. Sinha

Indian Statistical Institute

Kolkata, Indian

Date: April 30, 2004

Time: 14.00-15.00

Host: Department of Mathematics, Faculty of Science, Mahidol University

Location: Rm. M 302 M. Building, Faculty of Science, Mahidol University

on

Some Singular Homogenization Problems in Non-linear Elasticity and Pseudo-plasticity

2

Prof. Dr. Christian Licht

Laboratoire de Mécanique et Génie Civil,

Université MONTPELLIER II, France

Date: May 31, 2004

Time: 10:30 - 11:30

Location: Rm. M 202 M. Building, Faculty of Science, Mahidol University Host: Department of Mathematics, Faculty of Science, Mahidol University

# On a Family of Apportionment Indices and Its Limiting Properties

Prof. Dr. Bikas K. Sinha
Stat-Math Unit,
Theoretical Statistics and Mathematics Division,
Indian Statistical Institute
Kolkata, India

Date: August 16, 2004 Time: 11.00 – 12.00

Location: Rm. M 301 M. Building, Faculty of Science, Mahidol University Host: Department of Mathematics, Faculty of Science, Mahidol University Rama 6 Rd., Bangkok 10400 Tel. 02-644-5419 Fax. 02-201-5343

### **Delay- and Nonlinear Fokker-Planck Equations**

Beyond Conventional Fokker-Planck Equations: Delay- and Nonlinear Fokker-Planck Equations	Date: August 23, 2004 Time: 13.30-14.30 Location: Rm. M202 M. Building
Stochastic Processes Described by Conventional Fokker-Planck Equations	Date: August 25, 2004 Time: 13.30-14.30 Location: Rm. M202 M. Building
Solutions of Delay Fokker-Planck Equations	Date: August 27, 2004 Time: 13.30-14.30 Location: Rm. M202 M. Building
Data Analysis in Stochastic Systems with Time-Delayed Feedback	Date: August 31, 2004 Time: 13.30-14.30 Location: Rm. M202 M. Building
Solutions of Nonlinear Fokker-Planck Equations	Date: September 2, 2004 Time: 13.30-14.30 Location: Rm. M202 M. Building

By
Dr. Till Daniel Frank
Institute for Theoretical Physics, University of Muenster,
Muenster, Germany

Host: Department of Mathematics, Faculty of Science, Mahidol University Tel: 02-644-5419 Fax: 02-201-5343

### Three formulations of the problem of finding equilibrium configurations

Date:

24 September 2004

Time:

13.30 - 16.30

Location: Rm. K 130 Chalerm Prakiat Building

### Solving the problem by using Lax-Milgram Lemma

Date:

25 September 2004

Time:

13.30 - 16.30

Location: Rm. K 130 Chalerm Prakiat Building

### Solving the problem through Optimization Theory- Equivalency

Date:

1 October 2004

Time:

13.30 - 16.30

Location: Rm. K 130 Chalerm Prakiat Building

### The direct method of Calculus of Variation

Date:

2 October 2004

Time:

13.30 - 16.30

Location: Rm. K 130 Chalerm Prakiat Building

### Some elements of Convex Analysis

Date:

8 October 2004

Time:

13.30 - 16.30

Location: Rm. K 130 Chalerm Prakiat Building

### Some elements of Convex Analysis (continued)

Date:

9 October 2004

Time:

13.30 - 16.30

Location: Rm. K 130 Chalerm Prakiat Building

by Professor Christian Licht University of Montpellier II, France

Host:

Department of Mathematics, Faculty of Science, Mahidol University, Rama 6 Rd., Bangkok 10400

Tel. 02-644-5419 Fax. 02-201-5343

# Three Applications of Common N-Gram Method

By
Prof. Nick Cercone, Dean
Faculty of Computer Science
Dalhousie University, Canada

Date: September 28, 2004 Time: 13.00 – 16.00 Host: Department of Mathematics, Faculty of Science, Mahidol University Location: Rm. B 201 B. Building, Faculty of Science, Mahidol University Rama 6 Rd., Bangkok 10400 Tel. 02-644-5419 Fax. 02-201-5343

#### "Partial Actions of Groups on Algebras"

Topic	Date - Time - Location
• Introduction	Date : October 4, 2004
Partial actions	Time : 10:00 – 12:00
,	Location: Rm. 8-3-5 Building
Enveloping actions	Date : October 5, 2004
	Time : 10:00 – 12:00
	Location: Rm. M-305 Building
<ul> <li>Partial skew group rings</li> </ul>	Date : October 6, 2004
The associativity question	Time : 10:00 – 12:00
	Location: Rm @-305 Building
Partial action	Date : October 7, 2004
on semiprime algebras	Time : 10:00 – 12:00
	Location: Rm. M-305 Building
Morita equivalence	Date : October <b>8</b> , 2004
1 -	Time : 10:00 – 12:00
	Location: Rm. M-305 Building
<ul> <li>Partial skew polynomial rings</li> </ul>	Date : October 11, 2004
	Time : 10:00 – 12:00
i i	Location: Rm. M-305 Building
Partial Galois theory	Date : October 12, 2004
of commutative rings	Time : 10:00 – 12:00
← Some questions	Location: Rm. 17-305 Building
to be considered	
Discuss and Exchange ideas	Date : October 13 - 14, 2004
,	Time : 10:00 – 14:00
: ii	Location: Rm -M-305 Building

#### By

#### Professor Dr. Miguel Ferrero

Department of Mathematics, Federal University of Rio Grande do Sul, Porto Alegre, Brazil

Host: Department of Mathematics, Faculty of Science, Mahidol University Tel: 02-644-5419 Fax: 02-201-5343

# Introduction to dyadic Models for Social Network Analysis

Prof. Dr. Bikas K. Sinha
Stat-Math Unit,
Theoretical Statistics and Mathematics Division,
Indian Statistical Institute
Kolkata, India

Date: October 18, 2004 Time: 11.00 – 12.00 Host: Department of Mathematics, Faculty of Science, Mahidol University Location: Rm. B 201 B. Building, Faculty of Science, Mahidol University Rama 6 Rd., Bangkok 10400 Tel. 02-644-5419 Fax. 02-201-5343

# Exchange Properties for Modules and Rings

þ

### Professor Dr. John Clark

Department of Mathematics, Otago University, New Zealand

hate: November 22-23, 2004

Time: 10.00 - 12.00

Location: Rm. M 302 M Building

Date: November 24, 2004

Time: 10.00 - 12.00

Location: Rm. M 305 M. Building

Date: November 25, 2004

Time: 10.00 - 12.00

Location: Rm. K 136 Chalerm Prakiat Building

Date: November 26, 2004 Time: 10.00 - 12.00 Location: Rm. M 307 M. Building

Department of Mathematics, Faculty of Science, Mahidol University Rama 6 Rd., Bangkok 10400 Tel. 02-644-5419 Fax. 02-201-5343 Host:

on

### Calibration Curves with Heteroscedastic Errors Confidence Regions for Random-Effects

by

Assoc. Prof. Dr. Dulal K. Bhaumik

Department of Psychiatry and Biostatistics

University of Illinois at Chicago, USA.

Date: December 2, 2004

Time: 11:00 - 12:00

Host: Department of Mathematics, Faculty of Science, Mahidol University

Location: Rm. M 307 M. Building, Faculty of Science, Mahidol University

Special Seminar

on

# Lecture#1: Methods for Extracting Critical Parameters in Nerve Fiber Models

Lecture#2: Stationary States and Traveling Waves of Excitation in Neural Field Theory

þ

### Professor Jonathan Bell

Chair, Department of Mathematics and Statistics

University of Maryland, Baltimore County, USA.

Date: January 7, 2005

Time: 10:00 - 12:00

Host: Department of Mathematics, Faculty of Science, Mahidol University

Location: Rm. M 302 M. Building, Faculty of Science, Mahidol University

O

## Non-ejective and Non-extremal Fixed Point Theory

by

#### Dr. Dang Vu Giang

Hanoi Institute of Mathematics, Vietnam

Date: February 17, 2005

Time: 14:00 - 16:00

Location: Rm. M 307 M. Building, Faculty of Science, Mahidol University Host: Department of Mathematics, Faculty of Science, Mahidol University Rama 6 Rd., Bangkok 10400 Tel. 0 2644 5419 Fax. 0 2201 5343

Special Seminar

OU

## Spectrum of Laplacian in Paley-wiener Spaces

2

### Dr. Dang Vu Giang

Hanoi Institute of Mathematics, Vietnam

Date: February 18, 2005

Time: 14:00 - 16:00

Host: Department of Mathematics, Faculty of Science, Mahidol University

Location: Rm. M 303 M. Building, Faculty of Science, Mahidol University

 $0^{\mathrm{n}}$ 

# ML Estimation for Pareto Distribution: Role of Sequential Designs

 $\stackrel{\wedge}{\mathrm{B}}$ 

Prof. Dr. Bikas K. Sinha

Stat - Math Unit,

Theoretical Statistics and Mathematics Division,

Indian Statistical Institute. Kolkata, India

Date: February 28, 2005

Time: 13.30 – 14.30 PM.

Host: Department of Mathematics, Faculty of Science, Mahidol University

Location: Rm. M. 202 M. Building, Faculty of Science, Mahidol University

Special Seminar

Sequential Hypothesis Testing in the Distribution of Lifetime of the Oil Seals

by

### Dr. Chana Preecha

Ph.D. in Applied Statistics,

University of Northern Colorado, USA.

Date: February 28, 2005

Time: 15:00 p.m.

Host: Department of Mathematics, Faculty of Science, Mahidol University

Location: Rm. M 202 M. Building, Faculty of Science, Mahidol University

O

Limit theorems in Statisties with Applications.

þ

Prof. Bimal K. Sinha

Department of Mathematics and Statistics,

University of Maryland, Baltimore County, U.S.A

Date: March 22 - 25, 2005

Time: 10.00 - 12.00

Host: Department of Mathematics, Faculty of Scuence, Mahidol University

Location: Room M 202 M.Buiding, Faculty of Science, Mahidol University

Rama 6 Rd., Bangkok 10400 Tel 02-644-5419 Fax. 02-2015343

10 m

Special Seminar

O

Some new results on estimation of a common mean of two normals.

þ

Prof. Bimal K. Sinha

Department of Mathematics and Statistics,

University of Maryland, Baltimore County, U.S.A

Date: March 25, 2005

Time: 13.30 - 14.30

Host: Department of Mathematics, Faculty of Scuence, Mahidol University

Location: Room M 202 M.Buiding, Faculty of Science, Mahidol University

New Approach and Results: From Linear to Nonlinear Systems

þ

Prof. Dr. Vu Ngoc Phat Institute of Mathematics

Hanoi, Vietnam

Date: April 22, 2005

Time: 10.00 - 11.00 a.m.

Host: Department of Mathematics, Faculty of Science, Mahidol University

Location: Room M 202 M.Buiding, Faculty of Science, Mahidol University

=

Applications in Mathematical Control Problems

<u>S</u>

Prof. Dr. Vu Ngoc Phat Institute of Mathematics Hanoi, Vietnam

Date: April 29, 2005

Time: 10.00 - 11.00 a.m.

Host: Department of Mathematics, Faculty of Science, Mahidol University

Location: Room M 202 M.Buiding, Faculty of Science, Mahidol University

Rama 6 Rd., Bangkok 10400 Tei 02-644-5419 Fax. 02-2015343

Madizonal

大180.68

O

Hankel Operator on Bergman Space

2

Dr. Zen Harper

Department of Pure Mathematics

Leeds University, U.K.

Dáte: May 3,2005

Time: 10.00 - 11.00 am.

Host: Department of Mathematics, Faculty of Scuence, Mahidol University

ocation: Room M 202 M.Buiding, Faculty of Science, Mahidol University

00 --- on

Theory and Applications of Shadowing in Dynamical Systems

2

Prof. Kenneth Palmer

Department of Mathematics

National Taiwan University

Date: July 18, 2005

Time: 14.00 - 15.00 pm.

Host: Department of Mathematics, Faculty of Science, Mahidol University

Location: Room M.302, M.Building Faculty of Science, Mahidol University

 $\subseteq$ 

Semantic Representation and Machine Translation

ģ

Prof. Nick Cercone

Dalhousie University, Canada

Date: July 19, 2005

Time: 10,00 - 12.00 a.m.

Host: Department of Mathematics, Faculty of Science, Mahidol Uniyersity

Location: Room M.306 M.Building Faculty of Science, Mahidol University

Special Seminar

O

ONTOLOGY

þ

Prof. Nick Cercone

Dalhousie University, Canada

Date: July 20, 2005

Time: 13.30 - 15.30

Host: Department of Mathematics, Faculty of Science, Mahidol University

Location: Room M.306 M.Building Faculty of Science, Mahidol University